Forschungszentrum Jülich
in der Helmholtz-Gemeinschaft

Institut für Festkörperforschung

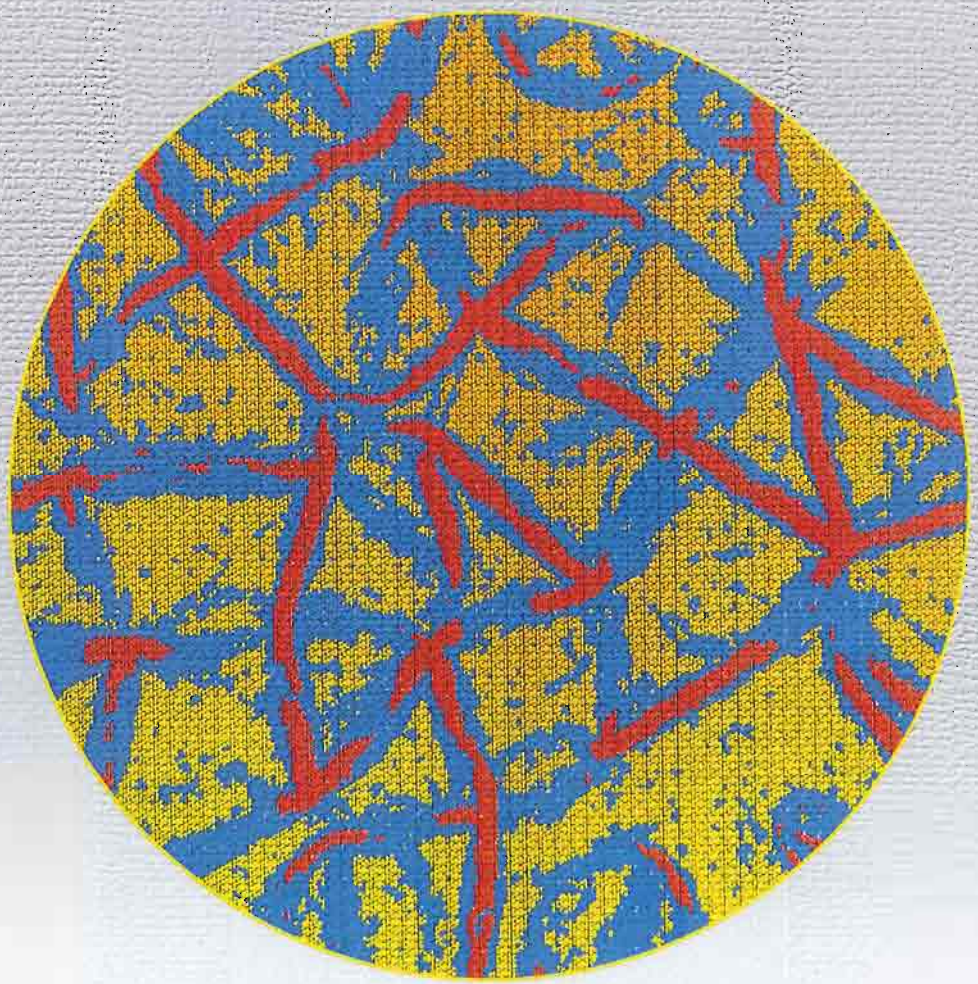

Scientific Report 2002/2003

Institut für Festkörperforschung

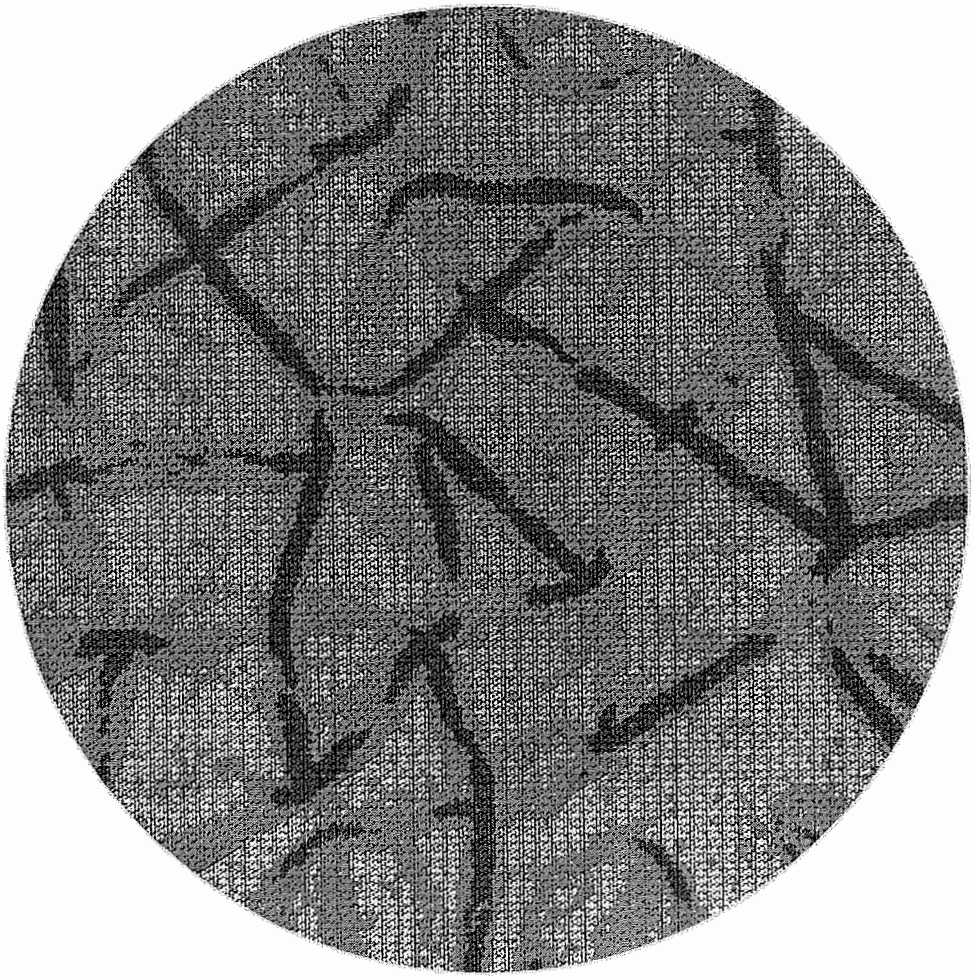

Scientific Report 2002/2003

Published by Forschungszentrum Jülich GmbH
D-52425 Jülich
Telephone: +49 2461 61-0 – Telex: 833556-0 kfa d
Responsible for content: the Managing Director of the IFF
tel: +49 2461 614465, fax: +49 2461 612410, e-mail: h.geisler@fz-juelich.de
Wholly set-up by BD-SG, Grafische Betriebe, Forschungszentrum Jülich GmbH
Time of going to press: 24.02.2003

Introduction

The "Institut für Festkörperforschung" (IFF) is devoted to condensed matter research. Topics range from the physics and chemistry of liquids, via membranes, clusters, surfaces and thin films to homogeneous and inhomogeneous bulk solids. The IFF has a department structure consisting of 9 institutes and service groups. Its wide spectrum of experimental facilities and individual expertise enables the IFF to successfully tackle complex problems in close collaboration between preparative, experimental and theoretical groups. Specialized laboratories and facilities exist for preparation of polymers, colloids and ceramics or the growth of thin films and bulk single crystals. Besides standard methods for characterization, highly sophisticated techniques are available and constantly further developed such as ultra high resolution electron microscopy, neutron- and synchrotron x-ray scattering, and femtosecond laser spectroscopy. Characteristic for an institute of the HGF (Hermann von Helmholtz Association of National Research Centers) is the fact that the IFF builds, operates and makes available to external users the neutron scattering instruments at the research reactor FRJ-2. Last but not least, the IFF has a long tradition in teaching and training of young researchers, not only through the approximately 29 IFF scientists teaching at universities, but in particular through the Spring Schools of the IFF and the annual Neutron Laboratory Course.

This annual report is intended to inform the international scientific community, including our scientific advisory board, about the scientific activities at the IFF during the past year. We have attempted to present a typical cross section through the research done at the IFF, including scientific highlights as well as results of long term developments, for example the construction of new large-scale instruments. The scientific activities of the IFF have lead this year to 393 publications, of which 301 articles were published in journals, and a total of 356 external talks of which 212 were invited. I hope you will enjoy learning about our activities.

Since 01.01.2002 Prof. H. **Müller-Krumbhaar** is Chairman of the Visiting Committee of the „ Minerva Center for Nonlinear Physics" at the Weizmann Institute, Rehovot, and the Technion, Haifa, Israel. On behalf of the Federal President, the Secretary of State of the Federal Ministry for Education and Research, Dr. Uwe Thomas, awarded Prof H. **Müller-Krumbhaar** the Bundesverdienstkreuz am Bande. Prof. H. **Müller-Krumbhaar** has been elected Member of the German Academy of Natural Scientists LEOPOLDINA. Dr. **Allgaier, Prof. Gompper, Prof. Richter, and others** received the „Erwin-Schrödinger-Prize 2002" for Interdisciplinary Research of the Stifterverband für die Deutsche Wissenschaft for their joint work on the subject „Amphiphilic Block Copolymers as Efficiency Boosters in Oil-Water-Surfacant". Prof. Th. **Brückel** was elected Chairman of the „Research with Neutrons" Committee. Dr. Hitoshi **Endo** was invited by the Rector of the Westfälische-Wilhelms-University of Münster to this year's awards to the authors of outstanding dissertations. Dr. Paul Siegfried **Bechthold** has been named Extraordinary Professor at the University of Köln. Prof. Dr. Peter **Grünberg** has been awarded an honorary doctorate at the Ruhr-University of Bochum. Dr. Simone **Wiegand** has been awarded the Habilitation at the University of Bremen (Biology/Chemistry).

Alexander von Humboldt Research Prize
Prof. B. Carter, Rutherford Appleton Laboratory, USA
Prof. F. Spaepen, Harvard University, Cambridge, USA

Alexander von Humboldt Scholars
Dr. Z. Dogic, Brandeis University, USA
Prof. S.K. Dattagupta, S.N. Base National Centre for Basic Sciences, Calcutta, Indien

Prof. Dr. Knut Urban
IFF Managing Director 2003

Contents

Institute for Solid State Research (IFF)

Management and Structure

Prof. Dr. K. Urban
Institute 'Microstructural Research'
IFF-Managing Director for 2003

H. Geisler (Permanent Deputy of the Managing Director)

Institutes:

Institute 'Theory I'
Prof. S. Blügel

Institute 'Theory II'
Prof. Dr. G. Gompper

Institute 'Theory III'
Prof. Dr. H. Müller-Krumbhaar

Institute 'Scattering Methods'
Prof. Dr. Th. Brückel

Institute 'Neutron Scattering'
Prof. Dr. D. Richter

Institute 'Electroceramic Materials'
Prof. Dr. R. Waser

Institute 'Soft Matter'
Prof. Dr. J. Dhont

Institute 'Microstructural Research'
Prof. Dr. K. Urban

Institute 'Electronic Properties'
Acting Director: Prof. Dr. Th. Brückel

Central Facilities:
'Networks and Numerics'
H. Geisler

'Accelerator'
DI R. Hölzle

'Construction'
H. Feilbach

'Mechanical Workshop'
K. Hirtz

'Administration'
H. Geisler

1. The Mission of the Institute for Solid State Research

The Institute for Solid State Research (IFF) pursues research on condensed materials in the solid or liquid state. Based on its studies of bulk properties of condensed phases, the IFF is concerned with inhomogeneous systems and with the consequences of reduced dimensionality. This refers in particular to the physics of boundaries, interfaces, thin films, and membranes. With regard to both theory and experiment, the institute's research can be understood in terms of three strategically distinct categories:

- **Phenomena oriented research:** The search for, the discovery and explanation of general phenomena and behaviour in condensed matter systems, including the mathematical and physical concepts and structures underlying this behaviour.

- **Materials oriented research:** The investigation of specific materials or classes of materials with a view of gaining an understanding of their special properties and, where appropriate, exploring their potential for practical application. Production of novel materials, and preparation as well as characterisation of well-defined samples.

- **Methods oriented research:** Development of new methods and the improvement of existing methods, both in the experimental and the theoretical/numerical sectors.

The general physical basis for these research areas is provided by statistical physics and quantum mechanics. Together they describe on a microscopic scale the behaviour and the reaction to external influences of electrons, atoms and molecules, the building blocks whose aggregation and cooperation is responsible for the formation of condensed phases. The issues to which these connections give rise in the context of current research form the basis of the work of *theoretical* and *experimental* groups within the institute.

Based on new techniques of preparation and characterization on a microscopic atomic scale, the *experimental* groups carry out research projects to develop devices and tailor materials systems with new properties. This, in turn, has triggered the *theoretical* groups, employing modern techniques, to describe and come to an understanding of the extremely complex behaviour of these new systems.

The following specific foci of work in the IFF are typical for the mission of a Helmholtz-Research-Centre:

- Contributions to the construction and operation of new experimental equipment and instruments for international sources of neutron and synchrotron radiation. In addition to the Jülich Research Reactor "DIDO", the neutron sources at Argonne, Berlin, Gaithersburg, Grenoble, München, Oak Ridge, Saclay and Appleton are used. Experiments with synchrotron radiation are carried out at BESSY, DELTA and HASYLAB in Germany, and internationally at Argonne (APS), Berkeley (ALS), Brookhaven (NSLS), Grenoble (ESRF), and Trieste (ELETTRA).

- Use of the Jülich Computer Centre, mainly for theoretical investigations and large-scale numerical simulations.

- Projects that require high levels of investment and/or the continuity of a highly qualified team of staff (in most cases in the context of national and international cooperative projects and services). Examples are the Centre for High-Resolution Microscopy, the operation of accelerators, the Electroceramics laboratory, superconductor technology and the development of sophisticated numerical algorithms and programs.

The research results of the IFF have led to a broad and internationally recognized status. Special technical and scientific excellence was achieved in the following areas: application of synchrotron radiation and neutron scattering, high-resolution electron-microscopy, electron spectroscopy, high-temperature superconductivity, magnetoelectronics, the physics of clusters, electron theory, dynamical features of phase transitions, quasicrystals, colloids, membranes and polymers.

A prerequisite for the focal areas of research in the IFF mentioned above and its position in the international community as a partner for cooperation is its strong position in basic research. The IFF carries out basic research in areas with potential for the future of condensed matter science, also as a springboard for applied research projects.

Genuine innovation (as distinct from continuous development) occurs typically as a by-product of curiosity-driven research. This is exemplified particularly well by the discovery of the "giant-magnetoresistance" effect, which has become a very active area in solid state research. The effect has attractive applications for magnetic sensors, e.g. as read-out heads for data storage and for control of moving parts. The license revenue from the patents on this effect represents the largest contribution to the total patent revenue of the Jülich Research Centre devolving from a single application! With this activity the IFF is also participating in the BMBF (Bundesministerium für Bildung und Forschung, i.e. Ministry of Education and Research) project "Magnetoelectronics".

2. Scientific and Technical Infrastructure

Research "at the cutting edge" requires the capability to build and maintain experimental facilities in high-tech areas. This holds as well for the basic research performed by the IFF at national and international sources as for its applied research. Equipment must meet high international standards, and especially so when the work performed is to be "relevant for industry". A basic requirement for the work of the Department is an infrastructure, within the IFF and the Research Centre itself, which supplies the necessary expertise, effectiveness, and facilities.

The group *Networks and Numerics* maintains the workstation cluster and computer networks, and supports scientific staff in the design and performance of experiments. It supplies expert assistance in hard- and software, maintains the system-software of the IFF-Workstation-Cluster and trains mathematical-technical assistants.

The *Accelerator Group* is responsible for the operation of the Compact-Cyclotron and the Tandetron.

Construction and *Workshop* develop and build equipment for the IFF, from simple mechanical components to sophisticated modern technology. The facility works closely together with the scientists and engineers of the Institute to achieve the ambitious quality and tolerance goals set by the experimentalists.

Staff members in the central facilities:

K. v. Ameln, F. Bläsen, H.P. Esser, A. Bremen, H. Cremer, P. Eickenberg, M. Emmerich, H. Feilbach, U. Funk-Kath, R. Gehlhaar, R. Heckmann, J. Heinen, D. Henkel, K. Hirtz, R. Hölzle, T. Jansen, K.H. Johnen, T. Kohnke, S. Krahe, J. Lingenbach, T. Matulewski, W. Noack, P. Pickartz, M. Pohl, B. Radermacher, H. Sachsenhausen, L. Schätzler, H. Schnitzler, J. Schnitzler, J. Schramm, P. Stefelmanns, W. Stellmacher, H. Terberger, R. Thomas, E. Westphal, K. Wingerath.

J. Hengesbach (INC), L. Kasterke (IME), H. Schwalbach (ISG)

3. Other Scientific Activities: Collaborations with Universities, Institutions, and Industry

The productivity of a Research Institute depends strongly on its capacity for scientific exchange and for scientific and technical cooperation. In this regard, the Jülich Research Center offers excellent possibilities. The Centre's top class infrastructure offers efficient assistance, also for visiting scientists. Modern neutron scattering instrumentation appropriate for cutting-edge studies are available to a large number of IFF guest scientists in the DIDO reactor hall and in the neutron guide hall ELLA. The wide variety of collaborations in which the institutes for Neutron Scattering and Scattering Methods of the IFF are involved leads to optimal usage of these large-scale instruments. On the other hand, the availability of complementary facilities at other institutions is essential for the IFF. With the construction of instruments the IFF contributed to the development and improved usage of external large-scale facilities such as ILL and CEN (Grenoble), APS (Argonne, USA), DELTA (Dortmund), HASYLAB (Hamburg), BESSY (Berlin), NSLS (Brookhaven), and NIST (Washington).

Bilateral agreements have been concluded with the Paul-Drude-Institute, Berlin, RWTH Aachen, and the Universities Bonn, Göttingen and Kiel for the use of the Jülich centre for high-resolution microscopy for specialized studies in the area of quantitative and high-resolution microscopy, and the use of the Jülich microscopes with correction of spherical abberation.

In the past years, the IFF has expanded its activities as a *sub-contractor* to large companies (e.g. Bosch, Siemens, Daimler-Benz, Thompson, Philips) and contract work has become the main focus of the scientific work of several groups, especially in the context of large national (German) and international projects. Of special importance is the IFF's participation in the BMBF-Project "Magnetoelectronics". Under the auspices of the Technology Transfer Bureau of the Jülich Research Centre, the IFF leases equipment to companies that have established themselves in the Jülich Technology Centre. In addition, the IFF has designed and built pilot equipment for industrial companies.

One of the most important duties of a Research Centre is to make its large-scale instruments available to universities and other research organisations for research projects that need not necessarily have a direct connection with active research programs of the Centre. In this context it is of paramount importance for the IFF to keep the 16 neutron scattering instruments at the research reactor DIDO operating and to improve them further. In the year 2002, neutrons were available for users at 185 days altogether. During this time 82 experiments were performed by IFF scientists and 116 experiments by external groups (38 groups from each national and international universities, 7 groups from national, and 15 from international research institutes).

Many staff members of the IFF serve in scientific committees (e.g. advisory boards for institutes and scientific societies, program committees for international meetings, editors of proceedings, journals, and databases, members or presidents of the boards of directors of scientific societies) as well as referees, e.g. for the German funding agencies, special research areas, and prize committees.

Institute Reports with Selected Research Results 2002

Institute Theory I

General Overview

Introduction:

The research activities of the Institute encompass several key areas of condensed matter theory: (i) electronic and structural properties of complex systems ranging from large organic molecules, low-dimensional magnets, magnetic multilayer and mesoscopic contacts to complex solids; (ii) transport properties across interfaces, electronic excitations and dynamical properties of molecular clusters, solids and solid surfaces, as well as the quasiparticle behaviour of transition metals and oxides resulting from electronic correlations; (iii) nano-scale tribology, friction, plastic deformation, adhesion and brittle fracture.

The principal goal of these studies is to achieve a microscopic understanding of complex phenomena on an electronic and atomic scale. Although most of these topics involve fundamental issues associated with many-body interactions, they are nevertheless relevant to a wide host of practical applications in modern materials science. In fact, the majority of research topics is directly motivated by the aim of providing a quantitative or qualitative physical basis for possible future technologies.

In line with the range of topics investigated a wide variety of conceptual and computational methods is currently employed: density functional theory, molecular dynamics calculations, genetic algorithms, data mining techniques, time-dependent generalization of density functional theory, diagrammatic perturbation approaches, classical and Quantum Monte Carle methods, exact diagonalization schemes, as well as analytical methods. Needless to say that the state-of–the-art use of these methods benefits greatly from the excellent computational facilities available at the research center. The unique combination of basic physics questions and possible practical applications, investigated with these theoretical tools in collaboration with experimentalists is the hallmark of modern condensed matter and computational materials science research.

Research Topics:

1. *Curie temperature from first-principles calculations:*
   The Curie temperature of Fe, Co, Ni, and Gd and the Néel temperature of Eu were calculated from a Heisenberg model in the mean-field and the random-phase approximation. The interaction parameters that determine the interatomic exchange interaction in the Heisenberg model were extracted from ab-initio calculations based on density functional theory. A good agreement of the critical temperatures in theory and experiment is only possible, if long-ranged exchange interactions are taken into account. For Gd, a strong dependence of the Curie temperature on the c/a ratio was found; an experimental verification is awaited. (G. Bihlmayer, S. Blügel; in collaboration with I. Turek)

2. *Ballistic electron transport through mesoscopic contacts:*
   A previously developed method to determine the conductivity of nano-contacts based on semiconductor-heterostructures will be extended to the case of junctions via single molecules. (A. Bringer)

3. *Femtosecond spectroscopy of molecular clusters:*
   "Pump and probe" experiments are an important tool to study the dynamics of quantum systems in the range of femto-seconds. Normally lifetimes of excited quantum states are deduced assuming that the

dynamics is relaxational. This is not necessarily the case. In short intervals of time the dynamics must be described by a time dependent Schrödinger-equation. This will be done for simple situations (atoms, small molecules). (A. Bringer)

4. *Mathematical modelling using a genetic algorithm:*
Many quantities of considerable interest (such as the electrical conductivity of a real material) cannot be predicted by first principles theory. However, by mining existing data for hidden correlations (using e.g. the genetic algorithm) it may be possible to generate mathematical models for such quantities that use readily computed descriptors and which are able to predict these quantities with a certain degree of reliability. (J. Harris; A. Bringer)

5. *Computation of thermal and mechanical properties using density functional methods:*
A body of recent work has shown that the DFT method with well-established exchange-correlation energy functionals describes the small changes necessary to compute quantities such as the stiffness matrix (elastic moduli) of even quite complicated crystals. Furthermore application of full Grüneisen theory gives a good description of thermo-mechanical properties like the coefficient of thermal expansion. These are currently supercomputer applications, however, requiring a very careful treatment of phonon spectra. A lower level of theory (Debye-Grüneisen) is available but so far has been tested only for some elemental metals. The current status of the programme is to establish procedures for implementing Debye-Grüneisen theory in general and testing its area of applicability. (J. Harris; in collaboration with J. Rodgers, Y. LePage, P. Schmidt)

6. *Magnetic imaging with the scanning tunnelling microscope:*
Up to now, a successful imaging of magnetic structures on surfaces with the scanning tunnelling microscope was only possible using magnetic tips. Exploiting the dependence of the tunnelling current on the spin-orbit interaction, it has been shown both theoretically and experimentally that an investigation of the local orientation of the magnetization is even possible with non-magnetic tips. (S. Heinze, X. Nie, G. Bihlmayer, S. Blügel)

7. *Energy surfaces, structures and reactions of polymers and organic molecules:*
The electronic and structural properties of organic molecules are evaluated using density functional theory and molecular dynamics methods with the aim of understanding in detail the mechanism of reactions between polymer chains, and the catalysts and additives used in their production. The density functional programs run on the T3E supercomputers and are very demanding of computer resources for systems of the complexity studied here. The resulting energy surfaces, however, provide a consistent and extendible data base for developing simplified models that allow calculations on much larger systems. Of particular interest are: (i) the refinement of classical force fields for use in molecular dynamics and Monte Carlo simulations, (ii) the development of a model of "living polymers" that allows one to study the polymerization process in polycarbonate and other materials over a wide range of temperatures and densities. (R.O. Jones; in collaboration with J. Akola, P. Ballone, Bayer AG)

8. *Coulomb correlations in photoemission spectra:*
For the bulk and the surface of SrVO3, an electronically strongly correlated material, the quasi-particle spectrum is evaluated using the dynamical mean field theory (DMFT). In agreement with experiment, it is shown that as a result of the reduced coordination numbers of surface atoms correlations effects are stronger at the surface than in the bulk. This result is of considerable importance for the interpretation of photoemission experiments. (A. Liebsch)

9. *Magneto-optical Kerr effect for non-equilibrium electron distributions:*
There is currently great interest in understanding the dynamical response of magnetic surfaces to excitations via ultra fast lasers (e.g., recent experiments in this area in the institute IFF-IEE). In order

to investigate to what extant the Kerr signal provides information on the time-varying magnetization of the sample, the optical conductivity tensor is evaluated for non-equilibrium electron distributions generated by the initial pump laser. Of particular interest is the so-called bleaching effect (closing of certain excitation channels) at high laser intensities. (A. Liebsch; in collaboration with P. Oppeneer)

10. *Trajectories and their discrete counterparts:*
It is generally believes that trajectories can well be represented by their discrete counterparts, the so called Poincaré maps (PM) which quite often are much easier to handle (e.g. numerically). It is shown, that in repelling systems (transient chaos) the PM gives misleading results. Even the sign of drifts can be erroneous. Modifying the PM by including the return time (time between two intersections) leads to correct results. At present correlation functions and diffusion are computed and compared by using PM and the modified PM. (H. Lustfeld; in collaboration with Z. Kaufmann)

11. *Characterization of tracer gas concentrations in the atmosphere:*
In the atmosphere small scale fluctuations of tracer gas, in particular pollutant, concentrations occur signalizing that the concentrations are singular functions. It is shown that these singularities have to be characterized not by just one Hölder exponent but by an ensemble classifying the strength of these singularities. The situation is quite analogous to that of trajectories: These have to be classified by an ensemble of Lyapunov exponents as well. Just one exponent is not sufficient. (H. Lustfeld; in collaboration with Z. Neufeld)

12. *Friction, nano-sale tribology:*
A research activity related to many practical applications concerns the area of tribology, in particular, friction and related topics such as plastic deformation, adhesion and brittle fracture. The influence of surface roughness on adhesion between elastic bodies is also investigated. Furthermore, Molecular Dynamics calculations are performed to understand the transition between lubrication and hydrodynamic lubrication. An important result was obtained within a recently developed theory of contact mechanics between randomly rough surfaces, where the solids are assumed to deform elastically when the stress is below the yield stress, and plastically when the stress reaches the yield stress. Of key interest is the dependence of the (apparent) area of contact on the magnification. In most cases the area of real contact is proportional to the load, If the rough surfaces, however, is self-affine fractal (Hurst exponent H) up to the lateral size L of the nominal contact area, and assuming no plastic deformation, then the real contact area is proportional to LH. (B.N.J. Persson; in collaboration with A. Volokitin, V. Samoilov, S. Zilbermann).

13. *Rubber Friction:*
When rubber slides on a hard, rough substrate, the surface asperities of the substrate exert oscillating forces on the rubber surface leading to energy "dissipation" via the internal friction of the rubber. A recently developed theory shows how the resulting friction force depends on the nature of the substrate roughness and on the sliding velocity both for stationary and non-stationary sliding. Numerical results were obtained for the case when the substrate surface has a self affine fractal structure and are in good agreement with experimental observations. The theory is now used be tire companies in developing new rubber compounds for tires. At present the theory is extended to take into account the flash temperature in the rubber-substrate contact areas. (B.N.J. Persson)

14. *Dynamical correlations in the electron gas:*
To understand dynamical correlations in the electron gas beyond the RPA, lowest order corrections in the dynamically screened. Coulomb interaction are evaluated numerically. The corresponding irreducible polarization diagrams have been known for 40 years but have resisted computation because of their complexity. By analytical means the resulting 7-dimensional integrals were now reduced to 3-dimensional integrals. For (k, w) outside the particle-hole continuum, dynamical correlations consist of two-particle-hole-pair, two-plasmon and coupled particle-hole-pair-plasmon

excitations. The results in this range compare well with experiments. Presently the calculations are extended to (k, w) inside the particle-hole continuum with the aim of analyzing additional available data. (K. Sturm; in collaboration with A. Gussarov, H. Lustfeld)

15. *Ballistic transport through realistic interfaces:*
A new ab-initio method for the calculation of ballistic electron transport has been developed on the basis of the density functional theory. The ballistic transport is described by the formula of Landauer-Büttiker reformulated in terms of Green functions. By means of an implementation in the FLAPW method and by applying the embedding method to calculate the Green functions it is possible to investigate the transport properties of e.g. realistic magnetic tunnelling barrier systems such as Fe/MgO/Fe. (D. Wortmann, H. Ishida, G. Bihlmayer, S. Blügel)

Stefan Blügel

Personnel 2002/2003 and areas of activity:

Scientific Staff

Dr. G. Bihlmayer	Development of FLAPW method, electronic structure and complex magnetism	E2310207
Prof. S. Blügel	Institute Director Electronic structure calculations, low dimensional magnetism, nano-spintronics, organic molecules on surfaces	E2310207
Dr. A. Bringer	Problems of electron correlation, genetic algorithms for materials research	E2310207
Dr. J. Harris	Practical applications of computational and informational methods to materials research	E2310207
Dr. R.O. Jones	Structure and dynamics of clusters, molecules, and disordered systems; Project: "Chemistry Laboratory Computer"	E2310207
Dr. A. Liebsch	Electronic response at surfaces; correlated systems; ultrafast demagnetization	E2310207
Dr. H. Lustfeld	Theory of nonlinear systems; atmospheric chemistry; dynamical electron correlations in metals	E2310207
Dr. B.N.J. Persson	Electronic response at surfaces, adsorbate modes, atomic friction, crack propagation	E2310207

Technical Staff

U. Winkler	Secretary	E2310207

Guests

Prof. P. Ballone	(University of Messina) Development and applications of the MD/DF method, Monte Carlo calculations	E2310207
Prof. K. Fischer	(FZ Jülich, retired) Vortices in high Tc superconductors	E2310207
Prof. H. Ishida	(Nihon University, Tokyo) Electronic properties of surfaces, transport through interfaces	E2310207
Dr. Y. Koroteev	(Academy of Science, Tomsk, Russian) Surface states and life time of surface states	S216010
K. Rytkönen	(University Jyväskylä, Finland) Adsorption on graphite layers	E2310207
Prof. V. Samoilov	(Moskau State University) Theory of friction	E2310207

Prof. K. Sturm	(FZ Jülich, retired since 1.4.2001) Dynamical correlations	E2310207
Dr. M. Trioni	(INFM UdR, Milano Bicoccia) Greenfunction embedding method	S216010
Prof. A. Volokitin	(Samara University, Russia) Theory of friction	E2310207
Dr. I. Sievebaek	(Tech. University Copenhagen) Theory of friction	E2310207

Postdocs

Dr. J. Akola	(University Jyväskylä, Finland) Structure and dynamics of organic molecules	E2310207
Dr. V. Caciuc	(University of Osnabrück) Development of parallelized PAW program, applications to AFM	extern
Dr. Y. Liu	(Nagoya University) Carbon nanotubes	E2310207
Dr. T. Ohwaki	(Tokyo University) Electronic structure theory of field emission	E2310207

Graduate Students

S. Baud	(Besancon, France) Magnetic chains	S216010
D. Boukhvalov	(Ekaterinburg, Russia) Molecular magnets	E2310207
M. Heide	Nanomagnetism, non-collinear magnetism	E2310207
M. Lezaic	Spin-gap materials	extern
Y. Mokrousov	Development of FLEUR code for one-dimensional systems, magnetic chains	extern
S. di Napoli	(Comision Nacional de Energia Atomica, Buenos Aires, Argentina) Non-collinear magnetism in IGMR compounds	S216010
D. Wortmann	Embedded Green-Function method, magneto-electronics	S216010
S. Zilbermann	(Tel Aviv University) Theory of friction	E2310207

E2310207	Condensed Matter
S216010	HGF Strategy fond magneto electronic

Liquid sulphur – a "simple" polymer?

R. O. Jones and P. Ballone†
Institute Theory I

In recent years we have reported on density functional (DF) and Monte Carlo calculations on organic polymers, particularly bisphenol-A polycarbonate (BPA-PC). DF calculations provide essential information on the energy surfaces of the polymer and its reactants, and the results are used to derive the parameters of a simplified force field model. Monte Carlo calculations with this model have then provided new information about the polymerization and its driving force. We are extending these ideas to study liquid sulphur, often viewed as the simplest of all polymer systems. We describe DF calculations for the structures and cohesive energies of sulphur clusters and their reactions with each other. These provide essential input for Monte Carlo calculations now in progress.

F&E-Nr: E2310207

Density functional (DF) calculations provide a means of computing the geometrical and electronic properties of molecules, and of simulating the behaviour of bulk systems. Such such calculations avoid the use of parameterized force fields common in the study of polymers, but they are very demanding of computing resources. Our first applications to polymers were to cyclic tetramers of bisphenol-A polycarbonate (BPA-PC) reacting with nucleophilic molecules ("active sites") such as LiOPh, shown schematically in Fig. 1. This reaction is a particular form of ring-opening that produces an active site at the end of the chain. This can then react with another ring, leading to a "living polymer". The DF calculations provide reliable estimates of energy barriers and the overall enthalpy change, and this information was used to develop a model force field for use in Monte Carlo and molecular dynamics calculations for systems with many thousands of particles. The model demonstrates a clear tendency towards polymerization that is enhanced by increasing the temperature T and particularly the packing fraction. Polymerization is highly reversible, i.e. it decreases upon decreasing the system density, and the transition is driven by the entropy associated with the bond distribution [1,2].

The liquid-liquid phase transition in sulphur at 159°C is often described as ring-opening polymerization, and it is natural to ask whether the transition can be described by a similar model. Above the melting point (113°C) sulphur is believed to comprise mainly S_8 rings with small concentrations of homocyclic rings with up to 23 atoms [3]. At 159°C, there are dramatic changes in viscosity, specific heat, and other properties, and this liquid-liquid phase transition is often described as a ring-opening polymerization of the S_8 rings. Its apparent simplicity has made it the subject of many experimental and theoretical investigations, but there is no consensus on the origin. For example, neutron scattering results have been interpreted as indicating percolation rather than polymerization.

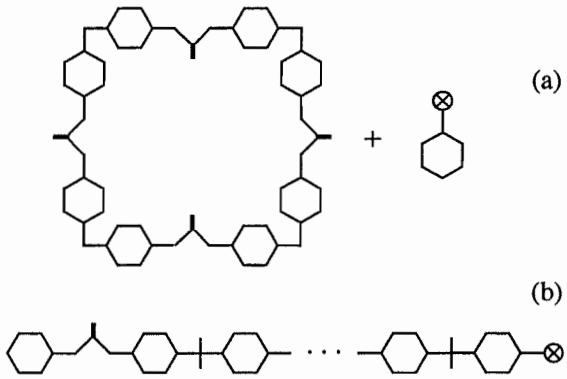

FIG. 1. Reaction of LiOPh with cyclic tetramer of BPA-PC. The product (b) is a Li-terminated chain.

Liquid sulphur is not only a relatively simple system with a single element, but sulphur has the most solid allotropes of any element. The ring structures that occur provide an extensive data base for testing the parameters of force fields that can be used for long simulations for many particles. We have performed calculations on more than 60 isomers of sulphur clusters with two to 18 atoms, focusing on the trends in structures, binding energies, and vibration frequencies. Full details will be published elsewhere [4].

Examples of the structures found are shown in Fig. 2 for nine and ten-atom clusters. In addition to the ring structures **9a** and **10a**, we have a variety of chain structures. Rings are more stable than chains, although the number of chain isomers is much greater. Chain structures with planar tetramer terminations are the most stable. The overall agreement with other calculations and with x-ray diffraction measurements is very good.

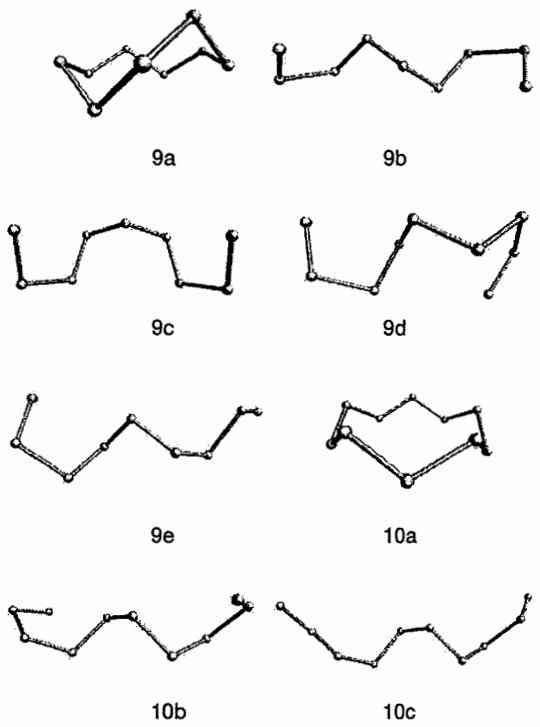

FIG. 2. Structures of isomers of S_9 and S_{10}.

The calculated cohesive energies (Fig. 3) of the most stable isomers of S_n clusters show some interesting trends. S_8 and S_{12} are the most stable, but all larger clusters show similar cohesive energies.

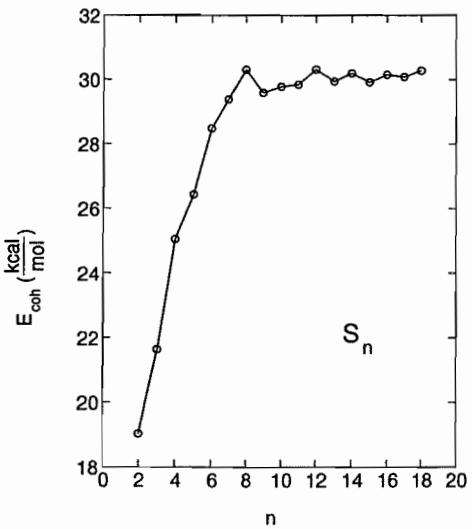

FIG. 3. Cohesive energies of sulphur clusters S_n, $n = 2 - 18$).

The common picture of polymerization in liquid sulphur involves the opening of S_8 rings to chains, followed by their reactions to longer chains. However, the energy required to open the crown-shaped S_8 isomer is ca. 28 kcal/mol, and the interaction of two S_8 ring singlets is repulsive (Fig. 4(a,b)), and the most likely reaction path is

$$\textit{cyclo}\text{-}S_8 \longrightarrow \textit{chain}\text{-}S_8^{\cdot\cdot} \ (+nS_8) \longrightarrow S_{poly}^{\cdot\cdot} \qquad (1)$$

where the double dots indicate a triplet radical. The course of this reaction is shown in Fig. 4(c-f), and the calculated energy barrier is only 5.4 kcal/mol, in reasonable agreement with experimental estimates. These structures and energies have been used as database behind a force field for sulphur interactions that we are using to study the thermodynamic properties of liquid sulphur.

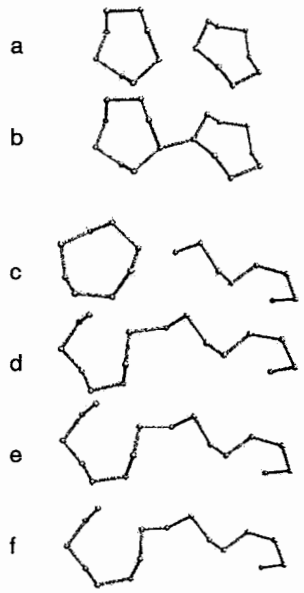

FIG. 4. Reactions of (a-b) two S_8 (D_{4d}) rings, (d-f) an S_8 chain (triplet) with an S_8 ring (D_{4d}). The shortest distances between the units are: (a) 2.53 Å, (b) 2.32 Å, (c) 2.58 Å, (d) 2.38 Å, (e) 2.28 Å, (f) 2.13 Å.

---

† Permanent address: Università degli Studi di Messina, Dipartimento di Fisica, I-98166 Messina, Italy.

[1] P. Ballone and R. O. Jones, J. Chem. Phys. **115**, 3895 (2001).
[2] P. Ballone and R. O. Jones, J. Chem. Phys. **116**, 7724 (2002).
[3] R. Steudel, R. Strauss, and L. Koch, Angew. Chem. **97**, 58 (1985).
[4] R. O. Jones and P. Ballone, J. Chem. Phys. (submitted).

Surface vs. bulk Coulomb correlations in photoemission spectra of perovskites

A. Liebsch
IFF Theory I

Photoemission spectra of the perovskite series $Sr_xCa_{1-x}VO_3$ reveal strong modifications associated with surface contributions. To study the effect of Coulomb correlations in the bulk and at the surface the quasi-particle spectra are evaluated using the dynamical mean field theory. It is shown that as a result of the reduced coordination number of surface atoms correlation effects are stronger at the surface than in the bulk, in agreement with experiment.

Photoemission is a key spectroscopy for the investigation of electronic properties of strongly correlated materials. Because of its surface sensitivity there is growing concern to what extent the data are representative of bulk properties and whether they need to be corrected for surface effects influencing the one- and many-electron properties. To study these questions Maiti *et al.* [1] and Sekiyama *et al.* [2] performed photoemission measurements on $Sr_xCa_{1-x}VO_3$ using a wide range of photon energies. As a result of the frequency dependent escape depth of the photoelectron, the spectra reveal striking variations evidently associated with surface modifications of the electronic structure: emission from the coherent peak near the Fermi level is reduced and correlation-induced satellites have larger weight than in the bulk. The same trend is observed on $SrRuO_3$ and $La_xCa_{1-x}VO_3$.

The understanding of surface effects in photoemission spectra of transition metal oxides is important in order to distinguish them from correlation phenomena in the bulk. Although the electronic properties of strongly correlated materials are currently a field of intense experimental and theoretical investigation surface effects have so far received little attention. Here, we use the dynamical mean field theory (DMFT)[3] to evaluate the surface and bulk quasi-particle spectra of $SrVO_3$[4]. We show that because of the planar electronic structure of perovskite systems and the concomitant narrowing of the surface local density of states correlation effects at the surface are more pronounced than in the bulk. We calculate the self-energy for a multi-band system using a realistic local density of states appropriate for $SrVO_3$ and find qualitative agreement with photoemission data.

Electronic structure calculations for $SrVO_3$ within the local density approximation (LDA) show that the conduction bands near E_F consist of degenerate t_{2g} bands derived from V^{4+} ($3d^1$) ions. The filled O 2p bands are separated from the t_{2g} levels by a gap of about 1 eV, and the cubic crystal field of the V-O octahedron shifts the e_g bands above the t_{2g} bands. Fig. 1 (a) shows the t_{2g} bulk bands of $SrVO_3$. According to the predominantly planar electronic structure, the bulk density of states $\rho_b(\omega)$ exhibits the characteristic asymmetric peak related to the van Hove singularity at the X point (see Fig. 1 (b)). At the surface, the t_{2g} degeneracy is lifted since only the d_{xy} band exhibits strong dispersion within the surface plane (the z axis defines the surface normal). To evaluate the surface density of states we use a Green's function formalism for semi-infinite tight-binding systems. Fig. 1 (b) shows the local density of states $\rho_s(\omega)$ of the $d_{xz,yz}$ bands for the surface layer of $SrVO_3$. Its spectral weight is reduced at low and high energies but enhanced at intermediate energies. Thus, the effective width of $\rho_s(\omega)$ is smaller than that of $\rho_b(\omega)$ although their total widths are identical. In contrast to the $d_{xz,yz}$ density, the density of d_{xy} states nearly coincides with the bulk density, reflecting the planar nature of the t_{2g} states.

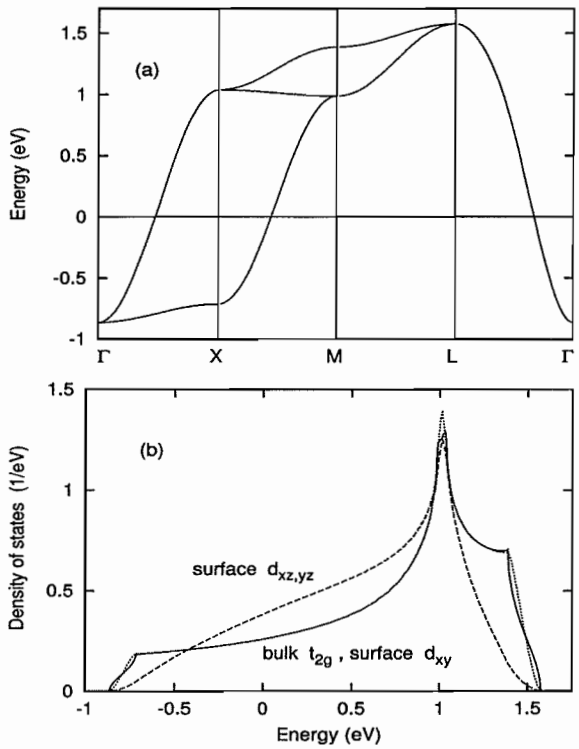

FIG. 1: (a) Tight-binding fit to LDA t_{2g} bulk bands of $SrVO_3$ ($E_F = 0$). (b) Solid curve: isotropic bulk density of states; dashed and dotted curves: local density of $d_{xz,yz}$ and d_{xy} states in the first layer of $SrVO_3$.

To interpret the experimental photoemission data we evaluate the quasi-particle spectra by accounting for local Coulomb correlations. According to the one-electron properties discussed above we are dealing with a non-isotropic system where two narrow bands interact with a wider band. The key quantity characterizing the effect of

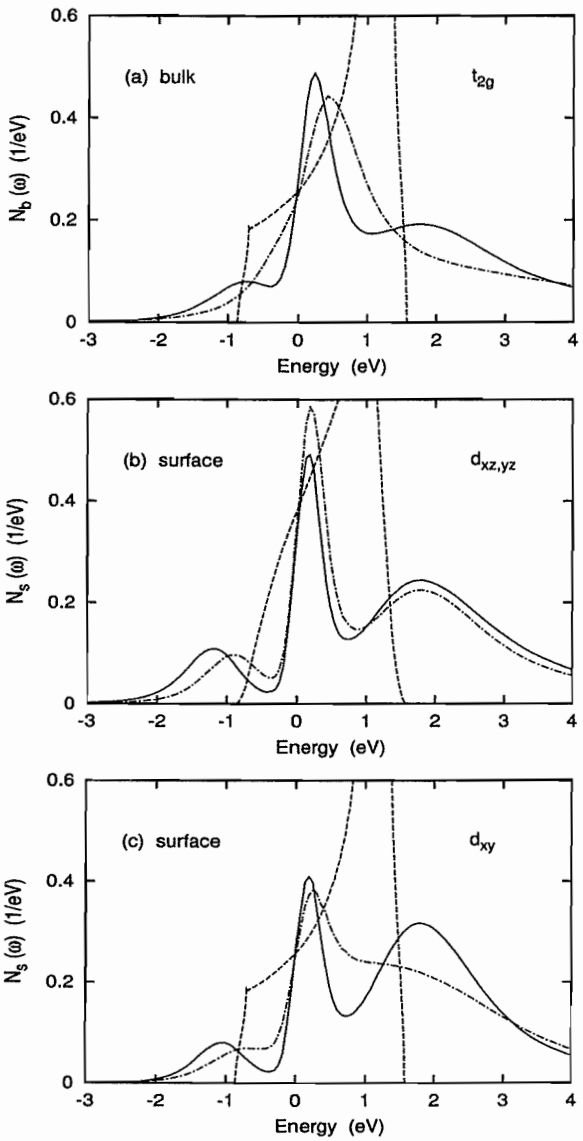

FIG. 2: Quasi-particle density of states of $SrVO_3$ derived from DMFT. (a) bulk t_{2g} states, (b) surface $d_{xz,yz}$ states, (c) surface d_{xy} states. Solid curves: $U = 4.3\,\mathrm{eV}$; dot-dashed curves: $U = 4.0\,\mathrm{eV}$; dashed curves: bare densities.

Coulomb correlations is the complex self-energy. Since we neglect the weak hybridization between t_{2g} bands, $\Sigma(\omega)$ is diagonal in orbital space and depends on the local density of states within each layer.

Fig. 3 (a) shows the bulk quasi-particle density of states of $SrVO_3$ for two Coulomb energies: $U = 4.0\,\mathrm{eV}$ and $4.3\,\mathrm{eV}$, with $J = 0.7\,\mathrm{eV}$. These results show that in the bulk U must be larger than $4\,\mathrm{eV}$ to obtain the satellite observed in photoemission spectra. The peak near 2 eV above E_F agrees with inverse photoemission data. Although for $U = 4\,\mathrm{eV}$ there is considerable correlation-induced band narrowing and an emerging satellite shoulder, the increase of U to $4.3\,\mathrm{eV}$ yields an even narrower coherent feature near E_F, with the missing weight shifted to the lower and upper Hubbard bands.

The surface quasi-particle spectra for $SrVO_3$ are shown in Fig. 3 (b) and (c). The lower Hubbard peak of the $d_{xz,yz}$ states is clearly visible already for $U = 4\,\mathrm{eV}$ because of the narrower local density of states in the first layer. A larger U shifts the satellite to higher binding energies. The comparison with the spectra shown in Fig. 3 (a) demonstrates that correlation effects for a fixed value of U are stronger at the surface than in the bulk: The coherent peak near E_F is narrower at the surface and the incoherent satellite feature is more pronounced than in the bulk, in agreement with experiment.

The surface quasi-particle density of d_{xy} states in Fig. 3 (c) is intermediate between $N_b(\omega)$ and $N_s(\omega)$ for $d_{xz,yz}$. Although there is little single-electron hybridization between t_{2g} bands, the local Coulomb interaction mixes them so that the d_{xy} surface spectrum involves contributions arising from the more strongly correlated $d_{xz,yz}$ states. The coupling between narrow and wide bands is a genuine multi-band effect and underlines the fact that single-particle bands in the presence of local Coulomb interactions cannot be considered independently.

Note that the many-body reduction of the quasi-particle band width is much larger than the surface-induced one-electron band narrowing. On the other hand, since the on-site Coulomb energy is not far from the critical value for a metal-insulator transition, the band narrowing substantially enhances the influence of correlations at the surface.

In summary, we have performed DMFT quasi-particle calculations for $SrVO_3$ in the bulk and at the surface. As a result of the planar nature of the t_{2g} states and the surface narrowing of the local density of states on-site correlation effects are more pronounced at the surface than in the bulk, in agreement with photoemission data. The two-dimensional character of d states near E_F is one of the hallmarks of transition metal oxides. The surface-induced enhancement of correlation effects discussed in the present work should therefore be a phenomenon observable in many materials.

[1] K. Maiti, D.D. Sarma, M.J. Rozenberg, I.H. Inoue, H. Makino, O. Goto, M. Pedio, and R. Cimino, Europhys. Lett. **55**, 246 (2001).

[2] A. Sekiyama, H. Fujiwara, S. Imada, H. Eisaki, S.I. Uchida, K. Takegahara, H. Harima, Y. Saitoh, and S. Suga, cond-mat/0206471.

[3] A. Georges, G. Kotliar, W. Krauth, and M.J. Rozenberg, Rev. Mod. Phys. **68**, 13 (1996).

[4] A. Liebsch, submitted to Phys. Rev. Lett.

Adhesion between elastic bodies with randomly rough surfaces

B.N.J. Persson
Institute Theory I

I have developed a theory of adhesion between an elastic solid and a hard randomly rough substrate. The theory takes into account that partial contact may occur between the solids on all length scales. For self-affine fractal surfaces, when the fractal dimension is close to 2, complete contact typically occurs in the macro asperity contact areas. For a fractal dimension larger than 2.5, the area of (apparent) contact decreases continuously when the magnification is increased.

Even a highly polished surface has surface roughness on many different length scales. When two bodies with nominally flat surfaces are brought into contact, the area of real contact will usually be only a small fraction of the nominal contact area.

How large is the area of *real* contact between a solid block and the substrate? This fundamental question has extremely important practical implications. For example, it determines the contact resistivity and the heat transfer between the solids. It is also of direct importance for sliding friction [1,2], e.g., the rubber friction between a tire and a road surface, and it has a major influence on the adhesive force between two solid blocks in direct contact. I have developed a theory of contact mechanics [3], valid for randomly rough (e.g., self affine fractal) surfaces, but neglecting adhesion. Here I consider adhesion for randomly rough surfaces for the most general case where *partial* contact occurs at the interface on many different length scales, see Fig. 1.

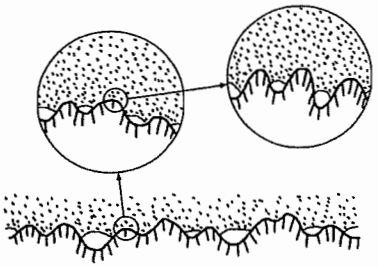

FIG. 1. A rubber block (dotted area) in adhesive contact with a hard rough substrate (dashed area). The substrate has roughness on many different length scales and the rubber makes partial contact with the substrate on all length scales. When a contact area is studied at low magnification it appears as if complete contact occur, but when the magnification is increased it is observed that in reality only partial contact occurs.

The present theory is based on the contact mechanics theory developed in Ref. [3]. This theory recognizes that it is essential not to exclude *a priori* any roughness length scale from the analysis. Thus, if $A(\lambda)$ is the (apparent) area of contact on the length scale λ [more accurately, we *define* $A(\lambda)$ to be the real contact area (projected on the xy-plane) if the surface would be smooth on all length scales shorter than λ], then we study the function $P(\zeta) = A(\lambda)/A(L)$, which is the relative fraction of the rubber surface area where contact occurs on the length scale $\lambda = L/\zeta$ (where $\zeta \geq 1$), with $P(1) = 1$. Here $A(L) = A_0$ denotes the macroscopic (nominal) contact area [L is the diameter of the macroscopic contact area so that $A_0 \approx L^2$].

Consider a rubber ball (radius R_0) in adhesive contact with a perfectly smooth and hard substrate. The elastic deformation of the rubber can be determined by minimizing the total energy, which is the sum of the (positive) elastic energy stored in the deformation field in the rubber ball, and the (negative) binding energy between the ball and the substrate at the contact interface. The free energy minimization gives the JKR pull-off force: $F_c = (3\pi/2)R_0\Delta\gamma$, where $\Delta\gamma = \gamma_1+\gamma_2-\gamma_{12}$ is the change in the surface free energy (per unit area) upon contact due to the rubber-substrate interaction. Consider now the same problems as above, but assume that the substrate surface has roughness described by the function $z = h(\mathbf{x})$ and that the width L of the nominal contact area is much larger than the long-distance cut-off (or roll-off) length $\lambda_0 = 2\pi/q_0$ of the surface roughness power spectra. In this case we can still use the result for F_c above (even when only partial contact occur at the interface), but with $\Delta\gamma$ replaced by $\gamma_{\rm eff}(1)$ given below.

Consider the system at the length scale $\lambda = L/\zeta$, where L is of order the diameter of the nominal contact area. We define $q_L = 2\pi/L$ and write $q = q_L\zeta$. Let $P(\sigma,\zeta)$ denote the stress distribution in the contact areas under magnification ζ. The function $P(\sigma,\zeta)$ satisfies the differential equation (see Ref. [3]):

$$\frac{\partial P}{\partial \zeta} = f(\zeta)\frac{\partial^2 P}{\partial \sigma^2}, \tag{1}$$

where

$$f(\zeta) = \frac{\pi}{4}\left[\frac{E}{1-\nu^2}\right]^2 \zeta^3 {q_L}^4 C(\zeta q_L), \tag{2}$$

where E is the elastic modulus and ν the Poisson ratio. The surface roughness power spectra

$$C(q) = \frac{1}{(2\pi)^2}\int d^2x\ \langle h(\mathbf{x})h(\mathbf{0})\rangle e^{-i\mathbf{q}\cdot\mathbf{x}}, \tag{3}$$

where $z = h(\mathbf{x})$ is the height of the surface above a flat reference plane (chosen so that $\langle h\rangle = 0$), and $\langle ...\rangle$ stands for ensemble average.

The relative (apparent) area of contact (projected on the surface xy-plane) when the system is studied under the magnification ζ can be written (see Ref. [3]):

$$P(\zeta) = \int_{-\sigma_a}^{\infty} d\sigma \; P(\sigma, \zeta), \tag{4}$$

where the *detachment stress* $\sigma_a = \sigma_a(\zeta)$ is defined below. $P(\sigma, \zeta)$ can be obtained by solving Eq. (1) subjected to the boundary conditions:

$$P(-\sigma_a(\zeta), \zeta) = 0, \quad P(\infty, \zeta) = 0. \tag{5}$$

These equations state that detachment occurs when the local stress on the length scale L/ζ reaches $-\sigma_a(\zeta)$, and that there is no infinitely large stress at the interface.

Let us consider the system on the characteristic length scale $\lambda = L/\zeta$. The quantity $\sigma_a(\zeta)$ is the stress necessary to induce a detached area of width λ, which is given by the theory of cracks:

$$\sigma_a = \left[\frac{\gamma_{\rm eff}(\zeta) E q}{2(1-\nu^2)}\right]^{1/2} \tag{6}$$

where $q = 2\pi/\lambda = \zeta q_L$. Here $\gamma_{\rm eff}(\zeta)$ is the change in the effective surface energy upon contact, which can be determined from $P(\zeta)$ as described in Ref. [4].

Fig. 2 shows (a) the effective interfacial energy $\gamma_{\rm eff}(1)$ and (b) the normalized area of real contact, $P(\zeta_1) = A(\zeta_1)/A_0$ (as obtained by studing the interface at the highest magnification $\zeta = \zeta_1$), as a function of of $q_0 h_0$ (where h_0 is the rms roughness amplitude). Results are shown for $q_0\delta = 0.1$, 0.2, 0.4 and 0.8, where $\delta \sim \Delta\gamma/E$. Note that for $q_0\delta = 0.4$ and 0.8 the macroscopic interfacial energy first increases with increasing amplitude h_0 of the surface roughness, and then decreases. The increase in $\gamma_{\rm eff}$ arises from the increase in the (contact) surface area, while the decrease result from the elastic energy stored at the interface. As shown in Fig. 2(b), for small h_0 the two solids are in complete contact, and, as expected, the complete contact remains to higher h_0 as $\delta \sim \Delta\gamma/E$ increases. Note also that the contact area is nonzero even when $\gamma_{\rm eff}(1)$ is virtually zero: the fact that $\gamma_{\rm eff}(1)$ (nearly) vanishes does not imply that the contact area vanishes (even in the absence of an external load), but implies that the (positive) elastic energy stored at the interface just balances the (negative) adhesion energy from the area of real contact. The stored elastic energy at the interface is given back when the block is removed, and when $\gamma_{\rm eff}(1) \approx 0$ it is just large enough to break the block-substrate bonding. Since it is the area of real contact that is important in sliding friction, it is clear that the *adhesion interaction may affect the friction force strongly even when no adhesion can be detected in a pull-off experiment.*

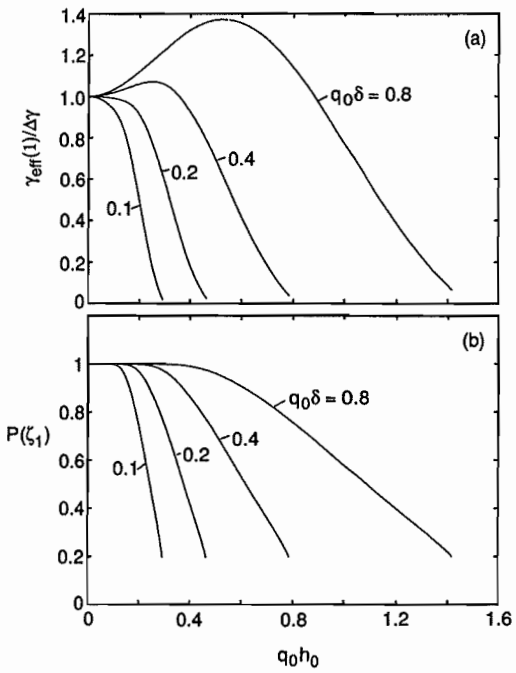

FIG. 2. (a) The macroscopic interfacial energy, and (b) the normalized area of real contact, $P(\zeta_1) = A(\zeta_1)/A_0$, as a function of of $q_0 h_0$. For $q_0\delta = 0.1$, 0.2, 0.4 and 0.8 as indicated, and with the roughness exponent $H = 0.8$.

The results presented in Fig. 2 are in good qualitative agreement with the experimental data of Fuller, Tabor, Briggs, Briscoe and Roberts. Unfortunately, those authors did not measure the surface roughness power spectra so no quantitative comparison is possible. A collaboration is underway, where the theory will be quantitatively tested with measurements performed on rough surfaces for which the full surface roughness power spectra has been measured [5].

[1] B.N.J. Persson, *Sliding Friction: Physical Principles and Applications*, Second Edition (Springer, Heidelberg, 2000).

[2] J.N. Israelachvili, *Intermolecular and Surface Forces*, Academic Press, London, 1995.

[3] B.N.J. Persson, Phys. Rev. Lett. **87**, 1161 (2001); B.N.J. Persson, J. Chem. Phys. **115**, 3840 (2001); B.N.J. Persson, F. Bucher and B. Chiaia, Phys. Rev. B**65**, 184106 (2002).

[4] B.N.J. Persson, Eur. Phys. J. E**8**, 385 (2002); Phys. Rev. Lett. **89**, 245502 (2002).

[5] W. Hild, G. Heinrich and B. Persson, in preparation.

An Embedded Green-function approach to the ballistic electron transport

D. Wortmann,[1] H. Ishida,[2] G. Bihlmayer,[1] and S. Blügel[1]

[1]*Institute "Theory I"*

[2]*College of Humanities and Sciences, Nihon University, Sakura-josui, Tokyo 156, Japan*

We present an efficient method for calculating the conductance of ballistic electrons through an interface from first-principles using the embedding approach of Inglesfield. In our method the Landauer-Büttiker formula for ballistic transport is expressed in terms of two quantities that are available in the embedded Green-function formalism without additional calculations. As a proof of principle we calculate on the basis of the density functional theory the spin-resolved electron transmission through a model system of ferromagnetic Co monolayers sandwiched between bulk Cu.

Studying electron transport through a thin interface layer or through a nanoscale contact between two electrodes forms a base of future technologies such as molecular electronics and spin electronics. According to the Landauer-Büttiker[1] formula for ballistic transport, the conductance across the interface is determined by the transmission probability of electrons at the Fermi energy ϵ_F. In other words, the conductance calculation is reduced to a scattering problem for an electron impinging on the interface.

The embedding approach of Inglesfield[2] provides a general framework to treat electronic states at the interface sandwiched between two bulk systems. Inglesfield showed that the effects of the bulk crystals beyond the embedding surfaces on both sides of the interface can be represented by an energy-dependent potential acting on the embedding surfaces. By simply adding the matrix elements of the embedding potentials to the Hamiltonian of an isolated slab, one can obtain the Green function of the entire system.

We start with defining the one-electron Green function with a real energy ϵ,

$$\left[-\frac{1}{2}\Delta + v(\vec{r}) - \epsilon\right] G(\vec{r},\vec{r}\,';\epsilon) = -\delta(\vec{r}-\vec{r}\,'), \qquad (1)$$

where $v(\vec{r})$ denotes the one-electron potential. In the embedding method the boundary condition of this Green function is controlled by means of the so called "embedding potential" $G^{-1}_{S_\alpha}$ which relates the value and normal derivative on S_α of an outgoing solution of the Schrödinger equation with energy ϵ by

$$\partial_n \psi^{\alpha o}_\nu(\vec{x}) = 2\int_{S_\alpha} G^{-1}_{S_\alpha}(\vec{x},\vec{x}\,')\,\psi^{\alpha o}_\nu(\vec{x}\,')\,d\vec{x}\,'. \qquad (2)$$

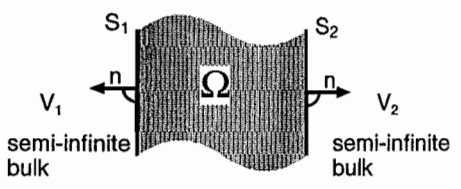

FIG. 1: Setup used in embedding calculations. The region of interest is a slab Ω between the two boundaries S_1 and S_2. Ω is infinite in two dimensions and of finite size normal to the boundaries. Outside the region Ω two semi-infinite bulk regions V_1 and V_2 are attached.

Applying Green's theorem, one may show that $\psi(\vec{r})$, a solution of the Schrödinger equation for energy ϵ, satisfies

$$\psi(\vec{r}) = -\frac{1}{2}\sum_{\alpha=1,2}\int_{S_\alpha}\left[G(\vec{r},\vec{x})\,\partial_n\psi(\vec{x}) - \partial_n G(\vec{r},\vec{x})\psi(\vec{x})\right] d\vec{x}, \qquad (3)$$

where $\vec{r}$ is any position in region Ω, $\vec{x}$ is any position at the interface S_α, and ∂_n denotes a surface normal derivative with n pointing outwards from Ω. In Eq. (3) we omitted the energy dependence of the Green function for simplicity.

In the following we use the first superscript, 1 or 2, to distinguish between states in V_1 and those in V_2, the second superscript, i or o, to distinguish between incoming and outgoing states, and the subscript, b or e, to distinguish between Bloch and evanescent waves. For example, $\psi^{1i}_b(\vec{r})$ stands for a Bloch state in volume V_1 propagating toward the interface. Let us define an expectation value of the normal component of the current operator on S_α by

$$J_\alpha(\phi,\psi) = \frac{1}{2i}\int_{S_\alpha}\left[\,\phi^*(\vec{x})\,\partial_n\psi(\vec{x}) - \partial_n\phi^*(\vec{x})\,\psi(\vec{x})\,\right] d\vec{x}. \qquad (4)$$

$J_\alpha(\phi,\psi)$ remains constant if S_α is moved around inside the bulk crystal suppose that ϕ and ψ are solutions of the Schrödinger equation, thus we have,

$$J_\alpha(\psi^{\alpha o}_e,\psi^{\alpha o}_{e'}) = 0, \qquad (5a)$$
$$J_\alpha(\psi^{\alpha o}_e,\psi^{\alpha o}_b) = J_\alpha(\psi^{\alpha o}_b,\psi^{\alpha o}_e) = 0, \qquad (5b)$$
$$J_\alpha(\psi^{\alpha o}_b,\psi^{\alpha o}_{b'}) = \delta_{bb'}, \qquad (5c)$$

where Eq. (5c) provides a condition for normalizing the Bloch states.

By substituting Eq. (2) in Eq. (4) we obtain a useful expression,

$$J_\alpha(\psi^{\alpha o}_\nu,\psi^{\alpha o}_{\nu'}) = 2\int_{S_\alpha}[\psi^{\alpha o}_\nu(\vec{x})]^*\Im G^{-1}_{S_\alpha}(\vec{x},\vec{x}\,')\psi^{\alpha o}_{\nu'}(\vec{x}\,')d\vec{x}d\vec{x}\,'. \qquad (6)$$

Now we consider a scattering process in which a Bloch state b incident from the interior of the bulk crystal V_1 is scattered at the interface and either reflected back into V_1 or transmitted into V_2. The corresponding wave function can be expressed as

$$\psi(\vec{r}) = \begin{cases} \psi_b^{1i}(\vec{r}) + \sum_\nu r_{b\nu}\, \psi_\nu^{1o}(\vec{r}) & , \vec{r} \text{ in } V_1 \\ \sum_{\nu'} t_{b\nu'}\, \psi_{\nu'}^{2o}(\vec{r}) & , \vec{r} \text{ in } V_2 \end{cases}, \quad (7)$$

where $r_{b\nu}$ and $t_{b\nu'}$ denote reflection and transmission coefficients, respectively, with subscripts ν and ν' running through both Bloch and evanescent states. As the Green function in Eq. (3) fulfills the outgoing boundary condition on S_1 and S_2 the reflected and transmitted waves in Eq. (7) do not contribute to the integral in Eq. (3). As a result, Eq. (3) is simplified to

$$\psi(\vec{r}) = -\frac{1}{2}\int_{S_1} \left[G(\vec{r},\vec{x})\, \partial_n \psi_b^{1i}(\vec{x}) - \partial_n G(\vec{r},\vec{x}) \psi_b^{1i}(\vec{x}) \right] d\vec{x}, \quad (8)$$

The Green function with the outgoing boundary condition can be expanded as

$$G(\vec{r},\vec{r}\,') = \sum_{\nu,\nu'} g_{\nu\nu'} \psi_\nu^{1o}(\vec{r}) \psi_{\nu'}^{2o}(\vec{r}\,'), \quad (9)$$

for $\vec{r}$ in V_1 and $\vec{r}\,'$ in V_2. Let us denote the complex conjugate of $\psi_b^{1i}(\vec{r})$ by $\psi_{b^*}^{1o}(\vec{r})$, which is a Bloch state propagating toward infinity. With this in mind, substituting Eq. (9) in Eq. (8) one has

$$\psi(\vec{r}) = \sum_{\nu'} i\, g_{b^*\nu'} \psi_{\nu'}^{2o}(\vec{r}), \quad \vec{r} \text{ in } V_2. \quad (10)$$

Comparing Eq. (10) and Eq. (7) yields

$$t_{b\nu'} = i\, g_{b^*\nu'}. \quad (11)$$

According to the formulation of Landauer the conductance Γ of ballistic electrons tunneling at a small bias voltage through the interface Ω can be expressed in terms of the transmission probability of all the Bloch states at the Fermi energy ϵ_F as

$$\Gamma = \frac{1}{2\pi} \sum_{bb'} |\, t_{bb'}\, |^2 = \frac{1}{2\pi} \sum_{b^*b'} |\, g_{b^*b'}\, |^2 . \quad (12)$$

With the use of Eq. (5), the above equation may read

$$\Gamma = \frac{1}{2\pi} \sum_{\mu\nu} \sum_{\mu'\nu'} g^*_{\mu\nu} J_1(\psi_\mu^{1o}, \psi_{\mu'}^{1o}) J_2(\psi_\nu^{2o}, \psi_{\nu'}^{2o}) g_{\mu'\nu'}. \quad (13)$$

Using Eqs. (6) and (9), one obtains

$$\Gamma = \frac{2}{\pi} \int_{S_1} d\vec{x}_1 d\vec{x}_1\,' \int_{S_2} d\vec{x}_2 d\vec{x}_2\,' G(\vec{x}_1,\vec{x}_2) \times \Im G_{S_2}^{-1}(\vec{x}_2,\vec{x}_2\,')\, G^*(\vec{x}_2\,',\vec{x}_1\,')\, \Im G_{S_1}^{-1}(\vec{x}_1\,',\vec{x}_1), \quad (14)$$

or after introducing a shorter matrix notation

$$\Gamma = \tfrac{2}{\pi} Tr(G_{12} \Im G_{S_2}^{-1} G_{21}^* \Im G_{S_1}^{-1}).$$

We implemented the embedding formalism within the framework of the FLAPW method[3,4]. Like in standard FLAPW electronic structure calculations we introduce a finite basis set of functions with a different representation within muffin-tin spheres around the atoms and the remaining interstitial region. Using the LAPW-basis functions Eq. (1) turns into a matrix equation and the Green-function matrix is obtained by a matrix inversion.

Figure 2 depicts the spin-resolved reflection coefficients for Cu electrons scattered by a ferromagnetic 5 monolayer Co film determined by Eq. (14). These results are in very good argeement with those in Refs. [5,6]. The dashed line corresponds to the majority spin channel while results for the minority spin are shown by the squares connected by solid lines. In the majority spin channel the reflectivity of the Co layers is low and varies smoothly over a wide energy range. This is easily understood from the bulk bandstructures of Cu and Co which both show a single band of the same 2D-symmetry character around the Fermi energy. For the minority spin, however, we find a strong energy dependence of the reflection coefficient. The nearly perfect reflectivity below -0.7 eV is due to the absence of Co states which are allowed to couple to the incoming Cu wavefunction.

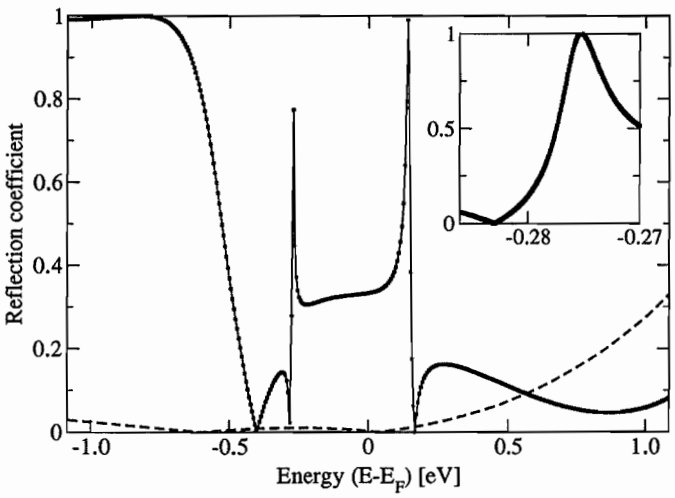

FIG. 2: Spin-resolved reflection coefficient for a ferromagnetic Cu/5 ML Co/Cu(001) layer for $\vec{k}_\parallel = 0$. The zero of energy was chosen to be the Fermi level. Note that the resonance peaks actually reach a value of one as shown in the inset. The difference between two energy grid points was 5.5 meV (inset: 0.08 meV).

References

1. Büttiker, Phys. Rev. Lett. **57**, 1761 (1986)
2. Inglesfield, J. Phys. C V.**14**,3795 (1981)
3. Wortmann, Ishida, Blügel, Phys. Rev. B **65**, 165103 (2002)
4. Wortmann, Ishida, Blügel, Phys. Rev. B **66**, 075113 (2002)
5. Riedel et al., Phys. Rev. B **63**, 195403 (2001)
6. Wildberger et al., Phys. Rev. B **58**, 13721 (1998)

Wavepacket Motion across a Nanoscale Contact

Andreas Bringer
IFF Theory I

Wave-packet motion of an electron through a ring-shaped nano-contact is investigated. The wave-packet will usually be split into various independent parts corresponding to different internal processes in the contact region. The example, shown here, demonstrates, that reflection comes from inlet and outlet of the ring.

Modern electronic devices are based nanoscale contacts between electrodes. The electron transport through such contacts can be easily manipulated by electric and magnetic fields and signals can be transmitted. The contacts can be realized in semiconducting sandwich structures, as "break"-contacts between metallic electrodes, or as "molecular"-bridges consisting of an organic molecule.

Electron transport in nanoscale devices is ballistic, in contrary to transport over larger scales, where the electron motion is diffusive. It requires a quantum-mechanical treatment. The conductance is given by the transmission probability for electron waves at the Fermi-energy [1].

A striking consequence of the quantum nature of ballistic transport through nanostructures is the quantisation of conductance. The conductance jumps discontinuously, when the Fermi-energy is varied in the contact region via gate-electrodes. The number of open transport channels changes abruptly at fixed energies depending on the geometry of the contact. A large variety of interference phenomena may arise from the geometry of the contact. The most prominent one is the Aharanov-Bohm effect in ring-shaped contacts. The conductance of the contact changes periodically with an applied magnetic field [2].

The device of Appenzeller et al. [2] was formed in an InGaAs-InP layer structure by reactive ion etching. Shape and size of the contact between the electrodes are shown in figure 1.

A 2-dimensional electron gas exists in the InP boundary layer. At low temperatures (< 1K) the mean free path of the electrons is larger than the contact size, i.e. the electrons move like free electrons in a plane with an effective mass determined by the conduction band of InP, $m^* = .037m_e$. To determine the conductance of the ring a free-particle Schroedinger-equation in 2 dimensions was solved with boundary conditions and the transmission as function of energy determined up to 40meV [3]. Over this range of energies the Fermi-energy can be varied changing the density of the electron gas by gate-electrodes. The quantization of momenta vertical to the walls produces a complicated finestructure in the spectrum. Waves with up to four radial nodes appear with increasing energy and interfere with each other. Figure 2 shows a closeup of the spectrum of the solution, incoming without node, between 15 and 16 meV. The closeup demonstrates a further important mechanism in transport through geometrical restrictions. The incoming particles couple resonantly to the internal modes of the geometry, in this case the orbital modes of the closed ring at 15.35 and 15.7 meV.

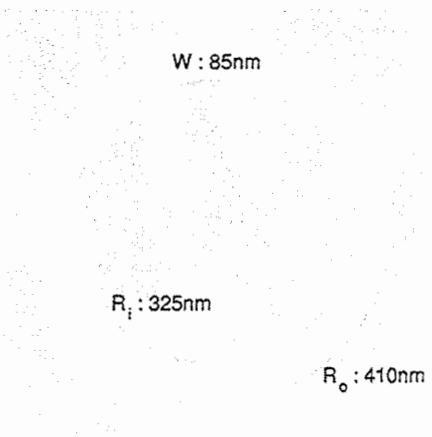

FIG. 1: schematic drawing of the ring contact showing the values of the inner and outer radii and the width of the ring.

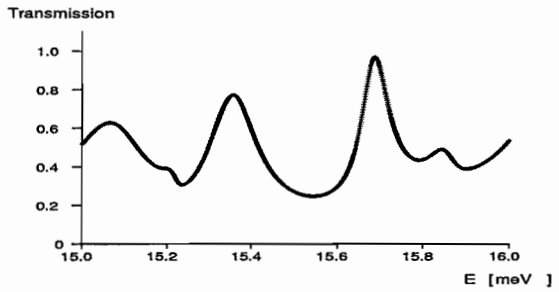

FIG. 2: transmission-spectrum channel 1

With the detailed knowledge of the spectrum it is easy to set up an incoming wavepacket outside the contact in the "source" electrode, propagate it in time and study transmission of a single electron into the "drain" electrode. At the end of the process the packet will be split into a transmitted and a reflected part with weights corresponding to the total transmission and reflection probabilities. Even more information is contained in the outgoing wavepacket. As outlined above the component of the momentum of an electron vertically to the boundary may be changed discontinously. The outgoing wavepackets contain parts moving faster or slower than the incoming packet. Furthermore an electron may be reflected be-

fore entering the ring or after one roundtrip, which leads to a time delayed part.

As a specific example an Gaussian wavepacket at 15.35 meV with a halfwidth of .1 meV (corresponds roughly to the experimental temperature) is discussed here. With the experimental values for size and width of the ring and the effective mass quoted above the proper timescale is picoseconds. Classically an electron would pass the ring in roughly 6 ps. The spread in energy corresponds to a spread of 10 ps in time. The spread in space is roughly twice the diameter of the contact. In figure 3 the packet is shown just after entering the ring. The direction of current is always from top to bottom.

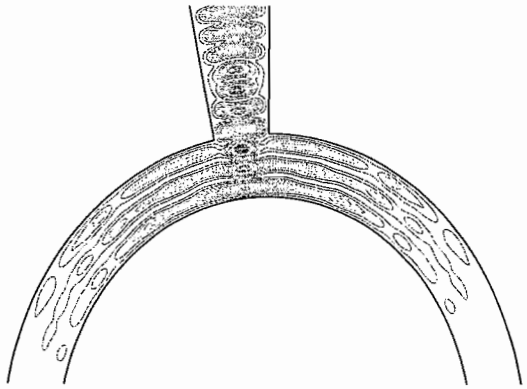

FIG. 3: contour-plot of the probability density of a Gaussian wave-packet entering the ring

The wavelength of the incoming wave generates two nodes inside the ring. The wave propagates with two nodes in the ring. 7 ps later the wave-packet reaches the drain

FIG. 4: contour-plot of the probability density of a Gaussian wave-packet reaching the drain.

The probability of reflection into the source is maximal. Again 6 ps later the rest of the packet is concentrated close to the drain.

The probability of transmission is maximal. Now the rest of the packet makes a roundtrip back to the source, which is reached 6 ps later.

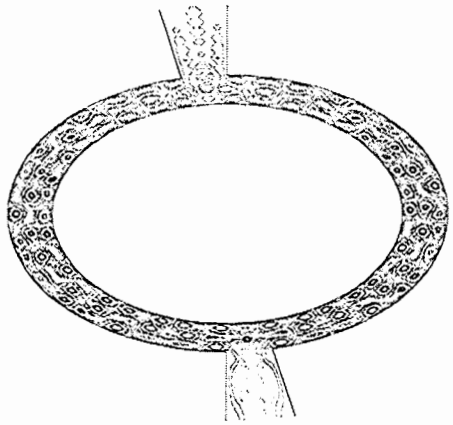

FIG. 5: wave-packet concentrated at the drain, highest probability of transmission,

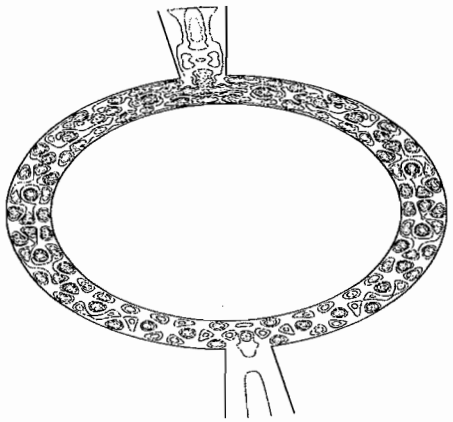

FIG. 6: roundtrip of the rest of the packet completed, reflection into the source starts again

Reflection into the source starts again and the whole process is finished a few ps later.

The method of wave-packet propagation is an alternative to stationary state calculations. It will get important again in the context of femtosecond spectroscopy.

[1] Büttiker,Phys. Rev. Lett. 57,1761 (1986)

[2] J. Appenzeller, Th. Schäpers, H. Hardtdegen, B. Lengeler, and H. Lüth, Phys. Rev. B **51**, 4336 (1995).

[3] A. Bringer, IFF-Jahresbericht 1996

Publications in journals

Akola,J.; Ballone,P.*; Jones,R. O.
Reactions of polycarbonates with cyclohexene oxide and phosphites : a density functional study
Macromolecules, 35 (2002), S. 2327 - 2334

Akola,J.; Manninen,M.*
Aluminum-lithium clusters : first-principles simulation of geometries and electronic properties
Physical review B, 65 (2002), S. 245424

Antons,A.; Schroeder,K.; Voigtländer,B.; Cherepanov,V.; Berger,R.; Blügel,S.
Element specific surface reconstructions of islands during surfactant-mediated growth on Si(111)
Physical review letters, 89 (2002), 23, S. 236101

Ballone,P.*; Jones,R. O.
Density functional/Monte Carlo study of ring-opening polymerization
Computer physics communications, 147 (2002), S. 325 - 330

Ballone,P.*; Jones,R. O.
Equilibrium polymerization of cyclic carbonate oligomers III branching and the gel transition
Journal of chemical physics, 117 (2002), S. 6841 - 6851

Ballone,P.*; Jones,R.O.
Equilibrium polymerization of cyclic carbonate oligomers II role of multiple active sites
Journal of chemical physics, 116 (2002), S. 7724 - 7732

Bene,J.*; Bröcheler,S.*; Lustfeld,H.
Simulating 2D flows with viscous vortex dynamics
Journal of statistical physics, 101 (2000), S. 567

Bode,M.*; Heinze,S.*; Hennefarth,M.*; Pietzsch,O.*; Kubetzka,A.*; Getzlaff,M.*; Wiesendanger,R.*; Nie,X.; Bihlmayer,G.; Blügel,S.
Structural, electronic and magnetic properties of a Mn monolayer on W(110)
Physical review B, 66 (2002), S. 014425

Bode,M.*; Heinze,S.; Kubetzka,A.*; Pietzsch,O.*; Nie,X.; Bihlmayer,G.; Blügel,S.; Wiesendanger,R.*
Magnetization-direction-dependent local electronic structure probed by scanning tunneling spectroscopy
Physical review letters, 89 (2002), S. 237205

Cao,Y.; Zheng-Kuan,J.*; Antons,A.; Schroeder,K.; Blügel,S.
Stable structure of Sb monolayer on a strained Ge(111) substrate
Chinese journal of physics, 19 (2002), S. 259

Cao,Y.; Zheng-Kuan,J.*; Antons,A.; Schroeder,K.; S. Blügel,S.
Relaxation of small molecules, an ab initio study
Communications in theoretical physics, 37 (2002), S. 597

Galanakis,I.; Bihlmayer,G.; Bellini,V.*; Papanikolaou,N.*; Zeller,R.; Blügel,S.; Dederichs,P.H.
Broken bond counting rule for the surface energies of noble metals
Europhysics letters, 58 (2002), S. 751

García-Lekue,A.*; Pitarke,J.M.*; Chulkov,E.V.*; Liebsch,A.; Echenique,P. M.*
Role of surface plasmons in the decay of image potential states on silver surfaces
Physical review letters, 89 (2002), S. 096401

Heinze,S.*; Kurz,Ph.; Wortmann,D.; Bihlmayer,G.; Blügel,S.
Complex magnetism in ultra-thin films : atomic-scale spin structures and resolution by the spin-polarized scanning tunneling microscope
Applied physics A, 75 (2002), S. 25

Himpsel,F. J.*; Altmann,K. N.*; Crain,J. N.*; Kirakosian,A.*; Lin,J.-L.*; Liebsch,A.; Zhukov,V.P.*
Photoelectron spectroscopy of atomic wires
Journal of electron spectroscopy and related phenomena, 126 (2002), S. 89 - 99

Hirnet,A.*; Schroeder,K.; Blügel,S.; Torrelles,X.*; Albrecht,M.*; Jenichen,B.*; Gierer,M.*; Moritz,W.*
A novel Sb induced reconstruction of the (113) surface of Ge
Physical review letters, 88 (2002), S. 226102

Ishida,H.*; Liebsch,A.
Static and quasistatic response of Ag surfaces to a uniform electric field
Physical review B, 66 (2002), S. 155413

Komeda,T.*; Kim,Y.*; Kawai,M.*; Persson,B.N.J.; Ueba,H.*
Lateral hopping of molecules induced by excitation of interna vibrational mode
Science, 295 (2002), S. 2055

Kurz,Ph.; Bihlmayer,G.; Blügel,S.
Magnetism and electronic structure of hcp Gd and the Gd(0001) surface
Journal of physics: condensed matter, 14 (2002), S. 6353

Kurz,Ph.; Bihlmayer,G.; Hirai,K.*; Blügel,S.
Itinerant magnets on a triangular Cu(111) lattice
Phase transitions, 75 (2002), S. 101 - 112

Lustfeld,H.; Pohlmeier,A.

Electric potential and reaction rates at charged surfaces in asymmetric electrolytes-an analytic approach
Journal of colloid and interface science, 181 (2001), S. 45

López Bastidas,C.*; Maytorena,J.A.*; Liebsch,A.
Hot-electron dynamics at noble metal surfaces
Physical review B, 65 (2002), S. 035417

Maus-Friedrichs,W.*; Frerichs,M.*; Gunhold,A.*; Krischok,S.*; Kempter,V.*; Bihlmayer,G.
The characterization of SrTiO3(001) with MIES, UPS(HeI) and first-principles calculations
Surface science, 515 (2002), S. 499 - 506

Persson,B. N. J.
Adhesion between elastic bodies with randomly rough surfaces
Physical review letters, 89 (2002), S. 245502

Persson,B. N. J.
Adhesion between elastic bodies with randomly rough surfaces
European physical journal E, 8 (2002), S. 385

Persson,B. N. J.
Comment on : Nanoadhesion between rough surfaces
Physical review letters, 88 (2002), S. 129601

Persson,B. N. J.
Persson replies to : comment on elastoplastic contact between randomly rough surfaces
Physical review letters, 88 (2002), S. 069602-1

Persson,B. N. J.; Bucher,F.*; Chiaia,B.*
Elastoplastic contact mechanics between randomly rough surfaces
Physical review B, 65 (2002), S. 184106

Persson,B. N. J.; Ueba,H.*
Theory of inelastic tunneling induced motion of adsorbates on metal surfaces
Surface science, 502-503 (2002), S. 18

Persson,B. N. J.; Volokitin,A.I.*
Theory of rubber friction : nonstationary sliding
Physical review B, 65 (2002), S. 134106

Persson,B.N.J.; Samoilov,V.N.*; Zilberman,S.*; Nitzan,A.*
Squeezing molecularly thin Xe, CH4 and C16H34 lubrication films between smooth and rough solid surfaces with long-range elasticity
Journal of chemical physics, 117 (2002), S. 3897

Schroeder,K.; Antons,A.; Berger,R.; Blügel,S.
Surfactant mediated heteroepitaxy versus homoepitaxy : kinetics of group-IV atoms on As-passived Si(111) and Ge(111)
Physical review letters, 88 (2002), S. 046101

Schröder,K.; Antons,A.; Berger,R.; Blügel,S.
Ad-atom kinetics on surfactant-covered Si(111) : ab initio calculations
Phase transitions, 75 (2002), S. 91 - 99

Schröder,K.; Antons,A.; Berger,R.; Blügel,S.
Surfactant mediated heteroepitaxy versus homoepitaxy : kinetics for group-IV adatoms on As-passivated Si(111)
Physical review letters, 88 (2002), S. 046101

Volokitin,A.I.*; Persson,B.N.J.
Radiative heat transfer and vacuum friction between nanostructures
Physics of low-dimensional structures, 5/6 (2001), S. 151

Wortmann,D.; Ishida,H.*; Blügel,S.
An ab initio Green-function formulation of the transfer matrix : application to complex bandstructures
Physical review B, 65 (2002), S. 165103

Wortmann,D.; Ishida,H.*; Blügel,S.
Embedded Green-function approach to the ballistic electron tran sport through an interface
Physical review B, 66 (2002), S. 075113

Wortmann,D.; Kurz,Ph.; Heinze,S.*; Hirai,K.*; Bihlmayer,G.; Blügel,S.
Resolving noncollinear magnetism by spin-polarized scanning tunneling microscopy
Journal of magnetism and magnetic materials, 240 (2002), S. 57 – 63

Book chapter

Jones,R. O.
Material Science
NIC Symposium 2001 : 5.-6. December 2001, Forschungszentrum Jülich ; proceedings / ed.: H. Rollnik ... - Jülich, 2002. - (NIC series ; 9). - 3-00-009055-X. - S. 211 - 212

Invited talks

Atodiresei,N.; Kromen,Wi.; Blügel,S.; Schroeder,K.
The neutral Cd-vacancy complex in Si and Ge
DPG-Frühjahrstagung : Regensburg
Regensburg: 11.03.2002 - 15.03.2002

Bihlmayer,G.; Kurz,Ph.; Förster,F.; Blügel,S.
Non-collinear ab-initio calculations with the FLAPW-method
ESF/TMR Workshop : Noncollinear Magnetism
Wien: 08.03.2001

Blügel,S.
Magnetism under the microscope
International Symposium on Scientific and Industrial Nanotechnology 2002 : (ISSIN-2002)
Osaka, Japan: 12.12.2002 - 13.12.2002

Blügel,S.
Magnetism under the scanning tunneling microscope

ESCM-2002 : Electronic Structure and Computational Magnetism
Washington, DC : 14.07.2002 - 17.07.2002

Blügel,S.
Magnetism under the scanning tunneling microscope
ECOSS-20 : European Conference on Surface Science
Krakow, Polen: 04.09.2001 - 07.09.2001

Blügel,S.
Theory and potential of spin-polarized STM/STS : to unraval complex magnetic structures on the atomic scale
IVC-15 : 15th International Vacuum Congress
San Francisco, CA: 28.10.2001 - 02.11.2001

Blügel,S.
Theory of complex magnetism at the atomic scale
Workshop Properties of Magnetic Nanostructures
Sincrotrone Trieste, Italien: 30.10.2002

Blügel,S.
Theory of magnetic anisotropy in metals and multilayers
EGSCM : European Graduate School on Condensed Matter
Prag, Tschech. Republik: 24.06.2001 - 29.06.2001

Blügel,S.
Theory of magnetic anisotropy in metals and multilayers
258. WE-Heraeus-Seminar on Electronic Origin of Magnetoelastic Anisotropy and Stress in Atomic Layers
Tegernsee: 09.09.2001 - 12.09.2001

Blügel,S.
Theory of magnetism under the microscope
Discussion Meeting : Magnetism at the Special Limit
Ringberg, Germany: 09.09.2002 - 11.09.2002

Blügel,S.
Theory of magnetism under the scanning tunneling microscope
MML'01 : 4th International Symposium on Metallic Multilayers
Aachen: 12.06.2001

Blügel,S.
Theory of thin film magnetism
Swedish Summer School of Magnetism
Backagarden, Schweden: 01.07.2002 - 04.07.2002

Blügel,S.; Heinze,S.*; Wortmann,D.; Bihlmayer,G.
Theorie komplexer magnetischer Strukturen in dünnen Schichten und deren Auflösung mittels des spin-polarisierten STM
DPG-Frühjahrstagung
Hamburg: 26.03.2001 - 30.03.2001

Bode,M.*; Pietzsch,O.*; Kubetzka,A.*; Heinze,S.*; Kleiber,M.*; Ravlic,R.*; Nie,X.; Blügel,S.; Wiesendanger,R.*
Spin-polarisierte Rastertunnelmikroskopie
DPG-Frühjahrstagung
Hamburg: 26.03.2001 - 30.03.2001

Förster,F.; Bihlmayer,G.; Blügel,S.
Structure and magnetism of thin Fe films on Cu(100)
Symposium on Surface Science 2002
St. Christoph am Arlberg: 03.03.2002 - 09.03.2002

Harris,J.
Historical reflections on density functional theory
Electronic Structure of Solids : TU Dresden
Dresden: 05.07.2002

Heide,M.; Nie,X.; Bihlmayer,G.; Blügel,S.
Ab initio investigations of Fe/W(110) : magnetic structure of domain-walls
DPG-Frühjahrstagung
Regensburg: 11.03.2002 - 15.03.2002

Jones,R. O.
The structure of carbon clusters - how much do we really know?
Norman March Symposium : Universität Antwerpen
Antwerpen, Belgien: 01.02.2002

Jones,R. O.
Thermal expansion in silicate glass ceramics - why are cooktops so atable?
Workshop Electronic Structure of Solids : IFW Dresden
Dresden: 05.07.2002

Jones,R. O.; Ballone,P.*
Silicon segregation from SiO (2-x) suboxides : dynamical Monte Carlo study
National Meeting : American Chemical Society
Boston, MA, USA: 18.08.2002

Jones,R.O.; Ballone,P.*; Akola,J.
Accurate and efficient many-body potential for hydrogen bonding-application to water
National Meeting : American Chemical Society
Boston, MA, USA: 20.08.2002

Lustfeld,H.
Characterization of active tracer fields by a set of Hoelder exponents
27th General Assembly of the EGS
Nizza: 26.04.2002

Lustfeld,H.
Electric potential and reaction rates at charged surfaces in asymmetric electrolytes-an analytic approach
DPG-Tagung
Leipzig: 19.03.2002

Lustfeld,H.

Ordinary differential equation solver applied to differential equations of realistic pollutants in the troposphere
DPG-Tagung
Leipzig: 19.03.2002

Persson,B. N. J.
Sliding friction
WE Heraeus Seminar 2002 : Integrating Friction and Wear Research
Ilmenau: 26.05.2002 - 29.05.2002

Persson,B. N. J.
Sliding friction
9th Joint Vacuum Conference
Graz, Österreich: 16.06.2002 - 20.06.2002

Persson,B. N. J.
Sliding friction
APS Meeting
Indianapolis, USA: 18.03.2002 - 22.03.2002

Persson,B. N. J.
Sliding friction
ACS Meeting
Orlando, Florida: 07.04.2002 - 11.04.2002

Persson,B. N. J.
Sliding friction
Tribology Gordon Research Conference
USA: 04.08.2002 - 09.08.2002

Schroeder,K.; Antons,A.; Berger,R.; Blügel,S.
Simulation von STM-Bildern von Stufenkanten auf As-bedecktem Si(111)
DPG-Frühjahrstagung
Regensburg: 11.03.2002 - 15.03.2002

Other talks

Akola,J.
Improved force field for hydrogen bonding - applications to water and carbonic acid
Projekttreffen des MaTech-Kompetenzzentrums Werkstoffmodellierung : Swiss Center for Scientific Computing CSSC
Manno, Schweiz: 28.05.2002

Akola,J.
Improved force field for hydrogen bonding - applications to water and carbonic acid
HLCS-Euroconference : XI. Workshop on Computational Materials Science (CMS2002)
Villasimius, Sardinien: 23.09.2002 - 29.09.2002

Blügel,S.
Magnetismus im Nanokosmos
Physikalische Kolloquium : Universität Duisburg
Duisburg: 12.11.2002

Blügel,S.
Magnetismus unter dem Mikroskop
Institut für Festkörperphysik : Forschungszentrum Karlsruhe
Karlsruhe: 12.07.2002

Blügel,S.
Spin-polarized electrons tunneling into the future of spintronics
Institut für Theorie : Fritz-Haber-Institut Berlin
Berlin: 13.06.2002

Harris,J.
Historical reflections on density functional theory
Kolloquium : TU Dresden
Dresden: 05.07.2002

Jones,R. O.
Reactions and phase transitions in polycarbonate - what can theory contribute?
Kolloquium : General Electric Global Research Center
Schenectady, NY, USA: 26.08.2002

Jones,R. O.
Reaktionen und Phasenumwandlungen in Polymeren - Dichtefunktional- und Kraftfeldrechnungen
Kolloquium : Institut für Physikalische Chemie ; Technische Universität Dresden
Dresden: 14.05.2002

Lustfeld,H.
Appropriate Hoelder exponents for an active tracer field
Seminar and Workshop on Microscopic Chaos and Transport in Many-Particle Systems
Dresden: 23.08.2002

Lustfeld,H.
Appropriate Hoelder exponents for an active tracer field
Seminar and Workshop on Chemical and Biological Activity in Flows
Dresden: 20.09.2002

Lustfeld,H.
Properties of realistic tracer gas chemistry in the atmosphere
Seminar and Workshop on Chemical and Biological Activity on Flows
Dresden: 25.09.2002

Persson,B. N. J.
Sliding friction
Twannberg Workshop on Nanoscience
Twannberg, Schweiz: 30.09.2002 - 04.10.2002

Persson,B. N. J.
Sliding friction
German-Japanese Workshop
Hayama, Japan: 10.09.2002 - 13.09.2002

Persson,B. N. J.
Sliding friction
1st ESF-Nanotribology Workshop
Portovenere, Italien: 19.10.2002 - 23.10.2002

Posters

Akola,J.
Improved force field for hydrogen bonding - applications to water
HGF-Workshop : Forschungszentrum Jülich
Jülich: 06.11.2002

Antons,A.; Schroeder,K.; Berger,R.; Blügel,S.
The neutral Cd-vacancy complex in Si and GeClusters and Steps on Si(111) :
surfactant effect due to As and Sb
Physics Congress : European Physical Society (Condensed Division)
Bristol: 07.04.2002 - 11.04.2002

Heide,M.; Heinze,S.*; Nie,X.; Bihlmayer,G.; Blügel,S.
Ab initio investigations of Fe/W(110) : magnetism, domain-walls, STM-images 269
WE-Heraeus Seminar on Magnetism on the Sub-Micrometer Scale : Interactions and Microscopy
Bad Honnef: 07.01.2002 - 09.01.2002

Heide,M.; Nie,X.; Bihlmayer,G.; Blügel,S.
Ab initio investigations of Fe/W(110) : magnetic structure of domain-walls
2nd Annual Meeting of the RTN (Computational Magnetoelectronics)
Oleron Island, France: 05.10.2002 - 09.10.2002

Heide,M.; Nie,X.; Bihlmayer,G.; Blügel,S.
Ab initio investigations of Fe/W(110) : magnetic structure of domain-walls 281
WE-Heraeus Seminar on Spin-Orbit Interaction and Local Structure
Wandlitz: 12.06.2002 - 15.06.2002

Lustfeld,H.; Neufeld,Z.*
Active tracer fields in mildly chaotic flows and higher Hoelder exponents
3. Dresdner Herbstseminar des Arbeitskreises Nichtlineare Physik
Dresden: 03.12.2002

Wortmann,D.; Ishida,H.*; Blügel,S.
A transfer matrix method for ballistic transport : MgO/Fe(001)
Physical Society Meeting of the European Physical Society CMD19CMMP
Brighton, UK: 07.04.2002 - 11.04.2002

Wortmann,D.; Ishida,H.*; Blügel,S.
An embedded Green-function approach to the ballistic electron transport through an interface
RTN Magnetoelectronics Mid-Term Meeting
Oleron, France: 05.10.2002 - 09.10.2002
Wortmann,D.; Ishida,S.*; Blügel,S.
An embedded Green function approach to the ballistic electron transport through an interface
Trends in Nanotechnology Conference
Santiago de Compostela, Spain: 09.09.2002 - 13.09.2002

Institute Theory II

General Overview

Introduction: Soft Matter Research

The main research topic of the Institute is the theory of "complex fluids" and "soft matter" systems. Soft matter physics is an interdisciplinary research area encompasing statistical physics, material science, chemistry, and biology. The systems are characterized by

- Supramolecular structure and self-assembly
- Typical length scales ranging from nano- to micro-meters
- Typical energy scales comparable to the thermal energy k_BT.

Classical examples of complex fluids are

- Polymer solutions, mixtures, and melts
- Mixtures of block copolymers and homopolymers
- Lyotropic liquid crystals
- Amphiphilic systems, i.e. mixtures of oil, water and amphiphiles
- Colloidal suspensions.

While these areas remain active fields of research, the focus has recently shifted to more complex systems which are obtained by combining two or more of the components listed above. A few examples are

- Colloidal particles in polymer solutions
- Mixtures of surfactants and amphiphilic block-copolymers
- Mixtures of several surfactants or lipids
- Colloids in liquid crystals

This brings the systems which are studied in physics closer to applications in material science or biology.

Since the structures in soft matter systems often contain a large numer of molecules, *mesoscale modelling* is typically required to bridge the length- and time-scale gap between the microscopic domain — of atoms and their interactions — and the emerging properties of supramolecular assemblies on meso- or macroscopic scales. Microscopic models are employed to study properties of complex systems on the molecular scale, and to provide a link of mesoscale models to molecular architecture.

A large variety of methods is used to study soft matter systems. In fact, a combination of analytical and numerical methods is often needed to successfully characterize these complex systems. In particular, simulation methods (Monte Carlo, molecular dynamics), computational hydrodynamics, field theory, perturbation theory, and exact solutions are employed in our institute.

A characteristic feature of soft-matter research is the fruitful interaction between theory and experiment. With a third of the IFF institutes [Neutron Scattering (Richter), Theory II and Soft Matter (Dhont)] now focusing on soft matter research, many of the essential aspects of these systems are investigated here.

Research projects and results:

(in alphabetic order)

1. *Mesoscopic solvent simulations: Multi-particle-collision dynamics of three-dimensional flows:*
   Due to the large length- and time-scale gap, in simulations of complex-fluid flow the solvent often has to be modeled by a mesoscopic model. We apply a recently developed mesoscale simulation technique, multi-particle-collision dynamics (MPCD), to three dimensional solvent flows in a channel with and without a spherical obstacle. The advantage of a gravitationally-driven flow of the solvent over the flow induced by a pressure gradient in the calculation of the solvent viscosity is demonstrated. Three different algorithms for stochastic collision step are investigated and compared. Our simulation results for the recirculation length of stationary vortices behind a spherical obstacle as a function of the Reynolds number are in good agreement with previous experimental measurements. (E. Allahyarov, G. Gompper)

2. *Cell Motility and Migration:*
   The motility and locomotion of biological cells is based on signal-mediated polymerization of their cytoskeletons. It has been shown recently by researchers from the institute how the the random motion and the chemotaxis of a cell can be explained based on a model of the autocatalytic polymerization kinetics of the cytoskeletal actin network. The current work is mainly concerned with investigations how the chemotaxis is induced by a complex signaling network of actin-regulating proteins inside the cell. These studies are aimed to explain the specific migration patterns of cells found, e.g., during embryogenesis. Most of the studies use computer simulations, but also mathematical models are employed. (A.Baumgärtner, S.Satyanarayana, B.Nandy)

3. *Molecular Signal Transduction across Biomembranes:*
   The transduction of signals across the membranes of cells and organelles is an important feature of all living organisms. Important examples are the proton transport in protein pumps, as bacteriorhodopsin (bR), and the permeation of ions through ion channels. Our recent work was mainly concerned with molecular dynamics (MD) simulations of all-atom models of bR and the KcsA potassium channel. In the case of bR we used as the template structure the one obtained at the institute IBI-2, the structure of the KcsA channel was obtained from the protein data bank. Important information were obtained concerning the distribution of water inside bR, which constitute pathways for proton conduction. The actual proton transfer, concomitant to a sequence of conformational transitions of bR, is the current challenging topic of MD studies. In the case of the KcsA channel, a certain type of steered MD simulation method helped to clarify the "supplanting" process of ions while passing the selectivity filter. The aim of the current investigations is the simulation of the complete channel, including the N- and C-terminii, which are not resolved in crystallographic experiments. These parts of the protein are essential in order to understand the gating of the ion channel. (A.Baumgärtner, K. Votyakov, S.Grudinin, J.-F.Gwan)

4. *Polymer depletion interaction between an anisotropic colloidal particle and a wall:*
   We investigate the interaction between a colloidal particle of *ellipsoidal* shape and a wall which is induced by long flexible and nonadsorbing polymer chains. Besides a force the interaction provides a *torque* on the particle. We concentrate on the case in which the particle size is much smaller than typical polymer lengths such as the radius of gyration $\mathcal{R}_g$ and in which a rigid polymer approximation of the Asakura-Oosawa type cannot be applied. Our explicit *analytical* results for ideal polymers show that for particle-wall distances z large compared to $\mathcal{R}_g$ an orientation of the ellipsoid *perpendicular* to the wall is favored while the *parallel* orientation is favored for z small compared to $\mathcal{R}_g$ (but z still large compared to the particle size). (E. Eisenriegler, A. Bringer, R. Maassen)

5. *The Freezing Transition of Flexible Membranes:*
   The freezing transition of flexible, tensionless membranes fluctuating about a planar reference state is investigated by Monte Carlo simulations and scaling arguments. Out-of-plane fluctuations are expected to reduce the free energy of dislocations sufficiently to make the crystalline phase unstable for any finite temperature. To study the hexatic-to-fluid transition, the bond-orientational order-parameter susceptibility is analyzed for different values of the bending rigidity κ. It is found that for sufficiently large κ the low temperature hexatic phase melts via a universal Kosterlitz-Thouless transition. These

results are consistent with recent theoretical predictions that the crumpled-to-crinkled transition occurs via disclination melting for all bending rigidities. However, our simulations provide evidence that the transition becomes first order at very low bending rigidity. (G. Gompper, D.M. Kroll)

6. *Giant Hexagonal Superstructures in Diblock Copolymer Membranes:*
Amphiphilic diblock copolymers can form bilayer vesicles (polymersomes), just as the vesicles made from lipid molecules (liposomes). While previous experiments show vesicles of spherical topology, we have observed for the first time polymersomes of high genus, with their vesicle wall organized on the micrometer scale either in a double bilayer connected by a lattice of passages, or a tubular network with hexagonal symmetry. Experimentally found shape classes are identified within a theoretical phase diagram based on the bending energy of the polymer membrane. Pronounced morphological changes could be induced and controlled by temperature. (C.K. Haluska, W.T. Góźdź, H.-G. Döbereiner, S. Förster, G. Gompper)

7. *Free energy cost to immerse a colloidal particle in a dilute or semidilute polymer solution:*
The free energy cost F of immersing a spherical colloidal particle in a solution of nonadsorbing polymers depends in a crucial way on the particle to polymer size ratio and the degree of interchain overlap. We use an approximate renormalization method to describe the crossovers between the known limits of large and small spheres in dilute and semidilute polymer solutions and to predict F for arbitrary values of the size ratio and interchain overlap. Our results are free from adjustable parameters and compare well with simulation data both for the overlap-dependence of the polymer-induced surface tension of a large particle and for the size ratio dependence of F at a fixed overlap value in between the dilute and semidilute limits. (R. Maassen, E. Eisenriegler)

8. *Criterion for phase separation in one-dimensional driven systems:*
We found a criterion for the existence of phase separation in driven density-conserving one-dimensional systems which suggests that phase separation is related to the size dependence of the steady-state currents of domains in the system. A quantitative criterion for the existence of phase separation is conjectured using a correspondence made between driven diffusive models and zero-range processes. The criterion is verified in all cases where analytical results are available, and predictions for other models are provided. (G.M. Schütz, Y. Kafri, E. Levine, D. Mukamel, J. Török)

9. *The distribution function of a semiflexible polymer and random walks with constraints:*
We have studied the end-to-end distribution function $G(r, N)$ of a worm-like chain. Using the propagator method we established that the combinatorial problem of counting the paths contributing to $G(r, N)$ is equivalent to the problem of random walks with constraints. Utilizing this mapping we derived (i) an exact expression of the Fourier-Laplace transform of the distribution function, $G(k, p)$, as an inverse of an infinite rank matrix and (ii) a recursion relation permitting to compute $G(k, p)$ directly. The moments $< r^{2n} >$ of $G(r, N)$ can be calculated exactly by calculating the $(1, 1)$-matrix element of the $2n$-th power of a truncated matrix of rank $n + 1$. (G.M. Schütz, S. Stepanow)

10. *Shocks and excitation dynamics in a driven diffusive two-component system:*
We have considered classical hard-core particles hopping stochastically on two parallel chains with an inter- and intra-chain interaction. From microscopical considerations we derived the collective velocities and shock stability conditions. The findings are confirmed by comparison to Monte Carlo data of a multi-parameter class of driven two-lane models. We also derived the hydrodynamic limit and clarified analogies of our results with those known in the theory of partial differential equations. The singularity problem is discussed and a dissipative term that selects the physical solution is identified. (G.M. Schütz, V.Popkov)

11. *Kinetics of depletion interactions:*
Depletion interactions between colloidal particles dispersed in a fluid medium are effective interactions induced by the presence of other types of colloid and give rise to interesting equilibrium and non-equilibrium phase behaviour. These interactions are not instantaneous but build up in time through a diffusive collision process between the two species. We show by means of Brownian dynamics simulations that the fluctuations in the depletion force between two guest particles in a host dispersion of differently sized colloids do not decay exponentially with time, but show a power-law dependence.

A simple scaling theory accurately describes the dependence of the magnitude of these fluctuations on time. The consequences in particular for the dynamics of colloidal mixtures are discussed. (G. Vliegenthart, P. van der Schoot)

12. *Universal scaling behavior of directed percolation and the pair contact process in an external field:*
Models which show a continuous phase transition from an active state (density of active particles ρ larger zero) to a *unique* absorbing state ($\rho = 0$) belong to the universality class of directed percolation (DP). We compare the scaling behavior in an external field of one such model, i.e. directed site percolation, to that of the pair contact process (PCP), which has *infinitely many* absorbing states. The external field is conjugated to the order parameter and is realized as a spontaneous creation of particles. We determine numerically the equation of state in 1+1 dimensions for both models by extensive Monte Carlo simulations and show that both models are characterized by the same universal scaling function. This universality has also be derived analytically within the mean-field approach. (R.D. Willmann, S. Lübeck)

13. *Dynamics of linear and ring alkane molecules in a melt:*
The conformational and dynamical properties of linear and ring alkane molecules in a melt are studied by molecular dynamics simulations and analytical theory. Using a semiflexible chain model, the equilibrium properties can consistently be described for all chain lengths. Moreover, the dynamics is partially captured by the semiflexible chain dynamics. In particular, the mean square displacement of the longest chains exhibits deviations from the analytical result indicating the onset of entanglement effects. The calculation of the chain length dependence of the diffusion coefficient yields an dependence close to $D \sim N^{-2}$, characteristic for reptation dynamics. This suggests the presence of a mechanism which slows down the dynamics before entanglements are relevant. The comparison of the dynamics of the ring alkanes with the linear molecules displays a faster internal dynamics for the rings, consistent with analytical results. (R.G. Winkler, D.Y. Yoon, K. Hur)

14. *Conformational properties of weakly charged polyelectrolyte chains:*
The conformational properties of weakly charged polyelectrolyte chain have been studied by a perturbation scheme. The persistence length of a semiflexible reference chain is determined in such a manner that the mean square end-to-end distances of the reference chain and the charged chain agree with each other. To take into account screening effects by added salt and counterions, the charge interactions among the individual monomers of a chain are described by a Debye-Hückel potential. Considering the scaling behavior of the mean square end-to-end distance with respect to chain length, we obtain a transition from a rodlike behavior to an excluded volume type dependence with increasing chain length. For very short screening lengths, chain monomers experience short range interactions only. No Gaussian regime is observed between the rodlike and the excluded volume regime, which contradicts resent scaling considerations but is in agreement with computer simulation results. (R.G. Winkler)

Some Remarks:

- A workshop *Biology meets Physics* was organized by G. Gompper (Theory II) on February 20, 2002, to bring together the institutes of the Forschungszentrum Jülich, which are interested in research at the boundary between biology and physics. Speakers from 12 institutes (IFF-NS, IFF-WM, IFF-T2, NIC, ISG-2, ISG-4, IBI-1, IBI-2, ICG-III, ICG-IV, IBT-1, IME) presented their work.
- An international one-day symposium on *Cooperativity in Biophysical Systems* was organized by G. Schütz (Theory II), P. Grassberger (Neumann Institute for Computing, FZJ) and E. Frey (Hahn-Meitner-Institut, Berlin) on October 7, 2002. Seven invited speakers gave introductory lectures as well as more specialized talks about their current research. Eight of the about 45 participants also contributed posters.
- An international workshop, the *Jülich Soft Matter Days 2002*, was organized by J. Dhont (IFF Soft Matter), G. Gompper (Theory II) and D. Richter (IFF Neutron Scattering) at the Congresscentrum Rolduc in Kerkrade (NL) on Nov. 19-22, 2002. The program consisted of 4 plenary talks, 21 invited talks, 10 contributed talks, and about 90 posters. The workshop was attended by 175 participants.
- The paper of S. Lübeck and R. Willmann about *Exact Hurst exponent and crossover behavior in a limit order market model*, which was published in the November issue of *J. Phys. A*, has been chosen by *IOP Select* as one of the most significant articles in IOP journals in its December issue.

Awards etc.:

- J. Allgaier (IFF Neutron Scattering), G. Gompper (Theory II), D. Richter (IFF Neutron Scattering), T. Sottmann (University of Cologne) and R. Strey (University of Cologne) have received the Erwin-Schrödinger award for interdisciplinary research of the Stifterverband der Deutschen Wissenschaften and the Helmholtz Society.
- Dr. Tamotsu Kohyama (Department of Physics, Faculty of Education, Shiga University, Japan) has received a fellowship of the Japanese Ministry of Education, Science and Culture to visit the Institute Theory II for 10 months (March–December 2002).
- Richard Willmann has received a Minerva fellowship to visit the Weizmann-Institut (Rehovot, Israel) for 6 months (March–August 2002)
- Matthias Paessens has received a DAAD fellowship to visit the University of Nancy (France) for four months (May–August 2002)

Gerhard Gompper

Personnel 2002/2003 and areas of activity

Scientific Staff

Dr. A. Baumgärtner	Statistical mechanics of proteins and membranes;	23.102
Prof. E. Eisenriegler	Polymers near surfaces, colloid-polymer mixtures	23.102
Prof. G. Gompper Institute Director	Statistical mechanics of amphiphilic systems	23.102
Dr. G. Schütz	Non-equilibrium Statistical Mechanics; Polymer dynamics	23.102
Dr. G. A. Vliegenthart	Colloid-polymer mixtures, polymerized membranes	23.102
Prof. R. G. Winkler	Charged and uncharged macromolecular systems	23.102

Technical Staff

H. Paffen	Secretary	

Postdocs

Dr. E. Allakhiarov	Charged Colloids	23.102
Dr. A. Cherstvy	Polyelectrolyte Complexes	23.102
Dr. K. Mussawisade	Hydrodynamics of Complex Fluids	23.102
Dr. V. Popkov	Driven Diffusive Systems	23.102
Dr. A. Rakos	Driven Diffusive Systems	23.102
Dr. M. Ripoll	Hydrodynamics of Complex Fluids	23.102

Diploma and Graduate Students

T. Auth	Polymers at membranes	23.102
R. Maassen	Polymer depletion interaction	23.102
M. Paeßens	Finite-size effects in entangled polymers	23.102
R. Willmann	Polymer dynamics in disordered media	23.102

Guests

W. Vos	(University of Wageningen, The Netherlands) Simulations of membrane proteins (Jan. - March 2002)	23.102
Dr. K.P.N. Murthy	(Indira Ghandi Centre for Atomic Research, Kalpakkam, India) Random Walks on Lattices (Feb. - April 2002)	23.102
S. Grosskinsky	(Technische Universität München) Boundary-induced phase transitions (March 2002)	23.102
Prof. T. Burkhardt	(Temple University, Philadelphia, USA) Semi-flexible polymers (June - July 2002)	23.102
K. Hur	(University Schillim-Dong, Seoul, South-Korea) Polymer conformations (July - Sept. 2002)	23.102
Prof. T. Kohyama	(Shiga University, Japan) Shapes and fluctuations of vesicles (March - Dec. 2002)	23.102
Dr. A. Lamura	(CNR, Bari, Italy) Hydrodynamics of complex fluids (July 2002)	23.102

Water Molecules and Hydrogen-Bonded Networks in Bacteriorhodopsin : Molecular Dynamics Simulation Completes Crystal Structure

S. Grudinin[‖*+], G. Büldt*, and A. Baumgaertner[+]
[‖] *Center for Biophysics and Physical Chemistry of Supramolecular Structures, Moscow, Russia,*
**FZJ, IBI-2, and [+]FZJ, IFF, Theory 2*

The spatial distribution of water molecules and their corresponding hydrogen-bonded network inside bacteriorhodpsin (bR) in its ground state conformation were investigated by molecular dynamics simulation. The protein was embedded in a fully hydrated lipid bilayer membrane. A much higher average number of internal water molecules (44) than observed in crystal structures (18) was found in our simulation. This discrepancy is due to the high mobility of these water molecules between different positions. The simulations provides new and valubale insights into the structure and lifefetime of water-mediated hydrogen-bonded networks used for proton translocation during the photocyle of bR.

F&E-Nr. 23.102

The protein bacteriorhodopsin (bR) resides in the membrane of the archaebacterium *Halobacterium salinarum* and uses photonic energy for transmembrane proton pumping. Our current knowledge of the structure and the photocycle of bR has been reviewed [1,2]. Since certain dynamical features of bR cannot be captured by crystallographic techniques, molecular dynamics simulations (MD) have been used to elucidate, among others, conformational fluctuations [3] and bR-water mobility (see e.g. [4] and references therein). Still, the amount of buried ("internal") water molecules in bR [5,6] which are assumed to play a decisive role in providing proton pathways and to be involved in the molecular mechanism leading to proton translocation, is still unclear.

Very recently, we have reported on MD simulations [7] which have provided new details of the amount and the distribution of internal water molecules, and of the related hydrogen-bonded networks in bR that constitute proton pathways. In addition, this work provides important information on hydrogen-bonded networks in bR fluctuating on the ps to ns time scale which is not seen in crystallographic studies.

Distribution of Water Molecules. Using molecular dynamics simulations the number of internal water molecules in bR have been estimated. In addition, "diffusive" and "trapped"water molecules have been discriminated. From the simulations the average number of diffusive water has been estimated to 24 and the average fluctuation is about 1.5. The equilibrium distribution of internal water molecules (IWM) in bR is shown in Fig.1. The number density $n_w(z)$ has been calculated with respect to the z-axis, i.e., the average number of IWM within a slab of thickness $\delta z = 1$ Å. The origin $z = 0$ is placed at the center of mass of the protein. The first remarkable information from the distribution $n_w(z)$ is that a migration of water between the extracellular and cytoplasmic part does not take place within the simulation time. This is concluded from the gap in the distribution of diffusive molecules. This gap reflects a kind of structural "watershed" in the protein. The existence of this impenetrable structural interface between the cytoplasmic and the extracellular part of bR was already concluded from crystallographic data and is a necessary feature of the protein in its ground state prohibiting a spontaneous transport of protons across the membrane.

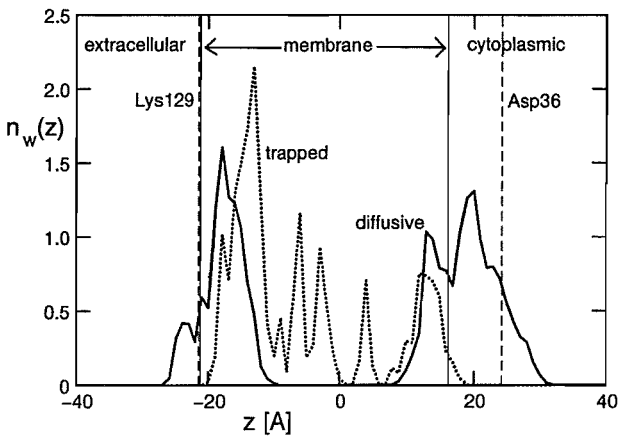

FIG. 1. One-dimensional number density $n_w(z)$ of water molecules in bR as found by simulations.

The distribution of IWM (diffusive and trapped) as detected by crystallographic data [5] and as found during our simulations are in qualitative agreement as far as the overall shape is concerned : less water molecules near the center of the protein, more outside. However, from the quantitive point of view, they differ considerably. The crystallographic data of Sass et al. [5] contain in total 77 water molecules, out of which only 18 are inside the protein whereas the simulation data provide a much higer amount of IWM, 44. The explanation for the large discrepancy of the number of IWM as found during simu-

lation and as compared to the crystallographically found IWM is the high exchange rate of water molecules between internal and external locations. Consider a particular ensemble of IWM and denote by $N_w^{(e)}(t)$ the average number of remained IWM after time t. From MD simulation we found that the decay follows an exponential law according to $N_w^{(e)}(t) \sim exp(-t/\tau_{cor})$, where the correlation time $\tau_{cor} \approx 180$ ps characterizes the time evolution of the "exchange" process of those IWM which penetrate deeply into bR. Due to this short time scale it is very difficult to detect by crystallographic methods the accurate amount of water molecules inside bR.

Structure of Hydrogen-Bonded Network. During the photocycle, protons are vectorially transported from the cytoplasmic side to the extracellular environment. This implies that hydrogen-bonded pathways must exist between the cytoplasmic surface of the protein and the Schiff base via the side chain Asp96 as shown by infrared spectroscopy. Therefore we have addressed the question about the quantitative contribution of water molecules to generate hydrogen-bonded pathways between the bR's aqueous environment and the core of bR. We have considered the following constructs of hydrogen-bonded chains. The hydrogen-bonded pathway was described by the "Grotthuss relay mechanism" or "structural proton diffusion model" for proton transport [8]. There, ordered chains of water molecules are considered, where one path consists of an alternating sequence of hydrogen bonds between water molecules, H$\cdots$O, separated by O–H bonds of water molecules. In this case, the protons are assumed to hop in a rate-limiting process along such a path which results in a reorientation of the participating water molecules. In our study, the Grotthuss-path model was used as a static geometrical construct rather than a dynamical one. A detailed analysis of the Grotthuss pathways between the protein surface and various tritrable amino acids (Asp96,Lys41, Asp38 and Asp36) have provided valuable information about the proton conduction pathway. In particular, it has been shown that the the distribution of bonds are localized in a certain regime of bR. It is suggested that the hydrogen-bonded network targeted to the core of bR works as a kind of "funneling" requisite for protein translocation. In particular, the probability distribution $P(N_p)$ of the number N_p of hydrogen-bonded pathways has been calculated and the average number $N_G(L)$ of Grutthuss paths consisting of L hydrogen bonds has been estimated. The typical length of a Grotthuss-path (in units of a hydrogen bond) is of the order of L = 4.

Dynamics of Hydrogen-Bonded Network. Each hydrogen-bonded path is transient and exists only for a certain life time. Since these paths are assumed to constitute proton pathways, it is important to estimate their life times which can provide some insights into the efficiency of the proton translocation. From MD simulation, the probability density distribution $P_L(\tau_p)$ of the life times τ_p of hydrogen-bonded paths has been calculated. The data indicated that the distribution can be described by a a stretched exponential, $P_L(\tau_p) = c_L \ exp[-\sqrt{\tau_p/b}]$, where where b and c_L are constants depending on L. Since it is well known that re-protonation of Asp96 takes several milliseconds it is of interest to correlate this time to the probability distribution $P_L(\tau_p)$. Assuming a proton hopping time $\tau_H \approx 1.5$ ps [9] between hydronium and water, and the applicability of the Einstein relation for diffusion along a one-dimensional path $a_H^2 = 2\ D\ \tau_H$, one can estimate a diffusion coefficient [10,8] $D = 2.1$ Å^2/ps by assuming a hopping length of the hydrogen-bond length $a_H = 2.5$ Å. For a typical hydrogen-bonded pathway of length $L = 5$, then the proton would need on the average a time $\tau_L = (L\ a_H)^2/2D \approx 37$ ps to travel along a path between protein surface and Asp96. According to the probability $P_L(\tau_p)$ to find a pathway existing for a traveling time τ_L leads to an unreasonable long waiting time, $\tau_{wait} \sim \langle\tau_p\rangle/P_L(\tau_L)$, which excludes the possibility of a diffusional proton translocation between the protein surface and Asp96. The key problem is the long traveling time τ_L. This time, however, would be much shorter if local electric fields E due to the surrounding residues would induce a drift of the proton along the path and along the direction of the electric field according to $v = \mu_H\ E$ where v is the proton drift velocity, $\mu_H = 36$ Å^2/V ps the proton mobility [9]. Assuming a field in the order of the membrane electric field $E = 0.05$ V/Å (see e.g. [11]) yields $v = 1.8$ Å/ps. From the drift relation $L\ a_H = v\ \tau_L$ one obtains for a typical length L=4 a traveling time $\tau_L = 5.5$ ps, which leads to a waiting times τ_{wait} =8 ms which is in reasonable agreement with experiments.

[1] Heberle,J. 2000. *Biophys. Biochim. Acta*, 1458:135–147.
[2] Lanyi, J. K. 2001. *Biochemistry (Moscow)* 66:1192–1196.
[3] Edholm,O. O.Berger, F.Jähnig. 1995. *J.Mol.Biol.* 250:94-111.
[4] Baudry,J., E. Tajkhorshid, F. Molnar, J. Phillips, and K. Schulten. 2001. *J. Phys. Chem. B* 105:905-918.
[5] Sass, H.J., Büldt, G. Gessenich, R., Hehn, D., Neff, D., Schlesinger, R., Berendzen, J., Ormos, P. 2000. *Nature* 406:649-653.
[6] Luecke, H. 2000. *Biochim. Biophys. Acta* 1460:133-156.
[7] Grudinin, S., G.Büldt, and A. Baumgaertner. 2002 (preprint 2002)
[8] Agmon, N. 1995. *Chem. Phys. Lett.* 244:456-462.
[9] Eigen, M. 1964. *Ang. Chem. Intern. Ed.* 3:1-72.
[10] Meiboom, S. 1961. *J. Chem. Phys.* 34:375-388.
[11] Lin,J.H., N.A. Baker, J.A. McCammon. 2002. *Biophys. J.* 83:1374-1379.

Polymer depletion interaction of small anisotropic particles

E. Eisenriegler, A. Bringer[1], and R. Maassen
Institute Theory II, [1]*Institute Theory I*

We discuss the depletion interaction between a wall and a mesoscopic particle of *ellipsoidal* shape which is induced by long, flexible, nonadsorbing polymer chains. Both a force and a *torque* are exerted on the particle. We concentrate on the case in which the particle size is much smaller than typical polymer lengths, such as the radius of gyration $\mathcal{R}_g$, where a rigid polymer approximation of the Asakura-Oosawa type cannot be applied. Explicit *analytical* results are obtained for *ideal* polymers. The preferred orientation of the ellipsoid changes from perpendicular to parallel to the wall on decreasing the particle-wall distance from large to small values compared to $\mathcal{R}_g$. The perturbation of the polymer system due to the small particle is represented by a series of point-operators in the corresponding field theory, with next-next to leading anisotropic derivative-operators characterizing the particle orientation. For the interaction between a *spherical* particle and a wall the simple analytical results predicted by the proposed small particle expansion beyond leading order are corroborated by direct numerical computation.

F&E-Nr.: 23.102

Colloid science covers a broad class of substances encompassing milk, blood, and paints. A major goal is to understand the effective interactions between mesoscopic colloidal particles. These can be tuned in various ways by manipulating the solvent. One way is by adding nonadsorbing free polymer chains. For entropic reasons nonadsorbing chains avoid the space between two particles, leading to an unbalanced pressure which pushes the two particles towards each other. Depletion forces for an isolated pair of immersed particles or for a single immersed particle near a wall were measured in recent experiments. The polymer depletion interaction is also of relevance for the separation of proteins.

The polymer depletion interaction depends on the degree of inter-chain overlap and on the size ratio between the colloidal particle and the polymer chains. For a dilute solution of polymer chains with radius of gyration $\mathcal{R}_g$ much smaller than the particle size, a qualitatively correct description is obtained by viewing the polymer coils as non-deformable hard spheres [1], with a radius of the order of $\mathcal{R}_g$. This approach has been applied both to large spherical colloidal particles and to anisotropic particles such as disks or platelets [2, 3]. However, for particle size much smaller than $\mathcal{R}_g$ (but much larger than the polymer persistence length), polymer conformations coiling around the particle are important, and the above Asakura-Oosawa treatment does not apply.

The perturbation of the polymer system due to a small spherical particle can, in leading order, be viewed as a δ function potential repelling the chain-monomers with an amplitude that equals a universal number times the particle radius raised to a universal exponent. The exponent is the scaling dimension $3 - 1/\nu$ of the monomer density with ν the Flory exponent. This is an operator relationship similar in spirit to operator-product expansions in field theory. Since the amplitude is independent of distant perturbations such as other particles or a wall, the same power of the radius and the same universal number appear in the free energy of immersing a particle in bulk polymer solution and in the effective interaction between two particles or between a particle and a wall. Moreover, replacing the mesoscopic particle acting via boundary conditions on the polymer system by a simple density operator considerably simplifies the evaluation of these interactions, by relating them to the density-density correlation function in bulk polymer solution or to the density profile in a polymer solution in the half space bounded by a wall [4].

The point-operator representation or 'small particle expansion' can be extended to *anisotropic* particles of ellipsoidal shape in a polymer solution [5]. The anisotropic effects of small particles, such as prolate or oblate ellipsoids of revolution, are related to operators containing anisotropic spatial derivatives. These have a higher scaling dimension than the density operator, which is isotropic, and thus are accompanied by the particle size raised to a greater power than the exponent $3 - 1/\nu$. In order to consider anisotropy, the small particle expansion must be extended beyond the leading order.

Here we consider the simplest case of *ideal* polymers in which $3 - 1/\nu = 1$ and the scaling dimension of the leading anisotropic operators turns out to be 3. Thus the anisotropic effects of, e.g., a small circular disk are proportional to the third power of the radius of the disk.

There are also *isotropic* operators beyond the leading density operator. The dominant ones are the next-to-leading operator of scaling dimension 2 and three next-to-next-to-leading operators of scaling dimension 3. These higher isotropic operators survive, even in the special case of a *spherical* particle, in which the amplitudes of the anisotropic operators vanish, and describe corrections in the physical properties which are of higher order in the radius R of the sphere.

As an example [5] the next-to-next-to-leading contribution of order R^3 to the polymer induced free energy cost for immersing the sphere at a distance z_S from a

planar wall is shown in Fig. 1. The full line is a plot of the *analytic* expression predicted by the operator expansion for the regime $R \ll z_S, \mathcal{R}_g$. Here the necessary universal amplitudes in front of the three operators and a so-called contact term have been determined from a study of the *single* sphere problem without a wall. The excellent agreement with results from a direct numerical evaluation shown as squares, circles, and asterisks in Fig. 1 indicates that the proposed expansion is a reliable and useful tool for evaluating small particle behavior even beyond the leading order.

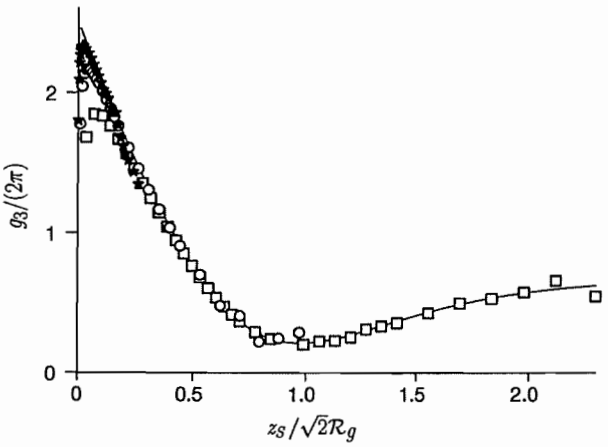

FIG. 1: Third order contribution $pR^3 g_3(z_S/\mathcal{R}_g)$ in the particle radius of the free energy required to immerse a small spherical particle with its center at a distance z_S from a planar wall. Here p is the ideal gas pressure of the ideal polymer chains in the bulk. The analytic prediction of the operator expansion (full line) is compared with a direct numerical evaluation of the free energy following the method of Ref. 4 for size ratios $R/\mathcal{R}_g = 0.05$ (squares), 0.0125 (circles), and 0.0031 (asterisks). For $R \ll z_S, \mathcal{R}_g$ the data convincingly collapse onto the predicted curve.

Consider now an *anisotropic* particle with the shape of an oblate or prolate ellipsoid of revolution. In this case the small particle expansion up to the third order contains apart from the above mentioned five isotropic operators also two anisotropic operators [5] of uniaxial symmetry and scaling dimension 3. The amplitudes in front of all the operators now depend on the aspect ratio l/s between the sizes l and s of the large and small ellipsoid axes. Again they are independent of distant perturbations such as a wall or another particle and can be obtained from considering the simple case of a *single* ellipsoidal particle in a polymer solution in free space.

As an application we discuss the interaction between a small ellipsoidal particle such as a circular disk of radius $R_{\rm disk}$ and a planar wall. The leading term

$$F_{\rm leading} = 8\,p\,R_{\rm disk}\,\mathcal{R}_g^2\,\mathcal{M}_h(z_E/\mathcal{R}_g) \qquad (1)$$

of the free energy cost F to immerse the disk is linear in the radius of the disk and arises from the density operator. It depends on the distance from the wall z_E of the center of the disk but is independent of its orientation. Here $\mathcal{M}_h$ is the bulk-normalized polymer density profile near a wall in absence of the particle. The leading term with orientational dependence is given by

$$F_{\rm leading\ anisotropic} = (\cos\vartheta)^2\,p\,R_{\rm disk}^3\,\mathcal{A}_{\rm disk}(z_E/\mathcal{R}_g) \qquad (2)$$

and arises from the two anisotropic operators. Here ϑ is the angle between the surface normals of the disk and the wall and $\mathcal{A}_{\rm disk}(\zeta)$ is the simple expression $8\{-{\rm erfc}\zeta + [{\rm erfc}(\zeta/2)]/3\}$ shown in Fig. 2. The leading contribution

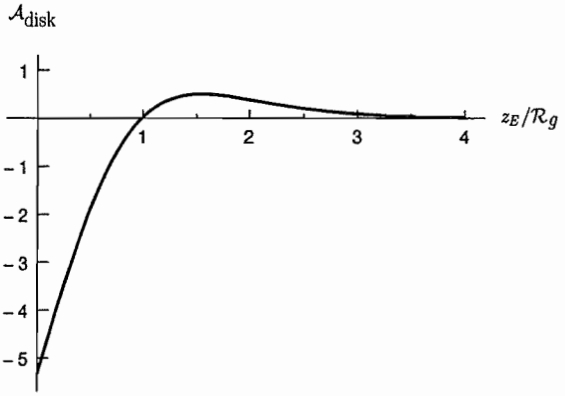

FIG. 2: The amplitude $\mathcal{A}_{\rm disk}$ which specifies the dependence (2) of the free energy on the orientation of the small disk with respect to the wall. $\mathcal{A}_{\rm disk}$ changes sign at $z_E/\mathcal{R}_g = \zeta_0 = 0.99$. For $z_E/\mathcal{R}_g > \zeta_0$ and $< \zeta_0$ the most favorable orientation of the disk is perpendicular and parallel to the wall with $\cos\vartheta = 0$ and 1, respectively, compare Eq. (2).

(1) for a disk should be compared with the corresponding contribution for a spherical particle of radius R in which $8R_{\rm disk}$ is replaced by $4\pi R$. Thus the free energy cost for a disk is smaller by a factor $2/\pi$ than for a sphere of the same radius, as expected since polymer depletion is weaker in the former case.

Eq. (2) implies that the free energy for the larger particle-wall separations $z_E/\mathcal{R}_g > \zeta_0$ is lowest if the disk is aligned perpendicular to the wall with $\vartheta = \pi/2$, and for the smaller separations $z_E/\mathcal{R}_g < \zeta_0$ if it is aligned parallel to the wall with $\vartheta = 0$.

[1] S. Asakura and F. Oosawa, J. Chem. Phys. **22**, 155 (1954); J. Polym. Sci. **33**, 183 (1958).
[2] M.A. Bates and D. Frenkel, Phys. Rev. E **62**, 5225 (2000).
[3] F.M. van der Kooij, M. Vogel, and H.N.W. Lekkerkerker, Phys. Rev. E **62**, 5397 (2000).
[4] A. Bringer, E. Eisenriegler, F. Schlesener, and A. Hanke, Eur. Phys. J., B **11**, 101 (1999).
[5] E. Eisenriegler, A. Bringer, and R. Maassen, to be published.

Giant Hexagonal Superstructures in Diblock Copolymer Membranes

C. K. Haluska[1], W. T. Góźdź[2,4], H.-G. Döbereiner[1], S. Förster[3] and G. Gompper[4]

[1] *Max-Planck-Institut für Kolloid- und Grenzflächenforschung, Am Mühlenberg 1, 14476 Golm*

[2] *Institute of Physical Chemistry Polish Academy of Sciences, Kasprzaka 44/52, 01-224 Warsaw, Poland*

[3] *Institut für Physikalische Chemie, Universität Hamburg, Bundesstrasse 45, 20145 Hamburg*

[4] *Institute Theory II*

We have observed polymersomes of high genus with their vesicle wall organized on the micrometer scale either in a double bilayer connected by a lattice of passages or a tubular network with hexagonal symmetry. Experimentally found shape classes are identified within a theoretical phase diagram based on the bending energy of the polymer membrane. Pronounced morphological changes could be induced and controlled by temperature.

F&E-Nr: 23.102

Controlled structuring of materials on all length scales is required to tune their specific chemical and physical properties. In this respect, the complex molecular organisation of block copolymer melts has been the focus of intense efforts over the last two decades [1]. Adding solvent to amphiphilic block copolymers melts produces an even richer zoo of marvelous morphologies on a supramolecular scale of 10 to 100 nm. Finally, advances are being made to extend structuring into the micrometer domain. Recently, giant bilayer vesicles with a typical size of 10 μm made of an homogenous diblock copolymer membrane, so called polymersomes, could be obtained in aqueous solution [2]. We report here [3] the remarkable property of polybutadiene(32)-b-polyethylenoxide(20) (PB-PEO) molecules [4] to self-assemble into giant vesicles with a wall formed either by a double bilayer, which is connected by a lattice of passages, or a tubular network with hexagonal symmetry. In Fig. 1, we show examples for these morphologies. The vesicles we consider here have a high-genus topology, with a genus on the order of $g \simeq 100$ or even larger. We are not interested in global vesicle shapes, but rather want to characterize and model the local membrane shape on the scale of a typical structural unit.

The viscoelastic properties of a PB-PEO bilayer membrane have already been investigated in Ref. [5] for giant quasi-spherical vesicles (with genus $g = 0$). The bending and stretching elastic moduli of the polymer membrane were found to be $\kappa = 42\ k_BT$ and $K = 470\ dyn/cm$, respectively, very similar to the values commonly found for lipid membranes, and also in an earlier study for an aqueous solution of the diblock copolymer polyethylethylene(37)-b-polyethylen oxide(40) [2]. However, the membrane viscosity is increased almost 1000-fold as compared to typical lipid membranes [5]. Thus, as in the case of lipid membranes, we may model the block copolymer membrane as a fluid elastic sheet allowing bending deformations but essentially no area dilatation due to the high stretching elastic modulus.

Our theoretical analysis of the local membranes shapes is therefore based on the curvature energy of doubly-periodic membranes with the constraints of fixed volume V and membrane area S. The walls of the polymersomes, which are formed of a double bilayer connected by passages, can be well approximated by doubly-periodic surfaces when the distance between the bilayers is small compared to the size of the polymersomes. We study a lattice of passages of hexagonal symmetry. For simplicity, we ignore the existence of lattice defects, in particular those which are induced by the spherical topology of the polmersome shapes, see Fig. 1. Membrane shapes with passages, which are symmetric with respect to the midplane between the two bilayers, can be parametrised by [6]

$$\cosh^2(z) = a_0 + \sum_{i=1}^{N} a_i \sum_{j=1}^{N_i} \cos\left(\frac{2\pi}{L}\mathbf{k}_j^{(i)} \cdot \mathbf{r}\right), \qquad (1)$$

where $\mathbf{r} = (x, y)$, and N is the number of Fourier amplitudes. There are N_i reciprocal lattice vectors $\mathbf{k}_j^{(i)}$ in the i-th shell. L is the lattice constant.

The elastic properties of diblock copolymer bilayers are described by the curvature energy

$$\mathcal{H} = \frac{\kappa}{2} \int dS\, (C_1 + C_2 - 2C_0)^2 \qquad (2)$$

where the integral extends over the whole membrane area. C_1, C_2 are the local principal curvatures at each point of the membrane. The spontaneous curvature C_0 is induced by the different sugar solutions on the two sides of the polymer membrane [7]. A second contribution to C_0 arises from the different number of polymer molecules in the two sheets of the bilayer, which typically occurs during the formation process.

We examine the stability of local membrane shape as a function of dimensionless variables $v = V/S^{3/2}$ and $c_0 = C_0 S^{1/2}$. Here, volume V and membrane area S are calculated for the unit cell of the hexagonal lattice. We have found several families of shapes: small and large passages, budded vertices, tubes, and spindles, which are stable for different values of v and c_0. Experimental membrane morphologies can be matched nicely with

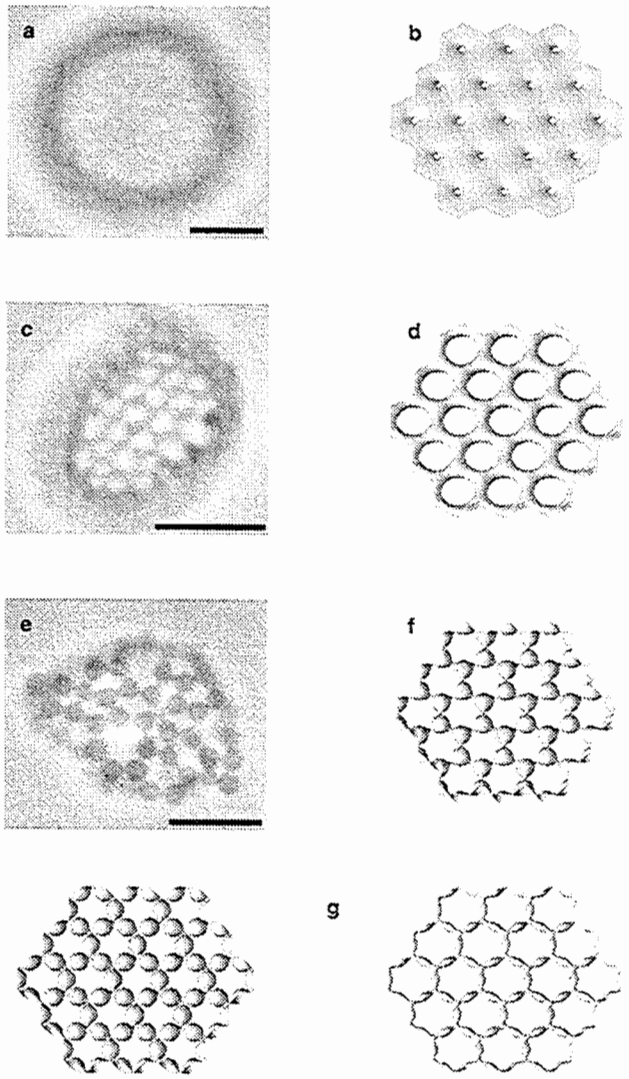

FIG. 1: Comparison of experimental and theoretical membrane shapes. The scale bars correspond to 10 μm. Experimental images with (a) narrow passages, (c) wide passages, (e) budded vertices. Theoretical shapes resulting from minimization of the functional (2) with $N = 15$ in Eq. (1) for (b) $v = V/S^{3/2} = 0.098$ and $c_0 = C_0 S^{1/2} = 0.3$ (small passages), (d) $v = 0.076$ and $c_0 = 2.7$ (large passages), (f) $v = 0.065$ and $c_0 = 4.4$ (budded vertices), (g) $v = 0.053$ and $c_0 = 5.7$, $v = 0.043$ and $c_0 = 5.9$ (spindles). The lattice of touching spheres (e) is deformed by strong thermal fluctuations.

their respective corresponding theoretical counterparts, as demonstrated in Fig. 1. The regions of stability of these phases can be seen in the phase diagram of Fig. 2.

The most common shapes are membranes connected by circular passages. For $v \lesssim 0.10$, shapes of two families of circular passages exist for the same values of v and c_0 over some range of spontaneous curvature. The shapes of these two families differ mainly by the size of the passage, where one family — see Fig. 1a,b — is characterized by a small ratio of passage radius to lattice constant, while the other — see Fig. 1c,d — is characterized by a large ratio.

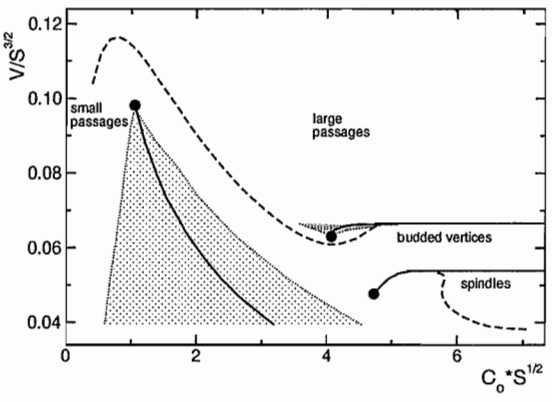

FIG. 2: Theoretical phase diagram, calculated for $N = 15$ Fourier amplitudes in Eq. (1). The full lines indicate phase transitions, where the energies of two different families of shapes are equal. All transitions are first-order and end in criticial points (•). The dashed lines are locations of minimal energy when the volume constraint is released. The shaded areas show the regions where shapes of two different families are (meta-)stable.

The transition from small to large passages with increasing c_0 is discontinuous for small reduced volume v, and ends in a critical point. The transition is accompanied by the change of the lattice constant L of the order of a few percent. Other families of shapes, which resemble either spheres located on the vertices of the hexagonal lattice connected by small necks (Fig. 1e,f), or spindle-like object located along the edges of a hexagonal lattice and connected at the vertices (Fig. 1g). are found to be stable at lower reduced volumes.

Structuring polymeric interfaces on micrometer length scales may prove useful for applications requiring materials with giant pores. In a biomimetic context, we note the striking resemblance of the large-passage membrane structure Fig. 1c-d to the tests of certain sea urchins [8]. It seems promising to employ superstructures of diblock copolymer membranes in order to cast desired mineral materials into micron-sized geometrical shapes.

[1] F.S. Bates, and G.H. Fredrickson, Physics Today **52**, 32 (1999).
[2] B.M. Discher *et al.*, Science **284**, 1143 (1999).
[3] C.K. Haluska, W.T. Góźdź, H.-G. Döbereiner, S. Förster, and G. Gompper, Phys. Rev. Lett. **89**, 238302 (2002).
[4] S. Förster, and E. Krämer, Macromolecules **32**, 2783 (1999).
[5] R. Dimova, U. Seifert, B. Pouligny, S. Förster, and H.-G. Döbereiner, Eur. Phys. J. E **7**, 241 (2002).
[6] W.T. Góźdź, and G. Gompper, Phys. Rev. Lett. **80**, 4213 (1998); Phys. Rev. E **59**, 4305 (1999).
[7] H.-G. Döbereiner, O. Selchow, and R. Lipowsky, Eur. Biophys. J. **28**, 174 (1999).
[8] K. Simkiss, and K.M. Wilbur, Biomineralization (Academic Press 1989).

Criterion for phase separation in one-dimensional driven systems

Y. Kafri[(a)], E. Levine[(a)], D. Mukamel[(a)], G. M. Schütz[(b)], J. Török[(a)]
(a) Department of Physics of Complex Systems,
Weizmann Institute of Science, Rehovot, Israel 76100.
(b) Institute Theory II.

A general criterion for the existence of phase separation in driven density-conserving one-dimensional systems is proposed. It is suggested that phase separation is related to the size dependence of the steady-state currents of domains in the system. A quantitative criterion for the existence of phase separation is conjectured using a correspondence made between driven diffusive models and zero-range processes. The criterion is verified in all cases where analytical results are available, and predictions for other models are provided.

F&E-Nr: 23.102

While phase separation and spontaneous symmetry breaking are well known not to take place in one dimension in thermal equilibrium, several models of driven one dimensional systems with local dynamics have recently been demonstrated to exhibit both [1]. Whether or not a given model exhibits phase separation is in many cases not a simple question to answer, and it may depend on numerical evidence which could be rather subtle.

For example, in a recent 3-species model introduced by Arndt *et al* [2] (AHR), it has been suggested that one should expect two distinct phase separated states: one in which the three species are fully separated from each other (related to the phase separation observed by Evans *et al* [3] in a related model), and the other is a more subtle mixed state whose existence is supported by extensive numerical simulations of systems of finite length and by a mean-field treatment. Subsequently, an exact analytical analysis of the model has shown that the mixed state is in fact disordered, and that in order to see this in simulations one has to study extremely long systems (of the order of 10^{70}) [4], far beyond existing numerical capabilities.

In another example introduced by Korniss *et al* a two lane extension of a 3-species driven system was studied [5]. It has been suggested that while for this model the one lane system does not exhibit phase separation [6], this phenomenon does exist in the two lane model. The studies rely on numerical simulations of systems of length up to 10^4. This result is rather surprising and not well understood. It may very well be the case that as for the AHR model, the two lane model does not actually exhibit phase separation in the thermodynamic limit, and that this could be seen only by studying extremely long systems. It would thus be of great importance to find other criteria, which could distinguish between models supporting phase separation from those which do not.

In [7] we introduced a simple general criterion for the existence of phase separation in density-conserving one-dimensional driven systems. Phase separation is usually accompanied by a coarsening process in which small domains of, say, the high density phase coalesce, eventually leading to macroscopic phase separation. This process takes place as domains exchange particles through their currents. When smaller domains exchange particles with the environment with faster rates than larger domains, a coarsening process is expected, which may lead to phase separation. Our criterion quantifies this mechanism, and relates the existence of phase separation to the steady-state currents through which domains exchange particles. The criterion is readily applicable even in cases which cannot be decided by direct numerical simulations.

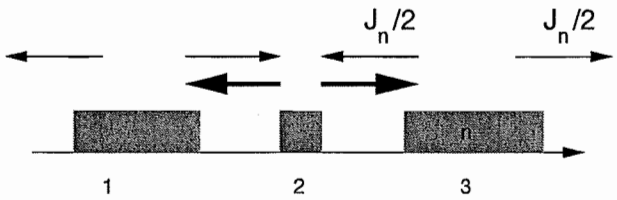

FIG. 1: Domain growth of larger domains on the expense of smaller domains. The current J_n out of domain 3 of size n is smaller than the current out of the smaller domain 2

In order to explicitly state the criterion we note that in many models which carry a non-zero current in the thermodynamic limit the current of a finite domain of size n takes the form $J_n = J_\infty(1 + b/n)$ to leading order in $1/n$. For $b > 0$ the current of long domains is smaller than that of short ones, which leads to a tendency of the longer domains to grow at the expense of smaller ones. According to our criterion phase separation takes place at high-densities only for $b > 2$. Moreover if the current decays to its asymptotic value as $J_n = J_\infty(1+b/n^\sigma)$, the model is predicted to phase separate at any density for $\sigma < 1$ while it is always homogeneous for $\sigma > 1$. In some models $J_\infty = 0$, although, due to lack of detailed balance, the current J_n of a finite system is non-vanishing. In this case the system is predicted to phase separate at any density.

The results presented above emerge from a careful analysis of a zero-range process (ZRP) which could be viewed as a generic model for domain dynamics in one-dimension. To define this process we consider a one-

dimensional lattice of M sites, or "boxes", with periodic boundary conditions. Particles, or "balls", are distributed among the boxes with the box i occupied by n_i balls. The dynamics is defined in the following way: a box i is chosen at random and a particle is removed from it and transferred to a left (right) neighbor with rates pw_{n_i} $((1-p)w_{n_i})$ where $0 \leq p \leq 1$. The rate w_{n_i} depends only on the number of balls in that box. The model may either be unbiased ($p = 1/2$), or biased ($p \neq 1/2$).

In a grand canonical ensemble, namely an ensemble where the number of boxes M is fixed while the number of balls is allowed to fluctuate with their average number controlled by a fugacity z, the steady state weight of a configuration of the ZRP is known to be [8]

$$W_{\mathrm{ZRP}}(\{n_i\}) = \prod_{i=1}^{M} z^{n_i} \mathcal{F}_{n_i} \,. \qquad (1)$$

Here $\mathcal{F}_k = \prod_{m=1}^{k} 1/w_m$ for $k \geq 1$ and $\mathcal{F}_0 = 1$. In this ensemble boxes are statistically independent with a single-site occupation distribution function given by $P(k) \sim z^k \mathcal{F}_k$. It is known [8] that condensation occurs at any density when $w_n \to 0$ with $n \to \infty$, or when it decreases to a non-vanishing asymptotic value as b/n^σ with $\sigma < 1$; no phase separation takes place for $\sigma > 1$; for $\sigma = 1$ phase separation takes place at high densities only for $b > 2$.

This model may be used to gain physical insight into the dynamics of driven one-dimensional systems. Occupied boxes represent domains of the high density phase. The currents leaving domains are represented by the rates of the ZRP. This is done by identifying the rate w_n associated with a box containing n balls with the currents J_n leaving a domain of n particles. A bias in the currents to a certain direction may be incorporated through p as defined above. The existence of a box with a macroscopic occupation in the ZRP corresponds to phase separation in the driven model.

In [7] we have considered several one-dimensional driven systems and studied their domain dynamics by introducing a corresponding zero-range process. By analyzing the ZRP, the existence of phase separation in the original model may be addressed. The AHR model is a three-state model on a ring. Each site is either empty (0), occupied by a positive (+) or a negative (−) particle. The model evolves by a random sequential dynamics in which a pair of nearest neighbor sites is chosen at random and exchanged with the rates:

$$+\,0 \xrightarrow{\alpha} 0\,+ \quad ; \quad 0\,- \xrightarrow{\alpha} -\,0 \quad ; \quad +\,- \underset{q}{\overset{1}{\rightleftarrows}} -\,+ \,. \qquad (2)$$

We showed that for the AHR model the corresponding ZRP yields its *exact* steady-state domain-size distribution. This ZRP does not exhibit phase separation, in agreement with the exact results of [4].

For the two-lane model [5] we argue that it, too, does not exhibit phase separation contrary to results of numerical simulations of finite systems. This model is a generalization of (2) with $q = 0$ to two lanes. Here in addition to the hopping process (2) within each lane, particles may hop to neighboring empty sites on the other lane with rate $\gamma\alpha$, and to exchange with a neighboring particle on the other lane with rate γ. Numerical studies of the model have suggested that for large enough α the system phase separates [5]. However, physical insight into the phenomenon is lacking. In particular it is not understood why the two-lane model seems to exhibit phase separation while its singled-lane version does not [6]. In order to apply the conjecture, the current J_n of a block of size n is calculated numerically for the two lane model. One finds that $b < 2$ [7]. Thus the conjecture suggests that the apparent phase separation found in numerical studies is due to simulations of systems much smaller than the typical domain size. We note that simulating the open systems and obtaining the asymptotic behavior of the current involves a relatively modest numerical effort, as one only needs to simulate rather small systems. This should be compared with the huge systems which are needed in order to demonstrate the lack of phase separation in direct simulations.

Applying the conjecture to a class of models with vanishing J_∞ these systems are expected to phase separate for any density. This is in agreement with results obtained from models with exponentially decaying currents which have been shown to exhibit a strongly phase separated state [1]. Although the criterion introduced in this Letter has not been proved to hold in general, the physical picture emerging from this analysis offers a rather robust mechanism for phase separation, suggesting a broad applicability.

[1] For a recent review see D. Mukamel in *Soft and Fragile Matter: Nonequilibrium Dynamics, Metastability and Flow*, Eds. M.E. Cates and M.R. Evans (Institute of Physics Publishing, Bristol, 2000).

[2] P. F. Arndt, T. Heinzel, V. Rittenberg, J. Phys. A **31**, L45 (1998).

[3] M. R. Evans, Y. Kafri, H. M. Koduvely, and D. Mukamel, Phys. Rev. Lett. **80**, 425 (1998).

[4] N. Rajewsky, T. Sasamoto, E. R. Speer, Physica A **279**, 123 (2000).

[5] G. Korniss, B. Schmittmann and R. K. P. Zia, Europhys. Lett. **45**, 431 (1999).

[6] C. Godrèche and S. Sandow , unpublished.

[7] Y. Kafri, E. Levine, D. Mukamel, G.M. Schütz, and J. Török, Phys. Rev. Lett. **89**, 035702 (2002).

[8] See, *e.g.*, O. J. O'Loan, M. R. Evans and M. E. Cates, Phys. Rev. E **58**, 1404 (1998).

Kinetics of depletion interactions

G. A. Vliegenthart
Institute Theory II

Depletion interactions between colloidal particles dispersed in a fluid medium are effective interactions induced by the presence of other types of colloid and give rise to interesting equilibrium and non-equilibrium phase behaviour. These interactions are not instantaneous but build up in time through a diffusive collision process between the two species. We show by means of Brownian dynamics simulations that the fluctuations in the depletion force between two guest particles in a host dispersion of differently sized colloids do not decay exponentially with time, but show a power-law dependence. A simple scaling theory accurately describes the dependence of the magnitude of these fluctuations on time. The consequences in particular for the dynamics of colloidal mixtures are discussed.

F&E-Nr: 23.102

INTRODUCTION

Dispersions containing colloidal particles of different size and/or shape play an important role in many processes in the fields of chemistry, biology and physics. It is no surprise then that the topic has attracted a lot of attention from workers in these fields. A full statistical description of the structure and dynamics of multi-component dispersions has proven extremely difficult, which is why many approaches involve the reduction of the number of degrees of freedom. In the equilibrium theory of binary colloidal mixtures one such approach is the so-called 'integrating out' of one of the components [1]. The resulting renormalisation of the interaction potential between the remaining particles, in what has become an effective one-particle description, is often referred to as the depletion potential.

Depletion interactions play a central role in the current understanding of the phase behaviour of dispersions containing colloids of different size and/or shape and have a remarkably elegant physical interpretation, although strictly accurate only in the dilute limit. This interpretation hinges on the view that an imbalanced osmotic pressure pushes two test particles towards each other when they approach within a correlation length set by the other species.

Depletion potentials are often treated as true, instantaneous potentials even when considering time-dependent phenomena such as the kinetics of demixing and gelation [2]. This is problematical as depletion interactions need time to build up through many collisions between a pair of test particles and the particles of the other species. This is (also) the reason why both in experiments [3] and in computer simulations the (mean) depletion potential is only obtained after extensive averaging. Here we show by means of scaling theory and Brownian dynamics simulations that the static depletion interaction potential is only approached algebraically in time, i.e., the build-up of the depletion interaction is a slow process. Clearly, this must have an impact upon processes such as phase-separation kinetics, gelation and dynamics of mixtures in external fields where there is competition between an instantaneous field and fluctuating depletion interactions.

SCALING THEORY

Arguably, diffusive processes are at the root of the buildup of depletion forces, allowing us to estimate the kinetics thereof by fairly simple scaling arguments.

First we consider the case of two parallel plates of linear dimension σ_1 fixed at a distance R immersed in a dispersion of (ghost) particles of diameter σ_2 at a number density ρ_2. If R is smaller than σ_2, the presence of the ghost spheres induce a net attraction as they are excluded from the gap between the plates. According to the Asakura-Oosawa depletion theory, [5] the mean interaction force between the plates is given by $\langle F\rangle = -\Pi\sigma_1^2$ for separations $R \leq \sigma_2$, where $\Pi = k_BT\rho_2$ is the osmotic pressure of the host dispersion and k_BT the thermal energy. For $R > \sigma_2$, $\langle F\rangle = 0$.

The mean number of ghost colloids $\langle N_2(t)\rangle$ contributing to the build-up of net force $\langle F\rangle$ between the plates in a time interval of width t is equal to their mean density times the plate area times a diffusion length, and increases with time proportionally to $\rho_2\sigma_1^2\sqrt{D_2t}$ with D_2 the diffusivity of species 2. Assuming the ideal host dispersion to be in local equilibrium, it follows from standard statistical mechanics that the mean-square fluctuation of this number must also be of the order $\langle N_2(t)\rangle$. As a consequence, the mean-square fluctuation $\langle \Delta F^2\rangle$ of the depletion force should scale as $\rho_2(k_BT)^2\sigma_1^2/\sqrt{D_2t}$.

Using the Stokes-Einstein relation $D_2 \sim k_BT/\mu\sigma_2$ for the diffusivity of colloid species 2, with μ the viscosity of the solvent, we thus obtain

$$\langle \Delta F^2\rangle \sim \rho_2(k_BT)^{3/2}\sigma_1^2\sigma_2^{1/2}\mu^{1/2}t^{-1/2} \qquad (1)$$

for $R < \sigma_2$, showing an algebraic decay with time which is due to the diffusive nature of the coupling of the plates to the host dispersion. Note that eq. (1) implies that the buildup of the depletion forces must also be algebraic in time.

Our arguments carry over naturally to physically more interesting geometries such as pairs of large spheres immersed in dispersions of (ghost) spheres of different size, although that the available collision area and the diffusion volume are no longer trivial to evaluate, because they now depend on the size ratio of the spheres as well as on their separation. Here, we simply reproduce without proof for that particular case the final results for the mean and the mean-square fluctuation of the depletion force. The former reads $\langle F \rangle = -\pi\sigma_1^2(1+q)^2[1 - R^2/\sigma_1^2(1+q)^2]\rho_2 k_B T$ for $\sigma_1 < R \leq \sigma_1 + \sigma_2$ and $\langle F \rangle = 0$ for $R > \sigma_1 + \sigma_2$ (where $q = \sigma_2/\sigma_1$ is the size ratio) while the latter equals,

$$\langle \Delta F^2 \rangle \sim \frac{(1+q)}{l(t)[1+q+R/\sigma_1]} \times \frac{[\sigma_1^2(1+q)^2[1+R^2/\sigma_1^2(1+q)^2]k_B T]^2 \rho_2}{[3\sigma_1^2(1+q)^2/4 + 3\sigma_1(1+q)l(t)/2 + l(t)^2]} \quad (2)$$

for $\sigma_1 < R \leq \sigma_1 + \sigma_2$, where $l(t) = c\sqrt{D_2 t}$ is a diffusion length. Here, c is an unknown constant of proportionality that we fix by fitting to the results of the Brownian dynamics simulations. Equation 2 holds also for $R \geq \sigma_1 + \sigma_2$ provided we set $R = \sigma_1 + \sigma_2$. Notice the non-obvious dependence of $\langle \Delta F^2 \rangle$ on time t, distance R and the size ratio q. Here we only show the results for the time-dependence of the fluctuations while a more extensive discussion including the distance, and size dependence is given elsewhere [4].

BROWNIAN DYNAMICS SIMULATIONS

Brownian dynamics simulations were performed for two two test colloids fixed at a distance R and N_2 ghost particles in a simulation box of volume V.

The ghost particles interact with the test particles through a hard-core-like steep repulsive potential that scales as $\epsilon((1+q)\sigma_1/r)^{50}$, where ϵ is the interaction strength and r is the distance between the centers of mass of a test colloid and a host particle. Simulation time was divided in a sequence $i = 1, ..., N$ intervals of width t. For each interval i the net force $f_i(t)$ along the vector connecting the centers of mass of the pair of test particles was calculated. The variance of the distribution of forces we define as the fluctuation in the force. The mean depletion force is simply obtained as $\langle F \rangle = \sum_{i=1}^{N} f_i(t)/N$, while the mean squared fluctuation in that force is given by $\langle \Delta F^2 \rangle = \sum_{i=1}^{N} f_i^2(t)/N - (\sum_{i=1}^{N} f_i(t)/N)^2$.

Plotted in fig. 1 is the value of $\langle \Delta F^2 \rangle$ at contact, as a function of t for $q = 0.5$, $k_B T/\epsilon = 1$ at a ghost particle density $\rho_2 \sigma_2^3 = 0.0625$. The time t is normalised on the Brownian time $\tau_2^B = 3\pi\mu\sigma_2^3/k_B T$ of the ghost particles. Also indicated is the fitted scaling relation eq. (2). For small t, the diffusion length is small on the scale of the linear dimension of the test particles, and therefore approaches the result for the flat plate. For large times the

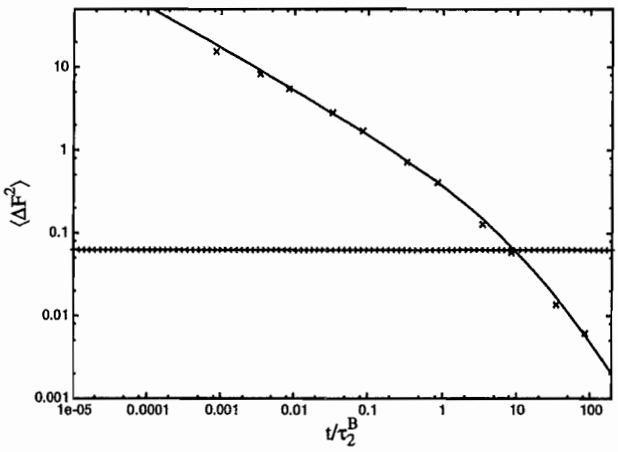

FIG. 1: The mean-square fluctuation of the depletion force as a function of the dimensionless time t/τ_2^B with τ_2^B the Brownian timescale of the ghost particles. The symbols indicate the simulation results and the full curve those of the scaling theory (eq. (2)). The horizontal, dashed line corresponds to the average force squared $\langle F \rangle^2$.

scaling crosses over to $t^{-3/2}$, approaching the time dependence of a radially symmetric diffusion volume. Best fits were obtained setting $c = 1$ although one would expect on basis of the quasi one-dimensional nature of the problem a value of $\sqrt{2}$. The description is quantitative over 5 decades in time. Also in the case of fig. 1 is the square-mean depletion force $\langle F \rangle^2$. Clearly, $\langle \Delta F^2 \rangle \ll \langle F \rangle^2$ only if $t \gg \tau_2^B$, i.e., for times very much larger than the diffusion time of the host particles. This means that for the case $q = 0.5$, the mean depletion force cannot fully build up at the diffusion time of the guest particles. Consequently, the actual depletion force felt by these particles must be dominated by fluctuations.

We have shown that the temporal fluctuations in the depletion force between two guest particles in a host dispersion of colloids of different size are significant. Our results imply that the dynamics of approach of two such colloids must be strongly influenced by these fluctuations and the slow buildup of the depletion force, a fact not commonly recognised.

[1] M. Dijkstra M. R. van Roij. and R. Evans, Phys Rev. E **59**, 5744 (1999).

[2] I. Bodnár, J.K.G. Dhont and H.N.W. Lekkerkerker, J. Phys. Chem B **100**, 19614 (1996).

[3] D. Rudhardt, C. Bechinger and P. Leiderer, Phys. Rev. Lett. **81**, 1330 (1998).

[4] G.A. Vliegenthart and P. van der Schoot, submitted to Europhys. Lett.

[5] S. Asakura and F. Oosawa, J. Chem. Phys. **22**, 1255 (1954).

Distribution functions and force-extension relations of semiflexible chains

R. G. Winkler
Institute Theory II

The conformational properties of semiflexible chains of Gaussian segments are studied for a constant force and constant extension ensemble. Qualitative differences are found for the force-extension relation and the end-to-end distribution when the persistence length is of the order of the chain length. The comparison of the force-extension relation with experimental results on DNA molecules exhibits excellent agreement. The proposed approach provides a simple analytical expression for the end-to-end distribution which is in excellent agreement with Monte Carlo simulations of the Kratky-Porod semiflexible chain model.

F&E Nr. 23.102

The functions and properties of biological systems crucially depend upon the conformational properties of the constituting (linear) macromolecules. Prominent examples are the polymers of the cytoskeleton, in particular actin filaments [1], and DNA. Like many other biological polymers, they are semiflexible chains. It is (among other aspects) the stiffness of actin which determines the mechanical properties of a cell. Insight into the conformational properties of individual molecules can be gained by fluorescence microscopy [2]. Measurements of the force-extension relation of DNA molecules by such techniques reveal the semiflexible character of biological molecules [3, 4].

Despite the success of the semiflexible chain approach there are various aspects of semiflexible chain behavior which are not satisfactorily solved. In particular, the distribution function of the end-to-end distance has attracted considerable attention recently [5, 6].

The basis of these approaches is the wormlike chain model of Kratky and Porod [5], which accounts for stiffness via inclusion of bending elasticity. Although physical reasonable, this model and its numerous, subsequent modifications have not provided analytically tractable results for equilibrium and dynamical properties of a chain of arbitrary stiffness. Results for the radial distribution function of the Kratky-Porod model have been obtained recently based on a perturbation theory with a rodlike chain as a reference [5].

The most promising candidate for an analytical tractable model is a chain of Gaussian segments, i.e., a chain with Gaussian distributed distances between successive points along the chain. For flexible chains, we demonstrated that even finite size can be taken into account by this model. However, the force constants have to be chosen adequately in order to satisfy macroscopic requirements, like a finite contour length. Numerous attempts have been undertaken to find the correct description for a semiflexible chain. Taking into account the chain ends properly, it has been shown that such an approach provides second moments which agree with those of the Kratky-Porod wormlike chain [7].

In order to interpret experimental data, it would be useful to have a clear and complete understanding of the predictions of the various models for wormlike chains. Such an understanding would reveal the strengths and deficiencies of a model in describing real polymers and serves as a bases for improved models. The major difference between the Gaussian description and the Kratky-Porod model is the intrinsic elasticity of the Gaussian approach. The comparison of experimental force-extension data on DNA with the predictions of the Kratky-Porod model yields deviations at large extensions [4], which are explained by an internal elasticity of DNA molecules.

Another major aspect is the understanding of the equilibrium and non-equilibrium dynamics of semiflexible chains. To obtain analytical solutions a sufficiently simple model is required which still captured the essential features of semiflexible chains. As we demonstrated, the Gaussian semiflexible chain provides such a model [8].

The partition function of a (continuous) chain can be obtained by the maximum entropy principle [7], where the distribution function is determined by a variational calculations from the entropy taking into account bond length and bond angle restrictions by constraints. For the constant force ensemble, an additional constraint for the average position of one of the chain ends is applied (to remove the translational degrees of freedom, the other chain end is fixed). In the constant extension ensemble the partition function has to be calculated with both end points fixed. Choosing appropriate constraints, the maximum entropy principle yields a path integral representation of the corresponding partition functions which are analytically tractable. The detailed calculation leads to the force-extension relation

$$F = \frac{3pk_BTa}{L\left(1-\frac{a^2}{L^2}\right)^2};\ pL \gg 1 \qquad (1)$$

for the constant force ensemble, where a is the extension, L the contour length, and $l_p = 1/(2p)$ the persistence length of the chain. Figure 1 compares our analytical result with measurements on B-DNA. As is obvious, the force-extension relation provides an excellent description of the experimental data. The least square fit of F to the experimental data yields a persistence length and a chain chain length in close agreement with previous results by Marko and Siggia [4].

The major difference between the Gaussian semiflexible chain and the Kratky-Porod model is the fact that the magnitude of tangent vector $\mathbf{u}(s)$ is not exactly one but only the average $\langle \mathbf{u}^2 \rangle = 1$ is constraint. As a conse-

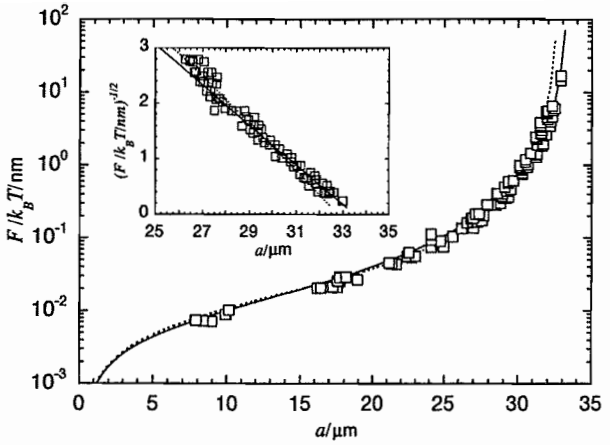

FIG. 1: Fit of the force-extension curve of the Gaussian semiflexible chain model (solid line) to experimental data of Smith et al. [9]. The fit parameters obtained from a logarithmic fit are $l_p = 53.5$ nm and $L = 33.5$ μm. The dotted line is calculated using the interpolation formula derived by Marko and Siggia [4] for the Kratky-Porod model with the parameters $l_p = 53$ nm and $L = 32.8$ μm, respectively.

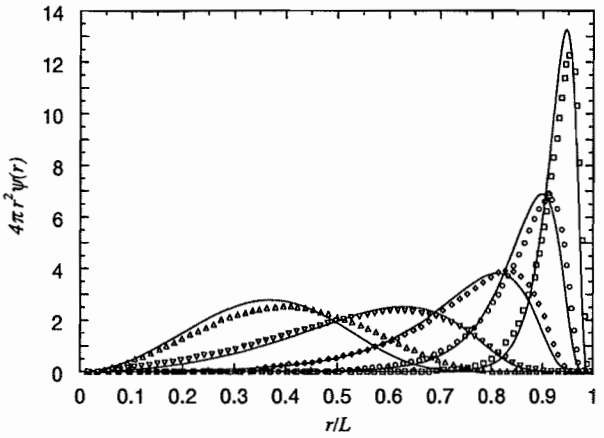

FIG. 2: Comparison of radial distribution functions obtained from Monte Carlo simulations (symbols) [5] and a Gaussian chain (solid lines) for $pL = 5$, 1.6, 0.66, 0.33, 0.166.

quence, the contour length is not a constant but fluctuates. Since we adopted a coarse grained description of a DNA, we expect that $\langle \mathbf{u}^2 \rangle$ exhibit some fluctuations due to the various monomers, and hence degrees of freedom, of the real chain incorporated in an effective segment. Naturally, the Gaussian chain can only partially capture such fluctuations [6].

Due to the contour length fluctuations inherent in the Gaussian model, the force-extension relation is slightly different from the relation following from the Kratky-Porod model. As a consequence, a somewhat larger contour length is obtained. This improves the quality of the fit to the experimental data at large extensions. This is related to the issue of the stretchability of DNA beyond the contour length determined by the fit to the Kratky-Porod model. In terms of the considered model, part of the stretching is due to contour length fluctuations. To clarify this point further comparisons with experimental data are necessary.

As long as $pL \gg 1$, the force-extension relations of a constant extension and a constant force ensemble are the same. The differences in the fluctuations inherent in the two ensemble, however, lead to different force-extension relations for $pL \lesssim 2.5$. Analysis of the equations for the constant extension ensemble shows that the force assumes the value zero for finite extensions and pL values below a certain threshold. As a consequence, a force has to be applied to move the chain ends towards each other for smaller extensions. At $a = 0$, however, the force is zero for each of the two ensembles. (For details see [6]).

Using the partition function and the free energy ($\mathcal{F}$) of a chain with fixed end points, the distribution function of a finite extensible chain with one free end can be calculated. The distribution function follows from the relation $\mathcal{F} \sim -k_BT \ln \psi(\mathbf{r})$, where $\psi(\mathbf{r})$ is the end-to-end distribution function of a free chain. The detailed calculation yields

$$\psi(\mathbf{r}) = N_c \left(1 - \frac{\mathbf{r}^2}{L^2}\right)^{-3/2} \left(2 - \frac{\mathbf{r}^2}{L^2}\right)^{-3} \times \exp\left(-\frac{3pL}{2(1 - \mathbf{r}^2/L^2)}\right) \quad (2)$$

for $pL \gg 1$. Here, N_c denotes the normalization constant.

Figure 2 compares the radial distribution function for the considered semiflexible chain model with Monte Carlo data of the Kratky-Porod model presented in Ref. [5]. The results of our approach obviously agree very well with the simulation data. Since we observe deviations on the order of a few percent only, our approach quantitatively describes the simulation data and can be used as a basis to analyze experiments.

In conclusion, our theoretical approach provides a useful description of equilibrium (and dynamical) properties of semiflexible chains. Extensions to a broad spectrum of problems, where the exact treatment of the constraint $\mathbf{u}^2 = 1$ is difficult, is possible.

[1] P. Janmey, *Cell Membranes and the Cytoskeleton*, volume 1A of Handbook of Biological Physics, Chapter 17 (Noth Holland, Amsterdam, 1995)
[2] T. T. Perkins, D. E. Smith, R. G. Larson, and S. Chu, Science **268**, 83 (1995)
[3] C. Bustamante, J. F. Marko, E. D. Siggia, and S. Smith, Science **265**, 1599 (1994)
[4] J. F. Marko and E. D. Siggia, Macromolecules **28**, 8759 (1995)
[5] J. Wilhelm and E. Frey, Phys. Rev. Lett. **77**, 2581 (1996)
[6] R. G. Winkler, J. Chem. Phys. **118** (7) (2003)
[7] R. G. Winkler, P. Reineker, and L. Harnau, J. Chem. Phys. **101**, 8119 (1994)
[8] R. G. Winkler, Phys. Rev. Lett. **82**, 1843 (1999)
[9] S. B. Smith, L. Finzi, and C. Bustamante, Science **258**, 1122 (1992)

Publications in journals

Allahyarov,E.; Gompper,G.
Mesoscopic solvent simulations : multiparticle-collision dynamics of three-dimensional flows
Physical review E, 66 (2002), S. 036702

Belitsky,V.; Schütz,G. M.
Diffusion and scattering of shocks in the partially asymmetric simple exclusion process
Electronic journal of probability, 7 (2002), 11, S. 1 - 21

Descas,R.*; Mussawisade,K.
Hopping diffusion of two coupled particles in random trap model
Physical review E, 66 (2002), S. 051103

Eisenriegler,E.; Maassen,R.
Center-of-mass distribution of a polymer near a repulsive wall
Journal of chemical physics, 116 (2002), S. 449

Gompper,G.; Kroll,D. M.
The freezing transition of flexible membranes
Europhysics letters, 58 (2002), 1, S. 60 - 66

Gozdz,W.T.*; Gompper,G.
Phase behavior of two-component membranes
Colloids and surfaces A:physicochemical and engineering aspects, 208 (2002), S. 241 - 251

Haluska,C. K.*; Gozdz,W. T.*; Döbereiner,H.-G.*; Förster,S.*; Gompper,G.
Giant hexagonal superstructures in diblock copolymer membranes
Physical review letters, 89 (2002), S. 238302

Kafri,Y.*; Levine,E.*; Mukamel,D.*; Schütz,G. M.; Török,J.*
Criterion for phase separation in one-dimensional driven systems
Physical review letters, 89 (2002), S. 035702

Lübeck,S.*; Willmann,R. D.
Universal scaling behaviour of directed percolation and the pair contact process in an external field
Journal of physics A, 35 (2002), S. 10205 - 10217

Maassen,R.; Eisenriegler,E.; Bringer,A.
Erratum : density depletion profile and solvation free energy of a colloidal particle in a polymer solution
Journal of chemical physics, 116 (2002), S. 1207

Müller,M.; Gompper,G.
Elastic properties of polymer interfaces : aggregation of pure diblock, mixed diblock, and triblock copolymers
Physical review E, 66 (2002), S. 041805

Paessens,M.; Schütz,G.M.
DMRG studies of the effect of constraint release on the viscosity of polymer melts
Physical review E, 66 (2002), S. 021806

Popkov,V.; Fouladvand,M. E.*; Schütz,G.M.
A sufficient criterion for integrability of stochastic many-body dynamics and quantum spin chains
Journal of physics A, 35 (2002), S. 7187 - 7204

Popkov,V.; Schütz,G. M.
Integrable Markov processes and quantum spin chains
Matematiceskaja fizika, analiz, geometrija, 3 (2002), S. 1 - 11

Schilling,T.; Gompper,G.
Wetting in ternary mixtures - with and without amphiphiles
Journal of chemical physics, 117 (2002), S. 7284 - 7294

Schäfer,L.; Ebert,U.; Baumgärtner,A.
Coherent scattering function in the reptation model : analysis beyond asymptotic limits
Physical review E, 65 (2002), S. 061505

Stepanow,S.*; Schütz,G. M.
The distribution function of a semiflexible polymer and random walks with constraints
Europhysics letters, 60 (2002), S. 546 - 551

Willmann,R.
Diffusion coefficient for reptation of polymers with kinematic disorder
Journal of chemical physics, 116 (2002), 7, S. 2688 - 2691

Willmann,R. D.; Schütz,G.M.; Challet,D.*
Exact Hurst exponent and crossover behavior in a limit order market model
Physica A, 316 (2002), S. 430 - 440

Winkler,R.
Virial pressure of periodic systems with long range forces
Journal of chemical physics, 117 (2002), S. 2449

Winkler,R.G.; Steinhauser,M.O.*; Reineker,P.*
Complex formation in systems of oppositely charged polyelectrolytes : a molecular dynamics simulation study
Physical review E, 66 (2002), S. 021802

Book chapter

Baumgärtner,A.
Polymer mixtures
Soft matter : complex materials on mesoscopic scale ; lecture manuscripts of the 33rd IFF winter school, this winter school was organized on March, 04 - 15, 2002 in the Forschungszentrum Jülich by the Institut für Festkörperforschung ... / ed.: J. K. G. Dhont. - Jülich, 2002. - (Schriften des Forschungszentrums Jülich, Reihe Materie und Material/Matter and Materials ; 10). - 3-89336-297-5. - S. B4.1 - B4.16

Baumgärtner,A.
Scaling laws of polymers
Soft matter : complex materials on mesoscopic scale ; lecture manuscripts of the 33rd IFF winter school, this winter school was organized on March, 04 - 15, 2002 in the Forschungszentrum Jülich by the Institut für Festkörperforschung ... / ed.: J. K. G. Dhont. - Jülich, 2002. - (Schriften des Forschungszentrums Jülich, Reihe Materie und Material/Matter and Materials ; 10). - 3-89336-297-5. - S. B3.1 - B3.13

Eisenriegler,E.
Polymers near surfaces
Soft matter : complex materials on mesoscopic scale ; lecture manuscripts of the 33rd IFF winter school, this winter school was organized on March, 04 - 15, 2002 in the Forschungszentrum Jülich by the Institut für Festkörperforschung ... / ed.: J. K. G. Dhont. - Jülich, 2002. - (Schriften des Forschungszentrums Jülich, Reihe Materie und Material/Matter and Materials ; 10). - 3-89336-297-5. - S. B10.1 - 10.16

Gompper,G.
Statistical mechanics of membranes
Soft matter : complex materials on mesoscopic scale ; lecture manuscripts of the 33rd IFF winter school, this winter school was organized on March, 04 - 15, 2002 in the Forschungszentrum Jülich by the Institut für Festkörperforschung ... / ed.: J. K. G. Dhont. - Jülich, 2002. - (Schriften des Forschungszentrums Jülich, Reihe Materie und Material/Matter and Materials ; 10). - 3-89336-297-5. - S. B9.1 - B9.46

Schütz,G. M.
Random motion in equilibrium
Soft matter : complex materials on mesoscopic scale ; lecture manuscripts of the 33rd IFF winter school, this winter school was organized on March, 04 - 15, 2002 in the Forschungszentrum Jülich by the Institut für Festkörperforschung ... / ed.: J. K. G. Dhont. - Jülich, 2002. - (Schriften des Forschungszentrums Jülich, Reihe Materie und Material/Matter and Materials ; 10). - 3-89336-297-5. - S. C1.1 - C1.24

Winkler,R.G.
Polyelectrolytes
Soft matter : complex materials on mesoscopic scale ; lecture manuscripts of the 33rd IFF winter school, this winter school was organized on March, 04 - 15, 2002 in the Forschungszentrum Jülich by the Institut für Festkörperforschung ... / ed.: J. K. G. Dhont. - Jülich, 2002. - (Schriften des Forschungszentrums Jülich, Reihe Materie und Material/Matter and Materials ; 10). - 3-89336-297-5. - S. B5.1 - B5.22

Invited talks

Baumgärtner,A.
The physics of cell locomotion
Jülich Soft Matter Days 2002
Kerkrade, Niederlande: 19.11.2002 - 22.11.2002

Baumgärtner,A.
The physics of cell locomotion
DAE Solid State Physics Symposium
Chandigarh, Indien: 26.12.2002

Gompper,G.
Structure and phase behavior of membran ensembles
Workshop Mathematical Aspects of Material Science : Soft Matter
Schloß Ringberg: 17.10.2002 - 02.11.2002

Gompper,G.
Structure and phase behavior of membrane ensembles
15th Marian Smoluchowski Symposium on Statistical Physics
Zakopane, Poland: 07.09.2002 - 12.09.2002

Schütz,G.
Phase separation in one-dimensional stochastic particle systems
VIth Brazilian School of Probability
Ubatuba, Brasilien: 05.08.2002 - 10.08.2002

Schütz,G. M.
Criterion for phase separation in one-dimensional driven systems
La Physique Statistique Hors Equilibre et Les Systemes Desordonnes : Universität Nancy
Nancy, Frankreich: 29.05.2002 - 31.05.2002

Schütz,G. M.
From single-file diffusion to molecular/colloidal traffic control
SFB-Symposium on Molecules in Interaction with Interfaces
Leipzig, Deutschland: 09.10.2002 - 11.10.2002

Schütz,G. M.

Phase separation in one-dimensional nonequilibrium systems
TH2002 : UNESCO
Paris, Frankreich: 22.07.2002 - 27.07.2002

Schütz,G. M.
Theory of boundary-induced phase transitions
Annual Conference of the Iranian Physical Society
Zanjan, Iran: 24.08.2002 - 27.08.2002

Vliegenthart,G.
Depletion induced phase transitions : possible relevance for red blood cell aggregation
11th International Congress of Biorheology and 4th International Conference on Clinical Hemorheology
Antalya, Türkei: 22.09.2002 - 26.09.2002

Vliegenthart,G.
Phase transitions and gelation of silica-polystyrene mixtures in benzene
Faraday Discussion 123 : Non-Equilibrium Phase Behaviour of Colloidal Dispersions
Edinburgh, UK: 09.09.2002 - 11.09.2002

Other talks

Baumgärtner,A.
Lipid-protein interactions at ion channels
COST D22 Meeting on Supramolecular Assemblies
Madrid, Spanien: 15.03.2002

Baumgärtner,A.
Molecular dynamics simulations of membrane proteins
Workshop Biology meets Physics :
Forschungszentrum Jülich
Jülich: 20.02.2002

Baumgärtner,A.
Polymer mixtures
Soft matter : complex materials on mesoscopic scales ; 33. IFF-Ferienkurs 2002, FZ Jülich
Jülich: 04.03.2002 - 15.03.2002

Baumgärtner,A.
Scaling laws of polymers
Soft matter : complex materials on mesoscopic scales ; 33. IFF-Ferienkurs 2002, FZ Jülich
Jülich: 04.03.2002 - 15.03.2002

Baumgärtner,A.
The hydrogen-bonded network in bacteriorhodopsin
COST D22 Workshop on Nanotechnologies of Membrane Mimetic Systems
Graz, Österreich: 11.10.2002

Baumgärtner,A.
Zellbewegung
Beiratsitzung IFF : Forschungszentrum Jülich
Jülich: 21.03.2002

Eisenriegler,E.
Polymers near surfaces
Soft matter : complex materials on mesoscopic scales ; 33. IFF-Ferienkurs 2002, FZ Jülich
Jülich: 04.03.2002 - 15.03.2002

Gompper,G.
Aktuelle Forschungsarbeiten des Instituts für Festkörperforschung :
Bericht des Geschäftsführenden Direktors
17. Sitzung des Wissenschaftlichen Beirats :
Forschungszentrum Jülich
Jülich: 21.03.2002

Gompper,G.
Statistical mechanics of membranes
Soft matter : complex materials on mesoscopic scales, 33. IFF-Ferienkurs 2002 ;
Forschungszentrum Jülich
Jülich: 04.03.2002 - 15.03.2002

Gompper,G.
Statistische Physik der Weichen Materie
Oberseminar der Sektion Physik und des CeNS :
Ludwig-Maximilians-Universität
München: 31.05.2002

Gompper,G.
Statistische Physik der Weichen Materie
HGF-Workshop Kondensierte Materie :
Forschungszentrum Jülich
Jülich: 06.11.2002

Gompper,G.
Weiche Materie : Amphiphile, Membranen, Schwamm-Phasen
Kolloquiumsvortrag : Martin Luther Universität
Halle-Wittenberg: 07.02.2002

Schütz,G.
Dynamical Matrix Product : Ansatz und Integrable Systems
Universidade Sao Paulo
Sao Carlos, Brasilien: 14.08.2002

Schütz,G.
Phasenseparation in eindimensionalen stochastischen Vielteilchensystemen
Universität Halle
Halle: 16.04.2002 - 16.04.2002

Schütz,G. M.
Diffusion and interaction of shocks in the asymmetric simple exclusion process
Universität Lausanne
Lausanne, Schweiz: 13.03.2002

Schütz,G. M.

Dynamical matrix product : Ansatz and integrable systems
Freie Universität Berlin
Berlin, Deutschland: 05.02.2002

Schütz,G. M.
Lattice gas model for relaxation of entangled polymers
Hahn-Meitner-Institut Berlin
Berlin, Deutschland: 04.02.2002

Schütz,G. M.
Microscopic structure and dynamics of interface in stochastic particle systems
Universität Leipzig
Leipzig, Deutschland: 10.04.2002

Schütz,G. M.
Random motion in equilibrium
Soft matter : complex materials on mesoscopic scales ; 33. IFF-Ferienkurs 2002, FZ Jülich
Jülich: 04.03.2002 - 15.03.2002

Schütz,G. M.
Relaxation of entangled polymers
Universität Freiburg
Freiburg, Deutschland: 02.12.2002

Schütz,G. M.
Relaxation verschlaufter Polymere
Universität Bonn
Bonn, Deutschland: 12.12.2002

Schütz,G. M.
Stochastische Vielteilchensysteme fern vom Gleichgewicht
Universität Köln
Köln, Deutschland: 22.04.2002

Winkler,R. G.
Dynamics of semiflexible macromolecules : from DNA in solution to polymer melts
Institut Charles Sadron
Strasbourg, France: 10.12.2002

Winkler,R. G.
Structure of polyelectrolyte solutions : from repulsion to attraction
Institut für Polymerforschung
Dresden, Deutschland: 07.11.2002

Winkler,R.G.
Polyelectrolytes
Soft matter : complex materials on mesoscopic scales, 33. IFF-Ferienkurs 2002 ;
Forschungszentrum Jülich
Jülich: 04.03.2002 - 15.03.2002

Ph.D. Theses

Maassen,R.
Mesoscopic particles in polymer solutions
2002
Düsseldorf, Univ., Diss., 2002

Institute Theory III

General Overview

The institute Theory III investigates the mechanisms of the formation of structures and their consequences in condensed matter. The research starts from electronic properties which define the shortest length and time scales, but it also encompasses the macroscopic consequences. The analytical and numerical investigations are in many ways closely connected with experimental studies performed in other groups of the IFF, and also with activities in other institutes of the Research Center Jülich.

Central points of interest for the research in Theory III are in the field of electronic structure of solids. Material classes under consideration are metals, semiconductors and related nanostructured materials specifically with respect to their importance for information technology. A second mainstream is formed by cooperative phenomena in condensed matter. Questions here aim at the dynamics of structure and pattern formation and the statistical mechanics of order and disorder processes. Specific activities concern the effect of long-range interactions like elastic effects in solids or hydrodynamic interactions in solid-liquid systems.

The research of Theory III employs a wide range of analytical and numerical techniques applicable to many-body problems in condensed matter. In addition the development of new methodological concepts and numerical procedures is part of our research interest. The development of parallel program codes adapted to massively parallel computers has received special attention in recent years.

The explanation of the microstructure and dynamics of real solids requires the understanding of the electronic properties. One of the most important methods for the calculation of the electronic structure of real solids is the density functional theory in connection with appropriate numerical procedures. While in recent years bulk properties of metals and semiconductors have been at the center of our interest a main concern now is directed towards the understanding of surface and interface properties, with particular emphasis on magnetism.

Theoretical efforts in the investigation of electronic effects, combining charge and spin properties for a future technology based on spin-electronics, presently are centered on the problem of spin-injection. Spin-injection is a prerequisite for semiconductor spin-electronics. We have considered spin-injection from Fe into ZnSe and GaAs in the ballistic limit. By means of the ab-initio SKKR method the ground state properties of epitaxial Fe/ZnSe and Fe/GaAs heterostructures were calculated. Three different injection processes were considered. The calculation of the electrical conductance shows that (001)-interfaces may act as almost ideal spin-filters, while other orientations give only small injection efficiencies. The high spin polarization can be traced back to symmetries of the bandstructure of iron.

The properties of high-tech materials for sensorics and information-technology depend usually on details of their surface structures and on the growth processes of these materials. The surface of the growing interface is often covered with a passivating material like Sb, in order to achieve layered growth rather than island growth. We can explain the experimentally observed

development of surface structures of a growing Ge film on Si(111), covered with a monatomic layer of Sb. For this purpose an ab-initio method (the Jülich EStCoMPP-code) was used for the calculation of the stability of different Ge(111):Sb structures. As one example, the (1x1) substitutional structure experimentally found on top of the Sb-covered hexagons, formed for a three-monolayer Ge film deposited on Si(111), can be traced back to an over-relaxation of the finite size hexagons caused by the Sb atoms on top and at the edge of the hexagons.

Glasses have properties with characteristic anomalies in comparison with regular solids or with liquids. Particularly significant is the so-called Boson-peak in the phonon-spectrum at low frequencies. A universal mechanism of Boson-peak formation in glasses has now been proposed. It is based on the concept of interacting quasi-local oscillators. Even in the case of weak interaction the ordinary low frequency-spectrum becomes unstable. Due to anharmonicity the system undergoes a transition into a new stable configuration. Below some characteristic frequency the renormalized density of states becomes a universal function of the frequency with Boson-peak characteristics. An analytical form of this function has been derived.

The formation of alloys in directional solidification and the appearance of structures in liquids may exhibit striking similarities. The phase transformation of a two-component liquid during condensation in a distillation apparatus is discussed. The liquid is assumed to flow in a temperature gradient towards decreasing temperature. Two different phase diagrams are considered. For a binary fluid with a critical point the separation occurs via spinodal decomposition as a convective instability. For a cigar-shaped phase diagram the phase-transformation is shown to evolve in analogy to the fingering-processes known from directional solidification.

Solids crack when the stresses are getting too strong. A satisfactory explanation for the dynamics of crack propagation has been missing so far. We present a continuum theory which describes the fast growth of a crack by surface diffusion. This mechanism overcomes the usual cusp singularity by a self-consistent selection of the radius of the crack tip. It is found that the maximal steady state crack velocity remains appreciably below the Rayleigh speed, while the crack-tip becomes blunt. Furthermore the theory suggests the possibility of a tip splitting instability for high applied tensions.

H. Müller-Krumbhaar, January 2003.

Personnel 2002/2003 and areas of activity

Scientific Staff

Dr. E. Brener	Kinetics of phase transformations	E2310203
Prof. P.H. Dederichs	Electronic structure and magnetism	E2310203
Dr. Ph. Mavropoulos (GR)	Half-metallic systems	E2310203
Dr. K. Mika	Structure maps for binary systems	E2310203
Dr. J. Minar	Spectroscopies of magnetic materials	E2310203
Prof. H. Müller-Krumbhaar - Institute Director -	Non-linear dynamics of dissipative systems	E2310203
Dr. R. Rzehak	Polymer dynamics and hydrodynamic flow	E2310203
Dr. K. Sato	Diluted magnetic semiconductors	E2310203
Dr. H. Schober	Statics and dynamics of glasses, defects and phonons	E2310203
Prof. K. Schroeder	Surfaces and interfaces: structure and defect kinetics	E2310203
Dr. J. da Silva	Adsorption of molecules on metals	E2342003
Dr. R. Zeller	Electronic structure and magnetic properties of metals	E2310203
L. Snyders	Secretary	

Visitors

Dr. V. Caciuc (RO)	Atomic force microscopy	E2342003
Prof. S. Dattagupta (IND)	Disordered Systems	E2310203
Dr. I. Galanakis (GR)	Half-metallic ferromagnets	E2310203
Prof. V. Gurevich (GUS)	Low energy modes in glasses	E2310203
Prof. S. Iordanski (GUS)	Kinetics of Bose condensation	E2310203
Dr. D. Kienle	Transport coefficients in polymer solutions	E2310203
Dr. S. Malinin (GUS)	Friction of soft materials and stick-slip motion	E2310203
Prof. V. Marchenko (GUS)	Pattern formation in elasticity and hydrodynamics	E2310203
Dr. D.A. Parshin (GUS)	Low energy modes in glasses	E2310203
Dr. V. Popescu (RO)	Relativistic KKR-codes	E2310203
Dr. D. Temkin (GUS)	Pattern formation at interfaces	E2310203

PhD and Diploma Students (University = RWTH Aachen)

MSc. N. Atodiresei	Small organic molecules on surfaces	E2342003
Dipl.-Phys. A. Antons	Surfactant-mediated growth on semiconductors	E2310203
Dipl.-Phys. F. Gutheim	Cluster growth on surfaces	E2310203
Dipl.-Phys. M. Hartmann	Collective effects of cracks and dislocations	E2310203
Dipl.-Phys. H. Höhler	Defect complexes in semiconductors	E2310203
Dipl.-Phys. R. Spatschek	Collective effects of cracks in solids	E2310203
Dipl.-Phys. O. Wunnicke	Spin injection	E2310203

Research program E2310203: "Condensed Matter"
Research program E2342003: "Materials, processes and devices for the micro- and nanoelectronics"

Ballistic Spin Injection from Fe into ZnSe and GaAs

O. Wunnicke, Ph. Mavropoulos, R. Zeller, and P.H. Dederichs
Institute Theory III

We consider the spin injection from Fe into ZnSe and GaAs in the ballistic limit. By means of the *ab initio* SKKR method we calculate the ground state properties of epitaxial Fe|ZnSe and Fe|GaAs heterostructures for the (001), (111) and (110) orientation. Three injection processes are considered: injection of hot electrons and injection of "thermal" electrons with and without an interface barrier. The calculation of the conductance by the Landauer formula shows, that (001) oriented interface acts like a nearly ideal spin filter, while the other orientations give only small injection efficiencies. The high spin polarization can be traced back to the symmetry of the band structure of Fe(001) for normal incidence.

The controlled injection of a spin polarized current into a semiconductor (SC) is one of the central problems in the new field of spin electronics ("spintronics"), since it is a prerequisite for the development of new spin dependent devices. Recently some important successes have been achieved. Firstly the injection from magnetic semiconductors into GaAs has been demonstrated by two groups; however these experiments are restricted to low temperatures. Therefore the injection from a ferromagnet with a large Curie temperature such as Fe would have strong advantages. Such attempts, though, have not been very successful in the past, i.e., the reported spin injection efficiency was low, and Schmidt *et al.* and Fert *et al.* have explained the reasons and the possible cure for this problem. Only recently the Ploog-group were successful in demonstrating the spin injection at room-temperature from Fe(001) into GaAs with an efficiency of 2% which they attributed to tunneling through a Schottky barrier.

Recently two calculations from Grundler and Hu *et al.* for the ballistic spin injection process have been published, which rely on a free-electron description of the majority and minority spin bands. Grundler could argue in this way that the Fe|SC interface can act as a spin filter, however, with an efficiency of a few percent only. Motivated by this work we have performed [1, 2] *ab initio* calculations of the ground state properties and the ballistic transport through the Fe|ZnSe and Fe|GaAs interfaces for the (001), (111) and (110) orientations. In contrast to the above mentioned methods our calculations include the whole complexity of the band structures of the ferromagnet and the SCs as well as the even more complex properties of the interface. The important result of our calculation is, that the considered Fe|SC(001) interfaces act like nearly ideal spin filters, with spin injection ratios as high as 99%. We can attribute this to the different symmetries of the majority and minority d-bands of Fe(001) at the Fermi level, a behavior which cannot be described in the free-electron model.

Our method is based on the local density approximation of the density functional theory and applies the screened KKR-method. The heterostructure consists of an Fe halfspace and a SC (either ZnSe or GaAs) halfspace, both oriented in the (001) direction and being epitaxially bonded at the interface, so that the SC lattice constant is double the Fe constant ($a_{\mathrm{Fe}}^{\mathrm{exp}} = 5.425$ a.u. is used in the calculation). The two halfspace Green's functions are determined by the decimation technique. In the interface region the potentials of the Fe and SC layers are determined selfconsistently. The potentials of all other ML are identified with the asymptotic bulk values. The ballistic conductance G is calculated by the Landauer-Büttiker formalism for $T = 0$. Here we use an expression adjusted to the asymptotic Bloch character of the wave functions and the two-dimensional translation symmetry of the system. The in-plane component $\mathbf{k}_{\|}$ of the $\mathbf{k}$-vector enumerates then the scattering channels, and we can express the $\mathbf{k}_{\|}$-dependent conductance $G(\mathbf{k}_{\|})$ wholly in terms of the Green's function of the system.

As we will demonstrate in this paper, the spin injection process is to a large extent determined by the symmetries of the bulk band structures. To show this we discuss in the following the Fe/SC(001) heterostructure in detail. Fig. 1 shows in the left panel the spin split majority and minority band structure of Fe and in the middle the one of ZnSe for Bloch electrons $\mathbf{k} = (0, 0, k_z)$ with normal incidence on the (001) interface. These are the states relevant for the injection process, since in the SC only states close to the conduction band minimum E_C will be populated, having $\mathbf{k}_{\|} \approx 0$. As usual the different bands in (001) direction are indexed by Δ_1, Δ_2, etc. indicating the symmetries of the wave functions. The Fermi energy (E_F) is assumed to be located in the middle of the SC gap. Most important is here that the lowest conduction states have Δ_1^{SC}-symmetry; they are invariant under all symmetry operations of the zinc-blende lattice, that transform the Bloch vector $\mathbf{k} = (0, 0, k_z)$ in itself. These operations form the symmetry group C_{2v}, which is at the same time identical with the symmetry of the whole Fe|SC(001) interface. It is now important to single out those Fe states, which are compatible with this C_{2v} symmetry. In Fe, the Δ-nomenclature refers to the C_{4v} symmetry group, since, contrary to the zinc-blende lattice, in the bcc lattice the (001) direction is a fourfold axis. Thus, not only the Δ_1^{Fe}-states, consisting locally of s, p_z

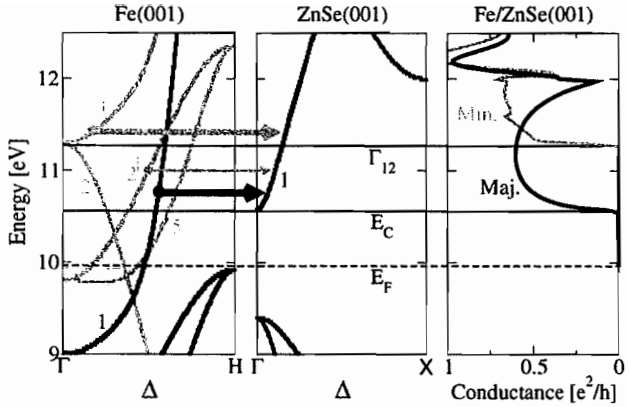

FIG. 1: Band structure of Fe(001) and ZnSe(001) and the conductance through the Fe/ZnSe(001) interface. Black lines denote the majority and grey ones the minority spin direction. The arrows symbolize the coupling strength between both bands and no arrow means the coupling is forbidden due to symmetry. The numbers indicate the Δ symmetry of the bands.

and d_{z^2} orbitals, can couple to the Δ_1^{SC}-band states, but also the $\Delta_{2'}^{Fe}$-states consisting locally of in-plane d_{xy} orbitals. On the other hand the Fe states of Δ_2^{Fe}-symmetry as well as the Fe states with Δ_5^{Fe}-symmetry cannot couple to the Δ_1^{SC}-states, since they do not show the full symmetry C_{2v} of the heterostructure. For the spin injection it is now important, that in the majority band at E_F and above there exists a Δ_1^{Fe}-band while in the minority band only a $\Delta_{2'}^{Fe}$-band exists that can couple to the Δ_1^{SC}-states. The minority Δ_1^{Fe}-band starts only at 1.3eV above E_F.

Firstly we discuss the injection process of hot electrons with Fe states well above E_F. Although for hot spin injection states with non-zero $\mathbf{k}_\parallel$ values also play a role, we consider here for simplicity only states with normal incidence. The calculated transmission probabilities for injection into ZnSe are shown in the right panel of Fig. 1 for both spin directions for a Zn terminated interface. The results for the Se termination and for Fe/GaAs(001) are qualitatively the same. The transmission starts at the energy E_C of the SC conduction band minimum. In the majority band the conductance strongly increases to values of around 0.6 e^2/h, while the conductance in the minority band is much smaller. As a result, the spin polarization of the injected current is larger than 97%. However, the situation completely changes, if the energy of the injected Fe electrons exceeds the value $E_{\Gamma_{12}}$ (1.3eV above E_F) of the minimum of the minority Δ_1^{Fe}-band. There the transmission in the minority band increases very sharply and even overcomes the majority transmission, so that the spin polarization changes sign. This clearly illustrates, that the absence of the Δ_1^{Fe}-state in the minority band leads for lower energies to the very large spin polarization of the current. The strong spin polarization can be understood from the different spatial orientation and extent of the Δ_1^{Fe} and $\Delta_{2'}^{Fe}$-states. The other investigated orientations (111) and (110) do not have this symmetry mismatch in the majority and minority band and therefore do not show a strong symmetry enforced spin polarization. So we will discuss in the following only the (001) oriented heterostructures.

Furthermore we have investigated the injection process of electrons at E_F with and without a Schottky barrier by appropriately lowering the potentials in the SC halfspace. Without a Schottky barrier a spin polarization of more than 97% is found in Fe/ZnSe(001) and practically 100% in Fe/GaAs(001) for Fermi energies around 10meV above the conduction band minimum. To simulate a Schottky barrier the potential step at the interface is smeared out to a barrier of up to 150 ML thickness. In this case a new effect from resonant interface states in the minority band arises resulting in lower spin polarizations for thicker barriers. This interface state is the analogue to the localized Δ_1-surface state of the (001) surface, and lies in the minority Δ_1-gap of the bulk. The interface state becomes important, if its energy nearly coincides with the Fermi level. This is approximately the case for the Zn terminated Fe/ZnSe(001) interface where the spin injection efficiency is reduced below 80%, but is not important for the other interfaces.

In summary our calculations show that the ideal (001) interfaces of Fe/ZnSe(001) and Fe/GaAs(001) act as nearly ideal spin filters. The results assume an ideal interface structure. Any defects will break the $\mathbf{k}_\parallel$-conservation, thus invalidating the simple symmetry rules leading to the high spin polarization. Together with the recent observation of spin injection for Fe/GaAs(001), our results give a bright prospect for spin injection. Much larger spin polarizations might be achievable, in particular if ballistic experiments can be realized.

[1] O. Wunnicke, Ph. Mavropoulos, R. Zeller, P.H. Dederichs, and D. Grundler, Phys. Rev. B **65**, R241306 (2002).

[2] Ph. Mavropoulos, O. Wunnicke, and P.H. Dederichs, Phys. Rev. B **66**, 024416 (2002).

Strained Sb-covered Ge-films: Understanding Ge growth on Si(111):Sb(1 ML)

A. Antons, Y. Cao[1], B. Voigtländer[1], R. Berger, K. Schroeder, S. Blügel[2]
IFF-Theorie III, [1]Institut für Schichten und Grenzflächen, and [2]IFF-Theorie I

Using STM and *ab initio* total energy calculations, we have investigated the stability of different structures found on Ge films grown on Si(111):Sb(1 ML)[2]. We find that the (2×1) chain-reconstruction of Ge(111):Sb experimentally found to be stable at the equilibrium lattice constant of Ge has a range of stability between about 5.5% compression and 1% expansion. For larger dilatations the (1×1)-structure becomes stable. With the calculated equilibrium structures we can explain the experimentally observed development of the surface structure of a growing Ge film on Si(111):Sb.

For optimal electronic devices (lasers, transistors) one often desires materials combinations which cannot easily be matched. An important example is the growth of Ge on Si: due to the lattice mismatch Ge grows epitaxially in large three-dimensional (3D) islands (Stranski-Krastanov growth) on a clean Si surface whereas with the proper choice of a "surfactant", i.e. by depositing a (sub-)monolayer of group-V atoms (As, Sb or Bi) on the surface of the growing crystal, the growth mode of Ge on Si(111) or Si(001) turns to layer-by-layer (Frank-van der Merwe) growth [3]. Especially, Sb has been successfully applied, and a MOSFET with an active p-doped Ge layer on a Si substrate has been built recently[4].

The short period units of bonded adsorbate atoms found experimentally on Si and Ge (111) surfaces are shown in Fig. 1. All arrangements satisfy the bonding requirements: Every Si or Ge atom has four covalent bonds, and every group-V atom has three covalent bonds and one lone pair of non-bonding electrons. This yields a low surface energy. In three structures (Fig. 1(a-c)) the surfactant atoms sit on top of a full substrate double layer (DL), whereas in the substitutional geometry, Fig. 1(d), the adsorbate atoms replace the substrate atoms in the upper half of a double layer.

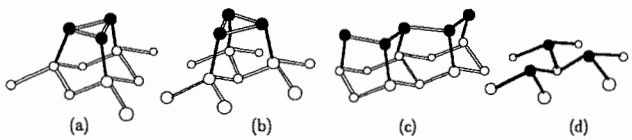

FIG. 1: Geometries for group-V adsorbate layers: (a) H3-trimer centered above a hexagon composed of first and second layer substrate atoms, (b) T4-trimer centered above a second layer substrate atom (Si(111):(Bi, Sb)), (c) chain (Ge(111):Sb), and (d) substitutional (Si(111):As). The adsorbate atoms are shown black, while the substrate atoms are shown as open spheres.

We have performed a detailed STM analysis of the surface structure of a growing and relaxing Ge film on Sb-covered Si(111). An analysis of the strain in the growing film has been performed by Horn-von Hoegen[5] using electron scattering. Both studies agree that growth of Ge on Si(111):Sb proceeds in several steps (see Fig. 2): (i) The Sb layer on Si(111) shows the $(\sqrt{3} \times \sqrt{3})$ T4-trimer structure, Fig. 2(a). (ii) After deposition of three MLs of Ge (1 ML = $7.8{\times}10^{14}$ atoms cm^{-2}) in a wide temperature range a homogeneous wetting layer develops which shows 1 ML deep trenches. At high temperatures ($\approx 660^0$C) a long-range ordered hexagonal $(6\sqrt{3} \times 6\sqrt{3})$ structure appears. The hexagons are separated by micro-ditches and consist of triangular sections with the (1×1) structure with Sb atoms on substitutional sites, Fig. 2(b). (iii) Growth proceeds with a roughness of several layers until (iv) the Ge film largely relaxes by the formation of misfit dislocations at the Ge/Si interface when 10 -12 Ge layers are deposited. (v) Further growth proceeds on the relaxed Sb-covered Ge film which shows the (2×1) surface structure, Fig. 2(c).

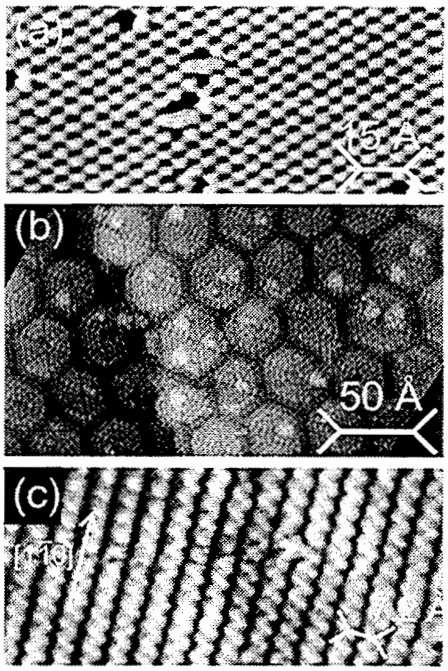

FIG. 2: STM images of the surface structures of the growing Sb-covered Ge film on Si(111):Sb as a function of film thickness. (a) On Si(111):Sb the $(\sqrt{3} \times \sqrt{3})$ T4-trimer structure is found, (b) for 3 ML Ge long-range ordered flat hexagons in a $(6\sqrt{3}{\times}6\sqrt{3})$ arrangement are found, which consist of triangles showing the (1×1) structure, (c) for thick (> 10 ML) relaxed Ge films the (2×1) chain structure is found.

In order to understand the structures of the growing and relaxing Ge film deposited on the Sb-covered Si(111) substrate we have investigated the surface energies for the four different structures as a function of lateral lattice constant a. We have carried out first-principle calculations with the EStCoMPP code [6]. The surfaces are modeled by slabs which are periodically repeated in the direction perpendicular to the surface. For reliable energy comparisons of structures with different lateral periodicities, a comparable well-converged sampling with identical k-point densities in the reciprocal lattice is essential. We chose k-point sets which correspond to a set of 6×6 k-points in the surface Brillouin zone for the (1×1) unit cell. To establish minimum energy configurations the forces acting on the atoms are relaxed to less than 0.1 mRy/a.u..

To obtain the surface energy of Sb-covered Ge we used laterally strained Ge bulk and Sb_4-molecules as reference configurations. The calculated surface energies E_s with varying lateral lattice constants for the different structures are shown in Fig. 3. The surface energy of the chain

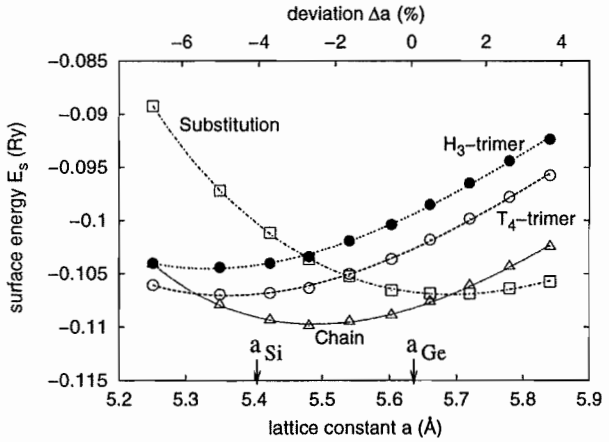

FIG. 3: Surface energies E_s per Sb atom deposited on Ge(111), plotted against lateral lattice constant a for different structures. The filled circles, empty circles, triangles, and squares represent the H3-trimer, T4-trimer, chain, and substitutional geometries, respectively. The arrows indicate the theoretical Si and Ge lattice constants.

geometry is lower than for the other three geometries at the theoretical and experimental equilibrium lattice constants of bulk Ge ($a_{th}(Ge)$=5.632 Å and $a_{exp}(Ge)$=5.657 Å). This shows that the chain geometry is the most stable structure, the substitutional geometry is slightly higher in energy than the chain. The H3-trimer configuration has the highest-energy over the entire range of lattice constants tested.

We find that the (2×1)-reconstruction of Ge(111):Sb is stable in the entire range from the Si lattice constant ($a_{th}(Si)$=5.403 Å) to the Ge lattice constant. It is also stable for slightly dilated Ge films (<1%). For larger dilatations the (1×1)-structure becomes stable. For highly compressed Ge films the ($\sqrt{3} \times \sqrt{3}$) T_4-structure (found experimentally on Si(111):Sb) becomes competitive. It stable for lattice constants compressed more than 5.5%.

This means one would expect the (1×1)-structure on a growing Ge film on Si(111) if the lattice constant was *over-relaxed* for some reason. To model the finite size hexagons separated by trenches as found in the equilibrium structure for a Sb-covered 3 ML Ge film grown on Si(111) (see Fig. 2(b)), we have calculated the structure of a narrow terrace (width 5 nearest neighbor distances) for this system. The result is shown in Fig. 4. We find

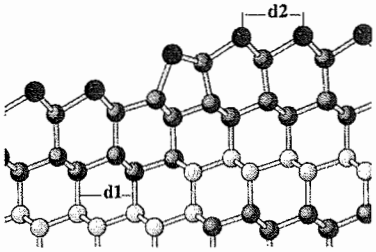

FIG. 4: Calculated structure of two narrow terraces on Sb-covered 3 ML Ge film grown on Si(111) (Sb: dark, Ge gray, Si light). Notice, that at the step edge one Sb atom is bound to Ge atoms of the higher and lower terrace, and pulls the Ge atoms apart at the free edge. This results in an over-relaxation of the Ge film. The in-plane lattice constant of the top layer ($d2$) is 8% larger than the Si lattice constant, although the Si layer in the middle of the slab is fixed at the Si lattice constant ($d1$).

an over-relaxation of the Sb-covered Ge film, whose lateral lattice constant is about 8% larger than the lattice constant of Si bulk. This coincides very well with the measured lattice constants on top of the hexagons found in our STM studies for the 3 ML Ge film on Si(111) and earlier by Voigtländer and Zinner [7].

[1] present address: Department of Physics, Zhejiang University, Hangzhou 310027, P.R. China.

[2] A. Antons, Y. Cao, B. Voigtländer, R. Berger, K. Schroeder, and S. Blügel, submitted to Europhys. Lett..

[3] C. Y. Fong, M. D. Watson, L. H. Yang, and S. Ciraci, Modelling Simul. Mater. Sci. Eng. **10**, R61 (2002)

[4] D. Reinking *et al.*, Electr. Lett. **35**, 503 (1999).

[5] M. Horn-von Hoegen, Z. Kristallogr. **214**, 591 (1999); **214**, 684(1999).

[6] EStCoMPP: Electronic Structure Code for Materials Properties and Processes, Forschungszentrum Jülich, 1999. R. Berger *et al.*, Proceedings of the Workshop on Molecular Dynamics on parallel Computers (Editors: R. Esser, P. Grassberger, J. Grotendorst and M. Lewerenz), p. 185, (World Scientific, 2000).

[7] B. Voigtländer and A. Zinner, Surf. Sci. **351**, L233 (1995).

On the theory of Boson peak in glasses

V. L. Gurevich[1], D. A. Parshin[2], and H. R. Schober[3]
A. F. Ioffe Institute,Saint Petersburg, Russia[1]
Saint Petersburg State Technical University,Saint Petersburg, Russia[2]
Institute IFF-Theory III[3]

A universal mechanism of the Boson peak formation in glasses is proposed. The mechanism is based on the concept of interacting quasi-local oscillators. Even in the case of weak interaction the low-frequency spectrum becomes unstable. Due to anharmonicity the system undergoes a transition into a new stable configuration. Below some characteristic frequency the renormalized density of states becomes a universal function of ω with a Boson peak feature, i.e. the reduced density of states $g(\omega)/\omega^2$ has a maximum at a frequency $\omega_b \ll \omega_c$. We derive an analytical form of this function.

The Boson peak (BP) is observed in a wide temperature range in the inelastic light and neutron scattering intensities at low frequencies, corresponding to a maximum in the reduced density of vibrational states $g(\omega)/\omega^2$ [1]. The position of this maximum correlates with a low temperature bump in the reduced specific heat $C(T)/T^3$ where T is the temperature. Despite numerous efforts, there is no widely accepted theory of the Boson peak phenomenon. A crucial question is that whether this peak corresponds to phonon degrees of freedom or to some additional harmonic excitations in glasses, quasi-localized (resonant) modes (QLM). We base our theory of the Boson peak on harmonic excitations in glasses which coexist and interact with long wavelength acoustic phonons (sound waves).

The QLM (or broken up, low lying optical modes) can be described as harmonic oscillators (HO) that interact with the phonons [2,3]. QLM are also found by numerical simulations, see [4] and references therein. Due to their interaction with phonons they should inevitably interact with one another. This interaction can cause a mechanical instability of the system and the Boson peak phenomenon [5].

For illustration, consider a system of two interacting HO with a potential energy

$$U_{\rm har}(x_1,x_2) = M_1\omega_1^2x_1^2/2 + M_2\omega_2^2x_2^2/2 - I_{12}x_1x_2. \quad (1)$$

Here M_i are the masses and ω_i the frequencies of the two oscillators. The interaction strength is given by

$$I_{12} = g_{12}J/r_{12}^3, \quad J \equiv \Lambda^2/\rho v^2 \quad (2)$$

where g_{12} accounts for the relative orientation of the HO, r_{12} is their distance, ρ the mass density of the glass and v a sound velocity. The interaction between the HO is due to the coupling between a single HO and the surrounding elastic medium (the glass). Possible additional short range interactions do not introduce qualitative differences. The HO-phonon coupling has the form [3] $\mathcal{H}_{\rm int} = \Lambda x\varepsilon$, where Λ is the coupling constant and ε the strain.

Diagonalization of Eq. (1) yields two frequencies

$$\widetilde{\omega}_{1,2}^2 = \frac{\omega_1^2+\omega_2^2}{2} \pm \sqrt{\left(\frac{\omega_1^2-\omega_2^2}{2}\right)^2 + \frac{I_{12}^2}{M_1M_2}}. \quad (3)$$

The smaller value, $\widetilde{\omega}_2^2$, becomes negative when I_{12} exceeds the threshold (critical) value $I_c \equiv \omega_1\omega_2\sqrt{M_1M_2}$. A negative $\widetilde{\omega}_2^2$ indicates an instability of the corresponding eigenstate, *vibrational instability* — the previous minimum at $x_1 = x_2 = 0$ becomes a saddle point of the potential energy $U_{\rm har}(x_1,x_2)$.

This instability persists also in a system of many interacting HO. However, in a real glass an unstable HO is always stabilized by anharmonic forces into a nearby minimum of the potential energy. The position of this minimum depends on the interaction between HO. The new frequencies, in these new minima, are real and different from the original ones. Thus the vibrational spectrum is reconstructed. This is the mechanism of the Boson peak formation.

Let us consider a system of randomly distributed, interacting HO with an initial DOS, $g_0(\omega)$, where $g_0(\omega)$ is a monotonously increasing function of ω in the frequency range from 0 to ω_0 (it is normalized to 1). For the harmonic part of the interaction we take the generalization of Eq. (1) and add an anharmonic term to stabilize the system

$$U_{\rm anhar} = (A/4)\sum_i x_i^4. \quad (4)$$

We will consider the interaction I_{ij} between the oscillators to be a *small parameter* of our theory. Namely, we assume that the typical random interaction I between neighboring HO is much smaller than the typical values of the product $M\omega_0^2$. As $|I| \ll M\omega_0^2$ the frequencies of the order of ω_0 will be practically unaffected by the interaction whereas HO with frequencies

$$\omega < \omega_c \simeq |I|/M\omega_0 \ll \omega_0 \quad (5)$$

will be displaced to new minima.

Since the concentration of unstable HO is much smaller than the one of the stable ones a low frequency oscillator is usually surrounded by high frequency ones. Therefore

we can split our problem into two parts. First we consider a cluster containing a low frequency oscillator with frequency $\omega_1 \lesssim \omega_c$ which is surrounded by a large number N of HO with much higher frequencies $\omega_j \sim \omega_0$. To determine the eigenfrequencies of the interacting oscillators belonging to the cluster one should solve the secular equation of the order of $N+1$ in ω^2. However, the variations of the high eigenfrequencies should be small and can be discarded as they are proportional to the small parameter $I/M\omega_0^2$. As a result, one gets for the smallest eigenfrequency a linear equation. It can easily be solved, and one can show that such cluster becomes unstable under the condition

$$M_1\omega_1^2 < k \quad \text{where} \quad k \equiv \sum_j \frac{I_{1j}^2}{M_j\omega_j^2}. \tag{6}$$

For the unstable situation one has to take the anharmonicity, Eq. (4), into account. The new low frequency of the coupled oscillators is then given by

$$\widetilde{\omega_1}^2 = \begin{cases} \dfrac{1}{M_1}(M_1\omega_1^2 - k), & k < M_1\omega_1^2 \\ \dfrac{2}{M_1}(k - M_1\omega_1^2), & k > M_1\omega_1^2 \,. \end{cases} \tag{7}$$

It is remarkable that the anharmonicity which has been used in deriving the second Eq. (7) does in the end not enter this equation, as well as our final result, Eq. (8).

We have shown that the reconstructed density of states has a universal shape [6]

$$\frac{g(\omega)}{\omega^2} = \frac{3C}{\pi\omega^\star}\left(\frac{\omega^\star}{\omega}\right)^4 \left[z_1^2(\omega) + z_2^2(\omega)\right]^{-1} \left[\frac{1}{2z_1(\omega)} \ln \frac{z_1(\omega)+1}{z_1(\omega)-1} + \frac{1}{z_2(\omega)} \mathrm{arctg}\, \frac{1}{z_2(\omega)}\right] \tag{8}$$

where

$$z_{1,2}(\omega) = \frac{1}{2}\sqrt{\sqrt{9 + 8(\omega^\star/\omega)^6} \pm 3}.$$

The function $g(\omega)/\omega^2$ is plotted in Fig. 1. It depends on a single parameter, $\omega^\star$. The maximum of $g(\omega)/\omega^2$, i.e. the Boson peak, is at $\omega_b \approx 1.1\omega^\star$. For large frequencies, $\omega \gg \omega_b$, $g(\omega) \propto \omega$ while for small frequencies, $\omega \ll \omega_b$, $g(\omega) \propto \omega^4$. Also shown is a comparison of our theoretical curve with Raman scattering data for lithium borate glasses [7] of different compositions. These results are in good agreement with the experimental data and support the idea of a universal form of the Boson peak [8].

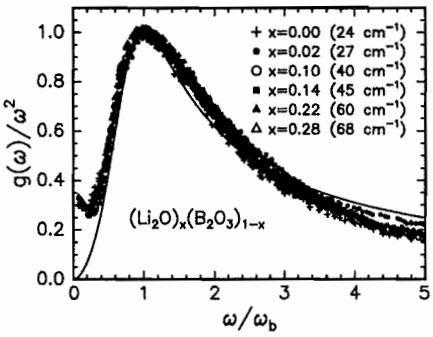

FIG. 1. The Boson peak in reduced units: Eq. (8) (solid line) and Raman data for lithium borate glasses [7]. The positions of the Boson peak (for different compositions x) are given in brackets.

In this report we dealt with the case of weak interaction between HO. If the interaction is increased the characteristic frequencies ω_b and ω_c grow and the gap between them narrows and finally disappears. Then our Boson peak in $g(\omega)/\omega^2$ superimposes the "boundary peak" in $g_0(\omega)$ at the edge of the original vibrational spectrum. The Boson peak can no longer be distinguished from the boundary peak in $g(\omega)$ or from a possible equivalent maximum in $g_0(\omega)$.

[1] *Amorphous Solids. Low Temperature Properties*, edited by W. A. Phillips, (Springer-Verlag, Berlin:1981).

[2] V. G. Karpov, M. I. Klinger, and F. N. Ignatiev, Sov. Phys. JETP **57**, 439 (1983); V. G. Karpov, D. A. Parshin, Sov. Phys. JETP Lett. **38**, 648 (1983); Sov. Phys. JETP **61**, 1308 (1985).

[3] U. Buchenau, Yu. M. Galperin, V. L. Gurevich *et al.* Phys. Rev. B **46**, 2798 (1992).

[4] B. B. Laird, H. R. Schober, Phys. Rev. Lett. **66**, 636 (1991); H. R. Schober, B. B. Laird, Phys. Rev. B **44**, 6746 (1991); H. R. Schober, and C. Oligschleger, Phys. Rev. B **53**, 11469 (1996); C. Oligschleger, Phys. Rev. B **60**, 3182 (1999).

[5] V. L. Gurevich, D. A. Parshin and H. R. Schober, JETP Lett. **76**, 553 (2002).

[6] V. L. Gurevich, D. A. Parshin and H. R. Schober, Phys. Rev. B in print.

[7] S. Kojima and M. Kodama, Physica B **263**, 336 (1999).

[8] V. K. Malinovsky and A. P. Sokolov, Solid State Commun. **57**, 757 (1986); V.K.Malinovsky V.N. Novikov, P.P. Parshin *et al.* Europhys. Lett. **11**, 43 (1990).

Liquid-Liquid Phase Change in Systems with Flow

R. Rzehak and H. Müller-Krumbhaar
Institute IFF-Theory III

The phase transformation of a two component liquid during the condensation in a distillation apparatus is discussed. The liquid is assumed to flow in a temperature gradient towards decreasing temperature. Two different phase diagrams are considered. For a binary fluid with a critical point the separation occurs via spinodal decomposition as a convective instability. For a cigar-shaped phase diagram the phase transformation is shown to evolve in analogy to the processes known from directional solidification.

Separation of phases forms the basis of important technological processes like distillation, rectification or extraction. In industrial applications these phase changes inevitably occur in the presence of flow of the fluids involved. We here present two scenarios for such processes depending on the qualitative features of the phase diagram near the operating point, taking into account a simple type of flow.

To be specific, we consider in each case a fluid which at high temperatures $T > T_1$ is a homogeneous mixture of two chemical components. We refer to these components as solute and solvent without implying that the concentration c_0 of the solute is small. At lower temperatures $T < T_1$ the homogeneous fluid has a tendency to phase-separate into two fluids with different composition. We assume that the fluid is flowing with velocity v in the positive x-direction, from high to low temperatures along a fixed temperature profile $T(x)$ which at $x = 0$ equals T_1, such that a phase transformation may occur for $x > 0$. For simplicity the flow field is taken to be uniform. Furthermore, we assume the system to be homogeneous in the direction across the channel such that only the streamwise direction needs to be considered.

In the first scenario we assume that the phase diagram of the fluid has a critical point at $T_{crit} = T_1$, $c_{crit} = c_0$. When the system is quenched from a temperature $T_0 > T_1 \equiv T_{crit}$ to a temperature $T_2 < T_1 \equiv T_{crit}$ separation of the initial homogeneous high-temperature phase into two two phases, one with higher and one with lower concentration than c_0, proceeds via an instability. This process is called spinodal decomposition [1].

Assuming diffusion of heat to be fast compared to diffusion of solute we consider the temperature to be fixed at each point in the liquid. Then the instability can be modeled by a free energy $\mathcal{F}$ which as a function of the order parameter $\phi \equiv c - c_{crit}$ has a maximum at the critical point. To lowest order this requires a quadratic contribution to $\mathcal{F}$. Higher order stabilizing terms are not relevant to the analysis of the initial instability and will be omitted. The free energy of the fluid in the vicinity of the critical point thus possesses the following form [2]:

$$\mathcal{F} = \int \frac{\alpha}{2} (T - T_{crit}) \phi^2 + \frac{\gamma}{2} (\nabla\phi)^2 \, d\mathbf{r} \,. \tag{1}$$

The dynamics of the conserved order parameter is described by a modified Cahn-Hilliard equation

$$\frac{\partial \phi}{\partial t} = \nabla \cdot M \nabla \frac{\delta \mathcal{F}}{\delta \phi} - \mathbf{v} \cdot \nabla \phi \,, \tag{2}$$

where the last term accounts for advection by the flow.

In a prescribed temperature profile the separation process sets in when the fluid passes the point where $T(x) = T_{crit}$. We assume that $T(x)$ is just a step function. Then we can ignore the stable region $x < 0$ and impose some reasonable boundary condition at $x = 0$.

With appropriate normalization by introducing length- and timescales $(M\gamma/v)^{1/3}$ and $v^{-4/3}(M\gamma)^{1/3}$ the stability problem is to find modes and associated growth rates of

$$\frac{\partial \phi}{\partial t} = -\frac{\partial^4 \phi}{\partial x^4} + h \frac{\partial^2 \phi}{\partial x^2} - \frac{\partial \phi}{\partial x} \tag{3}$$

together with boundary conditions, which can be rather arbitrary as long as they do not force completely trivial solutions. The dimensionless control parameter h is defined by $h = (M/v)^{2/3}\gamma^{-1/3}\alpha(T - T_{crit})$

The stability problem for Eq. (3) has been solved in Ref. [3] in terms of eigenfunctions and corresponding eigenvalues. Since the operator on the *rhs* of Eq. (3) is not self-adjoint, the spectrum contains a complex part. The corresponding modes are traveling waves.

For positive values of h the system (3) is absolutely stable. This means that any perturbation at $x = 0$ decays towards increasing $x > 0$. For h being negative but larger than some critical value

$$h_c = -(1 + \sqrt{7}) \left(\frac{3 - \sqrt{7}}{4} \right)^{2/3} \,, \tag{4}$$

a convective instability occurs. Fluctuations will be amplified with time but they are driven away sufficiently fast, such that the amplitudes do not grow at any point fixed in the laboratory system. For $h < h_c$ this convective instability turns into an absolute instability. Any small fluctuation will grow unlimited in time and space - within the linear model under consideration. After the initial instability, phase separation, of course, proceeds through several further stages: coarsening, Ostwald ripening, surface tension driven flow, turbulent flow etc. When h is

not constant but varies in space, a critical position x_c is defined by the condition, that $h(x)$ exceeds the value for absolute instability.

For the second scenario, we have a cigar-shaped phase diagram in mind, many features of which are contained also in a simplified phase diagram with two parallel coexistence lines. Such a phase diagram is characterized by two quantities, the slope $m_A = m_B = m$ of the coexistence lines and the miscibility gap Δc, *i.e.* the difference in solute concentration of the two coexisting phases which is independent of temperature.

Let the system initially consist entirely of liquid A at a solute concentration of c_0. Upon cooling, a phase transformation begins at $T = T_1$ where the upper coexistence line is crossed. At this temperature the first liquid B appears with a solute concentration of $c_1 = c_0 - \Delta c$. When the temperature is lowered further, the amount of liquid B increases while that of liquid A decreases. At the same time also the solute concentration in the liquid B phase increases while that in the liquid A phase decreases such that the total mass of solute is conserved. The phase change is completed when the last amount of liquid A vanishes at $T = T_2$ where the lower coexistence line is crossed. This last amount of liquid A has a solute concentration of $c_2 = c_0 + \Delta c$, while the solute concentration in the liquid B phase then has reached the value of c_0.

Expecting the existence of a sharp front separating the two phases we introduce separate concentration fields for each of them. The two fields are coupled via boundary conditions at the interface, the position $\xi(z,t)$ of which is not known in advance but must be determined as part of the solution. This requires an additional relation involving the normal interface velocity $\dot{\xi}\sqrt{1+(\partial z/\partial\xi)^2}$. The evolution equations describing advection and diffusion of the solute in terms of scaled variables $u_X = (c_X - c_0)/\Delta c$ are:

$$\begin{aligned} \frac{\partial u_A}{\partial t} &= D_A \nabla^2 u_A - v\frac{\partial u_A}{\partial x} \quad \text{for} \quad x < \xi \\ \frac{\partial u_B}{\partial t} &= D_B \nabla^2 u_B - v\frac{\partial u_B}{\partial x} \quad \text{for} \quad x > \xi\,. \end{aligned} \tag{5}$$

Here D_A and D_B are the diffusion coefficients which may be different in both phases A and B and v is the flow velocity. A relation for the interface velocity relative to the flow derives from continuity of the mass flux as

$$\dot{\xi}\sqrt{\left(1-\frac{v}{\dot{\xi}}\right)^2 + \left(\frac{\partial z}{\partial \xi}\right)^2} = \hat{n}\cdot(D_A\nabla u_A - D_B \nabla u_B)\,. \tag{6}$$

Boundary conditions at the interface, expressing thermal equilibrium are

$$\begin{aligned} u_A(\xi) &= -dK - \frac{\xi}{\ell_T} \quad \text{and} \\ u_B(\xi) &= u_A(\xi) - 1\,, \end{aligned} \tag{7}$$

where $K = \frac{\partial^2\xi}{\partial z^2}\left(1+\left(\frac{\partial\xi}{\partial z}\right)^2\right)^{-\frac{3}{2}}$ is the curvature of the interface and $d = T_2\sigma/Lm\Delta c$ is the capillary length.

The stationary solution of Eqs. (5)-(7) is a non-moving plane front at position $x = \ell_T = m\Delta c/G$ with a solute concentration profile

$$\begin{aligned} u_A &= -\frac{\xi}{\ell_T}\exp\left(\frac{v}{D_A}(x-\ell_T)\right) \\ u_B &= 0\,. \end{aligned} \tag{8}$$

Since our model indeed admits a solution describing a sharp front it offers a consistent description of the phase separation process.

The length scale $\ell_D = D_A/v$ of the concentration profile that is established is the result of a balance between diffusion and advection of the excess solute. The front is stable as long as this concentration profile lies completely outside the two-phase coexistence region. A sufficient condition for stability thus is:

$$\ell_D > \ell_T\,. \tag{9}$$

Otherwise the plane interface may be unstable with respect to modulations such that the full 2-dimensional problem has to be solved. An increase in velocity above the threshold indicated in (9) destabilizes the interface and leads to fingering. The instabilities and pattern selection that occur in this case have been studied extensively in the literature on directional solidification [4].

To summarize, in the first scenario, where the system goes through a critical point, phase separation sets in as an instability which is of convective nature below a critical flow velocity. In the intermediate stage of the separation process spatiotemporal chaos may occur. The linear approach given here should be sufficient to calculate the point is space, where the phase separation sets in. In the second scenario a rather sharp front between the high-temperature and the low-temperature phases exists at not too large flow velocities. Complicated flow patterns and a mushy zone are expected at higher flow rates. Thus an increase in flow rate increases stability in the first scenario while it decreases stability in the second scenario.

[1] K. Binder, in *Phase transformations*, Vol. 5 of *Materials Science and Technology*, edited by R. W. Cahn, P. Haasen, and E. J. Kramer (VCH, Weinheim, 1991), Chap. 7, p. 406.

[2] J. W. Cahn and J. E. Hilliard, J. Chem. Phys. **28**, 258 (1958).

[3] J. S. Langer and H. Müller-Krumbhaar, Phys. Rev. A **27**, 499 (1983).

[4] H. Müller-Krumbhaar and W. Kurz, in *Phase transformations*, Vol. 5 of *Materials Science and Technology*, edited by R. W. Cahn, P. Haasen, and E. J. Kramer (VCH, Weinheim, 1991), Chap. 10, p. 554.

Fast crack propagation by surface diffusion

Efim A. Brener and Robert Spatschek

We present a continuum theory which describes the fast growth of a crack by surface diffusion. This mechanism overcomes the usual cusp singularity by a self-consistent selection of the crack tip radius. It predicts the saturation of the steady state crack velocity appreciably below the Rayleigh speed and tip blunting. Furthermore, it includes the possibility of a tip splitting instability for high applied tensions.

One of the most challenging puzzles in nonequilibrium physics and materials science is the phenomenon of fracture. It is important for the vast field of material failure and probably also for friction processes. Despite its relevance even the motion of a single crack is poorly understood. Experimentally, the maximum attained crack velocities are far lower than the theoretically expected Rayleigh speed. Beyond a critical velocity, a so far unpredictable tip splitting of the crack can happen and produce strange oscillations of the crack speed [1].

Here we demonstrate that the *linear theory of elasticity* is sufficient to describe consistently crack propagation, driven by *surface diffusion* along the crack surfaces. Of course, in many situations plasticity is very important, but the beauty of our approach is that it predicts, in a simple and well controlled continuum theory, steady state crack growth, the tip splitting instability and also slow deformations of already existing cracks [2, 3]. The goal of this paper is to present a completely new description of crack propagation by a *consistent* set of equations of motion.

Our basic mechanism is related to the Asaro-Tiller-Grinfeld (ATG) instability [4], which predicts a morphological instability of a uniaxially stressed solid interface due to surface diffusion. Relatively long-wave perturbations of the interface lead to a reduction of the elastic energy of the system, whereas short-wave corrugations are hampered by surface energy. In the long time behavior, deep grooves can form, producing shapes similar to cracks. According to previous theories, which used only the *static* theory of elasticity, the notches propagate with increasing velocity and decreasing tip radius and collapse to a finite-time cusp singularity.

Usually, it is believed that surface diffusion is slow, but, surprisingly enough, it should not be ignored even in fast fracture processes.

Steady state crack growth — On the surfaces of the crack the normal stress σ_{nn} and the shear stress $\sigma_{n\tau}$ vanish, whereas the tangential stress $\sigma_{\tau\tau}$ usually does not. The chemical potential at the interface is given by

$$\mu = \Omega\left(\frac{1-\nu^2}{2E}\sigma_{\tau\tau}^2 - \alpha\kappa\right). \tag{1}$$

Here α is the surface energy, κ the curvature of the interface and Ω the atomic volume. E and ν are Young's modulus and Poisson ratio, respectively. Non-hydrostatic stresses drive a surface flux proportional to the gradients of the chemical potential along the surface; in turn the normal velocity equals the divergence of this flux due to conservation of material,

$$v_n = -\frac{D}{\alpha\Omega}\frac{\partial^2\mu}{\partial s^2} \tag{2}$$

where $\partial/\partial s$ denotes the tangential derivative and D (dimension $\mathrm{m^4 s^{-1}}$) is proportional to the surface diffusion coefficient.

First, we are interested in steady state solutions of the equation of motion, with a crack moving in positive x-direction with velocity v (see Fig. 1); In co-moving polar coordinates, $x = r(\theta)\cos\theta, y = r(\theta)\sin\theta$, the steady state equation for the shape $r(\theta)$ reads after one integration of Eq. (2)

$$vr\sin\theta = -\frac{D}{\alpha\Omega}\frac{1}{\sqrt{r^2+r'^2}}\frac{d\mu}{d\theta}. \tag{3}$$

In the tail region stresses decay and the shape equation is a third order linear differential equation $Dy''' = vy$ with two growing (and oscillating) and one decaying solution. Only the latter, $y(x \to -\infty) = A\exp[(v/D)^{1/3}x]$, asymptotically describes physical shapes and is allowed. Integration over the upper interface $\theta > 0$ requires the suppression of two growing exponentials at the tail, which imposes two boundary conditions. For a given external loading, these conditions can be fulfilled by a proper selection of the tip radius r_0 and growth velocity v. By this argument the situation seems to be fully described. However, as we mentioned already earlier, the use of a *static* theory of elasticity does not allow a selection of the tip radius. The reason is, that both contributions to the chemical potential, surface energy $\mu_s \sim \kappa$ and elastic energy $\mu_{el} \sim \sigma^2$, behave as r_0^{-1} close to the tip: In the tip approximation, stresses behave as $\sigma_{ij} = \frac{K}{r^{1/2}} f_{ij}(\theta)$ with the static stress intensity factor K. The universal stress distribution f_{ij} depends only on the orientation relative to the crack. Therefore, a dimensionless rescaling of all lengthscales, e.g. $\tilde{r} = r/r_0$, and of the growth velocity $\tilde{v} = vr_0^3/D$ leaves the equation of motion invariant and, thus, cannot determine the lengthscale r_0. Consequently, a steady state solution does not exist. This is the reason for the already mentioned cusp singularity of the ATG instability.

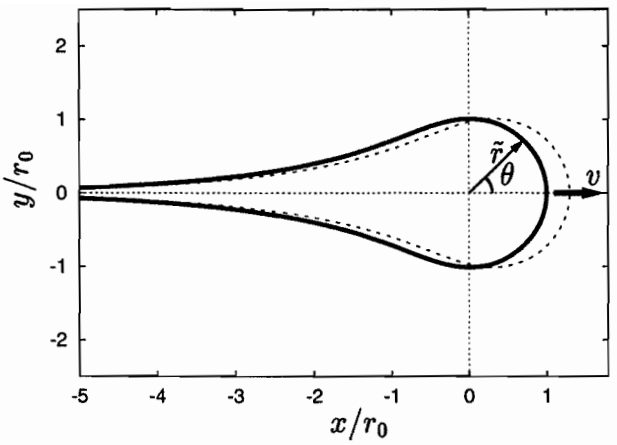

FIG. 1: Calculated shape of the crack (without elastic displacements) driven by surface diffusion for $\Delta = 2$. The advance of the crack in positive x direction is indicated by the dashed curve. This requires the redistribution of matter along the crack by a transport mechanism.

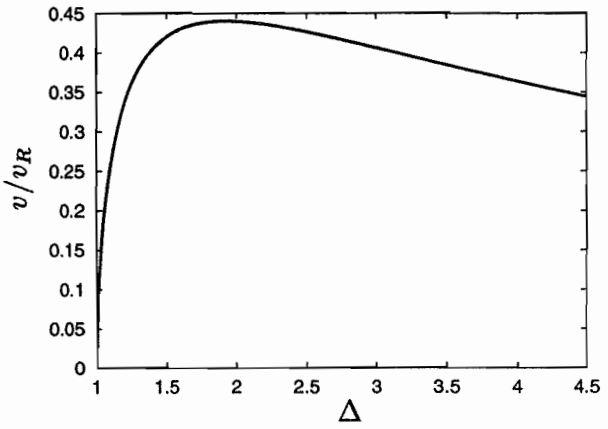

FIG. 2: Steady state velocity of the crack versus dimensionless driving force Δ.

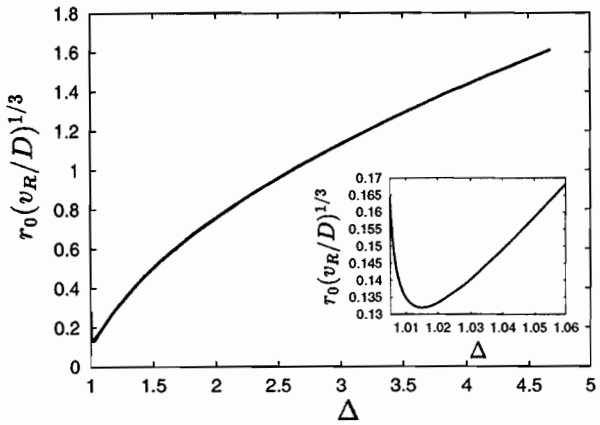

FIG. 3: Dimensionless crack tip radius r_0 versus dimensionless driving force Δ.

The main idea of this paper is based on the fact that a full *elastodynamic* description restores the selection of this lengthscale. It is known that at least for higher crack speeds the angular distribution f_{ij} become strongly dependent on the ratio v/v_R (v_R is the Rayleigh speed). The dynamical stress intensity factor K_{dyn} is related to the static one used here by an extra velocity dependent function $g(v/v_R)$, $K_{dyn} = Kg(v/v_R)$. The crucial observation is, that velocity appears now in two different combinations in the equation of motion, vr_0^3/D and v/v_R. Thus, by introduction of the new parameter v/v_R, a selection of both v and r_0 happens.

From these general arguments we conclude that fast steady state crack propagation by surface diffusion is indeed possible.

The local crack tip model — We mimic the tangential stress by a *local* description, as depending on the propagation velocity and only on the local properties of the interface. It takes both the velocity dependence of the angular distribution and the decrease of the dynamical stress intensity factor into account:

$$\sigma_{\tau\tau} = K\left[\sqrt{1-(v/v_R)^2}\cos(\theta/2) + (v/v_R)^2\sin^4\theta\right]/r^{1/2}. \quad (4)$$

We obtain both the crack shape (Fig. 1) and a selection of v/v_R and r_0 as functions of the dimensionless driving force $\Delta = K^2(1-\nu^2)/2E\alpha$. The results are given in Figures 2 and 3.

One of the main results is that the upper limit for the steady state crack velocity is appreciable below the Rayleigh speed, as known from experimental results.

Stability — Our solution is subject to the ATG instability above a critical threshold of the driving force Δ. The de-stabilizing effects stem from the non-local elastic contributions which we neglected in our model, but which are obviously present in the real problem. This can be proved by simple dimensional analysis arguments: The characteristic wavelength of the ATG instability is $\lambda \sim E\alpha/\sigma_{\tau\tau}^2$ [4]; in the tip region it reads $\lambda^{(tip)} \sim r_0/\Delta$. Thus, as soon as a certain critical driving force Δ_c is exceeded, the characteristic wavelength of instability fits into the tip region. Hence we expect the ATG instability to be the relevant mechanism for the experimentally observed microbranching instability.

[1] E. Sharon and J. Fineberg, Nature **397**, 333 (1999).

[2] E. A. Brener and V. I. Marchenko, Phys. Rev. Lett. **81**, 5141 (1998).

[3] R. Spatschek and E. A. Brener, Phys. Rev. E **64**, 046120 (2001).

[4] R. J. Asaro and W. A. Tiller, Metal. Trans. **3**, 1789 (1972); M. A. Grinfel'd, Sov. Phys. Dokl. **31**, 831 (1986).

Publications in journals

Antons,A.; Schroeder,K.; Voigtländer,B.; Cherepanov,V.; Berger,R.; Blügel,S.
Element specific surface reconstructions of islands during surfactant-mediated growth on Si(111)
Physical review letters, 89 (2002), 23, S. 236101

Baranov,A. N.*; Stepanyuk,V.S.*; Hergert,W.*; Katsnelson,A. A.*; Settels,A.; Zeller,R.; Dederichs,P.H.
Full-potential KKR-calculations for MgO and divalent impurities in MgO
Physical review B, 66 (2002), S. 155117

Brener,E.; Kessler,D.*
Comment on solidification of a supercooled liquid in a narrow channel
Physical review letters, 88 (2002), S. 149601

Brener,E.; Marchenko,V.*
Frictional shear cracks
JETP letters, 76 (2002), S. 211

Brener,E.; Temkin,D.*
Theory of diffusion induced grain boundary migration : is mass transport along free surfaces important?
Acta materialia, 50 (2002), S. 1707

Cabria,I.; Nonas,B.; Zeller,R.; Dederichs,P.H.
Orbital magnetism of transition metal adatoms and clusters on the Ag and Au(001) surfaces
Physical review B, 65 (2002), S. 054414-1

Cao,Y.; Zheng-Kuan,J.*; Antons,A.; Schroeder,K.; Blügel,S.
Stable structure of Sb monolayer on a strained Ge(111) substrate
Chinese journal of physics, 19 (2002), S. 259

Cao,Y.; Zheng-Kuan,J.*; Antons,A.; Schroeder,K.; S. Blügel,S.
Relaxation of small molecules, an ab initio study
Communications in theoretical physics, 37 (2002), S. 597

Caprion,D.*; Schober,H. R.
Influence of quench rate and pressure on the glass transition temperature in selenium
Journal of chemical physics, 117 (2002), S. 2814

Dederichs,P.H.; Mavropoulos,Ph.; Wunnicke,O.; Papanikolaou,N.; Bellini,V.; Zeller,R.; Drchal,V.*; Kudrnovsky,J.*
Importance of complex band structure and resonant states for tunneling
Journal of magnetism and magnetic materials, 240 (2002), S. 108 - 113

Drchal,V.*; Kudrnovsky,J.*; Bruno,P.*; Dederichs,P. H.; Turek,I.*; Weinberger,P.*
Electron transport in magnetic multilayers : effects of disorder
Physical review B, 65 (2002), S. 214414-1

Freyss,M.; Mavropoulos,P.; Papanikolaou,N.; Bellini,V.; Zeller,R.; Dederichs,P.H.
Tunneling transport in ferromagnet/insulator/ferromagnet junctions
Phase transitions, 75 (2002), 1/2, S. 159 - 166

Freyss,M.; Papanikolaou,N.; Bellini,V.; Zeller,R.; Dederichs,P. H.
Electronic structure of Fe/semiconductor/Fe(001) tunnel junctions
Physical review B, 66 (2002), S. 014445

Freyss,M.; Papanikolaou,N.; Bellini,V.; Zeller,R.; Dederichs,P.H.; Turek,I.*
Transport properties and electronic structure of epitaxia tunnel junctions
Journal of magnetism and magnetic materials, 240 (2002), S. 117

Galanakis,I.; Bihlmayer,G.; Bellini,V.*; Papanikolaou,N.*; Zeller,R.; Blügel,S.; Dederichs,P.H.
Broken bond counting rule for the surface energies of noble metals
Europhysics letters, 58 (2002), S. 751

Galanakis,I.; Papanikolaou,N.; Dederichs,P. H.
Applicability of the broken bond rule to the surface energy of fcc metals
Surface science, 511 (2002), S. 1

Gurevich,V.*; Parshin,D.A.*; Schober,H. R.
On the theory of the Boson peak in glasses
JETP letters, 76 (2002), S. 650

Gurevich, V.L., Parshin, D.A., Schober, H.R.
On the theory of Boson peak in glasses
JETP letters, 76 (2002), 9, S. 553-557

Hartmann,M.; Trinkaus,H.
Evolution of gas-filled nanocracks in crystalline solids
Physical review letters, 88 (2002), S. 055505-1

Hauck,J.; Erkens,W.; Mika,K.; Wingerath,K.
Structure maps for polymer structures
International journal of modern physics B, 16 (2002), 23, S. 3449 - 3457

Hirnet,A.*; Schroeder,K.; Blügel,S.; Torrelles,X.*; Albrecht,M.*; Jenichen,B.*; Gierer,M.*; Moritz,W.*
A novel Sb induced reconstruction of the (113) surface of Ge
Physical review letters, 88 (2002), S. 226102

Kudrnovsky,J.*; Drchal,V.*; Turek,I.*; Dederichs,P. H.; Weinberger,P.*; Bruno,P.*

Ab-initio theory of perpendicular transport in layered magnetic systems
Journal of magnetism and magnetic materials, 240 (2002), S. 177

Levy,P. M.*; Wang,K.*; Dederichs,P. H.; Heide,C.*; Zhang,S.*; Szunyogh,L.*
An approximate calculation for transport in magnetic tunnel junctions in the presence of localised states
Philosophical magazine B, 82 (2002), S. 763

Luysberg,M.; Kirch,D.; Trinkaus,H.; Holländer,B.; Lenk,St.; Mantl,S.; Herzog,H.-J.*; Hackbarth,T.*; Fichtner,P.F.P.*
Effect of helium ion implantation and annealing on the relaxation behaviour
of pseudomorphic Si1-xGex/Si(100) buffer layers on Si (100) substrates
Journal of applied physics, 92 (2002), S. 4290 - 4295

Mavropoulos,Ph.; Wunnicke,O.; Dederichs,P.H.
Ballistic spin injection and detection in Fe/semiconductor/Fe junctions
Physical review B, 66 (2002), S. 024416

Müller-Krumbhaar,H.; Abel,T.; Brener,E.; Hartmann,M.; Eissfeldt,N.; Temkin,D.*
Growth morphologies in solidification and hydrodynamics
JSME international journal series B - fluids and thermal engineering, 45 (2002), S. 129

Papanikolaou,N.; Zeller,R.; Dederichs,P.H.
Conceptual improvements of the KKR-method
Journal of physics: condensed matter, 14 (2002), S. 2799

Rzehak,R.; Zimmermann,W.*
Dynamics of strongly deformed polymers in solution
Europhysics letters, 59 (2002), S. 779

Schober,H. R.
Collectivity of motion in undercooled liquids and amorphous solids
Journal of non-crystalline solids, 307 (2002), S. 40

Schober,H.R.
Atomic motion in amorphous solids
Acta physica Polonica A, 102 (2002), S. 83

Schober,H.R.
Pressure dependence of diffusion in simple glasses and supercooled liquids
Physical review letters, 88 (2002), S. 145901

Schroeder,K.; Antons,A.; Berger,R.; Blügel,S.
Surfactant mediated heteroepitaxy versus homoepitaxy : kinetics of group-IV atoms on As-passived Si(111) and Ge(111)
Physical review letters, 88 (2002), S. 046101

Schroeder,K.; Antons,A.; Berger,R.; Blügel,S.
Ad-atom kinetics on surfactant-covered Si(111) : ab initio calculations
Phase transitions, 75 (2002), S. 91 - 99

Schroeder,K.; Antons,A.; Berger,R.; Blügel,S.
Surfactant mediated heteroepitaxy versus homoepitaxy : kinetics for group-IV adatoms on As-passivated Si(111)
Physical review letters, 88 (2002), S. 046101

Trinkaus,H.; Heinisch,H. L.*; Barashev,A. V.*; Golubov,S.I.*; Singh,B.N.*
1D to 2D diffusion-reaction kinetics of defects in crystals
Physical review B, 66 (2002), S. 060105 (R)

Trinkaus,H.; Ullmaier,H.
Does pulsing in spallation neutron sources affect radiation damage?
Journal of nuclear materials, 296 (2001), S. 101
M03
Nachtrag 2001

Turek,I.*; Kudrnovsky,J.*; Drchal,V.*; Weinberger,P.*; Dederichs,P.H.
Ab-initio theory of transport in FeRh-based natural magnetic multilayers
Journal of magnetism and magnetic materials, 240 (2002), S. 162

Turek,I.*; Kudrnovsky,J.*; Drchal,V.*; Weinberger,P.*; Dederichs,P.H.
Theory of electron transport in FeRh-based natural magnetic multilayers
Czechoslovak journal of physics, 52 (2002), S. 203

Wunnicke,O.; Mavropoulos,Ph.; Zeller,R.; Dederichs,P.H.; Grundler,D.*
Ballistic spin injection from Fe(001) into ZnSe and GaAs
Physical review B, 65 (2002), S. 241306(R)

Wunnicke,O.; Papanikolaou,N.; Zeller,R.; Dederichs,P.H.; Drchal,V.*; Kudrnovsky,J.*
Effects of resonant interface states on tunneling magnetoresistance
Physical review B, 65 (2002), S. 064425

Book chapter

Schober,H. R.; Caprion,D.*
Atomistic studies on amorphous silicon
Physics and applications of disordered materials / ed.: M. A. Popescu. - INOE Publishing House, Bucharest, Romania. - 973-98742-8-2. - S. 390

Invited talks

Atodiresei,N.; Kromen,Wi.; Blügel,S.; Schroeder,K.
The neutral Cd-vacancy complex in Si and Ge
DPG-Frühjahrstagung : Regensburg
Regensburg: 11.03.2002 - 15.03.2002

Brener,E.; Marchenko,V.*
Frictional shear cracks
International Workshop on Nanotribology
Portoverne, Italy: 19.10.2002 - 23.10.2002

Brener,E.; Spatschek,R.
Crack propagation by surface diffusion
Workshop on Interfacial Dynamics in Pattern Forming Processes
Magdeburg: 10.06.2002 - 13.06.2002

Brener,E.; Spatschek,R.
Fast crack propagation
1st International Workshop Pattern Formation by Molecular Self-Organisation at Interfaces
Berlin: 04.03.2002 - 06.03.2002

Brener,E.; Spatschek,R.
Fast crack propagation by surface diffusion
Workshop on Computational Physics of Transport and Interface Dynamics
Dresden: 07.03.2002 - 08.03.2002

Brener,E.; Spatschek,R.
Fast crack propagation by surface diffusion
XXII. Dynamics Days Europe
Heidelberg: 14.07.2002 - 19.07.2002

Brener,E.; Temkin,D.*
Theory of DIGM
II. International Workshop on Diffusion and Stresses
Moscow, Russia: 25.05.2002 - 30.05.2002

Dederichs,P. H.
Ballistic spin injection from Fe into ZnSe and GaAs
International Workshop on Oxidic Interfaces : Lutherstadt Wittenberg
Wittenberg: 14.02.2002 - 17.02.2002

Dederichs,P. H.
Magnetic properties and Curie temperatures of diluted magnetic semiconductors
Workshop on Electronic Structure of Solids
Dresden: 03.07.2002 - 05.07.2002

Dederichs,P. H.
Magnetoelectronics
Workshop and Hands-on Course 'KKR and Spectroscopies'
München: 18.02.2002 - 23.02.2002

Dederichs,P. H.
Spin injection from Fe into ZnSe and GaAs
International Conference on the Science and Technology of Spin Transport in Nanostructures : ITCP
Trieste, Italien: 19.08.2002 - 22.08.2002

Dederichs,P.H.
Electronic structure of diluted magnetic semiconductors
Workshop on Electronic Structure Calculations
Uppsala, Schweden: 10.06.2002 - 11.06.2002

Galanakis,I.
Surface and interface magnetic properties Heusler alloys
International Workshop on Oxidic Interfaces : Lutherstadt Wittenberg
Wittenberg: 14.02.2002 - 17.02.2002

Galanakis,I.; Dederichs,P. H.
Origine and properties of the gap in half-ferromagnetic Heusler alloys
RTN Mini-Workshop on Magnetoelectronics
Orsay, Frankreich: 08.02.2002

Golubov,S.*; Singh,B.*; Trinkaus,H.
Treatment of microstructural evolution under cascade damage conditions within the framework of production bias model : status and perspectives
Second IEA Fusion Materials Agreement Workshop on Modeling and Experimental Validation
Les Diablerets, Schweiz: 30.09.2002 - 04.10.2002

Höher,H.; Zeller,R.; Dederichs,P. H.
Der Leerstelle-Cd Komplex in Si und Ge
Arbeitstreffen Forschung mit nuklearen Sonden und Ionenstrahlen
Bonn: 30.09.2002 - 02.10.2002

Mavropoulos,Ph.; Galanakis,I.; Dederichs,P.H.
Towards new half-metallic systems : zinc-blende compounds of transition elements with N, P, As, Sb, S, Se, and Te
2nd Annual Meeting of the RTN (Computational Magnetoelectronics)
Oleron Islands, Frankreich: 05.10.2002 - 09.10.2002

Sato,K.; Katayama-Yoshida,H.*
Ferromagnetism in III-V compound-based diluted magnetic semiconductors
European Physical Society Meeting : Brighton
Brighton, GB: 08.04.2002 - 11.04.2002

Sato,K.; Katayama-Yoshida,H.*; Dederichs,P. H.

Curie temperatures of III-V diluted magnetic semiconductors calculated from first-principles in mean field approximation
Physics and Applications of Spin Related Phenomena in Semiconductors : Würzburg
Würzburg: 23.07.2002 - 26.07.2002

Sato,K.; Katayama-Yoshida,H.*; Dederichs,P. H.
Electronic structure and Curie temperatures of diluted magnetic semiconductors
Computational Magnetoelectronics : Oleron Island
Oleron Island, France: 05.10.2002 - 09.10.2002

Schober,H. R.
Diffusion in Gläsern und Schmelzen
Meeting zur Struktur und Dynamik von unterkühlten Schmelzen und Gläsern : SFB 625 ; Universität Mainz
Mainz: 23.10.2002

Schober,H. R.
Diffusion in amorphous materials and their melts
Diffusion and Thermodynamics D&T'02
Brno, Tschechien: 04.09.2002 - 06.09.2002

Schober,H. R.
Diffusion zur Struktur und Dynamik
Meeting zur Struktur und Dynamik von unterkühlten Schmelzen und Gläsern : SFB 625 ; Universität Mainz
Mainz: 23.10.2002

Schober,H. R.; Caprion,D.*
Molecular dynamics simulation of amorphous selenium
XIIIth International Symposium on Non-Oxide Glasses and new Optical Glasses
Pardubice, Tschechien: 09.09.2002 - 13.09.2002

Schober,H. R.; Gurevich,V. L.*; Parshin,D. A.*
Wechselwirkung weicher anharmonischer Oszillatoren
DPG-Frühjahrstagung
Regensburg: 11.03.2002 - 15.03.2002

Schroeder,K.; Antons,A.; Berger,R.; Blügel,S.
Simulation von STM-Bildern von Stufenkanten auf As-bedecktem Si(111)
DPG-Frühjahrstagung
Regensburg: 11.03.2002 - 15.03.2002

Trinkaus,H.
Pulsed versus continuous irradiation - conditions for effects of radiation pulsing
Workshop on Fusion Materials Irradiation in Spallation Sources
Jülich: 21.01.2002 - 22.01.2002

Trinkaus,H.
The effect of cascade-induced gas resolution on bubble formation in metals
5th International Workshop on Spallation Materials Technology
Charleston, South Carolina: 19.05.2002 - 24.05.2002

Trinkaus,H.
Under which conditions could beam pulsing in spallation neutron sources affect radiation damage?
5th International Workshop on Spallation Materials Technology
Charleston, South Carolina: 19.05.2002 - 24.05.2002

Trinkaus,H.; Singh,B.*
He accumulation irradiated metals, where do we stand?
Second IEA Fusion Materials Agreement Workshop on Modeling and Experimental Validation
Les Diablerets, Schweiz: 30.09.2002 - 04.10.2002

Wunnicke,O.; Mavropoulos,P.; Zeller,R.; Dederichs,P.H.; Grundler,D.*
Ballistic spin injection from Fe into ZnSe and GaAs
PASPS Conference
Würzburg: 23.07.2002 - 26.07.2002

Wunnicke,O.; Mavropoulos,P.; Zeller,R.; Dederichs,P.H.; Grundler,D.*
Ballistic spin injection from Fe into ZnSe and GaAs
RTN Mini-Workshop "Magnetoelectronics"
Orsay, Frankreich: 08.02.2002

Wunnicke,O.; Mavropoulos,P.; Zeller,R.; Dederichs,P.H.; Grundler,D.*
Ballistic spin injection from Fe(001) into ZnSe and GaAs
19th Conference of the Condensed Matter Division of the EPS
Brighton, UK: 07.04.2002 - 11.04.2002

Wunnicke,O.; Mavropoulos,P.; Zeller,R.; Dederichs,P.H.; Grundler,D.*
Ballistische Spininjektion von Fe(001) in ZnSe und GaAs
Frühjahrstagung des Arbeitskreises Festkörperphysik der DPG
Regensburg: 11.03.2002 - 15.03.2002

Zeller,R.
Computational electronic-structure methods for large-scale and complex materials
Eröffnung des Zentrums für Computational Nanoscience : Universität Halle-Wittenberg
Halle-Wittenberg: 18.12.2002 - 18.12.2002

Other talks

Brener,E.; Spatschek,R.
Fast crack propagation by surface diffusion
University Colloquia : University of Manchester
Manchester, UK: 20.04.2002 - 28.04.2002

Dederichs,P. H.
Diluted magnetic semiconductors
Seminar am Donostia International Physics Center
San Sebastian, Spanien: 11.11.2002

Gutheim,F.; Müller-Krumbhaar,H.

Statistical analysis and feature selection
Grünenthal Applied Lifescience Analysis
Eschweiler/Stolberg: 21.02.2002

Mavropoulos,P.; Wunnicke,O.; Dederichs,P.H.
Ballistic spin injection from Fe into ZnSe and GaAs
Lehrstuhlseminar (Prof. D. Weiss)
Universität Regensburg: 23.05.2002

Rzehak,R.; Kienle,D.*; Zimmermann,W.*
Nonlinear stochastic dynamics of polymers in flow
3. Dresdner Herbstseminar
des Arbeitskreises Nichtlineare Physik
zum Thema : Nichtlineare stochastische Prozesse
Dresden: 01.12.2002 - 04.12.2002

Sato,K.; Katayama-Yoshida,H.*
Ferromagnetism of III-V diluted magnetic semiconductors
RTN Mini-Workshop : Paris
Paris, France: 08.02.2002

Schober,H. R.
Dynamik in Gläsern und Schmelzen
Seminar : TU München
München: 11.07.2002

Schober,H. R.; Caprion,D.*
Diffusion and relaxation in glasses and their melts
MRS Fall Meeting
Boston, USA: 02.12.2002 - 06.12.2002

Schroeder,K.
Einfluss von Surfactant-Schichten auf das epitaktische Wachstum :
Struktur, Diffusion, Clusterbildung und Stufenkanten auf As- und
Sb-bedeckten Si(111)-Oberflächen
Seminar des Institut für Kristallographie und Angewandte Mineralogie : LMU München
München: 14.06.2002

Spatschek,R.; Brener,E.
Fast crach growth by surface diffusion
University of California
Santa Barbara, CA: 19.03.2002

Posters

Antons,A.; Schroeder,K.; Berger,R.; Blügel,S.
The neutral Cd-vacancy complex in Si and GeClusters and Steps on Si(111) :
surfactant effect due to As and Sb
Physics Congress : European Physical Society (Condensed Division)
Bristol: 07.04.2002 - 11.04.2002

Brener,E.; Marchenko,V.*
Frictional shear cracks
Workshop on Interfacial Dynamics in Pattern Forming Processes
Magdeburg: 10.06.2002 - 13.06.2002

Galanakis,I.; Dederichs,P.H.
Origine and properties of the gap in half-ferromagnetic Heusler alloys
Gordon Conference om Magnetic Nanostructures
Il Ciocco, Italien: 12.05.2002 - 16.05.2002

Gurevich,V. L.*; Parshin,D. A.*; Schober,H. R.
Low frequency excitations and their interactions
19th General Conference of the EPS, Condensed Matter Division
Brighton, UK: 07.04.2002 - 11.04.2002

Rzehak,R.; Müller-Krumbhaar,H.; Marquardt,W.*
Liquid-liquid phase change in systems with flow
Liquid Matter Conference of the EPS
Konstanz: 13.09.2002 - 18.09.2002

Rzehak,R.; Zimmermann,W.*
Inertial effects in Brownian motion of a trapped particle in shear flow
Jülich Soft Matter Days
Kerkrade, Niederlande: 19.11.2002 - 22.11.2002

Sato,K.; Katayama-Yoshida,H.*
Electronic structure and ferromagnetism in III-V compound-based diluted magnetic semiconductors
Physics and Applications of Spin Related Phenomena in Semiconductors : Würzburg
Würzburg: 23.07.2002 - 26.07.2002

Sato,K.; Katayama-Yoshida,H.*
Electronic structure and ferromagnetism in III-V compound-based diluted magnetic semiconductors
International Conference on the Physics of Semiconductors : Edinburgh
Edinburgh, GB: 29.07.2002 - 02.08.2002

Sato,K.; Katayama-Yoshida,H.*; Dederichs,P. H.
An estimation of the Curie temperature for III-V diluted magnetic semiconductors within the mean field theory based on first-principles calculations
International Conference on the Physics of Semiconductors : Edinburgh
Edinburgh, GB: 29.07.2002 - 02.08.2002

Sato,K.; Katayama-Yoshida,H.*; Dederichs,P.H.
Electronic structure and Curie temperatures of III-V diluted magnetic semiconductors
Gordon's Conference : Magnetic Nanostructures ; Il Ciocco
Il Ciocco, Italy: 12.05.2002 - 16.05.2002

Schober,H. R.; Kluge,M.; Caprion,D.*
Collectivity of motion in undercooled liquids and amorphous solids
19th General Conference of the EPS, Condensed Matter Division
Brighton, UK: 07.04.2002 - 11.04.2002

Wunnicke,O.

Ballistic spin injection from Fe into ZnSe and GaAs
Annual Meeting RTN : Oleron
Oleron, France: 05.10.2002 - 09.10.2002

Wunnicke,O.; Mavropoulos,P.; Zeller,R.;
Dederichs,P.H.; Grundler,D.*
Ballistic spin injection from Fe(001) into ZnSe and GaAs
Dreikönigstreffen "Magnetism on the Sub-micrometer Scale : Interactions and Microscopy"
Bad Honnef: 07.01.2002 - 09.01.2002

Wunnicke,O.; Mavropoulos,Ph.; Zeller,R.;
Dederichs,P.H.
Ballistic spin injection from Fe into ZnSe and GaAs
HGF-Treffen : Forschungszentrum Jülich
Jülich: 06.11.2002

Wunnicke,O.; Mavropoulos,Ph.; Zeller,R.;
Dederichs,P.H.
Ballistic spin injection from Fe into ZnSe and GaAs
2nd Annual Meeting of the RTN (Computational Magnetoelectronics)
Oleron, Islands, Frankreich: 05.10.2002 - 09.10.2002

Wunnicke,O.; Papanikolaou,N.; Zeller,R.;
Dederichs,P.H.; Drchal,V.*; Kudrnovsky,J.*
Effects of resonant interface states on tunneling magnetoresistance
19th Conference of the Condensed Matter Division of the EPS
Brighton, UK: 07.04.2002 - 11.04.2002

Ph.D. Theses

Antons,A.
First-principles investigation of initial stages of surfactant mediated growth
on the Si(111) substrate
Jülich, Forschungszentrum, Zentralbibliothek,
Berichte des Forschungszentrums Jülich ;
JUEL-3941
Aachen, Tech. Hochsch., Diss., 2002

Berger,R.
Berechnung der Stufenkanten auf der As-bedeckten Si(111)-Oberfläche
mit einem parallelisierten ab initio Programm
Aachen, Techn. Hochsch., Diss., 2002

Institute for Scattering Methods

General Overview

Research Areas

Modern solid state physics goes far beyond a phenomenological description and bases the understanding of solid state properties and phenomena on atomistic theories. To obtain information about the atomic structure of solids, probes with sub-nanometer spatial resolution are needed. To study the excitation spectra, an appropriate energy resolution is necessary in addition. All these requirements can be met by scattering methods. In this sense, scattering methods provide the basis of our present understanding of the structure, excitations and phase transitions of condensed matter on a microscopic level.

At the Institute for Scattering Methods (ISM), synchrotron x-ray scattering and neutron scattering are employed for the investigation of condensed matter on an atomistic microscopic level. The emphasis lies on exploiting fully the complementarity of the two probes. Besides the application of scattering methods to solid state problems, major activities are concentrated on the methodology. This includes the further development of experimental techniques by improving instrument components and data treatment algorithms, the development of new experimental methods and the corresponding instruments and the development, construction and operation of scattering instruments at large-scale facilities. At present, ISM operates five instruments at the research reactor DIDO of the Research Center Jülich and two instruments at the Hamburger Synchrotronstrahlungslabor HASYLAB. In addition, we participate in the operation of a sector at the Advanced Photon Source APS in Argonne, USA. These instruments are open for the use by external groups from universities, research centers and industry. The instrument responsibles from ISM provide scientific and technical support during the experiment and the data processing. In order to secure the future of European neutron research, ISM made a strong commitment to the European Spallation Source project. Besides development of novel instrument concepts, ISM took the lead in research and development for the "heart of the ESS", the target and moderator block.

ISM is open for all research areas in condensed matter science, where scattering methods can be applied. At present, the research activities are concentrated in the fields: "solid state magnetism", "correlated electron systems", "magnetic nanostructures", "structural and magnetic disorder", "novel materials" and "ultrathin liquid films". For the purpose of this research, ISM is also engaged in sample preparation (e.g. by molecular beam epitaxy and single crystal growth) and characterisation (e.g. resistivity, AC and DC susceptibility and magnetisation measurements).

Highly Correlated Electron Systems
Certain materials, in particular transition metal oxides, exhibit marked deviations from a simple Fermi-liquid behaviour of the electronic system. Strong electronic correlations lead to macroscopic quantum phenomena and the systems exhibit a strong competition between several degrees of freedom. A prominent example is provided by colossal magneto-resistance (CMR) manganites, e. g. $La_{1-x}Sr_xMnO_3$. In a cooperation with RWTH Aachen, a series of high quality single crystals have been grown with compositions close to $x = {}^1/_8$ (low doping regime). In these crystals, various ordering phenomena occur, such as charge ordering, orbital ordering, spin ordering and lattice distortions. The interplay of these ordering phenomena can be studied by a combination of different scattering methods: scattering of high energy x-rays with $E > 100$ keV, anisotropic anomalous x-ray scattering at the Mn-K-edge and neutron scattering. For the latter, polarisation analysis is employed to clearly separate magnetic from lattice contributions. The nature of the charge- and orbital ordering in the intriguing ferromagnetic insulating ground state was comprehensively investigated by resonant x-ray scattering. For the first time, a novel superstructure was identified and intensively characterised. In addition, a x-ray induced switching between charge ordered and disordered states could be observed. In contrast to observations by other groups, our effect was entirely reversible. These results will have a significant impact on the understanding of the exotic electronic properties of these compounds.

Bulk Magnetism
The elementary excitations in 3D-antiferromagnets are well described by linear spin wave theory, which assumes purely transversal modes. In neutron scattering experiments using polarisation analysis, we were able to separate for the first time the spectra of transverse and longitudinal magnetic fluctuations for the model system MnF_2. The energy spectrum of longitudinal fluctuations is continuous and extends to about twice the frequency of the zone boundary modes. Longitudinal fluctuations result from non-linear processes due to multimagnon scattering. The dynamic magnetic response due to two magnon creation or annihilation is separated by a gap centered near

the spin wave frequency from the central peak corresponding to neutron-magnon scattering. The observed longitudinal spectra are in qualitative agreement with the theory for two magnon processes (see detailed report).
A phenomenological description of the sublattice magnetisation over a wide range of temperature has been proposed by using simple power laws for the low temperature behaviour and the critical behaviour. The low temperature behaviour clearly deviates from the predictions by Bloch (see detailed report). Of particular interest in this context are the transition metal carbonides $CuCO_3$ and $NiCO_3$, which have been synthesised by hydrothermal synthesis. These compounds show weak ferromagnetism, i. e. a coexistence of ferromagnetic and antiferromagnetic ordering.

Thin Film Systems
Research is ongoing on thin soft matter films, in particular in confined geometry and magnetic thin film systems. X-ray scattering under grazing incidence could be performed on confined polymers. Self-organisation of the polymer molecules under confinement is significantly different compared to non-confined thin films. The effect depends strongly on pressure, temperature and the number of polymer molecule layers. For thin magnetic films, we have continued the investigation of the Er/Tb multilayer for films of various thicknesses of the two components. A phase diagram as the function of film thickness could be established. By means of resonant x-ray scattering, a spin density wave of the conduction band electrons could be observed in the Er_{20}/Tb_5 sample. Thus, the element and band specificity of resonant magnetic x-ray scattering allows us to directly observe the coupling mechanism of the 4f-electrons in the Er-layers via the 5d-conduction band electrons (see detailed report). Magnetic multilayer systems are one-dimensional artificial structured magnetic systems. To explore the effect of an artificial structuring in a second dimension, we have produced a Fe/Cr/Fe multilayer, in which the last Fe-layer was structured into a regular grating by means of electron beam lithography and ion beam edging (collaboration with ISG). Applying an external field to this laterally structured multilayer, a competition arises between dipolar energy, Zeeman energy and exchange energy through the multilayer stack. Our aim is to understand the interaction between the magnetic nanostructures in detail. Polarised neutron scattering under grazing incidence has been measured on the HADAS reflectometer and shows that the domain pattern is significantly changed due to the lateral structuring (see detailed report). Bulk manganese has a very complicated magnetic structure. As an epitaxial thin film, a body centered tetragonal structure can be stabilised. To study the magnetic structure of this new phase of manganese, neutron reflectometry measurements on a Fe/Mn/Fe trilayer have been performed. These measurements indicate the existence of a net magnetic moment inside the 8 Å Mn layers. However, with neutrons, only a sensitivity in space can be achieved. We employed the technique of resonant soft x-ray magnetic scattering and could verify that the ferromagnetic moment is indeed intrinsic to the body-centered tetragonal manganese phase. In a Fe/Cr/Fe trilayer, the optical potential is such that for one neutron spin state, a quantum well structure is formed. With grazing incidence neutron scattering, we could observe a second order resonance where the amplitude of the wave-function is strongly amplified at the Fe/Cr interfaces, which enhances the sensitivity to magnetic roughness. Finally, with the new focusing small-angle camera KWS-3, ordering in a ferrofluid in an external field could be observed for the first time (collaboration with PNPI, Gatchina, and MPI, Stuttgart). The ferromagnetic particles align in chains oriented along the field (see detailed report).

Research and Advanced Materials
Scattering methods are applied for a wide range of novel materials or materials with particularly interesting properties. An example is the investigation of three-dimensional networks of platinum nanoparticles separated by organic spacer molecules (cooperation with MPI für Kohlenforschung) with the anomalous x-ray scattering method. The mechanism for synthesis of these networks could be elucidated. Another example is the research on novel storage phosphor and neutron converter materials for the use in neutron image plates. It could be shown that mixed LiF + KCl: Eu^{2+} features a significantly higher neutron over γ signal ratio compared to commercial available neutron image plates. The research on amorphous silicon-germanium alloys relevant for solar cell technology has been continued (together with Colorado School of Mines). Samples with a hotwire preparation technique using a small deposition rate showed a significantly reduced amount of Ge inhomogeneities on a length scale smaller 10 nm. In cooperation with the University of Liège, Belgium, we investigated a thermoelectric material - with Tl filled Sb Skutterudite. By measuring the phonon density of states we could demonstrate that Tl behaves as an Einstein oscillator with 5 meV excitation energy. Phonon scattering from the local and incoherent Tl modes gives rise to the strongly reduced thermal conductivity.

Research and Development for the European Spallation Source project ESS
The Forschungszentrum Jülich has taken a leading role in the research and development for a future next generation MW neutron source, the European Spallation Source ESS. The Institute for Scattering Method is developing innovative instrument concepts and is heavily engaged in research on target window materials, novel neutron moderators and the target-moderator arrangement. In particular, the embrittlement of candidate structure materials for spallation devices by implanted helium was studied in detail. It was found that the embrittlement of austenitic stainless steel by implanted helium is significantly lower than of martensitic steels. FATIMA, a piezo-driven fatigue test machine simulating the pulse stresses appearing in the ESS target container, has been built

and operated showing that pulse stress in the relevant range can be generated. Measures for the minimisation of erosion of target window materials due to cavitation following short proton pulses of high energy density were studied. Finally, in a search for an innovative cold moderator, the inelastic neutron spectra of various candidate materials has been measured. The resulting neutron flux as function of wavelength could be determined on the target moderator mock-up JESSICA (see detailed report).

Development of Instrumentation and Methods for Neutron and X-Ray Scattering
The new high resolution small angle scattering camera KWS-3 with focussing mirror could be successfully commissioned. With this world-unique instrument, a momentum space resolution down to 2 x 10^{-4} $Å^{-1}$ can be achieved. First successful user experiments were performed, see detailed report. A new instrument - named LAP-ND - for spherical neutron polarimetry in transmission was installed in the neutron guide hall and taken into operation. The primary spectrometer of a novel instrument for polarisation analysis with thermal neutrons SV-30 was erected in the reactor hall. The secondary spectrometer was completed, so that the instrument can take-up operation in 2003. By means of filter cells with nuclear spin polarised ^{3}He gas in combination with a position sensitive image plate detector, neutron polarisation analysis up to incident energies larger than 100 meV will become possible over a wide angular range. A significant progress has been made in the development of the image plate detector with low γ-sensitivity (in cooperation with University of Darmstadt) and also in the production of nuclear spin polarised ^{3}He, where we pursue the two alternative routes: spin exchange optical pumping and direct optical pumping of metastable ^{3}He. Finally a new method has been developed for vectorial (3D, spherical) polarisation analysis, which does not require the use of zero-field chambers, such as the complicated CRYOPAD device. The method is applicable for time-of-flight machines over a wide angular- and energy transfer range.

A major event for the institute in 2002 was the "International Workshop on Polarised Neutrons in Condensed Matter Investigations" PNCMI 2002, which was held at FZJ from 15 to 19 September. 126 scientists from 17 countries came to the Forschungszentrum to present 114 papers. The proceedings will be published as a special issue of Physica B: Condensed Matter. The PNCMI series of workshops bring together scientist concerned with the methodology of polarised neutrons, the development of the corresponding technology and the applications in condensed matter science. In view of the current spallation source projects, a special microsymposium was devoted to polarised neutron methods and instrumentation on existing and future pulsed sources. In connection with the workshop, we had organised the "First School on Polarised Neutron Scattering" from 10 to 14 September. In contrast to the two week long neutron laboratory course for students held at FZJ every year, this school was geared to neutron scientists wishing to obtain specialised training in the use of polarised neutrons. Lectures by some of the most experienced scientists who are at the forefront of the developments in the field were followed by hands-on experience on four polarised beam instruments at the FRJ-2 reactor as well as in the ^{3}He laboratory and with instrument simulation software. The lecture notes were published in the series *Matter and Materials* of Forschungszentrum Jülich.

I would like to close this report by thanking all members of the institute for their dedicated work during the past year.

Thomas Brückel

Personnel 2002/2003 and areas of activity

Scientists

Prof. Dr. Th. Brückel	Institute director; neutron and synchrotron x-ray scattering; magnetism.
Dr. L. J. Chang *- since 28.01.2002 -*	Hyperpolarised ^{3}He for neutron polarisation analysis by the spin-exchange method.
Dr. J. Chen	Mechanical tests and TEM on irradiated spallation materials. Fatigue behaviour of ESS structural materials.
Dr. H. Conrad	European Spallation Source project ESS: target and moderators.
Dr. G. Goerigk *- HASYLAB, Hamburg -*	Material research with anomalous small angle x-ray scattering (ASAXS); instrument responsible for Jülich's user-dedicated small-angle scattering facility JUSIFA.
Dr. H.-G. Haubold	Anomalous small angle x-ray scattering ASAXS and x-ray absorption spectroscopy XAS from highly dispersive systems; in-situ studies of electro-chemical processes.
Dr. A. Ioffe	Development of neutron scattering methods and instrumentation for polarisation analysis. Instrument responsible for the triple axis spectrometer SV-30 and the depolarisation instrument LAP-ND.
Dr. P. Jung	Radiation damage and hydrogen effects in metals and ceramics, thermal desorption spectroscopy. Development of ESS target module.
Dr. E. Kentzinger	Neutron and synchrotron x-ray scattering from magnetic thin film materials. Instrument responsible for the high resolution small angle camera and reflectometer KWS-3.
Dr. U. Köbler	Magnetisation and neutron diffraction studies of materials with fourth-order exchange interactions.
Dr. R. Mueller	Development of the ^{3}He filter for neutron polarisation analysis by the metastable exchange method.
J. Perßon *- since 01.12.2002 -*	Sample preparation and characterisation, crystal growth.
Dr. U. Rücker	Instrument responsible for the neutron reflectometer HADAS; preparation and characterisation of magnetic thin film systems.
Dr. W. Schweika	Diffuse neutron scattering for the investigation of short-range order in alloys, oxides, perovskites and quasi-crystals; instrument responsible for the diffuse neutron scattering instrument DNS.
Dr. O. Seeck *- HASYLAB, Hamburg -*	X-ray scattering from ultrathin liquid films in confined geometries; instrument responsible of the Wiggler beamline W1 at HASYLAB.
Dr. Y. Su	X-ray and neutron scattering from strongly correlated systems.
Dr. Th. Vad	Further development of the instrument control and data treatment programs for Jülich's user-dedicated small-angle scattering facility (JUSIFA); ASAXS measurements.

Technicians and Engineers

Dipl.-Ing. K. Bussmann	Electronic engineer; responsible for spectrometer control hard- and software.
A. Christ *- 19.01.2002 until 31.07.2002 -*	Laboratory assistant.
L. Dohmen	Project engineer for the small angle scattering instrument KWS III.
M. Abdel Fattah	Single crystal growth.
P. Foucart	Sample preparation, single crystal growth.
Dipl.-Ing. D. Hamann *- HASYLAB, Hamburg-*	Project engineer JUSIFA beamline.
Dipl.-Ing. P. Hiller	Project engineer for μCAT-collaboration at the Advanced Photon Source APS; Responsible for x-ray scattering laboratory.
Ms. C. Horriar-Esser	Ultra low-temperature magnetometry and ^{3}He filter project.
H. Jungbluth	Software development for x-ray small angle scattering.
H. Klein	Instrumentation and data processing, TEM, irradiation experiments.
Ms. B. Köppchen	Secretary.
Dipl.-Ing. E. Küssel	Project engineer for the new polarised thermal neutron scattering instrument SV-30.
B. Olefs	Magnetometry, electronics and PC responsible.
B. Schmitz	Triple axis spectrometer SV-30 and cryotechniques.
W. Schmitz *- until 31.04.2002 -*	SEM, irradiation experiments, specimen preparation.
T. Sorkalla *- until 28.08.2002 -*	Laboratory assistant.

J. Thelen	Small angle scattering KWS-3 and molecular beam epitaxy MBE.
M. Wündrich *- 03.06.2002 until 30.09.2002 -*	Diffuse neutron scattering instrument DNS; Reflectometer HADAS.

Thesis Students

Dipl.-Phys. W. Babik *- until 31.03.2002 -*	(RWTH Aachen) Interface morphology of GMR and TMR layer structures.
M. Sc. K. Istomin *- until 30.09.2002 -*	(RWTH Aachen) Interplay of charge, orbital and magnetic ordering in manganites.
Ms. M. Sc. M. Mihaylova *- HASYLAB, Hamburg -*	(RWTH Aachen) Liquids in confined geometry investigated by scattering methods.
Dipl.-Ing. M. Schlapp *- TU Darmstadt -*	(TU Darmstadt) Development of highly efficient materials and image plates for neutron detection.
Dipl.-Phys. J. Voigt	(RWTH Aachen) Influence of proximity and reduced dimensionality on structure and phase transition in rare earth superlattices.
Ms. cand. phys. N. Ziegenhagen *- until 31.07.2002 -*	(RWTH Aachen) Laterally structural multilayers.

Guests

Ms. Dr. J. Bos	(RWTH Aachen) Preparation of powder and single crystal samples; magnetic structures and phase transitions by neutron- and x-ray scattering.
D. Finarelli *- since 02.09.2002 -*	(Dip. Fisica Politecnico di Milano, Italy) ESS-project: target materials.
Dr. S. Massalovitch *- until 14.09.2002 -*	(Kurchatov Institute, Moscow, Russia) Development of a large-area image plate detector for thermal neutrons.
Prof. V. Plakhty *- 01.02.2002 until 14.06.2002 -*	(Petersburg Nuclear Physics Institute, Russia) Neutron scattering on chiral magnetic systems.
Dr. S. Romanzetti *- until 31.08.2002 -*	(Universita degli Studi di Ancona, Italy) ESS-project: target materials.
Dr. B. Toperverg	(Petersburg Nuclear Physics Institute, Russia) Theory for grazing incidence diffraction.
Z. Yao *- until 30.11.2002 -*	(China Institute of Atomic Energy (CIAE), Beijing, China) ESS-project: target materials.

Trainees

Ms. S. Bluhm
- until 04.10.2002 -
Ms. I. Schulte
- until 31.01.2002, since 18.09.2002 -

Longitudinal spin fluctuations in 3-D antiferromagnets

W. Schweika[1], S. V. Maleyev[1,2], Th. Brückel[1], V. P. Plakhty[1,2], and L.-P. Regnault[3]
[1] *Institut für Streumethoden, IFF*
[2] *Petersburg Nuclear Physics Institute, Gatchina, St. Petersburg 188300, Russia,*
[3] *CEA-Grenoble, DRFMC-SPSMS-MDN, 38054 Grenoble Cedex 9, France*

Usual spin waves in 3-D antiferromagnets are well described as transverse magnetic fluctuations in linear spin-wave theory. Here we investigated the non-linear response which leads to longitudinal fluctuations, as shown in an experiment with polarized neutrons on MnF_2 at temperatures well below the Néel temperature $T_N = 67$ K. It is found that the dynamic magnetic response due to two-magnon creation or annihilation is separated by a gap centered near the spin wave frequency from the central peak corresponding to neutron-magnon scattering (creation of one magnon and annihilation of another). The longitudinal energy spectrum extends to about twice the frequency of the zone boundary modes. This tail at high energies is fairly independent of momentum transfer. The observed longitudinal spectra are in qualitative agreement with the theory for two-magnon processes and are determined for large energy transfers ω by the density of states $D(\omega/2)$. [1]

Well below the Néel temperature T_N the transverse spin fluctuations namely spin-waves are well studied both theoretically and experimentally in a large amount of antiferromagnets (AF). Particularly, it was shown in the seminal paper by Harris *et al.* [2] that the interaction of the spin-waves is very weak and slightly renormalizes the spin-wave velocity. Hence, the linear spin-wave theory is a very good approximation for the description of the experimental data. Longitudinal spin fluctuations (LSF) (those along the sublattice magnetization) arise from higher order excitations. More precisely they consist of excitation and absorption of an even number of spin-waves. The main contribution to LSF should be due to two-magnon processes: (i) two magnon excitation (absorption) and (ii) absorption of one magnon and excitation of another one, which can be considered as neutron-magnon scattering. Excitations take place at all temperatures including $T = 0$, where absorption and scattering disappears. We have considered both parts of scattering separately showing that they take place in different parts of the ($\mathbf{Q}$,ω)-space [1]. For antiferromagnets with anisotropy, in the long-wavelength limit $q \to 0$, a gap is predicted in the dynamic spectra separating the scattering $S_{exc}(\mathbf{Q},\omega)$ due to two magnon excitation (absorption) from the one due to neutron-magnon scattering $S_{sc}(\mathbf{Q},\omega)$ [3,4]. From kinematic considerations the different regions of two-magnon scattering are defined, as shown in Fig. 1. Furthermore, it is found that the asymptotic behavior, in the limit of $q \ll 1/a$ and $\omega > 0$, of S_{ex} is essentially independent of the scattering vector and proportional to $D(\frac{\omega}{2})$, where $D(\omega)$ is the magnon density of states.

The neutron scattering experiments with polarization analysis have been performed on the triple-axes spectrometer IN22 at the ILL, Grenoble. The sample consists of several single crystals of MnF_2 with a total volume of 1.3 cm^3, oriented with the tetragonal a and c axes in the horizontal scattering plane. Polarized neutrons are used to separate the transverse spin fluctuactions from longitudinal spin fluctuactions, see Fig. 2.

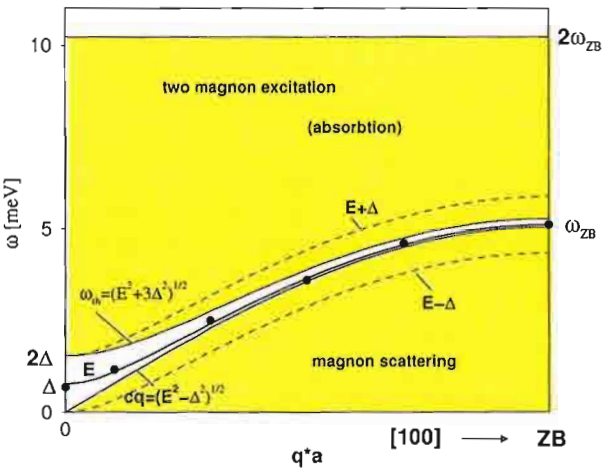

FIG. 1. Dispersion of the single magnon excitation $E(\mathbf{q})$ and regions of the longitudinal two-magnon spectra. The points denote the measured spin-waves at 50 K. The regions of possible excitation of two magnons and scattering are limited by twice the energy of the highest single magnon excitation (zone boundary mode), and as derived for low $\mathbf{q}$, by the threshold energy ω_{th} and cq, respectively. Therefore, a gap in the longitudinal (two-magnon) response, albeit fading out at higher $\mathbf{q}$, is to be found near to the much stronger scattering due to single magnon excitations.

As compared to the transverse spin waves, which are also shown (open symbols) on a reduced scale, the signal due to the longitudinal spin fluctuations is rather weak and has the expected continuous spectrum in energy, as shown in Fig. 3. The characteristic features are the wave-vector and temperature dependent central peak and the dip underneath the relatively strong peak due to

single spin wave excitation. Evidently, without polarization analysis this feature would not have been seen. The gap is affected by the experimental resolution, in particular, for the data taken at $T = 50\,\mathrm{K}$. Apart from this effect, the directional dependence of the spin-wave branches in MnF_2 leads to an intrinsic smearing of the gap at higher $\mathbf{q}$. For $\mathbf{h} = (1.15, 0, 0)$, where we measured also in the neutron energy gain mode ($\omega < 0$), we observed equivalent minima on both sides. Taking into account the Bose statistics and the (k_f/k_i) dependence of the dynamic scattering cross-section, we obtain a longitudinal susceptibility that is antisymmetric in energy. Comparing all spectra taken at different scattering vectors, see Fig.4., we observe a common asymptotic behaviour at higher energies as expected for two magnon scattering processes.

From the naive point of view the two spin-wave processes should saturate the longitudinal magnetic susceptibility and higher order processes can be neglected. According to [5,3], this is not necessarily the case for the longitudinal susceptibility. It was shown that in the isotropic exchange approximation at $\mathbf{q} = 0$ and $T = 0$ there is an infrared divergence (IRD) of the longitudinal susceptibility. It means that in the longitudinal scattering signal the interaction between spin-waves is expected to become strong. Processes involving many spin-waves should screen this IRD, and the $\chi_{AF}(\mathbf{q}, \omega)$ has to possess a weaker singularity than predicted by the two-magnon theory. Magnetic anisotropy suppresses the IRD. In the present case of MnF_2 one can expect that the longitudinal susceptibility is saturated by two-magnon processes. The IRD is expected to become stronger in lower dimensions [5,3]. Hence, with respect to the screening of the IRD it will be very interesting to measure the longitudinal spin fluctuations in 2-D antiferromagnets with very weak anisotropy in future experiments.

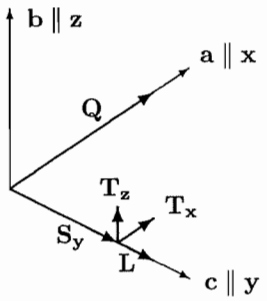

FIG. 2. Scattering geometry for measuring longitudinal fluctuactions. Only the spin components perpendicular to the scattering vector appear in magnetic neutron scattering. Spins are aligned parallel to c in the antiferromagnet MnF_2. For scattering vectors $\mathbf{Q} = (1 + \mathbf{q}, \mathbf{0}, \mathbf{0})$ the components $\mathbf{T_z}$ and $\mathbf{L}$ contribute. In order to separate these terms, neutrons are polarized parallel (and perpendicular) to one of these components which leads to a signal of non-spin flip (spin flip) scattering.

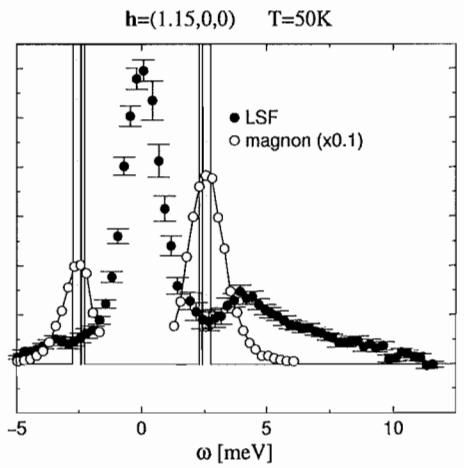

FIG. 3. Longitudinal spin fluctuation spectra. The predicted gap (*gray-shaded area*) separating the regions of two-magnon excitation (absorption) from magnon scattering coincides with the observed minima. For comparisons, the measured transverse magnon peaks are also shown, however, on a reduced scale (*open symbols*).

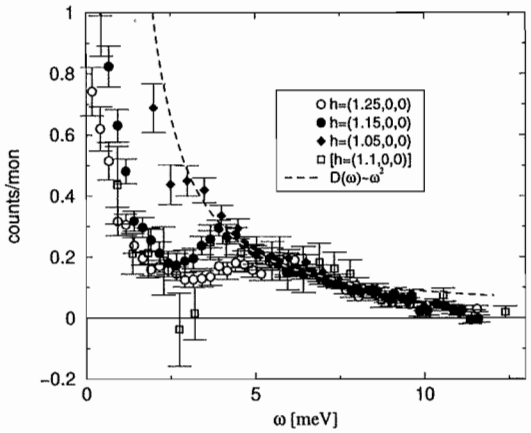

FIG. 4. The high energy tail of the longitudinal frequency spectrum is approximately q-independent and is determined by the density of states $D(\omega/2)$.

[1] W. Schweika, S. V. Maleyev, Th. Brückel, V. P. Plakhty, and L.-P. Regnault, Europhys. Lett. **60** (3) 446-452 (2002).

[2] A. B. Harris, D. Kumar, B. I. Halperin, P. C. Hohenberg, Phys. Rev. B**3**, 961, (1971).

[3] S. Braune, S. V. Maleyev, Z. Phys. B-Cond. Mat. **81**, 69-73 (1990).

[4] A. Bunker, D. P. Landau, Phys. Rev. Lett. **85**,2601(2000).

[5] R. Kubo, Phys. Rev. **87**, 568 (1952).

Amplitude, exponent and quantum state crossover phenomena in the spontaneous magnetization of pure spin magnets

U. Köbler[1], A. Hoser[1,2], O. Hupe[3] and J. Hesse[3]

[1] Institut für Streumethoden, IFF
[2] Institut für Kristallographie, RWTH-Aachen
[3] Institut für Metallphysik und Nukleare Festkörperphysik, TU-Braunschweig

It is shown experimentally that the temperature dependence of the magnetic order parameter can completely be described by a few temperature power functions with analytical changes (crossover) at the intersections of these functions. The standard behaviour consists in one power function for $T\rightarrow 0$ with exponent ε and the well known critical power law for $T\rightarrow T_c$ with exponent β. Additional crossover events can occur if the thermal variation of either the absolute value of the interactions or the exchange anisotropy exceeds a threshold value. In the itinerant ferromagnets Fe, Ni and Co a particular crossover due to a changing spin quantum number is observed.

Experimental investigations of many transition metal compounds with a quenched orbital moment and a well defined spin quantum number have shown [1] that the deviations of the magnetic order parameter from saturation at absolute zero can be described over a large temperature range by the simple power function

$$m_s(T) = 1 - c*T^{\varepsilon} \qquad (1)$$

Normally, this function holds up to the critical range at about $\sim 0.85*T_c$ where the analytical change (crossover) to the critical power law

$$m_s(T) \sim (T_c - T)^{\beta} \qquad (2)$$

occurs. The standard behaviour for $m_s(T)$ is therefore given by the crossover from eq.(1) to eq.(2) at the intersection of the two functions [2]. Fig.1 demonstrates this for FeF_2. This material has the tetragonal rutile structure and a spin of S=2. The relevant interactions are axial and the exponents are ε=3 (see Table I) and β=1/3.

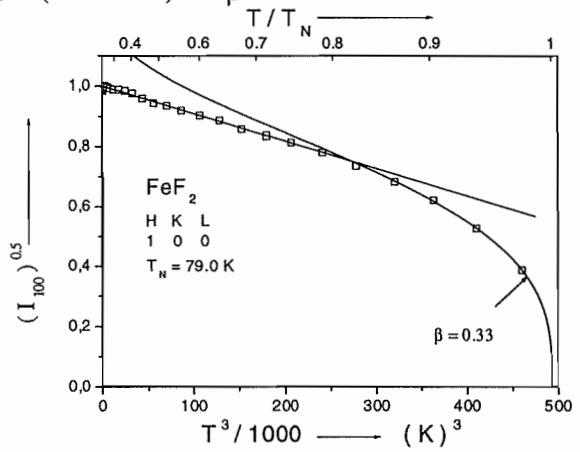

Fig.1 Antiferromagnetic order parameter of FeF_2 obtained from integrated (100) neutron scattering intensities vs. T^3. The two power functions according to eqs.(1) and (2) give an excellent fit using ε=3 and β=1/3.

In many materials more crossover events than only that one between eq.(1) and eq.(2) are observed [1,3]. At these crossover either the coefficient c (amplitude crossover) or the exponent ε (exponent crossover) changes discontinuously. Table I displays the six empirical universality classes for the exponent ε [1]. Note that the exponent ε is independent of the spin order type but that it is different for integer and half-integer spin quantum number. Moreover, ε depends –of course- on the dimensionality of the relevant magnetic interactions.

Table I
Empirical exponents ε according to eq.(1)

exchange interactions	*integer spin*	*half-integer spin*
3D	$T^{9/2}$	T^{2}
2D 3D anisotropic	T^{2}	$T^{3/2}$
1D 2D anisotropic	T^{3}	$T^{5/2}$

In cubic materials showing an isotropic magnetostriction the universality class is of the isotropic 3D type throughout but the exchange interactions can change their absolute strength with temperature. If this change is sufficiently strong an amplitude crossover can be induced. The cubic ferromagnets EuO (T_C=69.3K) and EuS (T_C=16.5K) with a spin of S=7/2 and therefore ε=2 are two suitable candidates to study the conditions for an amplitude crossover to occur. Since the spontaneous magneto-

striction of EuO is about twice as large as the spontaneous magnetostriction of EuS the exchange interactions can be expected to change much stronger with temperature for EuO compared to EuS. As fig.2 shows, an amplitude crossover occurs in the spontaneous magnetization of EuO but not in the spontaneous magnetization of EuS. Note that the weaker slope on the low temperature side indicates increasing interactions with decreasing temperature. From the ratio of the two slopes of ~0.65 it can be estimated that the interactions differ by ~18%. In EuS the anticipated increase of the interactions is evidently below threshold. As a consequence, no information on the temperature dependence of the exchange interactions can be obtained in this way.

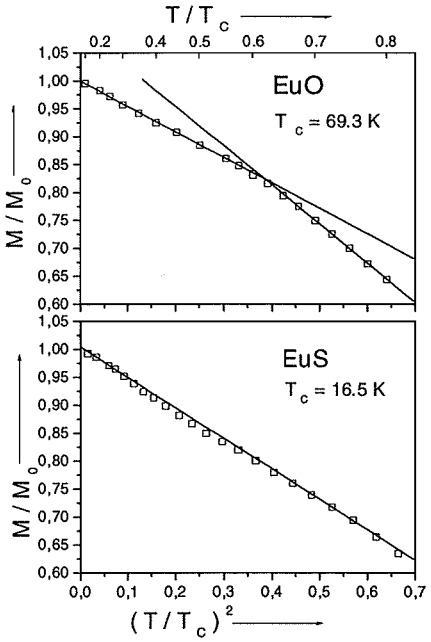

Fig.2 Spontaneous magnetization of EuO and EuS vs. squared reduced temperature. An amplitude crossover occurs for EuO but not for EuS.

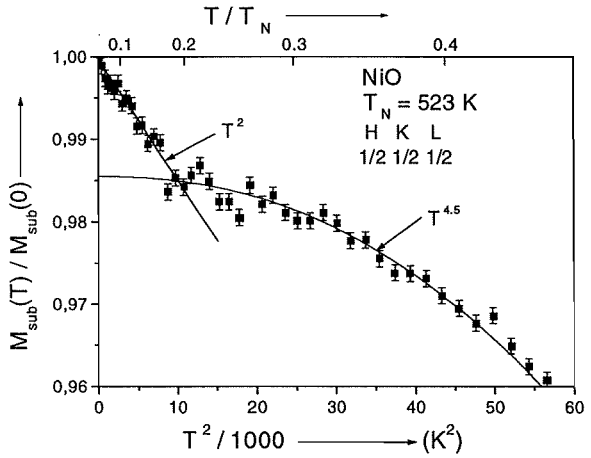

Fig.3 Exponent crossover from isotropic 3D interactions (ε=9/2) to anisotropic 3D interactions (ε=2) in cubic NiO induced by a triagonal exchange striction.

NiO with S=1 is cubic above the Néel temperature of T_N=523 K but undergoes a progressive trigonal lattice distortion with decreasing temperature. Due to the associated increasing exchange anisotropy the relevant interactions finally change from 3D isotropic (ε=9/2) to 3D anisotropic (ε=2). Fig.3 shows this exponent crossover, i.e. change of the universality class.

Originally, the exponents ε of Table I were established for insulators with well defined spin quantum numbers. Interestingly, these exponents apply also for the itinerant ferromagnets Fe, Ni and Co [4]. From the type of exponent crossover observed in cubic iron and nickel it can be concluded that the effective spin quantum number changes with temperature. At low temperatures ε=2 is well confirmed by the data of numerous authors [4]. This exponent is indicative for a half-integer spin. Our Mössbauer data in fig.4 show a clear crossover to ε=9/2 at 628 K, i.e. to an integer spin value. A semiquantitative analysis of the critical amplitude of the paramagnetic susceptibility suggests that S=2. We consider S=2 as an experimental evidence that ferromagnetic four-spin interactions are the relevant interactions in the high temperature region including the critical range.

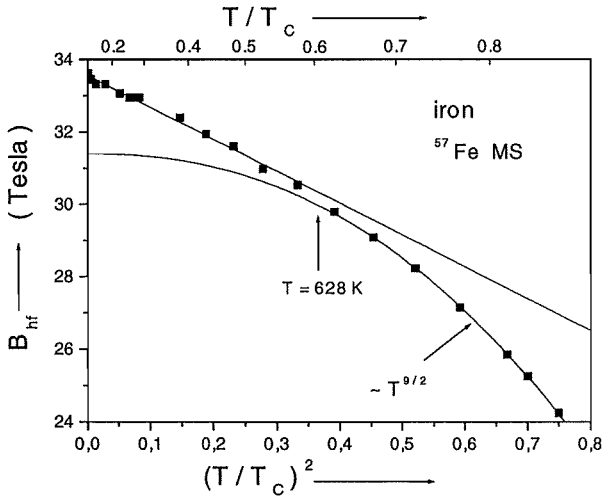

Fig.4 Exponent crossover from ε=2 to ε=9/2 in the ^{57}Fe hyperfine field of cubic iron indicating a change from a half-integer to an integer (S=2) spin quantum number.

As a conclusion, T=0 seems to be a singular point similar as $T=T_c$. In the vicinity of those points simple power functions hold exactly. At the validity limits of these power functions an analytical change (crossover) to another functional dependence can be expected. We have shown that in the simplest case the crossover is directly from the $T\rightarrow T_c$ power function to the $T\rightarrow 0$ power function. The spontaneous magnetization therefore consists of two (ore more) analytical sections.

[1] U.Köbler, A.Hoser, J.Englich, A.Snezhko, M.Kawakami, M.Beyss and K.Fischer, *J. Phys. Soc. Japan*, **70** 3089 (2001)
[2] U.Köbler, A.Hoser and D.Hupfeld, *Physica B*, to appear
[3] U.Köbler, A.Hoser, K.Fischer and M.Beyss, *Appl. Phys. A*, to appear
[4] U.Köbler, *J. Phys.:Condens. Matter*, **14** 8861 (2002)

Interlayer Exchange coupling in [Er|Tb] multilayers

J.Voigt,[1] Th.Brückel,[1] W.Schmidt,[2] and D.Wermeille[3]
[1] *IFF, Institut für Streumethoden*
[2] *IFF, Institut für Neutronenstreuung*
[3] *Advanced Photon Source, Argonne National Lab, Argonne, USA*

We report on a study of **R**esonant **X**-ray **M**agnetic **S**cattering (RXMS) from an [Er_{20}|Tb_5] multilayer. The study aims at a better understanding of the magnetic coupling in Rare Earth (RE) superlattices. The magnetic structure as resolved by neutron diffraction can be probed element-specific by the RXMS technique. Furthermore details of the interlayer exchange coupling can be accessed, since RXMS probes the relevant electronic states.

The magnetic coupling and its influence on the electronic properties in artificial superlattices attract the interest of scientists from a fundamental and a applied point of view. The different magneto-resistive effects are used for example in read-heads of hard disks or sensors for the anti-skid system in cars. But the basic physics behind the effects are still subject of investigations.
Magnetic superlattices containing RE metals were among the first systems, when the field of magnetic interlayer coupling came up again in the middle of the eighties. [1] and [2] report on long range ordered magnetic phases throughout a multilayer stack, even if the magnetic layers are separated by non-magnetic spacer layers (as a schematic view see figure 1). The thickness of a bilayer D ranges from 10-100 atomic planes. This coupling was

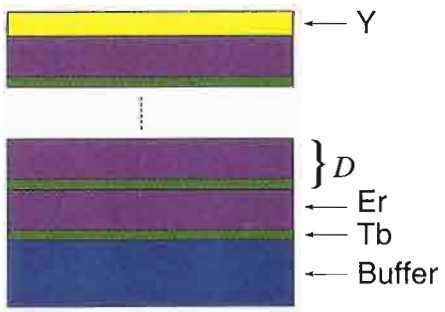

FIG. 1: Schematic view of a superlattice sample. The buffer layer provides the base for epitaxial growth, while the cap layer prevents the sample from oxidation

explained in terms of an extension to the conventional RKKY interaction, which is responsible for the magnetic order in RE metals. The conduction electrons in the spacer layer are polarized by the magnetic moments of the magnetic layers and mediate the magnetic information to the next bilayer. Complications arise, if one combines two magnetic layers with different magnetic structures. How does the resulting magnetic structure look like? The structure is determined not only by the RKKY interaction, but anisotropy and magneto-elastic forces must be taken into account.
We have investigated the magnetic structure of the [Er|Tb] system. The two materials have fairly different magnetic properties. Terbium orders at a temperature of $T_N = 230$ K in a helical structure, i.e. the magnetic moments in one basal plane of the hexagonal lattice are aligned parallel within the plane and turn by a given angle propagating along the c-direction. At $T_c = 220$ K the structure changes to a ferromagnetic alignment of all planes. In Erbium the anisotropy favors the alignment of magnetic moments perpendicular to the basal plane. At $T_N = 82$ K the c-axis component of the moment orders with a sinusoidal modulation when propagating along the c-direction. Below $T_{N1} = 54$ K a basal plane component develops, which is aligned in a helical way. A third phase transition at $T_C = 20$ K leads to a cone structure, i.e. the c-axis component orders ferromagnetically, while the basal plane component stays helical [3].
The standard tool to reveal magnetic structures is Neutron Scattering. In a diffraction experiment one resolves the structure of the sample on a atomic scale. Using neutrons as a probe, the arrangement of the nuclei and the magnetic moments of an atom define the diffraction pattern, since the neutron feels the nuclear forces and the magnetic field produced by the magnetic moment of the atom. The two interactions are comparable in strength. For RE metals it is fairly easy to distinguish the two contributions. Particularly the helical and sinusoidal phases of Erbium and Terbium lead to diffraction peaks with propagation vector 'τ' related to the layer turn angle.
This can be seen in the neutron diffraction pattern in figure 2. It shows the temperature dependent scattering from an [Er_{20}|Tb_5] superlattice, the subscripts denoting the number of atomic layers per bilayer. The bilayer unit was repeated 150 times. The main Bragg peak at (0002) doesn't change with temperature. In contrast to this structural signal the branches denoted with 'τ_{Er}' and 'τ^n_{Er}' increase in intensity and also change their position depending on the temperature. The 'branches' 'τ^n_{Er}' re-

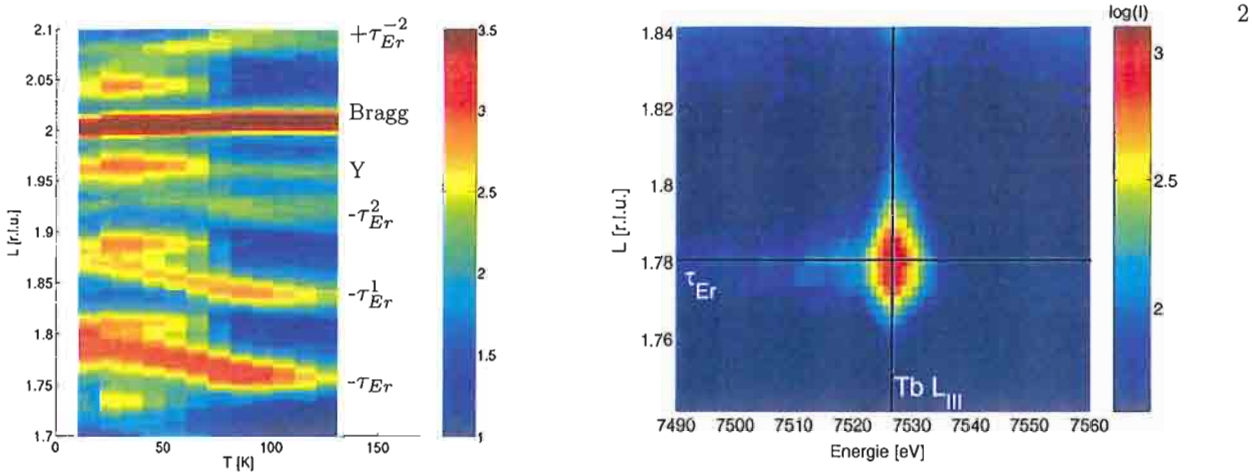

FIG. 2: Neutron diffraction (left) and RXMS (right) from an $[Er_{20}|Tb_5]$ superlattice.The color coded diffracted intensity is shown as a function of temperature respectively photon energy and reciprocal lattice coordinate corresponding to linear scans along $(000l)$.

flect the superimposed superlattice periodicity. From the existence of the satellites to the helix reflections and from the width of the helix peak we deduce a coherent magnetic helix with a coherence length of approximately 6 bilayers. The shifting position is due to a change of the turn angle from layer to layer with respect to the temperature. The value of this turn angle is about 40 °, which is close to the value of bulk Erbium. In contrast to the bulk Erbium behavior the phase transition occurs at a higher temperature and the magnetic moments in the basal plane order first into a pure helix state. At temperatures below 75 K more reflections appear, which can not be easily interpreted. We refer to [4] for details.

The magnetic neutron scattering gives the overall magnetic structure of a superlattice. The element specifity is the great advantage of RXMS. Usually magnetic scattering of photons is about six orders of magnitude weaker as compared to the charge scattering. But tuning the energy close to an absorption edge of a magnetic material can enhance the magnetic scattering by several orders of magnitude. Resonant scattering from the element in scattering condition dominates the magnetic signal. For the RE elements, large enhancements ($\geq$ 100) are observed at the L_{II} and L_{III} absorption edges. For Er and Tb, dipolar transitions $2p \rightarrow 5d$ are dominant, hence the magnetic state of the conduction electrons and not of the $4f$ electrons is probed. As mentioned above these electrons are also responsible for the transport of the magnetic information in the spacer layer. Hence the resonant scattering yields information about the coupling in our samples. The right part of figure 2 shows the scattering vector and energy dependent scattering close to the τ_{Er} peak in the vicinity of the Terbium L_{III} edge measured at a temperature of 30 K. To reduce the charge scattering we employed a polarization analyzer. The resonance enhancement of the magnetic peak is obvious. The conduction electrons in the Terbium layers are polarized according to the magnetic structure of the Erbium 4f electrons. Therefore we observe the coupling electrons responsible for the coherent magnetic structure directly.

The $[Er_{20}|Tb_5]$ superlattice shows a coherent magnetic structure with a propagation vector comparable to the one found in bulk Erbium. However, the sequence of the magnetic phases and the phase transition temperatures are changed drastically. In the artificial superlattice a magnetic structure develops in the conduction band, which fits to the quantum well structure and couples the 4f moments in the Erbium layers. This confirms the RKKY theory for the interlayer exchange coupling. Investigations of [Er|Tb] multilayers with a different composition especially on samples with thicker Terbium layers do not show the same behavior, but a long range ordering of the ferromagnetic Terbium structure [4].

The Midwest Universities Collaborative Access Team (MUCAT) sector at the APS is supported by the U.S. Department of Energy, Basic Energy Sciences, Office of Science, through the Ames Laboratory under Contract No. W-7405-Eng-82. Use of the Advanced Photon Source was supported by the U.S. Department of Energy, Basic Energy Sciences, Office of Science, under Contract No. W-31-109-eng-38.

[1] C.F.Majkrzak, J.W.Cable, J.Kwo, M.Hong, D.B.McWhan, Y.Yafet, J.V.Waszczak, C.Vettier, PRL 56, 2700(1986)

[2] M.B.Salomon, S.Sinha, J.J.Rhyne, J.E. Cunningham, R.W.Erwin, J.Borchers, C.P.Flynn, PRL 56, 259(1986)

[3] W.C.Koehler, *Magnetic Properties of Rare Earth Metals*, ed. by R.J.Elliot, Plenum Press, New York (1972)

[4] J.Voigt, p.h.d. thesis 2003

Magnetic domain formation in a laterally structured Fe / Cr multilayer

N. Ziegenhagen[1], U. Rücker[1], E. Kentzinger[1], B. Toperverg[1], Th. Brückel[1],
R. Lehmann[2], A. van der Hart[2]

[1]*IFF, Institut für Streumethoden*
[2]*Institut für Schichten und Grenzflächen, Abt. Lithographietechnik*

The top Fe layer of an Fe / Cr multilayer structure has been structured lithographically into stripes with 1 µm period. This serves as a model system for the investigation of the magnetic domain formation in layers with externally induced anisotropy due to the antiferromagnetic interlayer coupling between the structured layer and the individual unstructured layers.
Polarized neutron reflectometry and diffuse scattering under grazing incidence show strongly enhanced domain formation compared to the unstructured sample. The domains are vertically correlated throughout the multilayer. The lateral domain size is commensurable with the period of the stripe pattern of the surface layer.

Magnetic layered structures, e.g. Fe / Cr / Fe trilayers which exhibit the Giant Magnetoresistance effect, are today well-known for their applications as magnetic-field sensors or read heads of computer hard disk drives [1]. Today, much effort is undertaken for the development of a Magnetic Random Access Memory (MRAM). Due to the necessary miniaturization of such devices, the magnetic interaction between neighboring cells is becoming a more and more important parameter that has to be controlled. Furthermore, the efficiency of such a device can be reduced thoroughly by domain formation. Therefore, the influence of the geometry and the neighbourhood on the domain formation needs to be studied to be able to suppress it securely.

For measuring the magnetization and the domain pattern of layered structures, reflectometry and diffuse scattering of polarized neutrons is the method of choice, especially to access the buried magnetic layers. In contrast to integral methods such as Vibrating Sample Magnetometry or SQUID-Magnetometry, the magnetization of individual layers can be resolved, and in contrast to surface sensitive methods such as Magnetic Force Microscopy or Scanning Electron Microscopy with Polarization Analysis, the buried layers are accessible.

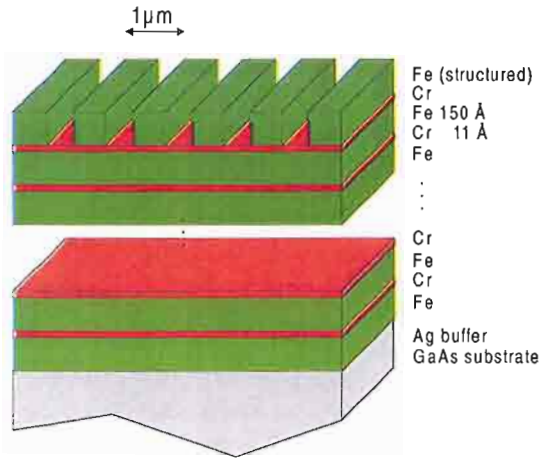

Fig. 1: Schematic sketch of the sample under investigation. The Cr interlayer thickness of 11 Å yields strong antiferromagnetic coupling between neighboring Fe layers.

Specular reflectivity (i.e. incident angle α_i = outgoing angle α_f) measures the laterally averaged structure. It is sensitive on the depth variation of the elementary composition and the mean magnetization. Diffuse or off-specular scattering (i.e. $\alpha_i \neq \alpha_f$) contains additional information about the lateral correlations, e.g. island or magnetic domain sizes. The difference between the non-spin-flip signals with spin + (R++) and spin – (R--) contains information about the magnetization components parallel and antiparallel to the external magnetic field, the spin flip signals R+- and R-+ contain information about magnetization components perpendicular to the external field. Here, + and – refer to the neutron polarization parallel and antiparallel to the external field, respectively. The first index denotes the polarization of the incident beam, the second the one of the scattered beam.

The model system under investigation is shown in Fig. 1. It is basically an epitaxial Fe / Cr (001) multilayer structure with 11 periods prepared on 1500 Å Ag buffer on a GaAs (001) single crystal. The thickness of the Fe layers is 150 Å, and the one of the Cr layers is 11 Å, yielding antiferromagnetic coupling between the neighboring Fe layers.

After deposition of the multilayer structure, the top Fe layer was patterned into stripes of 1 µm period using electron beam lithography and ion beam etching. The stripes are oriented parallel to the (100) easy magnetization axis of the Fe layers. Due to the magnetic interlayer coupling, the lateral structure of the top layer is coupled to the magnetization of the non-structured bottom layers.

Magnetization measurements with the magnetooptical Kerr effect (MOKE) show a variety of phases. When the magnetic field is oriented parallel to the stripes, the structure is saturated magnetically above $\mu_0 H$ = 35 mT. Between 35 and 17 mT, a region is identified, where the magnetizations of adjacent layers are oriented almost perpendicular to each other. This behaviour results from the competition between antiferromagnetic coupling, crystalline anisotropy and Zeeman energy. It is observed in the same way with the unstructured sample. Between 17 mT and 6 mT, a complex phase is observed, that is discussed below. This complex phase does not appear in the unstructured sample.

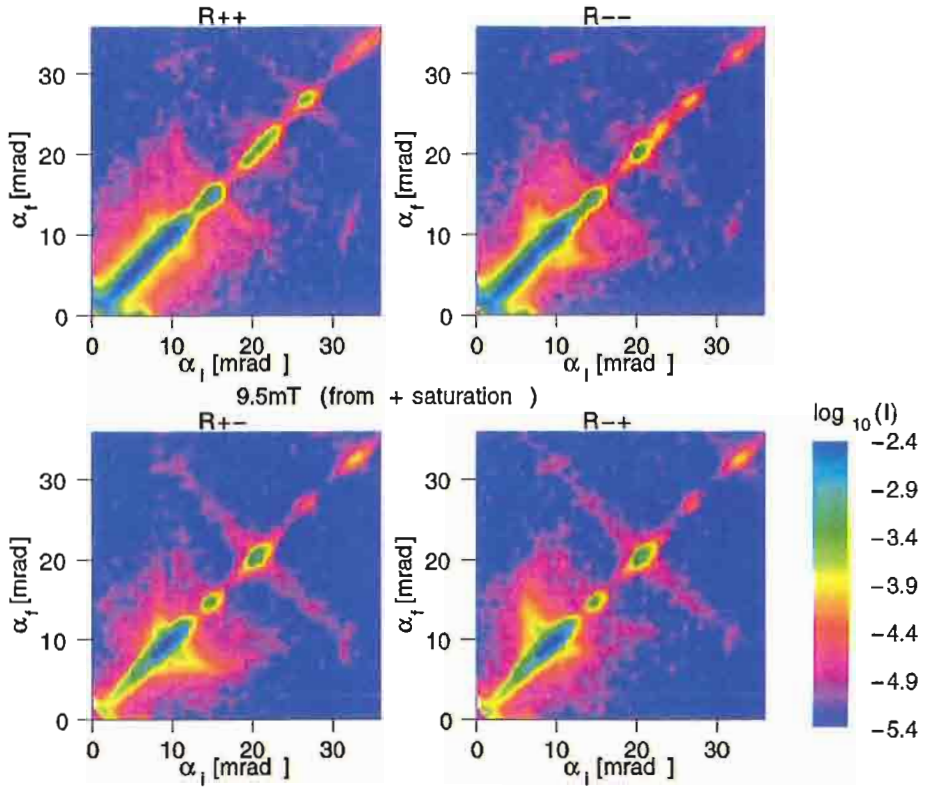

Fig. 2: Reflectivity and diffuse scattering under grazing incidence of polarized neutrons with polarization analysis as measured on the HADAS-reflectometer in ELLA (FRJ-2 Jülich). The scattered intensity (on a logarithmic colour scale) is plotted against incident angle α_i and outgoing angle α_f of the polarized neutrons. The specular reflectivity ($\alpha_i = \alpha_f$) is shown on the main diagonal in each plot. The four polarization channels are R++ non-spin-flip with the neutron spin along the direction of the applied magnetic field, R-- non-spin-flip with the neutron spin antiparallel to the magnetic field direction and R+- and R-+ spin-flip with the incident neutron spin parallel or antiparallel to the magnetic field, respectively.

Below 6 mT, a state without remanent magnetization is observed. As seen from polarized neutron reflectometry and off-specular scattering, the magnetic layered structure is completely split into columnar domains. In each single domain, the magnetization of the neighboring layers is oriented antiparallel to each other. No preferred orientation against the remaining external field and therefore no net magnetization is observed.

Reflectivity and diffuse scattering under grazing incidence of polarized neutrons with polarization analysis have been measured at the HADAS reflectometer [2] in the neutron guide hall ELLA at the Jülich research reactor FRJ-2 (DIDO). Fig. 2 shows the four different polarization channels, measured at $\mu_0 H$ = 9.5 mT, i.e. in the intermediate, complex magnetization state.

On the diagonal of each figure, the specular reflectivity ($\alpha_i = \alpha_f$) is displayed. Beginning at small angles, one can see the total reflection plateau (only in the non-spin-flip channels), a half order peak (representing the double of the period of the multilayer structure, not resolved from the plateau in R++), the first order multilayer peak at about α_i = 16 mrad, and the peaks with the orders 3/2, 2 and 5/2.

The appearance of the half order peaks is a clear indication of antiferromagnetic orientation of neighboring Fe layers. But it is clearly visible, that the 3/2 order and 5/2 order peaks are only sharp in the spin-flip channels, not in the non-spin-flip channels.

A lot of diffuse scattering is seen, that indicates domain formation within the sample. Compared to the unstructured sample, the diffuse scattering is enhanced by a factor of 3, and the extension away from the specular line is much longer, indicating a smaller domain size. The diffuse scattering is mainly concentrated in Bragg sheets around the half order specular peaks. This indicates a strong vertical correlation between the domain pattern in adjacent layers. So we observe columnar alternating domains throughout the complete multilayer stack.

At the Bragg sheet across the 3/2 order peak, in all four polarization channels the first order diffraction maximum of the lateral grating can be seen (at about $\alpha_i = 32$ mrad and $\alpha_f = 10$ mrad and vice versa). In contrast to that, at saturation field, the lateral diffraction maximum can only be observed in the R++ channel. This shows, that there is a tendency for the magnetic domains to order according to the pattern of the top layer. Furthermore, in the two spin-flip channels, a half order lateral diffraction maximum is observed, indicating that the domains in some part of the sample have twice the period of the patterned surface.

Up to now, we have not yet found a suitable model to describe quantitatively the complete diffuse scattering observed. Nevertheless, we have found a description of the specular reflectivity, that reproduces the different peak width in non-spin-flip and spin-flip for the half order peaks. They can be described assuming a structure, in that the component of the magnetization perpendicular to the stripes is alternating regularly, while the magnetization component parallel to the stripes shows one phase slip between the 3rd and the 4th layer (counted from the top). With this magnetic structure, a net magnetization along the field is achieved with minimal cost of exchange energy favoring the antiferromagnetic coupling.

[1] A. Fert, P. Grünberg, A. Barthélémy, F. Petroff, W. Zinn, *J. Magn. Magn. Mat.* **140-144**, 1 (1995)
[2] U. Rücker, E. Kentzinger, B. Alefeld, W. Bergs, Th. Brückel, *IFF Scientific Report* 2000 / 2001, 79; U. Rücker, W. Bergs, B. Alefeld, E. Kentzinger, Th. Brückel, *Physica B* **297**, 140 (2001)

Ordering in Ferrofluids Measured on the New Focusing-Mirror USANS Diffractometer KWS-3

A. Vorobiev[a,b], G. Gordeev[b], E. Kentzinger[c], B. Toperverg[c]
[a] *Max Plack Institut für Metalforschung, Stuttgart, Germany*
[b] *Petersburg Nuclear Physics Institute, Gatchina, 188350 St. Petersburg, Russia*
[c] *Institut für Streumethoden*

For the first time, ordering in real (opaque) ferrofluids have been measured by ultra-small angle neutron scattering (USANS) on the new and worldwide unique focusing-mirror SANS spectrometer in Jülich (KWS-3@FRJ-2). This experiment confirms the presence of nuclear scattering density correlations on a length scale two orders of magnitude greater than the single particle size, i.e. in the micrometer range.

Ferrofluids (FF) are stable colloidal suspensions of fine (10 nm in diameter) single domain magnetic particles coated with a non-magnetic molecular surfactant shell [1]. Since the time of FF's discovery they are an attractive subject for both fundamental science and industrial applications [2]. The same kind of objects, self- organized on a substrate, are thought to be the basis for the next step to increase the storage capacity of magnetic recording media (100 Tbits/in^2). [3]

An external magnetic field tends to order dipolar moments parallel to each other. Parallel orientation promotes chaining of particles, while it increases the repulsion between them in the plane perpendicular to the field, i.e. repulsion between chains. On the other hand, thermal motion of particles tends to destroy those field-induced structures reducing also the correlation length along the chains as well as their lifetime. Depending on the ferrofluid concentration, the magnetic field strength, the temperature, the type of surfactant and solvent, one can expect a variety of possible ordered structures, e.g., (anti-) ferromagnetic, spin-glass, or fractal objects.

Light scattering and optical microscopy studies have confirmed that FF particles can be arranged in various structures depending on the external magnetic field strength and direction. However, real (i.e. not diluted) FF are completely opaque. This is why small angle neutron scattering (SANS) remains the most suitable tool to carry out the investigation of the bulk structure of *real* FF with normal concentrations and thicknesses. In our early experiments [4,5] of polarized neutron small angle scattering carried out at PNPI we found some indications of possible spatial ordering in 4 % (volume concentration) FF while single particle parameters were well determined.

To get a better insight on the spatial ordering in real FF, we performed an USANS study on the new focusing-mirror SANS diffractometer in Jülich (KWS-3@FRJ-2). The principle of this instrument is an one-to-one image of an entrance slit (typically 2×2 mm^2) on a detector by neutron reflection on a double focusing elliptical mirror. The entrance slit is placed in a focus of the mirror, the detector in the other. The sample is placed just after the mirror [6]. Compared to a conventional pinhole SANS instrument of the same length, a focusing mirror SANS diffractometer has considerable intensity advantages for a scattering wave-vector resolution (δQ) below 7×10^{-3} Å^{-1}. For $\delta Q = 10^{-4}$ Å^{-1}, a focusing mirror SANS wins by about four orders of magnitudes and its intensity is still comparable to that of a pinhole SANS at $\delta Q = 10^{-3}$ Å^{-1} [7]. The big technical challenge was to build a high quality mirror with a shape as close as possible to an ellipsoid with a very smooth surface (structural roughness less than 5 Å rms) in order to suppress as much as possible off-specular scattering. Our mirror was manufactured using technology developed for x-ray space telescopes [8]. To date, KWS-3 is the worldwide unique neutron scattering machine running on this principle.

We present here two examples of measurements performed on a 3.3 % FF in deuterated solvent. In order to cover the whole cross section of the incident beam (10×2 cm^2), the sample was put in a cell 11 cm wide, 4 cm high and 1 mm thick, the longest edges being perpendicular to the incident beam. In FIG. 1 and 2, differences between measurements performed with and without field are displayed. In FIG. 1, those differences are displayed on a logarithmic scale, in FIG. 2 on a linear scale.

In the pictures on the left-hand sides, the field was applied horizontally, along the longest side of the sample cell, i.e. along the Q_x axis. The intensities vary and stay concentrated inside a vertical stripe, oriented along the Q_z axis. This shows that the ferromagnetic particles order in stripes oriented parallel to the applied field, as schematically represented on the left-hand side of FIG. 3. The average distance between the stripes is given by the distance between the two minima, i.e. approximately 2 μm.

In the pictures on the right-hand sides, the field was also applied horizontally, but this time along the primary beam, i.e. perpendicular to the two longest sides of the cell. In that case the ordering looks a bit more complicated than above. Two types of ordering seem to compete, both of them tending to order the ferrofluids along stripes perpendicular to the applied field. This tendency can be understood if one considers the cell geometry and the magnetic shape anisotropy that it induces. One ten-

dency, similar to the one above, tends to order the particles along stripes oriented along the longest side of the sample cell. The other one tends to order the particles into stripes along one of the two the diagonals of the cell, as schematically represented on the right-hand side of FIG. 3. As a matter of fact, the angle between the two types of ordering is very close to the one that makes one of the diagonals of the cell with respect to the horizontal. The fact that the second type of ordering appears along only one of the two diagonals can be explained by a slight misalignment of the magnetic field with respect to its nominal direction. The width perpendicular to the intensity modulation of the ordering along one of the diagonals of the cell is larger than the one perpendicular to the intensity modulations due to the ordering along the horizontal. This shows that, in the former case, the average length of the chains is smaller than in the latter case.

To conclude, for the first time we were able to measure the ordering in the bulk of real ferrofluids, having access to correlations in the micrometer range. For this we used the new and worldwide unique focusing mirror USANS machine recently installed in the guide hall ELLA of the research reactor in Jülich, KWS-3@FRJ-2. Depending on the orientation of the applied magnetic field, different types of ordering were observed. A simulation of the data will give access to the exact size, exact orientation, and the distance between the chains. Within the next months, polarized neutrons will be available at KWS-3, permitting to discriminate between nuclear and magnetic correlations.

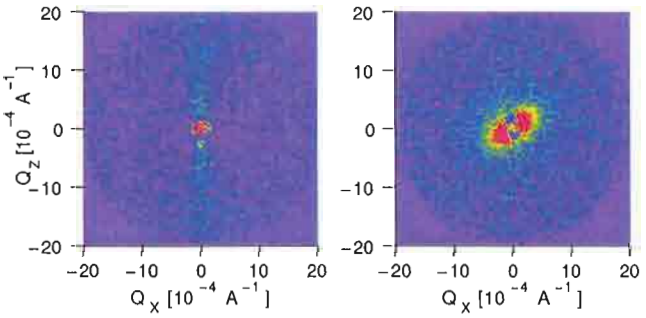

FIG. 1. Differences between intensities measured from a 3.3 % (volume concentration) ferrofluid under a magnetic field of 11.4 mT and under zero field. Intensities are displayed on a logarithmic scale and only differences greater than one are displayed. In the top picture, the field was applied along the Q_x-axis (i.e. perpendicular to the incident beam). In the bottom one, the field was applied perpendicular to the (Q_x-Q_z) plane (i.e. parallel to the incident beam). The color scale extends from 0 (violet) to 2 (red).

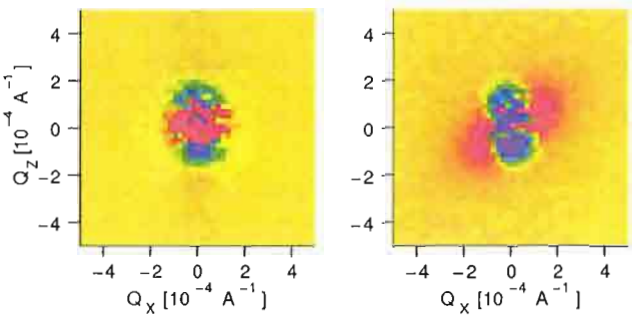

FIG. 2. Same as above. Here, the differences are displayed on a linear scale and the range of scattering wave vectors is smaller than above. The color scale extends from -1500 (violet) to 500 (red). 0 corresponds to yellow.

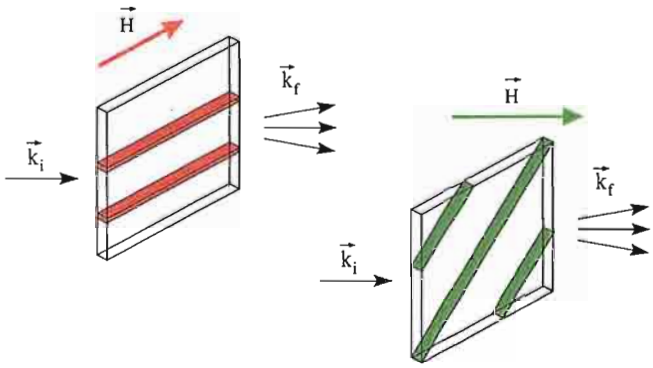

FIG. 3. Schematic representation of the two types of ordering encountered above. On the left-hand side the magnetic field H is applied along the longest side of the cell, on the right-hand side perpendicular to the cell

[1] R.E. Rosensweig, *Ferrohydrodynamics*, Cambridge University Press (1985)

[2] V.M. Berkovski , *Magnetic Fluids. Engineering applications* (1993)

[3] D. Weller, talk held at the "294. WE-Hereaus Seminar: Frontiers in Nanomagnetism" in Bad-Honnef, Germany, January 2003.

[4] B. Toperverg, A. Vorobyev, G. Gordeyev, A. Lazebnik, Th. Rekveldt, W. Kraan, Physica B **267-268**, 203 (1999)

[5] A. Vorobiev, B. Toperverg, L. Axelrod, G. Gordeev, V, Kraan, I. Lazebnik, D. Orlova, Th. Rekveld Physica B **276-278**, 694 (2000)

[6] B. Alefeld, L. Dohmen, D. Richter, Th. Brückel Physica B **283**, 330 (2000)

[7] B. Alefeld, L. Dohmen, D. Richter, Th. Brückel Physica B **276**, 52 (2000)

[8] B. Aschenbach, Rep. Prog. Phys. **48**, 579 (1985)

Sr^{2+}-Induced Collapse of Sodium Polyacrylate Chains as Assessed by Anomalous Small-Angle X-ray Scattering

G. Goerigk, R. Schweins[1], K. Huber[1] and M. Ballauff[2]

Institut für Streumethoden, IFF
[1]Fachbereich 13 Chemie und Chemietechnik, Universität Paderborn, Warburger Str. 100, 33098 Paderborn, Germany
[2]Polymer Institut, Universität Karlsruhe, Kaiserstr. 12, 76128 Karlsruhe, Germany

The distribution of Sr-counterions around polyacrylate chains in aqueous solution was studied by anomalous small-angle X-ray scattering. Different ratios of the concentrations of $SrCl_2$/[NaPA] reveal dramatic changes in the scattering curves. At the lower ratio the scattering curves indicate a coil like behavior, while at the higher ratio the scattering curves are contracted to smaller q-values, possibly caused by the collapse of the NaPA coil to pearl-like subdomains.

Polyelectrolytes are highly charged macromolecules. The density of charges along the polymer chain may cause a wide variety of conformations. A large variety of polyelectrolytes is found in nature, where the role of electric charges is essential for the proper functioning of nucleic acids, the numerous enzymes and proteins.

Due to the high charge density concentrated on the chain, polyelectrolytes show an unusual behavior in many ways. There is a strong interaction between the segments of the same chain and other macromolecules which clearly indicates a long range electrostatic potential. The latter has its image in the counterion distribution around charged polymer chains. The conformational and folding properties of polyelectrolytes and their specific functioning could be better understood if the spatial distribution of the various kinds of free ions of the solvent could be determined.

Anomalous small-angle X-ray scattering (ASAXS) with synchrotron radiation is a suitable experimental technique, which allows the structural characterisation of the counterion distribution around the macroions by tuning the energy in the vicinity of the absorption edge of the ion in question. The distribution of the counterions is not accessible by conventional SAXS measurements, because the scattering contributions of the counterions and the macroions superimpose and cannot be distinguished. The first ASAXS experiments of counterion distributions were reported by Stuhrmann [1] and more recent results are published in [2-4].

The present contribution deals with the conformation of the sodium salt of polyacrylic acid (NaPA) in aqueous solutions with 0.01 M NaCl and pH 9. NaCl was added in order to screen the electrostatic interaction between dissociated carboxylate groups, which leads to a coiled chain conformation of the polyanions. In contradiction to Na^+, Sr^{2+} binds specifically and more tightly to the carboxylate groups. This interaction neutralizes the polyanions to a large extent, and due to the hydrophobic nature of the backbone, leads to a collapse of the polyelectrolyte chains. Theoretical work on this shrinking process, based on scaling arguments and Monte Carlo simulations propose that polyeclectrolyte structure passes elongated intermediates like cigars or pearl necklaces [5,6] before reaching the spherical shape. However, these conformations have not yet been observed experimentally. If a large fraction of the carboxylate sites is occupied by Sr^{2+} ions, the spacial distribution of the Sr^{2+} ions should reflect the monomer density distribution within the collapsing chain and anomalous small angle X-ray scattering (ASAXS) may be a well-suited experimental technique to study the correlation of the macroion with its counterions [1-4].

First, a stock solution of NaPA (supplier: Polysciences, Eppelheim, Germany) was prepared in bidistilled water with 0.01 M NaCl and pH 9. After 3 days, this solution was combined with a $SrCl_2$ solution with pH 9 and $2[Sr^{2+}]+[Na^+]=0.01M$ [7]. The Sr^{2+} content thereby is set to 1.5 mM. In order to approach the precipitation limit, several polymer concentrations were produced by diluting with a solution with 1.5 mM $SrCl_2$, pH 9 and $[Sr^{2+}]+[Na^+]=0.01M$, i.e. with a constant concentration of cationic charges. Preliminary measurements using combined static and dynamic light scattering (ALV 5000E CGS) allowed us to get first information on the shape of the polymer chains in dependence on the ratio of $[Sr^{2+}]$/[NaPA]. Finally, two samples differing in the polymer concentration were chosen: P4KE corresponds to [NaPA] = 3.61 mM, i.e. $[Sr^{2+}]$/[NaPA] = 0.42, P4KU2 corresponds to [NaPA] = 3.25 mM, i.e. $[Sr^{2+}]$/[NaPA] = 0.46 which is close to the border line of phase separation. Compared to coiled chains in Sr^{2+}-free solutions, the polyanion dimensions of both

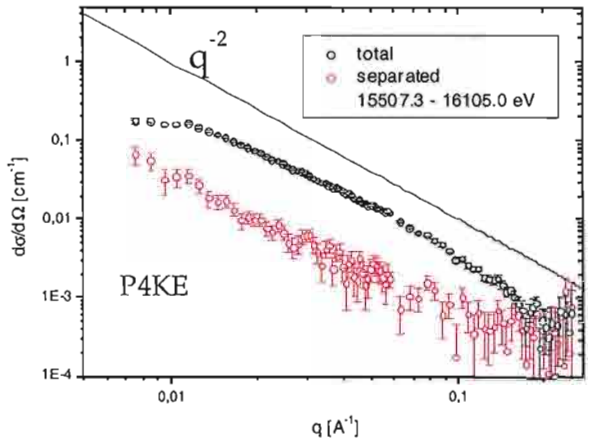

Figure 1: ASAXS measurements of the collapsed NaPA chains ([NaPA] = 3.61 mM; $[SR^{2+}]/[NaPA]=0.46$) at the Sr-K-absorption edge at 16.105 keV. The black scattering curve represents the scattering from the polymer and the Sr^{2+} ions. The red scattering curve is the separated scattering curve of the Sr^{2+} ions.

samples are significantly shrunken. The two samples as well as the solvent (containing the same amount of Sr^{2+}) were filled into capillaries from Hilgenberg GmbH, Malsfeld, Germany. The capillaries are made of borosilicate glass with an inner diameter of 4 mm and a wall thickness of 0.05 mm. The inner diameter of 4 mm is nearly the optimal size for the energy range of the Sr-K edge at 16.105 keV. The capillaries were closed with a pipette plug fixed by two component quick setting adhesive.

ASAXS measurements were performed at the JUSIFA beamline at HASYLAB, DESY Hamburg in the energy range of the K-absorption edge of Strontium at 16.105 keV. The energy dependence of the small angle X-ray scattering near the K-absorption edge of Sr is used to separate the scattering due specifically to the Sr-ions.

In Figure 1 the scattering curves of NaPA-chains at [NaPA]=3.61 mM (P4KE) obtained from SAXS measurements are shown. The total as well as the separated scattering curve follows a power law of $d\sigma/d\Omega \sim q^{-\alpha}$. The exponent α is close to 2 for both curves, indicating a coil like behavior [8]. However, it is worth mentioning that the separated curve reveals undulations which points to the occurence of spherical subdomains as would be expected for a pearl necklace [5].

The scattering curves (total and separated in Figure 2) of a second sample (P4KU2) with a smaller concentration of NaPA ([NaPA] = 3.25 mM), but the same $SrCl_2$ content as P4KE show a different behavior. However, the separated scattering curve (red) obtained from SAXS measurements at the two energies 15.507 and 16.105 keV exhibits a similar characteristic for $q > 0.02$ 1/Å with pronounced maxima, minima and shoulders indicating a scattering function, which again seems to be influenced by correlation effects between rather monodisperse subdomains within the collapsing chains. The total scattering curve (black) measured at 15.507 keV shows several shoulders and is compatible with the form factor of a polydisperse sphere, which is modulated by interparticle scattering contributions. The latter is indicated by additional SANS measurements extended to smaller q-values. Possibly the NaPA coil collapses to a sphere whereby the structure of pearl-like subdomains is preserved.

Thereby the measurements clearly reveal significant contributions from non-uniformly distributed Sr-counterions imaging the monomer distribution.

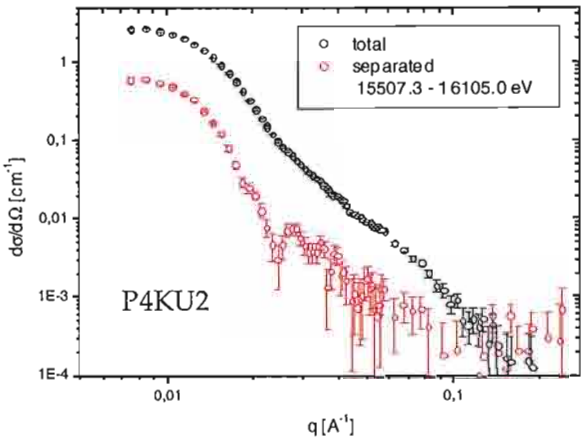

Figure 2: ASAXS measurements of the collapsed to sphere NaPA chains ([NaPA] = 3.25 mM; $[SR^{2+}]/[NaPA]=0.41$) at the Sr-K-absorption edge at 16.105 keV. The black scattering curve represents the scattering from the polymer and the counterions. The red scattering curve is the separated scattering curve of the Sr^{2+} ions.

[1] H B. Stuhrmann, Advances in Polymer Science 67, 123-163 (1985)

[2] Q. de Robilliard, X. Guo, N. Dingenouts, M. Ballauff, and G. Goerigk, Macromol. Symp. 164, 81 (2001)

[3] B. Guilleaume, M. Ballauff, G. Goerigk, M. Wittemann, and M. Rehahn, Colloid Polym. Sci. 279:829-835 (2001)

[4] B. Guilleaume, J. Blaul, M. Ballauff, M. Wittemann, M. Rehahn, and G.Goerigk, Eur.Phys.J. E8, 299-309 (2002)

[5] A P. Chodanowski and S. Stoll, J. Chem. Phys. 1999, 111, 6069ff; U. Micka, C. Holm, K. Kremer, Langmuir, 1999, 15, 4033ff

[6] A.V. Dobrynin, M. Rubinstein and S. P. Obukhov, Macromolecules 1996, 29, 2974ff

[7] R. Schweins and K. Huber, Eur. Phys. J. E, 2001, 5, 117ff

[8] M. Ragnetti and R.C. Oberthür, Coll. Polym. Sci., 1986, 32, 264ff

Development of the ESS-target-module

J.Chen[a], P.Jung[a], H.Klein[a], T.Koppitz[b], H.Soltner[b], A.Soukhanova[b], J.Wolters[b] M.Rödig[c], R.Herzog[d], B.Werner[d],
[a])Institut für Streumethoden, [b]) ZAT, [c])BD-Z, [d]) IWV2

In 2002 IFF contributed to the development of the ESS liquid mercury target module within the ESS-project mainly through the following tasks:

1) Experimental and computational studies of the effect of pressure pulses on the target structure, induced by the pulsed proton beam in the liquid metal.
2) Development and testing of means to mitigate these effects, mainly by introducing gas bubbles into mercury and by surface hardening of the structural materials.
3) Development of devices and study of high-cycle-fatigue and corrosion behaviour of structural materials in liquid mercury.
4) Studies on radiation damage of ESS candidate structural materials under proton and neutron irradiation, including investigations of the specific effects of the light transmutation products hydrogen and helium.

Two target stations for short (1.2 μs) and long (2 ms) pulses are planned for the European Spallation Source (ESS). According to a feasibility study [1], liquid mercury will be used as target material in both cases. Technical details of these targets, including fabrication as well as lifetime and cost estimates will be described in a baseline report at the end of 2003. This will comprise a detailed description of the target module itself, of surrounding moderators, reflectors, shielding as well as of auxiliary and ancillary systems, remote handling and building etc.. The work to this aim is coordinated in the FZJ Project European Spallation Source (PES). In the following four tasks are addressed which have mainly been performed at IFF. Other important contributions, e.g. on thermal-hydraulics and on fabrication technology have been performed elsewhere.

Pressure pulse effects

The pressure pulses in the liquid mercury, induced by the pulsed proton beam cause severe stresses on the mercury containment. These strongly restrict the choice of candidate structural materials. Fig.1 compares calculated maximum stress induced by ESS-typical 5 MW beam pulses and the thermal stresses induced by temperature differences to the respective yield strengths. Pulse and thermal stresses show 1/d and d^2 dependence on thickness, respectively, and increase about linearly with beam power. These results show for example that in austenitic stainless steels (316L) both pulse and thermal stresses are above the yield strength at all thicknesses. Even if the pulse stresses could be reduced by mitigation methods (see below), the thermal stresses would limit the possible window thickness to less than 1 mm in this material. Inconel 718 (IN718) and tantalum (Ta) are ruled out due to low radiation resistance and limited database, respectively. Thus, only martensitic steels (e.g. the 12%Cr steel MANET) remain as feasible structural materials for the ESS target

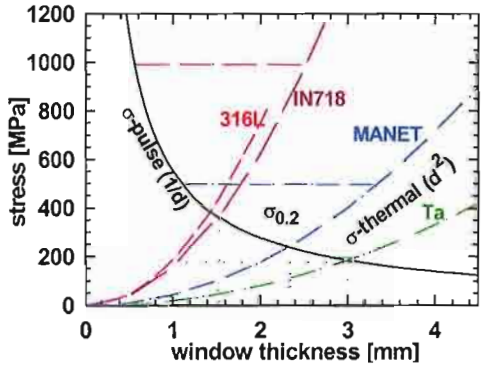

Fig.1 : Pulse (left), yield (horizontal) and thermal (right) stresses in four candidate structural materials of ESS. The cross-overs indicate optimum window thicknesses (vertical dotted lines).

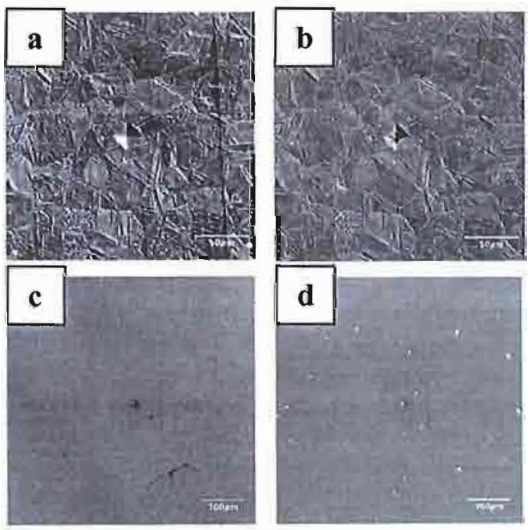

Fig.2 : SEM pictures of 12%Cr steel in hard (a, b) and standard (c, d) condition, before (a, c) and after (b, d) irradiation with 100 pulses of 0.8 GeV protons at LANSCE.

Aside from stresses, the pulsed nature of the ESS proton beam also induces surface damage on the structural materials, which is ascribed to cavitation. Fig.2 shows scanning electron microscope (SEM) pictures of a 12%Cr steel (DIN1.4922) irradiated with 100 pulses of 0.8 GeV protons in the WNR device at LANSCE, Los Alamos. In the standard condition (Fig.1d) a lot of small erosion pits are observed, but virtually none in the hardened material (Fig.1b). This indicates that the steel in the hardened condition is much more resistant to cavitation damage than in standard condition. On the other hand the higher ductility of the standard condition is indispensable for operation. Therefore the possibility of surface-hardening is examined by pulsing or scanning of electron- or laser-beams across the surface.

Wide extrapolation is necessary from the above relatively small number of pulses and low beam power to ESS relevant conditions. Therefore devices are developed to produce pressure pulses in liquid mercury outside such expensive and radioactive irradiation facilities. Mainly inductive techniques are employed to induce pulsed power into mercury, such as for example used in lithotripters. An advantage of Hg is, that the pulsed power can be directly coupled into the liquid metal.

Pressure pulse mitigation

While surface-hardening may reduce cavitation damage, methods are examined to reduce the pressure pulse itself. The two basic properties of mercury which are involved in the development and spreading of the pressure pulse are thermal expansivity α and compressibility κ. While the possiblities to reduce α (for example by alloying Hg with Tl) are rather limited, various methods to increase κ have been examined. The most promising seems to be introduction of tiny bubbles of uncondensable gas. To reach the needed small diameters of typically 20 µm, large shear forces are necessary due to the high surface energy of mercury. Several devices have been designed and proved successfully in water and in a substitute liquid metal (GaInSn) and will be tested soon in a large mercury loop at IPUL Riga.

High cycle fatigue and corrosion

The 1.2 µs pulses with 50 Hz repetition rate of the ESS short pulse target imposes stresses of an unique time structure on the target structure. Further uncommon environmental features are the presence of liquid Hg and of heavy irradiation. These conditions are simulated in conventional as well as pulsed high-cycle-fatigue (HCF) devices. Fig.3 shows a small device which has proven its ability to produce pulsed stresses of ESS-relevant time structure. The influence of irradiation is simulated by using spent target materials from spallation devices (LANSCE, ISIS, SINQ). In other more conventional experiments the effect of composition and surface treatment on HCF is studied.

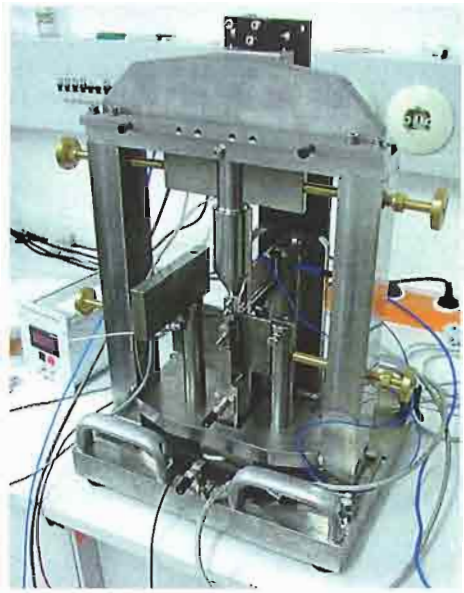

Fig.3 : HCF device for the application of pulsed stresses (FATIMA).

Radiation damage

The spent targets are also used to study the effect of irradiation on mechanical properties and microstructure [2]. Austenitic and martensitic steels, Ni-base alloys and pure tantalum have been investigated. For detailed studies on fracture behaviour a small-punch device is under construction. An outstanding feature of the high energy proton irradiation in ESS is the high production rate of spallation products, mainly hydrogen and helium. Their effect on tensile properties have been reported last year. This work performed at the Jülich compact cyclotron has been extended to a large regime of doses and temperatures [3]. The results show strong embrittlement by helium, mainly at lower temperatures. This indicates that the behaviour of materials in a spallation source cannot be simply extrapolated from behaviour in other devices. Therefore specimens are irradiated in SINQ (PSI), the only presently available spallation source for material testing.

This work was partially supported by the European Community under the SPIRE (Spallation and Irradiation Effects) project, Contract FIKW-CT-2000-00058. Part of the work was performed in collaboration with CEA-Saclay, IMH-FzKarlsruhe, IPUL-Riga, PSI-Villigen, TU-Ilmenau, TU-Braunschweig.

[1] The European Spallation Source Study, Vol.III, Report ESS-96-53-M (1996)
[2] J.Chen et.al., 5th IWSMT, Charleston 2002, accepted for J.Nucl.Mater.
[3] P.Jung et.al., ibid.

Inelastic Neutron Scattering from CH_4 - clathrate, THF- clathrate and Ice

H. Conrad[1], W. Kuhs[2], K. Nünighoff[3], M. Prager[4], W. Schweika[1]
[1] *Institute Scattering Methods, IFF*
[2] *Göttinger Zentrum Geowissenschaften, Universität Göttingen*
[3] *Institute for Nuclear Physics, FZJ*
[4] *Institute Neutron Scattering, IFF*

Inelastic neutron scattering with emphasis on energetically low lying modes has been performed on three prospective advanced cold moderator materials. Employing the time-of-flight instruments SV29 and DNS at the Jülich FRJ-2 reactor, spectra have been obtained from synthetic methane clathrate, tetrahydrofurane (THF) clathrate and light water ice at several temperatures between 2 K and 70 K. Clearly separated excitations at energy transfers of ±1 meV, +2 meV and +3 meV have been observed with synthetic methane clathrate. In hexagonal ice at T = 2 K up to now unreported low lying energy levels were found at energy transfers of 1.8 meV and 2.8 meV. An additional line at about 10 meV could be detected in the THF clathrate, which is most likely due to the embedded THF molecule.

The motivation for the investigations described in this note is the development of advanced cold neutron moderators in particular with respect to pulsed spallation sources. Solid methane at low temperatures, e.g. T = 20 K, is generally considered the best moderator medium for cold neutron sources. In contrast to liquid hydrogen at the same temperature it experimentally exhibits a Maxwellian spectrum with a "neutronic" temperature of about 23 K. The observation that neutrons are virtually in thermal equilibrium with methane at this temperature is attributed to the low lying energy levels, which in turn are believed to be due to the free rotations of a limited number of methane molecules in the solid phase. In addition, methane yields an intensity gain of a factor of 3 to 4 at neutron energies around 2 meV as compared to liquid hydrogen.

A not quite as perfect cold spectrum is observed with water ice at 20 K. On the other hand, ice shows an extended slowing down spectrum covering the so-called thermal neutron energy range (ambient temperature regime). This would entail narrower neutron pulse widths (better resolution for time-of-flight spectrometers) than those obtainable from common ambient temperature water moderators.

Therefore, a combination of methane and water at low temperatures could be the ideal moderator over a broad energy range from 2 meV up to, say, 100 meV. Indeed, there are inclusion compounds of gases or other molecules in water, the clathrates, which might exactly serve this purpose. A well-known example is methane clathrate, a substance, which even occurs naturally on the deep sea floor. Unfortunately, it is only stable under these conditions (high pressure and/or low temperature). On the other hand, inelastic neutron scattering on a few samples of natural deep sea methane clathrates revealed nearly the same low energy levels, which have been discovered long ago with pure solid methane [1].

Since the proper composition of natural methane clathrate is not predictable, we investigated the spectral properties of synthetic material with the correct stoichiometric ratio of one methane molecule per six water molecules. The results of the inelastic neutron experiments are presented below.

Due to the technical difficulties with the synthesis of methane clathrate (30 bars at 70 K), it seems worthwhile to search for a compound easier to produce, such as tetrahydrofurane (THF) clathrate. The room temperature liquid THF (C_4H_8O) and water mix easily and form an inclusion compound at 6°C. This hydrate composed of one THF per 17 water molecules can thereafter easily be cooled down to cryogenic temperatures.

In order to complete our studies with respect to searching for low lying excitations in solid cryogenic moderator media we also did some measurements with water ice, which is still a candidate for pulsed sources due to reasons described above. Furthermore, water ice not only is simple to produce, but at temperatures as low as 5 K has an extremely high thermal conductivity, which is important for removing the power deposited by the primary neutron source (nuclear heating).

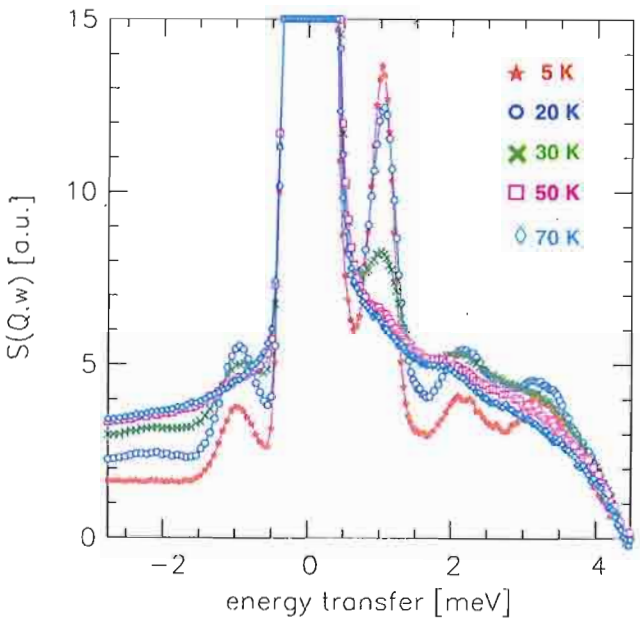

FIG. 1: Inelastic spectrum from synthetic methane clathrate at 5 different temperatures (E_0 = 7 meV, δE = 0.4 meV; Q_0 = 2.9 Å^{-1}).

The experiments have been conducted at the time-of-flight spectrometer for thermal neutrons, SV29, and the spectrometer for diffuse scattering, DNS, at the FRJ-2 reactor. In order to find the respective optimum range for energy transfer with simultaneously obtaining the required energy resolution, the measurements have been performed with

three different incoming energies, 7 meV, 26 meV and 41 meV. A distinct separation of the expected lowest rotational levels (±1 meV, +2 meV and +3 meV) from the elastic line was possible with 7 meV, as can be seen in Fig. 1. It should be noted that at the highest temperature of 70 K the discrete lines of the free rotations are smeared out to a quasi-elastic line due to diffusional motions. The energies of the observed lines at the lowest temperature corresponds perfectly to the lines found with natural deep sea methane clathrate [2].

The important point is that the production scheme for methane clathrate developed in Göttingen not only yields the desired quality with respect to the microscopic properties, but also is suitable for mass production. The latter is of utmost importance for a real cold neutron source, where amounts of the order of one liter are required. In fact, for the moderator experiments described below, about 900 g of this compound were used.

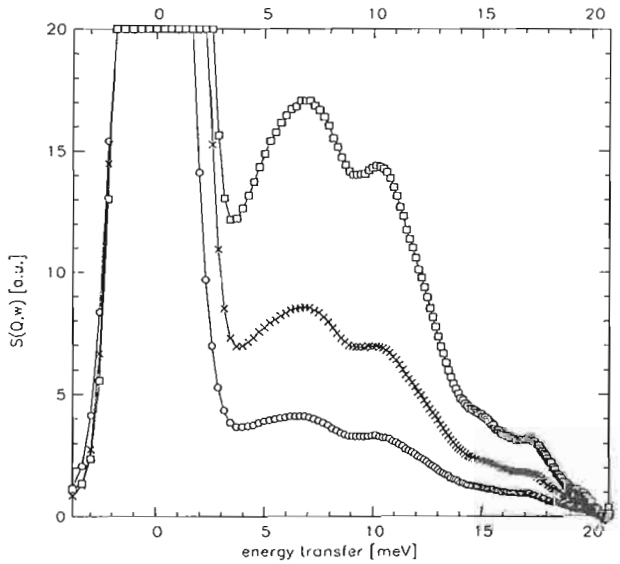

FIG. 2: Inelastic spectrum from THF clathrate at T = 2 K and three different scattering angles (E_0 = 26 meV, δE = 2.1 meV; Q_o = 3.0; 3.9 and 5.8 Å^{-1} resp.).

The spectrum from THF clathrate is shown in Fig. 2. It exhibits a feature at about ΔE = 10 meV not present in pure ice and therefore attributed to the THF molecule embedded in the ice crystal structure. The peaks at the lowest energy transfers (cf. Fig. 3), on the other hand, we have observed in ice as well. To our knowledge there is no report in the literature about a similar observation. The physical origin of these excitations is not understood yet.

In order to check the expected superior performance of a methane clathrate moderator compared to an ice moderator we have performed measurements at the Jülich spallation source mock-up JESSICA. In these experiments pulses of 1.3 GeV protons are deposited into a mercury target and the fast neutrons generated in and emitted from this target are partly intercepted and slowed down in adjacent moderators such as our ice or methane clathrate moderators. The volume of these moderators typically is of the order of one liter. The energy distribution of the slow neutrons is measured by a time-of-flight technique. First preliminary results are shown in Fig. 4. Despite the low statistical accuracy, increased intensity at energies below about 5 meV is evident. The spectra are normalized to the same densities.

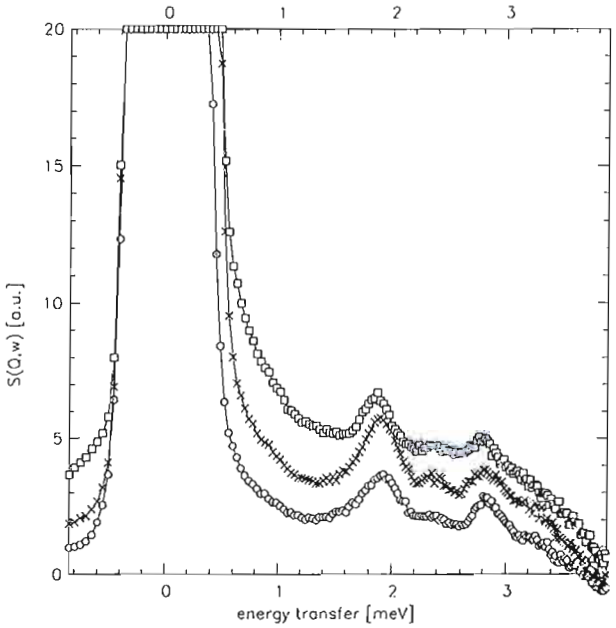

FIG. 3: Inelastic spectrum from THF clathrate at T = 2 K and three different scattering angles. (E_0 = 7 meV, δE = 0.4 meV; Q_o = 1.5; 1.9 and 2.9 Å^{-1} resp.).

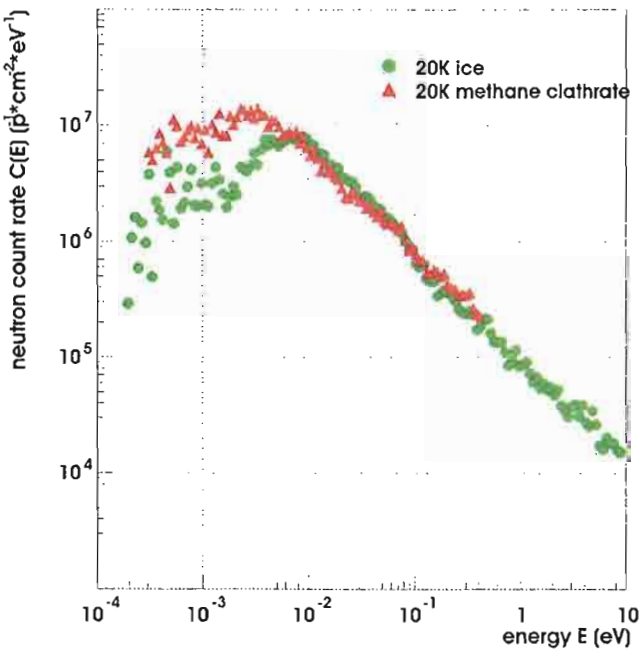

FIG. 4. Energy distribution of neutrons emitted from an ice and a methane clathrate moderator, respectively, measured at the Jülich spallation source mock-up JESSICA. The enhancement of the intensity at the lowest energies attributed to the methane is clearly seen.

REFERENCES

[1] H. Kapulla and W. Gläser; Neutron Inelastic Scattering IAEA-SM-155/G3; p 841 - 849 (1972)

[2] C. Gutt, B. Asmussen, W. Press, C. Merkl, H. Casalta, J. Greinert, G. Bohrmann, J.S. Tse and A. Hüller; Europhys. Lett., 48 (3), 269 (1999)

Publications in journals

Angermund,K.*; Bühl,M.*; Dinjus,E.*; Endruschat,U.*; Gassner,F.*; Haubold,H.-G.; Hormes,J.*; Köhl,G.*; Mauschick,F. T.*; Modrow,H.*; Mörtel,R.*; Mynott,R.*; Tesche,B.*; Vad,Th.; Waldöfner,N.*; Bönnemann,H.*
Nanoscopic Pt colloids in the 'embryonic state'
Angewandte Chemie-international edition, 41 (2002), 21, S. 4041 - 4044

Angermund,K.*; Bühl,M.*; Dinjus,E.*; Endruschat,U.*; Gassner,F.*; Haubold,H.-G.; Hormes,J.*; Köhl,G.*; Mauschick,F. T.*; Modrow,H.*; Mörtel,R.*; Mynott,R.*; Tesche,B.*; Vad,Th.; Waldöfner,N.*; Bönnemann,H.*
Nanoskopische Pt-Kolloide im "embryonalen Stadium"
Angewandte Chemie, 114 (2002), 21, S. 4213 - 4216

Bota,A.*; Goerigk,G.; Drucker,T.*; Haubold,H.-G.; Petro,J.*
Anomalous small-angle X-ray scattering on a new, nonpyrophoric raney-type Ni catalyst
Journal of catalysis, 205 (2002), S. 354 - 357

Bönnemann,H.*; Waldöfner,N.*; Haubold,H.-G.; Vad,Th.
Preparation and characterization of three-dimensional Pt nanoparticle networks
Chemistry of materials, 14 (2002), S. 1115 - 1120

Chen,J.; Romanzetti,S.*; Sommer,W. F.*; Ullmaier,H.
Helium bubble formation in 800 MeV proton-irradiated 304L stainless steel and alloy 718 during post-irradiation annealing
Journal of nuclear materials, 304 (2002), S. 1 - 7

Doan,T. D.*; Ott,F.*; Menelle,A.*; Humbert,P.*; Fermon,C.*; Prejbeanu,I. L.*; Rücker,U.
New evanescent neutron wave diffractometer at LLB
Applied physics A, 74 (2002), Suppl., S. S186 - S188

Guilleaume,B.*; Blaul,J.*; Ballauff,M.*; Wittemann,M.*; Rehahn,M.*; Goerigk,G.
The distribution of counterions around synthetic rod-like polyelectrolytes in solution
European physical journal E, 8 (2002), S. 299 - 309

Henry,J.*; Jung,P.; Chen,J.; Brachet,J.-C.*
Tensile properties and microstructure of 9Cr-1Mo martensitic steels containing a high helium concentration
Journal de physique IV, 12 (2002), Pr8, S. 103

Herms,M.*; Irmer,G.*; Goerigk,G.; Bedel,E.*; Claverie,A.*
Precipitation in low temperature grown GaAs
Materials science and engineering B, 91/92 (2002), S. 466 - 469

Hupfeld,D.; Schweika,W.; Strempfer,J.*; Caliebe,W.; Köbler,U.; Mattenberger,K.*; McIntyre,G. J.*; Yakhou,F.*; Brückel,Th.
Element-specific magnetic long- and short-range order and competing interactions in GdxEu1-xS
European physical journal B, 26 (2002), S. 273 - 289

Hupfeld,D.; Seeck,O. H.; Voigt,J.; Bos,J.; Fischer,K.; Brückel,Th.
X-ray resonance exchange scattering from ferromagnets : a new approach and its application to EuS
Europhysics letters, 59 (2002), 2, S. 284 - 290

Jung,P.
Irradiation effects and consequences on in-service properties under proton and neutron mixed spectra : an overview
Journal de physique IV, 12 (2002), Pr8, S. 59

Jung,P.
Radiation effects in structural materials of spallation targets
Journal of nuclear materials, 301 (2002), S. 15

Kolb,R.*; Schlapp,M.; Hesse,S.*; Schmechel,R.*; von Seggern,H.*; Fasel,C.*; Riedel,R.*; Ehrenberg,H.*; Fueß,H.*
The quasi-binary phase diagram BaF2-BaBr2 and its relation to the x-ray storage phosphor BaFBr:Eu2
Journal of physics D - applied physics, 35 (2002), S. 1914 - 1918

Köbler,U.
Temperature dependence of the spontaneous magnetisation of body-centred-cubic bulk iron, amorphous iron and thin iron films
Journal of physics: condensed matter, 14 (2002), S. 8861 - 8880

Köbler,U.; Hoser,A.; Fischer,K.; Beyss,M.
The impact of fourth-order exchange interactions on the thermal variation of the order parameter
Applied physics A, 74 (2002), Suppl. S. S604 - S606

Lauter,H. J.*; Lauter-Pasyuk,V.*; Toperverg,B.; Romashev,L.*; Ustinov,V.*; Kravtsov,E.*; Vorobiev,A.; Nikonov,O.*; Major,J.*
Spin-resolved unpolarised neutron off-specular scattering for magnetic multilayer studies
Applied physics A, 74 (2002), Suppl., S. S1557 - S1559

Lauter-Pasyuk,V.*; Lauter,H. J.*; Toperverg,B.; Petrenko,A.*; Schubert,D.*; Schreiber,J.*; Burcin,M.*; Aksenov,V.*
Interface and surface formation in self-assembled polymer multilayers by off-specular neutron scattering
Applied physics A, 74 (2002), Suppl., S. S528 - S530

Lauter-Pasyuk,V.*; Lauter,H. J.*; Toperverg,B.;

Romashev,L.*; Ustinov,V.*
Transverse and lateral structure of the spin-flop phase in Fe/Cr antiferromagnetic superlattices
Physical review letters, 89 (2002), 16, S. 167203-1 - 167203-4

Mackowski,S.*; Sobczak,E.*; Nietubyc,R.*; Goerigk,G.; Kret,S.*; Deuzewski,P.*; Szczepanska,A.*; Janik,E.*; Kossut,J.*; Karczewski,G.*
Three-dimensional quantum dot "crystal" formation in CdTe/ZnTe superlattices
Physica status solidi B, 229 (2002), S. 445 - 448

Massalovitch,S.; Ioffe,A.; Küssel,E.; Schlapp,M.; von Seggern,H.*; Brückel,Th.
Development of neutron image plate for low-flux measurements
Applied physics A, 74 (2002), Suppl., S. S118 - S120

Olligs,D.; Bürgler,D. E.; Wang,Y. G.; Kentzinger,E.; Rücker,U.; Schreiber,R.; Brückel,Th.; Grünberg,P.
Roughness-induced enhancement of giant magnetoresistance in epitaxial Fe/Cr/Fe(001) trilayers
Europhysics letters, 59 (2002), 3, S. 458 - 464

Polizzi,S.*; Riello,P.*; Goerigk,G.; Benedetti,A.*
Quantitative investigations of supported metal catalysts by ASAXS
Journal of synchrotron radiation, 9 (2002), S. 65 - 70

Rücker,U.; Kentzinger,E.; Toperverg,B.; Ott,F.*; Brückel,Th.
Layer-by-layer magnetometry of polarising supermirrors
Applied physics A, 74 (2002), Suppl., S. S607 - S609

Schlapp,M.; von Seggern,H.*; Massalovitch,S.; Ioffe,A.; Conrad,H.; Brückel,Th.
Materials for neutron-image plates with low gamma-sensitivity
Applied physics A, 74 (2002), Suppl., S. S109 - S111

Schweika,W.; Maleyev,S.; Brückel,Th.; Plakhty,V. P.; Regnault,L. P.*
Longitudinal spin fluctuations in the antiferromagnet MnF2 studied by polarized neutron scattering
Europhysics letters, 60 (2002), 3, S. 446 - 452

Seeck,O.; Kim,H.*; Lee,D. R.*; Shu,D.*; Kaendler,I. D.*; Basu,J.*; Sinha,S. K.*
Observation of thickness quantization in liquid films confined to molecular dimensions
Europhysics letters, 60 (2002), S. 376 - 382

Seydel,T.*; Tolan,M.*; Ocko,B. M.*; Seeck,O.; Weber,R.*; di Masi,E.*; Press,W.*
Freezing of capillary waves at the glass transition
Physical review B, 65 (2002), S. 184207 - 184213

Toperverg,B.
Off-specular polarised neutron scattering from magnetic fluctuations in thin films and multilayers
Applied physics A, 74 (2002), Suppl., S. S1560 - S1562

Vad,Th.; Haubold,H.-G.; Waldöfner,N.*; Bönnemann,H.*
Three-dimensional Pt-nanoparticle networks studied by anomalous small-angle X-ray scattering and X-ray absorption spectroscopy
Journal of applied crystallography, 35 (2002), S. 459 - 470

Voigt,J.; Kentzinger,E.; Rücker,U.; Schmidt,W.; Ohl,M.; Hupfeld,D.; Brückel,Th.
Interlayer coupling in [Er/Tb] superlattices
Applied physics A, 74 (2002), Suppl., S. S1517 - S1519

Voigt,J.; Rücker,U.; Nerger,S.; Kentzinger,E.; Hupfeld,D.; Schmidt,W.; Brückel,Th.
Structural and magnetic properties of [Er/Tb] superlattices
Journal of magnetism and magnetic materials, 240 (2002), S. 559 - 561

Vorobiev,A.*; Gordeev,G.*; Major,J.*; Toperverg,B.; Dosch,H.*
The structure of ferrofluids in the vicinity of an interface with silicon
Applied physics A, 74 (2002), Suppl., S. S817 - S819

Book chapter

Alefeld,B.; Conrad,H.; Dohmen,L.; Ioffe,A.; Kentzinger,E.; Küssel,E.; Prager,M.; Rücker,U.; Vehres,G.
Instrument modernisation program at the FRJ-2 reactor
European Conference Abstract Book : 16.-17.05.2002. - Bonn, 2002. - S. 43

Brückel,Th.
Magnetic X-ray and polarised neutron scattering
Polarized neutron scattering : lectures of the 1st summer school held at the Forschungszentrum Jülich from 10 to 14 September 2002 / eds.: T. Brückel and W. Schweika. - Jülich, 2002. - 3-89336-314-9. - S. 323 - 357

Brückel,Th.
Scattering
Soft matter : complex materials on mesoscopic scale ; lecture manuscripts of the 33rd IFF winter school, organized on March, 4 - 15, 2002 in the Forschungszentrum Jülich at the Institut für Festkörperforschung / ed. J. K. Dhont ... - Jülich, 2002. - (Schriften des Forschungszentrum Jülich, Reihe Materie und Material ; 10). - 3-89336-297-5. - S. A1.1 - A1.35

Chen,J.; Conrad,H.; Jung,P.; Soltner,H.; Wolters,J.;

Ullmaier,H.
Materialprobleme am Target-Moderator-Komplex der ESS
European conference abstract book : Bonn, 16. - 17.05.2002. - S. 27

Conrad,H.; Küssel,E.; Bayer,N.; Glückler,H.; Soltner,H.; Stelzer,H.
Entwicklung fortschrittlicher kalter Moderatoren für die ESS
European conference abstract book : Bonn, 16. - 17.05.2002. - S. 27

Dohmen,L.; Alefeld,B.; Kentzinger,E.; Rücker,U.; Stellbrink,J.; Springer,T.; Richter,D.; Brückel,Th.
KWS3 : a focusing small angle neutron scattering instrument and neutron refectometer at Jülich
European conference abstract book : Bonn, 16. - 17.05.2002. - S. 33

Fermon,C.*; Suck,J. B.*; Toperverg,B.; Vettier,C.*; Zabel,H.*
Microsystems and information technologies
New science and technology for the 21st century : the ESS project vol. 2. - 2002. - S. 6 - 7

Ioffe,A.
Wide angle high resolution spectroscopy at pulsed neutron sources
PNCMI-Workshop, Jülich, 16.-19.09.2002 : abstract book. - 2002. - S. M11

Kampmann,R.*; Haese-Seiller,M.*; Kudryashov,V.*; Deriglazov,V.*; Toperverg,B.; Schreyer,A.*; Sackmann,E.*
Perspectives for polarised reflectometry at the novel reflectometer REFSANS at FRM-II in Munich/Germany
PNCMI-Workshop, Jülich, 16.-19.09.2002 : abstract book. - 2002. - S. B29

Kentzinger,E.; Rücker,U.; Toperverg,B.; Brückel,Th.
Determination of the magnetic fluctuations in a Fe/Cr/Fe trilayer exhibiting a neutron resonance state
PNCMI-Workshop, Jülich, 16.-19.09.2002 : abstract book. - 2002. - S. A24

Kentzinger,E.; Toperverg,B.; Rücker,U.; Brückel,Th.
Simulation of reflectivity and off-specular scattering of polarised neutrons from laterally patterned magnetic multilayers
PNCMI-Workshop, Jülich, 16.-19.09.2002 : abstract book. - 2002. - S. A23

Klimko,S.*; Böni,P.*; Currat,R.*; Demmel,F.*; Fåk,B.*; Gähler,R.*; Mezei,F.*; Stadler,C.*; Toperverg,B.
Implementation of a zero field spin-echo option at the three-axis spectrometer IN3 (ILL, Grenoble) and first measurements of phonon linewidths
PNCMI-Workshop, Jülich, 16.-19.09.2002 : abstract book. - 2002. - S. V33

Köbler,U.; Hoser,A.*; Bos,J.; Schäfer,W.*; Mueller,R.; Fischer,K.
On the thermodynamic universality classes of Heisenberg type magnets
European conference abstract book : Bonn, 16. - 17.05.2002. - S. 26

Lauter,H. J.*; Lauter-Pasyuk,V.*; Toperverg,B.; Romashev,L.*; Ustinov,V.*; Vorobiev,A.*; Major,J.*
Neutron spin selection in off-specular scattering from magnetic multilayers
European conference abstract book : Bonn, 16. - 17.05.2002. - S. 53

Lauter,H. J.*; Lauter-Pasyuk,V.*; Toperverg,B.; Rücker,U.; Romashev,L.*; Milyaev,M.; Ustinov,V.*
Spin-flop transition in Fe/Cr multilayers
PNCMI-Workshop, Jülich, 16.-19.09.2002 : abstract book. - 2002. - S. V25

Lauter,H.*; Lauter-Pasyuk,V.*; Toperverg,B.; Romashev,L.*; Milyaev,M.*; Ustinov,V.*
Twisted ground state in antiferromagnetically coupled multilayers
Proceedings of the 7th International Conference on Surface X-ray and Neutron Scattering : Lake Tahoe, USA, 23. - 27.09.2002. - (2002). - S. 17

Lauter-Pasyuk,V.*; Lauter,H. J.*; Gordeev,G.*; Müller-Buschbaum,P.*; Toperverg,B.; Petry,W.*
Magnetic nanoparticles in self-assembled diblock-copolymer films
PNCMI-Workshop, Jülich, 16.-19.09.2002 : abstract book. - 2002. - S. A22

Lauter-Pasyuk,V.*; Lauter,H. J.*; Toperverg,B.; Müller-Buschbaum,P.*; Petrenko,A.*; Petry,W.*; Aksenov,V.*
Self-assembly of magnetite nanoparticles in thin block-copolymer films by off-specular neutron scattering
European conference abstract book : Bonn, 16. - 17.05.2002. - S. 53

Lauter-Pasyuk,V.*; Lauter,H. J.*; Toperverg,B.; Romashev,L.*; Milyaev,M.; Ustinov,V.*
The origin of the twisted ground state in magnetic multilayers in external magnetic field
PNCMI-Workshop, Jülich, 16.-19.09.2002 : abstract book. - 2002. - S. V22

Lauter-Pasyuk,V.*; Lauter,H.*; Gordeev,G.*; Müller-Buschbaum,P.*; Toperverg,B.; Petry,W.*
Self-assembled nanomaterials : magnetic nanoparticles in copolymer films studied by off-specular neutron scattering
Proceedings of the 7th International Conference on Surface X-ray and Neutron Scattering : Lake Tahoe, USA, 23. - 27.09.2002. - (2002). - S. 52

Lee,W.-T.*; te Velthuis,S. G. E.*; Felcher,G. P.*; Klose,F.*; Gredig,T.*; Dahlberg,D.*; Toperverg,B.
Measuring lateral magnetic structure in thin films using polarised neutron reflectometry
PNCMI-Workshop, Jülich, 16.-19.09.2002 : abstract book. - 2002. - S. A21

Massalovitch,S.; Ioffe,A.; Küssel,E.; Schlapp,M.; Brückel,Th.
Development of image plate based neutron detector
International Workshop on Position-Sensitive Neutron Detectors : Status and Perspectives. - 2002 (2). - S. 569 - 571

Massalovitch,S.; Ioffe,A.; Schlapp,M.; Von Seggern,H.*; Küssel,E.; Brückel,Th.
Low gamma-sensitivity neutron image plate detector
European conference abstract book : Bonn, 16. - 17.05.2002. - S. 89

Mueller,R.; Chang,L. J.; Appelt,S.
Polarized 3He in Jülich
European conference abstract book : Bonn, 16. - 17.05.2002. - S. 96

Mueller,R.; Chang,L. J.; Appelt,S.; Haesing,W.; Horriar-Esser,Ch.; Ioffe,A.; Brückel,Th.
Progress in the production of polarised 3He in Jülich
PNCMI-Workshop, Jülich, 16.-19.09.2002 : abstract book. - 2002. - S. B30

Plakhty,V. P.; Maleyev,S.*; Gavrilov,S. V.*; Bourdarot,F.*; Pouget,S.*; Barilo,S. N.*
Quantum phase transition in Pr2CuO4 to collinear state induced by magnetic field : a neutron diffraction study
European conference abstract book : Bonn, 16. - 17.05.2002. - S. 56

Rücker,U.; Toperverg,B.; Kentzinger,E.; Brückel,Th.
Resonant states in a ferromagnetic quantum well for neutrons
European conference abstract book : Bonn, 16. - 17.05.2002. - S. 43

Schweika,W.
Introduction to polarised neutron scattering
Polarized neutron scattering : lectures of the 1st summer school held at the Forschungszentrum Jülich from 10 to 14 September 2002 /eds.: T. Brückel and W. Schweika. - Jülich, 2002. - 3-89336-314-9. - S. 5 - 29

Schweika,W.
Time-of-flight and polarisation analysis for diffuse neutron scattering
PNCMI-Workshop, Jülich, 16.-19.09.2002 : abstract book. - 2002. - S. M9

Schweika,W.; Maleyev,S. V.; Brückel,Th.; Plakhty,V. P.; Regnault,L.-P.*
Longitudinal spin fluctuations in 3d antiferromagnets
PNCMI-Workshop, Jülich, 16.-19.09.2002 : abstract book. - 2002. - S. V9

Schweika,W.; Maleyev,S.*; Brückel,Th.; Plakhty,V.*; Regnault,L.-P.*
Longitudinal spin fluctuations in the antiferromagnet MnF2 studied by polarized neutron scattering
European conference abstract book : Bonn, 16. - 17.05.2002. - S. 36

Seeck,O.
Capillary waves on polymer thin films
Soft matter : complex materials on mesoscopic scale ; lecture manuscripts of the 33rd IFF winter school, organized on March, 4 - 15, 2002 in the Forschungszentrum Jülich at the Institut für Festkörperforschung / ed. J. K. Dhont ... - Jülich, 2002. - (Schriften des Forschungszentrum Jülich, Reihe Materie und Material ; 10). - 3-89336-297-5. - S. B7.1 - B7.15

Su,Y.; Istomin,K.; Schweika,W.; Fattah,A.; Foucart,P.; Meuffels,P.; Brückel,Th.; Kaiser,V.*
Polarization analysis of diffuse neutron scattering in lightly doped La1-xSrxMn03 single crystals
European conference abstract book : Bonn, 16. - 17.05.2002. - S. 26

Su,Y.; Istomin,K.; Schweika,W.; Fattah,A.; Foucart,P.; Meuffels,P.; Brückel,Th.; Kaiser,V.*
Polarization analysis of diffuse neutron scattering in lightly doped La1-xSrxMnO3 single crystals
PNCMI-Workshop, Jülich, 16.-19.09.2002 : abstract book. - 2002. - S. A13

Tasset,F.*; Regnault,L.-P.*; Brückel,Th.; Rupp,A.*; Eccleston,R.*; Török,G.*; Fermon,C.*; Heil,W.*
ENPI : the European neutron polarisation initiative
European conference abstract book : Bonn, 16. - 17.05.2002. - S. 95

te Velthuis,S. G. E.*; Felcher,G. P.*; Toperverg,B.; Vorobiev,A.*; Major,J.*
Domain states in exchange biased Co/CoO bilayers
PNCMI-Workshop, Jülich, 16.-19.09.2002 : abstract book. - 2002. - S. V19

Toperverg,B.
Larmor phase labelling in reflectometry, SANS and tomography
PNCMI-Workshop, Jülich, 16.-19.09.2002 : abstract book. - 2002. - S. V31

Toperverg,B.
Polarised neutron reflection and off-specular scattering
Polarized neutron scattering : lectures of the 1st summer school held at the Forschungszentrum Jülich from 10 to 14 September 2002 / T. Brückel (ed.) .. - Jülich, 2002. - 3-89336-314-9. - S. 247 - 288

Toperverg,B.

Supermatrix formalism to model off-specular neutron scattering
Proceedings of the 7th International Conference on Surface X-ray and Neutron Scattering : Lake Tahoe, USA, 23. - 27.09.2002. - (2002). - S. 51

Voigt,J.; Kentzinger,E.; Rücker,U.; Schmidt,W.*; Schweika,W.; Brückel,Th.
Magnetic structures of phase transitions in [Er-Tb] multilayers
European conference abstract book : Bonn, 16. - 17.05.2002. - S. 24

Vorobiev,A.*; Gordeev,G.*; Major,J.*; Toperverg,B.; Dosch,H.*
Transverse and lateral self-organisation in colloids of ferromagnetic nanoparticles
PNCMI-Workshop, Jülich, 16.-19.09.2002 : abstract book. - 2002. - S. V26

Vrana,M.*; Mikula,P.*; Lukas,P.*; Ioffe,A.; Nistler,W.*
Neutron interferometric measurements in NPI Rez
European conference abstract book : Bonn, 16. - 17.05.2002. - S. 11

Ziegenhagen,N.; Rücker,U.; Kentzinger,E.; Lehmann,R.; van der Hart,A.; Toperverg,B.; Brückel,Th.
Determination of the magnetic properties of laterally structured Fe/Cr multilayers
PNCMI-Workshop, Jülich, 16.-19.09.2002 : abstract book. - 2002. - S. V18

Ziegenhagen,N.; Rücker,U.; Kentzinger,E.; Lehmann,R.; van der Hart,A.; Toperverg,B.; Brückel,Th.
Magnetic properties of laterally structured Fe/Cr multilayers
European conference abstract book : Bonn, 16. - 17.05.2002. - S. 25

Zotov,N.*; Schäfer,W.; Jansen,E.; Kockelmann,W.*; Delaplane,R. G.*
Neutron diffraction studies of glasses in the collaborative research project SFB 408 Bonn, Germany
European conference abstract book : Bonn, 16. - 17.05.2002. - S. 23

Book

Brückel,Th. (Hrsg.); Schweika,W. (Hrsg.)
Polarized neutron scattering : lectures of the 1st summer school held at the Forschungszentrum Jülich from 10 to 14 September 2002
Jülich, Forschungszentrum, Zentralbibliothek, 2002
Schriften des Forschungszentrums Jülich, Reihe Materie und Material ; 12
3-89336-314-9

Invited talks

Bayer,N.; Conrad,H.; Glückler,H.; Küssel,E.; Soltner,H.; Stelzer,H.
Entwicklung fortschrittlicher kalter Moderatoren für die ESS
ESS-European Conference : Bonn, Alter Bundestag Bonn: 16.05.2002 - 17.05.2002

Brückel,Th.
Introduction to polarised neutron scattering
First Summer School on Polarised Neutron Scattering : FZJ, IFF
Jülich: 11.09.2002 - 14.09.2002

Brückel,Th.
Magnetic X-ray and polarised neutron scattering
First Summer School on Polarised Neutron Scattering : FZJ, IFF
Jülich: 11.09.2002 - 14.09.2002

Brückel,Th.
Magnetic X-ray scattering : status and perspectives
ERLSYN-Science2002 : International Workshop on Scientific Applications of Energy Recovery Linac Driven Synchrotron Light Sources ; Universität Erlangen
Erlangen: 27.09.2002 - 29.09.2002

Brückel,Th.
Magnetic X-ray scattering : status and perspectives
PETRA III Upgrade Workshop on Condensed Matter Applications : DESY Hamburg
Hamburg: 30.09.2002 - 02.10.2002

Brückel,Th.
Scattering
Soft matter : complex materials on mesoscopic scale ; lecture manuscripts of the 33rd IFF winter school
Jülich: 05.03.2002

Brückel,Th.
The colorful palette of magnetism : resonant magnetic X-ray scattering
Max-Planck-Institut : Stuttgart
Stuttgart: 16.07.2002

Brückel,Th.
Von korrelierten Elektronen zu komplexen Legierungen : Festkörperforschung am IFF
HGF-Workshop Kondensierte Materie : Forschungszentrum Jülich
Jülich: 06.11.2002

Chen,J.
HCF experiments for ESS
4th International Workshop on Mercury Target Development : Forschungszentrum Jülich
Jülich: 12.07.2002 - 16.07.2002

Chen,J.
Summary and conclusion from PIE of spent targets at FZ-Juelich
5th International Workshop on Spallation Materials Technology
Charleston, S.C.: 19.05.2002 - 24.05.2002

Conrad,H.
Konzepte zur Auslegung der Neutronentargets an Spallationsquellen
ESS-Tage
Bad Honnef: 15.04.2002

Conrad,H.
The new ESS moderator concept
4th International Workshop on Mercury Target Development : Forschungszentrum Jülich
Jülich: 15.07.2002

Goerigk,G.
Materialwissenschaftliche Untersuchungen mit anomaler Röntgen- Kleinwinkelstreuung
Vortrags- und Diskussionstreffen "Materialwissenschaften in Hamburg 2002" : Universität Hamburg, Chemie
Hamburg: 14.10.2002 - 15.10.2002

Goerigk,G.; Haubold,H.-G.; Lyon,O.*; Simon,J.-P.*
Review of anomalous ASAXS in materials science
SAS 2002 - Konferenz
Venedig, Italien: 25.08.2002 - 30.08.2002

Goerigk,G.; Williamson,D. L.*
Quantitative ASAXS of germanium inhomogeneities in amorphous silicon-germanium alloys
SAS 2002 - Konferenz
Venedig, Italy: 25.08.2002 - 30.08.2002

Hanslik,R.; Butzek,M.; Müller,A.
New design for ESS rotation shutter
4th International Workshop on Mercury Target Development : Forschungszentrum Jülich
Jülich: 12.07.2002 - 16.07.2002

Haubold,H.-G.; Vad,Th.; Waldöfner,N.*
From Pt molecules to catalyst nanoparticles : ASAXS / SAXS in-situ studies
SAS 2002 - Konferenz
Venedig, Italien: 25.08.2002 - 30.08.2002

Ioffe,A.
Neutron speed echo add-on to TAS : an increase in resolution without the use of polarized neutrons
Workshop on the Perspectives in Single Crystal Neutron Spectroscopy (SCNS) : ILL Grenoble
Grenoble, Frankreich: 12.12.2002 - 14.12.2002

Ioffe,A.
Wide angle high resolution spectroscopy at pulsed neutron sources
Workshop on Polarised Neutrons in Condensed Matter Investigations : Forschungszentrum Jülich
Jülich: 16.09.2002 - 19.09.2002

Jung,P.
Hydrogen in RAFM´s : diffusion and effects on tensile properties
IEA Workshop on Ferritic-Martensitic Steels
Garching: 14.11.2002

Jung,P.
Pitting mitigation strategies at ESS
4th InternationalWorkshop on Mercury Target Development : Forschungszentrum Jülich
Jülich: 12.07.2002 - 16.07.2002

Jung,P.
Strahlenschäden am ESS-Target
ESS Tage
Bad Honnef: 14.04.2002 - 16.04.2002

Jung,P.
The solid target concept
Technical Advisory Committee of ESS
Saclay, Frankreich: 04.11.2002 - 05.11.2002

Jung,P.; Henry,J.*; Chen,J.; Brachet,J.-C.*
Effect of implanted helium on tensile properties and hardness of 9%Cr martensitic stainless steels
5th International Workshop on Spallation Materials Technology
Charleston, USA: 19.05.2002 - 24.05.2002

Jung,P.; Yao,Z.; Liu,C.*
Migration and trapping of hydrogen in steel - effect of irradiation and helium-implantation
International Conference on Hydrogen Effects on Material Behaviour and Corrosion
Jackson Lake, USA: 22.09.2002 - 26.09.2002

Kentzinger,E.
First experiments on the focusing mirror USANS diffractometer KWS-3
European Users Meeting of the European Access to Research Infrastructure Project "Juelich Neutrons for Europe" : Kerkrade (Netherlands)
Kerkrade: 22.11.2002

Kentzinger,E.
KWS3, the new focusing mirror SANS instrument at Jülich
6th ESS-SAC Meeting
Bochum: 01.10.2002

Klimko,S.*; Böni,P.*; Currat,R.*; Demmel,F.*; Fåk,B.*; Gähler,R.*; Mezei,F.*; Stadler,C.*; Toperverg,B.
Implementation of a zero field spin-echo option at the three-axis spectrometer IN3 (ILL, Grenoble) and first measurements of phonon linewidths
Workshop on Polarised Neutrons in Condensed Matter Investigations : Forschungszentrum Jülich
Jülich: 16.09.2002 - 19.09.2002

Kranold,R.*; Kriesen,S.*; Haselhoff,M.*; Weber,H.-J.*; Goerigk,G.

SAXS study of the growth kinetics of CuCl nanocrystals in NaCl
SAS 2002 Konferenz
Venedig, Italien: 25.08.2002 - 30.08.2002

Lauter,H. J.*; Lauter-Pasyuk,V.*; Toperverg,B.; Rücker,U.; Romashev,L.*; Milyaev,M.; Ustinov,V.*
Spin-flop transition in Fe/Cr multilayers
Workshop on Polarised Neutrons in Condensed Matter Investigations : Forschungszentrum Jülich
Jülich: 16.09.2002 - 19.09.2002

Lauter,H.*; Lauter-Pasyuk,V.*; Toperverg,B.; Romashev,L.*; Milyaev,M.*; Ustinov,V.*
Twisted ground state in antiferromagnetically coupled multilayers
The 7th International Conference on Surface X-Ray and Neutron Scattering
Lake Tahoe, CA: 23.09.2002 - 27.09.2002

Lauter-Pasyuk,V.*; Lauter,H. J.*; Toperverg,B.; Romashev,L.*; Milyaev,M.; Ustinov,V.*
The origin of the twisted ground state in magnetic multilayers in external magnetic field
Workshop on Polarised Neutrons in Condensed Matter Investigations : Forschungszentrum Jülich
Jülich: 16.09.2002 - 19.09.2002

Lauter-Pasyuk,V.*; Lauter,H.*; Gordeev,G.*; Müller-Buschbaum,P.*; Toperverg,B.; Petry,W.*
Self-assembled nanomaterials : magnetic nanoparticles in copolymer films studied by off-specular neutron scattering
7th International Conference on Surface X-ray and Neutron Scattering
Lake Tahoe, USA: 23.09.2002 - 27.09.2002

Massalovitch,S.; Ioffe,A.; Küssel,E.; Brückel,Th.
Neutron image plate detector with low gamma-sensitivity
Seminar : Technische Universität München
Garching: 10.06.2002

Massalovitch,S.; Ioffe,A.; Schlapp,M.; Von Seggern,H.*; Küssel,E.; Brückel,Th.
Low gamma-sensitivity neutron image plate detector
ESS-Conference and TECHNI-Network Meeting
Bonn: 15.05.2002 - 17.05.2002

Schweika,W.
Time-of-flight and polarisation analysis for diffuse neutron scattering
Workshop on Polarised Neutrons in Condensed Matter Investigations : Forschungszentrum Jülich
Jülich: 16.09.2002 - 19.09.2002

Schweika,W.; Maleyev,S. V.*; Brückel,Th.; Plakhty,V. P.*; Regnault,L.-P.*
Longitudinal spin fluctuations in 3d antiferromagnets
Workshop on Polarised Neutrons in Condensed Matter Investigations : Forschungszentrum Jülich
Jülich: 16.09.2002 - 19.09.2002

Schweika,W.; Maleyev,S.*; Brückel,Th.; Plakhty,V. P.; Regnault,L.-P.*
Longitudinal spin fluctuations in the antiferromagnet MnF2 studied by polarized neutron scattering
Deutsche Neutronenstreutagung
Bonn: 15.05.2002 - 16.05.2002

Seeck,O.
Auto- and cross correlation functions of thin film systems determined by X-ray diffuse scattering
Röntgenseminar des IFPAN
Warschau: 20.03.2002

Seeck,O.
Capillary waves on polymer thin films
Soft matter : complex materials on mesoscopic scale ; lecture manuscripts of the 33rd IFF winter school
Jülich: 05.03.2002

Seeck,O.
X-ray experiments on confined liquids
MPI-MF Institutskolloquium
Stuttgart: 03.05.2002

Seeck,O.
X-ray reflectivity on thin film samples
Röntgenseminar des IFPAN
Warschau: 20.03.2002

te Velthuis,S. G. E.*; Felcher,G. P.*; Toperverg,B.; Vorobiev,A.*; Major,J.*
Domain states in exchange biased Co/CoO bilayers
Workshop on Polarised Neutrons in Condensed Matter Investigations : Forschungszentrum Jülich
Jülich: 16.09.2002 - 19.09.2002

Toperverg,B.
Diffuse neutron scattering on multilayers
XXXVI PNPI Winter School Condensed State Physics
St. Petersburg: 15.04.2002 - 20.04.2002

Toperverg,B.
Larmor phase labelling in reflectometry, SANS and tomography
Workshop on Polarised Neutrons in Condensed Matter Investigations : Forschungszentrum Jülich
Jülich: 16.09.2002 - 19.09.2002

Toperverg,B.
Neutron scattering at grazing incidence
Workshop RNIKS-2002 : PNPI
Gatchina, Russland: 14.10.2002 - 21.10.2002

Toperverg,B.
Polarised neutron reflection and off-specular scattering
First Summer School on Polarised Neutron Scattering : FZJ, IFF
Jülich: 11.09.2002 - 14.09.2002

Toperverg,B.

Supermatrix formalism to model off-specular neutron scattering
The 7th International Conference on Surface X-Ray and Neutron Scattering
Lake Tahoe, CA: 23.09.2002 - 27.09.2002

Toperverg,B.
Theoretical interpretation and quantitative analysis of data on reflectometry and off-specular scattering
Workshop Neutron Reflection: Progress in the Study of Interfaces
ILL, Grenoble: 24.10.2002 - 26.10.2002

Toperverg,B.
Theoretical interpretation of off-specular polarized neutron scattering from nanocomposite films
International Workshop on Nanocomposites : Materials, Neutrons and Data Interpretation : ANL
Argonne: 28.03.2002

Toperverg,B.
Towards 3-dimensional polarimetry in neutron reflectometry
16th PAC for Condensed Matter Physics Meeting
Dubna: 18.04.2002 - 19.04.2002

Vorobiev,A.*; Gordeev,G.*; Major,J.*; Toperverg,B.; Dosch,H.*
Transverse and lateral self-organisation in colloids of ferromagnetic nanoparticles
Workshop on Polarised Neutrons in Condensed Matter Investigations : Forschungszentrum Jülich
Jülich: 16.09.2002 - 19.09.2002

Ziegenhagen,N.; Rücker,U.; Kentzinger,E.; Lehmann,R.; van der Hart,A.; Toperverg,B.; Brückel,Th.
Determination of the magnetic properties of laterally structured Fe/Cr multilayers
Workshop on Polarised Neutrons in Condensed Matter Investigations : Forschungszentrum Jülich
Jülich: 16.09.2002 - 19.09.2002

Other talks

Brückel,Th.
Das Institut für Streumethoden
Beirats-Informationsveranstaltung : Forschungszentrum Jülich
Jülich: 21.03.2002

Brückel,Th.
Elastic scattering from many-body systems
Laboratory Course Neutron Scattering : FZJ-IFF
Jülich: 16.09.2002 - 20.09.2002

Brückel,Th.
Magnetic X-ray diffraction reveals elementspecific magnetic correlations
APS User Science Seminar
Argonne: 26.07.2002

Brückel,Th.
Magnetism
Laboratory Course Neutron Scattering : FZJ-IFF
Jülich: 16.09.2002 - 20.09.2002

Brückel,Th.
Science review : "FZJ @ MuCAT: examples for research activities"
APS Seminar : Argonne National Laboratory (ANL)
Argonne, USA: 21.11.2002

Conrad,H.
Inelastic neutron scattering from water-ice, tetrahydrofurane-hydrate and methane-hydrate
6th Meeting of the Collaboration on Advanced Cold Moderators (ACoM) : Forschungszentrum Jülich
Jülich: 11.09.2002

Conrad,H.
Neutron Sources
Laboratory Course Neutron Scattering : FZJ-IFF
Jülich: 16.09.2002 - 20.09.2002

Goerigk,G.
JUSIFA : Jülichs small angle X-ray scattering experiment at HASYLAB
Satellite meeting : status and perspectives of SAXS/WAXS HASYLAB
Hamburg: 24.01.2002

Goerigk,G.
Materialuntersuchungen mit anomaler Röntgen-Kleinwinkelstreuung
Institutsseminar : Universität Göttingen. I. Physikalisches Institut
Göttingen: 28.01.2002

Ioffe,A.
Principles of neutron speed echo spectroscopy
Seminar : Institut Max von Laue, Paul Langevin
Grenoble: 11.03.2002

Köbler,U.
Experimentelle Evidenzen gegen die Gültigkeit der klassischen Spinwellentheorie
Universitäts-Kolloquium : Bochum
Bochum: 16.07.2002

Nünighoff,K.; Conrad,H.; Filges,D.; Goldenbaum,F.; Neef,R.-D.; Pohl,C.; Schaal,H.; Stelzer,H.; Tietze-Jaensch,H.; Paul,N.; Wohlmuther,W.
The JESSICA experiment - part I : inprovements of the JESSICA experiment
ACoM-6 - 6th Meeting of the Collaboration on Advanced Cold Moderators : Forschungszentrum Jülich
Jülich: 11.09.2002 - 13.09.2002

Pohl,C.; Conrad,H.; Filges,D.; Goldenbaum,F.; Neef,R.-D.; Nünighoff,K.; Schaal,H.; Stelzer,H.;

Tietze-Jaensch,H.; Paul,N.; Wohlmuther,W.
The JESSICA experiment - part II : results from the JESSICA experiment
ACoM6 - 6th Meeting of the Collaboration on Advanced Cold Moderators : Forschungszentrum Jülich
Jülich: 11.09.2002 - 13.09.2002

Rücker,U.
Neutronenstreuinstrumentierung am FRJ-2
ZFR-Fachkundeseminar : Forschungszentrum Jülich
Jülich: 06.11.2002

Rücker,U.
Neutronenstreuinstrumentierung am FRJ-2
ZFR-Fachkundeseminar : Forschungszentrum Jülich
Jülich: 15.11.2002

Schweika,W.
Diffuse neutron scattering : time-of-flight and polarization analysis
ESS-Tage : Bad-Honnef
Bad-Honnef: 14.04.2002 - 16.04.2002

Schweika,W.
Polarization analysis
Laboratory Course Neutron Scattering : FZJ-IFF
Jülich: 16.09.2002 - 20.09.2002

Seeck,O.
Continuum description : grazing incidence neutron scattering
Laboratory Course Neutron Scattering : FZJ-IFF
Jülich: 16.09.2002 - 20.09.2002

Toperverg,B.
Larmor precession tracing, small angle scattering, depolarization, and the optical theorem
Workshop Progress in Neutron Larmor Precession Techniques
Delft: 29.05.2002 - 01.06.2002

Toperverg,B.
Lateral magnetic patterns in thin films and layered superstructures : polarized neutron off-specular scattering
Seminar Ruhr Universität Bochum
Bochum: 21.02.2002

Toperverg,B.
Neutron scattering at grazing incidence
IPNS / SNS Seminar : ANL
Argonne, IL: 30.09.2002

Toperverg,B.
Polarised neutron reflection and off-specular scattering
GKSS-Seminar
Geesthacht: 23.08.2002

Toperverg,B.
Theory of polarized neutron scattering and interpretation of experimental data on vector analysis
ILL Seminar
Grenoble: 14.02.2002

Voigt,J.; Kentzinger,E.
Untersuchung magnetischer Übergitter mit Neutronen und Synchrotronröntgenstrahlung
Workshop Magnetismus und Streumethoden : Forschungszentrum Jülich
Jülich: 07.06.2002

Posters

Alefeld,B.; Conrad,H.; Dohmen,L.; Ioffe,A.; Kentzinger,E.; Küssel,E.; Prager,M.; Rücker,U.; Vehres,G.
Instrument modernisation program at the FRJ-2 reactor
ESS Conference
Bonn: 16.05.2002 - 17.05.2002

Andreasen,J. W.*; Rasmussen,O.*; Feidenhans,R.*; Berg Rasmussen,F.*; Christensen,R.*; Molenbroek,A.*; Goerigk,G.
An in-situ cell for ASAXS investigations of nanocrystalline catalysts
SAS 2002 Konferenz
Venedig, Italien: 25.08.2002 - 30.08.2002

Bos,J.; Köbler,U.; Küssel,E.
Magnetische Besonderheiten an den hydrothermal synthetisierten Carbonaten
4. Vortragstagung Fachgruppe Festkörperchemie und Materialforschung : Technische Universität Dresden
Dresden: 24.09.2002 - 26.09.2002

Chang,L. J.; Mueller,R. M.; Appelt,S.; Häsing,F. W.
Polarized 3He in Jülich
ESS-Conference
Bonn: 16.05.2002 - 17.05.2002

Chen,J.; Conrad,H.; Jung,P.; Soltner,H.; Wolters,J.; Ullmaier,H.
Material problem of the target-moderator-complex in ESS
ESS European Conference
Bonn: 16.05.2002 - 17.05.2002

Dohmen,L.; Alefeld,B.; Kentzinger,E.; Rücker,U.; Stellbrink,J.; Ioffe,A.; Springer,T.; Richter,D.; Brückel,Th.; Drochner,M.; Engels,R.; Kleines,H.; Suxdorf,F.; Zwoll,K.
A high resolution small angle neutron scattering instrument and reflectometer with focusing mirror (KWS3) at Jülich
ESS-Conference
Bonn: 16.05.2002 - 17.05.2002

Dürr,H. A.*; Krause,B.*; Schreiber,F.*; Dosch,H.*; Seeck,O.

Interfacial morphology and thermal stability of metal contacts on organic thin films
HASYLAB User Meeting
Hamburg: 25.01.2002

Goerigk,G.
Anomalous small angle X-ray scattering in solid state physics, catalyst research and chemistry
HGF-Workshop "Kondensierte Materie"
FZJ, Jülich: 06.11.2002 - 06.11.2002

Goerigk,G.; Williamson,D. L.*
Anomalous small-angle X-ray scattering study of hotwire and plasma grown amorphous silicon-germanium alloys
HASYLAB User Meeting
Hamburg: 25.01.2002

Grigorian,S.*; Grenzer,J.*; Pietsch,U.*; Seeck,O.
Thermal diffuse scattering in grazing-incidence-diffraction
HASYLAB User Meeting
Hamburg: 25.01.2002

Haubold,H.-G.; Vad,Th.; Waldöfner,N.*
From Pt molecules to nanoparticles: ASAXS / SAXS in-situ studies
HGF-Workshop "Kondensierte Materie"
FZJ, Jülich: 06.11.2002 - 06.11.2002

Istomin,K.; Su,Y.; Fattah,M.; Foucart,P.; Hupfeld,D.; Seeck,O.; Brückel,Th.
Reexamination of the charge/orbital ordering in lightly doped LaSrMnO by synchrotron X-ray scattering methods
HGF-Workshop "Kondensierte Materie"
FZJ, Jülch: 06.11.2002 - 06.11.2002

Istomin,K.; Su,Y.; Fattah,M.; Seeck,O.; Hupfeld,D.; Brückel,Th.
Resonant scattering from lightly doped La1-xSrxMnO3 (x - 1/8)
HASYLAB User Meeting
Hamburg: 25.01.2002

Istomin,K.; Su,Y.; Schweika,W.; Hupfeld,D.; Fattah,M.; Foucart,P.; Brückel,Th.
Complementary X-ray and neutron scattering from lightly doped La1-xSrxMnO3 (x ~ 1/8) single crystals
Workshop on Neutron and Synchrotron X-ray Scattering in Condensed Matter Research : PSI Villigen
Villigen: 03.08.2002 - 06.08.2002

Kampmann,R.*; Haese-Seiller,M.*; Kudryashov,V.*; Deriglazov,V.*; Toperverg,B.; Schreyer,A.*; Sackmann,E.*
Perspectives for polarised reflectometry at the novel reflectometer REFSANS at FRM-II in Munich/Germany
Workshop on Polarised Neutrons in Condensed Matter Investigations : Forschungszentrum Jülich
Jülich: 16.09.2002 - 19.09.2002

Kentzinger,E.
KWS-3, a focusing mirror USANS diffractometer in Jülich
Deutsche Neutronenstreutagung
Bonn: 15.05.2002 - 16.05.2002

Kentzinger,E.; Rücker,U.; Toperverg,B.; Brückel,Th.
Determination of the magnetic fluctuations in a Fe/Cr/Fe trilayer exhibiting a neutron resonance state
Workshop on Polarised Neutrons in Condensed Matter Investigations : Forschungszentrum Jülich
Jülich: 16.09.2002 - 19.09.2002

Kentzinger,E.; Toperverg,B.; Rücker,U.; Brückel,Th.
Simulation of reflectivity and off-specular scattering of polarised neutrons from laterally patterned magnetic multilayers
Workshop on Polarised Neutrons in Condensed Matter Investigations : Forschungszentrum Jülich
Jülich: 16.09.2002 - 19.09.2002

Köbler,U.; Hoser,A.; Bos,J.; Mueller,R.
Das Heisenberg Modell und die reale magnetische Welt
HGF-Workshop "Kondensierte Materie"
FZJ, Jülich: 06.11.2002 - 06.11.2002

Köbler,U.; Hoser,A.; Bos,J.; Mueller,R.; Schäfer,W.; Fischer,K.
On the thermodynamic universality classes of Heisenberg type magnets
ESS-Conference
Bonn: 16.05.2002 - 17.05.2002

Lauter,H. J.*; Lauter-Pasyuk,V.*; Toperverg,B.; Romashev,L.*; Ustinov,V.*; Vorobiev,A.*; Major,J.*
Neutron spin selection in off-specular scattering from magnetic multilayers
ESS-Conference
Bonn: 16.05.2002 - 17.05.2002

Lauter-Pasyuk,V.*; Lauter,H. J.*; Gordeev,G.*; Müller-Buschbaum,P.*; Toperverg,B.; Petry,W.*
Magnetic nanoparticles in self-assembled diblock-copolymer films
Workshop on Polarised Neutrons in Condensed Matter Investigations : Forschungszentrum Jülich
Jülich: 16.09.2002 - 19.09.2002

Lauter-Pasyuk,V.*; Lauter,H. J.*; Toperverg,B.; Müller-Buschbaum,P.*; Petrenko,A.*; Petry,W.*; Aksenov,V.*
Self-assembly of magnetite nanoparticles in thin block-copolymer films by off-specular neutron scattering
ESS-Conference
Bonn: 16.05.2002 - 17.05.2002

Lee,W.-T.*; te Velthuis,S. G. E.*; Felcher,G. P.*;

Klose,F.*; Gredig,T.*; Dahlberg,D.*; Toperverg,B.
Measuring lateral magnetic structure in thin films using polarised neutron reflectometry
Workshop on Polarised Neutrons in Condensed Matter Investigations : Forschungszentrum Jülich
Jülich: 16.09.2002 - 19.09.2002

Massalovitch,S.; Ioffe,A.; Küssel,E.; Brückel,Th.; Schlapp,M.; Von Seggern,H.*
The optimization of neutron image plate detector with low gamma-sensitivity
ESS-Conference
Bonn: 16.05.2002 - 17.05.2002

Mihaylova,M.; Seeck,O.; Kim,H.*; Serero,Y.*
Polymer thin films investigated with X-ray reflectivity and diffuse scattering
HASYLAB User Meeting
Hamburg: 25.01.2002

Mueller,R.; Chang,L. J.; Appelt,S.; Haesing,W.; Horriar-Esser,Ch.; Ioffe,A.; Brückel,Th.
Progress in the production of polarised 3He in Jülich
Workshop on Polarised Neutrons in Condensed Matter Investigations : Forschungszentrum Jülich
Jülich: 16.09.2002 - 19.09.2002

Murphy,B.*; Stettner,J.*; Sprung,M.*; Weber,R.*; Grotkopp,I.*; Seeck,O.; Müller,M.*; Tolan,M.*; Press,W.*
Surface behaviour in NbSe2 at the charge density wave phase transition
HASYLAB User Meeting
Hamburg: 25.01.2002

Rücker,U.; Kentzinger,E.; Toperverg,B.; Ziegenhagen,N.; Brückel,Th.
Off-specular scattering from magnetic structures measured with full polarisation analysis using HADAS@DIDO, Jülich
REFILL-Workshop : Grenoble
Grenoble: 24.10.2002

Rücker,U.; Toperverg,B.; Kentzinger,E.; Brückel,Th.
Resonant states in a ferromagnetic quantum well for neutrons
ESS-Conference
Bonn: 16.05.2002 - 17.05.2002

Schlapp,M.; Massalovitch,S.; Ioffe,A.; Brückel,Th.; von Seggern,H.*
Simulations on properties of neutron image plates
ESS-Konferenz
Bonn: 16.05.2002 - 17.05.2002

Seeck,O.; Mihaylova,M.; Kim,H.*; Sinha,S. K.*; Lambreva,D.*; Serero,Y.*; de Jeu,W.*
Investigation of confined and thin polymer films using x-ray scattering methods
Konferenz 7SXNS
Tahoe City, CA, USA: 22.09.2002 - 27.09.2002

Su,Y.; Istomin,K.; Schweika,W.; Fattah,A.; Foucart,P.; Meuffels,P.; Brückel,Th.; Kaiser,V.*
Polarization analysis of diffuse neutron scattering in lightly doped La1-xSrxMnO3 single crystals
Workshop on Polarised Neutrons in Condensed Matter Investigations : Forschungszentrum Jülich
Jülich: 16.09.2002 - 19.09.2002

Su,Y.; Istomin,K.; Schweika,W.; Foucart,P.; Fattah,M.; Meuffels,P.; Brückel,Th.; Kaiser,V.*
Polarization analysis of diffuse scattering in lightly doped La1-xSrxMn03 single crystals
ESS-Conference
Bonn: 16.05.2002 - 17.05.2002

Su,Y.; Schweika,W.; Istomin,K.; Fattah,M.; Foucart,P.; Brückel,Th.
Polarized neutron scattering from magnetic and structural correlations in lightly doped LaSrMnO single crystals
HGF-Workshop "Kondensierte Materie"
FZJ, Jülich: 06.11.2002 - 06.11.2002

Vad,Th.; Haubold,H.-G.; Waldöfner,N.*; Bönnemann,H.*
ASAXS investigations of 3-D platinum nanoparticle networks
SAS 2002 - Konferenz
Venedig, Italien: 25.08.2002 - 30.08.2002

Vad,Th.; Haubold,H.-G.; Waldöfner,N.*; Bönnemann,H.*
ASAXS investigations of 3-D platinum nanoparticle networks
HGF-Workshop "Kondensierte Materie"
FZJ, Jülich: 06.11.2002 - 06.11.2002

Voigt,J.; Kentzinger,E.; Rücker,U.; Schmidt,W.; Schweika,W.; Brückel,Th.
Magnetic structures and phase transitions in [Er-Tb] multilayers
ESS-Conference
Bonn: 16.05.2002 - 17.05.2002

Voigt,J.; Rücker,U.; Kentzinger,E.; Toperverg,B.; Brückel,Th.
Von Domänen und Grenzflächen: diffuse Streuung nahe der Totalreflexion an [Er/Tb] Schichtsystemen
HGF-Workshop "Kondensierte Materie"
FZJ, Jülich: 06.11.2002 - 06.11.2002

Voigt,J.; Wermeille,D.*; Schweika,W.; Brückel,Th.
Magnetic structure of a thin Er0,7Tb0,3-film
Workshop on Neutron and Synchrotron X-ray Scattering in Condensed Matter Research : PSI Villigen
Villigen: 03.08.2002 - 06.08.2002

Walter,G.*; Kranold,R.*; Enke,D.*; Goerigk,G.
SAXS characterisation of porous glasses
SAS 2002 Konferenz
Venedig, Italien: 25.08.2002 - 30.08.2002

Weber,R.*; Grotkopp,I.*; Stettner,J.*; Press,W.*; Tolan,M.*; Seeck,O.
Metal-polymer interfaces : X-ray reflectivity studies near the glass transition temperature
HASYLAB User Meeting
Hamburg: 25.01.2002

Ziegenhagen,N.; Kentzinger,E.; Rücker,U.; Toperverg,B.; Brückel,Th.; van der Hart,A.; Lehmann,R.; Schelten,J.
Investigation of artificial lateral magnetic structures in Fe/Cr multilayers with scattering methods
DPG-Frühjahrstagung
Regensburg: 11.03.2002 - 15.03.2002

Ziegenhagen,N.; Rücker,U.; Kentzinger,E.; Lehmann,R.; van der Hart,A.; Toperverg,B.; Brückel,Th.
Magnetic properties of laterally structured Fe/Cr multilayers
ESS-Conference
Bonn: 16.05.2002 - 17.05.2002

Ph.D. Theses

Babik,W.
Grenzflächenmorphologie von GMR- und TMR-Schichtsystemen
2002
Aachen, TH

Institute for Neutron Scattering

General Overview

1. User program at the FRJ-2 reactor

In 2002 the EU funded access to the research infrastructure program (ARI) "Jülich – Neutrons for Europe" (HPRI-2001-00268) has completed its first year of operation. The program has started in November 2001 with the purpose to support users from other European countries to perform experiments at the Jülich research reactor.

Proposals submitted to the ARI program are refereed by an international panel headed by Prof. J. Colmenero from the University of the Basque Country. In order to allow fast access, proposals are received for three deadlines per year (February, July and November). For the same reason the refereeing procedure is done using internet communications rather than panel meetings. In order to handle the additional administrational duties, a user secretariat was established. Figure 1 displays the number of proposals received and the amount of beam time requested at the four first deadlines. The figure also displays the number of selected proposals and the amount of beam time given. The total approved beam time of 206 instrument days in the first year exceeded significantly the contractual deliverable time of 133 per year.

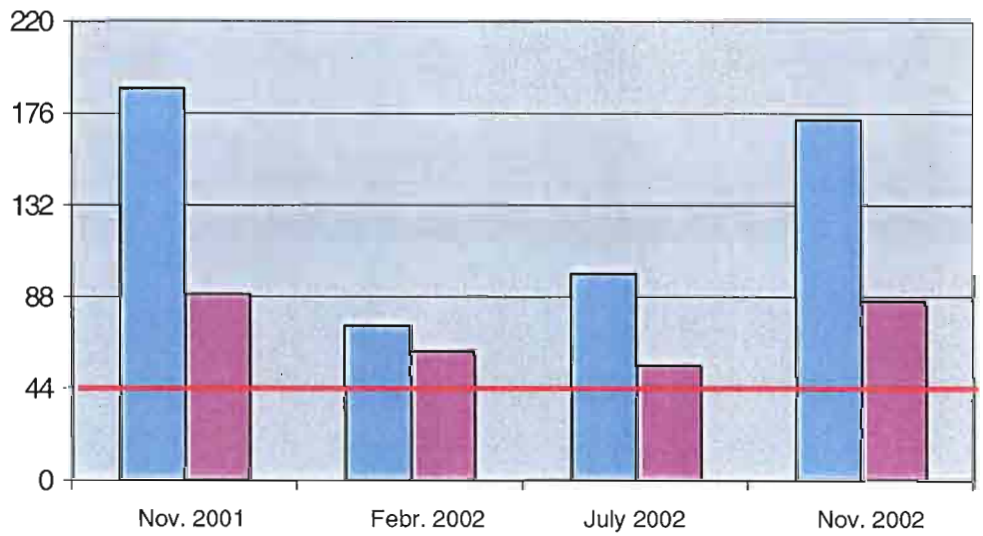

Figure 1 At the first four deadline requested (blue) and scheduled (red) beam time in the frame of the European access program. The red line displays the contractual deliverable beam time.

Figure 2 displays the scientific areas, where the proposals were placed. More than 50% were coming from soft matter science or biology, reflecting the distinctive strength of the Jülich instrumentation and scientific background in this field. We note that two proposals even dealt with topics from our cultural heritage, namely the study of archaeological findings. The proposals came from 10 European countries among which six do not have their own neutron

scattering facility. More than half of the users were new in the sense that they never did an experiment at the Forschungszentrum Jülich before. This clearly outlines the importance of the European funding for foreign scientists, who without this support would not have been able to access our facility.

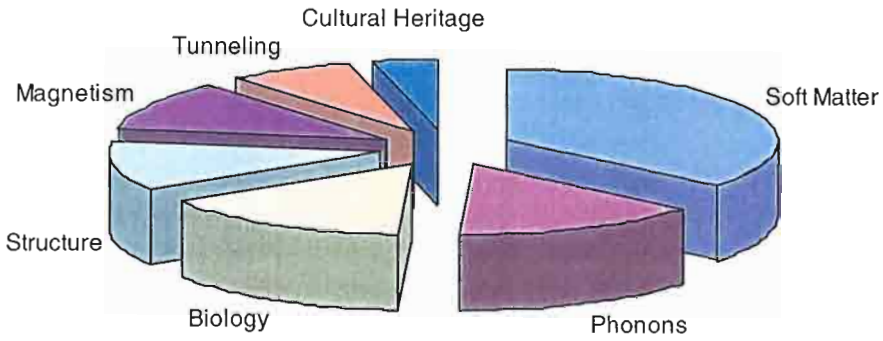

Figure 2: Distribution of the European proposals on different subject areas.

Aside of this European access program 59% of the experiments were performed by outside users. Figure 3 displays the origin of the different user groups classified into different categories.

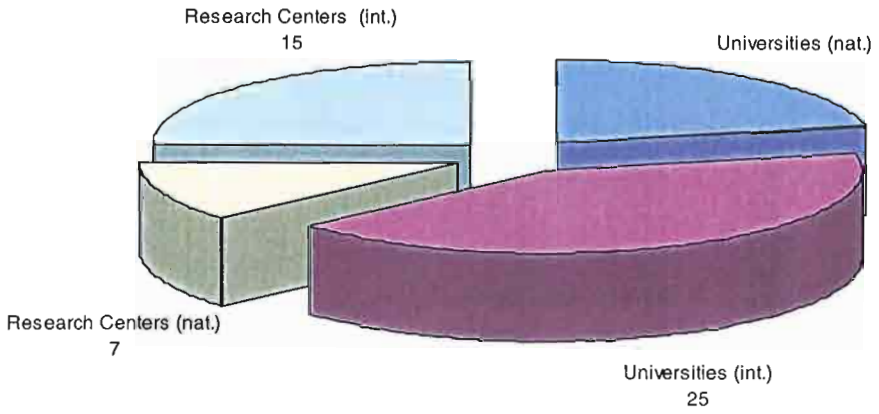

Figure 3: Origin of all external user groups classified into different categories.

Finally, in 2002 the "6th International Neutron Laboratory Course" took place. This training course for students was supported by the European Neutron Round Table. Again the number of applicants (89) surpassed largely the available places. From the 45 accepted participants 20 came from outside Germany.

2. Instrumentation (F&E No. 23.10.5)

New instrumentation and upgrading existing instrumentation is one of the focal points of the Institute for Neutron Scattering. In 2002 the following activities are noteworthy:

- The efforts to develop a "beyond the state of the art" neutron spin echo (NSE) instrument for the Megawatt Spallation Source SNS in the United States was followed with vigour. Test experiments and model calculations on the magnetic field properties in particular the field integral in homogeneities in superconducting coils were carried out (see report M. Ohl et al.). From these studies it became evident that in spite of flux pinning problems superconducting coils may be used even for ultra high resolution NSE instruments (F&E No. 23.60.0).

- The work on the backscattering instrument for the FRM-2 reactor in Munich came into its final phase. Most of the components are by now fabricated. Particularly noteworthy are the linear motor driven velocity drive gliding on aircushions of extremely high precision.

- At the Jülich facility the refurbishment of the two small angle scattering instruments KWS-1 and KWS-2 were in full swing. The new electronics and the new detector for KWS-1 are completed and are now being commissioned. Large parts of the new detector for KWS-2 have been built this year.

- Finally, the new technique of inelastic fixed window scans on the backscattering instrument lead to first results. Figure 4 displays such scans at an offset of 14.5μeV and Q = 1.88 for PEO/PPO block copolymers with and without salt. From such a scan the temperature dependence as well as the stretching of the relaxation function can be determined very quickly.

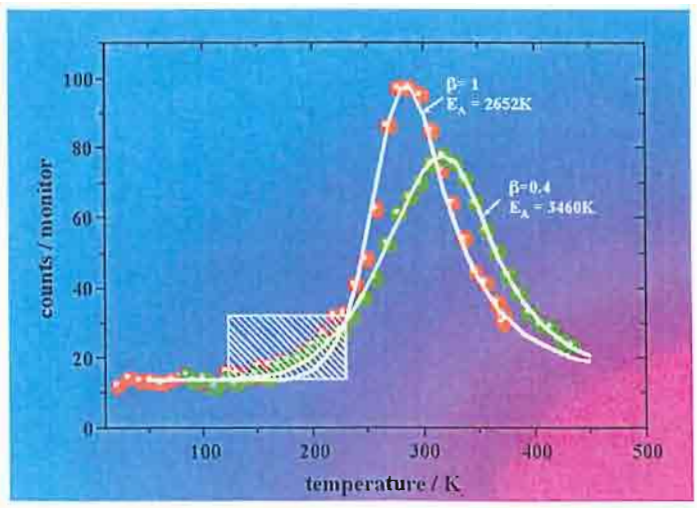

Figure 4:
Inelastic fixed window scan at the Jülich backscattering instrument at an offset energy of 14.5μeV. Sample PEO/PPO diblock copolymers with (•) and without salt (•). From the temperature dependent intensity both the activation energy and the stretching may be read off. Dashed area: contribution of CH_3 rotations.

3. Polymers, membranes and complex fluids (F&E No. 23.10.2)

The research of the institute concentrates on the field of soft condensed matter systems emphasizing polymers, complex fluids with a touch of biology. For this interdisciplinary research a close collaboration between chemists and physicists is mandatory. Soft matter materials are prepared and characterized in the chemistry laboratory of the institute. We all benefit also strongly from a close collaboration with the Institute Theory II of the IFF.

Polymer synthesis

Aside of the standard synthesis of homo- and blockcopolymers supporting the bulk of the research activities in the institute, a number of items specific to the chemistry need to be emphasized.

- Several model polyethylenes have been prepared by anionic polymerisation of butadiene and subsequent saturation of the double bonds. These polymers were triblock copolymers with protonated labels at various position along the chain. Additionally, a polyethylene three arm star block copolymer with a hydrogen label in the center of the star was synthesized.

- Careful studies of the refractive index increment of polybutadienes with various degrees of hydrogenation showed that the degree of deuteration can be determined easily and accurately by dn/dc measurements. Similarly, the microstructure may be such obtained.

- For the first time, we were able to relate in detail the monomer conversion and the initiation processes in anionic polymerisation with structural details in combining in-situ high resolution ^{1}H-NMR (500MHz) and in-situ small angle neutron scattering (SANS). These experiments appear to reveal completely new aspects of the anionic polymerisation mechanism. For example initiation occurs over a long time regime, where chain growth is already quite important. In addition, in the very early initiation stages, large scale aggregates are formed by cross association of the initiator molecules with the living chain.

- In the field of microemulsion efficiency boosting, new block copolymers were developed which are more simple to synthesize than the polyalkane-PEO systems. Furthermore, they allow to treat silicon oils which is not possible with the conventional boosters.

- The efficiency boosters used so far are not useful to stabilize emulsions. By changing the design of the polymers it was possible to obtain materials which now allow to stabilize emulsions.

Polymer dynamics

In 2002 our studies focused on (i) the large scale dynamics of polymers and its relation to rheological properties (molecular rheology) and (ii) dynamic studies, in order to elucidate the motions behind the α-relaxation in glass forming polymers

Large scale dynamics and molecular rheology

- From a combined measurement of the mean square segment displacement and the single chain coherent structure factor of a reptating chain a complete and consistent picture of the tube confinement in the reptation model evolved (see report A. Wischnewski et al.).

- After the observation of contour length fluctuations in a series of studies on reptating chains of different molecular weights, now by masking the outer parts of the chain by proper labelling it could explicitly be shown that the loosening of the confinement is related exclusively to the outer parts of the chain.

- In order to study constraint release, NSE measurements on long chains in different shorter chain matrices were performed. With decreasing matrix length an increasing loosening of

the confinement was observed. In the limit of a short chain matrix the transition to Rouse motion can be seen.

- In a second class of studies relaxation quench experiments were performed, in order to follow the chain relaxation in non-linear rheology. In this way, the chain retraction process after a non-linear stretch was identified (see report A. Blanchard et al.). On the basis of a thorough characterisation of model branched polymers (H-polymers and bi-products) we could confirm that backbone and arm relaxations of a branched polymer can be treated in a decoupled hierarchical way in time. We also showed that the tube dilution theories are valid over the investigated time range up to the length scale of the tube.

Dynamics of the α-relaxation

- A combined computer simulation and high resolution neutron scattering study covering an unprecedented large Q-range showed that the α-process may be understood as sublinear jump diffusion featuring finite jump lengths (see report A. Arbe et al.).

- Recent computer simulations on polyisobutylene suggested that the relaxation dynamics may be described as the combination of jumps between the split transconformations (tt jumps) and transgauche transition. It was claimed to have resolved the apparent inconsistencies between dielectric and NSE results on the one hand and NMR and ESR experiments on the other hand. With a combination of neutron time of flight and backscattering experiments on PIB samples with protons only at the backbone it could be shown that an evaluation following the scheme of the computer simulation leads to grossly inconsistent elastic incoherent structure factors for the tt jump, while the overall shape of the relaxation function can be accounted for. On the other hand the concept of a sublinear diffusion process is consistent with all data.

- The experiments on glass forming materials in mesoscopic confinement were extended from simple liquids to polymers. Researchers from the Federal Institute of Materials Research and Testing (Bundesanstalt für Materialforschung, BAM) were able to fill 25-200Å pores in a glass matrices with Polydimehtylsiloxane (PDMS). As in the simple liquid salol, a cut off of the glass typical low frequency vibrations (Boson peak) by the geometric confinement could be observed by inelastic neutron scattering. But the effect is weaker for the polymer.

Biomimetic mineralisation and cocrystallisation processes

Polymers are able to modify the crystallisation processes of anorganic and organic materials significantly. In this way, nature steers mineralisation processes like the growth of bones or shells. Our research in this field followed two lines

Mineralisation in the present of polymeric additives in calcium carbonate

- The role of the double hydrophilic block copolymer polyethyleneglycol-block-polymethacrylic acid (PEG-PMMA) on the morphogenesis of calcium carbonate was studied using contrast variation at the small angle scattering machine. The goal was to determine the partial scattering functions of the components. From the polymer partial scattering function we found clear evidence that the polymers are distributed inside the calcium carbonate crystals following a mass fractal distribution with an fractal exponent of $D_f = 2.7$. Time resolved SANS experiments under calcium carbonate contrast

confirmed these results and indicated that the crystallisation occurs via diffusion limited aggregation or percolation of clusters of nano-particles.

- The time evolution and growth of calcium carbonate mineralisation was also studied in the presence of additives like the protein Ovalbomin. While without the additive calcium carbonate nucleates into thin plates of a thickness less than 30Å and growths into porous micrometer large three dimensional particles, the additives convert the growth towards compact mineral structures. Ovalbomin itself denaturates during the mineralisation process from a globular to a rod like structure. The proteins seem to act as a nucleation center leading to a larger local accumulation of Ca^{2+} ions.

Cocrystallisation of partially crystalline polymers and paraffines

The influence of polymeric additives on the formation of wax crystals in crude oils and refined fuels are of scientific and practical interest. Wax crystal modification allows to modify pour points and cold filter plugging temperatures. Experiments on the random crystalline amorphous block copolymer of ethylene butene revealed that the biggest impact on wax crystal modification occurs if the polymer self assembly temperature coincides with the onset of crystallisation of the paraffin. SANS experiments gave insight into the various structures and cocrystallisation processes that occur.

Biophysics

Inelastic x-ray experiments were performed in order to study the longitudinal acoustic branch of DNA in various conformations along the helical axis. Advantages of this method are (i) that it accesses the zeroth Brillouin zone and (ii) that the sample volumes ($10mm^3$) are small. Therefore, such experiments allow to use artificial D-DNA as samples. Of disadvantage is the Lorentzian shape of the resolution function (FWHM $\cong$ 1.5meV). The experiments reduced a clearly visible sinusoidal LA branch which gives a reasonable sound velocity. The present modelling concentrates on the understanding of the damping mechanisms.

Complex fluids

After the polymer boosting effect has been established for the bicontinous microemulsions the influence of amphiphilic polymers was investigated also for droplet microemulsions. Thereby, asymmetric amphiphilic polymers of the PEO-PEP type were used.

- In the case of long water soluble blocks, homogenous distributions of polymer around the droplets were found and only a depletion zone around the droplet was avoided by the PEO block. No boosting was observed.

- If the oil soluble block was dominating, then the emulsification efficiency of the polymer doped surfactants strongly increased. At a maximum oil concentration a shape change from cylindrical to spherical structures was observed.

- The addition of homopolymers to bicontinous microemulsions allows to tune its viscosity. However, as an adversary effect the emulsification efficiency drops significantly. It was shown that this may be contour balanced by adding in addition diblock copolymers such that both efficiency and counter can be tuned simultaneously.

Soft colloids

Since 01.10.2002 our institute participates in the newly funded Transregio-Sonderforschungsbereich SFB-TR6 "Physics of colloidal dispersions in external fields". In this Sonderforschungsbereich we will use PEP-PEO block copolymer micelles as a tuneable model system for the investigation of the influence of external shear on the structure and phase behaviour of ultra soft colloids.

So far, we have studied the relation between the microscopic pair potential and the structure of ultra soft colloids. Star like (ultra soft) micelles display a microscopic gel transition around the overlap concentration C* which is reflected in the SANS data as a concentration dependent structure factor peak showing a strong discontinous transition around C*.

Further research activities

Tunnelling systems

- The main goal of our research in this area is the common interpretation of rotational tunnelling spectra, the phonon density of states and librations on the basis of the low temperature crystal structures and the intermolecular interactions parameterised e.g. as the universal force field (UFF). All methyl halides so far studied could be understood in such an approach.

- Ga- or In-trimethyl compounds which are used as doping sources in semiconductor production are an interesting case with a larger number of inequivalent methyl groups. The rotational potentials were identified in simultaneously studying quasielastic scattering and tunnelling.

- A new field is opened by test experiments on methyliodid water clathrates. This material crystallises in the same symmetry called cubic as a famous methane clathrate. First experiments reveal three tunnelling lines signifying different adsorption sites.

Dieter Richter

Personnel 2002/2003 and areas of activity

Scientific Staff

Dr. J. Allgaier	Polymer synthesis, microemulsions, emulsions	23.10.2
Prof. Dr. U. Buchenau (until 30.06.2002)	Dynamics of glassforming materials	23.10.2
Dr. H. Grimm	Molecular crystals, oriented macromolecules Instrument Responsible: Backscattering spectrometer BSS1	23.10.2
Dr. M. Monkenbusch	Dynamics of polymers and complex liquids, development of new spin echo techniques Instrument Responsible: Neutron Spinecho Spectrometer (NSE)	23.10.2
Dr. M. Ohl	Project scientist for NSE at SNS	23.10.5
Dr. M. Prager	Rotational tunneling Instrument Responsible: Thermal time of flight spectrometer SV 29	23.10.2
Dr. W. Pyckhout-Hintzen	Polymer networks; linear, branched and composite polymers; rheology;X-ray Instrument Responsible: Small angle neutron scattering KWS 1	23.10.2
Prof. Dr. D. Richter *Institute Director*	Structure and dynamics of polymers, glass transition, complex liquids ESS Science Director	23.10.2
Dr. D. Schwahn	Phase transitions in polymer systems, self assembly of crystalline copolymers, biomineralisation Instrument Responsible: Small angle neutron scattering KWS 1 and double crystal diffractometer DKD	23.10.2
Dr. J. Stellbrink	Star polymers, polymer/colloid mixtures and living polymerization, polymer colloids in external fields	23.10.2
Dr. L. Willner	Polymer synthesis, characterization kinetics of polymer micelles, polymer colloids in external fields	23.10.2
Dr. habil. R. Zorn	Rubbery electrolytes, glass transition, dynamics in confinement, water dynamics in glasses	23.10.2

Technical Staff

U. Bünten	Technician at KWS 1 and NSE	23.10.5
W. Bünten	Development work on neutron spin echo spectrometer for SNS	23.60.0
Ms. M. Hintzen	Technician in the polymer characterization laboratory	23.10.5
Dipl.-Ing. M. Heiderich	Engineer responsible for the KWS 1 and DKD instruments	23.10.5
Dipl.-Ing. T. Kozielewski	Engineer backscattering spectrometer FRM 2	23.10.5
V.T. Nguyen	Technician at SV29 spectrometer	23.10.5
Ms. U. Sausen-Malka	Electronic laboratory	23.10.5
Dipl.-Ing. R. Schätzler	Head of technical service group	23.10.5
Ms. C. Schnitzler	Secretary user office	23.10.5
T. Starc	Technician at BSS 1 spectrometer	23.10.5
R. Stollenwerk	Technician at KWS 2, electronic data processing	23.10.5
Dipl.-Ing. G. Vehres	Electronics engineer, head of electronics laboratory Second Instrument Responsible: Thermal time of flight spectrometer SV 29	23.10.5
Ms. S. Oubenkhir	Secretary	
Ms. T. Ziebarth (since 07.06.02)	Technician in the polymer characterization laboratory	23.15.0

Scientists

Dr. R. Biehl	Dynamics of gels Second Instrument Responsible: Neutron Spinecho Spectrometer (NSE)	23.10.2
G. Chen (since 16.10.02)	Microemulsion phases in polymer blends	23.10.2

A. Fomenko	Mineralisation at polymer templates	23.10.2
Dr. H. Frielinghaus	Microemulsions Instrument Responsible: Small angle neutron scattering facility KWS 2	23.10.2
Dr. Ms. M. Heinrich	Polymer processing, influence of branched polymers	23.10.2
Dr. Ms. H. Hermes	Structural investigation of polymer-silicate nanocomposites	23.10.2
Dr. O. Holderer (since 14.10.02)	NSE spectroscopy on supercritical fluid microemulsions	23.10.2
Dr. S. Kahle	Dielectric spectroscopy, relaxations in complex polymer systems, partially structure factor, glass transition Second Instrument Responsible: Backscattering spectrometer BSS 1	23.10.2
Dr. G. Kali	Instrument Scientist at the IN 15 spectrometer at the ILL	23.10.5
Dr. O. Kirstein (until 31.08.02)	Project scientist for backscattering instrument at FRM-II	23.10.5
Dr. Ms. A. Niu (since 04.02.02)	Living polymerisation, NMR techniques, SANS	23.10.2
Dr. A. Radulescu	Aggregation behavior of copolymers and wax crystallization Second Instrument Responsible: Small angle neutron scattering facility KWS 2	23.10.2
Dr. M. Rheinstädter (since 01.03.02)	Second Instrument Responsible: IN 12 at the ILL	23.10.2
Dr. G. Rother (since 07.10.02)	Polymer colloids in external fields	23.10.2
Dr. P. Rottländer (since 01.10.02)	Project scientist for backscattering instrument at FRM-II	23.10.2
Dr. W. Schmidt	Instrument Responsible: IN 12 at the ILL	23.10.5
Dr. A. Wischnewski	Polymer dynamics, ESS Scientific Advisory Committee (SAC) secretary	23.60.0

Thesis Students (University of Münster)

DI Ms. A. Blanchard	Relaxation mechanisms in entangled polymers by means of the small angle neutron scattering technique	23.10.2
Dipl.-Phys. D. Byelov	Investigation of the role of polymers in microemulsions by small angle neutron scattering	23.10.2
Dipl.-Phys. M. Laurati (since 01.03.02)	Depletion interactions in micellar/polymer mixtures	
Dipl.-Chem. R. Lund	Exchange kinetics between polymer micelles	23.10.2
Dipl.-Phys. V. Pipich	Formation of structure in mixtures of two homopolymers and a diblockcopolymers	23.10.2
Dipl.-Phys. Ms M. Zamponi	Dynamics of entangled polymers	23.10.2

Guests

Dr. M. Abdel-Goad (El-Minia Univ. Egypt)	Rheology of model polymers	23.10.2
Dr. Ms. A. Arbe (Univ. of the Basque Country, Spain)	Intermediate scale dynamics in polymer systems	23.10.2
Dr. L.J. Fetters (Cornell Univ., USA)	In-situ experiment on anionic polymerization	23.10.2
Prof. Dr. J. Colmenero (Univ. of the Basque Country, Spain)	Partial structure factors in polymer melts, computer simulation and self correlation function	23.10.2
Prof. E. Straube (Univ. Halle)	The influence of topological constraints at the microscopic level in polymer networks and blends	23.10.2

Trainees

J. Kurt	K. Kordelos
B. Pütz	T. Scymczyk

23.10.2	Condensed Matter
23.10.5	Operation and Further Development of the Neutron Source FRJ-2
23.60.0	Research and Development for the European Spallation Source ESS

Progress report for the construction of the new NSE spectrometer for the SNS

M. Ohl, W. Bünten and M. Monkenbusch

Institute for Neutron Scattering

To build a beyond state of the art NSE spectrometer with a resolution τ>1μs the spectrometer has to be equipped with superconducting (SC) precession coils for field integrals J>1Tm. A SC test system has been installed to asses the effects of flux trapping, 'hysteresis' field etc. on the field integral and to study the magnetic field in time and space. Within a simplified model we were able to describe the field integral contribution of the 'hysteresis' field quite sufficiently. An operational mode for superconducting coils to avoid any trapped flux by heating and subsequently cooling below T_C yields a magnetic field reproducibility of at least $\Delta B=8\ 10^{-6}$.

F&E-Nr: 23.60.0

Neutron spin echo instruments cover a broad range of applications in dynamics of polymer and glassy materials as well as phase transitions, disordered magnetic systems and transport phenomena. Due to the encoding of individual neutron velocity changes into spin precession angles it is possible - without affecting the high resolution - to use a very broad wavelength (velocity) spread. Thereby intensity is preserved. The resulting signal is, however, the intermediate scattering function, the Fourier transform $S(Q,\tau)$ of the spectral scattering function the intermediate scattering function [1, 2]. The most striking feature of NSE is decoupling of resolution from intensity. Whereas the resolution is given in terms of the Fouriertime τ :

$$\tau = \frac{\gamma m_n^2}{2\pi h^2} \lambda^3 \int B\,dl \propto \lambda^3 \int B\,dl \quad (1)$$

Obviously, the maximum resolution and - Fouriertime τ_{max} - is determined by the maximum wavelength λ_{max} and maximum field integral $J_{max} = \int B_{max}\,dl$ of the precession coils. Beside the use of highest wavelengths one is interested to increase the maximum field integral J_{max}. For the development of the worldwide highest resolution neutron scattering instrument for the SNS with a resolution τ_{max}=1μs two key technologies remain.

1. Use of superconducting coils for highest magnetic field integrals J_{max} > 1Tm and.
2. Development of high precession correction elements for a field integral homogeneity of about $\Delta J/J < 10^{-6}$.

These two key technologies directly lead to the frontier of feasibility. In this short report we would like to focus on the key technology dealing with the SC precession coil.

The major novel design goal for a next generation spin – echo spectrometer is the use of SC main solenoids providing a field integral J > 1Tm which should operate at least at a four times higher magnetic field integral than the NSE spectrometer IN15 at the ILL with the highest resolution in neutron scattering instruments. Fig. 1 already shows a schematic view of the NSE spectrometer for the SNS without the chopper system. SC precession coils had been foreseen which allow for optimal compensation with a negligible magnetic field in a distance d = 1.5m perpendicular to the scattering axis (see Fig. 1). However, the experience with a NSE set-up using SC solenoids to boost magnetic field integrals is limited so far [3,4].

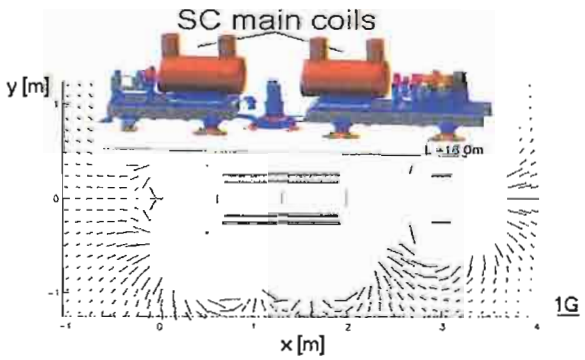

Fig. 1: Schematic view of the engineering design of the new NSE spectrometer and the stray field calculation for one main precession coil. The upper inset shows schematically the spectrometer with the two main precession coils.

Open questions still exist concerning a reliable operation in which the precession field changes for each Fouriertime τ. Field integral errors are due to unavoidable 'hysteresis' effects, 'flux pinning', influence of 'flux creeping' and 'flux jumping' during NSE operation and must be quantitatively estimated [5]. A feasibility study has been started in which the magnetic fields of a SC Nb-Ti Helmholtz - pair plus one auxiliary coil is under investigation (see Fig. 2 green and yellow region) and first results are presented. Fig. 2 shows the magnetic field in axial direction of the solenoids set after a central field of about B=1T as measured using a Hall probe. A remaining magnetic field of several Gauss has been pinned into the solenoid after the power supply has been switched off. When the coils reach the transition temperature $T_c = 8.9K$

this 'trapped field' vanishes continuously until all parts of them are above T_c.

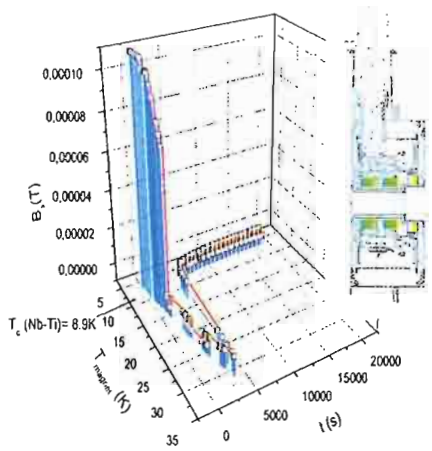

Fig. 2: Remaining magnetic field parallel to the symmetry – axis x of the Helmholtz - pair as pinned into the windings of the (SC) Helmholtz - pair while heating and subsequently cooling versus temperature T and time t.

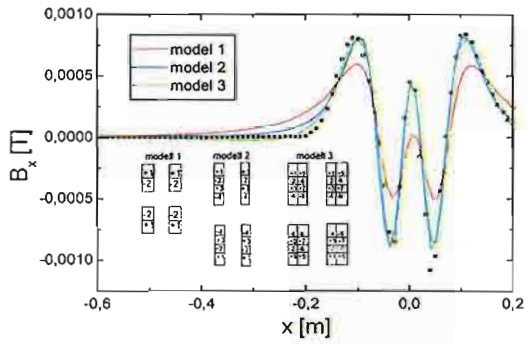

Fig. 3: Remaining axial magnetic field component on a path along the symmetry axis x through the coils assembly. Ring coil positions are at +4 cm and -4 cm, an extra coil at about 7 cm had not been excited but nevertheless trapped flux and contributes to the asymmetry of the curve. Model 1, 2 and 3 describe 2, 4 and 8 positive or negative currents pinned into the winding at positions schematically shown in the inset of the Figure.

Fig. 3 shows the field values B_x versus x-axis. The data show qualitatively a similar behaviour as expected for resistive coils carrying a finite current I_i=+I inside and I_o=-I in the outside section. A first coarse estimate indicates $J=\mu_0 N(I_o + I_i) \sim 0$, i.e. the influence on the key parameter for NSE is much smaller than inferred from looking on the absolute value of B at a single point. The exact difference of the field integral J due to trapped flux is currently being studied in more detail. This inset of Fig. 2 shows three models which describe the trapped flux in terms of positive and negative different currents. However, Model 2 and 3 were able to describe the data sufficiently with respect to the third SC coil which so far has not been taken into account.

For the stable operation especially the use of solenoids in combination with correction elements it is necessary to provide a radial distribution of the current as well as for the trapped flux which might also just trap into radial segments of the solenoid. However, we successfully described the magnetic field for several trajectories of the probe sensor assuming a radial distribution of currents. Thus we concluded the SC coils deliver the required radial symmetry of the magnetic field also for the trapped flux.

To achieve high reproducibility of the field integral and to avoid influences from previously 'pinned flux' one is able to operate SC coils with a defined current sequence after cooling below T_C and subsequently operating at a stable temperature. In a first test the magnetic field has been measured after the magnet system reached the stable operation temperature below T_c. Table 1 shows the results of such a measurement with the NMR sensor at a fixed position, whereas two solenoids Sol1 and Sol2 contribute to those windings as follows: $B = a\, I_{Sol1} + b\, I_{Sol2}$ whereas a = 5.0088724 10^{-2} T/A and b = 49.822 10^{-3} T/A.

No.	B [T]	I_1 [A]	I_2 [mA]	$(B_i - <B>)/<B>$
1	1.50408	30.0122	0.0164	2.49 10^{-6}
2	1.504065	30.0123	0.0159	7.47 10^{-6}
3	1.504085	30.0125	0.0156	5.81 10^{-6}
4	1.50408	30.0124	0.0160	2.49 10^{-6}
<>	1.50407625	30.01235	0.015975	---

Table 1: Magnetic field, currents of the two Helmholtz coils and normalized difference to the mean value <B> of the magnetic field.

The overall deviation lies within an error of about 8 10^{-6} which largely depends on the accuracy of the current and field measurement and SC effects [5]. Hence reproducibility of the magnet is certainly much better than 10^{-5}.

Despite the fact that residual 'hysteresis' fields of the order of several Gauss are encountered, the specific shape of these fields lead to a much smaller influence on the fields integrals. The first of the final goal of this study namely a modelling of the flux penetration and pinning effects in a realistic way that can be transferred to the final real coil pair for the NSE spectrometer has been made. Further refinements aim at quantitative assessment of the properties of the target system.

[1] F. Mezei : Z. Physik 255, 146 (1972.
[2] F. Mezei in 'The Principles of Neutron spin echo' in Neutron Spin Echo: proceedings of the ILL workshop, Grenoble 1979, ed. by F. Mezei (Lecture Notes in Physics 128, Springer Verlag, Heidelberg 1979 pp. 3 - 26).
[3] J. Kulda, E. Fahri, C. M. E. Zeyen, Phys. B 297 (2001) 37 – 39.
[4] S. Komura, T. Takeda, T. Miyazaki, M. Saga, S. Ueno, Nucl. Instr. Meth. Phys. Res. A 267 (1988) 425 – 435.
[5] Stability of Superconductors, Lawrence Dresner, 1995 Plenum Press, New York.

Segmental dynamics and topological confinement in polymer melts

A. Wischnewski, M. Monkenbusch, L. Willner, D. Richter
Institute for Neutronscattering

One salient property of long polymer chains in a melt is a constraint motion caused by a virtual tube along the chain profile as it has been proposed by deGennes in his famous Reptation model. This model proposes - next to the segment length - a second length scale in polymer melts, namely the tube diameter or entanglement distance. Neutron scattering can provide the single chain dynamic structure factor on the one hand and the time dependent segment mean squared displacement on the other hand. In the first case a protonated chain is measured in a deuterated matrix by neutron spin echo (NSE) - spectroscopy in the second the same method is applied to a fully protonated melt of polymer chains thereby providing information on the segment self correlation function. The different approaches, coherent and incoherent NSE, lead to the same tube diameter if the curvilinear segment motion along the contorted tube is accounted for.

F&E-Nr: 23.10.2

Beyond a certain length polymer chains in a melt are subject to topological constraints of motion due to entanglements. Microscopically the single chain structure factor $S(Q,t)$ as observed by NSE spectroscopy on deuterated melts containing a few h-labeled chains provides clear evidence for the restriction of motion and corrobates deGennes' dynamic structure factor for local reptation [1–3].
Thus the assumption of tube confinement, enforcing one-dimensional chain motion along the tube, is very effective in describing the chain dynamics for long chains. However, as it is known from broad cross-over phenomena like the molecular weight dependence of the melt viscosity, very important limiting mechanisms exist which effect the confinement and limit the reptation process. These processes increase in importance as the chain length decreases. Theoretically, constraint release, where a constraining chain moves out of the way of a given chain, and tube contour length fluctuations removing the constraints from the ends have been identified as the most important of those processes but only recently a direct microscopic observation of one of them could be performed [4]. In that work the comparison between the experimental chain length dependent dynamic structure factor and theoretical predictions clearly showed that in the time regime $t \leq \tau_R$, the Rouse time, the chain confinement inherent to the reptation picture is limited: Application of the pure Reptation model yields a significant molecular weight dependence of the apparent tube diameter. However, by introducing tube length fluctuations into the model for $S(Q,t)$ the fitted tube diameter d stays constant without any further assumption or parameter, i.e. it is possible to describe the full molecular weight dependence of $S(Q,t)$ in terms of local reptation and contour length fluctuation mechanism.
While in the coherent scattering the existence of a tube leads to a characteristic Q-dependence of the plateau at high Fourier times, given by the form factor of the tube, in the incoherent scattering, which measures the segmental self correlation, the tube should significantly change the temporal evolution of the extracted mean squared displacements at a time τ_e when the segments touch the "walls" of the virtual tube. The the predicted $\langle r^2(t)\rangle$ in the scenario of the reptation model are given by an initial Rouse motion ($\langle r^2(t)\rangle \propto t^{1/2}$) for $t < \tau_e$ while at τ_e the segmental diffusion slows down, further motion, termed local reptation, is a quasi one-dimensional Rouse relaxation along the contour of the virtual tube with $\langle r^2(t)\rangle \propto t^{1/4}$ [2].
Recently the first direct measurements of $\langle r^2(t)\rangle$ in terms of the proton self correlation function of diffusing segments in long chain polyethylene (PE) and polyethylene propylene (PEP)-melts have been performed at the NSE spectrometer in Jülich. We will focus here on PE. For the very long PE chains virtually all of the scattering intensity stems from "inner" segments. These should exhibit the same self-diffusion behavior and if the assumption of Gaussian shape of the diffusive displacement probability distribution would hold for all times one could extract the mean squared segment displacement directly from the scattering function

$$-6\ln[S_{\mathrm{inc}}(Q,t)]/Q^2 = \langle r^2(t)\rangle. \qquad (1)$$

Fig. 1 displays the hPE-data in this representation. As predicted by the standard Rouse theory [2] as well as by a number of computer simulations segment diffusion is described by the mean squared displacement due to

$$\langle r^2(t)\rangle = 2\sqrt{Wl^4/\pi}\, t^{\frac{1}{2}}. \qquad (2)$$

Inserting the previously determined value for the Rouse rate $W(509\,\mathrm{K})l^4 = 7 \pm 0.7\,\mathrm{nm}^4/\mathrm{ns}$ [5] from the analysis of the single chain structure factor of low molecular PE-melts, Eq. (2) is quantitatively corroborated.
Also a transition to a regime $\propto t^{\frac{1}{4}}$ is clearly visible. However, the crossover time is at about $\tau_e \simeq 1\,\mathrm{ns}$ which is much less than the textbook value [2] derived as $[\tau_e]_{\mathrm{DE}} = d^4\pi/(36Wl^4) \simeq 7\,\mathrm{ns}$, where the elementary step

length of the Gaussian contorted virtual tube is identified with the tube diameter ($d = 4.8$ nm [3,4]). Following Ref. [2] the mean squared segment displacement due to local reptation has been approximated as

$$\langle r^2(t)\rangle^{\text{locRep}} = d\sqrt{2/3}(Wl^4\, t/\pi)^{\frac{1}{4}} \qquad (3)$$

Inserting $d = 4.8$ nm leads to the dotted blue line in Fig. 1, its intersection with the $\propto t^{\frac{1}{2}}$ line defines $\tau_e = [\tau_e]_{\text{DE}}$, however the value of 7 ns is grossly wrong, fitting the data with d as a free parameter rather yields $d = 3$ nm.

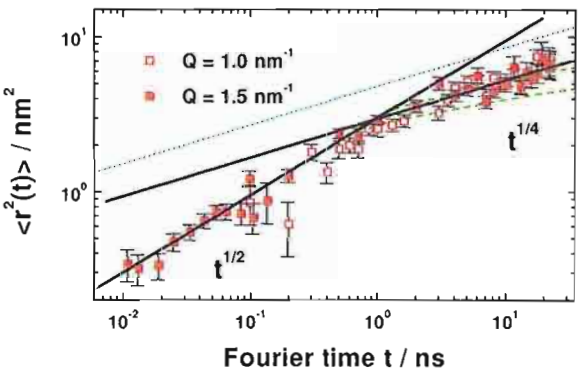

FIG. 1. NSE data obtained from the incoherent scattering from a fully protonated PE melt in a representation of $-6\ln[S_{\text{inc}}(Q,t)]/Q^2$ which is the mean squared displacement $\langle r^2(t)\rangle$ as long as the Gaussian approximation holds. Solid black lines describe the asymptotic power laws $\langle r^2(t)\rangle \propto t^{1/2}, t^{1/4}$. Dotted blue line: prediction from the Gaussian approximation, green dashed lines: see text.

In the derivation of Eq. (3) the Gaussian **width** after a diffusion time t of the single segment distribution along the 1D tube contour path coordinate, s, is taken for the time dependent **displacement**. Projecting this on the Gaussian contorted tube again corresponds to a Gaussian sublinear diffusion in real space (Eq. (3)). However, the real process has to be modelled by projecting the segment probability **distribution** due to curvilinear Rouse motion on the linear coordinate s onto the random walk like contour path of the contorted tube leading to a non-Gaussian probability distribution of the segment at times $t > \tau_e$. The necessity to perform the proper averaging has first been shown by Fatkullin & Kimmich [6] in the context of interpretation of field-gradient NMR diffusometry data [7] which yield results that are analogous to the incoherent neutron scattering functions however in another time and space regime covering mainly the regime $\tau_R < t < \tau_d$, the Reptation time. Their result

$$S_{\text{inc}}(Q, t > \tau_e) = \exp\left[\frac{Q^4a^2}{72}\frac{\langle r^2(t)\rangle}{3}\right]\text{erfc}\left[\frac{Q^2a}{6\sqrt{2}}\sqrt{\frac{\langle r^2(t)\rangle}{3}}\right] \qquad (4)$$

invalidates the Gaussian approxiamtion for times above τ_e. We note that Eq.4 is strictly valid only for $t >> \tau_e$ when $\langle r^2(t)\rangle \gg d^2$. The effect on the scattering function is that if (wrongly) interpretated in terms of the Gaussian approximation the cross over to local reptation appears to occur at significant lower values of τ_e.

Figure 1 shows a comparison of the scattering function $S_{\text{inc}}(Q,t)$ as predicted by Eqs. (1,4) (dashed green lines) with the incoherent NSE data. The parameters Wl^4 and d were fixed to the values taken from the single chain structure factor measurements. For Q = 1 nm^{-1} the free Rouse regime ($t < \tau_e$) as well as the local reptation regime is perfectly reproduced by a combination of Eq.1 and Eq.4. For Q = 1.5 nm^{-1} the prediction of Eq.4 lies slightly outside the error band of the data points (dashed green line).

With increasing Q-values the spatial resolution increases and agreement with theory may only be expected for Q - values $< 2\pi/d$. For the tube diameter of 4.8 nm in PE the "limiting" wavevector would be 1.3 nm^{-1} which may explain why at $Q = 1.5\,\text{nm}^{-1}$ deviations become visible. Since Eq.4 is strictly valid only when the segment displacement is large compared to the tube diameter, in the transition regime an unknown crossover function may modify its detailed behavior.

Thus, the measurement of the mean square segment displacement may be consistently interpreted in terms of the parameters derived from the single chain structure factor. Both approaches lead to a fully consistent description of the neutron data and validate the picture of a chain confining tube quantitatively. It will be now up to the interpretation of rheological data to find out why there too narrow chain confinement is predicted.

[1] P. DeGennes, Journal de Physique (France) **42**, 735 (1981).

[2] M. Doi and S. Edwards, *The Theory of Polymer Dynamics*, Vol. 73 of *International Series of Monographs on Physics* (Oxford University Press, Oxford, 1994).

[3] P. Schleger, B. Farago, C. Lartigue, A. Kollmar, and D. Richter, Physical Review Letters **81**, 124 (1998).

[4] A. Wischnewski, M. Monkenbusch, L. Willner, D. Richter, A. E. Likhtman, T. C. B. McLeish, and B. Farago, Physical Review Letters **88**, 058301 (2002).

[5] D. Richter, B. Farago, R. Butera, L. Fetters, J. Huang, and B. Ewen, Macromolecules **26**, 795 (1993).

[6] N. Fatkullin and R. Kimmich, Physical Review E (Statistical Physics, Plasmas, Fluids, and Related Interdisciplinary Topics) **52**, 3273 (1995).

[7] E. Fischer, R. Kimmich, U. Beginn, M. Moller, and N. Fatkullin, Physical Review E (Statistical Physics, Plasmas, Fluids, and Related Interdisciplinary Topics) **59**, 4079 (1999).

Relaxation mechanisms in deformed linear melts

A. Blanchard[1], M. Heinrich[1], W. Pyckhout-Hintzen[1], D. Richter[1], E. Straube[2]

[1] *Institut für Festkörperforschung, Neutronenstreuung, FZJ-Jülich*
[2] *Universität Halle, FB-Physik, Halle/Saale*

The dynamic properties of monodisperse high molecular weight model and entangled linear polymers are by now qualitatively understood to a high degree of sophistication and various processes have been taken into account to complete their full linear relaxation spectrum in both frequency and time domain. The use of scattering methods, i.e. the neutron spin echo method and lately also the small angle scattering technique is responsible for the latest developments which, after reptation, e.g. also allowed contour length fluctuations to be spatially correlated. The foregoing description bases on the tube model as an effective means to simulate the many-chain problem in a mean field approach. The situation is entirely different as soon as non-linear rheology is concerned. No consensus as to the description of start-up flow or microscopic details of the relaxation is present, not the least due to the lack of suitable experimental proof. This work aims at solving these problems and explores the whole time regime after a controlled step-strain experiment with subsequent relaxation.

F&E-Nr: 23.10.2

The scattering structure factor is an important tool in the investigation of chain deformations and segment fluctuations and the accessible wave vector in common experimental setups fits perfectly to the length scales of interests. Each length scale is connected to its own dynamical range or time domain in real space. The study of the microscopic polymer structure as a function of time after macroscopic uniaxial deformation can cope with intrinsically unsolvable assumptions, made in rubber elasticity theories or melt rheology. The equipment to do so is an elongational rheometer which was built earlier in order to investigate related processes in complicated branched polymeric structures.

FIG. 1: Elongational rheometer.

The system studied is a linear polyisoprene chain (glass temperature T_g ~ -70°C) with about 45 entanglements and a reptation time (τ_D) of the order of 20-30 seconds at ambient temperature. Through time-temperature equivalency, quantified in small amplitude linear shear, the dynamic processes on all length scales can be elegantly shifted into convenient time scales which allows an efficient control of handling and straining without loss of accuracy. The strain rate at -30°C is about 0.138 s^{-1} which is short compared to the Rouse time (τ_R) of the chain. Quenching at different states in time allows a unique visualization of the chain dynamics and its conformation. We have investigated the time domain between the immediately quenched state (t=0% of τ_R) and 50 times τ_R (i.e. 1/3 of τ_D). The deformation is highly non-linear (200%) and new relaxation processes are expected.

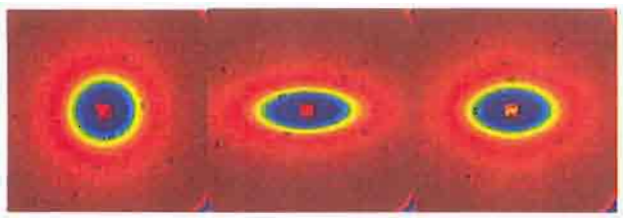

FIG. 2: Scattering at 6m for the isotropic state, the Rouse time and 30 times τ_R. The limits of the Q range are $Q.d_0=1$ and $Q.R_g=1$.

The proposed processes can be summarized as follows: after an (theoretically assumed) affine deformation of both the chain and the containing tube contour, a retraction mechanism appears to reduce the tube length to its equilibrium value. In this case, the chains must retract back in their still deformed tube of initial length but remain anisotropically oriented. After this first process, the path-length fluctuation sets in to introduce the later reptation process by which the final stress is relieved.

$$S(\vec{q},\lambda) = 2\int_0^x dx \int_0^{x'} dx' \prod_\mu exp\left\{ -(qR_g\lambda_\mu)^2 \frac{(x-x')}{\gamma} - (qR_g)^2(1-\lambda_\mu^2)\frac{d_\mu^2}{2\sqrt{6}R_g^2}\left(1-e^{-\frac{(x-x')2\sqrt{6}R_g^2}{\gamma . d_\mu^2}}\right)\right\}$$

Eq. 1: Static tube constrained structure factor.

The structure factor for a relaxing dilute chain in a melt of identical chains (to avoid random phase corrections and inter-chain contributions) is currently under construction (cooperation with theoreticians A. Likhtman, Leeds and E. Straube, Halle) and existing tube approaches (Warner-Edwards, Straube, Read) are modified as a short time solution in order to catch the possible details of the physical model.

In view of the time domain which was investigated, no contribution of reptational diffusion is to be expected and an analysis in terms of static rubber-elastic theories, corrected for chain extension, are justifiable. In a first approach, the retraction process is treated by reducing the effective chain length or equivalently speaking the Kuhn segment by a factor to be determined from SANS. These are compared to estimates from the Doi-Edwards theory. As this correction is isotropic in space, in the 2d scattering patterns the anisotropy should clearly increase as it enhances the relaxation of the parallel state but compresses the perpendicular even more. It is to be mentioned that this particular retraction process could not be confirmed in the last 20 years though severely tried by several research groups [1,2,3].

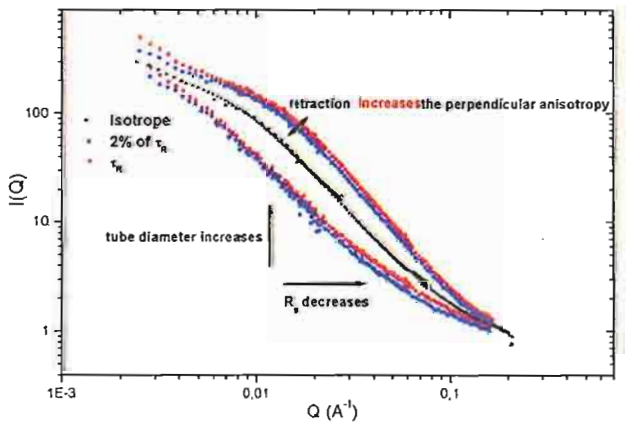

FIG. 3: Principal axes for times between affinely and relaxed chain scattering.

In Fig.3 and Fig. 4 we show the final experimental proof for the existence of the retraction process and its precursor - to be understood still - as well as the onset of reptation at long times. The different relaxation times available reveal more details on convective constraint release effects which are to be quantified in a next step.

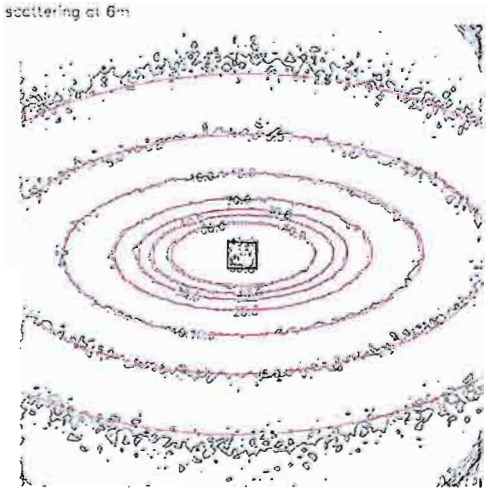

FIG. 4: 2-dimensional fits according to a Warner-Edwards confinement structure factor with retraction factor around 20%.

[1] F. Boué, "Polymer coil relaxation in uniaxially strained polystyrene observed by small angle neutron scattering", *J. Phys.* (Paris), **43**, 137 (1982)

[2] J.L. Viovy, "Chain retraction, length fluctuations, and small angle neutron scattering in strained polymer melts", *Journal of Polymer Science*, **24**, 1611 (1986)

[3] F. Boué, "Transient relaxation mechanisms in elongated melts and rubbers investigated by small angle neutron scattering", *Advances in Polymer Science*, **82**, 47-101, (1987)

Experimental evidence of a cross-over from Gaussian to non-Gaussian behavior in the α-relaxation of polyisoprene

A. Arbe, J.Colmenero, F. Alvarez
Unidad de Física de Materiales, San Sebastian, Spain

M. Monkenbusch, D. Richter
Institute for Neutronscattering

B. Farago, B. Frick
Institut Laue Langevin, Grenoble

By a combination of neutron spin-echo and backscattering spectroscopy the α-relaxation in polyisoprene has been explored over an unprecedented range in momentum transfer. Corroborating and validating earlier MD-simulations, the measurements reveal a crossover from a Gaussian regime of sublinear diffusion to a strongly non-Gaussian regime at short distances. A consistent interpretation in terms of a distribution of finite jumps underlying the α-process is possible. This model leads to a time dependent non-Gaussian parameter exhibiting all features revealed so far from various simulations.

F&E-Nr: 23.10.2

The heterogeneity in the dynamics of undercooled liquids and, connected with it, the deviations from Gaussianity of the dynamic correlation functions is one of the challenges along the way to understand glass formation. Recently the main dynamical process, the α-relaxation came into focus. Computer simulations as well as various experimental techniques have provided different and partially conflicting evidences for heterogeneous behavior or the absence of it (see e.g. [1] and references therein).

Incoherent neutron scattering (NS) experiments directly reveal the Fourier transform of the van Hove self correlation function $G_s(r,t)$: the intermediate scattering function $F_s(Q,t)$ or the dynamic structure factor $S_s(Q,\omega)$. For the α-relaxation $F_s(Q,t)$ assumes the form of a Kohlrausch-Williams-Watts (KWW) function

$$F_s(Q,t) = A \exp\left[-\left(\frac{t}{\tau_w(Q)}\right)^{\beta}\right], \qquad (1)$$

where A is a Lamb-Mössbauer-factor (LMF). A Gaussian correlation function implies a relation between the Q-dependence of τ_w and β as $\tau_w \sim Q^{-2/\beta}$ [2]. Extensive NS experiments on many different polymers have verified this Gaussian relationship in the low Q-regime ($Q \lesssim 1$ Å^{-1}) [3]. However, very recent MD-simulations on a polyisoprene melt (PI) revealed a clear crossover from $\tau_w \sim Q^{-2/\beta}$ to $\tau_w \sim Q^{-2}$ [4] at $Q \approx 1.3$ Å^{-1}. Furthermore, it was found to be connected with a strong increase of the non-Gaussian parameter $\alpha_2(t) = 3/5 \langle r^4(t) \rangle / \langle r^2(t) \rangle^2 - 1$. A monodisperse PI sample with deuterated methyl groups was investigated: -[CH_2-CH=$C(CD_3)$-CH_2]-$_n$ (PId3) by incoherent neutron scattering.

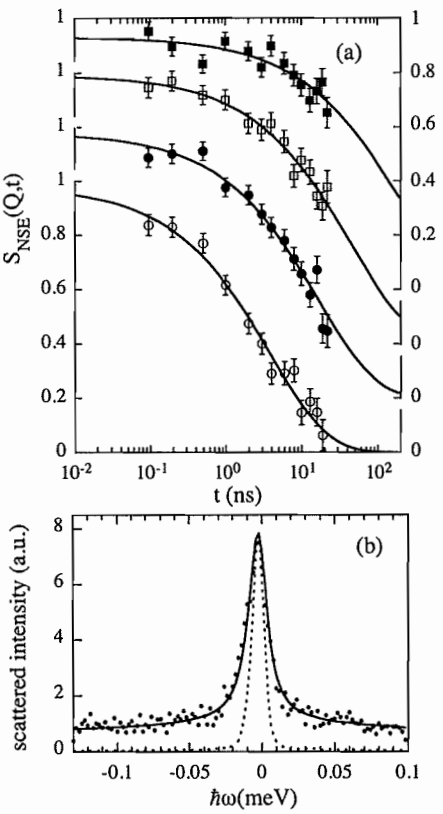

FIG. 1. Spectra obtained for PId3 (a) by the Jülich NSE at 340 K and Q= 0.10, 0.15, 0.20 and 0.30 Å^{-1} (top to bottom), and (b) by IN13 at 2.9 Å^{-1} and 300 K. Solid lines correspond to KWW descriptions with $\beta = 0.57$ (a) and $\beta = 0.50$ (b). The dotted line shows the IN13 instrumental resolution function obtained at 1.5 K.

To study the characteristic time $\tau_w(Q)$ in PI in a very extended Q-range ($0.1 \leq Q \leq 4.7\,\text{Å}^{-1}$) a suite of different instruments has been used: the Jülich-NSE, the ILL NSE spectrometers IN11, IN11c and the thermal backscattering spectrometer IN13. Results of a KWW analysis using stretching parameters $0.4 \leq \beta(T) \leq 0.57$ are shown in Fig. 2.

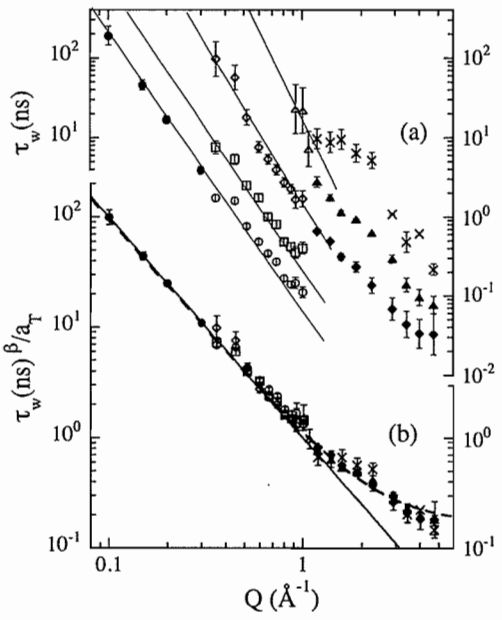

FIG. 2. (a): Q-dependence of τ_w obtained for PId3 by IN13 (×: 260 K; ▲: 280 K; ♦: 300 K), IN11c (△: 280 K; ◇: 300 K; □: 320 K; ○: 340 K) and Jülich NSE spectrometer (•: 340 K). (b): Master curve built with the data in (a). The straight solid lines display the Q-dependence expected from the Gaussian approximation. The dashed line shows the description of the master in terms of the anomalous jump diffusion model with $\ell_0 = 0.42$ Å.

A strong decrease of τ_w with increasing Q is encountered. To scrutinize the Gaussian character of $G_s(r,t)$, in Fig. 2(a) we have compared the Q-dependent characteristic times with the Gaussian prediction $\tau_w \sim Q^{-2/\beta}$ (solid lines). As the value of β slightly increases with T, the slopes of the predicted power laws decrease in absolute value towards higher T. Only above 1 Å^{-1} the times deviate and follow a weaker Q-dependence. In Fig. 2(b) all data from Fig. 2(a) are condensed to a single master curve: by first exponentiating $\tau_w(Q)$ to the power of β to eliminate the effect of a β variation assuming the Gaussian prediction $\tau_w^{\beta} \sim Q^{-2}$. Secondly, the T-dependence is removed applying shift factors a_T relative to a reference temperature T_R [300 K in Fig. 2(b)]. A Q^{-2} dependence of τ_w^{β} is obtained at low Q crossing over to a weaker power law at $Q \approx 1.3$ Å^{-1}. Thus, covering the largest $Q-t$ range ever in a single NS-experiment, we have experimentally established a crossover from Gaussian to non-Gaussian character of the α-relaxation similar to that reported for the simulated sample [4].

The likely origin of the deviation from Gaussianity at short length is a jump like character of the elemtary steps of motion. In jump diffusion models finite jump lengths tend to cause a bending of the dispersion for the diffusive relaxation times away from the Q^{-2} law.

$$F_s^{JD}(Q,t) = \exp\left[-\frac{\langle u^2 \rangle}{3}Q^2 - b(Q)\left(\frac{t}{\tau_0}\right)^{\beta}\right], \quad (2)$$

where $b(Q)$ depends on the particular geometry of the jumps involved, i.e., on the jump vectors $\vec{\ell}$. Assuming randomly oriented jump directions with an exponential distribution of jump lengths $f_0(\ell) = \ell\ \ell_0^{-2}\exp(-\ell/\ell_0)$, where ℓ_0 is the most likely jump distance, $b(Q) = Q^2\ell_0^2\ \left(1+Q^2\ell_0^2\right)^{-1}$. By comparing Eqs. (1) and (2), τ_w reads: $\tau_w = \tau_0\left[1+1/(Q^2\ell_0^2)\right]^{\frac{1}{\beta}}$ providing a good description of the experimental results displayed in Fig. 2(b) (dashed line). The non-Gaussianity parameter $\alpha_2(t)$ as computed from the jump model reproduces the main conjectures that are reported in the literature from simulations of glass forming systems in general (see e.g. [8–12]). In conclusion the measurements reveal a crossover in $\tau_w(Q)$ in perfect agreement with the simulation results. The Q-dependence of $\tau_w(Q)$ is described in terms of a jump length distribution underlying the sublinear diffusion present in the α-process. We find that this simple approach accounts for all universal features of $\alpha_2(t)$ reported so far in the literature for glass forming systems in general. See Ref. [13] for more details.

[1] H. Sillescu. *J. Non-Cryst. Solids*, 243:81, 1999.
[2] J. Colmenero, A. Alegría, A. Arbe, and B. Frick. *Phys. Rev. Lett.*, 69:478, 1992.
[3] A. Arbe, J. Colmenero, M. Monkenbusch, and D. Richter. *Phys. Rev. Lett.*, 81:590, 1998.
[4] J. Colmenero, F. Alvarez, and A. Arbe. *Phys. Rev. E*, 65:041804, 2002.
[5] B. Farago, A. Arbe, J. Colmenero, U. Buchenau, D. Richter *Phys. Rev. E*, 65:051803, 2002.
[6] O. Ahumada et al. *Macromolecules*, 35:7110, 2002.
[7] Ed. P. A. Egelstaff, *An Introduction to the Liquid State*,Oxford University Press, NY , 1992.
[8] D. Caprion, J. Matsui, and H. R. Schober *Phys. Rev. Lett.*, 85:4293, 2000.
[9] F. Sciortino, P. Gallo, P. Tartaglia, and S.-H. Chen. *Phys. Rev. E*, 54:6331, 1996.
[10] M. M. Hurley and P. Harrowell. *J. Chem. Phys.*, 105:10521, 1996.
[11] W. Kob et al. *Phys. Rev. Lett.*, 79:2827, 1997.
[12] S. Mossa, R. Di Leonardo, G. Ruocco, and M. Sampoli. *Phys. Rev. E*, 62:612, 2000.
[13] F. Alvarez et al. *Phys. Rev. Lett.*, 89:245701, 2002.

Thermal Composition Fluctuations and Phase Behavior of an A/B/A-B Homopolymer Blend / Diblock Copolymer Mixture

V. Pipich, D. Schwahn and L. Willner

Institute for Neutron Scattering

Thermal composition fluctuations were explored with SANS in a homopolymer blend dPB/PS of critical composition mixed with different amounts of a symmetric diblock copolymer dPB-PS. Phase boundaries of various ordered phases including two critical universality classes and the Lifshitz line (LL) were determined. Strong thermal fluctuations lead to a non-monotonic LL, droplet and bicontinuous micro emulsion phases, and a reentrant two-phase region near LL with an upper and lower critical solution temperature and a double critical point (DCP). The expected doubling of the Lifshitz critical exponent γ was observed approaching the DCP.

F&E-Nr: 23.10.2

Small additions of A-B diblockcopolymers (A and B characterize the monomer) in partly miscible A and B homopolymers lead to a better compatibility. It also influences the degree of thermal composition fluctuations and imposes a crossover from the universality class of 3D-Ising to isotropic Lifshitz critical behavior. Adding even larger amounts of diblock copolymer lead to an even more complex phase diagram of lamella ordered and microemulsion phases. Such phase behavior and the change of universality class can be qualitatively understood as binary homopolymer blends phase separate into macroscopically large domains and obey the universality class of 3D-Ising while diblock copolymers show an ordering transition into ordered phases of mesoscopic scale and obey the Brasovskiĭ universality class [1]. It is therefore quite apparent, that such systems are of strong scientific and of industrial interest. We particularly studied ternary mixtures of two A, B homopolymers of same molar volume and of critical composition and of symmetric A-B diblock copolymer of about five time larger molar volume.

Mean field theory predicts for the present blend a Lifshitz line of constant diblock concentration, a Lifshitz critical point with the critical exponents of susceptibility and correlation length of γ=1 and ν=1/4, respectively [2]. Those mean field critical exponents were observed in such a polymer system of rather large molar volume [3]. On the other hand, a sharp transition from 3D-Ising (γ=1.24, ν=0.63) to the isotropic Lifshitz critical behavior (γ=1.62 and ν=0.9) was found in a mixture of significantly smaller polymer molar volume [4,5]. The isotropic Lifshitz critical exponents could not yet be determined from theory [2].

In the Lifshitz critical regime thermal composition fluctuations play an important role and are responsible for several deviations from mean field predictions: (1) no Lifshitz critical point exists and instead a micro emulsion channel appears between the two-phase and lamella ordered regions, (2) the Lifshitz line shows a non-monotonic temperature dependence, (3) a reentant two-phase region is observed with an upper and lower critical solution temperature and a double critical point. These

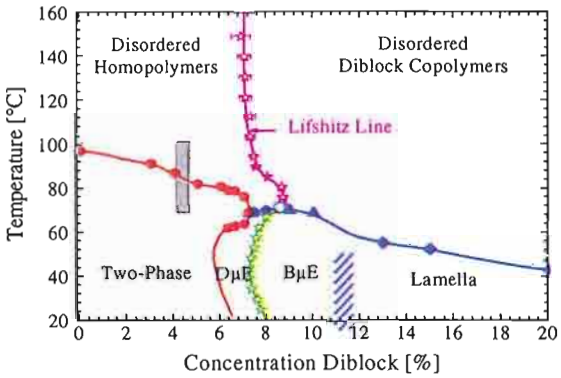

FIG. 1. Phase diagram of the ternary dPB/PS/dPB-PS blend

findings are visualized in the phase diagram (Fig.1) of the ternary blend of dPB/PS/dPB-PS representing the temperature versus diblock concentration plane. The acronym dPB and PS stands for deuterated poly(butadiene) (V_W=2720cm^3/mol), and poly(styrene) (V_W=2180 cm^3/mol), respectively. Samples of the critical blend dPB/PS (Φ_C(dPB)=0.42) were mixed with different concentrations of the dPB-PS symmetric diblock copolymer (V_W=15400cm^3/mol). Thermal composition fluctuations were measured with SANS as a function of temperature and diblock concentration from which the phase boundaries and critical universality classes were determined.

The Lifshitz Line divides the disordered region at high temperature into a „blend-like" and "diblock-like" part, and is determined when the peak position of S(Q) moves away from Q^*=0. Within mean field approximation the Lifshitz line is determined from the ratio of the molar volumes $\alpha = \sqrt{V_A V_B}/V_{A=B}$ and is estimated with 4.7% from $\Phi_{LL}=2\alpha^2/(1+2\alpha^2)$ for the present system [6]. The Lifshitz line in Fig.1, however, shows deviations. At high temperatures it is observed at a larger diblock contration of 7% and bends near the critical line to an even larger concentration. Such deviations are caused by thermal composition fluctuations as has been found from

renormalization group theory calculations [7]. The Lifshitz line terminates at Φ=0.085 and T=71°C at the transition line of the micro emulsion phases and represents a multicritical point. The line below this critical point separates the droplet (DμE) and bicontinuous micro emulsion (BμE) phase. Both lines were derived from isothermal scaling laws according to $Q^* \propto |\Phi - \Phi_{LL}|^{\alpha}$ in the range of $\Phi_{LL}<\Phi<1$; in the disordered phase an α=0.4 while in the bicontinuous phase a α=0.3 was observed.

„3D-Ising Critical Regime" The binary blend of dPB/PS shows a crossover from mean field behavior at high temperatures to 3D-Ising critical behavior at low temperature in the vicinity of the critical point. The temperature dependence of the susceptibility is adequately described by the Kiselev-Belyakov crossover function [8]. Small diblock additions within $0<\Phi<5\%$ do not change the universality class but lead to an improved compatibility and a sharp increase of the Ginzburg number from $1.3\cdot10^{-4}$ to $3.4\cdot10^{-3}$ for Φ=4%.

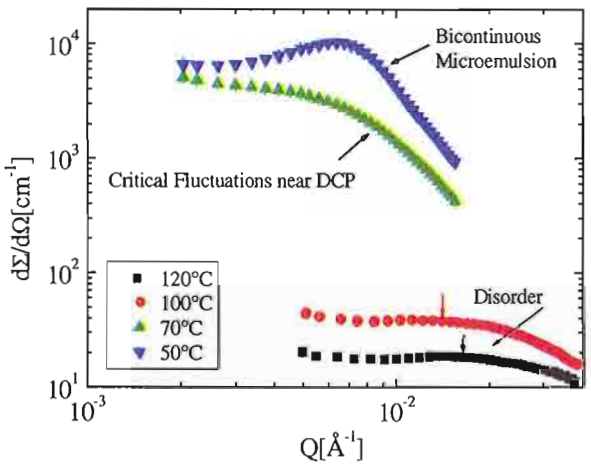

FIG. 2 . Scattering cross-section of a 8% sample at four different temperatures in the disordered phase, near the double critical point (DCP), and bicontinous phase

„Isotropic Lifshitz Critical Regime" Diblock copolymer concentrations larger than Φ=4% lead to a crossover to the isotropic Lifshitz universality class. This crossover can be understood from a reduced surface energy (first order gradient energy term of the Hamiltonian becomes zero at the Lifshitz line [2]) and thereby a reduced restoring force for thermal fluctuations. This means that in the Lifshitz universality regime thermal fluctuations are stronger and much more effective than in the Ising regime. So, mean field theory predicts the existence of an isotropic critical Lifshitz point at the position where two-phase, ordered lamellae, and disordered one-phase regimes come into contact. Such a critical point, however, is destroyed by strong thermal fluctuations and instead a channel of a bicontinuous microemulsion phase is observed [9]. Surprisingly, in the present system a reentrance coexistence phase is observed near the Lifshitz line between 6% and 7.1% diblock content. In this range the two-phase region is limited by the upper and lower critical solution temperatures T_{UCST} and T_{LCST}, respectively, and this gap decreases from 15K at Φ=6.6% to zero at the double critical point at Φ_{DCP}=7.1% and T_{DCP}=71°C. Theory predicts twice as large critical exponents which can be understood from the tangential approach to the critical point and the quadratic nature of the critical line. A differently defined reduced temperature, however, including both critical temperatures according to $\tau_{UL} = |(T - T_{UCST})(T - T_{LCST})|/T^2$ leads to a scaling behavior with the conventionally defined critical exponents [10]. The critical exponent γ from both reduced temperature fields have been depicted in Fig.3 versus diblock content. The filled diamonds correspond to τ_{UL} while the full dots to τ. A crossover from the Ising exponent to the isotropic Lifshitz critical exponent is found in consistence with an earlier study [5].

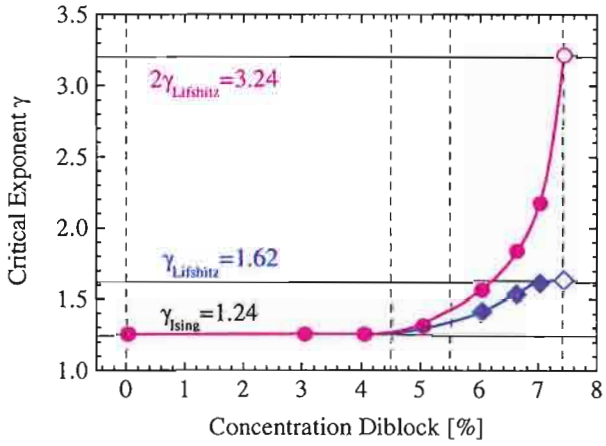

FIG. 3. Critical exponent of the susceptibility γ vs. diblock copolymer content

"Diblock-like behavior" At diblock content larger than the Lifshitz line the system follows a "diblock-like" behavior with an order-disorder transition at low temperatures. Above 12% diblock content a clear indication of an ordering transition is obtained from the observation of a second order peak and a characteristic change of the susceptibility. A lamella ordered phase is expected because a symmetric diblockcopolymer was added.

[1] K. Binder, *Adv. Polym. Sci.*, **112**, 181 (1994).
[2] R. Holyst et al. *J. Chem. Phys.* **96** , 7728 (1992).
[3] F.S. Bates et al. *Phys. Rev. Lett.* **75**, 4429 (1995).
[4] D. Schwahn et al. *Phys. Rev. Lett.*, **82**, 5056 (1999).
[5] D. Schwahn et al. *J. Chem. Phys.*, **112**, 5454 (2000).
[6] D. Broseta et al. *J. Chem. Phys.* **96**, 7728 (1990).
[7] A. Kudlay et al. *Macromol. Theory and Simulations*, **11**, 16 (2002).
[8] M.Y. Belyakov et al. *Physica A*, **190**, 75 (1992).
[9] F. Bates et al. *Phys. Rev. Lett*, **79**, 849 (1997).
[10] B.V. Prafulla et al. *Phys.Rev.A*, **46**, 7456 (1992).

Lattice dynamics and methyl rotational tunneling of the methyl halides based on universal force fields

O. Kirstein [1,2], M. Prager[1]
[1] *Institute for Neutron Scattering,*
[2] *Australian Nuclear Science and Technology Organisation,*
Lucas Heights, PMB1, Menai, NSW 2243 Australia

Methyl halides are the most simple molecules containing methyl groups. Beside of hydrogen and carbon with their well established interaction potentials methyl halides contain just one additional other atom. This offers the possibility to test actually used parametrizations of interaction potentials between hydrocarbons and halide atoms. Their reliability is judged on the basis of a comparison of the calculated lattice dynamics and methyl rotational tunneling based on the low temperature crystal structure with inelastic neutron scattering experiments.

F&E-Nr: 23.10.5

The single particle model (SPM) of rotational tunneling [1] is a mean field approach. Despite the more recent detection of systems with coupling between rotors and other degrees of freedom the prominent number of molecular crystals can be well described by the SPM. A data analysis beyond a phenomenological use of the SPM has to reproduce the lattice dynamics and rotational potentials on the basis of the crystal structure and fundamental intermolecular interactions. More and more systems are analysed this way [2]. Their number is mainly limited by the lacking knowledge of precise low temperature crystal structures. Vice versa these tests may contribute to an improved parametrization of intermolecular potentials.

The low temperature crystal structures of CH_3F and CH_3Br are described in the literature. The one of CH_3I is established at $T = 4K$ in a recent unpublished diffraction experiment. The crystal structure of CH_3Cl is only known at elevated temperature. The low temperature structure of methyl fluoride is monoclinic $P2_1/n$ while methyl iodide and bromide assume an orthorhombic structure Pnma. The molecules are arranged in chains along the c axis with alternating orientations. The molecules in the unit cell of CH_3Br are shown in fig. 1. Below its melting point CH_3Br transforms into space group $Cmc2$ with all molecules parallel. This is also the crystal structure of CH_3Cl at high - and likely all - temperatures.

The density of states and the tunneling spectra of all methyl halides are published [4,5].

Beside the interatomic distances obtained from the crystal structures intermolecular interaction potentials are needed as second ingredient of the calculations. An established concept of intermolecular interactions are the transferable pair interaction potentials. While there are specific parametrizations for special subsets of atoms like the hydrocarbons the accumulated knowledge on all elements of the periodic system is condensed into the universal force field (UFF) [3]. The application of intermolecular interaction potentials to methyl halides must be based on UFF. The pair interaction of the UFF is a modified Born-Meyer potential

$$V_{ij}^{vdW}(r) = [D_{ij}(\frac{6}{\zeta - 6})exp(\zeta)]exp(-\zeta(r/x_{ij}))$$

$$-[D_{ij}(\frac{\zeta}{\zeta - 6})x_{ij}^6]/r^6 \qquad (1)$$

with strength parameters D_{ij} and interaction distances x_{ij} characteristic of a pair i,j of atoms and a specifical adjustable parameters ζ. To guarantee transferability the interaction between different atoms is derived from the one between identical atoms by the relations $D_{ij} = \sqrt{(D_i \times D_j)}$ and $x_{ij} = (x_i + x_j)/2$. To quantify the origin of deviations of calculated and measured spectra we introduce two fit parameters [6].

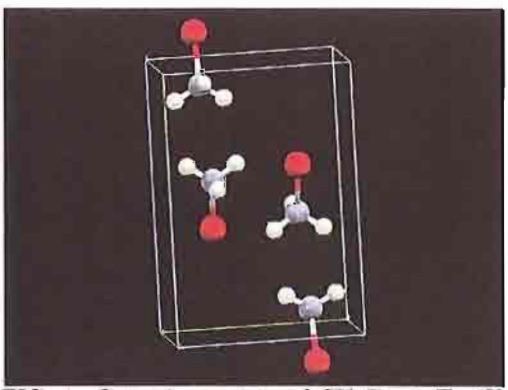

FIG. 1. Crystal structure of CH_3Br at T=4K. The space group is Pnma, Z=4, a=4.5115Å, b=6.5040Å, c=9.3504Å.

At first, by scaling r the overall strength of the potential had to be increased by 5%, secondly the repulsive term between hydrogen and *all* other atoms had to be softened in case of the fluoride and chloride. In case of bromide and iodide only the interaction to the halides is weakened. The calculations presented used the such modified UFF potentials. Beside the vdW the Coulomb interaction is taken into account. The charges needed were

obtained from GAUSSIAN98 calculations.

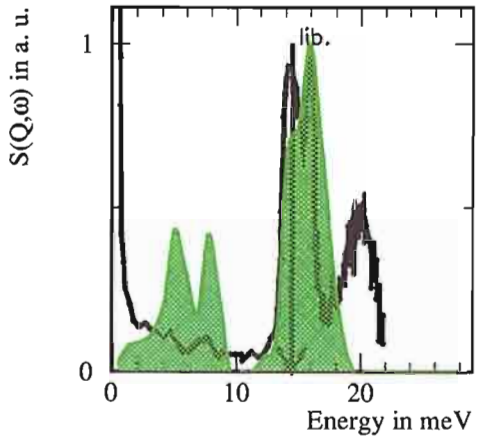

FIG. 2. Measured (solid line) and calculated (green area) densities of states of CH_3Br. The lower line of the doublett shows the methyl libration, the higher one a libration of the whole molecule around its centre of mass perpendicular to the molecular symmetry axis. Both, the eigenvectors and the eigenenergies are well reproduced by the calculation.

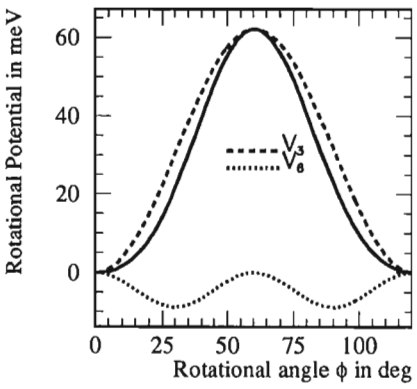

FIG. 3. Methyl rotational potential of CH_3Br calculated from the single particle model. The antiphase of the V_3 and the V_6 terms (dashed lines) broadens the minimum of the potential. This enlargens the tunnel splitting while the libration is reduced in good agreement with experiment.

Dispersion curves and the weighted density of states (DOS) were calculated in harmonic approximation [7] using the program DYNCAL [8]. The DOS is compared with neutron time-of-flight spectra from polycrystals.

The tunnel splittings $\hbar\omega_t$ and librational energies E_{01} of methyl groups are calculated in the SPM. In this approximation the rotational potential up to order 2

$$V(\varphi) = \sum_{n=1}^{2} V_{3n}(1 - cos(3n\varphi - \alpha_{3n}) \qquad (2)$$

is obtained by rotating the symmetrized methyl group about its symmetry axis in a rigid environment and summing up all pair interaction potentials between its three protons and the atoms of the lattice.

The results for methyl bromide are shown in the figures 2 and 3. A comparison of some measured and calculated eigenenergies is shown for all methyl halides in Tab. I.

mol.	$\hbar\omega_t/\mu eV$	E_{01}/meV	V_3/meV	V_6/meV	α_3/deg
CH_3F					
calc.	20.5	10.4	24.3	-3.2	-16
exp.	23.1	10.0	26.6	0.0	
CH_3Cl					
calc.	0.04	17.4	104	-18	-1.5
exp.	0.1	18.1	77	0.0	
CH_3Br					
calc.	0.7	14.4	62.2	-8.8	-1.5
exp.	0.9	14.8	50.7	0.6	
CH_3I					
calc.	2.6	12.0	48.2	9.0	-1.5
exp.	2.44	13.3	41.0	1.9	

TABLE I. Comparison of measured methyl rotational potentials with calculations based on the low temperature crystal structures and UFF intermolecular potentials [3].

The agreement between experiments and theory is very promising. The equilibrium orientations are well reproduced for all methyl halides beside of CH_3F. The calculated potentials agree within ~20% with those derived from the measured eigenenergies. The largest deviations of the tunnel splittings is by a factor 2.5.

[1] W. Press, 'Single Particle Rotations in Molecular Crystals', Springer Tracts in Modern Physics 92, Springer, Berlin, 1981

[2] M.R. Johnson, M. Neumann, N. Nicolai, P. Smith, G.J. Kearley, Chem. Phys. **215**,343(1997)

[3] A.K. Rappé, C.J. Casewitt, K.S. Colwell, W.A. Goddard III, W.M. Skiff, J. Am. Chem. Soc. **114**,10024(1992)

[4] M. Prager, J. Stanislawski, W. Häusler, J. Chem. Phys. **86**,2563(1987)

[5] M. Prager, J. Chem. Phys. **89**,1181(1988)

[6] J. Kalus, M. Monkenbusch, I. Natkaniecz, M. Prager, J. Wolfrum, F. Wörlen, Mol. Cryst. Liqu. Cryst. **268**,1(1995)

[7] P. Brüesch, 'Phonons: Theory and Experiments I', Solid State Sciences 34, Springer, Berlin, 1982

[8] M. Monkenbusch, local software

The Role of Interfacial Tension for the Structure of PEP-PEO Micelles

R. Lund, L. Willner, A. Radulescu, and D. Richter
Institute for Neutron Scattering

We report results of the aggregation behaviour of a highly assymmetric PEP-PEO block copolymer in water/DMF mixtures. Both are good solvents for PEO and non-solvents for PEP with a large difference in interfacial tension, γ, of PEP with the respective solvent. By using mixtures of water and DMF we were able to vary the interfacial tension over a wide range and, accordingly, the aggregation behaviour of the block copolymer. Small angle neutron scattering was used for the structural determination of the micelles. Interfacial tensions were measured by pendant drop tensiometry of a PEP homopolymer in the corresponding solvent mixtures. The aggregation number, P, of the micelles decreases steadily from 120 in pure water to 1 in DMF. A double logarithmic plot of γ versus P reveals a linear dependence with a slope of 6/5 for large γ. This is in a good agreement with a scaling law predicted for starlike micelles. Some deviations at small P and γ are observed most likely due to the limit of the validity range of the scaling approach.

F&E-Nr: E 23.10.2

Polymeric micelles have received continuous attention for a long time, both from theoretical and experimental point of view. Experimentally, poly(ethylene-alt-propylene)-polyethylene oxide (PEP-PEO) block copolymers are known to form well-defined micelles with segregated core-shell structures and large aggregation numbers in aqueous solution [1]. This is essentially due to the high incompatibility of PEP and water which is expressed in a large interfacial tension between these two components. The influence of block copolymer molecular weight and composition has been studied previously [2, 3]. Different morphologies ranging from long cylinders to spherical micelles either with starlike or homengeneous profile were observed. From a theoretical point of view models have been proposed which we coarsly can divide into mean field [4] and scaling approaches [5]. Mean field theories commonly ignore the effects of excluded volume on the corona structure and assume a constant density. For PEP-PEO micelles this has proved to be valid for micelles having short soluble PEO-blocks. For more asymmetric micelles with longer PEO-blocks the scaling predictions for starlike micelles were found to be appropriate.

In this report we present a systematic study of the effect of interfacial tension on the micellisation of a PEP1K-PEO20K block copolymer. The strong asymmetry in the block molecular weights was chosen since a starlike structure of the micelles can be anticipated that then facilitates the assignment to an adequate micellar theory. As selective solvent we have used water/dimethylformamide (DMF) mixtures in order to exploit the large difference in interfacial tension between PEP and water, γ=46 mN/m, and PEP and DMF γ=8.6 mN/m. In FIG. 1 typical SANS-curves of 0.25% block copolymer solutions in pure water, in water/DMF-mixtures and in pure DMF are presented.

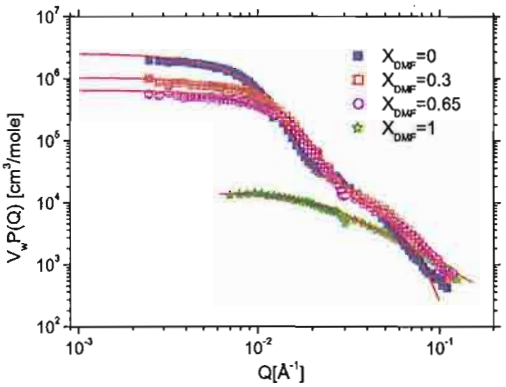

FIG. 1: Typical scattering curves for PEP1K-PEO20K in pure water, in water/DMF mixtures and in pure DMF.

Except for DMF all scattering curves exhibit features characteristic for starlike micelles: A high scattering intensity at low Q in the Guinier regime, a strong decay at intermediate Q and after a shallow maximum a power law decay, Q^{-x}, with an exponent x close to 1.7 as predicted for swollen chains in a good solvent. The curves presented in FIG.1 further reveal a decrease in the forward scattering indicating a decrease of the aggregation number with larger DMF content. The data were analysed by a spherical core-shell model with constant density distribution for the core and a radially decreasing density profile for the shell, $n(r)=r^{-x}$, with x=4/3 for starlike structures. Fits are shown as solid lines in FIG.1. In pure DMF no micelles are formed. The intensity at Q=0 corresponds to the molecular weight of the block copolymer as de-

termined by a fit with the Beaucage form factor. The fitted aggregation numbers vary from 120 in pure water to 1 in DMF. The observed trend can quantitatively be related to the interfacial tension by measuring γ in the respective solvent mixtures. These measurements were performed on a PEP1K homopolymer using a Pendant Drop Tensiometer. This method is based upon placing a drop of one phase, e.g. the polymer, in another phase, e.g. the solvent. The shape of the obtained drop is given by the balance of gravitational force and buyoancy elongating the drop into vertical direction and surface tension pulling it back to spherical geometry. Using digital image recognition techniques for analyzing the drop profile optically, γ can be extracted with high accuracy provided that the difference in density is large and its values are precisely known. In FIG.2 the results of PEP1K in different DMF/water mixtures are depicted. It can be seen that the interfacial tension decreases as the DMF content increases indicating that the interfacial free energy of the corresponding micelles can be tuned over a wide range.

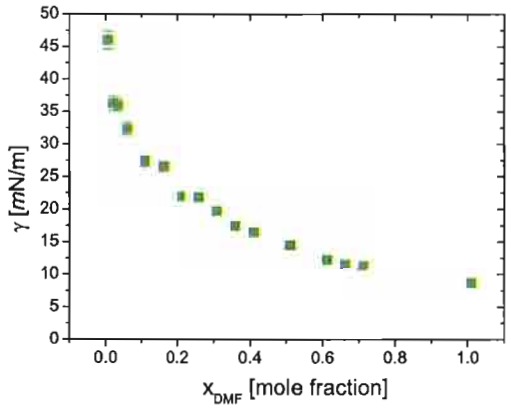

FIG. 2: Interfacial tension versus mole fraction DMF in the selective solvent mixture.

The obtained results are now discussed in terms of the starlike model proposed by Halperin. Generally, the free energy of a single micelle is approximated by the sum of three contributions:

$$F_{micelle} = F_{interface} + F_{core} + F_{corona} \qquad (1)$$

$F_{interface}$ is associated with the core-solvent interface. This term represents the driving force for micellisation. The two terms F_{core} and F_{corona} are due to the stretching of the core and corona chains and counteract micellar growth. For starlike micelles, where the degree of polymerization of the core chain is much smaller than the one of the corona, the contribution of F_{core} can be neglected. Thus, balancing interface and corona free energies gives the following expression:

$$F_{mic}/kT \approx (\gamma a^2/kT)P^{-1/3}N_B^{2/3} + P^{1/2} \qquad (2)$$

where a denotes a monomer size and N_B the degree of polymerization of the insoluble block. Minimization with respect to P yields:

$$P \approx (\gamma a^2/kT)^{6/5}N_B^{4/5} \qquad (3)$$

In order to compare the experimental results with the derived scaling prediction a double logarithmic plot of the aggregation number versus the interfacial tension is shown in FIG.3.

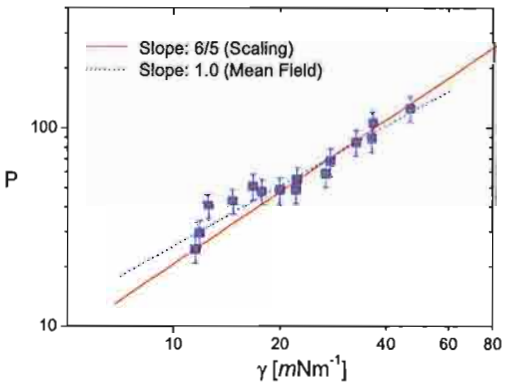

FIG. 3: Aggregation number versus Interfacial tension

It can be seen that a linear dependence is obtained for large γ and P. The slope of 6/5 corresponds nicely to the starlike prediction. At low values of γ and P deviations to the mean field prediction with a slope of 1 are visible before P drops to 1 at γ=8.6 mN/m. Since it is evident from the scattering profiles that the micelles exhibit a starlike shape these deviations are related to the limit of the validity range of the scaling prediction which demand large aggregation numbers and strong segregation but also to increasing experimental uncertainties in the analysis of micelles with smaller aggregation numbers.

By combining sophisticated SANS and tensiometric techniques we have demonstrated that beside changing molecular weight and composition the aggregation of block copolymers in a selective solvent can be easily tuned by variation of the interfacial tension. The results confirm the predicted scaling of starlike micelles.

REFERENCES

[1] A. Poppe, L. Willner, J. Allgaier, J. Stellbrink, and D. Richter Macromolecules 30 (1997) 7463.
[2] L. Willner, A. Poppe, J. Allgaier, M. Monkenbusch, P. Lindner, and D. Richter Europhys. Lett. ,51 (6) (2000) 628.
[3] H. Kaya, Ph. D. thesis, Universität Münster, 2002.
[4] R. Nagarajan and K. Ganesh J. Chem. Phys.90(10) (1989) 5843.
[5] A. Halperin Macromolecules 20 (1987) 2943.

Publications in journals

Alvarez,F.*; Arbe,A.*; Colmenero,J.*; Zorn,R.; Richter,D.
Partial structure factors of a simulated polymer melt
Computational materials science, 25 (2002), S. 596 - 605

Arbe,A.*; Colmenero,J.*; Alvarez,F.*; Monkenbusch,M.; Richter,D.; Farago,B.*; Frick,B.*
Non-Gaussian nature of the alpha-relaxation of glass-forming polyisoprene
Physical review letters, 89 (2002), S. 245701

Ashbaugh,H. S.*; Radulescu,A.; Prud'homme,R.K.*; Schwahn,D.; Richter,D.; Fetters,L.J.*
Interaction of paraffin wax gels with random crystalline/amorphous hydrocarbon copolymers
Macromolecules, 35 (2002), S. 7044 - 7053

Botti,A.; Pyckhout-Hintzen,W.; Richter,D.; Straube,E.*
An in situ rheological and SANS investigation of the crosslinking reaction
of polyisoprene and dicumyl peroxide
Rheologica acta, 41 (2002), S. 475 - 482

Botti,A.; Pyckhout-Hintzen,W.; Richter,D.; Straube,E.*
Filled elastomers : polymer chain and filler characterization by a SANS-SAXS approach
Physica A, 304 (2002), S. 230 - 234

Buchenau,U.; Wischnewski,A.; Zorn,R.; Hadjichristidis,N.*
Relaxations in the glass phase of silica and poly(methylmethacrylate) PMMA
Philosophical magazine B, 82 (2002), S. 209 - 222

Farago,B.*; Arbe,A.*; Colmenero,J.*; Faust,R.*; Buchenau,U.; Richter,D.
Intermediate length scale dynamics of polyisobutylene
Physical review E, 65 (2002), S. 051803

Fetters,L. J.*; Lohse,D. J.*; Garcia-Franco,C. A.*; Brant,P.*; Richter,D.
Prediction of melt state poly(alpha-olefin) rheological properties : the unsuspected role of the average molecular weight per backbone bond
Macromolecules, 35 (2002), S. 10096 - 10101

Frielinghaus,H.; Schwahn,D.; Willner,L.; Freed,K. F.*
Small angle neutron scattering studies of a polybutadiene/polystyrene blend with small additions of ortho-dichloro-benzene for varying temperatures and pressures - part II : phase boundaries and Flory-Huggins parameter
Journal of chemical physics, 116 (2002), S. 2241 - 2250

Gohr,K.*; Schärtl,W.*; Willner,L.; Pyckhout-Hintzen,W.
SANS investigation of PS-PB block copolymer micelles in a short chain PB
homopolymer matrix
Macromolecules, 35 (2002), S. 9110 - 9116

Heinrich,M.; Pyckhout-Hintzen,W.; Allgaier,J.; Richter,D.; Straube,E.*; Read,D.J.*; McLeish,T.C.B.*; Groves,D. J.*; Blackwell,R. J.*; Wiedenmann,A.*
Arm relaxation in deformed h-polymers in elongational flow by SANS
Macromolecules, 35 (2002), S. 6650 - 6664

Iatrou,H.*; Hadjichristidis,N.*; Meier,G.; Frielinghaus,H.; Monkenbusch,M.
Synthesis and characterization of model cyclic block copolymers of styrene and butadiene : comparison of the aggregation phenomena in selective solvents with linear diblock and triblock analogues
Macromolecules, 35 (2002), S. 5426 - 5437

Izawa,K.*; Ogasawara,T.*; Masuda,H.*; Okabayashi,H.*; Monkenbusch,M.; O'Conner,C. J.*
Growth process for fractal polymer aggregates formed by perfluorooctyltriethoxysilane : time-resolved small-angle X-ray scattering spectra and the application of the unified equation
Colloid and polymer science, 280 (2002), S. 725 - 735

Keiper,J. S.*; Simhan,R.*; DeSimone,J. M.*; Wignall,G. D.*; Melnichenko,Y. B.*; Frielinghaus,H.
New phosphate fluorosurfactants for carbon dioxide
Journal of the American Chemical Society, 124 (2002), 9, S. 1834

Kirstein,O.; Prager,M.; Johnson,M.R.*; Parker,S.F.*
Lattice dynamics and methyl rotational excitations of 2-butyne
Journal of chemical physics, 117 (2002), S. 1313 - 1319

Koizumi,S.*; Monkenbusch,M.; Richter,D.; Schwahn,D.; Farago,B.*; Annaka,M.*
Observation of concentration fluctuations in polymer gels performed by neutron spin echo
Journal of neutron research, 10 (2002), S. 155 - 162

Krishnamoorti,R.*; Graessley,W.W.*; Zirkel,A.*; Richter,D.; Hadjichristidis,N.*; Fetters,L.J.*; Lohse,D. J.*
Melt state polymer chain dimensions as a function of temperature
Journal of polymer science B - polymer physics, 40 (2002), S. 1768 - 1776

Melnichenko,Y.B.*; Wignall,G.D.*; Schwahn,D.
Universal aspects of macromolecules in polymer blends, solutions, and supercritical mixtures
Physical review E, 65 (2002), S. 061802

Menge,H.*; Pyckhout-Hintzen,W.; Meier,G.; Straube,E.*
Butadiene rubbers : topological constraints and microscopic deformations by mechanical and small angle neutron scattering investigation
Polymer bulletin, 48 (2002), S. 183 - 190

Mihailescu,M.; Monkenbusch,M.; Allgaier,J.; Frielinghaus,H.; Richter,D.; Jakobs,B.*; Sottmann,T.*
Neutron scattering study on the structure and dynamics of oriented lamellar microemulsions
Physical review E, 66 (2002), S. 041504

Montes,H.*; Monkenbusch,M.; Willner,L.; Rathgeber,S.; Richter,D.; Fetters,L.J.*; Farago,B.*
Direct observation of domain wall excitations in symmetric diblock copolymer melts at and above the order-disorder transition
Europhysics letters, 58 (2002), S. 389 - 394

Moral,A.*; Arbe,A.*; Alegria,A.*; Colmenero,J.*; Pyckhout-Hintzen,W.; Richter,D.; Farago,B.*; Frick,B.*
Heterogenous structure of poly(vinylchloride) as the origin of anomalous dynamical behaviour
Journal of chemical physics, 117 (2002), S. 1336 - 1350

Prager,M.; Combet,J.*; Parker,S.F.*; Desmedt,A.*; Lechner,R.*
The methyl rotational potentials of Ga(CH3)3 derived by neutron spectroscopy
Journal of physics: condensed matter, 14 (2002), S. 10145 - 10157

Prager,M.; Grimm,H.; Parker,S.F.*; Lechner,R.*; Desmedt,A.*; McGrady,S.*; Koglin,E.*
Methyl group rotation in trimethylaluminium
Journal of physics: condensed matter, 14 (2002), S. 1833 - 1845

Prager,M.; Press,W.*; Asmussen,B.*; Combet,J.*
Phase III of methane : crystal structure and rotational tunnelling
Journal of chemical physics, 117 (2002), S. 5821 - 5826

Prager,M.; Schiebel,P.*; Combet,J.*
Rotational tunneling and molecular disorder in 4-iodo-toluene
Journal of chemical physics, 276 (2002), S. 69 - 79

Prager,M.; Schiebel,P.*; Grimm,H.
Rotational tunneling of NH4 and NH3D and dipolar interaction in (NH3.6D0.4)2PtCl6
Journal of chemical physics, 116 (2002), S. 10338 - 10342

Rathgeber,S.; Monkenbusch,M.; Kreitschmann,M.*; Urban,V.*; Brulet,A.*
Dynamics of star-burst dendrimers in solution in relation to their structural properties
Journal of chemical physics, 117 (2002), S. 4047 - 4062

Richter,D.; Monkenbusch,M.; Willner,L.; Wischnewski,A.; Arbe,A.*; Colmenero,J.*
Experimental aspects of polymer dynamics
Polymer international, 51 (2002), S. 1211 - 1218

Schwahn,D.; Frielinghaus,H.; Willner,L.
Small angle neutron scattering studies of a polybutadiene/polystyrene blend with small additions of ortho-di-chlorine-benzene for varying temperatures and pressure fields - part I : mean field to 3D-ising crossover behavior
Journal of chemical physics, 116 (2002), S. 2229 - 2240

Schwahn,D.; Richter,D.; Lin,M.*; Fetters,L.J.*
Cocrystallization of a poly(ethylene-butene) random copolymer with C24 in n-decane
Macromolecules, 35 (2002), S. 3762 - 3768

Schwahn,D.; Richter,D.; Wright,P.J.*; Symon,C.*; Fetters,L.J.*; Lin,M.*
Self-assembling behavior in decane solution of potential wax crystal nucleators based on poly(co-olefins)
Macromolecules, 35 (2002), S. 861 - 870

Schwahn,D.; Willner,L.
Phase behavior and Flory-Huggins interaction parameter of binary polybutadiene copolymer mixtures with different vinyl content and molar volume

Macromolecules, 35 (2002), S. 239 - 247

Senapati,S.*; Keiper,J.S.*; DeSimone,J.M.*; Wignall,G.D.*; Melnichenko,Y.B.*; Frielinghaus,H.; Berkowitz,M. L.*
Structure of phosphate fluorosurfactant based reverse micelles in supercritical carbon dioxide
Langmuir, 18 (2002), S. 7371 - 7376

Stellbrink,J.; Allgaier,J.; Willner,L.; Richter,D.; Slawecki,T.*; Fetters,L.J.*
Real time SANS study on head group self-assembly for lithium based
anionic polymerizations
Polymer, 43 (2002), S. 7101 - 7109

Ulrich,C.*; Kondo,S.*; Reehuis,M.*; He,H.*; Bernhard,C.*; Niedermayer,C.*; Bourée,F.*; Bourges,P.*; Ohl,M.; Ronnow,H.M.*; Takagi,H.*; Keimer,B.*
Structural and magnetic instabilities of La2-xSrxCaCu2O6
Physical review B, 65 (2002), S. 220507

Voigt,J.; Rücker,U.; Nerger,S.; Kentzinger,E.; Hupfeld,D.; Schmidt,W.; Brückel,Th.
Structural and magnetic properties of [Er/Tb] superlattices
Journal of magnetism and magnetic materials, 240 (2002), S. 559 - 561

Volkmer,D.*; Bredenkötter,B.*; Tellenbröker,J.*; Kögerler,P.*; Kurth,D.G.*; Lehmann,P.*; Schnablegger,H.*; Schwahn,D.; Piepenbrink,M.; Krebs,B.*
Structure and properties of the dendron-encapsulated polyoxometalate (C52H60NO12)12[(Mn(H2O))3(SbW9O33)2], a first generation dendrozyme
Journal of chemical physics, 124 (2002), S. 10489 - 10496

Wischnewski,A.; Richter,D.
ESS-SAC and European science groups evaluate ESS impact on Europe's priority research themes
Neutron news, 13 (2002), S. 4 - 5

Wischnewski,A.; Monkenbusch,M.; Willner,L.; Richter,D.; Likhtman,A. E.*; McLeish,T.C.B.*; Farago,B.*
Molecular observation of contour length fluctuations limiting topological confinement in polymer melts
Physical review letters, 88 (2002), S. 058301

Yang,B.S.*; Lal,J.*; Mihailescu,M.; Monkenbusch,M.; Richter,D.; Huang,J.-S.*; Kohn,J.*; Russel,W.B.*; Prud'homme,R.K.*
Neutron spin-echo study of dynamics of hydrophobically modified polymer doped surfactant bilayers
Langmuir, 18 (2002), S. 6 - 13

Zorn,R.
Logarithmic moments of relaxation time distributions
Journal of chemical physics, 116 (2002), S. 3204 - 3209

Zorn,R.
Multiple scattering correction of polarized neutron diffraction data
Nuclear instruments and methods in physics research section A, 479 (2002), S. 568 - 584

Zorn,R.; Frick,B.*; Fetters,L.J.*
Quasielastic neutron scattring study of the methyl group dynamics in polyisoprene
Journal of chemical physics, 116 (2002), S. 845 - 853

Zorn,R.; Hartmann,L.*; Frick,B.*; Richter,D.; Kremer,F.*
Inelastic neutron scattering experiments on the dynamics of a glass forming material in mesoscopic confinements
Journal of non-crystalline solids, 307-310 (2002), S. 547 – 554

Book chapter

Allgaier,J.
Polymer synthesis
Soft matter : complex materials on mesoscopic scale ; lecture manuscripts of the 33rd IFF winter school, this winter school was organized on March, 04 - 15, 2002 in the Forschungszentrum Jülich by the Institut für Festkörperforschung ... / ed.: J. K. G. Dhont. - Jülich, 2002. - (Schriften des Forschungszentrums Jülich, Reihe Materie und Material/Matter and Materials ; 10). - 3-89336-297-5. - S. A4.1 - A4-16

Buchenau,U.
Glassy polymers
Soft matter : complex materials on mesoscopic scale ; lecture manuscripts of the 33rd IFF winter school, this winter school was organized on March, 04 - 15, 2002 in the Forschungszentrum Jülich by the Institut für Festkörperforschung ... / ed.: J. K. G. Dhont. - Jülich, 2002. - (Schriften des Forschungszentrums Jülich, Reihe Materie und Material/Matter and Materials ; 10). - 3-89336-297-5. - S. C3.1 - C3.16

Dohmen,L.; Alefeld,B.; Kentzinger,E.; Rücker,U.; Stellbrink,J.; Springer,T.; Richter,D.; Brückel,Th.
KWS3 : a focusing small angle neutron scattering instrument and neutron refectometer at Jülich
European conference abstract book : Bonn, 16. - 17.05.2002. - S. 33

Kahle,S.
Dielectric spectroscopy
Soft matter : complex materials on mesoscopic scale ; lecture manuscripts of the 33rd IFF winter school, this winter school was organized on March, 04 - 15, 2002 in the Forschungszentrum Jülich by the Institut für Festkörperforschung ... / ed.: J. K. G. Dhont. - Jülich, 2002. - (Schriften des Forschungszentrums Jülich, Reihe Materie und Material/Matter and Materials ; 10). - 3-89336-297-5. - S. A3.1 - A3.18

Monkenbusch,M.
Membrane and microemulsion dynamics
Soft matter : complex materials on mesoscopic scale ; lecture manuscripts of the 33rd IFF winter school, this winter school was organized on March, 04 - 15, 2002 in the Forschungszentrum Jülich by the Institut für Festkörperforschung ... / ed.: J. K. G. Dhont. - Jülich, 2002. - (Schriften des Forschungszentrums Jülich, Reihe Materie und Material/Matter and Materials ; 10). - 3-89336-297-5. - S. C6.1 - C6.31

Richter,D.
Polymer dynamics
Soft matter : complex materials on mesoscopic scale ; lecture manuscripts of the 33rd IFF winter school, this winter school was organized on March, 04 - 15, 2002 in the Forschungszentrum Jülich by the Institut für Festkörperforschung ... / ed.: J. K. G. Dhont. - Jülich, 2002. - (Schriften des Forschungszentrums Jülich, Reihe Materie und Material/Matter and Materials ; 10). - 3-89336-297-5. - S. C2.1 - C2.37

Schwahn,D.
Investigations of polymers by small angle neutron scattering
Soft matter : complex materials on mesoscopic scale ; lecture manuscripts of the 33rd IFF winter school, this winter school was organized on March, 04 - 15, 2002 in the Forschungszentrum Jülich by the Institut für Festkörperforschung ... / ed.: J. K. G. Dhont. - Jülich, 2002. - (Schriften des Forschungszentrums Jülich, Reihe Materie und Material/Matter and Materials ; 10). - 3-89336-297-5. - S. B6.1 - B6.17

Zorn,R.
Colloidal glasses
Soft matter : complex materials on mesoscopic scale ; lecture manuscripts of the 33rd IFF winter school, this winter school was organized on March, 04 - 15, 2002 in the Forschungszentrum Jülich by the Institut für Festkörperforschung ... / ed.: J. K. G. Dhont. - Jülich, 2002. - (Schriften des Forschungszentrums Jülich, Reihe Materie und Material/Matter and Materials ; 10). - 3-89336-297-5. - S. C5.1 - C5.19

Zorn,R.
Inelastic neutron scattering : dynamics of polymers
Neutrons, X-rays and light : scattering methods applied to soft
condensed matter / ed.: P. Lindner ... - North Holland, Amsterdam,
2002. - 0-444-51122-9. - S. 221 - 255

Book

Richter, D. (Hrsg.)
The ESS Project, Volume II: New Science and Technology for the 21st Century
Jülich, ESS Central Projekt Team, c/o Forschungszentrum Jülich, 2002, ISBN 3-89336-302-5

Invited talks

Allgaier,J.; Buchenau,U.; Endo,H.; Gompper,G.; Monkenbusch,M.; Pyckhout-Hintzen,W.; Richter,D.; Willner,L.; Arbe,A.*; Colmenero,J.*
Future prospects of soft matter science at the European Spallation Source
Joint Symposium of the Research Center Jülich and the Jaggiellonian University in Krakow in co-operation with the Max-Planck Society
Krakow, Poland: 11.11.2002 - 13.11.2002

Allgaier,J.; Endo,E.; Gompper,G.; Monkenbusch,M.; Pyckhout-Hintzen,W.; Willner,L.; Arbe,A.*; Colmenero,J.*; Richter,D.
Neutrons in soft matter science
Spanish Neutron Scattering Association (SETN) User Meeting
San Sebastian, Spain: 03.10.2002 - 04.10.2002

Buchenau,U.
Energy landscape - a central concept for the dynamics of
liquids and glasses
III. Workshop on Non-Equilibrium Phenomena in Supercooled Fluids, Glasses and Amorphous Materials
Pisa, Italy: 22.09.2002 - 27.09.2002

Buchenau,U.
Energy landscape - a central concept for the dynamics of glasses

INF Meeting (Treffen des italienischen Instituto Nazionale per la Fisica della Materia)
Bari, Italy: 24.06.2002 - 28.06.2002

Buchenau,U.
Experimente zur Dynamik glasbildender Materialien Glasdynamik und Strukturbildung : WE-Heraeus-Ferienschule der Universität Chemnitz
Chemnitz: 25.08.2002 - 06.09.2002

Buchenau,U.
Inelastic neutron and X-ray scattering
Workshop on Spectroscopic Investigation of the Collective Dynamics in Disordered Systems
Trieste, Italy: 17.06.2002 - 28.06.2002

Byelov,D.; Frielinghaus,H.; Endo,H.; Allgaier,J.; Richter,D.
Polymer boosting effect in the droplet phase studied by small angle neutron scattering
Sixth European School on Scattering Methods Applied to Soft Condensed Matter
Bombannes, Frankreich: 25.05.2002 - 01.06.2002

Frielinghaus,H.; Byelov,D.; Allgaier,J.; Richter,D.; Jakobs,B.*; Sottmann,T.*; Strey,R.*
Small angle neutron scattering studies of microemulsions in the droplet phase with polymer as an efficiency booster
XII. International Conference on Small Angle Scattering
Venice, Italy: 25.08.2002 - 29.08.2002

Heinrich,M.; Pyckhout-Hintzen,W.; Allgaier,J.; Richter,D.; McLeish,T.C.B.*; Read,D.*; Straube,E.*; Wiedenmann,A.*
Time evolution of strain relaxation in a model H-branched polymer by SANS
XII. International Conference on Small Angle Scattering
Venice, Italy: 24.08.2002 - 29.08.2002

Kahle,S.
High resolution inelastic neutron scattering spectroscopy
Joint ICTP-INFM School and Workshop on Spectroscopy Investigation of the Collective Dynamics in Disordered Systems
Trieste: 17.06.2002 - 28.06.2002

Kahle,S.
Local dynamics in polymers
Joint ICTP-INFM School and Workshop on Spectroscopy Investigation of the Collective Dynamics in Disordered Systems
Trieste: 17.06.2002 - 28.06.2002

Monkenbusch,M.
Neutron spin echo study on the modification of surfactant membrane properties due to polymer addition
American Conference on Neutron Scattering (ACNS)
Knoxville, USA: 23.06.2002 - 27.06.2002

Monkenbusch,M.
Segmental dynamics and confinement in polymer melts
Jülich Soft Matter Days 2002
Kerkrade, Niederlande: 19.11.2002 - 22.11.2002

Ohl,M.; Monkenbusch,M.; Bünten,W.; Richter,D.; Lieutenant,K.*; Zsigmond,G.*; Krist,T.*; Pappas,C.*; Mezei,F.*
High resolution NSE spectrometer for spallation sources
Conference on Polarized Neutrons in Condensed Matter Investigations : Forschungszentrum Jülich
Jülich: 16.09.2002 - 19.09.2002

Ohl,M.; Monkenbusch,M.; Richter,D.
Progress on NSE correction devices
Techni-Meeting 2002 : Orsay, Paris
Paris: 17.10.2002 - 18.10.2002

Pipich,V.
Critical behavior of a ternary polymer blend near the Lifshitz line
Sixth European School on Scattering Methods Applied to Soft Condensed Matter
Bombannes, France: 25.05.2002 - 01.06.2002

Prager,M.
Rotational potentials studied by spectroscopy and relaxation
6th International Conference on Quasielastic Neutron Scattering
Potsdam: 04.09.2002 - 07.09.2002

Pyckhout-Hintzen,W.
Polymers and fibers
ESRF Workshop
Grenoble, Frankreich: 11.02.2002 - 13.02.2002

Pyckhout-Hintzen,W.
Polymers and fibers
Deutsche Neutronenstreutagung
Bonn: 15.05.2002

Pyckhout-Hintzen,W.
Polymers and fibers
XII. International Conference on Small Angle Scattering
Venedig, Italien: 25.08.2002 - 29.08.2002

Richter,D.
ESS - new horizons for science and technology
ESS European Conference
Bonn: 16.05.2002 - 17.05.2002

Richter,D.
European spallation neutron source project
International Meeting of the European Spallation Source on Flexibility and Function of Proteins : Universität Heidelberg
Heidelberg: 25.01.2002 - 27.01.2002

Richter,D.
The European Spallation Source - a beacon for research
10. Jahrestagung der Deutschen Gesellschaft für Kristallographie (DGK) 2002 : Universität Kiel
Kiel: 04.03.2002 - 07.03.2002

Richter,D.
Wax control by self-assembling polymers - a science approach
6th International Symposium on the Science and Technology of Polymer Assembly : the Global Strategy in 21st Century
Kyoto, Japan: 31.01.2002 - 01.02.2002

Richter,D.; Monkenbusch,M.; Willner,L.; Wischnewski,A.; Arbe,A.*; Colmenero,J.*
Polymer dynamics from large to small scales
American Conference on Neutron Scattering (ACNS)
Knoxville, USA: 23.06.2002 - 27.06.2002

Richter,D.; Monkenbusch,M.; Willner,L.; Wischnewski,A.; Arbe,A.*; Colmenero,J.*
Polymer dynamics from large to small scales
XII. International Conference on Small Angle Scattering (SAS)
Venice, Italy: 25.08.2002 - 29.08.2002

Schwahn,D.
Nucleation and growth of CaCO3 minerals on biomimetic templates studied by small angle neutron scattering
XII. International Conference on Small Angle Scattering
Venice, Italy: 25.08.2002 - 29.08.2002

Willner,L.; Lund,R.; Radulescu,A.; Monkenbusch,M.; Richter,D.
Time-resolved SANS for the determination of polymer exchange kinetics in block copolymer micelles
XII. International Conference on Small Angle Scattering
Venice, Italy: 25.08.2002 - 29.08.2002

Wischnewski,A.
Status of the ESS project
Conference on Perspectives of Neutron Scattering for the Earth Sciences with the ESS
Cambridge, UK: 05.01.2002 - 08.01.2002

Other talks

Allgaier,J.
Amphiphile Blockcopolymere zur Effizienzsteigerung von Tensiden
Firma Böhme
München: 13.11.2002

Frielinghaus,H.; Byelov,D.; Allgaier,J.; Richter,D.; Sottmann,T.*; Strey,R.*
Mikroemulsionen mit Polymerbeigaben untersucht mit Neutronenkleinwinkelstreuung
Kolloquium : Universität Münster
Münster: 14.11.2002

Grimm,H.
Statics and dynamics of DNA
Universität Konstanz
Konstanz: 23.04.2002

Grimm,H.
Statics and dynamics of DNA as seen by neutrons
Workshop on Biology meets Physics : Forschungszentrum Jülich
Jülich: 20.02.2002

Kahle,S.
Segmental dynamics in polyisobutylene : comparison between neutron scattering and computer simulations
7. Labortreffen Relaxationsdynamik
Rostock: 16.12.2002 - 17.12.2002

Kahle,S.
Untersuchung der lokalen Relaxation von Polymeren mittels Neutronenstreuung
6. Labortreffen Relaxationsdynamik
Halle: 18.02.2002 - 19.02.2002

Kirstein,O.; Kozielewski,T.; Prager,M.; Andersen,K. H.*

The 0.9 My eV backscattering spectrometer for the ESS
Jülich ESS Days
Bad Honnef: 15.04.2002 - 16.04.2002

Monkenbusch,M.
Instrumentierung für die ESS
ESS Tage
Bad Honnef: 15.04.2002 - 16.04.2002

Monkenbusch,M.
Neutronenspinechospektroskopie und Bewegungen in weicher Materie
SFB Workshop Zeitskalen und Spektroskopie : Universität Halle
Halle: 27.03.2002

Ohl,M.; Bünten,W.
Progress of the feasibility study for a highest resolution NSE spectrometer
Workshop NSE for the SNS : Forschungszentrum Jülich
Jülich: 11.11.2002 - 12.11.2002

Ohl,M.; Monkenbusch,M.; Bünten,W.; Richter,D.; Lieutenant,K.*; Zsigmond,G.*; Krist,T.*; Pappas,C.*; Mezei,F.*
Neutron spin echo technology at pulsed sources : a feasibility study
ESS Tage
Bad Honnef: 15.04.2002 - 16.04.2002

Prager,M.
A walk through the tunnel landscape with special emphasis to instrumentation
Toni Heidemann Symposium
Grenoble, France: 29.11.2002

Prager,M.
Status and experience with the time-focusing thermal TOF-spectrometer SV29 at Jülich
PSI Villigen
Villigen: 05.02.2002

Richter,D.
Die Europäische Spallationsquelle (ESS) - European Source of Science
Kolloquium : Universität Köln
Köln: 17.12.2002

Richter,D.
ESS project overview
Kolloquium : Universität Tokai
Tokai, Japan: 04.02.2002

Richter,D.
European spallation neutron source project
Kolloquium bei der Akademie der Wissenschaften
Düsseldorf: 06.02.2002

Richter,D.
Neutron backscattering : from the early days to polymer glasses and non-Gaussianity
Toni Heidemann Symposium
Grenoble, France: 29.11.2002

Richter,D.
Neutron spin echo in soft matter science
Kolloquium : Firma ExxonMobil
Annandale, USA: 24.10.2002

Richter,D.
Neutrons in soft matter science
Seminar : Firma ExxonMobil
Annandale, USA: 23.10.2002

Richter,D.
Soft-Matter-Forschung am IFF : eine Einführung
HGF Workshop Kondensierte Materie : Forschungszentrum Jülich
Jülich: 06.11.2002

Richter,D.
The European Spallation Source
Kolloquium : Universität Paderborn
Paderborn: 10.01.2002

Richter,D.
The European Spallation Source
Kolloquium : Magnushaus Berlin
Berlin: 11.06.2002

Schwahn,D.
Grundlagen der Neutronenbeugung im Kleinwinkelbereich
Workshop Grundlegende Aspekte der Biomineralisation im DFG-Schwerpunktprogramm Prinzipien der Biomineralisation
Bochum: 07.10.2002

Schwahn,D.
Methode der Kleinwinkelstreuung mit Neutronen zur Untersuchung nano- und mesoskopischer Strukturen
Kolloquium : Universität Mainz
Mainz: 07.02.2002

Schwahn,D.
Untersuchungen zur Keimbildung und dem Kristallwachstum von CaCO3 in wäßriger Lösung an biomimetisch strukturierten Grenzflächen mittels Neutronenkleinwinkelstreuung
1. Berichtskolloquium Prinzipien der Biomineralisation
Bonn-Röttgen: 20.06.2002

Sottmann,T.*; Müller,S.*; Strey,R.*; Richter,D.; Allgaier,J.
Giant structures in microemulsions : SANS versus SLS
ACS Meeting
Boston, Mass.: 18.08.2002 - 22.08.2002

Stellbrink,J.
Streumethoden zur Untersuchung 'Weicher Materie'
Seminar : Fachhochschule Jülich
Jülich: 05.11.2002

Zorn,R.
Dynamics of confined glass-forming systems observed by neutron
scattering
Seminar : Texas Technical University
Lubbock, USA: 26.11.2002

Zorn,R.; Richter,D.; Hartmann,L.*; Kremer,F.*; Frick,B.*
Dynamics of glass forming liquids in spatial confinement
Workshop on Slow Dynamics of Soft-Matter and Biological Molecules Studied by Neutron Scattering
Tsukuba, Japan: 07.03.2002 - 08.03.2002

Posters

Blanchard,A.; Pyckhout-Hintzen,W.; Heinrich,M.; Richter,D.
Relaxation mechanisms in a stretched linear polymer melt studied by SANS
Jülich Soft Matter Days 2002
Kerkrade, Niederlande: 19.11.2002 - 22.11.2002

Blanchard,A.; Pyckhout-Hintzen,W.; Heinrich,M.; Richter,D.
Relaxation mechanisms in a stretched linear polymer melt studied by SANS
HGF Workshop Kondensierte Materie : Forschungszentrum Jülich
Jülich: 06.11.2002

Botti,A.; Pyckhout-Hintzen,W.; Richter,D.; Straube,E.*; Urban,V.*
Filled elastomers : polymer chain and filler characterization by a SANS-SAXS approach
HGF Workshop Kondensierte Materie : Forschungszentrum Jülich
Jülich: 06.11.2002

Byelov,D.; Frielinghaus,H.; Allgaier,J.; Richter,D.; Müller,S.*; Sottmann,T.*; Strey,R.*
SANS studies of bicontinuous microemulsions with homopolymer and diblock copolymer additions
ESS European Conference
Bonn: 15.05.2002 - 17.05.2002

Byelov,D.; Frielinghaus,H.; Allgaier,J.; Richter,D.; Müller,S.*; Sottmann,T.*; Strey,R.*
SANS studies of bicontinuous microemulsions with homopolymer and diblock copolymer additions
HGF Workshop Kondensierte Materie : Forschungszentrum Jülich
Jülich: 06.11.2002

Byelov,D.; Frielinghaus,H.; Allgaier,J.; Richter,D.; Müller,S.*; Sottmann,T.*; Strey,R.*
SANS studies of bicontinuous microemulsions with homopolymer and
diblock copolymer additions
Jülich Soft Matter Days 2002
Kerkrade, Niederlande: 19.11.2002 - 22.11.2002

Frielinghaus,H.; Allgaier,J.; Byelov,D.; Richter,D.
Small angle neutron scattering results on the polymer boosting effect in the droplet phase
14. SIS Conference
Barcelona, Spain: 09.06.2002 - 14.06.2002

Frielinghaus,H.; Byelov,D.; Allgaier,J.; Richter,D.; Jakobs,B.*; Sottmann,T.*; Strey,R.*
Small angle neutron scattering studies of microemulsions in the droplet phase with polymer as an efficiency booster
Deutsche Neutronenstreutagung
Bonn: 15.05.2002

Frielinghaus,H.; Byelov,D.; Allgaier,J.; Richter,D.; Jakobs,B.*; Sottmann,T.*; Strey,R.*
Small angle neutron scattering studies of microemulsions in the droplet phase with polymer as an efficiency booster
Jülich Soft Matter Days 2002
Kerkrade, Niederlande: 19.11.2002 - 22.11.2002

Heinrich,M.; Pyckhout-Hintzen,W.; Richter,D.; Straube,E.*; Wiedenmann,A.*
Relaxation dynamics of entangled branched polymers investigated by SANS

Jülich Soft Matter Days 2002
Kerkrade, Niederlande: 19.11.2002 - 22.11.2002

Heinrich,M.; Pyckhout-Hintzen,W.; Richter,D.; Straube,E.*; Wiedenmann,A.*
Time evolution of strain relaxation in a model-branched H-polymer by SANS
Deutsche Neutronenstreutagung
Bonn: 15.05.2002

Heinrich,M.; Pyckhout-Hintzen,W.; Richter,D.; Straube,E.*; Wiedenmann,A.*
Time evolution of strain relaxation in a model-branched H-polymer by SANS
HGF Workshop Kondensierte Materie : Forschungszentrum Jülich
Jülich: 06.11.2002

Hermes,H. E.; Willner,L.; Kreitschmann,M.*; Pyckhout-Hintzen,W.; Richter,D.; Nijenhuis,A.*
Small angle scattering investigation of linear and star trifluoroacetylated nylon-6
Jülich Soft Matter Days 2002
Kerkrade, Niederlande: 19.11.2002 - 22.11.2002

Kahle,S.; Monkenbusch,M.; Richter,D.; Ryckaert,J.P.*; Karatasos,K.*; Koza,M.*
Segmental dynamics in polyisobutylene: Comparison between neutron scattering and computer simulations
Jülich Soft Matter Days 2002
Kerkrade, Niederlande: 19.11.2002 - 22.11.2002

Kahle,S.; Monkenbusch,M.; Richter,D.; Ryckaert,J.P.*; Karatasos,K.*; Koza,M.*
Segmental dynamics in polyisobutylene: Comparison between neutron scattering and computer simulations
HGF Workshop Kondensierte Materie : Forschungszentrum Jülich
Jülich: 06.11.2002

Kahle,S.; Monkenbusch,M.; Richter,D.; Ryckaert,J.P.*; Koza,M.*
Local dynamics in polymers
ESS European Conference
Bonn: 16.05.2002 - 17.05.2002

Kirstein,O.; Kozielewski,T.; Prager,M.
Status of the high flux backscattering spectrometer RSSM for the FRM-II reactor in Munich
ESS European Conference
Bonn: 15.05.2002 - 17.05.2002

Kirstein,O.; Kozielewski,T.; Prager,M.; Andersen,K. H.*
A 0.9 My eV direct backscattering spectrometer for the 50Hz target station of the European Spallation Source ESS
ESS European Conference
Bonn: 15.05.2002 - 17.05.2002

Kirstein,O.; Prager,M.
Lattice dynamics and methyl group rotations of the methyl halides CH_3X, X = F, Cl, Br, I
ESS European Conference
Bonn: 15.05.2002 - 17.05.2002

Kirstein,O.; Prager,M.
The dynamics of methyl halides CH_3X, X = F, Cl, Br, I
6th International Conference on Quasielastic Neutron Scattering
Potsdam: 04.09.2002 - 07.09.2002

Laurati,M.; Stellbrink,J.; Lund,R.; Willner,L.; Richter,D.
PEP-PEO diblock copolymers as 'tunable' star polymers
ESS European Conference
Bonn: 15.05.2002 - 17.05.2002

Laurati,M.; Stellbrink,J.; Willner,L.; Rother,G.; Richter,D.
Frozen block copolymer micelles as 'tunable' model system for soft colloids
HGF Workshop Kondensierte Materie : Forschungszentrum Jülich
Jülich: 06.11.2002

Lund,R.; Willner,L.; Monkenbusch,M.; Radulescu,A.; Richter,D.
Time resolved SANS for the determination of unimer exchange kinetics of polymeric micelles
ESS European Conference
Bonn: 16.05.2002 - 17.05.2002

Lund,R.; Willner,L.; Monkenbusch,M.; Radulescu,A.; Richter,D.
Time resolved SANS for the determination of unimer exchange kinetics of polymeric micelles
HGF Workshop Kondensierte Materie : Forschungszentrum Jülich
Jülich: 06.11.2002

Lund,R.; Willner,L.; Radulescu,A.; Monkenbusch,M.; Richter,D.
Tuning of chain exchange kinetics and structure in PEP-PEO block copolymer micelles
Jülich Soft Matter Days 2002
Kerkrade, Niederlande: 19.11.2002 - 22.11.2002

Meinnel,J.*; Hernandez,O.*; Grimm,H.; Prager,M.
Assignment of the 3 methyl tunnelling lines in a trichloromesitylene single crystal
Jülich Soft Matter Days 2002
Kerkrade, Niederlande: 19.11.2002 - 22.11.2002

Ohl,M.; Monkenbusch,M.; Richter,D.; Pappas,C.*; Lieutenant,K.*; Mezei,F.*
The new NSE spectrometer for the SNS
American Conference of Neutron Scattering (ACNS)
Knoxville, USA: 23.06.2002 - 27.06.2002

Ohl,M.; Monkenbusch,M.; Richter,D.; Pappas,C.*; Lieutenant,K.*; Mezei,F.*
The new NSE spectrometer for the SNS
HGF Workshop Kondensierte Materie : Forschungszentrum Jülich
Jülich: 06.11.2002

Pipich,V.; Schwahn,D.; Willner,L.
Complex phase behavior near the Lifshitz line in a ternary polymer blend
ESS European Conference
Bonn: 15.05.2002 - 17.05.2002

Pipich,V.; Schwahn,D.; Willner,L.
Double critical behavior of a binary A,B polymer blend mixed with a symmetric A-B diblock copolymer near the Lifshitz Line
XII. International Conference on Small Angle Scattering
Venice, Italy: 25.08.2002 - 29.08.2002

Pipich,V.; Schwahn,D.; Willner,L.
Double critical behavior of a binary A,B polymer blend mixed with a symmetric A-B diblock copolymer near the Lifshitz Line
Jülich Soft Matter Days
Kerkrade, Niederlande: 19.11.2002 - 22.11.2002

Pipich,V.; Schwahn,D.; Willner,L.
Double critical behavior of a binary A,B polymer blend mixed with a symmetric A-B diblock copolymer near the Lifshitz Line
HGF Workshop Kondensierte Materie : Forschungszentrum Jülich
Jülich: 06.11.2002

Prager,M.; Parker,S.F.*; Lechner,R.*; Desmedt,A.*
Characterization of complex molecular systems by concerted neutron spectroscopy : trimethyl gallium
ESS European Conference
Bonn: 16.05.2002 - 17.05.2002

Radulescu,A.; Schwahn,D.; Richter,D.; Fetters,L. J.*
Co-crystallization of poly(ethylene-butene) copolymers and paraffin molecules in decane solution investigated by SANS
ESS European Conference
Bonn: 15.05.2002 - 17.05.2002

Radulescu,A.; Schwahn,D.; Richter,D.; Fetters,L.J.*
Co-crystallization of poly(ethylene-butene) copolymers and paraffin molecules in decane solution investigated by SANS
HGF Workshop Kondensierte Materie : Forschungszentrum Jülich
Jülich: 06.11.2002

Radulescu,A.; Schwahn,D.; Richter,D.; Fetters,L.J.*
Co-crystallization of poly(ethylene-butene) copolymers and paraffin molecules in decane solution investigated by SANS
XII. International Conference on Small Angle Scattering
Venice, Italy: 24.08.2002 - 29.08.2002

Rheinstädter,M.C.; Kityk,A. V.*; Klöpperpieper,A.*; Knorr,K.*
Dipolar ordering and relaxations in acetonitrile-b-hydroquinone clathrate
SCNS Workshop 2002
Grenoble, France: 12.12.2002 - 14.12.2002

Schmidt,W.; Ohl,M.; Ruppert,H.*; Buchenau,U.
A new instrumental set-up for polarized neutron scattering experiments
ILL Workshop (SCNS)
Grenoble, France: 12.12.2002 - 14.12.2002

Schmidt,W.; Rheinstädter,M.C.; Ohl,M.; Raymond,S.*; Ruppert,H.*; Buchenau,U.
Current activities on IN12
ESS European Conference
Bonn: 16.05.2002 - 17.05.2002

Schwahn,D.; Balz,M.*; Bartz,M.*; Fomenko,A.; Tremel,W.*
Nucleation and growth of CaCO3 minerals on biomimetic templates studied by small angle neutron scattering
ESS European Conference
Bonn: 15.05.2002 - 17.05.2002

Schwahn,D.; Balz,M.*; Bartz,M.*; Fomenko,A.; Tremel,W.*

Nucleation and growth of CaCO3 minerals on biomimetic templates studied by small angle neutron scattering
Jülich Soft Matter Days 2002
Kerkrade, Niederlande: 19.11.2002 - 22.11.2002

Schwahn,D.; Balz,M.*; Bartz,M.*; Fomenko,A.; Tremel,W.*
Nucleation and growth of CaCO3 minerals on biomimetic templates studied by small angle neutron scattering
HGF Workshop Kondensierte Materie : Forschungszentrum Jülich
Jülich: 06.11.2002

Stellbrink,J.
Partial structure factors in star polymer/colloid mixtures
Liquid Matter 2002
Konstanz: 14.09.2002 - 20.09.2002

Stellbrink,J.
Partial structure factors in star polymer/colloid mixtures
Jülich Soft Matter Days 2002
Kerkrade, Niederlande: 19.11.2002 - 22.11.2002

Stellbrink,J.; Allgaier,J.; Monkenbusch,M.; Richter,D.; Ehlers,G.*; Schleger,P.*
Dynamics of ordered multi-arm star polymer solutions
ESS European Conference
Bonn: 15.05.2002 - 17.05.2002

Stellbrink,J.; Allgaier,J.; Monkenbusch,M.; Richter,D.; Ehlers,G.*; Schleger,P.*
Dynamics of ordered multi-arm star polymer solutions
HGF Workshop Kondensierte Materie : Forschungszentrum Jülich
Jülich: 06.11.2002

Stellbrink,J.; Allgaier,J.; Richter,D.; Moussaid,A.*; Narayanan,T.*; Dolbnya,I.*; Bras,W.*; Poon,W.C.K.*; Pusey,P.N.*; Lindner,P.*
Partial structure factors in star polymer/colloid mixtures
HGF Workshop Kondensierte Materie : Forschungszentrum Jülich
Jülich: 06.11.2002

Stellbrink,J.; Allgaier,J.; Richter,D.; Moussaid,A.*; Schofield,A.B.*; Poon,W.C.K.*; Pusey,P.N.*; Lindner,P.*
Star polymer/colloid mixtures
ESS European Conference
Bonn: 15.05.2002 - 17.05.2002

Stellbrink,J.; Niu,A.; Allgaier,J.; Willner,L.; Richter,D.; Fetters,L.J.*
Real-time SANS experiments during 'living' anionic polymerization
ESS European Conference
Bonn: 15.05.2002 - 17.05.2002

Stellbrink,J.; Niu,A.; Allgaier,J.; Willner,L.; Richter,D.; Fetters,L.J.*
Real-time SANS experiments during 'living' anionic polymerization
HGF Workshop Kondensierte Materie : Forschungszentrum Jülich
Jülich: 06.11.2002

Wischnewski,A.; Monkenbusch,M.; Willner,L.; Richter,D.; Likhtman,A. E.*; McLeish,T.C.B.*; Farago,B.*
Constraints of motion in polymer melts : a coherent and incoherent neutron spin echo study
HGF Workshop Kondensierte Materie : Forschungszentrum Jülich
Jülich: 06.11.2002

Wischnewski,A.; Monkenbusch,M.; Willner,L.; Richter,D.; Likhtman,A. E.*; McLeish,T.C.B.*; Farago,B.*
Constraints of motion in polymer melts : a coherent and incoherent neutron spin echo study
Jülich Soft Matter Days 2002
Kerkrade, Niederlande: 19.11.2002 - 22.11.2002

Wischnewski,A.; Monkenbusch,M.; Willner,L.; Richter,D.; Likhtman,A. E.*; McLeish,T.C.B.*; Farago,B.*
Molecular observation of contour length fluctuations limiting topological confinement in polymer melts
HGF Workshop Kondensierte Materie : Forschungszentrum Jülich
Jülich: 06.11.2002

Zamponi,M.; Monkenbusch,M.; Richter,D.; Willner,L.; Wischnewski,A.; Likhtman,A. E.*; McLeish,T.C.B.*; Farago,B.*
NSE study on the influence of contour length fluctuations on the reptation process
Jülich Soft Matter Days 2002
Kerkrade, Niederlande: 19.11.2002 - 22.11.2002

Zamponi,M.; Monkenbusch,M.; Richter,D.; Willner,L.; Wischnewski,A.; Likhtman,A. E.*; McLeish,T.C.B.*; Farago,B.*
NSE study on the influence of contour length fluctuations on the reptation process

HGF Workshop Kondensierte Materie :
Forschungszentrum Jülich
Jülich: 06.11.2002

Zorn,R.
Jülich neutrons for Europe
ESS European Conference
Bonn: 16.05.2002 - 17.05.2002

Institute of Electroceramic Materials

General Overview

Research Areas

The research areas of the institute comprise (1) technologies for the integration of electroceramic materials into microelectronics and nanoelectronics, (2) dielectric and ferroelectric properties of oxide ceramics, and (3) the defect structure in the vicinity of internal and external interfaces in oxides. These areas are complementary to the research areas of the Institute for Electronic Materials 2 (IWE 2) at the Aachen Technical University (RWTH). Project groups often comprise staff members and students from both institutes.

As an updated and significantly enlarged version of the 32nd IFF-Ferienschule which we organized in 2001, we completed the edition of the textbook *Nanoelectronics and Information Technology - Advanced Electronic Materials and Novel Devices*. This textbook as well as the next IFF-Ferienschule on *Fundamentals of Nanoelectronics* are supporting the preparation of the new research program *Nanoelectronic Systems* in the frame-work of the HGF research area *Key Technologies*. One aspect of the new organization within the HGF will put more emphasis on the interdisciplinary of the research activities. In this respect, our activities are strengthening the bridge between the IFF and the ISG (Institut für Schichten und Grenzflächen).

Integration Technologies and Scaling Effects

The major project in the area of integration technologies and scaling effects is our HGF project *'Piccolo* – Scaling Effects in Integrated Electroceramic Materials' (2000 – 2003). This project is embedded in the former information technology program PGI (Physikalische Grundlagen der Informationstechnologie) of the Research Center Jülich. Beyond the (1) Institut für Elektrokeramische Materialien, the (2) Institut für Mikrostrukturforschung IMF headed by K. Urban, (3) the Theorie III, headed by H. Müller-Krumbhaar, and (4) the Ion Technology (IT) group at the ISG headed by S. Mantl are involved. Several national and international universities and research centers participate in "Piccolo", too. The main focus of the proposal "Piccolo" is a fundamental as well as applied research on scaling effects of electroceramic materials. Today, typically polycrystalline films exhibit grain sizes much smaller than the feature sizes of the microelectronic devices. However, along with the sustaining trend towards further miniaturization, the decreasing feature sizes in microelectronic technology will approach the typical crystallite sizes of the perovskite-type oxide structures. Specific scaling effects are anticipated along this route, due to the long-range nature of the ferroelectric interaction of the oxides involved. The project aims at an (1) elucidation of the physical origin of these scaling effects, (2) an exploitation and extension of the limits to which the ferroelectric properties and high permittivities of the oxides involved can be used, and (3) the development of technological design rules for the integration of the perovskite-type oxides on a decreasing scale. The spectrum of designated results of the project comprises (semiquantitative) models for the superparaelectric limit of ferroelectric (FE) oxides, the dead layer at interfaces, the phase stability and segregation processes of perovskite films during annealing, the nucleation and growth of films by MOCVD (Metal Organic Chemical Vapor Deposition), recipes for the deposition of single grain capacitors and ultrathin FE films as well as for reactive ion etching and a ferroelectric field-effect transistor (FE-FET) as a demonstrator. Scanning Probe Microscopy (SPM) techniques such as AFM and STM play an essential role in studying interrelationships on a microscopic base. Hence, the project "Piccolo" is an initiative to pursue research on the basic properties of electroceramic materials under scaling and on the relevance of these effects for the integration of perovskite-type oxides into microelectronics.

In cooperation with AIXTRON AG, our multiwafer MOCVD planetary reactor has been upgraded by the TriCent injector system which allows, in principle, the atomic layer-by-layer deposition of ultrathin films. This will be needed in the new Medea+ project which aims at the formation of alternative gate-oxide for future sub-100nm main-stream FETs and is useful as well for our FE-FET project.

As a supplement, we use high pressure oxygen sputtering for the deposition of ultrathin PZT film within the Piccolo project. For the patterning of the ceramic films and electrode / ceramic film stacks, the Reactive Ion Beam Etching (RIBE) technique is employed. In contrast to the situation in the standard Si and compound semiconductor technologies, dry etching processes of oxide ceramics have hardly been investigated yet and therefore represent a research area in which basic studies and industrially funded applied research can be linked in a beneficial manner. The integration processes are complemented by metallization methods based on electron beam and sputter techniques. Within this area, our studies aim at a better understanding of the processes and

material parameters which govern the adhesion, the mechanical stress, the microstructure, and their effect on the dielectric and ferroelectric properties.

Furthermore, organic molecules gain importance in electronic applications. In a cooperation with Infineon Technologies and headed by the FZ Karlsruhe, we have started a joint research project on resistive random access memories based on oxidic nanostructures and molecular electronic components.

Dielectric and ferroelectric properties

The second research area focuses on the *dielectric and ferroelectric properties* of oxide thin films and – for comparison – bulk ceramics, which are being investigated in Jülich as well as in Aachen. The material systems are based on compositions used for practical devices and model systems, e.g. $SrTiO_3$, $BaTiO_3$, $SrBi_2Ta_2O_9$, $Pb(Zr,Ti)O_3$. One of the research topics is the microscopic understanding of ferroelectric hysteresis including new approaches for the separation of *reversible* and *irreversible* contributions to polarisation based on the analysis of frequency-dependent small and large signals.

The polarisation studies are linked to the *aging* (imprint) phenomenon, i.e. the polarisation-dependent shift of the hysteresis curve with time and to the ferroelectric *fatigue* process, i. e. the reduction of the remanent polarisation by cycling. Both aging and fatigue processes play an important role in the operation of the novel non-volatile memories (Ferroelectric Random Access Memories, FeRAM). Impedance spectroscopy in the lower GHz regime is employed to determine the relaxation of the ferroelectric *domain wall* motion and to separate this contribution from the contribution of the crystal lattice. By varying the microstructure of the ceramics and by comparison between bulk ceramics and thin films, the model of Arlt will be extended with respect to the impact on 2D constraints imposed by mechanical stress due to the presence of substrates. The investigations of the ferroelectric properties are now additionally focussed on the scaling properties and nano-size effects. For *dielectric* ceramics, impedance spectroscopy is used to elucidate the interrelation of *extrinsic* losses and lattice defects. In the case of ferroelectric materials, existing theories are further developed and extended towards a more quantitative description of the dielectric, piezoelectric, and elastic properties.

Lattice disorder in the vicinity of internal interfaces

Our third research area comprises the *lattice disorder in the vicinity of internal interfaces* (grain boundaries) and external interfaces (surfaces and electrode interfaces) and their impact on electronic and ionic (oxygen ions and protons) charge transport. In the case of acceptor and donor doped titanate ceramics, the studies are focused on the formation of space charge depletion layers at grain boundaries as well as the related potential barriers and the transport of charge carriers along and across the grain boundary barrier. A hot-pressing technology has been developed to decorate the grain boundary area with additional dopants and to study the influence of these artificial grain boundary states. The coupling of the space-charge formation and the defect equilibria at the surface in the case of donor-doped titanates led us to a comprehensive explanation for long pending questions concerning the redox kinetics.

In some material systems, it is necessary to determine the equilibrium constants of the defect reactions and the diffusion constants of the system in order to create the basis for the research on interfaces. In this respect, the comparison of bulk ceramics and thin films of the same composition is of vital interest. In thin film systems, the significant influence of the electrode metals, the unexpectedly high stability under conditions of dc-voltage-induced resistance degradation, the tolerance of the lattice concerning the incorporation of non-stoichiometries as well as the relationship to nanocrystalline bulk ceramics represent current research topics.

Rainer Waser

Institute of Electroceramic Materials

Head: Prof. Dr.-Ing. Rainer Waser
Secretary: Maria Garcia
Tel. +49(0)2461 61 5811; Fax: +49(0)2461 61 2550
e-mail: r.waser@fz-juelich.de/m.garcia@fz-juelich.de

Personnel 2002/2003 and their areas of activity

SCIENTISTS:

Dr. R. Dittmann	Pulsed laser deposition of epitaxial oxide thin films, multilayers and nanostructures	23.42.0
Dr. P. Ehrhart	MOCVD methods for electroceramic thin films; X-ray diffraction	23.42.0
Dr. R. Elsebrock	Processing of electroceramic bulk materials; microwave characterization; dielectric properties	23.42.0
Dr. S. Hoffmann-Eifert	High-permittivity electroceramic thin films: MOCVD, dielectric properties, charge transport, defect chemistry	23.42.0
Dr. S. Karthäuser	Self-assembly processes of oxidic and metallic nanostructures	23.42.0
Dr. H. Kohlstedt	Reactive ion beam etching of ceramic and metallic materials, magnetic and ferroelectric tunnel junctions	23.42.0
Dr. P. Meuffels	Synthesis and processing of electroceramic materials; studies of the defect chemistry	23.10.2
Dr. Ch. Pithan	Processing of hot pressed nanocrystalline and grain boundary decorated bulk electroceramics	23.10.2
Prof. T. Schober	High temperature proton conduction, ionic conduction, fuel cell studies, impedance spectroscopy, transmission electron microscopy	23.10.2
Dr. H. Schroeder	Technology and properties of (metal) electrodes for electroceramic thin films; mechanical properties and electromigration in thin films and interconnects	23.42.0
Dr. K. Szot	Study of the surface layer of perovskite materials of ABO_3 structure	23.42.0
Prof. R. Waser	Electronic oxides and integration of electroceramic thin films	23.42.0

TECHNICAL ENGINEERS:

H. Bierfeld	Ceramic technology and sputtering techniques	23.10.2
DI J. Friedrich	Thermogravimetric analysis; Transmission electron microscopy	23.10.2
M. Gebauer	Metal organic chemical vapor deposition (MOCVD) of oxides; electrical measuring setups for atomic force microscopy (AFM)	23.42.0
M. Gerst	Measuring techniques; network administration	
DI H. Haselier	Metallization and thin film technology; clean-room technology	23.42.0
B. Hermanns	RIBE, sputtering of magnetic materials	23.42.0
DI H. John	Clean-room technology, microlithography and optical laboratory; LRP	23.42.0
DI C. Makovicka	Ceramic technology; powder processing	23.10.2

Ph.D. STUDENTS

M. Fitsilis (Univ. of Thessaloniki)	Simulation and design concepts of ferroelectric field effect transistor circuits	23.42.0
R. Ganster (TH Aachen)	MOCVD growth of alkaline earth titanate-zirconate thin films; optimization of growth processes and electrical characterization	23.42.0
A. Gerber (Uni Köln)	Epitaxial ferroelectric layers on silicon substrates and their use as field effect transistors	23.42.0
B. Lüssem (TH Aachen)	Technology of molecular-electronic test chips	23.42.0
Y. Mustafa (TH Aachen)	Circuit design of ferroelectric memories	23.42.0
Ch. Ohly (TH Aachen)	Electrical conductivity characteristics of nanocrystalline and thin film titanates under changing oxygen ambients	23.42.0
St. Regnery (TH Aachen)	MOCVD planetary reactor processes	23.42.0
J. Rodriguez (Uni Köln)	Ferroelectric capacitors with oxide electrodes and tunneling	23.42.0
S. Stein (Uni Köln)	Spin injection devices	23.42.0

GRADUANTS:

M. Weides (Uni Köln)	Brillouin light scattering on magnetic tunnel junctions	23.42.0
F. Peter (TH Aachen)	Characterization of scanning force microscopy cantilever for local piezoresponse measurements	23.42.0

GUEST SCIENTISTS:

Dr. N. Pertsev A.F. Ioffe Institute St. Petersburg, Russia	Theoretical calculations on the effects of strain and stress on the dielectric response of ferroelectric thin films grown on sole substrates	23.42.0
Dr. W. Hong Xi'an Jiaotong Univ, China	Microwave ceramics and devices	23.42.0

POST-DOC:

Dr. X. Guo	Near-interface defect chemistry of doped titanates	23.10.2
Dr. A. Magrez	Synthesis of ceramic proton conductors and construction of a fuel cell	23.10.2
Dr. A. Teren	Alternative gate oxides: MOCVD, characterization and optimization of film properties	23.42.0
Dr. R. Thomas	Evaluation and optimization of modified precursors for the MOCVD of complex oxide thin films	23.42.0
Dr. E. Vasco Matias	Nucleation and growth of epitaxial thin films and nanostructures by pulsed laser deposition	23.42.0

23.10.2 Condensed Matter

23.42.0 Materials, processes and devices for the micro- and nanoelectronics

Leakage currents through thin film insulators: A new approach

H. Schroeder, S. Schmitz and P. Meuffels

Institute of Electroceramic Materials

Thin film high permittivity materials such as perovskite-type mixed oxide insulators are promising candidates to replace SiO_2/SiN_x in future ultra-large-scale integrated Gbit-DRAM chips, e.g. as dielectric in capacitors of memory cells or as gate oxide in MOSFETs. As too high leakage currents are a big concern we have performed systematic experimental studies on leakage currents through metal/insulator/metal (MIM) planar capacitors using high permittivity alloys such as $SrTiO_3$ (STO) and $(Ba_xSr_{1-x})TiO_3$ (BST) as thin film dielectrics and a wide variation of external parameters (dielectric thickness, applied field and temperature, etc.). We also have used a new approach for describing the electronic transport through the insulator and performed finite difference simulation studies with this newly developed model. The main results are reported showing good agreement between the experimental and simulation data, indicating that the leakage currents in these materials with low electronic mobility are film "bulk" limited, in contrast to the often postulated interface ("Schottky-barrier") limitation.

F&E-Nr: 23.42.0

Thin film insulators such as mixed oxides with perovskite-type crystal structure gain more and more interest in the fast-growing information technology industry because of their unique electrical properties: Very high permittivity, ferroelectricity, piezoelectricity. They are or will be used e.g. in micro-electro-mechanical systems (MEMS) or as components in ultra-large-scale integrated (ULSI) silicon-based chips such as Gbit dynamical random access memories (DRAMs), ferroelectric memories (FeRAMs) presently used in smart-cards or future field-effect transistors with ferroelectric gate oxide (FeFET) [1].

Although some oxides, e.g. $(Ba,Sr)TiO_3$ or $Pb(Zr,Ti)O_3$, are already suitable for the above mentioned applications the underlying mechanisms for their superior properties are not fully understood which calls for mechanistic studies on these material systems. We therefore have systematically investigated the leakage properties of metallized thin oxide films (STO, BST with Pt electrodes) with controlled and wide variation of many external parameters.

STO films were grown by chemical solution deposition (CSD) and crystallized at 750°C for 30' in oxygen leading to columnar grains with mean diameter of about the film thickness. The grains have a strong <111>-fiber texture. The BST films were made by MOCVD as described in [2].

The results of leakage current densities are plotted in Figs. 1a and b vs. the square route of the applied field, i.e. the "Schottky-Plot", for STO and BST, respectively, with the measuring temperature T as additional parameter. The curves can be approximated by straight lines, especially at higher temperatures as shown for the BST sample at 200°C. Therefore, the leakage current quite often is interpreted to be interface limited by thermionic emission over the interface barrier Φ_0 including field enhanced barrier lowering $\Delta\Phi$ ("Schottky effect"):

$$j = A^* T^2 \exp[-(\Phi_0 - \Delta\Phi)/kT];\ \Delta\Phi = \sqrt{e^3 E(x \approx 0)/4\pi\varepsilon_0\varepsilon_{r,opt}} \quad (1)$$

A^* is the effective Richardson constant, k the Boltzmann constant, and ε_0 the vacuum permittivity. Using the applied field for $E(x \approx 0)$ unfortunately results in an unphysical optical permittivity $\varepsilon_{r,opt}$ of 0.17 (<1!). This can be corrected by introducing low permittivity ($\varepsilon_{int} < \varepsilon_{film}$) interface layers, so-called "dead" layers which increase the electrical field at the injecting electrode ($x \approx 0$) by the ratio $\varepsilon_{film}/\varepsilon_{int}$. For the curve discussed this ratio has to be 33 to give the correct

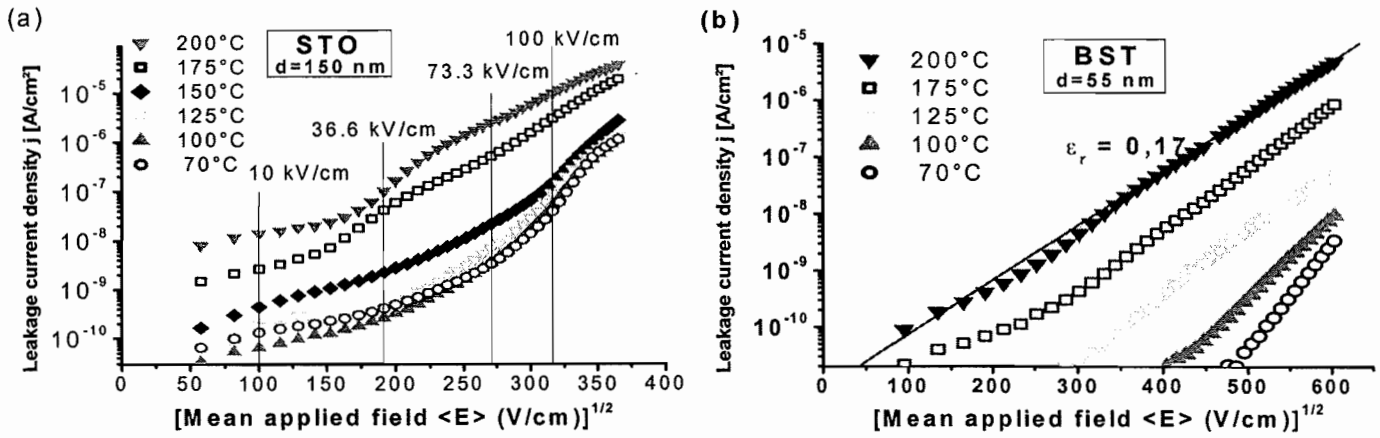

Fig. 1: Leakage current density j vs. <applied field $E>^{1/2}$ at different temperatures. (a) STO; (b) BST

optical constant of 5.6 for BST from the slope, as can be seen from Eq.(1). On the other hand the interface current limit (Eq. (1)) can only be reached if this current can be conducted through the insulator without any significant disturbance, which is questionable for low mobility materials such as STO or BST ($\mu \approx 1$ cm^2/Vs compared to e.g. about 1500 cm^2/Vs for Si at RT).

Therefore, we used a new approach to describe the measured current [3]: We have used a charge injection/recombination term for both interfaces (as it was introduced by Crowell and Sze [4] for current transport over the barrier at a metal-semiconductor Schottky contact (diode)) as boundary conditions for the transport equation (drift and diffusion) in the film bulk including the "dead" layers. As this equation cannot be solved analytically in general we have performed simulation studies using finite difference method with 200 slabs.

A comparison between measured and simulation data is shown in Fig. 2. The simulation data have been optimized to give the best fit for the experimental data at 425 K. The result is nearly perfect. For the 475 K simulation data the same parameter set was used but the temperature dependence needs some improvement. It should be noted that only three parameters were adjusted, i.e. the zero-field barrier height (1.52 eV; reasonable for Pt/BST interface), the space charge concentration (10^{18} cm^{-3} donors in this example assumed constant in the dielectric), and the thickness of the interface "dead" layer (1.1 nm, consistent with theoretical predictions [5]). All other parameters are given by separate measurements

One important result is that for the low mobility materials (BST, STO) the current is film bulk limited (although strongly influenced by the effective barrier height and thus the injection rate at the interface) while for high mobility materials (common semiconductors, e.g. Si) the thermionic emission (Schottky) limit is reached within a few percent, i.e. for these materials Eq.(1) is a very good approximation.

The deviations from the Schottky limit for the low mobility materials are most significant at low applied fields as indicated in Fig.2 for 475 K. The deviation of the Schottky limit at low applied fields from the high field straight line is due to internal fields by donor space charges.

Another important, possibly surprising experimental result

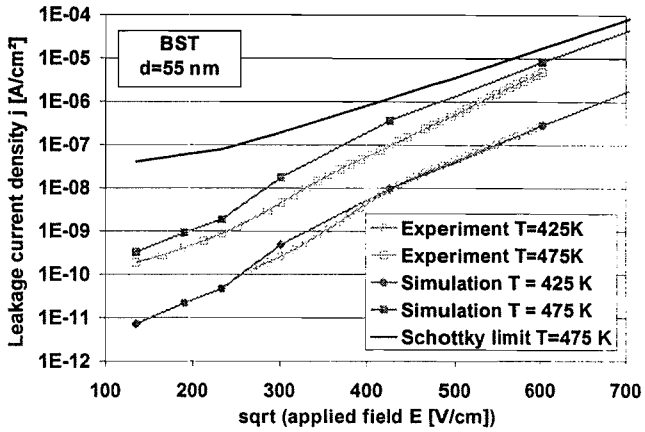

Fig. 2: Leakage current density j *vs.* <*applied field* E>$^{1/2}$ *at two temperatures: Comparison experiment-simulation.*

is shown in Fig. 3a, that is the thickness dependence of the leakage current density at constant applied field. It was measured for dielectric thicknesses between 20 and 109 nm. Clearly the current is largest in the thickest sample and than decreasing with decreasing thickness. The current difference between the thinnest and thickest sample is quite striking, more than 3 orders of magnitude. For the thicknesses in between the order is not perfect at all fields, a result of the large scatter of leakage current measurements of ± half an order of magnitude.

The new model approach could also verify this dependence as the simulation data demonstrate in Fig. 3b. Up to now we have did not try to optimize the input parameters for quantitative description of the experimental data. This is one task for future simulation studies. It should also be extended for arbitrary space charges, mobile ionic defects and additional injection contributions by tunnelling through the barrier.

In conclusion the new model approach could successfully describe a set of consistently generated experimental data suggesting that the leakage is film bulk limited in these low electronic mobility dielectrics.

[1] D.E. Kotecki et al., *IBM J. Res. Develop.* **43**, 367 (1999)
[2] P. Ehrhart et al., MRS Symp. Proc. **655**, CC9.4.1 (2001)
[3] H. Schroeder et al., *Appl. Phys. Letters* **82**, (Febr. 2003)
[4] C.R. Crowell and S.M. Sze, *Solid-State Electr.* **9**, 1035 (1966)
[5] C. Zhou and D.W. Newns, J. Appl. Phys. **82**, 3081 (1997)

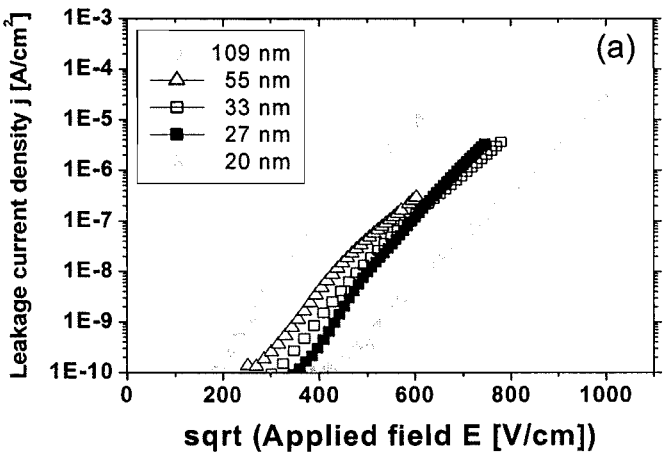

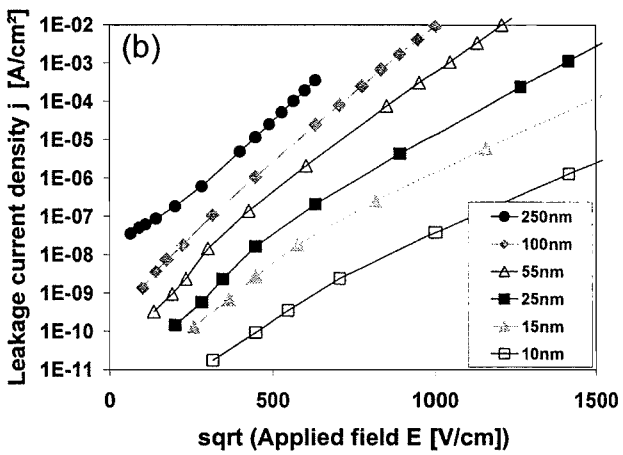

Fig. 3: Leakage current density j vs. <*applied field E*>$^{1/2}$ *for BST films of different thickness: (a) Experiment; (b) Simulation.*

The correlation between internal interfaces and the high temperature conduction behavior of nanocrystalline and thin film titanates

Christian Ohly and Susanne Hoffmann-Eifert

Institute of Electroceramic Materials

State-of-the-art integrated devices combine the classical semiconductors with electroceramic materials in order to further increase the degree of miniaturization and to show up new functional properties like for example non-volatility in ferroelectric memories (FeRAMs). As a consequence of decreasing feature sizes, the dimensions of the integrated ceramic thin films are reduced to several ten nanometers on the lateral scale and down to a few nanometers in thickness. Still one of the major difficulties in the physical description of the films, which is necessary for a precise tailoring of materials, is that properties become drastically different with decreasing dimensions. This point is addressed in our studies with respect to the analysis of the conductivity characteristics of $SrTiO_3$ thin films with different morphologies and nanocrystalline $BaTiO_3$ ceramic.

F&E-Nr: 23.42.0

Among electroceramic materials the titanates with their perovskite structure are intensely investigated materials due to their outstanding properties. For implementation in modern and future electronic devices, like memories, capacitors or sensors, recent research addresses especially the dielectric, ferroelectric and conductivity characteristics [1]. A key issue of these efforts focuses on the interplay between charge carrier transport properties and the microstructure of the material.

The conduction behavior of titanates exhibits a very characteristic dependence on the oxygen partial pressure [2]. For comparison the high temperature conduction behavior of a $SrTiO_3$ single crystal is depicted in Fig. 3 as solid lines. Under reducing conditions, oxygen is lost to the atmosphere according to $O_O^x \rightleftarrows V_O^{\bullet\bullet} + 2e' + \frac{1}{2}O_2 \uparrow$.

So with increasingly reducing atmospheres, more and more electrons are generated. This 'n-type' region is typified by a (–¼) slope in the log σ - log pO_2 - plot. Moving to higher oxygen concentrations, an intrinsic minimum is passed before entering the 'p-type' region, where intrinsically present oxygen vacancies are filled successively. This defect reaction generates holes, and the conductivity now increases with a slope of (+ ¼).

Our studies focused on the investigation of the high temperature conductivity characteristics of titanate thin films and the correlation to the thin film morphology. Applying different deposition techniques it was possible to vary the films' microstructure from polycrystalline to epitaxial which is portrayed in Figure 1. The left micrograph shows the typical cross section of a polycrystalline $SrTiO_3$ thin film grown on a sapphire substrate by means of a CSD (chemical solution deposition) technique. The film exhibits a columnar grain structure with a mean column diameter of ~ 50 nm and a thickness of about 500 nm. On the right of Figure 1, a 1 µm thick, single crystalline $SrTiO_3$ thin film is shown, grown heteroepitaxially on a MgO substrate by PLD (pulsed laser deposition). In the following we compare the conduction behavior of both types of films and investigate the effect of the density of interfaces, dominantly grain boundaries.

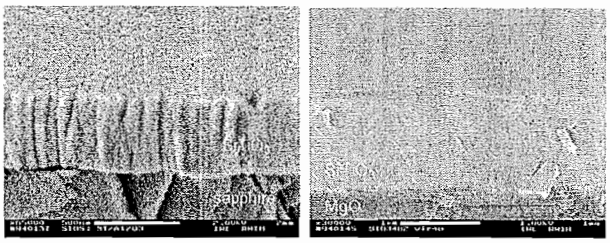

Fig. 1: Left: SEM micrograph of a CSD prepared polycrystalline $SrTiO_3$ thin film on sapphire (500 nm thick). Right: Heteroepitaxial $SrTiO_3$ thin film (1 µm thick) grown on MgO by means of PLD (J. Schubert, ISG).

Figure 2 shows the conductivity behavior of a polycrystalline CSD grown $SrTiO_3$ film (Fig. 1, left) in dependence of the oxygen partial pressure (pO_2) for temperatures between 700 °C and 1000 °C. The pO_2 was varied continuously from reducing conditions (10^{-20} bar) to pure oxygen (1 bar). Compared to the well known bulk behavior, the characteristics differ significantly. The most remarkable features are a drop of σ in the pO_2 regime of 10^{-15} to 10^{-10} bar, which is followed by a broad plateau region up to 10^{-5} bar. Instead of a 'p-type' region, a further decline of the conductivity under oxidizing ambient is revealed.

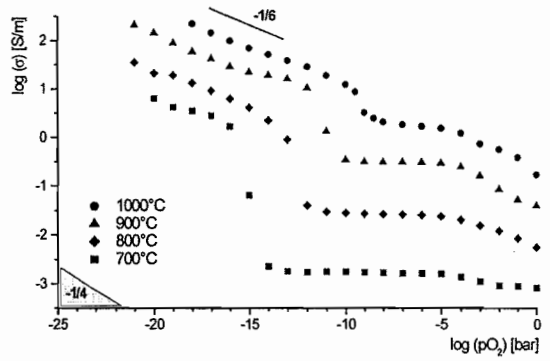

Fig. 2: Electrical conductivity as a function of the ambient oxygen partial pressure of a 500 nm thick polycrystalline CSD prepared $SrTiO_3$ thin film (see also Fig. 1, left).

This general behavior was found for a variety of films, including acceptor (Mn), and donor doped (La) ones, $BaTiO_3$ films, or solid solutions like $(Ba,Sr)TiO_3$ as well as for polycrystalline, PLD grown samples [3]-[5].

The calculation of the thermal activation energy for the conductivity in the plateau region yields a value of ~2.5 eV. In contrast, the conductivity in the plateau region of a classical donor doped titanate exhibits only a slight temperature dependence originating from the temperature dependent mobility of the electrons. Therefore, the origin of the plateau observed for the polycrystalline thin films is still to analyze.

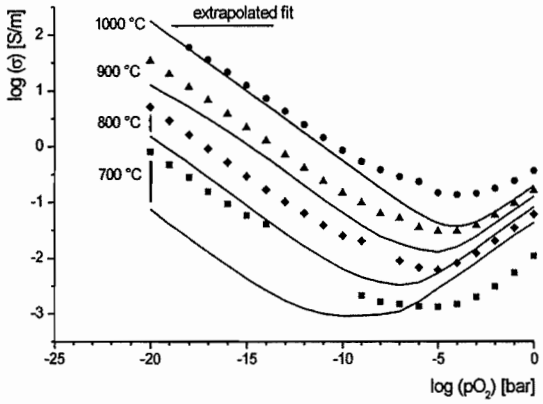

Fig. 3: Conductivity characteristic of a 1 µm thick $SrTiO_3$ film heteroepitaxially grown on MgO by PLD (symbols). The lines indicate the behavior of a $SrTiO_3$ single crystal.

The conductivity of the epitaxial $SrTiO_3$ film exhibits a totally different characteristic as shown in Figure 3. This behavior nearly resembles the single crystal characteristic (solid lines) although the activation energies for the 'n-type' and 'p-type' regime are different.

From the comparison with *epitaxial* films it is apparent that the drastic changes found for the *polycrystalline* thin films are correlated to the unprecedented high grain boundary density in these films. To further confirm this relation between conduction characteristic and morphology, a nanocrystalline $BaTiO_3$ ceramic has been prepared with a mean grain size of about 100 nm (see Figure 4). The extremely fine starting powder was synthesized via a microemulsion technique which is described in the article of C. Pithan in this report [6].

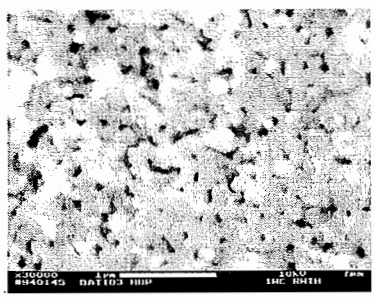

Fig. 4: SEM picture of a nanocrystalline $BaTiO_3$ ceramic with a mean grain size of about 100 nm synthesized by hot uniaxial pressing (HUP); see also [6].

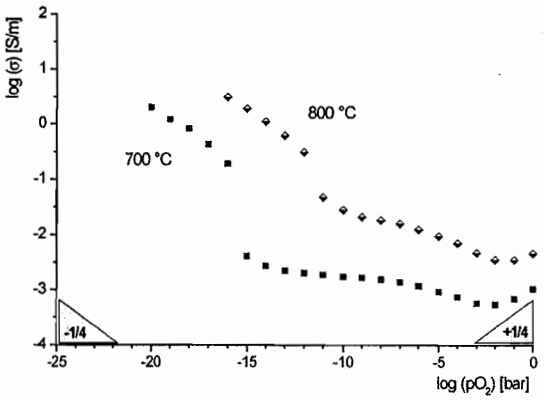

Fig. 5: Conductivity characteristics of a nanocrystalline $BaTiO_3$ ceramic. The mean grain size is about 100 nm.

The conductivity characteristics of this nanocrystalline ceramic are depicted in Figure 5. It is really remarkable to what extend these characteristics are similar to those of the polycrystalline thin films. This equivalence gives evidence to the idea that the main origin for the different characteristic of polycrystalline thin films is related to the high density of grain boundaries typical for nanocrystalline materials.

The results are summarized the following:

1. Polycrystalline titanate thin films exhibit a $\log \sigma$ - $\log pO_2$ characteristic which significantly differs from this of single crystals, and cannot be explained by the classical point defect chemistry model.
2. Epitaxially grown titanate films of 1 µm thickness show a behavior which resembles this of single crystals apart from a change in the activation energies.
3. A comparable characteristic like this of the polycrystalline films is found for nanocrystalline titanate bulk ceramics.

From the comparison of the various systems it is concluded that the different conductivity characteristics of nanocrystalline titanates, either thin films or bulk ceramics, are dominated by the influence of the grain boundaries. Here, a certain density of boundaries is necessary to observe the distinctive behavior.

Acknowledgement

The authors would like to thank J. Schubert (ISG) for the PLD grown films and C. Pithan for the nanocrystalline $BaTiO_3$ bulk ceramic.

References

[1] R. Waser, ed., 'Nanoelectronics and Information Technology', Wiley-VCH 2003.
[2] N. H. Chan, R. K. Sharma, D. M. Smyth, *J. Electrochem. Soc.* **128**, 1762 (1981).
[3] Ch. Ohly, S. Hoffmann, K. Szot and R. Waser, *Integr. Ferroelectr.* 33, 363 (2001).
[4] Ch. Ohly, S. Hoffmann-Eifert, K. Szot and R. Waser, *Integr. Ferroelectr.* **39**, 229 (2001).
[5] Ch. Ohly, S. Hoffmann-Eifert, K. Szot and R. Waser, *J. Eur. Ceram. Soc.* **21**, 1673 (2001).
[6] C. Pithan, this report

The formation of regular $SrRuO_3$ nanopatterns in the early stage of growth on $LaAlO_3$

E. Vasco, R. Dittmann, S. Karthäuser and R. Waser

Institute of Electroceramic Materials

The early stage of the epitaxial growth of $SrRuO_3$ deposited on $LaAlO_3$ by pulsed laser deposition has been studied by atomic force microscopy. After 1 nm, the $SrRuO_3$ film surface presents a ripple structure that serves as template for the development of a nano-pattern of flat islands that coalesce anisotropically forming a regular array of "infinite" nanowires at a thickness of 12 nm. With increasing thickness, the nanowires coarse and the surface row symmetry disappears for thicknesses higher than 20 nm. The lattice mismatch has been determined and the influence of the resulting stress on the evolution of the $SrRuO_3$ surface will be discussed.

F&E-Nr.:23.42.0

The fabrication of oxide nanostructures is on the one hand interesting from the scientific point of view, because it enables one to investigate novel electric, magnetic, optic and ferroelectric properties based on the confinement effect. On the other hand, it is an important technological step towards the design and implementation of future nanoscale devices.

The method of fabricating nanostructures by "self-assembly" has been intensely studied for semiconducting materials. One possible approach takes advantage of stress-induced surface modulations to create coherent arrays of 3 dimensional structures [1,2].

In spite of the increasing technological interest attracted by perovskite-like oxides, so far, self-organizing methods have only been rarely studied in these materials [3].

$SrRuO_3$ (SRO) is an metallic conducting oxide, well known as epitaxial electrode material for ferroelectric thin films [4], which becomes ferromagnetic below T_c=160 K [5]. The nano-scale integration of SRO with ferrolectric or dielectric materials is a real technological challenge. Furthermore, SRO represents a potential candidate for magnetic and magnetoresistive memories.

In this work, we investigated the possibility to grow stress-induced 3 dimensional patterns of $SrRuO_3$ on $LaAlO_3$ (LAO) substrates with a lattice mismatch of 3-4%.

The SRO films were deposited on (100)LAO by pulsed laser deposition (PLD) and the morphology was characterized by atomic force microscopy (AFM).

Fig. 1 displays the morphology of SRO films with a thickness from 1 nm to 20nm. The surface symmetries provided by their height-height correlation maps are included in the corresponding insets. The surface of the 1 nm (2-3 unit cells) thick film (Fig. 1b) grown on flat LAO (Fig. 1a) shows a periodic rippled structure. This means that after a few unit cells, the film releases stress by the creation of additional surface roughness.

The ripple structure produces a non-uniform distribution of stress at the film surface, thus the inter-ripple areas remain stressed and unfavorable for the nucleation. Therefore, for the 2.5 nm thick film (Fig. 1c), 3D irregular islands have developed from the nucleation centres on top of the ripples.

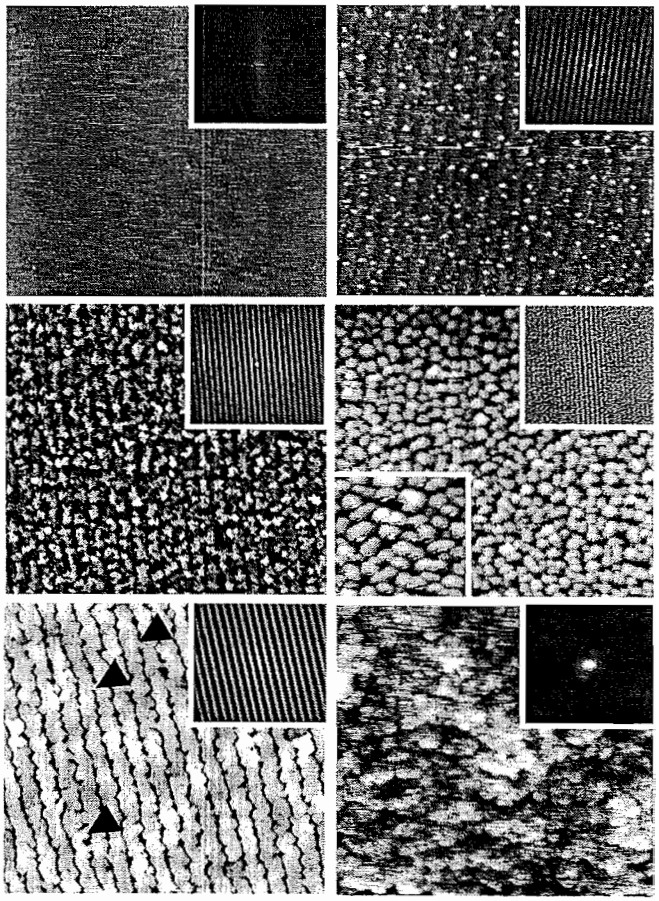

Fig. 1: Evolution of the surface morphology of SRO with film thickness: (a) 0 nm or LAO (001) surface, (b) 1 nm, (c) 2.5 nm, (d) 5 nm, (e) 12 nm and (f) 20 nm. The upper insets show the corresponding height-height correlation maps. The inferior inset in d displays 1x1 μm^2 details. The scanned area by AFM was 5x5 μm^2. Areas of early wire coalescence are pointed out in e.

The islands are grouped in unconnected rows and meanwhile remain laterally confined forming a nano-assembled pattern.The islands coarse to more regular forms and uniform sizes as the film thickness is increased (Fig 1d). The inset in Fig. 1d demonstrates that although a more disordered surface structure emerges, the row symmetry of

the growing surface is preserved. The anisotropic grain coalescence in the non-confined direction produces a compact and regular array of wires separated by abrupt boundaries (Fig. 1e). This anisotropy is likely connected to the fact that the surface stress relaxation hinders partially the diffusion of the mobile species between ripples by increasing the hopping barrier in this direction. Early evidences of wire coalescence have been pointed out in some areas in Fig. 1e. Finally, as a result of this coalescence the surface row symmetry disappears from thicknesses higher than 20 nm (Fig. 1f).

We calculated the roughness w and the lateral dimensions $\xi_\perp$ (grain size perpendicular to the ripples) and $\xi_{||}$ (ripple period) of our nanopatterns from the 10x10μm^2 AFM scans in order to determine the mechanisms that operate during the film growth. Fig. 2 shows the dependence of these parameters on the films thickness d in a double-logarithmic scale. The roughness and the grain average size increase monotonously with d up to film thicknesses around 10 nm (i.e. $w \sim d^\beta$, $\xi_\perp$ and $\xi_{||} \sim d^p$; being β and p the growth and coarsening coefficient, respectively). Above 10nm, the roughness decreases abruptly and remains constant ($w \approx 0.5$ nm). Since w and $\xi_{||}$ increase with the same exponent ($\beta = p_{||} = 0.75$) the 3D grains maintain their form (height/diameter ratio≈const.) during their coarsening. According to the dynamic scaling theory [6], from the strong increase of w ($\beta > 0.5$) one can conclude that the growth is controlled by stress-induced instabilities which hinder the surface relaxation by inhibiting the lateral redistribution of incident particles. The slow increase ($p_\perp = 0.25$) of the ripple period reveals the progressive stress relaxation with the film.

In order to investigate the origin of the anisotropy in the SRO growth mode, we performed x-ray measurements to study the epitaxial arrangement between the nano-assembled SRO film and the LAO (001) surface [7]. The ϕ-scan spectra reveal the existence of at least two epitaxial arrangements SRO<110>//LAO<001> (arrangement type A) and SRO<001>//LAO<001> (arrangement type B). The lattice mismatch of each arrangement, m, was roughly estimated from the lattice parameters obtained from the x-ray diffraction measurements. We obtain for the arrangement A: $m_{//SRO[001]} \approx -3.5\%$ and $m_{//SRO[-110]} \approx -3.6\%$; while for the arrangement B: $m_{//SRO[100]} \approx -3.9\%$ and $m_{//SRO[010]} \approx -3.3\%$. That means that the anisotropy degree produced by the arrangement B is meaningfully higher and the formation of the ripple structure may be attributed to the existence of this arrangement. However, both arrangements produce a significant biaxial compression of the SRO film.

In conclusion, nano-patterned epitaxial SRO has been successfully prepared on LAO by pulsed laser deposition. The compressive biaxial stress originated in the coherent SRO/LAO interface induces a ripple structure in the SRO growing surface, which plays a crucial role in the development of nano-arrays of islands and wires.

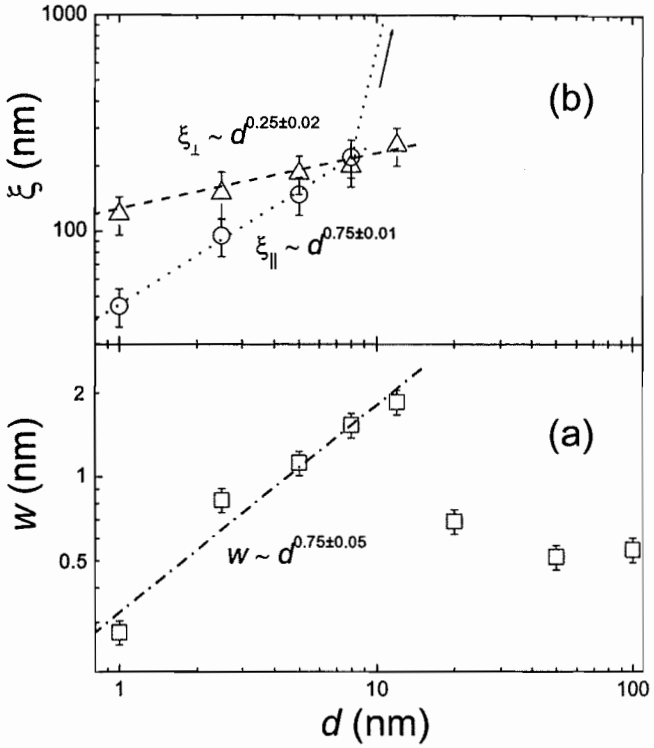

Fig. 2: Evolution of: (a) surface roughness, (b) ripple period and the grain average with the SRO film thickness. The lines correspond to linear fitted scaling expressions whose coefficients are included.

Scaling and x-ray analysis suggest that the stress instabilizes anisotropically the growing surface giving place to a Stranski-Krastanov growth mode.

REFERENCES

[1] H. Brune, M. Giovannini, K. Bromann, and K. Kern, Nature **394**, 451 (1998)

[2] O.G. Schmidt, N.Y. Jin-Phillipp, C. Lange, U. Denker, K. Eberl, R. Schreiner, H. Gräbeldinger, and H. Schweizer, Appl. Phys. Lett. **77**, 4139 (2000)

[3] M. Alexe, J.F. Scott, C. Curran, N.D. Zakharov, D. Hesse, and A. Pignolet, Appl. Phys. Lett. **73**, 1592 (1998)

[4] C. B. Eom, R. B. Van Dover, Julia M. Phillips, D. J. Werder, J. H. Marshall, C. H. Chen, R. J. Cava, R. M. Fleming, and D. K. Fork, Appl. Phys. Lett. **63**, 2570 (1993)

[5] A. Callaghan, C.W. Moeller, and R. Ward, Inorg. Chem. **5**, 1572 (1966)

[6] A. L. Barabási and H. E. Stanley, "*Fractal concepts in surface growth*" Cambridge University Press, New York (1995)

[7] E. Vasco, R. Dittmann, S. Karthäuser and R. Waser, submitted to Appl. Phys. Lett.

Stoichiometry effects in $(Ba_{0.7}Sr_{0.3})TiO_3$ thin films grown by MOCVD

F.Fitsilis[1], S. Regnery[1,2], P. Ehrhart[1]

[1] *Institute of Electroceramic Materials*
[2] *AIXTRON AG, Aachen*

The growth of $(Ba_xSr_{1-x})TiO_3$, BST, thin films on Pt-(111) surfaces was investigated within a wide parameter field. The deposition temperature was varied between 560°C and 650°C, which yields films with microstructures ranging from randomly oriented polycrystalline to perfectly (100)-textured columnar structures. Starting with $(Ba_{0.7}Sr_{0.3})TiO_3$ the Group-II/Ti content was varied from 0.9 to 1.1 and drastic changes in the surface morphology were observed. As the dielectric permittivity and the leakage current depend strongly on the film thickness, the thickness was varied between 5 and 100 nm and the data were analyzed using the phenomenological dead layer model. The relations between the stoichiometry dependence of the microstructural and electrical properties are emphasized.

F&E-Nr: 23.42.0

$(Ba_xSr_{1-x})TiO_3$, (BST), is one of the prime candidates as a high-K-dielectric in integrated high-density capacitors for future multi-GBit DRAM memory cells[1] as well as for tunable devices. BST properties critically depend, however, on the microstructure and the stoichiometry of the films. Detailed knowledge of the nucleation and growth behavior is therefore necessary for an optimization of the processes. The dependence of the film microstructure on deposition temperature has been investigated in detail previously[2] and the present discussion concentrates on stoichiometry effects and especially the Group-II/Ti content. This stoichiometry dependence is a characteristic feature of low temperature deposited thin films and is not observed for bulk ceramics, as the excess elements are precipitated at grain boundaries at the higher processing temperatures.

Films were grown in an AIXTRON 2600G3 Planetary Reactor®, which can handle five 6-inch wafers simultaneously and which has been described previously. The microstructure was investigated by X-ray diffraction and the composition of the films was determined by X-ray fluorescence analysis. Details of the microstructure were investigated by scanning electron microscopy (SEM) and by high-resolution transmission electron microscopy (HRTEM). The surface topology was investigated by scanning force microscopy (SFM). For the electrical characterisation Pt top electrodes were deposited by magnetron sputtering and structured by a lift-off process.

For films deposited at high temperatures (650-595°C) on (111)-textured Pt-electrodes, we generally observed perfectly (100)-oriented columnar grains and clean interfaces were observed by HRTEM[2]. At lower temperatures we observed a transition to a more random orientation of the grains. These structures were nearly independent of the stoichiometry and only in the transition region, around 595°C, we observed a stronger (100)-texture for Gr-II-rich films. The films were under a tensile stress of 500 to 900 MPa with no systematic dependence on the deposition parameters[2]. There is, however, a systematic difference in the lattice parameter: no change is observed for the Ti-rich samples (Gr-II/Ti $\leq$ 1) and a steady increase with higher Gr-II-content is observed for Gr-II/Ti $\geq$1. These observations may be attributed to a different incorporation of the excess elements: Gr-II elements in the form of Ruddlesden-Popper phases or micro-twins and the excess Ti within grain boundary precipitates of amorphous TiO_x.

More details on the grain structure can be seen from cross-sectional SEM at fracture surfaces. The micrographs of Fig.1 show examples for samples grown at 655°C. Generally, high-T_{growth} results in the formation of perfectly columnar grains regardless of the total film thickness[3]. The stoichiometry has, however, a significant impact on the surface morphology and grain size. The Gr-II rich films show rather large columnar grains of similar size, which seem to be faceted at the surface. This grain structure is reflected by the surface roughness observed by AFM, Fig.2.

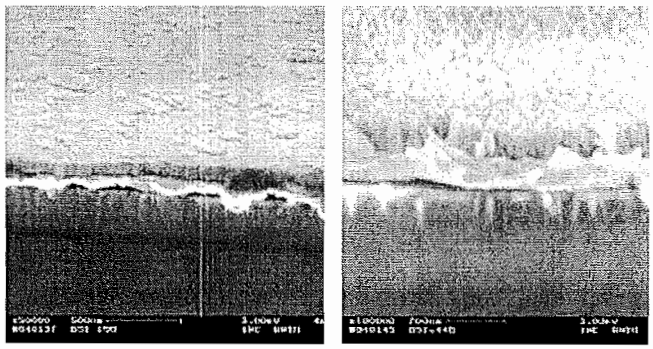

Fig. 1: SEM micrographs of a Ti- rich (left) and a GrII-rich film (right) deposited at 655°C. The film thickness is 75 and 91 nm respectively.

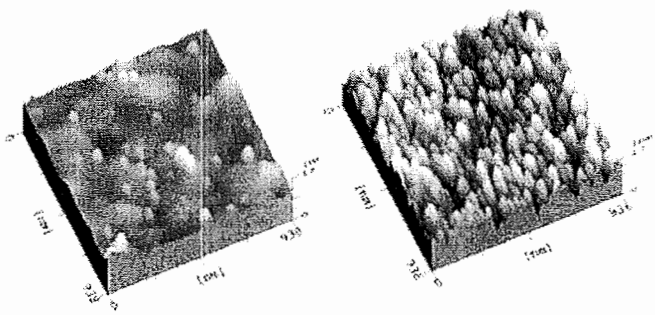

Fig. 2: AFM images of the surface of a Ti-rich (left) and a GrII- rich film (right) of 32 nm thickness.

Ti excess yields the formation of smaller and less well resolved grains with a locally flat surface; however, the formation of larger bumps is observed again. The differences in the surface morphology may indicate different growth modes, e.g., growth on strongly inclined (111) or (110) facets for Gr-II rich films and close to (100) for Ti-rich films. Although the Ti-rich films are locally more flat, the irregular bumps yield a rms roughness which is similar to that of the Gr-II rich films. This locally disturbed growth may be related to the incorporation of the Ti excess in the grain boundaries and perhaps also to the so-called irregular grain growth observed for Ti-rich $BaTiO_3$ ceramics.

It is generally observed that the permittivity of thin films shows some thickness dependence, which can be phenomenological described by a so-called dead layer or interface layer. This model assumes a bulk region of thickness, t, and the two interface regions adjacent to the electrodes with thickness, t_i, which yield two capacitors of a lower permittivity. Considering the two electrodes as identical the resulting reciprocal capacitance of the film is given by equation 1. By further approximating $(t-2t_i)$ by t, the slope of a plot of 1/C versus thickness reveals the bulk permittivity, while the intercept represents the interface capacitance, 2A/C. From this capacitance we deduce the value of ε_i/t_i for the average of the two interfaces.

$$\frac{A}{C} = \frac{2 \cdot A}{C_i} + \frac{A}{C_B} = \frac{2 \cdot t_i}{\varepsilon_0 \cdot \varepsilon_i} + \frac{t - 2t_i}{\varepsilon_0 \cdot \varepsilon_B} \qquad (1)$$

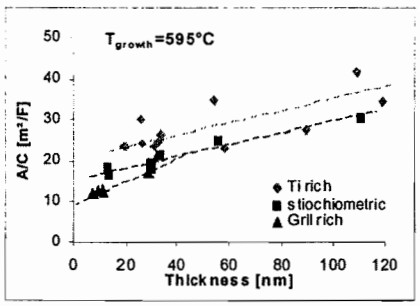

Fig. 3: Thickness dependence of the reciprocal permittivity for BST(70/30) with different Gr-II/Ti content

Fig. 3 shows the results for BST samples with a different Gr-II/Ti ratio grown at 595°C. In spite of some scatter, the data can be reasonably fit by a line, which means that the model can be applied to these data sets and table 1 summarizes the results.

T_{growth} (°C)	GrII/Ti ratio	Interface cap. ε_i/t_i (nm^{-1})	Bulk perm. ε_{bulk}
565	0.90-0-98	9.7	249
595	0.93-0.97	10.7	862
595	0.98-1.02	13.7	865
595	1.03-1.11	21.8	489
655	0.91-0.95	13.8	837
655	1.03-1.10	27.7	449

Table 1: Results for the interface and bulk permittivity

The bulk permittivity shows a strong increase from 565 to 595°C and seems constant within the uncertainties at higher temperatures. It reaches the highest values of 800-900 for Ti-rich and stoichiometric films. The interface capacitance shows a slight but systematic increase with deposition temperature for the Ti-rich samples and is systematically higher for Gr-II-rich films. Hence, a change of the stoichiometry between interface and bulk might offer a possibility for further optimisation of the total permittivity of the capacitor.

Leakage currents show also a strong thickness dependence, which cannot be explained in simple models and which corroborates a direct comparison of the results from different publications. The additional influence of the stoichiometry, which might be related to the higher interface capacitance, is shown in the Schottky plots of Fig.4. The thickness dependence and other details of the leakage current can be understood using the dead layer model developed for the permittivity. The important point for the thickness dependence is the inhomogeneous field distribution due to the rather large drop of the electric field within the low-ε interface layer; for details see the contribution of H. Schroeder et al..

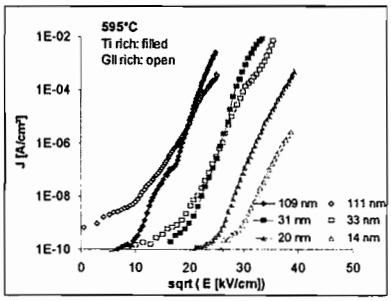

Fig. 4: Field dependence of the leakage current for films of different Gr-II/Ti ratio; T_{dep}=595°C

In summarizing, we observed major changes of film microstructure and related electrical properties with deposition temperature as well as with film stoichiometry, which is the main interest of the present report. With increasing the Gr-II content, from Ti rich to Gr-II rich films, we observe a change in the excess atom incorporation mode, in grain structure, and in surface morphology. The correlated difference in the electrical permittivity is characterized by a different behavior for the bulk and the interface. The leakage current is also strongly dependent on the film thickness and a stoichiometry dependence is only poorly visible. The observed thickness and field dependence can be explained by a low permittivity interfacial layer and thus the consistent description of permittivity and leakage current yields a strong support for the physical existence of a 'dead layer'.

1. A.I. Kingon, S.K. Streiffer, C. Basceri, S.R. Summerfelt, *MRS Bulletin* **21**, 7, 46 (1996)
2. F. Fitsilis et al., Integrated Ferroelectrics, **38** (2001) 211
3. P. Ehrhart et al., Integrated Ferroelectrics, **45** (2002) 59

Alternative Gate oxides grown by MOCVD

A. Teren[1], S.Regnery [1,3], J.Q.He[2], C.L. Jia[2], P. Ehrhart[1]
[1] *Institute of Electroceramic Materials,* [2]*Institute of Microstructure Research*
[3] *AIXTRON AG, Aachen*

We investigated the growth of a simple oxide, HfO_2, and a complex oxide, $SrTiO_3$, on Si(100) and SiO_2/Si(100) substrates. For the case of $SrTiO_3$, the growth kinetics of the amorphous SiO_x interlayer was investigated in detail by high-resolution transmission electron microscopy. The interlayer thickness showed a fast initial increase, which is much faster than the corresponding growth of amorphous SiO_2 in the absence of the precursors, and seemingly approached saturation after a short time. The thickness of the interfacial layer increases with the oxygen partial pressure during deposition and a reduction to a value acceptable for gate-oxide applications has been achieved for the minimum pressure given by the oxygen content of the present precursors. However, this comes at the expense of a dramatic increase of the carbon content of the film. For the case of HfO_2 we additionally discuss the influence of different precursors containing oxygen (Hafnium butoxide-mmp and -dmae) or not (Hafnium diethyl amide). With the amide precursor the highest low temperature, 300-500°C, deposition rate was achieved. The electrical properties of the MOS capacitors were determined for films of different thickness. The results are discussed in terms of the film microstructure, amorphous vs. crystalline, and of the post-annealing in different atmospheres.

F&E-Nr: 23.42.0

High-K gate oxides are of actual interest because the conventionally used SiO_2 gate dielectrics in metal-oxide-semiconductor (MOS) devices have to be reduced in thickness along with the continuous reduction of the device scale. Due to increased tunneling currents a fundamental scaling limit seems to be reached soon. Therefore the gate oxide has to be replaced by a material with higher permittivity which allows for a larger physical thickness[1]. In replacing SiO_2 it remains a challenge to achieve the required properties for films directly grown on the silicon substrates. Especially difficult is the elimination of interfacial layers with low-K values and/or high interfacial trap densities. Amorphous metal oxides, like Al_2O_3, HfO_2, and ZrO_2, are considered as the most promising near term replacement. Such amorphous gate oxides or silicates (e.g. $HfSiO_x$,) yield K-values in the range of 8 to 20. For even higher K-values crystalline materials, especially STO, are considered as epitaxial layers and, in spite of the possible complications by grain boundaries, also in the form of polycrystalline films. Based on our experience with perovskites we started with STO on Si and included Hf and Ti oxides.

The STO films were grown in an AIXTRON 2600G3 Planetary Reactor®, which can handle five 6-inch wafers simultaneously and the HfO_2 films in an AIX-200 research reactor which have been described previously[2,3]. The microstructure was investigated by X-ray diffraction and the composition of the films was determined by X-ray fluorescence analysis. Details of the microstructure were investigated by high resolution transmission electron microscopy (HRTEM). For the electrical characterisation Pt top electrodes were deposited by magnetron sputtering and structured by a lift-off process.

We started with detailed HRTEM studies on the growth of STO on Si. These investigations were complemented by investigations at reference samples oxidized in the absence of precursor molecules in order to elucidate the kinetics of the formation of the SiO_x interlayer under different conditions. Cross-sectional low-magnification lattice image show that the STO thin film deposited at 650°C has a polycrystalline structure. An amorphous layer evidently exists between the film and the substrate. The interface between the crystalline film and the amorphous layer looks flat, while the top surface of the STO film is quite rough. AFM microscopy yields a rms roughness of 3-5nm.

We observe a fast initial growth of the amorphous layer and the approach of a saturation thickness after 10-20 sec. In addition we observe a strong dependence on the oxidizer type (O_2 or a mixture of O_2 and N_2O) and flow rate. Fig.1 summarizes the growth rates taken after a deposition time of 440s, which yields a 'saturation thickness'. The starting value of 0.6nm is grown during heating and thermal stabilization at 655°C. The growth rates under deposition conditions are much larger than the values for thermal oxidation which are included for comparison. Such a behavior can be explained by an initially kinetically controlled fast growth, where catalytic effects might be important, and a transition to a slow diffusion limited growth as soon as there is a sufficiently thick closed film.

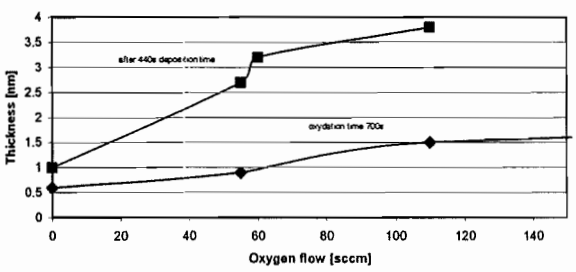

Fig. 1: Thickness of the amorphous layer between the STO film and the Si(100) substrate versus oxygen flow rate. Values are taken at a deposition time of 440s, which yields a 'saturation thickness'. Thermal oxidation rates after 700s for the same oxygen flow are included for comparison.

The importance of the details of the reaction paths is further stressed by the observation of the reduction of the growth rate by the addition of N_2O (55sccm O_2 data point in Fig,1). Hence, an appropriate choice of the oxidizer might help to suppress the growth of the amorphous interlayer.

Using the precursor without additional oxidizer we succeeded in reducing the amorphous layer thickness dramatically; at some places there actually seems to be direct crystal contact with the Si substrate. Hence the layer thickness may be reduced to a level which is acceptable for application as a gate-oxide. However, incomplete precursor reactions and a related dramatic increase of the carbon content of the films is revealed by secondary neutral-atom mass spectrometry for these conditions. A more detailed discussion is available [4].

For the case of HfO_2 we discuss the influence of different precursors containing oxygen (Hafnium butoxide-mmp and -dmae) and (Hafnium diethyl amide). The phase formation and structure of the HfO_2 films was investigated using X-ray diffraction. For films prepared with the amide precursor the amorphous to crystalline transition occurred for a deposition temperature of 450-500°C, which was 50°C higher than for the butoxide precursors. For higher temperatures, which represent the mass transport-limited growth regime, the growth rate was on the order of 10 nm/min for all the precursors. In the low temperature range (300-500°C) the growth rate for the amide precursor substantially higher than for both the butoxide precursors. Since amorphous films are of interest for the gate oxide applications, the amide precursor has the advantage in terms of growth rate at the lower deposition temperatures.

The thickness of the films was determined by x-ray reflectivity techniques and the mass density by Rutherford backscattering spectrometry (RBS). From the planar atomic mass density the thickness can be calculated assuming that the film is stoichiometric HfO_2 with the bulk density of 10.1 g/cm^3 or 8.668E22 atoms/cm^3. The thickness obtained with reflectivity measurements is typically higher by several nanometers compared to RBS. This discrepancy must be attributed to a lower-than-bulk density for the as-deposited films. The main factor that affected the density in the as-deposited films was the deposition temperature. However, a densification could also be achieved by post deposition annealing.

Electrical properties of the oxide films, were obtained from capacitance-voltage (C-V) measurements made on MOS capacitors, $Pt/HfO_2/p\text{-}Si/Ga_{0.85}In_{0.15}$ with a typical frequency of 100 kHz. Figure 2 shows a C-V curve for an as-deposited film and after annealing in N_2. For this example the C-V of the as deposited film shows no saturation in accumulation, which is indicative of a high leakage current and a well behaved MOS characteristic is only achieved after annealing.

From the maximum capacitance in accumulation the equivalent oxide thickness (EOT or t_{eq}), was obtained:

$$t_{eq} = \varepsilon_o \varepsilon_{SiO2} A / C_{max}$$

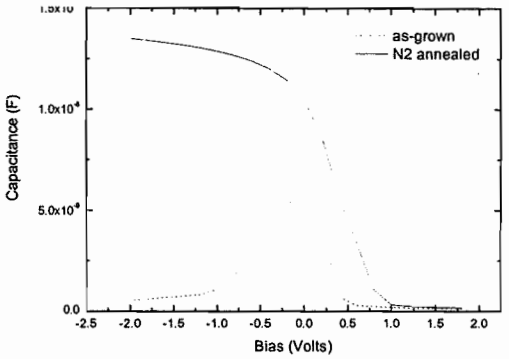

Fig. 2: C-V curves of HfO_2 MOS capacitors before and after N_2 annealing at 600°C for a 3 nm-thick film.

where ε_{SiO2} is set to 3.9 and A= 1mm^2. A graph of the equivalent oxide thickness versus the physical thickness for films prepared with the mmp and amide precursors at 400°C is shown in Figure 3. From the intercept, the interlayer thickness of 1-3 nm is obtained, which agrees with the measurement obtained from HRTEM. From the slope of the linear fit, a dielectric constant of 10 is obtained for the mmp precursor and a dielectric constant of 14 for the amide precursor.

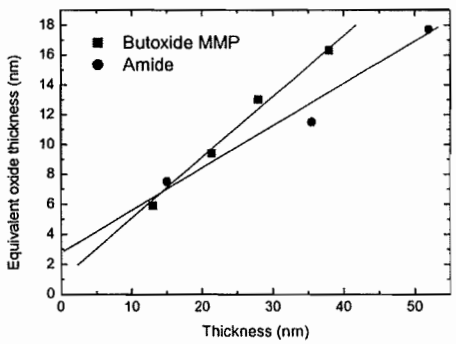

Fig. 3: EOT values versus physical thickness for as-deposited films prepared with different precursors.

In contrast to these relatively thick films, films with a thickness of < 15 nm usually displayed poorly-behaved C-V profiles, Fig.2 and both post-growth and post-electrode annealing was successfully applied. It is likely that the improvements in the C-V behaviour are due in part to the densification of the film and the removal of carbon species. This annealing process allowed the achievement of an EOT as low as 2.5 nm. Further work is necessary to optimise the annealing process.

1. A.I. Kingon, J.P. Maria, S.K. Streiffer, Nature, **406,** 2000, 1032
2. F. Fitsilis, et al., Intergrated Ferroelectrics, **38**, 2001, 211
3. P. Schäfer et al., Intergrated Ferroelectrics, **30**, 2000, 165
4. J.Q. He, S. Regnery, C.L. Jia, Y.L. Qin, F. Fitsilis, P. Ehrhart, R. Waser , K. Urban, and R.H. Wang, JAP, **92** (2002) 7200

Microemulsion mediated synthesis and ceramic processing of nano-crystalline $BaTiO_3$ powders

C. Pithan

Institute of Electroceramic Materials

Nano-crystalline $BaTiO_3$ powders with an average primary particle size of approximately 10 nm have been prepared by applying a microemulsion mediated synthesis technique. The powders were characterized with respect to their stoichiometry (ICP-OES, XRF), purity (XRD, FTIR, Analysis of C-content), crystalline structure (XRD), morphology (TEM, FE-SEM) and particle size distribution (XRD-line broadening, BET, SAXS). Compared to a commercial reference powder (primary particle size: 50 – 70 nm) the powders of our study clearly showed improved sinter activity, since the onset of densification is significantly shifted to lower temperatures. However, the preparation of highly densified nanocrystalline bulk $BaTiO_3$ ceramics requires the application of pressure assisted consolidation methods in order to reduce undesired grain-growth and porosity arising from differential sintering.

F&E-Nr: 23.10.2

The trend in the development of modern, highly volume efficient electroceramic multilayer devices such as for instance MLCCs (Multilayer Ceramic Capacitors), is driven by a continuous reduction in layer thickness. Conventional green bodies for MLCCs built up of hundreds of layers with a thickness of 1µm or more respectively, are usually manufactured by tape casting and lamination. For the technical realization of much thinner structures an alternate application of dielectric layers and electrodes by screen printing of suspensions prepared from nano-crystalline powders ("dielectric or metallic inks") is currently of strong interest. In both cases the final consolidation into bulk devices occurs via solid state sintering. The most important class of dielectric materials for MLCC is based on compositions derived from the well-known ferroelectric perovskite compound $BaTiO_3$.

In the present study nano-crystalline $BaTiO_3$ powders with high sinter activity have been prepared by applying micro-emulsion mediated synthesis according to the method suggested by Hempelmann et al. [1]. Powders synthesized by this route could eventually have some relevance for the above-mentioned technical applications and therefore some of their main characteristics and properties related to ceramic processing such as stoichiometry, purity, crystalline structure, particle size, powder morphology and sintering behaviour have been investigated. In order to realize nanostructured bulk ceramics from these powders pressure assisted consolidation techniques, such as sinter forging and hot isostatic pressing (HIP) have been applied. Highly densified and bulk $BaTiO_3$ ceramics with an average grain size between 50 nm and 300 nm, depending on the compaction method and the process parameters, have been obtained. First results on the high temperature electric conductivity behaviour of these samples as a function of oxygen partial pressure are reported in another contribution of this annual report [2].

Powder preparation and characterization

For the synthesis of the powders a solution of Barium Isopropoxide $(Ba[OCH(CH_3)_2]_2$ in Isopropanol was mixed with Titanium Isopropoxide $Ti[OCH(CH_3)_2]_4$ in a stoichiometric ratio Ba:Ti =1. To this mixture a microemulsion [1] consisting of Cyclohexane, deionized water, Tergitol NP 35 (Sigma Aldrich) as surfactant and 1-Octanol as co-surfactant has been added. Since the formation of the powder particles during the reaction of the alcoholic and heterometallic alkoxide solution is spatially confined to the aqueous nano-droplets of the microemulsion, controlled particle-nucleation and growth may be achieved. The resulting primary particles were approximately 10 nm in diameter. They consisted of essentially crystalline $BaTiO_3$ with only some traces of $BaCO_3$ and residual surfactant (Figure 1)

- Mean particle size: 10 nm (FWHM of XRD peaks ≈ 1 °)
- BET-surface: 117,3 m^2/g
- Stoichiometry: Ba/Ti: 1,009 (ICP)
- C-content: 4,44 wt.-% (organic)
  0,22 wt.-% (inorganic)

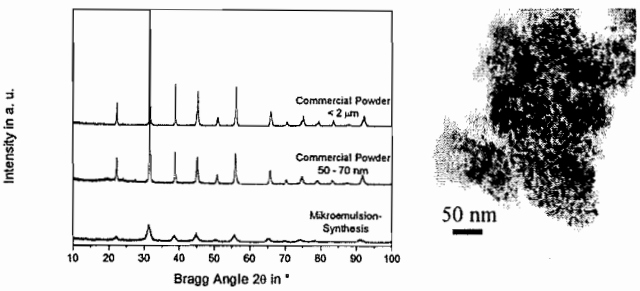

Fig. 1.: Typical properties of the synthesized raw powders.

SAXS-measurements confirmed, that the particle size distribution is quite narrow with a well defined degree of polydisperisty [3].

Consolidation behaviour

The densification behaviour of the microemulsion derived $BaTiO_3$ nano-powders has been investigated by dilatometric measurements, sintering experiments, and by determining the pore size distribution through BET (N_2-adsorption). Sintering of uniaxially pressed green compacts of the nano-crystalline $BaTiO_3$ powders begins at approximately 530°C (Figure 2). At this temperature shrinkage due to de-composition and elimination of residues originating from organic phases can be excluded: as the results of thermogravimetric studies clearly reveal, the main part of all organic impurities have already decomposed (Figure 3).

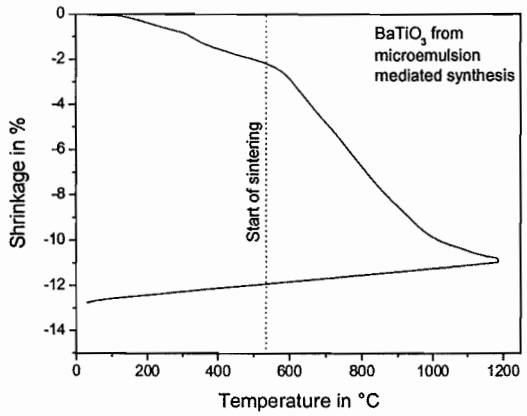

Fig. 2: Shrinkage behaviour of a uniaxially precompacted green body prepared from the nano-crystalline $BaTiO_3$ powder.

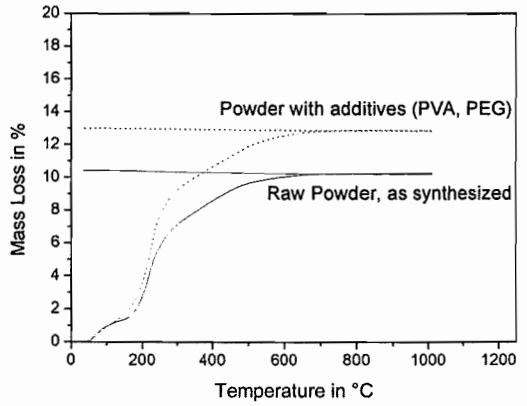

Fig. 3: Thermogravimetric characterization of nano-crystalline $BaTiO_3$ powder.

The microstructure of a sample that has been sintered for 1 h at 1000 °C is shown in Figure 4 (a). The mean size of the crystallites has significantely increased form 10 nm to approximately 200 nm and a still rather porous structure can be observed. Figure 4 (b) shows the microstructure of a sample that has been compacted by hot isostatic pressing at 860°C under 2000 bar pressure. It is evident, that the average grain size in the latter sample is much smaller (approximately 100 nm). Although still some larger pores can be recognized the connectivity between the grains is much more improved compared to the pressureless sintered sample.

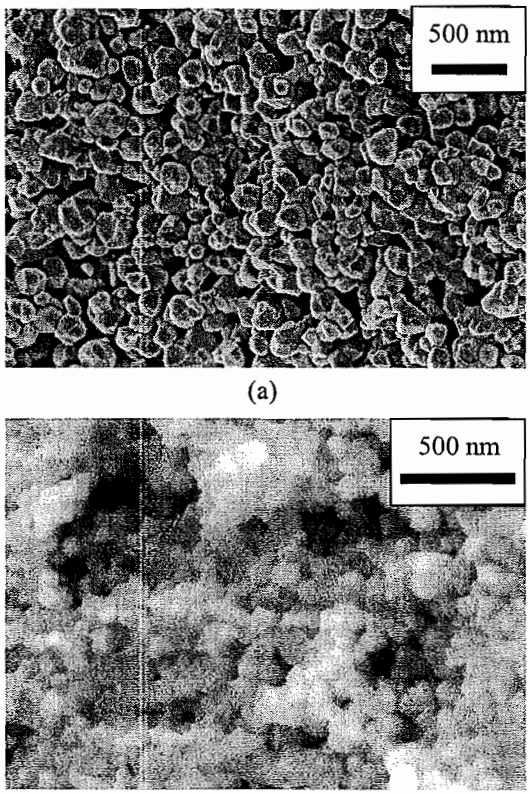

Fig. 4: Microstructure of a pressureless sintered sample and a sample that has been compacted by HIP.

ACKNOWLEGEMENTS

The very helpful support of B. Coenen (IWV 1) and C. Ohly (IFF) during the HIP-experiments is gratefully acknowledged.

Fruitful collaboration and discussions with J. Dornseiffer (ICG II) and F.-H. Haegel (ICG IV) are also gratefully acknowledged.

REFERENCES

[1] Ch. Beck, W. Härtl, R. Hempelmann: J. Mater. Res. 13 (1998) 3174.

[2] C. Ohly, S. Hoffmann-Eifert: this report.

[3] T. Vad, C. Pithan, G. Haubold: HASYLAB-Annual Report (2002) in print.

Publications in journals

Bachhofer,H.*; Reisinger,H.*; Steinlesberger,G.*; Nagel,N.*; Cerva,H.*; von Philipsborn,H.*; Schroeder,H.; Waser,R.
Interfacial layers and their effect on leakage current in MOCVD-deposited SBT thin films
Integrated ferroelectrics, 39 (2002), S. 189

Bachhofer,H.*; Reisinger,H.*; Steinlesberger,G.*; Nagel,N.*; Cerva,H.*; von Philipsborn,H.; Schroeder,H.; Waser,R.
Interfacial layers and their effect on leakage current in MOCVD-deposited SBT thin films
Integrated ferroelectrics, 39 (2002), S. 289

Ehrhart,P.; Fitsilis,F.; Regnery,S.; Waser,R.; Schienle,F.; Schumacher,M.*; Juergensen,H.*; Krumpen,W.
Growth of (Ba,Sr)TiO3 thin films by MOCVD : stoichiometry effects
Integrated ferroelectrics, 45 (2002), S. 59 - 68

Ellerkmann,U.*; Liedtke,R.*; Waser,R.
Influence of the film-electrode interface in thin-film capacitors
Ferroelectrics, 271 (2002), S. 315 - 320

Emelyanov,A. Y.*; Pertsev,S.*; Hoffmann-Eifert,S.; Boettger,U.*; Waser,R.
Grain-boundary effect on the Curie-Weiss law of ferroelectric ceramics and polycrystalline thin films : calculation by the method of effective medium
Journal of electroceramics, 9 (2002), S. 5 - 16

Ganpule,C. S.; Nagaranjan,V.; Hill,B. K.; Roytburd,A.L.; Williams,E.D.; Ramesh,R.; Alpay,S. P.; Roelofs,A.; Waser,R.; Eng,L. M.
Imaging three-dimensional polarization in epitaxial polydomain ferroelectric thin films
Journal of applied physics, 91 (2002), 3, S. 1477 - 1481

Grossmann,M.*; Lohse,O.*; Bolten,D.*; Boettger,U.*; Schneller,T.*; Waser,R.
The interface screening model as origin of imprint in PbZrx/Ti1-x/O3 thin films 1 : dopant, illumination, and bias dependence
Journal of applied physics, 92 (2002), S. 2680 -2687

Hofer,C.*; Hoffmann,M.*; Boettger,U.*; Waser,R.
Relaxors as high-E- materials for multilayer and thin film capactors
Ferroelectrics, 270 (2002), S. 179 - 184

Hoffmann,M.*; Hofer,C.*; Schneller,T.*; Böttger,U.*; Waser,R.
Preparation and ageing behavior of chemical-solution-deposited (PbMg(0.33)Nb(0,67)O3)1-x-(PbTiO3)x thin films without seeding layers
Journal of the American Ceramic Society, 85 (2002), S. 1867 - 1869

Hölbling,T.*; Waser,R.
Simulation of the charge transport across grain boundaries in P-type SrTiO3 ceramics
Ferroelectrics, 268 (2002), S. 215 - 220

Hölbling,T.*; Waser,R.
Simulation of the charge transport across grain boundaries in p-type SrTiO3 ceramics under dc load : Debye relaxation and dc bias dependence of long-term conductivity
Journal of applied physics, 91 (2002), 5, S. 3037 - 3043

Jia,C.L.; Rodriguez - Contreras,J.*; Poppe,U.; Kohlstedt,H.*; Waser,R.; Urban,K.
Lattice strain and lattice expansion of the SrRuO3 layers in SrRuO3/PbTr0.52Ti0.48O3/SrRuO3 multilayers thin films
Journal of applied physics, 92 (2002), 1, S. 101

Kueppers,H.*; Leuerer,T.*; Schnakenberg,U.*; Mokwa,W.*; Hoffmann,M.*; Schneller,T.*; Boettger,U.*; Waser,R.
PZT thin films for piezoelectric microactuator applications
Sensors and actuators A, 97-98 (2002), S. 680 - 684

Ohly,C.; Hoffmann-Eifert,S.; Szot,K.; Waser,R.
Defects in alkaline earth titanate thin films - the conduction behavior of doped BST
Integrated ferroelectrics, 38 (2001), S. 229 - 237

Prume,K.*; Franken,K.*; Böttger,U.*; Waser,R.; Maier,H.*
Modelling and numerical simulation of the electrical, mechanical and thermal coupled behaviour of MLCs
Journal of the European Ceramic Society, 22 (2002), S. 1285 - 1296

Quin,Y.L.*; Jia,C.L.*; Urban,K.; Liedtke,R.*; Waser,R.
Structural and morphologic evolution of Pt/Ba0,7Sr0,3TiO3/Pt capacitors with annealing processes
Journal of applied physics, 80 (2002), 15 , S. 2728 - 2730

Ritter,S.; Hoffmann-Eifert,S.; Bolten,D.
(Pb1-xBax)TiO3 thin films prepared by liquid delivery MOCVD : influence of the process parameters on film formation and electrical properties

Ferroelectrics, 268 (2002), S. 563 - 568

Roelofs,A.*; Pertsev,N.A.*; Waser,R.; Schlaphof,F.*; Eng,L. M.*; Ganpule,C.*
Depolarization-field-mediated 180° switching in ferroelectric thin films with 90 ° domains
Journal of applied physics, 80 (2002), 8, S. 1424 - 1426

Schneller,T.*; Waser,R.
Chemical solution deposition of ferroelectric thin films - state-of-the-art and recent trends
Ferroelectrics, 267 (2002), S. 293 – 301

Steinlesberger,G.*; Reisinger,H.*; Bachhofer,H.*; Schroeder,H.; Werner,W.*
Dielectric relaxation and charge carrier transport mechanisms in (Ba, SR) TiO3 thin films
Integrated ferroelectrics, 38 (2001), S. 249

Book chapter

Rodriguez Contreras,J.; Schubert,J.; Poppe,U.; Trithaveesak,O.; Szot,K.; Buchal,Ch.; Kohlstedt,H.; Waser,R.
Structural and ferroelectric properties of epitaxial PbZr 0,52 Ti 0,48 O3 and Ba TiO3 thin films prepared on SrRuO3/SrTiO3(100) substrates
Materials Research Society Symposium proceedings. - 688 (2002). - S. C8.10

Kügeler,C.*; Hoffmann,M.*; Böttger,U.*; Waser,R.
Integration, electrical and electromechanical properties of PZT and PMN-Pt thin films for MEMS applications
Proceedings of SPIE. - 4699 (2002). - S. 114 - 123

Schroeder,H.; Schmitz,S.
Leakage current measurements of STO and BST thin films interpreted by the 'dead' layer model
14th International Ferroelectrics (ISIF) 2002
Nara, Japan

Schneller,T.*; Waser,R.
Contribution to the microscopic understanding of the chemical mechanisms in solution based PZT thin film deposition
1. Working Group Meeting : Cost 528
Hamburg

Schober,T.
Applications of oxidic high temperature proton conductors
11th International Conference on Proton Conductors, SSPC11
Guildford, UK

Schober,T.
On the use of Pd filters on proton conducting SOFC ceramics
9th Euro Conference on Ionics
Ixia, Rhodos

Schober,T.
Solid state iIonics applications in vacuum technology
OSSEP Workshop der ESF on SOFC and Proton Conductivity
Roskilde, DK

Schroeder,H.
Deposition methods
MRS Fall Meeting 2002 : Tutorial on Ferroelectric Thin Films
Boston, Mass.

Schroeder,H.
Electro-optical devices
MRS Fall Meeting 2002 : Tutorial on Ferroelectric Thin Films
Boston, Mass.

Schroeder,H.
Ausgewählte Kapitel der Metallphysik
Vertiefungsfach II : Fakultät für Bergbau, Hüttenwesen und Geowissenschaften der RWTH Aachen
WS 01/02

Invited talks

Haegel,F.H.; Schwuger,M.J.; Pithan,C.; Waser,R.
Electroceramic materials made from nanoparticle powders - investigation of properties related to industrial application
National Meeting of the American Chemical Society : Symposium of Fundamentals and Applications of Uniform Fine Particles

Hoffmann-Eifert,S.; Ohly,C.; Schubert,J.; Waser,R.
The effect of microstructure on the high temperature conductivity of strontium titanate thin films
78th International Bunsen Discussion Meeting on Complex Oxides : Defect Chemistry, Transport and Chemical Reaction
Vaals, Niederlande

Hoffmann-Eifert,S.; Ohly,C.; Waser,R
The correlation between internal interfaces and the high temperature conduction behavior of nanocrystalline and thin film titanates
MRS Fall Meeting 2002
Boston, Mass.

Kügeler,C.*; Hoffmann,M.*; Böttger,U.*; Waser,R.

Integration, electrical and elctromechanical properties of PZT and PMN-Pt thin films for MEMS applications
9th International Symposium on Smart Structures and Materials : SPIE
San Diego, CA

Pithan,C.; Malic,B.*; Ringgaard,E.*; Waser,R.
Processing and characterization of pressure consolidated lead free piezoceramics based on alkaline niobates
International Joint Conference on the Applications of Ferroelectrics 2002
Nara, Japan

Pithan,C.; Waser,R.
Dissemination activities within POLECER
First Annual Meeting of the Thematic European Network on Polar Electroceramics
Interlaken, CH

Ohly,C.; Hoffmann-Eifert,S.; Waser,R.
The role of grain boundaries on the high temperature conduction behavior of nanocrystalline titanate thin films
International Joint Conference on the Applications of Ferroelectrics (IFFF) 2002
Nara, Japan

Regnery,S.; Ehrhart,P.; Fitsilis,F.; Waser,R.; Schienle,F.; Schumacher,M.*; Juergensen,H.*
Nucleation and growth of thin (Ba,Sr)TiO3 films in a MOCVD reactor
MRS Fall Meeting 2002
Boston, Mass.

Rodriguez Contreras,J.; Gerber,A.; Schubert,J.; Poppe,U.; Szot,K.; Jia,C.; Haeni,J.; Biegalski,M.; Kohlstedt,H.; Schlom,D.G.*; Waser,R.
Scaling effects in ferroelectrics
Panamerican Advanced Studies Institute (PASI) Workshop
Rosario, Argentinien

Rodriguez Contreras,J.; Schubert,J.; Poppe,U.; Szot,K.; Jia,C.L.; Kohlstedt,H.; Waser,R.
Scaling effects in ferroelectrics and tunnel junctions with ferroelectric barrier
Panamerican Advanced Studies Institute (PASI) Workshop
Rosario, Argentinien

Rodriguez Contreras,J.; Schubert,J.; Szot,K.; Jia,C.; Haeni,J.; Biegalski,H.; Kohlstedt,H.; Waser,R.; Schlom,D.G.*
Structural and ferroelectric properties of MBE-grown BaTiO3/SrRuO3 thin films
Workshop on Oxide Electronics (WOE 9)
St. Petersburg, Florida

Schneller,T.*; Roelofs,R.*; Waser,R.
CSD derived nanosized single crystalline ferroelectric grains for future non-volatile memory generations
8th International Conference on Ceramic Processing Science
Hamburg

Other talks

Waser,R.
Am Vorabend der nächsten Evolutionsstufe?
Infineon Corporate Research Seminar

Waser,R.; Schroeder,H.
Neue Materialien und Bauelemente für die Informationstechnik I
Vertiefungsfach II : Fakultät für Elektrotechnik der RWTH Aachen
WS 01/02

Ohly,C.
The role of grain boundaries on the high temperature conduction behavior of titanate thin films
Sitzung des Wissenschaftlichen Beirats des IFF
Jülich: 21.03.2002

Rodriguez Contreras,J.; Schubert,U.; Poppe,U.; Szot,K.; Kohlstedt,H.; Waser,R.
Influence of patterning method on ferroelectric properties of PbZr 0,52 Ti 0,48 O3
Workshop on Oxidic Surfaces 2002
Halle

POSTERS

Schroeder,H.; Schmitz,S.
Leakage current experiments in STO and BST thin films
MRS Fall Meeting 2002 : Symposium on Ferroelectric Thin Films
Boston, Mass.

Schroeder,H.; Schmitz,S.; Meuffels,P.
Simulation of steady state leakage current in thin films
MRS Fall Meeting 2002 : Symposium on Ferroelectric Thin Films XI
Boston, Mass.

Schroeder,H.; Schmitz,S.; Meuffels,P.; Liedtke,R.
Simulation of leakage current thin films with dead layers
14th International Symposium on Integrated Ferroelectrics (ISIF) 2002

Nara, Japan

Ehrhart,P.; Fitsilis,F.; Regnery,S.; Waser,R.; Schienle,F.; Schumacher,M.*; Juergensen,H.*; Krumpen,W.
Growth of (Ba,Sr)TiO3 thin films by MOCVD : stoichiometry effects
14th International Symposium on Integrated Ferroelectrics
Nara, Japan

Ganster,R.; Hoffmann-Eifert,S.; Waser,R.
Growth of Zr substituted barium titanate thin films from the vapor phase
MRS Fall Meeting 2002 : Symposium Ferroelectric Thin Films XI
Boston, Mass.
I01

Karthäuser,S.; Szot,K.; Waser,R.
Termination control of SrTiO3 (100) surfaces
Nato-Workshop : ASINATO Scanning Probe Microscopy
Albufeira, Portugal

Kügeler,C.*; Liedtke,R.*; Waser,R.
Leakage current properties of Ba0,7 Sr0,3 TiO3 thin films depending on the film thickness
ISAF
Nara, Japan

Ohly,C.; Hoffmann-Eifert,S.; Waser,R.
The influence of doping on the high temperature conduction behavior of polycrystalline strontium titanate
78th International Bunsen Discussion Meeting on the Complex Oxides : Defect Chemistry, Transport and Chemiacl Reaction
Vaals, Niederlande

Paul,A.; Damm,T.; Bürgler,D.E.; Stein,S.; Kohlstedt,H.; Grünberg,P.
Correlation of magnetotransport and structure evolution in sputtered Co/Cu multilayers
HGF-Workshop Kondensierte Materie : Forschungszentrum Jülich
Jülich: 06.11.2002

Pithan,C.
POLECER : European thematic network on polar electroceramics
International Joint Conference on the Applications of Ferroelectrics 2002
Nara, Japan

Pithan,C.; Waser,R.; Haegel,F.H.; Dornseiffer,J.
Nanocrystalline BaTiO3-ceramics prepared via microemulsion synthesis - powder characteristics and consolidation behaviour
International Joint Conference on the Applications of Ferroelectrics 2002
Nara, Japan

Pithan,C.; Waser,R.; Malic,B.*; Ringgaard,E.*
Sinter forged lead-free piezoceramics based on alkaline niobates - preparation and properties
Polecer-Workshop on Piezoelectric Materials for the End User
Interlaken, CH

Regnery,S.; Ehrhart,F.; Waser,R.; Ding,Y.; Jia,C.L.; Schumacher,M.*; Schienle,F.; Juergensen,H.
(Ba,Sr)TiO3 thin films growth in a batch processing MOCVD reactor
8th International Conference on Ceramic Processing Science (8th ICCPS)
Hamburg

Rodriguez Contreras,J.; Schubert,J.; Poppe,U.; Szot,K.; Jia,C.L.; Kohlstedt,H.; Waser,R.
Memory device based on a ferroelectric tunnel junction
Device Research Conference (DRC)
Santa Barbara, USA

Rodriguez Contreras,J.; Schubert,J.; Stein,S.; Gerber,A.; Poppe,U.; Szot,K.; Jia,C.L.; Kohlstedt,H.; Waser,R.
Size effects and charge transport through ultrathin ferroelectric barriers
Workshop on Oxide Electronics (WOE 9)

Schneller,T.*; Roelofs,R.*; Waser,R.
Self-assembled growth of nanosized single crystalline ferroelectric grains for future memory applications - a bottom up approach
International Joint Conference on the Applications of Ferroelectrics (IFFF) 2002
Nara, Japan

Ph.D. Theses

Sam Schmitz
Abhängigkeit des Leckstromes und der Dielektrizitätskonstanten in SrTiO3- und (Ba,Sr)-TiO3-Dünnschichtkondensatoren von der Kontakt-metallisierung

Fotios Fitsilis
MOCVD of High-K Ceramic Thin Films for the Gbit DRAM Technology

Jürgen Rickes
Advanced Circuit Design of Gigabit-Density
Ferroelectric Random-Access Memories

Christian Ohly
Nanocrystalline Alkaline earth Titanates and their
Electrical Conducitity Characteristics under Changing
Oxygen Ambients

Patents

Erfindungsmeldung PT 0.2248
Verfahren zur Herstellung einer B-terminierten
Oberfläche auf Perowskit-Einkristallen
K.Szot, IFF, W. Speier, WTP

Institute for Soft Matter

General Overview

The Institute "Weiche Materie" was founded in jan. 2000. The main focus of the Institute is to understand macroscopic properties and microstructural order of colloidal systems, under equilibrium- and non-equilibrium conditions, on a microscopic level. To make progress in this area it is necessary to be able to synthesize model colloidal systems, where monodispersity of the desirable interaction potential and shape is one of the main goals. The properties of these model systems should be tuned in such a way that it exhibits the phenomena that one wishes to study.

The research in the Institute is done within "projects", which will be described below:

Non-equilibrium Phenomena

The subjects under investigation in this project are :

Shear-banding and Rheology of "hairy Colloids" and Suspensions of rod-like Particles (P. Lettinga)
Shear-banding is a hydrodynamic instability in systems under flow that occurs whenever the stress decreases with increasing shear-rate, or the stress is a multivalued function of the shear-rate. The stationary state is now a state where regions of different microstructure and sometimes different shear-rates "coexist". The kinetics of the shear-banding instability and the possible stationary states that can occur are studied for two kinds of systems : "hairy colloids" (colloidal spheres coated with long polymer chains) and rigid rod-like particles. A system of hairy colloids where shear-banding has been observed will be investigated in cooperation with Dr. J. Vermant (University of Leuven). Another, well-defined hairy colloid has been developed in the Institut for Neutron Scattering (see the next theme). So far, our investigations are focused on the shear-induced polymer brush defoprmation at lower concentrations. Simulations on hairy colloids in shear flow will be performed in the Insitute Theory II. We recently observed a very clear shear-banding transition in suspensions of fd-virus (a semi-flexible colloid). By adding free polymer, the rate of the transition can be tuned, so that kinetic studies will be feasible in these systems. At this moment we are determining, by rheology and light scattering, the full non-equilibirum phase diagram of these kind of systems (where the shear-rate is on of the control variables). The shear-banding transition lines will be located as well. There is an ongoing collaboration with prof. W. Briels (University of Twente) on the theory of the shear-banding transition in systems of rigid rods.

Shear induced Polymer Brush Deformation (S. Rathgeber)
Colloidal micellar particles of PEO-PEP diblock copolymers with a small core in comparison to the length of the amphiphilic part of the polymers have been developed in the Institute for Neutron Scattering by Dr J. Allgaier and Dr. L. Willner. These "hairy colloids" exhibit deformation, as detected by neutron scattering under shear flow. High shear rates are needed to achieve appreciable deformation, due to their relatively small size. We are therefore currently investigation the possibility of using, in addition, small colloidal silica cores coated with very long polymers. We plan to investigate deformation at very low and higher concentrations, where interactions between the deformed brushes become important. These investigations are part of a European project (HUSC, Hard to Ultra Soft Colloids).

Critical Phenomena under Shear Flow (P. Lettinga, H. Wang))
In mixtures of stearyl silica spheres and small PDMS polymers (Poly Di Methyl Siloxane) in cyclohexane, depletion attractions can give rise to gas-liquid phase separation. Non-linear microstructural response to stationary and oscillatory shear flow near the gas-liquid critical point in these systems have been studied by means of time resolved small angle light scattering. The results of both the static and oscillatory experiments can be interpreted in terms of an earlier theory on near critical microstructure under shear flow, provided that the shear induced displacement of the critical point is taken into account. The shear induced microstructural distortion of short ranged correlations, which are responsible for the displacement of the critical point, render critical phenomena under shear flow non-universal in the sense that these depend on the details of the pair-interaction potential.

Dynamics and Structure of "Polymer-colloids" (S. Rathgeber)

Suspensions of polymeric particles of a colloidal size are studied by means of small angle neutron scattering and neutron spin echo experiments. This concerns the shape, internal structur and dynamics of the colloidal particles. The systems that are studied are two different kinds of dendrimers, cellulose derivatives and bottlebrush macomolecules, in cooperation with T. Pakula (Max Planck Institute for Polymer Research in Mainz). Scattering experiments and rheology measurements at higher concentration are planned.

Structure and Dynamics of Colloids at Interfaces and near Walls
Project leader : Dr. P. Lang

The subjects under investigation in this project are :

Structure and Dynamics of Interfaces between Coexisting Phases
The colloidal systems that will be investigated are rigid rods, like silica coated boehmite rods and semi-flexible fd-virus (in isotropic-nematic coexistence), soft systems like internally crosslinked cylindrical micelles (in isotropic-columnar coexistence), and spheres (in gas-liquid or liquid-crystal coexistence). A surface sensitive dynamic and static light scattering set up is being built at this moment.

Structure and Dynamics close to a Wall and Interactions with a Wall
Rods and spheres, mixed with several kinds of depletants (like semi flexible polymers and polyelectrolytes) will be investigated. We also plan to investigate concentration profiles, dynamics and depletion forces near a wall in mixtures of long polymers and small colloidal spheres. This will be done in cooperation with Dr. E. Eisenriegler and Dr. R Winkler (Institute Theory II). A Total Internal Reflection Microscope (TIRM) has been built for this purpose.

Dynamics in Equilibrium Systems
Project leader : Dr. G. Meier

The subjects under investigation in this project are :

Dynamics of Polymer Mixtures and Colloids under high Pressure
Pressure is an external variable that can be used to continuously vary the compatibility of polymers. The polymers can either be free polymers or polymers bound to the surface of colloidal particles. Besides by pressure, monomer-monomer pair-interaction potentials can also be changed systematically by changing the H/D composition of the polymers. This offers the possibility to gain insight in the microscopic origin of the rich phase behaviour and dynamics of these systems. The phase behaviour and (critical) dynamics of polymer mixtures and mixtures of polymers and polymer-coated colloidal particles will be the topic of this project.

Phonon Dispersion in heterogeneous Systems
Colloidal systems represent heterogeneous systems, in which the dynamics of acoustic modes will be studied. There will almost certainly be a dependence of the properties of acoustic exitations on the structural properties of the colloidal suspensions. The degree of heterogeneity can be changed continously by changing the size and/or concentration of the colloidal particles.

Rotational Diffusion of Rods near Phasetransition Lines
Rotational diffusion of rod like colloids and polymers in the neighbourhood of a gas-liquid and isotropic-nematic phase boundary will be studied. Near a gas-liquid phase transition line, the attractive interactions between the rods will probably lead to a severe change of the rotational diffusion coefficient, since attractions favor parallel alignment of neigbouring rods over perpendicular alignment. On approach of the isotropic-nematic spinodals, the rotational diffusion coefficient tends to zero in a way that is not known, that is, the critical exponent for the rotational diffusion coefficient is as yet unknown.

Rotational Diffusion away from Phasetransition Lines (P. Lettinga)
Rotational diffusion coefficients of colloidal spheres and rods in bulk solution and within porous media are investigated by means of Time resolved Phosphorescence Anisotropy (TPA) and Recovery After Photobleaching (FRAP). These experiments are performed at the University of Utrecht in collaboration G. Koenderink and prof. A.P. Philipse. Also of

interest is rotational diffusion of rigid rods under stationary shear flow, where FRAP and heterodyne dynamic light scattering experiments are planned.

We are building a combination of set ups which allows one to investigate dynamics in the time range 10^{-13}-10^{2} s. Dynamic light scattering covers a dynamic range of 10^{-7}-10^{2} s. A Sandercock tandem interferometer will be used to cover the time range 10^{-9}-10^{-11}s. The gap between these time ranges can be covered employing a confocal interferometer. The very fast dynamics will be studied by means of Raman scattering

Biopolymers
Project leader : Dr. R. Tuinier (started 1 nov. 2001)

This project deals with composite materials of colloids and biopolymers. Not much have been done so far experimentally, since the biology laboratory is not yet finished.

Phenomena in Temperature Gradients
Project leader : Dr. S. Wiegand (started 1 jan. 2003)

This project deals with the study of termodiffusion and macroscopic phenomena under temperature gradients. For thermodiffusion experiments we are currently building a Forced Rayleigh Scattering set up, specialized to measure the Soret effect.

Correlation between Interactions and ordered Structures
Project leader : Dr. J. Hauck

Dr. J. Hauck has been at the IFF for a longer time. His work in the Institute Weiche Materie is a continuation of part of the work that has been done by J. Hauck during the past, applied to ordered structures in various colloidal systems.

Synthesis
Project leaders : Dr. J. Buitenhuis
Dr. W. Sager

The aim of this project is the development of new colloidal systems, the investigation of synthesis mechanisms and the synthesis of (known) colloidal systems for cooperation projects.

Synthesis of known Colloidal Model Systems
The synthesis facility should supply and further develop the synthesis of known model systems with which physical experimentation will be done within the projects mentioned above. In this respect our contacts with the University of Utrecht are very valuable.

Development of new model systems
The following activities for the synthesis of novel model systems are in progress :
Preparation of Nanostructured Materials in Self-organising Systems (W. Sager)
This project is concerned with the characterisation of microemulsions as precipitation media for inorganic materials with at least one dimension in the nanometer range and the development of synthesis routes for nanostructured inorganic/organic composites employing the different structures encountered in microemulsion systems as templates. It is part of the PhD-project of Aurelie Autin and is performed together with Prof. R. Nolte at the University of Nijmegen.
Though microemulsions have increasingly been utilised over the last 2 decades, and in some cases even established themselves as precipitation medium for the preparation of small uniform inorganic particles of mostly spherical geometry, little systematic work has been performed on what actually controls the size, shape, crystallinity and stability of the particles formed. Until now there is no global picture at hand describing nucleation and growth processes for the different microemulsion morphologies investigated and a generally valid theory is still out of reach.
In this project we want to perform a systematic study on precipitation in well defined and characterised microemulsions with different morphology ranging from droplet-type microemulsions to cylindrical aggregate structures and bicontinuous microemulsions. The latter consist of an interwoven network of water and oil channels stabilised by the interfacial surfactant film. To establish a direct relation between microemulsion structure and particle morphology, the

microemulsions and the precipitated inorganic materials will be characterised by phase diagram and conductivity studies, electron and atomic force microscopy, X-ray diffraction and scattering techniques. Underlying nucleation and growth processes will be studied with respect to microemulsion morphology, specific inorganic nuclei/surfactant interactions and properties of the interfacial surfactant film. Emphasis will be laid on solidifying bicontinuous structures which is of special interest for inorganic/organic nanocomposites. Employing microemulsions systems as templates for nanostructured composite materials has the advantage of offering the possibility of both simultaneous and consecutive formation of the organic and the inorganic solid phase by bringing in one precursor with the water and the other with the oil phase or the interfacial surfactant layer.

Synthesis of Silica Coated fd-virusses (J. Buitenhuis)

The fd-virus is a slightly flexible rod of about 800 nm length and 6 nm width. The aim is to coat the virus by a silica layer to obtain rigid rods of variable diameter, which after using a variety of standard coatings of the silica, can be dispersed in apolar solvent to obtain cylinders with a variety of well defined interactions. This subject is just starting, in collaborayion with the University of Utrecht.

Colloidal Platelets (J. Buitenhuis)

Sinilar to the synthesis of colloidal boehmite rods, platelets can be synthesized. The monodispersity can be improved and surface treatment renders these platelets compatible to organic solvents. This synthesis has been developed in Utrecht.

Synthesis of Soft Colloidal Rods (P. Lang, L. Willner)

The aim is to develop a model system for soft colloidal rods. These rods are synthesized by radically crosslinking of cylindrical micelles, which consist of amphiphilic blockcopolymers.. This will lead to flexible colloidal rods, of which the length is about 200 nm and the aspect ratio about 20. The main problem will be to fractionate the system in order to reduce the polydispersity in length.

The polymer synthesis know how that is available in the Institute for Neutron Scattering (Dr. L. Willner and Dr. J. Allgaier) will be of great advantage in developing certain classes of new colloidal systems.

Theory

Project leader : Dr. G. Naegele

The aim of this project is two-fold : (i) developing theory on subjects that are, or may become, of experimental interest to the Institute, and (ii) to assist experimentalists with devising new experiments and with data interpretation.

Interdiffusion and Spinodal Decomposition

Interdiffusion in mixtures of differently sized colloidal spheres will be investigated by means of mode coupling theory. In relation to this, spinodal decomposition kinetics in binary mixtures will be studied.

Electrokinetic Effects in Colloids

In particular, electrolyte friction is studied on the basis of mode coupling theory for a binary system : the large colloidal particles and the counter ions. A remarkable result is that hydrodynamic interactions play an essential role. A treatment of non-linear electrolyte friction response is within the validity of the present approach.

Linear Viscoelastic Behaviour of spherical Colloids

A Green-Kubo formula for the linear shear viscosity of colloids, where hydrodynamic interactions are important, has been derived and evaluated numerically on the basis of a mode coupling approach.

Jan Dhont

Personnel 2002/2003 and areas of activity

Scientific Staff

Dr. J. Buitenhuis (since 01.03.01)	Synthesis	23.102.08
Prof. Dr. J.K.G. Dhont	Non-equilibrium structure and dynamics	23.102.08
Dr. J. Hauck	Structures and Interactions of Colloids, Polymers, Lipids and Bacteriae	23.102.08
Dr. P. Lang	Structure and dynamics of interfaces in colloidal systems	23.102.08
Dr. P. Lettinga	Study of the non-linear and linear viscoelastic, response of colloidal dispersions	23.102.08
Dr. G. Meier	Dynamics of mixtures, critical scattering, high pressure techniques	23.102.08
Prof. G. Nägele (since 01.01.01)	Theory and Simulation	23.102.08
Dr. W. Sager (since 01.04.01)	Synthesis	23.102.08

Technical Staff

Ms. K. Sellinghoff	Technician	23.102.08
Dipl.-Ing. H..-J. Hoffmann (since 01.01.02)	Head of the Electronics Laboratory	23.102.08
Dipl.-Ing. D. Triefenbach	Chemical Engineer	23.102.08
		23.102.08
Ms M.-L. Göcking	Secretary	

Scientists

Dr. P. Carletto (since 01.06.01-31.07.02)	Shear-banding of very soft colloids	23.102.08
Dr. Z. Dogic (since 01.11.00-01.06.02)	Synthesis and phase behaviour of di-block colloids	23.102.08
Dr. M. Kollmann (since 01.05.01-30.06.02)	Electrokinetic effects in colloidal systems	23.102.08
Dr. H. Kriegs (since 01.11.02)	Phonons and shear flow of colloidal systems	23.102.08
Dr. T. Lenstra (since 01.03.01)	Inhomogeneous flow of colloids	23.102.08
Dr. S. Rathgeber	Structure and dynamics of polymer – colloids, polymer & colloid mixtures and biological colloids	23.102.08
Dr. R. Tuinier (since 01.11.01)	Phase behaviour, phase separation kinetics	23.102.08
Dr. H. Wang (since 01.04.01)	Structure under shear flow	23.102.08

Guests

Prof. A. Patkowski (PL)	(Univ. Poznan) Fluorescence correlation function of rod like molecules	23.102.08
Dr. J. Gapinski (PL)	(Univ. Poznan) Interferometric studies of rotational diffusion	23.102.08
Prof. H. Zhang (C)	(Univ. Shanghai) Interdiffusion in colloidal mixtures	23.102.08

Trainees

M. Hölzle	Technician	23.102.08

F&E: 23.102.08 (Condensed Matter)

Isotropic/Nematic Pre–transition of Polybutadiene-b-poly(ethyleneoxide) micelles induced by a wall

Peter Lang
Institut für Festkörperforschung
Teilinstitut Weiche Materie

We have investigated the influence of the flat interface between a silicon single crystal and aqueous polybutadiene-b-poly(ethyleneoxide) solutions on the solutions' isotropic to nematic phase transition (I/N). An I/N pre–transition is induced by the wall at volume fractions of the polymer which are about 15% smaller than required for the phase transition in the bulk. Contrary to theoretical predictions for hard rod fluids and semi-flexible polymer systems this pre–transition is not followed by complete wetting of the interface by the nematic phase upon further increase of the polymer volume fraction.

In aqueous solution blockcoplymers (BCP) of the type polybuatdiene-b-poly(ethyleneoxide) (PBPEO) form cylindrical micelles, if the respective block lengths are about balanced. Solutions of this kind show an isotropic to nematic (I/N) phase transition at sufficiently high volume fractions $\phi_{I/N}$ of the polymer [1]. Theoretical and simulation studies [2] predict that the I/N transition of a hard rod fluid in the vicinity of a hard wall should comprise two step, i. e. the continuous transition from a uniaxial to a biaxial symmetry in a thin layer at the interface at bulk volume fractions of $\phi \approx 0.85 \times \phi_{I/N}$, followed by complete wetting of the wall by the nematic phase. In this case the thickness, d_N of the initially formed nematic layer is of the order of the rod length, L. On the other hand, Chen et al [3] predicted a first order I/N pre–transition in a layer close to a wall followed by complete wetting for semi–flexible polymer chains, where the segments were treated as Onsager–type rods [4], i. e the segments are infinitely thin. In this case d_N is of the order of the chain segment length, b.

A powerful tool to investigate the influence of a hard wall on the structure of an adjacent colloidal suspension is neutron reflectivity (NR), since the Fourier–transform of the reflectivity from an interface is related to the scattering length density profile along the interface normal.

Using this technique, we have investigated the influence of the flat interface between a silicon single crystal and solutions of the protonated polymer $PB_{1.5}PEO_{1.5}$ in D_2O and of the deuterated polymer d-$PB_{1.7}$d-$PEO_{1.8}$ in non–reflecting water (NRW) on the solutions' I/N phase transition. The subscripts indicate the blocks' molar mass in kg/mol. The bulk phase transition occurs at a volume fraction of $\phi_{I/N}$=0.078 in the case of the protonated polymer in D_2O and at $\phi_{I/N}$=0.066 for solutions of the deuterated polymer in NRW. The structural parameters of the micelles in dilute solution, which have been determined by small-angle neutron scattering beforehand [5] are collected in Table I. From this values it is obvious that the micelles have to be regarded as semi–flexible cylinders rather than rigid rods. It is worth to note that in both cases the segment length, b, is smaller than the cross section diameter. Therefore one might expect that a hard wall should induce an I/N pre–transition in a layer with a thickness which is of the order of the micellar cross–section diameter and not of the order of the micellar contour length.

TABLE I: Contour length, L_c, segment length, b, and cross–section radius, R_{cs} of the BCP micelles

System	L_c /Å	b/Å	R_{cs}/Å
$PB_{1.5}PEO_{1.5}$ / D_2O	3468	67	67
d-$PB_{1.7}$d-$PEO_{1.8}$ / NRW	964	45	79

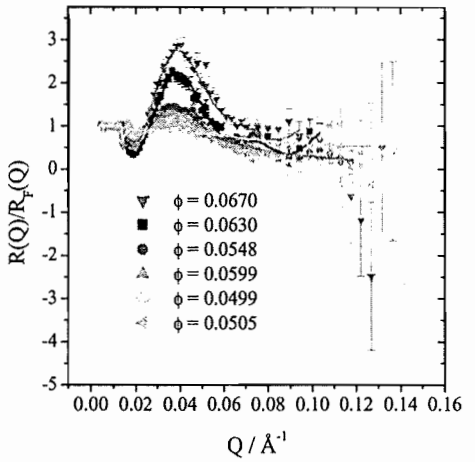

FIG. 1: Reflectivity scans from the interface between a Si single–crystal and solutions of $PB_{1.5}PEO_{1.5}$ in D_2O, normalized to the Fresnel–reflectivity. The symbols are experimental data and the full lines are best fits according to the scattering length density profiles shown in Fig. 3.

The reflectivity curves displayed in Figs. 1 and 2 show that in both cases undulations occur at a volume fraction which is about $\phi \approx 0.85 \times \phi_{I/N}$. The amplitude of these undulations increases with increasing ϕ, while its period is constant. The data were analysed using the so called box-model approach [6] and the model independent groove tracking algorithm [7], which both yielded the normalized scattering length density (SLD) profiles

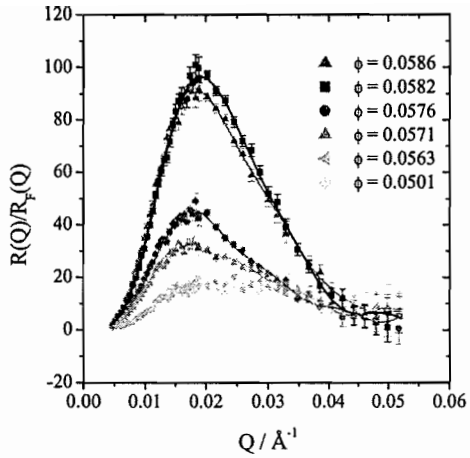

FIG. 2: Reflectivity scans from the interface between a Si single–crystal and solutions of d–$PB_{1.7}$–d–$PEO_{1.8}$ in non reflecting water, normalized to the Fresnel–reflectivity. The symbols are experimental data and the full lines are best fits according to the scattering length density profiles shown in Fig. 4.

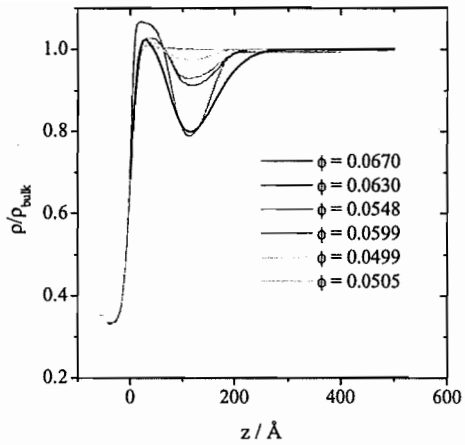

FIG. 3: Scattering length density profiles normalized to the bulk value, determined from the reflectivity data shown in Fig 1. Note that for the given contrast, a minimum of the scattering length density corresponds to a maximum of the polymer segment density.

shown in Figs. 3 (note that for protonated micelles dispersed in D_2O, a minimum of the scattering length density corresponds to a maximum of the polymer segment density) and 4 . The evolution of the SLD–profiles with increasing polymer volume faction is interpreted as the formation of an interfacial layer, the thickness of which is in the range of the micellar cross–section diameter and does not depend onϕ. On the other hand, the polymer segment density in the layer increases with increasing.

We therefore conclude that the our experimental data are in qualitative accord with the theoretical prediction by Chen et al. as far as the formation of a nematically ordered interfacial layer at $\phi \approx 0.85 \times \phi_{I/N}$ and the thickness of this layer is concerned. Although the formation of this layer occurs in a very narrow range of volume fraction it is not really possible to decide if the pre–transition is first order, as predicted. However, the experiments show clearly that the layer thickness does not increase with the polymer volume fraction, i. e. the nematic phase does not wet the interface completely, which is in contradiction to the theoretical expectation. This discrepancy may be due to either of or the combination of two reasons. First, the segments do probably not interact as hard bodies, but there might be a short ranged attractive part of the interaction potential. Second and probably much more important, as to be seen from Table I the segments may not be regarded as Onsgager–like rods. We therefore plan to do computer simulations to clarify the influence of the finite segment cross–section diameter.

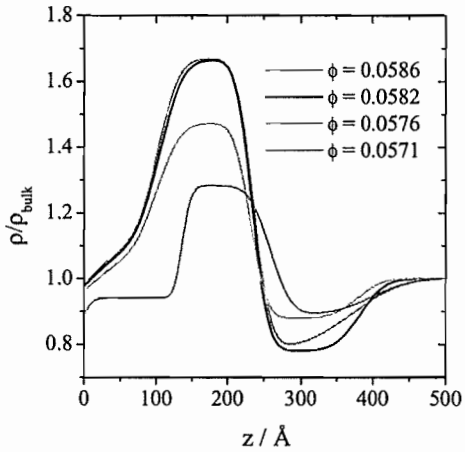

FIG. 4: Scattering length density profiles normalized to the bulk value, determined from the reflectivity data shown in Fig 2.

[1] Won, Y. Y; Davis, H. T.; Bates, F. S. *Science* **283**, 960 (1999).

[2] Roij, R.; Dijkstra, M.; Evans, R. *J. Chem. Phys.* **113**, 7689 (2000).

[3] Chen, Y. C.; Cui, S.-M. *Phys. Rev. E* **52**, 3876 (1995).

[4] Onsager, L. *Ann. N. Y. Acad. Sci.* **51**, 627 (1949).

[5] Lang, P., Willner, L. submitted to *Macromolecules*

[6] Als-Nielsen, J.; Jacquemain, D.; Kjær, K.; Leveiller, F.; Lahav, M.; Leiserowitz, L. *Physics Reports* **251**, 246 (1994).

[7] Zhou, X.-L.; Chen, S.-H. *Phys. Rev. E* **3174**, 47 (1993).

Shear-Banding in Suspensions of fd-Virus

M. P. Lettinga, Z. Dogic and J. K. G. Dhont
Institut für Festkörperforschung
Teilinstitut Weiche Materie
(Dated: January 14, 2003)

Shear-banding is the phenomenon where macroscopically large regions (the "bands"), with differing microstructural properties, coexist under the influence of shear flow. Banded structures are found at very low shear-rates, far below the shear-rate where the Taylor instability occurs. The final stationary state often depends on whether the flow is applied under controlled stress or shear-rate conditions [1, 2]. In a cylindrical geometry, bands are either alternately stacked in the vorticity direction or layered around the inner cylinder in the gradient direction. A well studied system that exhibits this complex behavior are dispersions of wormlike micelles under shear. Depending on the concentration of monomers and flow conditions, a variety of phase transitions and structural changes are observed [1, 3]. These experiments are theoretically described by Cates [4]. Wormlike micelles have a significant chain flexibility and they permanently exchange material (i.e. they can break and recombine). This complicates the physics of shear-banding considerably.

In order to gain fundamental insight in the origin of the shear-banding transition, we performed experiments on a much simpler system : fd-virus suspensions. Fd-virus is a good model system of hard rods [5] and displays an isotropic-nematic (I-N) phase transition. The location of phase transition lines is shifted to lower concentration on applying shear flow, since shear flow stabilizes nematic order. The shear dependent location of I-N spinodals of fd-virus suspensions has been determined in ref.[6] by means of time resolved birefringence measurements. Due to very slow nucleation rates it has not been possible to determine the shear-rate dependent location of binodals and shear-banding transition lines. In the present work we added polymer to the fd-virus suspension, which widens the biphasic region, resulting in increased nucleation rates [7] and shear-banding transition rates. The behaviour of this dispersion under shear flow is studied using an optical, cylindrical shear-cell, which is positioned between two polarizers in order to probe local orientational order. This shear cell allows for time resolved, small angle light scattering experiments in the flow-vorticity plane, where scattered light from one gap is blocked by means of a pinhole that is positioned in the middle of the inner cylinder. Formation of inhomogeneities on the micrometer scale were studied both by small angle light scattering (SALS) and microscopy.

We observed that the nematic phase is stable for shear-rates larger than a critical binodal shear-rate $\dot{\gamma}_{bin} \approx 1.5\,s^{-1}$, even though the sample without shear flow is in the I-N biphasic region. Such a critical shear-rate is predicted by a Doi-Edwards like theory and is confirmed by means of birefringence experiments [6]. For shear-rates larger than $\dot{\gamma}_{bin}$ the sample hardly scatters light. When a quench is made from the stable nematic phase at high shear-rates into the biphasic region by suddenly lowering the shear-rate below the binodal shear-rate (i.e. $\dot{\gamma} < \dot{\gamma}_{bin}$), phase separation occurs, the kinetics of which can be followed with SALS. In Fig.1 the evolution of the scattering pattern for two different quenches is shown. In the initial stage of phase separation, the scattering pattern shows four lobs, which indicates the formation of micron-sized paranematic regions within the nematic, which regions are tilted with respect to the flow direction (a paranematic state is a shear-aligned, otherwise isotropic state). After a few miniues, an intermediate state exists in which these regions are aligned along the flow direction.

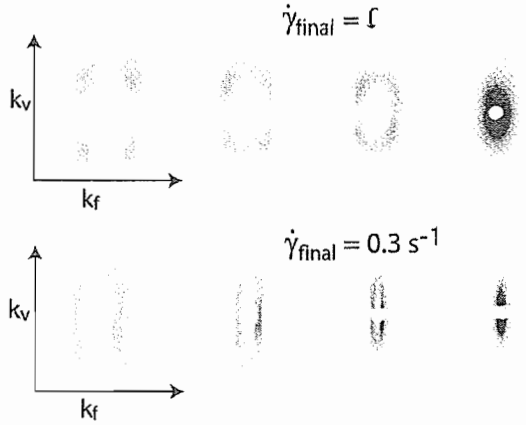

FIG. 1: SALS images taken between 5 seconds and five minutes after a shear-rate quench from $\dot{\gamma} = 2\,s^{-1}$ to $\dot{\gamma} = 0\,s^{-1}$ (top) and $\dot{\gamma} = 0.3\,s^{-1}$ (bottom). The first images on the left are taken a few seconds after the quench, while the images on the right are taken after about three minutes. k_v and k_f indicate the vorticity and flow direction, respectively.

In the shear-rate regime $\dot{\gamma} = 0.1 - 0.4\,s^{-1}$, in addition to the fast phase separation described above (few minutes) an additional process of band formation is observed on much longer time scales (few hours), see Fig.2. These bands are alternately stacked in the vorticity direction and can only be detected under crossed polarizers. The

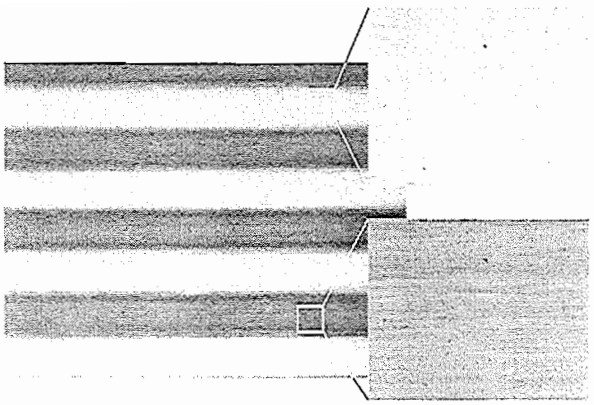

FIG. 2: The final, shear-band state, with two close-ups taken with a home-made polarization microscope. The shear-bands are about $2\,mm$ in height. The typical height of the inhomogeneities within the bands is about 10 to $20\,\mu m$.

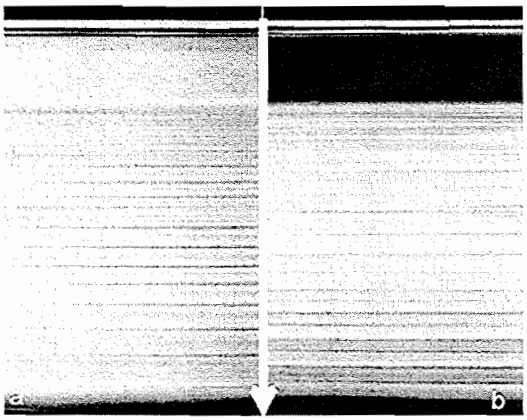

FIG. 3: a) Shear-bands of a sample that has been sheared for a week. During this time some sedimentation of the more dense nematic regions takes place. b) Same as figure (a), but immediately after the cessation of shear flow. In this sample bands fully disappear over a period of an hour.

bands can be as broad as $2\,mm$, depending on the composition of the sample. Bands are formed within a limited virus concentration range. The lower concentration at which banding still occurs is set by the lower branch of the binodal. For samples that are outside the two-phase region, no shear-banding along the vorticity direction is observed. This is illustrated in Fig.3a, where an image is shown of a sample that has been sheared for a week. During this time a gradient in density is established due to density differences of coexisting paranematic and nematic phases. The top part of the sample has a concentration that is equal to the lower binodal concentration. This part of the sample is a uniform paranematic phase that shows no banded flow and appears uniformly birefringent due to shear alignment. After cessation of shear flow, this paranematic phase almost instantaneously becomes isotropic, that is, the birefringence disappears and the corresponding part of the image turns black, as can be seen in Fig.3b. Note that the size of the bands increases towards the bottom of the shear cell where the concentration of the rods is higher. Preliminary rheology experiments indicate that the high concentration limit for the occurrence of banded flow is set by the concentration where tumbling is observed right after a shear-rate quench. Here, a few damped oscillations in the stress response are observed after an instantaneous change of the shear-rate. It seems that tumbling sets in at a concentration where shear-band formation is not observed anymore, that is, tumbling probably destroys the shear-banding instability.

A striking feature of the shear-bands is that they have an inhomogeneous internal structure, as is shown in the micrograph in Fig.2. This type of internal structure already exists during the process of band formation, and is probably reminiscent to the micron sized structures that are formed right after the quench as seen by SALS. This is in contrast to micellar systems, where the bands of either low or high viscosity appear homogeneous.

In conclusion, we have presented preliminary studies of the behavior of rods with attractive interactions in shear flow. In the process of shear-banding, where bands are formed along the vorticity direction, there is a fast process (minutes) where micron-sized inhomogeneities are formed, as measured by SALS, after which bands are formed on a very much longer time scale (hours), as seen through crossed polarizers. Banding is only observed in the two-phase region at concentrations below the concentration where tumbling is found. The goal of our further research will be to measure the entire non-equilibrium phase diagram and to understand the banding transition on a microscopic level. It might be that the micron-sized inhomogeneities that are formed due to phase separation are responsible for the occurrence of banding. If this is indeed the case, a linear stability analysis of appropriate equations of motion will not reveal the true nature of this instability. Equations of motion which include possibly very large gradients in suspension properties should be derived, and must be solved numerically.

[1] E. M. D. P. P. Boltenhagen, Y. Hu, Phys. Rev. Lett. **79**, 2359 (1997).
[2] E. Fischer and P. T. Callaghan, Phys. Rev. E **64**, 011501 (2001).
[3] P. L. J.-F. Berret, D.C. Roux, Eur. Phys. J. B **5**, 67 (1995).
[4] M. Cates, Macromolecules **20**, 52289 (19987).
[5] J. Tang and S. Fraden, PRL **71**, 3509 (1993).
[6] Z. D. T. A. J. Lenstra and J. K. G. Dhont, J. Chem. Phys. **114**, 10151 (2001).
[7] Z. Dogic and S. Fraden, Phil. Trans. R. Soc. Lond. A. **997**, 997 (2001).

Dynamics of Strongly Asymmetric Magnetic and Neutral Colloidal Mixtures

Gerhard Nägele, Haiyan Zhang and Markus Kollmann
Institut für Festkörperforschung
Teilinstitut Weiche Materie

Dynamic and static properties of strongly asymmetric binary mixtures of spherical colloidal particles are studied using Brownian dynamics (BD) computer simulations and analytical methods. Our study comprises mixtures of super-paramagnetic particles confined to an air-water interface, and mixtures of colloidal hard spheres. The strong interaction asymmetry in the magnetic particles leads to unusual features in the pair distribution functions, and to hydrodynamically enhanced self-diffusion. Rotational and translational diffusion of a tracer component in a hard-sphere host dispersion is examined in dependence on the tracer-host size ratio and host concentration. A continuum limiting behavior is reached for progressively enlarged tracer size, characterized by Stokes-Einstein (SE) relations between tracer diffusion coefficients and viscosities. To reach the continuum behavior, larger tracer sizes are required for rotational than for translational diffusion.

There is considerable interest in understanding the various mechanisms of diffusion in model suspensions of colloidal spheres, and their relations to viscoelastic properties, from the knowledge of the microscopic interactions. The additional presence of solvent-mediated hydrodynamic particle interactions (HI) distinguishes the essentially inertia-free dynamics of colloidal systems from the Newtonian dynamics of simple liquids. The HI are at the origin of interesting and, quite often, surprising dynamic effects. While a lot of work has been done on translational diffusion in monodisperse colloidal suspensions, the dynamic properties of colloidal mixtures and polydisperse systems, which are abundant in synthetic and naturally occurring colloidal fluids, is far less understood. This lack of knowledge has prompted us to explore various translational and rotational diffusion processes in three-dimensional and quasi-two-dimensional mixtures of electrically neutral, charged and magnetic colloidal spheres. We have determined the dynamics and microstructure of these systems using Brownian dynamics (BD) computer simulations and analytical methods.

BD results for the partial radial distribution functions, $g_{\alpha\beta}(r)$, and for the reduced mean-squared displacements (self-diffusion functions), $D_\alpha(t) = W_\alpha(t)/(D^0_\alpha\, t)$, of quasi-two-dimensional binary dispersions of super-paramagnetic particles at a water-air interface are shown in Figs. 1a and b, in comparison with experimental video imaging results [1]. The particles interact via dipolar magnetic forces, induced by a magnetic field applied perpendicular to the planar interface. The interaction energy among the particles of type 1 is about 100 times larger than the one for the the 2-particles. This extreme interaction asymmetry gives rise to unusual features, viz. the splitting of the primary peak of $g_{11}(r)$ into two twin peaks of approximately same height. The reason for the peak splitting is that the innermost next neighbor shell formed around a 1-particle, which contains 1-particles as characterized by the first twin peak in $g_{11}(r)$, includes a larger fraction of 2-particles than the more distant second subshell, characterized by the second twin peak in $g_{11}(r)$.

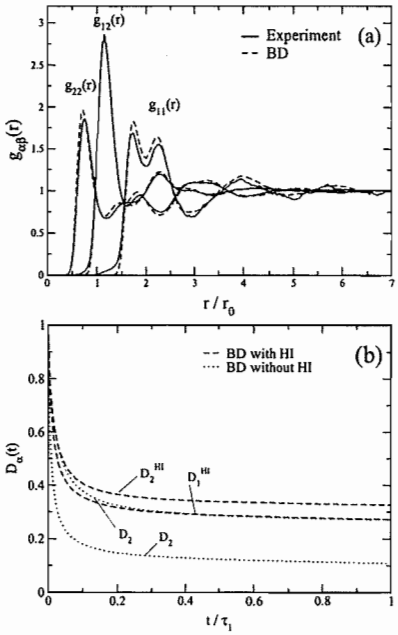

FIG. 1: Binary suspension of super-paramagnetic particles at a liquid-air interface. (a) Partial radial distribution functions, $g_{\alpha\beta}(r)$, versus reduced distance. (b) Reduced self-diffusion functions, $D_\alpha(t)$, versus reduced time t/τ_1 (from [1]).

There is nearly quantitative agreement between the BD and experimental data for $g_{\alpha\beta}(r)$, in spite of the profound interaction asymmetry. Fig. 1b shows BD results for $D_\alpha(t)$ versus reduced time with and without HI. The significant hydrodynamic enhancement of self-diffusion, characteristic of systems with strong and long-range particle repulsion, is clearly observed. The enhancement is stronger for the more weakly interacting component 2.

In another study of asymmetric binary mixtures we have explored the rotational and translational self-diffusion of a dilute tracer component in a dispersion of host spheres, in dependence on the tracer-to-host size ratio $\lambda = a_T/a_H$, the host volume fraction Φ, and the

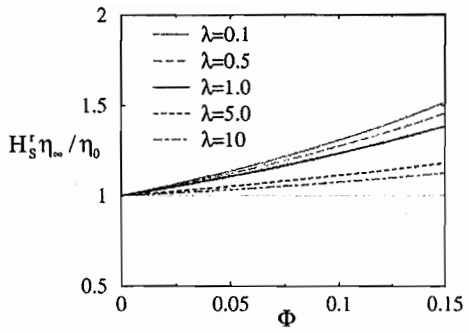

FIG. 2: Reduced rotational self-diffusion coefficient, $H_S^r = D_S^r/D_0^r$, times reduced high-frequency shear viscosity η_∞/η_0. The dots represent the generalized SE relation (from [2]).

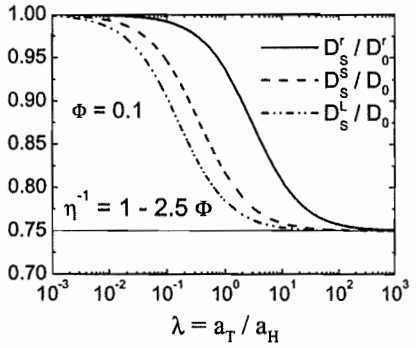

FIG. 3: Reduced rotational and translational short-time self-diffusion coefficients, D_S^r/D_0^r and D_S^S/D_0, and reduced translational long-time self-diffusion coefficient, D_S^L/D_0, versus λ, for a host volume fraction of $\Phi = 0.1$ (from [4,5]).

host viscosity. With increasing λ, the tracer experiences the host suspension more and more as an unstructured continuum, characterized by its macroscopic viscosity. It is thus of interest to identify the conditions for which the continuum behavior is reached. Therefore, we have calculated the rotational and translational short-time self-diffusion coefficients, D_S^r and D_S^S, of the tracer species, immersed in a host suspension of colloidal hard spheres, up to quadratic order in Φ [2,3]. Our calculations are based on a truncated rooted cluster expansion, with two- and three-body HI contributions included. Results for rotational short-time case, i.e. for $D_S^r/D_0^r \times \eta_\infty/\eta_0$ vs. Φ, where η_∞ is the high-frequency shear viscosity of the host dispersion, are depicted in Fig. 2. Note the rather slow convergence with increasing λ towards the rotational SE-Debye relation, $D_S^r = k_BT/(8\pi\eta_\infty(\Phi)a_T^3)$. The monotonic decline of the rotational/translational tracer diffusion coefficients from their infinite dilution values at $\lambda = 0$, towards the SE continuum limit $D_S = D_0\eta/\eta_0 = D_0(1 - 2.5\Phi) + \mathcal{O}(\Phi^2)$ for $\lambda \to \infty$, is illustrated in Fig. 3. The continuum limit is approached most quickly for increasing λ by the long-time translational tracer-diffusion coefficient D_S^L.

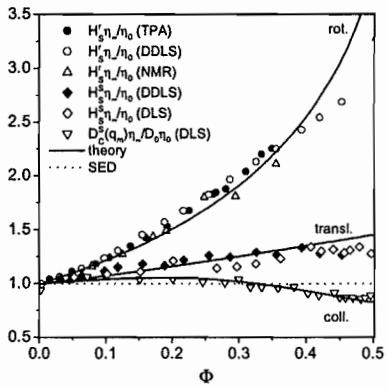

FIG. 4: Test of the validity of various generalized short-time Stokes-Einstein relations for rotational/translational self-diffusion, and collective diffusion at wave number q_m. The lines are theoretical predictions for hard spheres; symbols are experimental data obtained from various techniques [4,5].

It is rewarding to find generalizations of the single-tracer SE relations, which allow one to relate diffusional properties in concentrated colloidal suspensions to effective suspension viscosities. A valid SE relation can be used to determine a viscoelastic property in a non-invasive way and for small sample volumes (so-called microrheology). A test of various short-time translational/rotational SE relations for monodisperse colloidal hard spheres is shown in Fig. 4: only the short-time collective diffusion coefficient, $D_C^S(q_m)$, obeys approximately a generalized SE law. In contrast to the hard-sphere case, however, the same SE relation is clearly violated for charged spheres. Due to long-range electrostatic interactions, a charged particle experiences particularly strongly the discontinuous nature of its environment (cf. [4,5]).

In a recent study, we have analyzed the interdiffusion process in semi-dilute mixtures of hard spheres. Interdiffusion describes the relaxation of fluctuations in the relative concentration of two selected components. Our calculations show that interdiffusion is dominated by near-field HI. Moreover, one can not express the interdiffusion coefficient only in terms of the self-diffusion coefficients of the individual components.

[1] M. Kollmann, R. Hund, B. Rinn, G. Nägele, K. Zahn, H. König, G. Maret, R. Klein and J.K.G. Dhont, Europhys. Lett. **58**, 919 (2002)

[2] H. Zhang and G. Nägele, J. Chem. Phys. **117**, 5908 (2002)

[3] G.H. Koenderink, H. Zhang, M.P. Lettinga, G. Nägele and A.P. Philipse, Phys. Rev. E **64**, 022401 (2001)

[4] G. Nägele, J. Phys.: Condens. Matter **15**, S401 (2003)

[5] G.H. Koenderink, H. Zhang, M.P. Lettinga, D. Aarts, A.P. Philipse, G. Nägele, Faraday Discuss. **123**, 335 (2003)

Phase separation and membrane formation characteristics in ternary and quaternary EVAL-systems*

W.F.C. Sager[1], M.E. Avramescu[1,2] and M. Wessling[2]

[1] *Institut für Festkörperforschung-Teilinstitut Weiche Materie*
[2] *Membrane Technology Group, University of Twente, The Netherlands*

*This contribution is dedicated to M.H.V. Mulder, who died November 17, 2002

In this study we investigated phase separation and membrane formation in nonsolvent/solvent/polymer systems for a random ethylene vinyl alcohol copolymer (EVAL) with an ethylene content of 44 mol%. Polymeric membrane materials with hydrophilic and functionalizable groups are of special interest in biological and biomedical applications.

F&E-Nr: 23.102.08

A standard technique to prepare polymeric porous membranes is based on diffusion induced phase separation in nonsolvent/solvent/polymer systems (*immersion precipitation*). To obtain the membranes, a thin film of a homogenous polymer solution is immersed into a non-solvent bath, whereby the diffusional exchange of solvent and nonsolvent brings the film solution into an instable state resulting in liquid-liquid (*l-l*) and/or solid-liquid (*s-l*) demixing, depending on the type of polymer and the precipitation conditions employed.

In this study we investigated the phase separation characteristics for ternary and quaternary systems with ethylene vinyl alcohol (EVAL), a semi-crystalline random copolymer consisting of hydrophobic ethylene and hydrophilic vinyl alcohol segments that has become a promising biomedical material, to prepare microporous membranes for affinity separation processes. Ethylene-vinyl alcohol (EVAL) crystallizes over the entire ethylene composition range, since the melting point of poly(vinyl)alcohol is about 100° higher than that of polyethylene. Earlier phase diagram studies on the ternary *nonsolvent/DMSO/EVAL* system with water or short and medium chain length alcohols as nonsolvent and EVAL with an ethylene content of 44 mol% [1] revealed that the (calculated) binodals fall at room temperature within the crystallization lines. In the region that is meta-stable with respect to *s-l* demixing a gel forms from the collapsed polymer coils that consists of interconnected submicrometer-sized spherically shaped particles. With increasing temperature, the crystallization line is shifted towards the nonsolvent-EVAL side of the diagram, while the position of the binodal changes only little. For water, an intersection of both lines takes place at 65°C. Supersaturation with respect to crystallization and thus *s-l* demixing is therefore favored at high polymer concentration and low temperature.

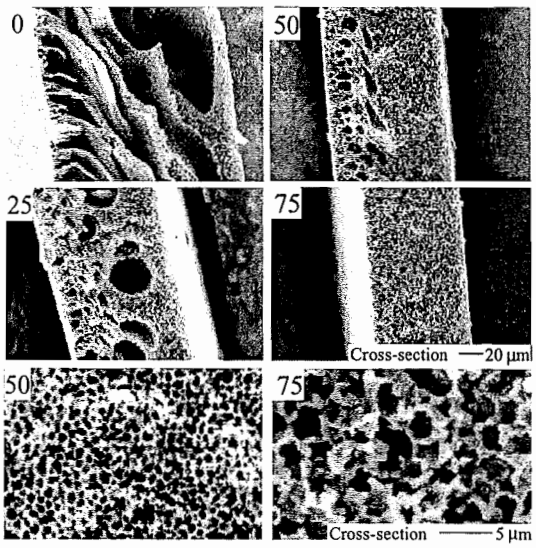

Fig.1: SEM-micrograph cross-sections (overview and detail) of membranes prepared from the *ternary* water/DMSO/EVAL system by dispersing films of 10% EVAL in DMSO into an aqueous coagulation bath containing different amounts of DMSO (0-75%) at 50°C. The membranes are shown with the top surface (film/bath interface) on the left.

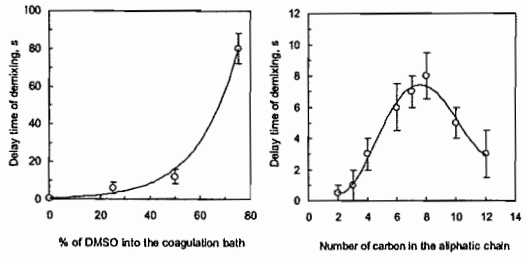

Fig.2: Measured delay times (t_d) before phase separation occurs after immersing the polymeric film into the coagulation bath. **Left:** t_d as function of the amount of DMSO in the coagulation bath for the *ternary water/DMSO/EVAL* system. **Right:** t_d as function of the aliphatic chain length (C2-C12) of the n-alcohols employed as nonsolvent additive in the casting solution.

In our investigation, we started with the ternary *water/DMSO/EVAL* system with DMSO being a good solvent and water a strong nonsolvent for the polymer. *Fig.1* shows cross-sections of membranes prepared by casting polymeric films from a solution of 10% EVAL in DMSO on a glass plate which were then immersed into an aqueous coagulation bath containing varying amounts of DMSO at 50°C in order to suppress crystallization. When pure water was used in the coagulation bath, the strong nonsolvent character and the high affinity between water and DMSO led to fast demixing conditions. The resulting asymmetric membrane (*Fig.1*-0) displays a continuous thin dense top layer (skin) and extended macrovoid formation in the cellular porous support, which are both characteristic for rapid *l-l* demixing. *Fig.2-left* shows the delay time t_d before phase separation sets in, obtained by measuring the light transmission across the immersed film [2]. Addition of solvent to the coagulation bath decreases the driving force for the exchange of solvent and nonsolvent and thus leads to delayed demixing conditions. Due to the high affinity to water, substantial delay is obtained only at a high content of DMSO. With rising amounts of DMSO in the coagulation bath (*Fig.1*-25 and 50), macrovoid formation is increasingly suppressed. More pores are present in the top layer and the polymeric walls surrounding the macrovoids, while the pore-interconnectivity of the cellular support remains, however, low. At 75% DMSO, *l-l* demixing is suppressed to such an extent (t_d=80 s) that crystallization of the polymer segments could take place. The obtained symmetric membrane (*Fig.1*-75) consists of submicron diameter particles packed into a bicontinuous porous structure. At 10% EVAL, the number of crystalline particles is rather low, so that the size of the pores that are formed by the interstitial space of the aggregated particle network lies in the micrometer range.

Fig.2-right and *Fig.3* display measured delay times and cross-sections for membranes prepared using a series of n-alcohols (C2-C12) as nonsolvent additive in the casting solutions (quaternary system) and water at 50°C as coagulation bath. At a fixed alcohol concentration of 10%, t_d shows a maximum for heptanol and octanol, which is reflected in a minimum in the amount of macrovoids present in the porous support. The mutual solubility between water and n-alcohols decreases significantly in the range between C3-C6. With increasing hydrophobicity of the alcohol, less alcohol flows from the polymeric film into the water and the tendency to prevent the water from flowing into the film increases. As a consequence, t_d should rise and reach a plateau value for alcohols with longer aliphatic chain length, when the changes in the hydrophobicity become small (>C6). Besides the affinity to water also the affinity to EVAL changes with the chain length of the alcohol. To obtain a first insight, we display in *Fig.4-left* the difference of solubility parameters of the alcohols and the polymer $|\Delta\delta_{a\text{-}p}|$ as a function of the aliphatic alcohol chain length, which shows a minimum for heptane and octane. For the long chain alcohols investigated (>C8), the nonsolvent character becomes prevalent and increases the tendency of the polymeric film to undergo *l-l* demixing.

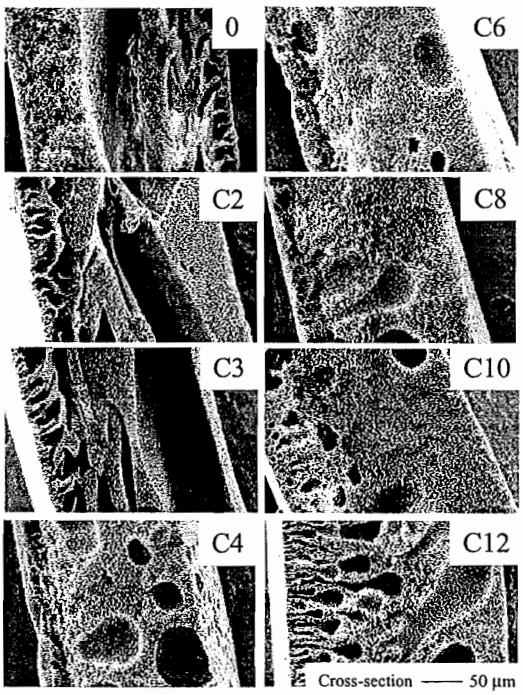

Fig.3: SEM-micrograph cross-sections of membranes prepared from the *quaternary* water/alcohol/DMSO/EVAL system with 10% n-alcohol (C2-C12) as nonsolvent additive in the casting solution and water as coagulation bath at 50°C.

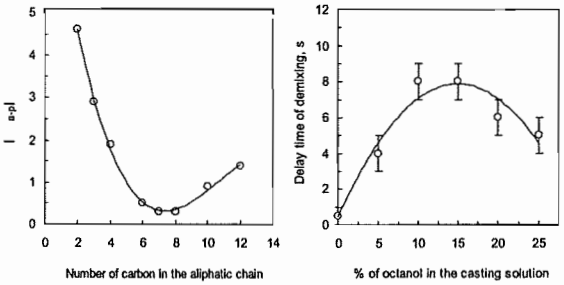

Fig.4: Left: Variation of the solubility parameter difference $|\Delta\delta_{a\text{-}p}|$ as a function of the hydrocarbon chain length of n-alcohols. **Right:** t_d as function of the amount of octanol (C8) used as nonsolvent additive in the casting solution.

Following this argument, one would also expect a chain length-dependent concentration dependence for t_d and the appearance of macrovoids. *Fig.4-right* shows t_d as a function of the octanol concentration. At concentrations where t_d is maximal, macrovoid free membranes with a high pore interconnectivity are obtained that are shown in *Fig.5*.

All EVAL membranes prepared with the n-alcohols as nonsolvent additive in the casting solution displayed no particulate structures or other features characteristic for *s-l* demixing, whereas symmetric particulate membranes were earlier obtained [3] from ternary systems with 2-propanol or 1-octanol used as nonsolvent bath. Macrovoids are often found under fast demixing conditions. In this case, the composition of the polymeric film falls directly after immersion within the binodal envelope. Phase separation sets in, before desolvation can take place over the entire film. At the film/bath interface the polymer concentration is high, whereas the concentration in the underlaying film remains nearly unchanged. The corresponding polymer profile then displays a steep increase near the film/bath interface, leading to a dense skin layer and a porous support. Under delayed demixing conditions desolvation can proceed for a longer time without triggering *l-l* demixing, leading to a more homogeneous polymer distribution (flat profile), more symmetric membrane structures and a more open top layer. Macrovoids are assumed to form from nuclei of the polymer-lean phase directly underneath the skin. If the coagulation front is hindered to proceed by the skin formed, the macrovoids can grow by (diffusional) flow of solvent that is expelled from the surrounding polymer solution. During the increase of the non-solvent concentration in the immersed polymer solution, the polymer molecules change to a less expanded conformation (syneresis) before *l-l* demixing takes place. The primary nuclei underneath the skin layer can only grow into larger voids when the composition in front of the nuclei remains stable against *l-l* demixing. Under these conditions the formation of new nuclei is suppressed or delayed and the macrovoids can grow until the polymer concentration becomes so high that the macrovoid/solution interface solidifies. Suppression or elimination of macrovoids formation is achieved under delayed *l-l* demixing conditions caused by the addition of DMSO to the coagulation bath (see *Fig.1*-25 and 50). When the phase separation sets in, the composition in front of the first nuclei has already become instable against *l-l* demixing and new nuclei can form. Another way to generally destabilize the polymer solution in front of the first nuclei formed, is to add a (weak) nonsolvent to the casting solution (quaternary system). For the n-alcohols used macrovoid suppression starts with butanol. Since d_t is increased between C3 and C8 it is not possible to conclude whether the formation of macrovoid is only suppressed due to the delayed *l-l* demixing conditions or also due to the fact that a nonsolvent is added to the casting solution. For octanol concentrations >25% the casting solution phase separates without water addition. The high interconnectivity of the pores might indicate that also secondary phase separation processes take place.

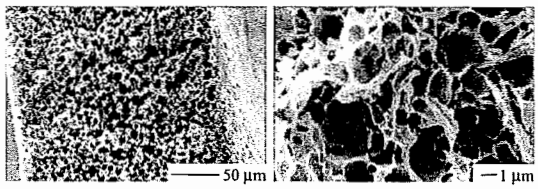

Fig.5: SEM-micrograph cross-sections (overview and detail) for a membrane prepared with 20% n-octanol in the casting solution.

Employing the quaternary system with the n-alcohols as nonsolvent additive in the casting solution delayed *l-l* demixing to such an extend that it was possible to find conditions to prepare macrovoid-free membranes with a high pore interconnectivity, but still to avoid crystallization and *s-l* demixing. More details on the characterization can be found in [2].

[1] L.P.Cheng, T.H. Young, W.M. You, J. Membr. Sci., **145**, 77 (1998)

[2] M.E. Avramescu, W.F.C. Sager, M.H.V. Mulder and H. Wessling, *J. Membr. Sci.*, **210**, 155 (2002)

[3] L.P. Cheng, T.H. Young, W.Y. Chuang, Polymer, **42**, 443 (2001)

Long-ranged attraction between proteins due to non-adsorbing polysaccharide

R. Tuinier

Institut für Weiche Materie

Using small-angle neutron scattering (SANS) experiments, the effect of a relatively long non-adsorbing polysaccharide (dextran) on the structure factor of a protein solution (lysozyme) was studied. A theoretical prediction from depletion theory is in fair agreement with the measured structure factor of lysozyme, as affected by non-adsorbing dextran.

F&E-Nr: 23.102.08 (9-Punkt-Schrift)

The stability of polysaccharide-protein mixtures is an important issue since both biopolymers are present in many food products and in biological systems [1]. The properties of polymer-protein mixtures have been intensively studied over the last decades [2] and it was found that usually a depletion interaction is responsible for the phase behavior. Although significant theoretical progress was made [3-7], a sufficient synergy with experimental work is still lacking. The early work of de Gennes [3] demonstrated that the depletion-induced attraction is weak when $R<\xi$, where ξ is the characteristic polymer length scale and R is the protein radius. Most polysaccharide-protein mixtures are examples of $R<\xi$; in their native state proteins have a diameter of a few nm whereas polysaccharides have a correlation length often one or two magnitudes larger.

In polysaccharide-protein mixtures the attraction is long-ranged and it is expected that the effective protein-protein structure factor is affected significantly in the presence of long non-adsorbing polymer chains. We have measured the effective protein-protein structure factor in the presence of a non-adsorbing polysaccharide with small-angle neutron scattering (SANS). As system to study polysaccharide-induced interactions between proteins a mixture of lysozyme and dextran was chosen. Lysozyme is a globular protein with an effective radius of 2.5 nm [8] and has a specific volume of 0.702 ± 0.003 L/kg [9]. The experiments reported were made in 0.10 M phosphate buffer at pH 6.0 where lysozyme molecules have a net charge of approximately 9.0 [10], are well soluble and crystallize at protein volume fractions, ϕ, above 0.1 [11]. Dextran is a polysaccharide and the sample used has a radius of gyration (R_g) 20 ± 1 nm in aqueous solution, and average molar masses of 260 kg/mol (number) and 387 kg/mol (weight) [12]. The overlap concentration, defined as $c^*=3M/N_{av}4\pi R_g^3$, is 13±3 g/L or 19±4 g/L (weight-average).

SANS measurements were performed with the PAXE spectrometer (Saclay, France) of the Laboratory Léon Brillouin at the Orphée reactor [12]. Dextran was made 'invisible' in aqueous solution by choosing $x_D=0.25$, where x_D is the H_2O/D_2O ratio. Dilute dextran solutions were prepared with a final concentration of 4 g/L in 0.10 M phosphate buffer at p'H' 6.0. Lysozyme was added to a concentration of 50 g/L ($\phi=0.035$) and a pure lysozyme solution ($\phi=0.035$) was used as reference system. Theoretically, the structure factor S(Q), where Q is the scattering wave vector, can be calculated when c(Q), the Fourier transform of the direct correlation function c(r), where r is the distance between the centers of the colloidal spheres with radius R, is known. Here c(r) is approximated as the Percus-Yevick direct correlation function for hard spheres inside the sphere and as a Mayer function of the depletion potential outside the sphere. This is accurate at least up to an order above the volume fractions relevant for this study and W(r) is the depletion interaction potential using the theory described in ref. [13]. In Fig.1 (left) the structure factor S(Q) is plotted as a function of $Q\sigma$ (where $\sigma=2R$) for three colloid-polymer size ratios, $R/R_g=0.1$, 0.3, and 0.5, for a volume fraction of the colloids of 0.035 (which is the lysozyme volume fraction in this study) as dashed curves for $c/c^*=0.3$, where c is the polymer concentration and c^* is the overlap concentration. The full curve is the hard sphere result. It is obvious that the attractions lead to an upswing of S(Q) at small Q. The larger the relative size of the polymer, the smaller the wave vector at which S(Q) increases; longer-ranged attractions are probed at smaller wave vectors, as was shown earlier with scaling theory by Sear [7]. The increase of S(Q) at small wave vectors is stronger as the relative polymer size increases. We compared the theoretical analytical results (curves) with computer simulation results (data points) for $q=R_g/R=2$ in Fig.1 (right) [14]. The computer simulation was made by sampling many configurations of spheres, which have a depletion interaction (following the theory in [13]) with the other spheres. The agreement between the computer simulation results and the theory is satisfying for small colloid volume fractions and is even better for larger q-values. The curves in Fig.1 (right) all go through an isosbestic point at $Q\sigma\approx2.1$ independent of polymer concentration. Previously, Louis *et al.* [15] noticed the appearance of this isosbestic point and recently demonstrated that various shapes of a like-ranged attractive potential yield similar isosbestic points [16]. Further, we found that the range of the potential determines the Q-value of the isosbestic point [14]. This is interesting since the range of the attraction is then directly measurable via the structure factor. The (corrected) measured scattering intensity of the pure lysozyme solution at $x_D=0.25$ is plotted as a function of the wave vector Q in Fig.2 (open triangles). The solid curve (the lower curve at small Q) shows the theoretical result for lysozyme in solution calculated by $I(Q)=\text{const}\times S_{HS}(Q)\ c\ P(Q)$, where $S_{HS}(Q)$ is the Percus-Yevick hard sphere structure factor, c the protein concentration and with the Guinier approximation:

$P(Q)=\exp(-[Q^2a_g^2/3])$, with the radius of gyration of the sphere a_g=1.5 nm (R=2.0 nm) [8]. The constant was fitted such that the curve is shifted best towards the experimental data. The results for a mixture of lysozyme with (invisible) 4 g/L dextran (at x_D=0.25) are also plotted in Fig.2. For this mixture it is noted that we are far below the phase separation threshold [12]. It follows from Fig.2 that the results (with and without dextran) are very comparable for Q>0.03Å, except for Q>0.07Å where the scattering intensity for the mixture seems to be somewhat larger.

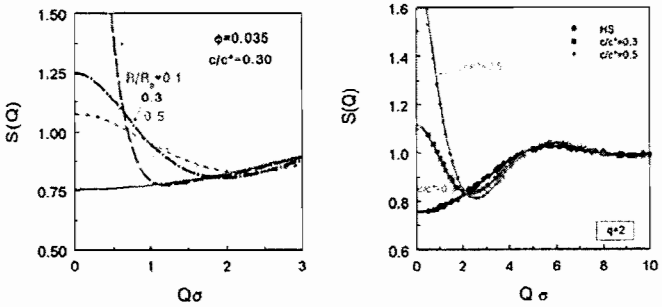

Fig.1: Effect of the polymer-colloid size ratio on the structure factor S(Q). Left:(dashed curves for R/R_g=0.1, 0.3, and 0.5 as indicated for small colloids, as compared to the hard sphere structure factor (full curve). The polymer concentration c/c=0.3 and the colloid volume fraction is 3.5 vol%. Right: Comparison of analyticla theory (curves) with computer simulation results of the structure factor of pure hard spheres with a volume fraction of 0.035 (spheres) and of hard spheres with an additional attraction for c/c*=0.3 (squares) and 0.5 (diamonds) for q=2.*

This could be an effect of the larger statistical errors for Q>0.07 Å. The main difference is found at small Q. The results are described as I(Q)=const×S(Q)P(Q), where the shifting constant and P(Q), the form factor of lysozyme, were kept the same as before. In the calculations of the depletion potential W(r), lysozyme was treated as a hard sphere with an interaction radius of 2.5 nm, so R_g/R=8.

A reasonable description of the experimental data could be obtained when using a concentration of polymers of c/c*=0.2 in the calculations. This is not unreasonable since the dextran concentration is 4 g/L and the (weight-averaged) overlap concentration is 19 g/L. The theoretical prediction obtained in this way (at low Q: upper curve in Fig.2) gives a fair description of the experimental results. The long-range attraction between the lysozyme molecules results in an increase in the scattering intensity at very small Q. We therefore have an indication therefore that SANS is a promising method to directly measure the long-ranged interaction potential between proteins in solutions with non-adsorbing polysaccharides. This may help to understand the phase behavior of biopolymer mixtures.

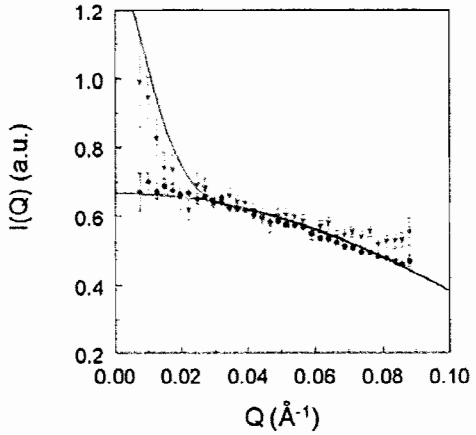

Fig.2: SANS intensity of a 3.5 vol% lysozyme dispersion (open triangles) and of a 3.5 vol% lysozyme / 4.0 g/L dextran mixture (closed circles) at x_D=0.25. Full curves are theoretical results for c/c=0.2 and a colloid volume fraction of 3.5 vol% for R_g/R=8.*

References

[1] Doublier, J.-L., Garnier C., Renard, C., Sanchez, C., *Curr. Opin. Coll. Int. Sci.* **5** (2000) 184.

[2] Grinberg, V.Ya., Tolstoguzov, V.B., *Food Hydrocolloids* **11** (1997) 145.

[3] De Gennes, P.G., *C.R. Acad.Sci. B* **288** (1979) 359.

[4] Eisenriegler, E., Hanke, A., Dietrich, S., *Phys. Rev. E.*, **54** (1996) 1134.

[5] Odijk, T., *Physica A* **278** (2000) 347.

[6] Eisenriegler, E., *J. Phys.: Condens. Matter,* **12** (2000) A227; *J. Chem. Phys.* **113** (2000) 5091.

[7] Sear, R.P., *Eur. Phys. J. B,* **1** (1998) 313.

[8] Castelletto, V., Arêas, E.P.G., Arêas, J. A.G., Craievich, A.F., *J. Chem. Phys.* **109** (1998) 6133.

[9] Chalikian, T.V., Totrov, M., Abagyan, R., Breslauer, K.J., *J. Mol. Biol.* **260** (1996) 588.

[10] Weber, P.C., Chapter 2 in: 'Methods in Enzymology; Macromolecular Crystallography, part A' **276** (1997) p. 36/37.

[11] Poon, W.C.K., Egelhaaf, S.U., Beales, P.A., Salonen, A., Sawyer, L., *J. Phys. Condens. Matter,* **12** (2000) L569.

[12] Tuinier, R., Brûlet, A., accepted for publication in *Biomacromolecules* (2003).

[13] Tuinier, R., Vliegenthart, G.A., Lekkerkerker, H.N.W., *J. Chem. Phys.* **113** (2000) 10768.

[14] Tuinier, R., Vliegenthart, G.A., *unpublished results* (2002).

[15] Louis, A.A., Finken, R., Hansen, J.-P., *Eur. Phys. Lett.* **46** (1999) 741.

[16] Louis, A.A., arXiv: cond-mat/0212073.

Shear-Induced Distortion of the Microstructure in near-Critical Colloids

H. Wang, M. P. Lettinga
Teilinstitut Weiche Materie, Institut für Festkörperforschung

We discuss small angle light scattering (SALS) by a near-critical colloidal system under shear flow. A newly developed optical shear cell allows for accurate SALS measurements under shear flow, and thus enables to directly compare the experimental structurefactor with the theoretical predictions [1,2]. The structurefactor relates to macroscopic quantities, such as the critical divergence of the shear-viscosity, the non-analytic dependence of turbidity on shear-rate and the critical behavior of flow induced dichroism. Contrary to the theoretical prediction, we find experimentally a significant distortion of the structurefactor at small scattering angles in directions perpendicular to the flow direction. We show that shear-induced distortion of short-ranged correlations (once was neglected in an earlier theory [1,2]) are responsible for the observed distortion of long-ranged correlations perpendicular to the flow direction. The importance of distortions on small scale for the distortion on large scale critical microstructure partly destroys universality as it is known for the critical behaviour of systems in the absence of shear flow, in the sense that critical microstructure under shear flow depends on short-ranged correlations, and thereby on the details of the pair-interaction potential. The integrated quantities mentioned above (such as the viscosity) are not very sensitive to distortions in directions perpendicular to the flow direction, since a finite distortion is found only within a limited region in wavevector space at small wavevectors, where the corresponding integrands are relatively small.

ROLE OF THE SHEAR-INDUCED DISTORTION OF SHORT-RANGED CORRELATIONS

Essential steps for the derivation of an equation of motion for the shear-rate dependent, total-correlation function can be found in refs [1] and [2]. These steps lead to an equation of motion for the total-correlation function for large distances, which in turn determines the structurefactor at small scattering angles. In the absence of shear flow the resulting structurefactor is just the Ornstein-Zernike (OZ) structurefactor. An important idea in the old theory is to neglect the effect of shear flow on short-ranged correlation, which seems to be straightforward since shear flow affects small scale structures to a much lesser extent as the extended near critical structures. The significance of distortion of short- and long-ranged correlations are measured by the bare Peclet number Pe^0 and dressed Peclet number λ, respectively,

$$Pe^0 = \frac{\dot\gamma\, R_V^2}{2\, D_0}, \qquad \lambda = \frac{\dot\gamma\, \xi^2}{2\, D^{eff}}, \tag{1}$$

where D_0 is the Stokes-Einstein diffusion coefficient, R_V is the range of the pair-interaction potential, D^{eff} is the effective diffusion coefficient at zero wavevector, $D^{eff} = D_0\, \beta\, \frac{d\Pi}{d\bar\rho}$, and the correlation length ξ of the unsheared suspension is given by $\xi = \sqrt{\Sigma / \frac{d\Pi}{d\bar\rho}}$, where $\beta = \frac{1}{k_B T}$, Π is the osmotic pressure of the unsheared suspension, $\bar\rho$ is the number density of spheres and Σ is a constant proportional to the Cahn-Hilliard square gradient coefficient. On approach of the critical point the dressed Peclet number λ can be very large as $D^{eff} \ll D^0$ and $\xi \gg R_V$ even for small bare Peclet numbers, quantifying the intuition that large structures with slow dynamics are much more easily distorted than small structures with fast dynamics. Nevertheless, a careful consideration reveals that in the equation of motion for the total correlation function, terms of order Pe^1 should be compared in magnitude with terms $\sim \beta\, d\Pi/d\bar\rho$ which also decay to zero on approach of the critical point (not with the Pe^0 term itself). This short-ranged distortion of the correlations can not be negelcted for a near-critical system and as we will see, it's crucial for the explanation of the experimentally found distortion of the structurefactor in directions perpendicular to the flow direction.

Instead of fully neglecting the shear-rate dependence of the short-range part of the pair-correlation function, as was done in the theory in refs.[1,2], we shall now take into account its leading order distortion, that is,

$$g(\mathbf{r}) \;=\; g^{eq}(r)\left[1 + \,|Pe^0|\, f_0(r) \;-\; 2\, Pe^0\, \hat x\, \hat y\, f_1(r)\right], \tag{2}$$

where g^{eq} is the pair-correlation function of the unsheared system, and the second term and the third term in the square brackets account for the isotropic distortion and anisotropic distortion of the short-ranged correlation function, respectively. Repeating the analysis in refs.[1,2], but now using eq.(2) for the short-ranged part of the correlation function, one finds the following stationary equation of motion for the critical part of the structurefactor

$$\lambda K_1 \frac{\partial S}{\partial K_2} \;=\; K^2(1+K^2)(S - S^{eq}) + \epsilon K^2 S + \alpha\, K_1 K_2\, [S-1]\;, \tag{3}$$

with the dimensionless wavevector $\mathbf{K} = \mathbf{k}\xi$, and with S^{eq} the OZ structurefactor. The dimensionless numbers

ϵ and α are equal to integrals of the functions f_0 and f_1 respectively. The above equation shows that the behaviour of the critical structure factor under shear flow conditions depends on the details of the short-ranged part of the pair-correlation function, and thereby on the details of the pair-interaction potential, contrary to the OZ structure factor of the unsheared suspension. Note that in directions perpendicular to the flow direction, where $K_1 = 0$, the revised theory predicts that,

$$S(\mathbf{K}) = \frac{\xi^2}{\beta\Sigma} \frac{1}{1 + \epsilon(\dot{\gamma}) + K^2}. \qquad (4)$$

This is only equal to S^{eq} in case $\epsilon = 0$, that is, with the neglect of the effect of shear flow on isotropic short-ranged correlations. Hence, the isotropic contribution to short-ranged distortions in eq.(2) is responsible for a finite distortion in directions perpendicular to the flow direction.

EXPERIMENTAL RESULTS

Data were obtained using a SALS set up where the wavevector dependence of the structure factor in the flow-vorticity $[K_1, K_3]$- plane is probed. The system used in this study is a mixture of silica spheres grafted with stearyl alcohol and Polydimethylsiloxane. Due to the attractive depletion forces this system undergoes a gas-liquid phase transition. The distance to the critical point can be tuned by gently evaporating or adding solvent to the dispersion. Scattering patterns were taken for six different correlation lengths ξ between $\xi = 300$ and $1450\,nm$, and with shear-rates in the range of $\dot{\gamma} = 0$ to $35\,s^{-1}$. We shall show here data obtained for a system with a correlation length of $\xi = 650\,nm$. The correlation length is obtained from the OZ structure factor in the absence of shear flow.

Fits were performed on ten cross sections in the $[K_1, K_3]$-plane per scattering pattern : five cross sections at fixed values of K_1 as functions of K_3, and five at fixed K_3 as functions of K_1. Besides the experimental parameters like intensity and background, scattering patterns are fitted with respect to the theoretical parameters $\lambda/\dot{\gamma}$ and $\epsilon/\dot{\gamma}$. The parameter α is set equal to 0 since it did not significantly improve fits.

Typical fitting results are given in Fig.1. The significant distortion in directions where $K_1 = 0$ is quantitatively described by the above discussed, revised theory. Fitting without the additional term $\sim \epsilon$ (the dotted curves) clearly leads to results that are qualitatively different from the experimental data. The revised theory predicts that $\lambda/\dot{\gamma}$ varies like $\sim \xi^4$ and $\epsilon/\dot{\gamma}$ varies like ξ^2. This is indeed what we found, as shown in Fig.2. In the double logarithmic plot in Fig.2 for the fit parameters, we found slopes of 4.4 ± 0.5 and 2.2 ± 0.3, respectively,

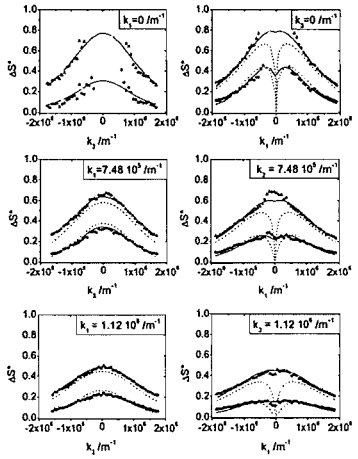

FIG. 1: Typical fitting results for a correlation length of $\xi = 650\,nm$. $\Delta S^* \equiv \frac{\beta\Sigma}{\xi^2}\{S^{eq}(K) - S(\mathbf{K})\}$. The points are experimental data, the dotted line is a best least square fit to the old theory while the solid lines are best fits to the revised theory. The wavevector at which a cross section is taken is indicated in the right upper corner of each figure.

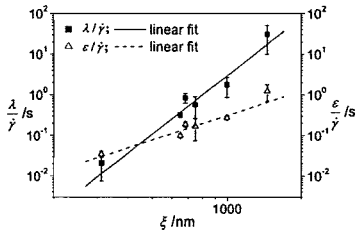

FIG. 2: The best least square fit results for $\lambda/\dot{\gamma}$ and $\epsilon/\dot{\gamma}$ versus the correlation length ξ of the unsheared suspension.

in agreement with the predictions. The deviation between experimental dichroism data and the older theory on close approach of the critical point is probably not due to non-mean field effects (as stated in ref.[2]), but are most likely due to the shear-induced short-ranged correlations as described in eq.(2).

REFERENCES

[1] J.K.G. Dhont, An Introduction to Dynamics of Colloids, Elsevier, Amsterdam, 1996.

[2] J.K.G. Dhont and G. Nägele, Phys. Rev. E. **58**, 7710 (1998).

Publications in journals

Aarts,D.G.A.L.*; Tuinier,R.; Lekkerkerker,H. N. W.*
Phase behaviour of mixtures of colloidal spheres and excluded-volume polymer chains
Journal of physics: condensed matter, 14 (2002), S. 7551 - 7561

Avramescu,M. E.*; Sager,W.; Mulder,M.H.*; Wessling,M.*
Preparation of ethylene vinylalcohol copolymer membranes suitable for ligand coupling in affinity separation
Journal of membrane science, 210 (2002),155-173

Beiner,M.*; Fytas,G.*; Meier,G.; Kumar,S.*
Strong isotopic labelling effects on the pressure dependent thermodynamics of polydimethylsiloxane/polyethylmethylsiloxane blends
Journal of chemical physics, 116 (2002), S. 1185 - 1192

Dhont,J. K. G.; Briels,W. J.*
Stresses in inhomogeneous suspensions
Journal of chemical physics, 117 (2002), S. 3992 - 3999

Ecker,S.*; Hoffmann,S.; Meier,G.; Alig,I.*
Composition fluctuations in a non-critical binary polymer blend studied by ultrasonic and light scattering experiments
Physical chemistry chemical physics, 4 (2002), S. 2594 - 2603

Eckert,S; Meier,G.*; Alig,I.*
Phase behaviour of mixtures of polyethylene glycol and polypropylene glycol : influence of hydrogen bond clusters on the phase diagram
Physical chemistry chemical physics, 4 (2002), S. 3743 - 3749

Figoli,A.*; Sager,W.; Wessling,M.*
Synthesis of novel nanostructured mixed matrix membranes
Desalination, 148 (2002), S. 401 - 405

Fytas,G.*; Nothofer,H. G.*; Scherf,U.*; Vlassopoulos,D.*; Meier,G.
Structure and dynamics of nondilute polyfluorene solutions
Macromolecules, 35 (2002), S. 481 - 488

Hauck,J.; Erkens,W.; Mika,K.; Wingerath,K.
Structure maps for polymer structures
International journal of modern physics B, 16 (2002), 23, S. 3449 - 3457

Hauck,J.; Mika,K.
Structure maps for crystal engineering
Crystal engineering, 5 (2002), S. 105 - 121

Hauck,J.; Mika,K.
Two- and three-dimensional surfaces
Zeitschrift für physikalische Chemie, 216 (2002), S. 1281 - 1293

Hauck,J.; Henkel,D; Mika,K.
Ordnung in Sprachen, Proteinen und Konferenzsälen
Zeitschrift für Kristallographie, 19 (2002), S. 62

Rathgeber,S.; Gast,A. P.; Hedrick,J. L.
Structural properties of star-like dendrimers in solution
Applied physics A, 74 (2002), S. 396 - 398

Iatrou,H.*; Hadjichristidis,N.*; Meier,G.; Frielinghaus,H.; Monkenbusch,M.
Synthesis and characterization of model cyclic block copolymers of styrene and butadiene : comparison of the aggregation phenomena in selective solvents with linear diblock and triblock analogues
Macromolecules, 35 (2002), S. 5426 - 5437

Koenderink,G.*; Lettinga,M. P.; Philipse,A.*
Rotational dynamics of charged colloidal spheres: role of particle interactions
Journal of chemical physics, 117 (2002),7751-7764

Kollmann,M.; Hund,R.*; Rinn,B.*; Nägele,G.; Zahn,K.*; König,H.*; Maret,G.*; Klein,R.*; Dhont,J. K. G.
Structure and tracer-diffusion in quasi-two-dimensional and strongly asymmetric magnetic colloidal mixtures
Europhysics letters, 58 (2002), S. 919 - 925

Marczuk,P.*; Lang,P.; Findenegg,G. H.*; Mehta,S. K.*; Möller,M.*
Gibbs films of semi-fluorinated alkanes at the surface of alkane solutions
Langmuir, 18 (2002), S. 6830 - 6838

Menge,H.*; Pyckhout-Hintzen,W.; Meier,G.; Straube,E.*
Butadiene rubbers : topological constraints and microscopic deformations by mechanical and small angle neutron scattering investigation
Polymer bulletin, 48 (2002), S. 183 - 190

Montes,H.*; Monkenbusch,M.; Willner,L.; Rathgeber,S.; Richter,D.; Fetters,L.J.*; Farago,B.*
Direct observation of domain wall excitations in symmetric diblock copolymer melts at and above the order-disorder transition
Europhysics letters, 58 (2002), S. 389 - 394

Rathgeber,S.; Monkenbusch,M.; Kreitschmann,M.*; Urban,V.*; Brulet,A.*
Dynamics of star-burst dendrimers in solution in relation to their structural properties
Journal of chemical physics, 117 (2002), S. 4047 - 4062

Scholten,E.*; Tuinier,R.; Tromp,R. H.*; Lekkerkerker,H. N. W.*
Interfacial tension of a decomposed biopolymer mixture
Langmuir, 18 (2002), S. 2234 - 2238

Stiakakis,E.*; Vlassopoulos,D.*; Likos,C.*; Roovers,J.*; Meier,G.
Polymer-mediated melting in ultrasoft colloidal gels
Physical review letters, 89 (2002), 20, S. 208302-1 - 208302-4

Stiakakis,E.*; Vlassopulos,D.*; Loppinet,B.*; Roovers,J.*; Meier,G.
Kinetic arrest of crowded soft spheres in solvents of varying quality
Physical review E, 66 (2002),S. 051804-1 - 051804-9

Tuinier,R.; de Kruif,C.G.*
Stability of casein micelles in milk
Journal of chemical physics, 117 (2002);1290-1295

Tuinier,R.; Lekkerkerker,H. N. W.*; Aarts,D.G.A.L.*
Interaction potential between two spheres mediated by excluded volume polymers
Physical review E, 65 (2002), S. 060801

Tuinier,R.; Petukhov,A.V.*
Polymer polydispersity effect on depletion interaction between colloidal particles
Macromolecular theory and simulations, 11 (2002), S. 975 - 984

Tuinier,R.; Rolin,C.*; de Kruif,C.G.*
Electrosorption of pectin onto casein micelles
Biomacromolecules, 3 (2002), S. 632 - 638

Vass,S.*; Haimer,K.*; Meier,G.; Klapper,M.*; Borbély,S.*
Small-angle neutron scattering study of poly(methyl methacrylate-block-sodium acrylate-block-methyl methacrylate) and poly(sodium acrylate-block-methyl methacrylate-block-sodium acrylate) triblock copolymers in aqueous solutions
Colloid and polymer science, 280 (2002),S. 245 - 253

Wang,H.; Lettinga,M. P.; Dhont,J. K. G.
Microstructure of a near-critical colloidal dispersion under stationary shear flow
Journal of physics: condensed matter, 14 (2002), S. 7599 – 7615

Book chapter

Buitenhuis,J.
Colloid synthesis
Soft matter complex materials on mesoscopic scales ; lecture manuscripts of the 33rd IFF winter school, this winter school was organized on March, 04 - 15, 2002 in the Forschungszentrum Jülich by the Institut für Festkörperforschung ... / ed.: J. K. G. Dhont. - Jülich, 2002. - (Schriften des Forschungszentrums Jülich, Reihe Materie und Material/Matter and Materials ; 10). - 3-89336-297-5

de Kruif,C. G.*; Tuinier,R.
Colloidal stability of casein micelles in milk
Soft matter : complex materials on mesoscopic scale ; lecture manuscripts of the 33rd IFF winter school, this winter school was organized on March, 04 - 15, 2002 in the Forschungszentrum Jülich by the Institut für Festkörperforschung ... / ed.: J. K. G. Dhont. - Jülich, 2002. - (Schriften des Forschungszentrums Jülich, Reihe Materie und Material/Matter and Materials ; 10). - 3-89336-297-5

Dhont,J. K. G. (Hrsg.)
Rotational Brownian Motion of colloidal rods
Soft matter : complex materials on mesoscopic scale ; lecture manuscripts of the 33rd IFF winter school, this winter school was organized on March, 04 - 15, 2002 in the Forschungszentrum Jülich by the Institut für Festkörperforschung ... / ed.: J. K. G. Dhont. - Jülich, 2002. - (Schriften des Forschungszentrums Jülich, Reihe Materie und Material/Matter and Materials ; 10). - 3-89336-297-5

Lang,P.
Fluid interfaces and amphiphiles at surfaces
Soft matter : complex materials on mesoscopic scale; lecture manuscripts of the 33rd IFF winter school, this winter school was organized on March, 04 - 15, 2002 in the Forschungszentrum Jülich by the Institut für Festkörperforschung ... / ed.: J. K. G. Dhont. - Jülich, 2002. - (Schriften des Forschungszentrums Jülich, Reihe Materie und Material/Matter and Materials ; 10). - 3-89336-297-5

Lettinga,M. P.
Phase separation kinetics
Soft matter : complex materials on mesoscopic scale ; lecture manuscripts of the 33rd IFF winter school, this winter school was organized on March, 04 - 15, 2002 in the Forschungszentrum Jülich by the Institut für Festkörperforschung ... / ed.: J. K. G. Dhont. - Jülich, 2002. - (Schriften des Forschungszentrums Jülich, Reihe Materie und Material/Matter and Materials ; 10). - 3-89336-297-5

Meier,G.
Nuclear magnetic resonance
Soft matter : complex materials on mesoscopic scale ; lecture manuscripts of the 33rd IFF winter school, this winter school was organized on March, 04 - 15, 2002 in the Forschungszentrum Jülich by the Institut für Festkörperforschung ... / ed.: J. K. G. Dhont. - Jülich, 2002. - (Schriften des Forschungszentrums Jülich, Reihe Materie und Material/Matter and Materials ; 10). - 3-89336-297-5

Nägele,G.
Ornstein-Zernike theories of fluid microstructures

Soft matter : complex materials on mesoscopic scale ; lecture manuscripts of the 33rd IFF winter school, this winter school was organized on March, 04 - 15, 2002 in the Forschungszentrum Jülich by the Institut für Festkörperforschung ... / ed.: J. K. G. Dhont. - Jülich, 2002. - (Schriften des Forschungszentrums Jülich, Reihe Materie und Material/Matter and Materials ; 10). - 3-89336-297-5

Rathgeber,S.
Practical rheology
Soft matter : complex materials on mesoscopic scale ; lecture manuscripts of the 33rd IFF winter school, this winter school was organized on March, 04 - 15, 2002 in the Forschungszentrum Jülich by the Institut für Festkörperforschung ... / ed.: J. K. G. Dhont. - Jülich, 2002. - (Schriften des Forschungszentrums Jülich, Reihe Materie und Material/Matter and Materials ; 10). - 3-89336-297-5

Sager,W. F. C.
Microemulsion templating
Soft matter : complex materials on mesoscopic scale ; lecture manuscripts of the 33rd IFF winter school, this winter school was organized on March, 04 - 15, 2002 in the Forschungszentrum Jülich by the Institut für Festkörperforschung ... / ed.: J. K. G. Dhont. - Jülich, 2002. - (Schriften des Forschungszentrums Jülich, Reihe Materie und Material/Matter and Materials ; 10). - 3-89336-297-5

Book

Dhont,J. K. G. (Hrsg.); Gompper,G. (Hrsg.); Richter,D. (Hrsg.)
Soft matter : complex materials on mesoscopic scale
Jülich, Forschungszentrum, Zentralbibliothek, 2002
Schriften des Forschungszentrums Jülich : Reihe Materie und Material/Matter and Materials ; 10
3-89336-297-5

Invited talks

Dhont,J. K. G.
Shear-banding of suspensions of rods
European Colloid and Interface Society (ECIS)
Paris, Frankreich: 22.09.2002 - 27.09.2002

Dhont,J.; Lettinga,M. P.; Dogic,Z.; Lenstra,T.; Wang,H.; Rathgeber,S.; Carletto,P.; Willner,L.; Frielinghaus,H.; Lindner,P.*
Shear-banding and microstructure of colloids in shear flow
Faraday Discussion 123 on Non-Equilibrium Behaviour of Colloidal Dispersions
Edinburgh, United Kingdom: 09.09.2002 - 12.09.2002

Nägele,G.
Electrolyte friction and diffusion
Jülich Soft Matter Days 2002
Kerkrade, NL: 19.11.2002 - 22.11.2002

Nägele,G.
Viscoelasticity and diffusional properties of colloidal model dispersions
5th Liquid Matter Conference
Konstanz: 14.09.2002 - 18.09.2002

Rathgeber,S.; Pakula,T.*; Wilk,A.*; Matyjaszewski,K.*
Regular branched macromolecules : structure of bottlebrush polymers in solution
XII International Conference on Small-Angle Scattering
Venezia, Italy: 25.08.2002 - 29.08.2002

Other talks

Buitenhuis,J.
Colloid synthesis
Soft matter : complex materials on mesoscopic scales ; 33. IFF Ferienkurs
Jülich: 04.03.2002 - 15.03.2002

Carletto,P.
Shear induced polymer brush deformation and rheology of ultrasoft colloids
HUSC-Meeting (Hard to Ultra Soft Colloids)
Kreta: 13.05.2002 - 15.05.2002

de Kruif,C. G.*; Tuinier,R.
Colloidal stability of casein micelles in milk
Soft matter : complex materials on mesoscopic scales ; 33. IFF-Ferienkurs
Jülich: 04.03.2002 - 15.03.2002

Dhont,J. K. G.
Long-time self-diffusion of brownian rods
Kolloquiumsvortrag
Mainz: 02.07.2002

Dhont,J. K. G.
Rotational Brownian Motion of colloidal rods
Soft matter : complex materials on mesoscopic scale ; 33. IFF-Ferienkurs
Jülich: 04.03.2002 - 15.03.2002

Dhont,J.K.G.
Shear-banding in complex fluids
Kolloquium des Sonderforschungsbereiches 448 \"Mesoskopisch strukturierte Verbundsysteme\"
Berlin: 29.01.2002 - 30.01.2002

Hauck,J.
Eine allgemeine Beziehung zwischen Struktur und Wechselwirkung
Seminar im Kristallographischen Institut : ETH Zürich
Zürich: 24.05.2002

Hauck,J.
Ordnung in Sprachen,Proteinen und Konferenzsälen
DGK Jahrestagung
Kiel: 04.03.2002 - 07.03.2002

Hauck,J.; Mika,K.
Interactions in ordered surfactants
ECIS 2002
Paris: 22.09.2002 - 27.09.2002

Hauck,J.; Mika,K.
Ordered surfactant structures
SIS 2002
Barcelona: 09.06.2002 - 14.06.2002

Hauck,J.; Mika,K.
Relation between structure and interactions
SSC 2002
Bratislava, Slowakai: 07.07.2002 - 12.07.2002

Lang,P.
Fluid interfaces and amphiphiles at surfaces
Soft matter : complex materials on mesoscopic scales ;
33. IFF-Ferienkurs
Jülich: 04.03.2002 - 15.03.2002

Lettinga,M. P.
Phase separation kinetics
Soft matter : complex materials on mesoscopic scales ;
33. IFF-Ferienkurs
Jülich: 04.03.2002 - 15.03.2002

Meier,G.
Nuclear magnetic resonance
Soft matter : complex materials on mesoscopic scales ;
33. IFF-Ferienkurs
Jülich: 04.03.2002 - 15.03.2002

Nägele,G.
Dynamik und Viskoelastizität von Kolloiden
Seminar im Institut für Theoretische Physik : Universität Düsseldorf
Düsseldorf: 18.07.2002

Nägele,G.
Ornstein-Zernike theories of fluid microstructures
Soft matter : complex materials on mesoscopic scales ;
33. IFF-Ferienkurs
Jülich: 04.03.2002 - 15.03.2002

Rathgeber,S.
Dynamics of star-burst dendrimers in solution in relation to their structural properties
HUSC Meeting (Hard to Ultra Soft Colloids)
Kreta: 13.05.2002 - 15.05.2002

Rathgeber,S.
Polymer Dynamik
Vortrag im Fachbereich Physik : TU Darmstadt
Darmstadt: 16.04.2002

Rathgeber,S.
Practical rheology
Soft matter : complex materials on mesoscopic scales ;
33. IFF-Ferienkurs
Jülich: 04.03.2002 - 15.03.2002

Sager,W. F. C.
Microemulsion templating
Soft matter : complex materials on mesoscopic scales ;
33. IFF-Ferienkurs
Jülich: 04.03.2002 - 15.03.2002

Tuinier,R.
Influence of polymer properties on the polymer-mediated interaction between colloidal particles
Seminar, Theoretische Physik II
Universität Düsseldorf: 04.12.2002 - 04.12.2002

Tuinier,R.
Polymer-mediated interaction between colloidal particles
Seminar at the Laboratoire Léon Brillouin
Saclay: 17.05.2002 - 17.05.2002

Wang,H.
Shear-induced microsturcture in near-critical systems
HUSC-Meeting (Hard to Ultra Soft Colloids)
Kreta: 13.05.2002 - 15.05.2002

Posters

Autin,A.*; Sager,W.; Nolte,R.*
Precipitation of nanostructured materials in self-organizing systems
Macromolecules
Lunteren/NL: 25.02.2002 - 26.02.2002

Buitenhuis,J.
Negative thixotropy of polymers solutions: a new model and experiments
Jülich Soft Matter Days 2002
Kerkrade, NL: 19.11.2002 - 22.11.2002

Eckert-Kastner,S.*; Meier,G.; Alig,I.*
Phase behavior of mixtures of PEG and PPG : influence of hydrogen bond clusters on the phase diagram and critical behavior
5. Kautschuk Herbst-Kolloquium
Hannover: 30.10.2002 - 01.11.2002

Hauck,J.
Interactions in ordered surfactants
Jülich Soft Matter Days 2002
Kerkrade, NL: 19.11.2002 - 22.11.2002

Lang,P.
Surface induced ordering of blockcopolymer micelles
Jülich Soft Matter Days 2002
Kerkrade, NL: 19.11.2002 - 22.11.2002

Lettinga,M. P.

On the behaviour of concentrated fd virus despersions under shear flow
Jülich Soft Matter Days 2002
Kerkrade, NL: 19.11.2002 - 22.11.2002

Lettinga,M. P.; Dogic,Z.; Dhont,J.K.G.
Shear band formation in fd-virus dispersions
5th Liquid Matter Conference of the European Physical Society
Konstanz: 14.09.2002 - 18.09.2002

Nägele,G.
Dynamic properties, scaling and related freezing criteria of 2C- and 3D dispersions
Gordon Research Conference - Colloidal Macromolecular and Polyelectrolyte Solutions
Ventura, Kalifornien: 03.02.2002 - 08.02.2002

Sager,W.
Characterization of nanosized oxide particles and ceramic nanocomposite coatings prepared via modified emulsion precipitation
Jülich Soft Matter Days 2002
Kerkrade, NL: 19.11.2002 - 22.11.2002

Stiakakis,E.*; Vlassopoulos,D.*; Likos,C. N.*; Roovers,J.*; Meier,G.
Polymer-mediated melting in crowded ultrasoft colloids
Jülich Soft Matter Days 2002
Kerkrade: 19.11.2002 - 22.11.2002

Stiakakis,E.*; Vlassopoulos,D.*; Loppinet,B.*; Likos,C. N.*; Roovers,J.*; Meier,G.
Glass-like transitions in crowded ultrasoft spheres
Jülich Soft Matter Days 2002
Kerkrade: 19.11.2002 - 22.11.2002

Tuinier,R.
Chain flexibility influence on depletion interaction in polymer-colloid mixtures
Jülich Soft Matter Days 2002
Kerkrade; NL: 19.11.2002 - 22.11.2002

Tuinier,R.; coher,D.*; Lekkerkerker,H.*
Attraction between colloidal particles due to interacting polymers
5th Liquid Matter Conference
Konstanz: 14.09.2002 - 18.09.2002

Wilk,A.*; Gapinski,J.*; Patkowski,A.*; Pecora,R.*; Dhont,J. K. G.; Meier,G.; Buitenhuis,J.
Self-diffusion measurements of short and long rod-like particles by means of fluorescence correlation spectroscopy
Jülich Soft Matter Days 2002
Kerkrade: 19.11.2002 - 22.11.2002

Zhang,H.; Nägele,G.
Short-time tracer-diffusion in binary colloidal hard sphere suspensions
5th Liquid Matter Conference of the European Physical Society
Konstanz: 14.09.2002 - 18.09.2002

Zhang,H.; Nägele,G.
Short-time tracer-diffusion in binary colloidal hard-sphere suspensions
Jülich Soft Matter Days 2002
Kerkrade, NL: 19.11.2002 - 22.11.2002

Institute for Microstructure Research

General Overview

The Institut für Mikrostrukturforschung (Institute for Microstructure Research) is working in a number of fields selected with an emphasis on the atomistic and microstructural understanding of materials properties and the possibility to contribute to the development of technology. In some of these fields the competence spans the whole range from basic research to technical devices. In others access to interesting materials and problems is provided by qualified collaborations. Besides this general-physics and technology part of the institute there is a second part of special competence. This is structure research by means of modern transmission electron microscopy and scanning tunneling microscopy and the development of advanced investigation methods for these. This work is carried out within the Jülich Center for High-Resolution Electron Microscopy operated by the institute.

Research Fields

(1) *Ceramic Superconductors*: Thin-film and heterostructure production, Josephson effects, and their application in magnetometer systems, magnetic-field microscopy and spectroscopic techniques.

(2) *Semiconductors*: Structural investigations, mainly by transmission electron microscopy, of thin films and heterostructures. Study of electronic states in compound semiconductors by scanning tunneling microscopy employing a technique developed in our group. It permits, via the detection of the far-reaching Debye screening cloud at the surface, an investigation of charged doping or impurity atoms in the bulk.

(3) *Metallic Alloys*: This concerns two major fields, quasicrystalline alloys and structurally complex alloy phases (SCAP). We are growing large single quasicrystals and SCAP crystals for our own research but also for users worldwide. Our own work concentrates on phase-diagrams, plasticity and surface physics.

(4) *Electroceramics*: In this field we take advantage of our long-standing experience with respect to perovskitic materials both in preparation and in transmission electron microscopy. In collaboration with the Institut für Elektrokeramische Materialien (Prof. Waser) we dedicate a large research capacity to the investigation of the structural aspects of the production and properties of electroceramic thin films.

(5) *High-Resolution Electron Microscopy*: The theoretical, technical and methodical aspects of atomic-resolution transmission electron microscopy are one of the central fields of interest of our group. Computer program packages for the exit wave-function reconstruction developed in the institute are in use world-wide. The institute co-developed and houses the world's first aberration-corrected transmission electron microscope with a record resolution of 1.2 Å at 200 kV.

(6) The institute operates together with the Institut für Streumethoden (Prof. Brückel) the IFF laboratory for crystal growth.

Equipment

The institute operates sputtering deposition machines, some of them with three-target facilities, which were developed and built in the institute for the high-quality deposition of ceramic superconductor thin films and heterostructures. Copies of these machines could be sold successfully to laboratories around the world. For SQUID reference studies we have a magnetically shielded room. For device production local clean room, structuring and packaging facilities are available. The institute operates the Jülich Center for High-Resolution Electron Microscopy with two 400 kV JEOL machines of the type 4000 EX/FX, a JEOL 2000 EX, a PHILIPS CM20 FEG, the spherical-aberration corrected PHILIPS CM200 FEG and a JEOL 840A scanning microscope. The new DFG-funded **SATEM** instrument, an aberration corrected sub-Ångstrom TEM produced by ZEISS-LEO will be installed in autumn 2003. Our instruments for scanning tunneling microscopy: Two microscopes with *in-situ* cleaving facilities and *ex-situ* heating up to 750 °C and an *in-situ* heating STM (Omicron). For the work on alloy plasticity a Zwick mechanical testing system is available.

Special results and developments in 2002

The **$YBa_2Cu_3O_7$ *dc*-SQUID sensors**, developed and produced in our institute show the world's highest sensitivity and have already found many applications around the world. Distributed by TTB (FZJ) and Tristan Technologies Inc.(San Diego, California) our SQUIDs are used in commercial measurement systems. The market demands represent challenges to science and technology, and our work in this field will be continued as long as we can derive good science from it. Submicrometer wide high-Tc bicrystal Josephson junctions with a normal state resistance of about 10 Ω and a critical current density of about 2×10^4 A/cm^2 (I_cR_n product of about 400 μV) at 77.4 K were developed. We have significantly improved the noise properties of *dc* flip-chip magnetometers with submicrometer wide bicrystal junctions. We demonstrated a modulation voltage V_{pp} up to 80 μV compared to about 30 μV for the magnetometers with 1.5 μm junctions. The noise of the magnetometers with electronics was about 6 fT/√Hz at frequencies above 100 Hz and about 20 fT/√Hz at 1 Hz. An axial first order gradiometer system, gradient resolution of about 1 fT/cm√Hz at 77.4 K, was developed for biomagnetic meas-

urements. It was successfully used in a BMBF project on biomagnetism and application in clinical environment. For application in semiconductor industry a non-contact measurement system for the distribution of the photo-induced magnetic field from p-n junctions in devices using a laser SQUID microscope and our SQUID sensors was developed successfully in Japan.

In the framework of our collaboration with the Institute of Radio Engineering, Moscow, we pursue our development of **Hilbert-spectroscopy** for the far-infra red range. For this we have measured the critical current density (j_C) distribution of [001]-tilt $YBa_2Cu_3O_7$ bicrystal Josephson junctions by means of the laser probing technique. The topography of the grain boundaries for the junctions with maximum and minimum j_C was studied by AFM and high-resolution TEM. We could show: The boundaries with high j_C consist mainly of symmetrical while those with low j_C consist of asymmetrical facets. In junctions optimized on this basis we investigated the broadband spectral range from GHz to THz frequencies. The low-frequency limit of the Josephson effect could be shown to be due to the finite linewidth of the Josephson oscillations while the high-frequency limit is determined by interaction of Josephson oscillations with strong optical phonons in $YBa_2Cu_3O_7$. A Hilbert spectrometer for operation with pulsed far-infrared radiation has been developed and characterized. It employs a [001]-tilt $YBa_2Cu_3O_{7-x}$ bicrystal junction in an optical cryostat. The spectral range of the spectrometer extends from 30 to 1200 GHz at the junction temperature of 78 K and can be shifted to the higher frequencies by lowering the junction temperature. We have demonstrated earlier that Hilbert-spectroscopy has great potential for beam diagnostics in high-energy electron accelerators. New applications are in the testing of ultra-fast electronic devices.

A **scanning SQUID microscope** for the investigation of room temperature samples has been built and successfully tested (collaboration with ZEL). Its resolution surpasses that of commercial systems. The application of this type of microscope for information technology especially in the field of failure analysis of semiconductor devices, e.g. the non-destructive detection of package- or chip level shorts of micro circuits, or the investigation of magnetic storage devices looks promising.

Setting a benchmark in quantitative **diffraction contrast imaging**, the gas pressure of helium-filled nanocracks formed upon implantation and annealing of silicon was measured for individual cavities at high precision. This parameter, which plays an import role in the plastic relaxation of implanted semiconductors, has been directly measured for the first time.

Our laboratory is still the only one operating a **spherical-aberration corrected TEM**. The technique of multipole-aberration corrector systems pioneered by the institute together with CEOS, Heidelberg, and TU Darmstadt has started a new era in transmission electron microscopy. All TEM companies, ZEISS-LEO Oberkochen, FEI (USA, formerly Philips Electron Optics), JEOL and Hitachi (Japan) are working on new microscope designs containing correctors. Our institute receives a large number of international visitors every year who are interested in the new technology. On the other hand, the very high number of invited keynote lectures on international conferences underlines the pioneering role and high reputation of our group in this field. The international electron optics community reacted enthusiastically to our discovery that adjusting small *negative* spherical-aberration values (by overcompensation of the original instruments aberration) revolutionizes atomic-resolution imaging. Negative spherical aberration imaging allows, e.g., to image oxygen in perovskite ceramics (SCIENCE, in press) where the local oxygen content sensitively controls the electronic properties.

The **alloy physics group** has successfully started an extended research program in the new field of complex alloy phases (SCAP). This concerns intermetallics with giant unit cells containing hundreds to thousands of atoms on which essentially nothing is known with respect to physical properties. Procedures for the growth of centimeter-sized high-quality single crystals of a number of such alloys were developed. These constitute the first reliable samples for physical property measurements of this novel class of materials. A special Symposium was organized by us and Prof. Trebin, University of Stuttgart, at the DPG Frühjahrstagung 2002 in Regensburg. This field was selected (spring 2002) by the French and Germany ministers of science as a field of preference for French-Germany science collaboration in materials science. Structurally complex alloy phases is also the topic of a European Network of Excellence "CMA" (Coordinators: Profs. K. Urban, Jülich, J.-M. Dubois, Nancy, L. Schlapbach, Fribourg, J. Hafner, Wien) to be applied for in the 6th Framework Program of the EC. The Chinese-German research program on Modern Metallic Materials Design organized on behalf of the DFG and the NSFC by Profs. Herlach, Köln, and Urban, Jülich, has been granted by the DFG Senate in September 2002. The work of our group together with the Institute of Physics CAS and Wuhan University on SCAP has started in December 2002.

In recent years great efforts went into joint **doctor student programs with foreign universities**. Formal contracts were signed with the Russian Academy of Sciences, the University of Kiev, the Tsinghua University and the Institute of Physics, Beijing, the Dalian University and Wuhan University, China. In the framework of this special program the doctor students are working up to three years in Jülich on a grant supervised by the Jülich Doktorandenausschuß, but they will pass their examina in their home university. A number of doctor students from Moscow Institute of Science and Technology, of Dalian University and of Wuhan University where Prof. Urban holds a professorship are working at Jülich. Students from the Institute of Physics will follow during this year.

It was a great gain and honor for the institute to be the host for extended stays of the **Humboldt prizewinners** Prof. Frans Spaepen, Harvard University, Cambridge, Mass., and Prof. Berry Carter, University of Minnesota, Minneapolis.

Prof. Dr. Knut Urban

Institute for Microstructure Research

Personnel 2002 / 2003 and areas of activity

Scientific Staff	Field of Activity	No.
Dr. Y. Divin	Hilbert-spectroscopy	2342004
Dr. Ph. Ebert	Scanning tunneling microscopy of semiconductors and quasicrystals	2310204, 2342004
Dr. M. Faley	High-T_c-Superconductor SQUIDs, Multilayer structures, SQUID-Microscopy	2342004
Dr. M. Feuerbacher	Plasticity of quasicrystals	2310204
Dr. B. Grushko	Crystal growth, phase diagrams of alloys	2310204
Dr. C.L. Jia	Characterization of superconductors, diamond and electroceramic films by high-resolution electron microsopy	2342004
Dr. M. Lentzen	Reconstruction techniques in high-resolution electron microscopy, Cs-corrected transmission electron microscopy for imaging of interfaces in semiconductors and of superconducting materials	2310204, 2342004
Dr. M. Luysberg	Transmission electron microscopy of semiconductor heterostructures, low-temperature GaAs and microcrystalline silicon	2342004
Dr. U. Poppe	Superconductivity, tunneling spectroscopy, High-T_c superconductor thin films and multilayers, SQUID-Microscopy	2342004
Dr. A. Thust	Reconstruction techniques in high-resolution electron microscopy, Cs-corrected transmission electron microscopy for imaging of interfaces in semiconductors, electron microscopy of superconducting materials	2342004, 2310204
Prof. Dr. K. Urban	Head of Institute	2310204, 2342004
Technical Staff		
K. Fischer	Crystal growth, Materials preparation and characterization	2310204
DI K.-H. Graf	Electronics, Electronic data processing, scanning tunneling microscopy	2310204, 2342004
D. Meertens	Metallography, semiconductor preparation, scanning- and transmission electron microscopy	2310204, 2342004
W. Pieper	Technical supervisor, Centre for High Resolution Electron Microscopy	2310204, 2342004
I. Rische-Radloff	Secretary	
K. Schwill	Trainee	2310204
M. Schmidt	Trainee	2310204
R. Speen	SQUID-Microscopy, Sputtering systems	2342004
C. Thomas	Crystal growth, Materials preparation and characterization	2310204
G. Waßenhoven	Photolaboratory, photography technique	2310204, 2342004
E. Würtz	Metallography, semiconductor preparation, scanning and transmission electron microscopy	2310204
Junior scientists		
Dr. Y. Ding	Cs-corrected transmission electron microscopy of electroceramic thin films	2342004
Dr. L. Houben	Structure characterization of microcrystalline silicon thin films and solar cells. Investigation of potential distributions at grain boundaries in semiconductors and semiconductor devices by holographic imaging.	2342004
Dr. P. Schall	Feodor-Lynen-Program of the Humboldt Foundation	2310204
Dr. K. Tillmann	Quantitative analysis of semiconductor heterostructures by high-resolution transmission electron microscopy and finite element simulations	2342004
Dr. M. Yurechko	Scanning tunneling microscopy of semiconductors and quasicrystals	2310204, 2342004
Doctor students		

S. Balanetskyy	Formation of intermetallic phases in ternary alloys of aluminium with palladium and a second transition metal	2310204
J. He	Investigation of electroceramic thin films by high resolution electron microscopy	2342004
M. Heggen	Plasticity of quasicrystals and complex intermetallic phases	2310204
N. Hüging	Investigation of Strain Fields and Structural Defects in Helium Implanted Silicon	2342004
N. Jäger	Effects of individual dopant atoms on the electronic properties of GaAs investigated by scanning tunneling microscopy and spectroscopy	2342004
M. Liatti	Signal / noise optimisation in superconductor heterostructures	2342004
S. Mi	Formation of intermetallic and quasicrystalline phases in ternary alloys of aluminium with transition metals	2310204
U. Semmler	Diffusion and dynamic effects on compound semiconductor surfaces	2342004
Guests		
J. Gebauer	UC at Berkeley, STM of semiconductors	2342004

23102.04 **Condensed Matter**
23420.04 **Materials, processes and devices for the micro- and nanoelectronics**

Atomic Resolution Imaging of Oxygen in Perovskite-Based Ceramics Employing a Novel Imaging Mode

C. L. Jia, M. Lentzen and K. Urban
Institut für Festkörperforschung, Forschungszentrum Jülich GmbH, 52425 Jülich, Germany

Employing a novel imaging mode based on the adjustment of a negative value of the spherical-aberration coefficient of the objective lens of a transmission electron microscope, we successfully imaged all types of atomic columns in the dielectric $SrTiO_3$ and the superconductor $YBa_2Cu_3O_7$, in particular, the oxygen atoms [1]. This allowed us to detect local non-stoichiometries or the degree of oxygen-vacancy ordering. This technique offers interesting opportunities for research into the huge group of perovskite-derived electroceramic materials in which the local oxygen content sensitively controls the electronic properties.

F&E-Nr: E 2342004

The microstructure of perovskites can be studied by means of high-resolution transmission electron microscopy (HRTEM). Under suitable conditions it is possible to image the cation columns projected along the viewing direction. As the cations have a high nuclear charge, their scattering power is high, resulting in strong phase contrast. In comparison, due to the relatively low scattering power, it is difficult to image the oxygen sublattice. In this study we used a transmission electron microscope (TEM) with a field-emission gun operated at an accelerating voltage of 200 kV. It is equipped with an electromagnetic hexapole system which allows for the correction of the spherical aberration of the objective lens [2]. As measured by the Young's fringe technique this instrument offers an information limit better than 0.13 nm [3]. A comparison with the atomic distances occurring in the projection of $SrTiO_3$ along the crystallographic [110] direction (Fig. 1a) indicates that this should be sufficient to resolve all the atom positions in the compound, including those of oxygen, provided that there is sufficient contrast.

We find that the aberration correction system in our microscope, initially designed to compensate the original C_S = 1.23 mm to zero, offers the great advantage that, by proper excitation of the hexapoles, C_S can be continuously adjusted within wide limits. This means that we have now two parameters, C_S and the defocus ΔZ, available to tune the microscope for optimum contrast. We find that compensating the aberration not to zero but to the small residual value of 40 µm and combining this with an underfocus of ΔZ = −8 nm should result in good contrast up to the information limit of the microscope. The progress achieved in this way is demonstrated by the calculated images displayed in Fig. 1. The strongly blurred and inadequate image obtained from $SrTiO_3$ without aberration correction is given in (b). The image obtained under the new conditions is given in (c). The strontium atoms give strong contrast and in between a horizontal dark band occurs at the position of the titanium-oxygen atom rows.

Exploiting the excitation range of the hexapoles even further, we find that we can overcompensate the objective-lens aberration resulting in negative C_S values. The intriguing result is that combining this negative value with the adjustment of an overfocus the contrast not only becomes inverted, i.e. atoms appear bright on a dark background, but it also increases steeply. In Fig. 1 (d) calculated employing C_S = −40 µm and ΔZ = +8 nm the atomic images are now very sharp and oxygen can be seen well separated from titanium. That this imaging condition provides us with real atomic resolution can be tested by calculat-

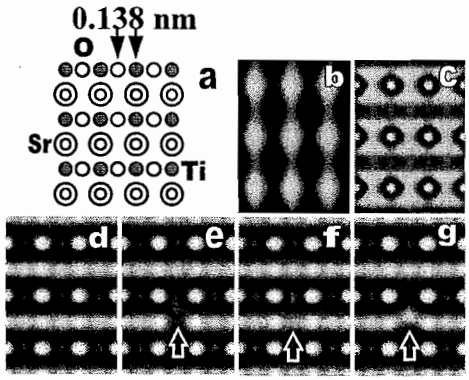

Fig. 1. Calculated images of $SrTiO_3$ demonstrating the improvement in point resolution. (A) Structure projected along the [011] crystal direction. (B) Image under Scherzer focus conditions in the uncorrected instrument; C_S = 1.23 mm, ΔZ = − 68 nm and 8.4 nm^{-1} for the diameter of objective lens aperture. (C) Image for C_S = +40 µm and ΔZ = −8 nm. (D) Image for the new imaging mode adjusting for C_S = − 40 µm and ΔZ = +8 nm. The calculations here are carried out for a specimen 4 nm thick. The fact that real atomic resolution is obtained is demonstrated by calculations for (E) an empty oxygen column, (F) a 50 % oxygen occupancy, and (G) a shift of the oxygen column by 0.05 nm. The effect on contrast is localized at the single atomic column (arrow).

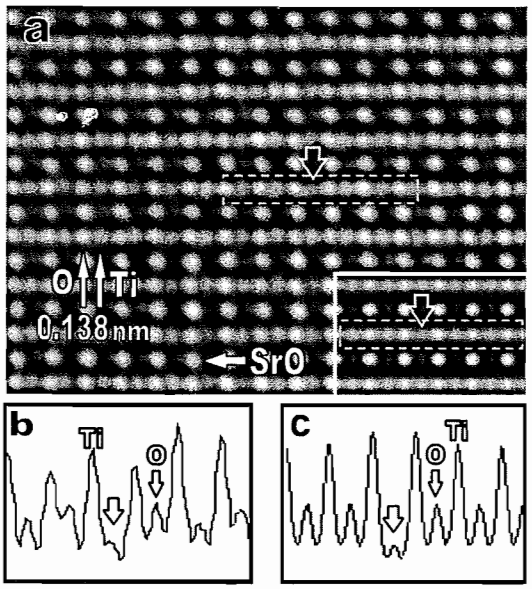

Fig. 2. (a) Experimental image of $SrTiO_3$ [110] with a specimen thickness of 4 nm, a spherical aberration of –40 μm, and a defocus of 8 nm: at the oxygen column marked with an arrow the local intensity is reduced. The inset shows a simulated image with an occupancy of 70% of one of the oxygen columns. (b) Intensity trace along the columns framed in (a): at the oxygen column marked with an arrow the local intensity is reduced. (c) Simulated intensity trace with an occupancy of 70% of one of the oxygen columns.

ing images for which the occupancy of a single atomic column of oxygen is set to 0 % (e) and to 50 % (f). The effect of displacing the column by 0.05 nm along the [001] direction is shown in (g). From the image it is apparent that the change in contrast is restricted to the selected atomic column. The contrast is rather robust with respect to a variation of the imaging conditions. The sample thickness can vary between 2.5 and 5.0 nm and the defocus value between 7 and 12 nm without seriously changing the contrast.

Fig. 2 shows an experimental image of $SrTiO_3$ [110] for C_S = –40 μm and ΔZ = +8 nm. It demonstrates the extraordinary quality of the images and the fact that the oxygen-atom columns can be seen and studied individually. At positions marked by an arrow the oxygen-atom contrast is weaker than in the neighbouring oxygen positions. This is shown by the intensity trace in (b). The calculated image in the inset, evaluated in the inset (c), perfectly matches the experimental data indicating that the occupancy of the oxygen columns is only 70 % of the stoichiometric value.

Fig. 3(a) shows the application of the negative-C_S imaging mode to $YBa_2Cu_3O_7$ [100]. Comparison with the structure model indicates that, besides the cations Ba, Y, and Cu, we image oxygen at atomic resolution in the CuO-chain planes marked by arrows, in the CuO_2-planes and in the BaO-planes. Dark contrast on both sides of the Y-atom supports the absence of oxygen in agreement with the structure model. Information on oxygen-vacancy ordering can be obtained by inspection of the [010] image of $YBa_2Cu_3O_7$ in Fig. 3(b) and a comparison of the atom contrast in the Cu-O-chain planes with that of Fig. 3(a). Since these two images show the two sample areas crystallographically tilted by 90° around a vertical axis with respect to each other, the horizontal atom rows seen in (a) are seen end-on in (b). We recognize that in (b), in the Cu-O-chain planes, the atom positions between the Cu-atoms are empty while they are occupied by oxygen in (a).

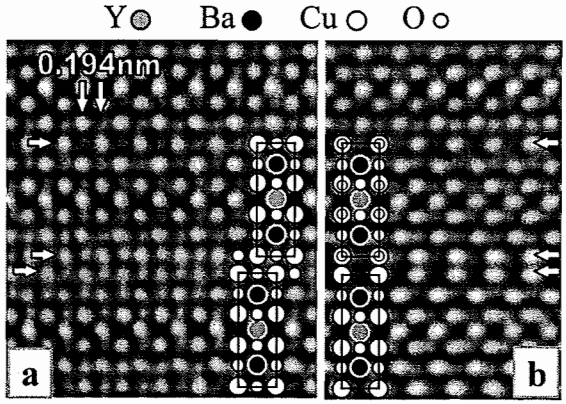

Fig. 3. (a) Experimental image of a stacking fault in $YBa_2Cu_3O_7$ [100] with a spherical aberration of –40 μm and a defocus of around 12 nm. (b) Experimental image of a stacking fault in $YBa_2Cu_3O_7$ [010] with spherical aberration of –40 μm, and a defocus of 12 nm.

In both images, Fig. 3(a) and (b), a stacking fault also occurs as indicated by two pairs of arrows. The two pictures were taken at different locations of the sample. They are, however, arranged in such a way that they represent two views, tilted by 90° with respect to the vertical axis, of the same type of fault. The shift by one half of the [010] lattice parameter in Fig. 3(a) and the occurrence of a Cu-O double layer in (b) indicates a so-called "124" fault since periodic arrangements of such faults occur in the structure of $YBa_2Cu_4O_8$ [4]. In Fig. 3(b) the enhanced white spot contrast of the Cu-O atom columns in the fault provides evidence of a high oxygen occupancy and highly perfect ordering. This can be explained by particularly strong Cu-O bonds along the [010] direction [5]. The study of such atomic detail including both the cation and the oxygen sublattices provides access to stoichiometric and structural defects in ferroelectric and superconducting heterostructures which have long been known to hamper their performance in microelectronic applications but could not so far be investigated in detail.

[1] C.L. Jia, M. Lentzen and K. Urban, Science, in press.
[2] M. Haider, et al., *Nature* **392**, 768 (1998).
[3] M. Lentzen, et al., *Ultramicroscopy* **92**, 233 (2002).
[4] H.W. Zandbergen, R. Gronsky and K. Wang, G. Thomas, *Nature* **331**, 596 (1988).
[5] D.E. Morris, et al., *Phys. Rev. B* **40**, 11406 (1989).

Ordering of Ruthenium Nanoscale Particles in the $SrRuO_3$ Buffer Layer in $SrTiO_3/SrRuO_3$ Bilayer Films on $SrTiO_3$ Substrate

Y.L. Qin[1], C.L. Jia[1], J.H. Hao[2] X.X. Xi[2], K. Urban[1]
[1]*Institut für Festkörperforschung, Forschungszentrum Jülich GmbH, D-52425 Jülich, Germany*
[2]*Department of Physics, The Pennsylvania State University, University Park, Pennsylvania 16802, USA*

A structural grate pattern is observed in the $SrRuO_3$ buffer layer in a $SrTiO_3/SrRuO_3$ bilayer system on (001) $SrTiO_3$ substrate. By means of high resolution transmission electron microscopy the grate fringes are identified as a band of planar defects with decoration of nanoscale precipitate particles. The planar defects are Sr-rich Ruddlesen-Popper defects occurring in the (100) and (010) planes. The precipitate particles are either Ru-rich phase or pure Ru crystals.

F&E-Nr: E 2342004

The microstructure and lattice defects of thin films have a dominant effect on the electrical properties, and therefore have attracted great attentions in perovskite oxide systems. In addition, there has been a broad interest in searching for methods to fabricate ordered structures for potential property engineering and technological applications [1]. A highly ordered structure pattern induced by strain was observed in $La_{1-x}Ca_xMnO_3$ (LCMO) films [2]. This pattern structure is believed to enhance the low field megnetorresistance.

In this work, we report on an ordered structure of Ru-rich nanoparticles in the $SrRuO_3$ (SRO) buffer layer in $SrTiO_3$(STO)/SRO bilayer films on STO substrate. The bilayer STO/SRO films were grown by PLD on single crystal STO substrates [3].

Fig. 1(a) is a low magnification transmission electron microscope (TEM) micrograph of a plan-view sample. An structural grate pattern can clearly be seen in the SRO film. The horizontal and vertical grate fringes are along the <100> directions of STO. At a high magnification the fringes look as ribbons with a width of about 6 nm. Fig. 1(b) shows the details of such a ribbon. It is evident that the ribbons are composed by small particles embedded in the faulted lattice areas. The average size of the particles is in the order of several nanometers. Along the ribbon/matrix boundary, stacking faults are frequently observed, as marked by arrows. Image simulation showed that the lines with brighter dots correspond to the SrO layers, while those with weak contrast are RuO_2 planes. The double row of strong dots at the boundary corresponds to double SrO plane with a projected displacement of *a/2*[110]. This planar defect is Ruddlesen-Popper (RP) type planar defect. The RP defects were also observed by Wu *et al.* in the SRO films grown on $LaAlO_3$ substrate [4].

In the cross-sectional samples these ribbons are found along the [001] direction only, i.e. the film growth direction. Fig. 2(a) shows a low magnification cross-sectional image of the bilayer STO/SRO film on

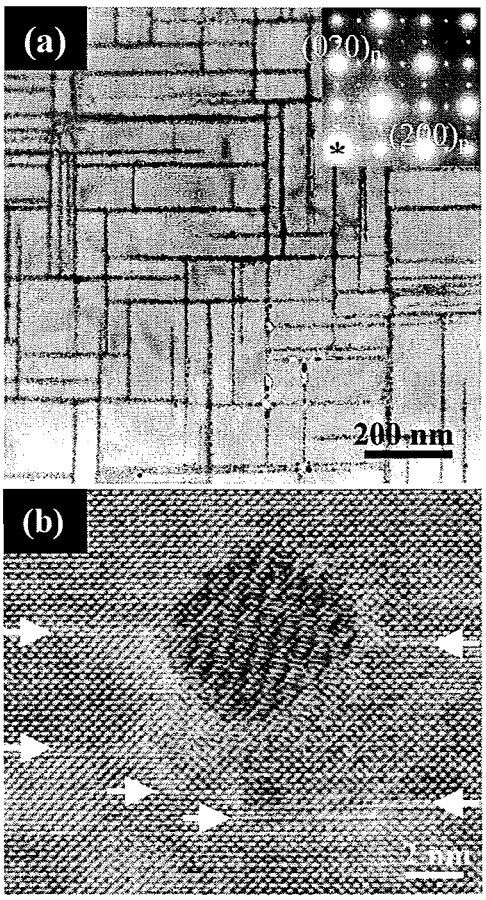

Fig. 1. (a) Plan-view TEM image of a $SrRuO_3$ film on the $SrTiO_3$ substrate. Inset is a quarter of an electron diffraction pattern. The central spots are indicated by an asterisk and indexing is based on the pseudo-cubic perovskite structure. (b) HREM image, showing the details of a ribbon. A particle is clearly seen at the boundary, arrows denote the boundaries.

STO taken along the [100] direction. High density defects were found in the top STO film. In contrast, except the ribbon structure, the SRO layer looks very clean. Most ribbons run from the substrate surface to the SRO layer. Fig. 2(b) is a low magnification HREM

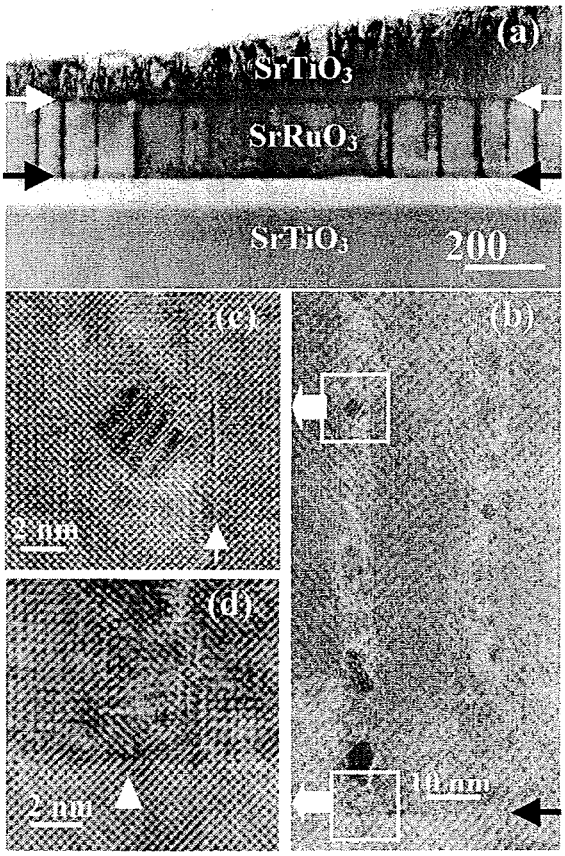

Fig. 2. (a) Cross-sectional picture of a STO/SRO bilayer on STO substrate taken along [100]. Arrows mark the interface between the STO and SRO films (white), and that between SRO film and STO substrate (black). (b) An HREM image at low magnification of a SRO film on the STO substrate, showing two ribbons with RP defects and small particles. The interface is marked by a black arrow. One of particles is shown in (c); and (d) shows the details of the interface between the left ribbon and substrate. A dislocation is indicated by an arrowhead.

image, showing two ribbons. The left ribbon grows from the interface (black arrow), and the right one is formed about 30 nm above the interface.

In the cross-sectional view, the ribbons show the same structure details as in the plan-view. Fig. 2(c) shows a small particles. The RP-defects can also be seen as marked by an arrow. Because of the small mismatch (~0.6 %) between SRO and STO, the perfect interface between SRO film and STO substrate is free of misfit dislocation.

However, dislocations are frequently observed in the ribbons either at the interface (the left one) or above the interface (the right one). Fig. 2(d) is a magnified picture of the area marked by the bottom frame in Fig. 2(b). A dislocation is indicated by an arrowhead. Employing a Burgers circuit, the Burgers vector of the dislocation is determined to be a[010].

By means of energy dispersive x-ray spectroscopy (EDX) much higher concentration of Ru was measured in the particles than in the film matrix. According to the image simulations, it is suggested that the particles are either Ruthenium oxides (RuO_2) or pure Ru crystal. More detailed work is necessary to unambiguously identify the two phases.

It is well known that strain and defects can provide energetically favorable sites for precipitate nucleation. The strain can result from either the lattice mismatch or/and the difference in thermal expansion coefficients between film and substrate. The ordered structure in LCMO films was identified to be induced by the strain resulting from the large difference in thermal expansion coefficients between film and substrate at high temperature [2]. In fact, LCMO has the same $GdFeO_3$-type structure as SRO but with a larger lattice mismatch than SRO to the STO substrate. From high-temperature structural studies [5], the thermal expansion coefficient of SRO is estimated to be 3.5×10^{-5}/T, which is not much different from that of STO (1.0×10^{-5}/T) [6]. Therefore, consideration of the strains induced from the lattice mismatch and thermal expansion difference only is not sufficient to explain the formation of the ordered structure in our SRO film.

From Fig. 1 and Fig. 2, the Ru-rich nanoparticles are always found to be combined with the RP defects. In the perovskite structure, the RP defect is a kind of non-conservative antiphase boundary in the {100} planes with a crystallographic displacement of a/2<111> [7]. It usually occurs in Sr-rich $(SrO)(SrTiO_3)_n$ phases, where n is the number of perovskite layers separating the defects [8]. This kind of planar defect is believed to be mainly introduced in the initial stage of film deposition and play an important role in the generation of misfit dislocation. We think that the pattern in our work can also be explained by this RP defect. At the initial stage of film growth, the deposition process may deviate from the stable conditions so that composition fluctuation is expected. The composition fluctuation may lead to the formation of the RP defects along the film growth direction. The formation of the RP planar defects results in a local Sr-deficient area, and leads to the formation of the Ru-rich precipitates.

[1] N. Bowden *et al.*, Nature (London) **393**, 146 (1998).
[2] H.B. Peng *et al.*, Phys. Rev. Lett. **82**, 362 (1999).
[3] H.C. Li, W.D. Si, A.D. West, and X.X. Xi, Appl. Phys. Lett. **73**, 190 (1998).
[4] J.S. Wu *et al.*, J. Crystal growth **234**, 603 (2002).
[5] B.J. Kennedy and B.A. Hunter, Phys. Rev. B **58**, 653 (1998).
[6] K. Char, L. Antognazza, and T.H. Geballe, Appl. Phys. Lett. **63**, 2420 (1993).
[7] S.N. Ruddlesden, and P. Popper, Acta Cryst. **11**, 54 (1958).
[8] R.J.D. Tilley, J. Solid State Chem. **21**, 293 (1977).

Dopant Induced Stabilization of LT-grown AlAs/GaAs:Be Multiple Quantum Wells and Superlattices against Thermally Activated Intermixing

K. Tillmann and M. Luysberg

Institut für Mikrostrukturforschung

The structural degeneration of interfaces in AlAs/GaAs:Be heterostructures epitaxially grown at low temperatures has been analysed by high-resolution transmission electron microscopy. Numerical data on the layer stoichiometry obtained by the quantitative analysis of high-resolution micrographs are used to calculate diffusion parameters controlling the exchange of aluminium and gallium atoms. Analyses demonstrate that beryllium doping of the GaAs layers decreases the interfacial mixing by up to one order of magnitude and results in an activation enthalpy enhanced by about 0.5 eV compared to the undoped heterostructures. The results lead to the conjecture that the diffusion process is governed by the defect related electronic properties close to the interfaces or the formation of defect complexes rather than by the pure concentration of gallium vacancies.

F&E-Nr: 2342 8000

Within recently AlAs/GaAs multiple quantum wells (MQWs) and superlattices (SLs) grown at low temperatures (LT) of about 200°C have become an object of intense research as they show great promise for ultrafast electronic device structures [1]. Due to a high concentration of gallium vacancies mediating the exchange of group III atomic species and the precipitation of excess aresenic these heterostructures, however, undergo an enhanced interfacial mixing compared to layers grown at standard temperatures [2]. On the other, beryllium doped GaAs:Be material shows a far better stability against the condensation of charged excess arsenic atoms towards precipitates [1], whose spatial distribution is well correlated with the local electrical field distribution of corresponding LT-AlAs/GaAs:Be MQWs [3]. Therefore, it is reasonable to assume that the doping with beryllium will also improve the stability of LT-grown AlAs/Gaas structures against intermixing upon thermal treatment.

In the present study high-resolution transmission electron microscopy (HRTEM) was used to quantify the impact of the beryllium dopant concentration on the interface stability of LT-grown AlAs/GaAs:Be MQW and SL structures. Heterostructures with nominal AlAs layer thicknesses d_n of 5.0 nm (equivalent to 17.7 (002)-monolayers; MQW) and of 1.7 nm (6.0 monolayers; SL) were grown by molecular beam epitaxy at a temperature of 210°C choosing a V/III beam equivalent pressure ratio of 20 and a growth rate of 0.5 μmh^{-1}. A reciprocal space modification [4] to classical chemical mapping [5] was implemented to measure concentration profiles x_{Al} *(z)* across interior interfaces. As sketeched in Figure 1, this approach bascially implies extracting the (002) beam intensity distribution I_{002} *(x, z)* from HRTEM images which is directly linked with the local layer composition [4].

Experimental data on the concentration profiles as expressed by the nominal AlAs layer thickness d_n together with the interfacial roughness parameters λ_{lo} and λ_{up} of the as-grown heterostructures and of samples annealed between 600°C and 900°C served as input parameters for numerical evaluation of the interdiffusion coefficient in dependence on the anneal temperature T applied. Assuming non-linear diffusion behaviour, the coefficient $D(T)$ for the

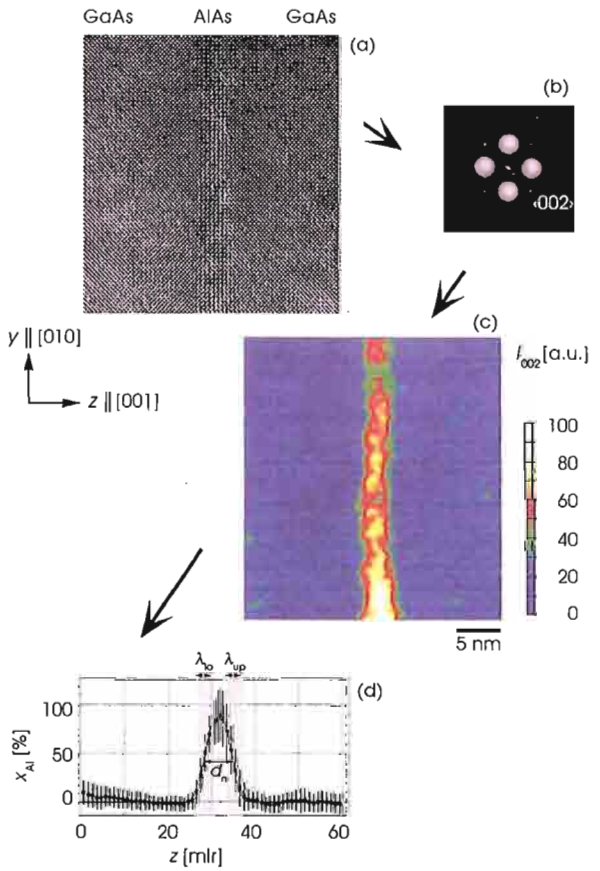

Figure 1: Schematic representation of basic procedures applied for the measurement of compositional profiles. (a) High-resolution micrograph taken with an aberration corrected Philips CM-200-C instrument under chemically sensitive imaging conditions showing a GaAs:Be/AlAs/GaAs:Be interface of a superlattice system annealed for 30 min at 750°C. (b) Diffractogram with the grey shaded areas indicating the positions of Gaussian apertures successively convoluted with the Fourier transform of the image and used to evaluate the (c) beam intensity distribution I_{002} (x, z). (d) Compositional profile x_{Al} (z) along the [001] growth direction of the SL. The solid curve represents a least square fit of the diffusion profile to the experimental data yielding d_n = 6.73 ± 0.30 mlr, λ_{lo} = 2.09 ± 0.29 mlr and λ_{up} = 2.17 ± 0.30 mlr for the nominal layer thickness

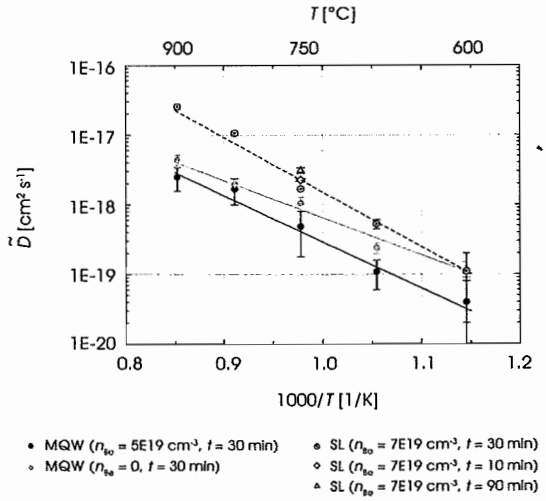

Figure 2: Diffusion coefficient D (T) for the intermixing of Al and Ga. Solid curves represent least square adaptions to the experimental data (•) obtained for the AlAs layers embedded in undoped GaAs (darker grey curve) and in beryllium doped GaAs:Be (black curve) of the MQWs together with the dashed curve fitted to the data measured for an AlAs/GaAs:Be SL.

intermixing between aluminium and gallium may be expressed in its most simple form as

$$D(T) = D_{Ga}(T)\,[x_{Al} + (1 - x_{Al})\,\xi] \qquad (1)$$

with $D_{Ga}(T)$ denoting the gallium diffusion coefficient in pure AlAs and ξ representing the ratio $D_{Ga}(T)/D_{Al}(T)$ for which previous analyses demonstrated a numerical value of about 15 independent of the anneal temperature applied [6].

Correspondingly obtained experimental results summarized in Figure 2, clearly demonstrate a reduced mixing for highly doped GaAs:Be (n_{Be} = 5e19 cm^{-3}) compared to undoped GaAs layers grown under identical conditions. The corresponding effective activation enthalpies H_{eff} amount to 1.0 eV (n_{Be} = 0) and to 1.4 eV (n_{Be} = 5e19 cm^{-3}) while even higher values of 1.7 eV are found when focusing on ultrathin AlAs/GaAs:Be superlattices (n_{Be} = 7e19 cm^{-3}) grown under similar conditions [7]. Independent of the doping concentration, these values are extraordinary low compared to $H_{eff} \approx 6$ eV as measured for heterostructures grown at standard temperatures of about 600°C. This difference is due to the fact that mobile gallium vacancies have first to be nucleated in intrinsic materials, thus requiring a formation enthalpy, which was shown to be in the order of 3.0 eV to 4.0 eV in addition to the migration enthalphy about 1.8 eV describing the motion process of the diffusion atoms [5], while a high concentration of vacancies is already present when layers are grown under LT conditions.

In the general, $D(T)$ values measured for the ultrathin SL system are higher compared to the MQW structures. This "apperently" higher degree intermixing will be due to the smaller nominal layer thickness of the superlattices. If the peak values of x_{Al} fall well below 1.0 the flux of aluminium atoms is no longer energised from a virtually infinite AlAs layer but from a layer which additionally needs to broaden to "provide" further atoms. In this case the intermixing takes mainly place between areas of low aluminium content, where the $D(T)$ values according to eqn. (1) will be locally increased compared to intermixing processes taking place in the high x_{Al} regime.

At least for mechanisms may be considered to explain the deceleration of the intermixing by means of the beryllium dopants, namely:

(i) a reduction of the gallium vacancy concentration due to an occupation of corresponding lattice positions by the beryllium dopant atoms which, however, may be ruled out with the utmost probability since positron annihilation measurements demonstrated no effect of the dopant concentration on the gallium vacancy concentration,

(ii) a lattice parameter reduction of the the doped GaAs:Be layers exacerbating the permeation of the larger aluminium atoms into the compressively strained GaAs:Be layers,

(iii) the formation of dopant-vacancy defect complexes whose binding energy has to be overcome to allow the gallium vacancies to contribute to intermixing processes thus yielding an additional contribution to the total activation enthalpy, and

(iv) changes in the position of the Fermi level induced by the beryllium dopants, which may alter the concentration of charged point defects close to the interfaces and thus have an impact on the concentration and the mobility of charged gallium and aluminium atoms. Indeed, detailed analyses demonstrate that the observed increase of H_{eff} values with increasing beryllium doping concentrations is well correlated with the dopant induced bending of the electronic bands thus influencing the movement of charged gallium vacancies and, consequently, the interfacial mixing [3].

Acknowledgements

The congenial co-operation with P. Specht, M. Cich and E.R. Weber (University of California, Berkeley, US) as well as with A. Fattah (IFF, Research Centre Jülich) is greatly acknowledged.

References

[1] Nolte, D.D., *J. appl. Phys.* **85**, 6259 (1999).
[2] Balasubramanian, S., Nolte, D.D. and Melloch, M.R., *J. appl. Phys.* **88**, 4576 (2000).
[3] Tillmann, K., Luysberg, M., Cich, M., Specht, P. and Weber, E.R., *Proc. 3rd Symp. on Non-Stoichiom. III-V Comp.*, edited by S. Malzer and T. Marek, Erlangen (Bavaria), 79 (2002).
[4] Tillmann, K., Luysberg, M., Specht, P. and Weber, E.R., *Ultramicroscopy* **93**, 123 (2002).
[5] Rouviere, J.L., Kim, Y., Cunningham, J., Rentschler, J.A., Bourret, A. and Ourmazed, A., *Phys. Rev. Lett.* **68**, 2798 (1992).
[6] Bracht, H., Haller, E.E., Eberl, K. and Cardona, M., *Appl. Phys. Lett.* **74**, 49 (1999).
[7] Tillmann, K., Luysberg, M., Specht, P. and Weber, E.R., *Inst.Phys. Conf. Ser.* **169**, 101 (2001).

Quantitative Transmission Electron Microscopy Analysis on the Gas Pressure of Helium Filled Nanocavities in Implanted Silicon

N. Hüging, K. Tillmann, M. Luysberg and H. Trinkaus[£]

Institut für Mikrostrukturforschung
[£]Institut Theorie III

For the first time, the gas pressure of crack-shaped nanocavities formed in silicon upon implantation with helium and subsequent annealing has been directly quantified from diffraction contrast features visible in transmission electron micrographs taken under dynamical two-beam conditions. For this purpose simulated images, based on the elastic displacements associated with a Griffith crack, have been matched to experimental micrographs thus yielding unambiguous data on the ratio p/μ of the cavity gas pressure to the silicon matrix shear modulus. Experimental results demonstrate cavity radii of some ten nanometres and p/μ values up to 0.22, which may be regarded as sufficiently high for the emission of dislocation loops from the nanocavities.

F&E-Nr: 2342 8000

Most recently, helium filled nanocavities formed in silicon upon implantation and subsequent thermal treatment have become an object of particular interest in microelectronics since, when nucleated in the substrate area of lattice mismatched GeSi/Si(001) heterostructures, the plastic relaxation of these overpressurized inclusions represents a highly efficient pathway in the reduction of the threading dislocation density inside the GeSi epilayers [1]. For these purposes, the elastic stress fields associated with the cavities, whose size and spatial arrangement may be well adjusted by proper process control during helium implantation and subsequent thermal annealing, act as nucleation sources during the formation of dislocation loops gliding to the heterointerfaces from the substrate area thus circumventing the formation of threading dislocations usually penetrating the epilayers from the free surfaces. In this context the ratio p/μ of the cavity gas pressure to the silicon matrix shear modulus is a most critical parameter with respect to the efficiency of the relaxation process [2].

In the present study nanocavities formed in silicon upon implantation with helium at room temperature and subsequent thermal annealing at 400 C for 1 min > t > 70 min have been subjected to a detailed structural analysis using quantitative transmission electron microscopy in tandem with specially developed numerical analysis and simulation algorithms. In general, electron diffraction contrast imaging is a versatile tool for the visualisation of local lattice strains with respect to an undisturbed crystal and full quantification requires the adoption of simulated images to experimental micrographs or, at least, the fitting of representative contrast features.

In the present case, arc shaped bright-dark diffraction contrast lobes visible in electron micrographs taken under dynamical two-beam excitation conditions, cf. Figure 1(a), have been used to measure the elastic strain fields in the proximity of the cavities. To this end the six outermost local extrema positions A_i extracted from intensity line profiles perpendicular to the crack plane, i.e. along the direction of the imaging vector **g**, cf. Figure 1(b), have been fitted by simulated profiles as shown in Figure 1(d). These simulations are based on analytical expressions of the elastic strain distribution associated with a Griffith crack [3] as described by the linear theory of elasticity. Dynamical electron scattering is taken into account in the framework of the column approximation using experimentally used imaging and specimen input parameters (specimen thickness t obtained by convergent beam electron diffraction, effective deviation parameter s measured from diffraction patterns and crack radii r_0 determined by large angle tilt experiments) together with a continuous variation of the p/μ ra-

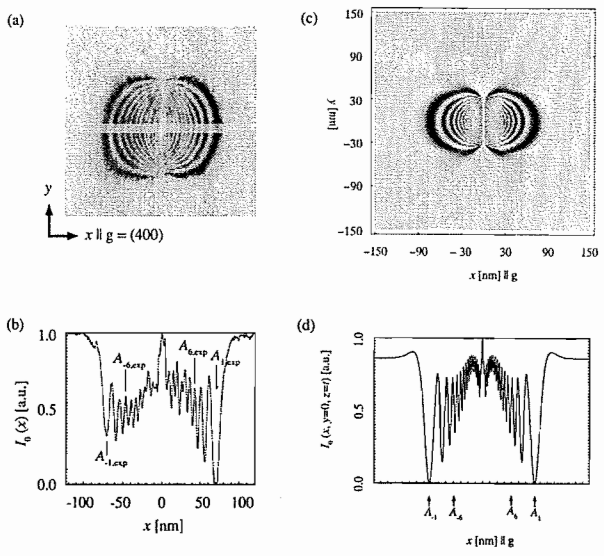

Figure 1: (a) Bright-field micrograph of a helium filled cavity in silicon taken from a cross-sectional sample oriented along the [110] direction and recorded under two-beam imaging conditions. (b) Intensity line profile measured perpendicular to the crack plane. (c) Calculated image assuming **g** *= (004), an effective deviation parameter s = 0.03, a sample thickness t = 300 nm, U = 200 kV, an imaginary part of the Fourier coefficient of the lattice potential of 0.05 thus taking absorption into account, a nanocavity radius r_0 = 30 nm and p/μ = 0.15 together with the (d) correspondingly calculated intensity line profile. Intensity extrema positions of the experimental profile (b) well coincide with the calculated positions (d) indicating an optimal adaption.*

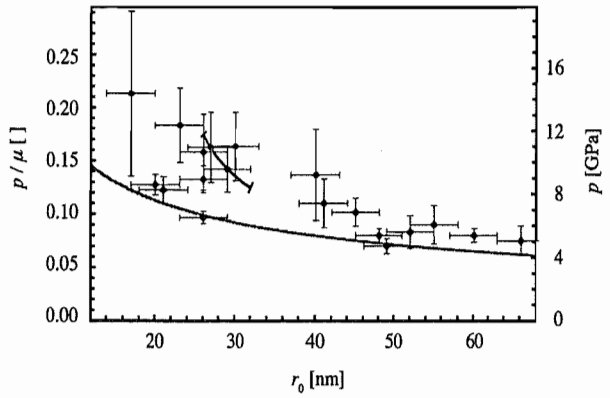

Figure 2: Experimentally measured nanocavity p/μ ratio in dependence on the radius r_0 of individual cavities together with an equilibrium curve for a Griffith crack assuming a specific free interface energy of 1.4 Jm^{-2}.

tio. Systematic analyses demonstrate that under suitable imaging conditions, the positions of the line profile intensity minima are most sensitive exclusively on the the p/μ ratio, which ensures a non-ambiguous determination of the nanocrack pressure [4,5].

Independent of the anneal time chosen, the experimental results demonstrate $0.07 < p/\mu < 0.22$ for cavity radii in the range 70 nm > r_0 > 20 nm, cf. Figure 2. The observed behaviour $p/\mu \propto 1/\ r_0$ gives evidence that the cavities are in approximate equilibrium with the silicon matrix under the anneal conditions applied. Minor deviations in the exact numerical values between experimental data and theoretical predictions [6] well below 20 % may be due to model assumptions concerning the linearity of the elastic material behaviour, the neglect of elastic anisotropy of silicon or due to increased free interface energies compared to previously reported data measured at significantly higher temperatures compared to our room temperature experiments [4, 7].

When not activating untypical glide systems at elevated temperatures, the nucleation and movement of mobile 60^0 dislocations usually takes place on {111} slip planes in silicon. Applying the criterion that shear stress values of about $\mu/2\pi$ 11 GPa will be necessary for expelling dislocation loops from areas close to the rim of the nanocavities, the shear stress distribution σ_b (ζ', ζ'') inside the (ζ', ζ'') slip plane shown in Figure 3 clearly indicates an intrinsic instability of the cavities to relax, e.g. by the formation of dislocation loops. This prediction, which needs further investigations, e.g. by performing microscopic *in-situ* experiments, will be especially true, when focusing on lattice mismatched heterostructures, e.g. GeSi epilayers on implanted silicon substrates, where image forces will additionally contribute to the pull out of dislocations from the overpressurized nanocracks.

Acknowledgements

The authors cordially thank B. Holländer and S. Mantl (ISG, Research Centre Jülich) for congenial co-operation during realization of the implantation experiments as well as for fruitful and inspiring discussions.

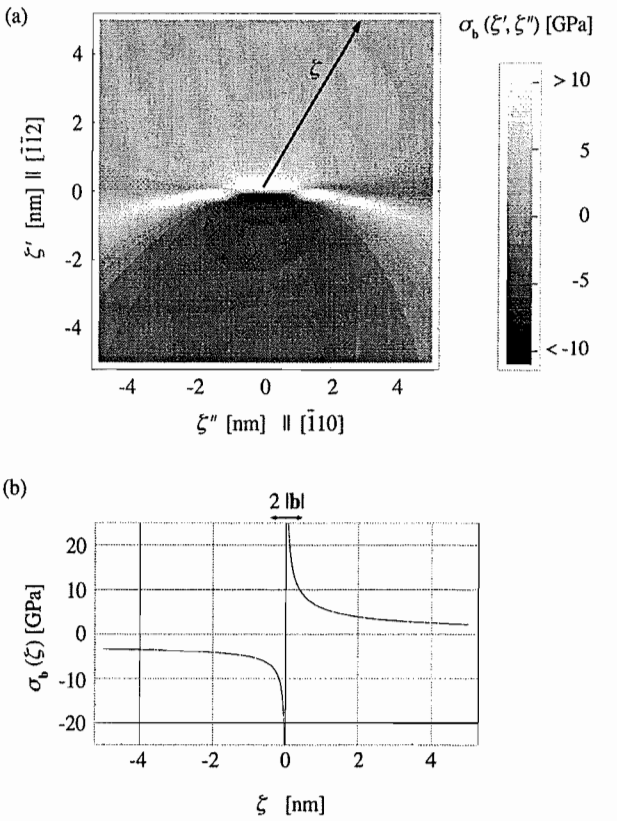

*Figure 3: (a) Contour representation of the elastic shear stress σ_b projected along the [110] direction of the Burgers vector **b**, which runs along the ζ direction inside the {111} slip plane together with (b) a line profile along the ζ direction touching the rim of the nanocrack at $\zeta = 0$.*

References

[1] Luysberg, M., Kirch, D., Trinkaus, H., Holländer, B., Lenk, S., Mantl, S., Herzog, H.J., Hackbarth, T. and Fichtner, P.F.P., *J. appl. Phys.* **69**, 4290 (2002).

[2] Trinkaus, H., Holländer, B., Rongen, S., Mantl, S., Herzog, H.J., Kuchenbecker, J. and Hackbarth, T., *Appl. Phys. Lett.* **76**, 3552 (2000).

[3] Sneddon, I.N, *Proc. Roy. Soc. London A* **187**, 229 (1946).

[4] Hüging, N., *Diploma Thesis* RWTH Aachen (2002).

[5] Hüging, N., Tillmann, K., Trinkaus, H. and Luysberg, M., *Proc. ICEM-15. Vol.* **1**, 99 (2002).

[6] Hartmann, M. and Trinkaus, H., *Phys. Rev. Lett.* **88**, 055505 (2002).

[7] Tillmann, K., Hüging, N., Trinkaus, H. and Luysberg, M., submitted to *Microscopy & Microanalysis* (2002).

Nanoscale dopant-induced dots and potential fluctuations in GaAs

N. D. Jäger [1], E. R. Weber [2], and Ph. Ebert [1]
[1] *Institut für Festkörperforschung, Forschungszentrum Jülich, 52425 Jülich, Germany*
[2] *University of California and Lawrence Berkeley Laboratory, Berkeley, CA 94720, U.S.A.*

We identified *p*-type nanoscale dopant-induced dots that are formed by fluctuations of the dopant atom distribution in thin GaAs *p-n* multilayers. Their electronic structure and the resulting potential variations were investigated by cross-sectional scanning tunneling microscopy and spectroscopy as a function of the number of dopant atoms within the dot. We find significant changes in the current-voltage characteristics of the dots compared to spatially non-confined material, due to a reduced ability to screen the tip's electric field. This indicates a limited ability to deplete the dots of free holes arising from the presence of confining potentials.

State-of-the-art semiconductor devices consist of structures with dimensions as small as 70 nm defined by the gate length of the transistors. Research is focusing on a further reduction to 20-30 nm. At such small dimensions the electrical potential distribution within the devices cannot be treated as continuous anymore. The potential is rather governed by individual, discrete ionized dopant atoms. Consequently, always present fluctuations in dopant distribution [1] limit the achievable miniaturization of semiconductor devices, by introducing variations in individual device characteristics, such as turn on voltage and noise level spectra. Although this problem is of key importance, it has turned out that a simultaneous direct experimental access to individual dopant atoms and the corresponding potential distributions is a very difficult task. We solved this task by using cross-sectional scanning tunneling microscopy (STM) and spectroscopy (STS) [2]. We present a direct experimental proof of local variations of electronic characteristics and potential induced by fluctuations of the dopant atom distribution on the tens of nanometer scale. We show that in *n-p-n* GaAs layer structures such fluctuations lead to localized nanoscale dopant-induced dots spatially confined by potential barriers, whose properties change drastically due to the spatial confinement of the free charge carriers even at room temperature.

The structure investigated consisted of alternating 30 nm thick *p*- and *n*-doped GaAs(001) layers grown by MBE, with C and Si dopant concentrations of $(5 \pm 1) \times 10^{18}$ cm^{-3} and $(4 \pm 1) \times 10^{18}$ cm^{-3}, respectively. The sample was cleaved in ultrahigh vacuum to expose a (110) cross-sectional view of the layers, which was imaged by STM with atomic resolution at room temperature.

Figure 1 shows a sequence of several *n*- and *p*-doped layers, which we identified on basis of the growth sequence and current-voltage spectra [3]. At the interface between *n*- and *p*-doped layers the presence of a depletion zone gives rise in STM to a dark line [4]. The bright hillocks are signatures of the individual dopant atoms [5]. For the present work the *p*-doped layer on the right hand side of Fig. 1 is of particular interest. It exhibits several encircled areas labeled d_2, d_4, and d_{14} according to the number of dopant atoms visible within the area. These areas are bordered along the growth direction by *n*-doped layers and perpendicular to the growth direction by zones with no dopant atoms (dark contrast areas labeled d_0). These zones with no dopant atoms exhibit tunneling spectra (Fig. 2) with typical characteristics of a depleted region. Thus the areas (d_2, d_4, and d_{14}) are semiconductor dots, whose confining potential for free holes is defined by the doping of the surrounding and thus by build-in potentials in the order of a few tenths of eV (border toward depleted zones) to 1.4 eV (toward *n*-doped layer).

During acquisition of the constant-current STM images we also measured current-voltage spectra at the different encircled areas in Fig. 1. Figure 2 shows that all spectra are essentially identical at positive sample voltages. In contrast, at negative voltages the current-voltage curves are shifted relative to each other. The fewer dopants are inside the cluster, the greater is the shift towards more negative voltages relative to the spectrum of the spatially extended *p*-doped layer (labeled p in Fig. 1).

The local variation of the dopant concentration apparent in Fig. 1 is a result of the combination of

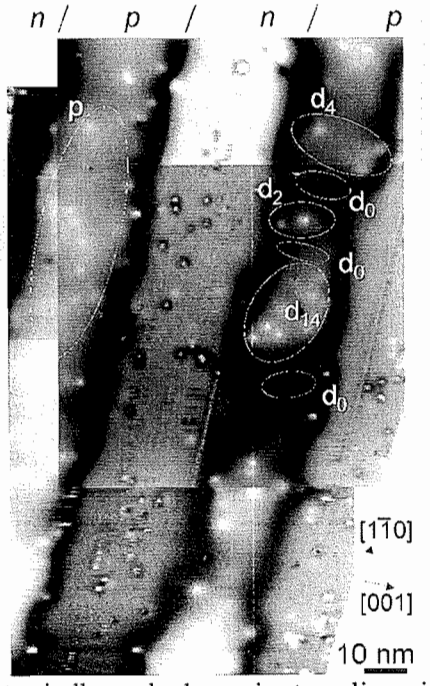

Fig. 1 Atomically resolved scanning tunneling microscope images of several *p*- and *n*-doped layers. The bright hillocks are signatures of dopant atoms. In the encircled areas the current voltage curves of Fig. 2 were recorded. The *p*-doped areas d_2, d_4, and d_{14} are dopant-induced dots confined by potential barriers due to the doping of the surrounding areas (*n*-type and lack of dopants). The growth direction is [001].

statistical incorporation and many-body effects in the repulsive screened Coulomb interactions between charged dopant atoms [1]. Unlike in bulk GaAs, in thin *p*-doped layers sandwiched between *n*-doped areas the electronic properties depend very sensitively on the exact dopant distribution governed by the individual statistical incorporation events: in our particular example this leads to one layer with nearly homogeneous electronic properties (marked p) and to another layer broken apart into electronically isolated dots (d_2, d_4, d_{14}) although the avarage dopant concentration is the same. The electronic separation of the dots within the thin *p*-doped layer is induced by the neighboring *n*-doped layers, which push down the valence band edge wherever *p*-dopant atoms are locally missing within the nominally *p*-doped layer. This explanation is supported by our tunneling spectra.

For a quantitative discussion of the spectra, we recall that the spectra consist of the current from valence and into conduction band states at negative and positive voltages, respectively, with the band gap region in

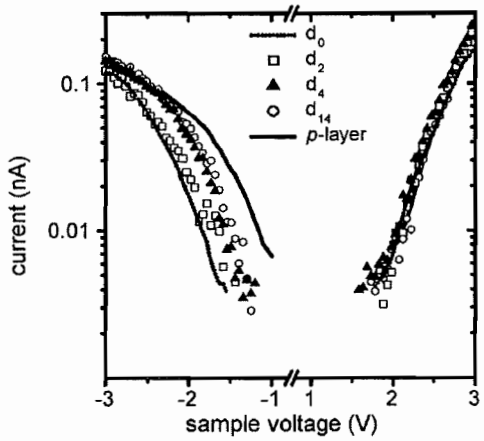

Fig.2 Current-voltage curves for the different dopant-induced dots marked in Fig. 1.

between. At a fixed voltage the tunneling current is determined by the energetic positions of the band edges underneath the tip:

At negative voltages, electrons tunnel from all filled valence band states lying between the valence band edge at the surface and the Fermi level of the tip. The size of this energy window is determined by the degree the tip bends the bands at the surface. Thus the shifts of the spectra at negative voltages indicate that the tip pulls downward the position of the valence band edge at the surface of our dopant-induced dots the more, the less dopants are enclosed within the dot. This suggests a reduced screening ability of the dots with smaller numbers of dopant atoms.

The electric field of the tip is screened by negatively charged acceptors, whose free holes have to be pushed away. On this basis, a reduction in the ability to screen the field of the tip is due to a combination of (i) the impossibility to deplete the dopant-induced dots from the free holes and (ii) the number of acceptors within the dot.

(i) The first effect depends on the size of the dot. If the dimension of the dot is much larger than the depletion width induced by the screening of the tip's field, i.e., the field can be screened entirely by the acceptors within the dot, then the band bending is determined by the concentration of dopant atoms in the dot. This effect is applicable to the spatially extended *p*-doped layer on the left hand side of Fig. 1, which is electronically homogeneous over dimensions of more than 100 nm, which is much larger than the estimated depletion width of 10 to 25 nm for our conditions.

If the dots' dimensions are similar to the width of the depletion zone, one needs to consider whether the holes can actually be pushed away sufficiently to accommodate the screening of the tip's electric field. For the small dot sizes, this means that holes need to be pushed out of the enclosed dot areas to deplete them. We recall that our dots are confined by potential wells. These wells act as a barrier for the free holes and impedes the holes to be pushed out, such that the remaining negatively charged acceptors could screen the electric field of the tip. Thus the band bending increases, causing lower tunneling currents than expected for infinitely sized bulk GaAs crystals with the same dopant concentration. In contrast, at *positive sample voltage* the electric field of the tip is screened by free holes accumulating at the *p*-doped surface. These holes feel no barrier to accumulate at the surface and their concentration is determined by the density of valence band states, which is the same for all investigated areas, because the material is the same. Thus the screening of the tip's field is equal for all dots in agreement with the spectra.

(ii) The above discussion also shows, that the ability to screen the electric field of the tip is directly proportional to the number of acceptors available within the electronically isolated dot. Thus the fewer acceptors within the dot, the larger the tip-induced band bending and the larger the voltage shift observed in the tunneling spectra. This explanation is in agreement with our observations.

In conclusion, we identified and characterized dopant-induced dots in GaAs *p-n* multilayers by scanning tunneling spectroscopy. Already at room temperature the properties of the dots are determined by the presence of confining potentials surrounding the dots, which reduce the ability to screen the tips' electric field compared to spatially non-confined material. The similarity of the dots' configuration with *n-p-n* transistors suggests that the effects found here will also affect future miniaturized semiconductor devices, once they reach dimensions as small as the fluctuations of the dopant concentration.

1. Ph. Ebert *et al.*, Phys. Rev. Lett. **83**, 757 (1999).
2. N.D. Jäger, K. Urban, E.R. Weber, and Ph. Ebert, submitted to Appl. Phys. Lett.
3. N.D. Jäger, K. Urban, E.R. Weber, and Ph. Ebert, Phys. Rev. B **65**, 235302 (2002).
4. N.D. Jäger, M. Marso, E.R. Weber, K. Urban, and Ph. Ebert, submitted to Phys. Rev. B.
5. Ph. Ebert, Surf. Sci. Rep. **33**, 121 (1999).

Application of Hilbert Spectroscopy to Pulsed Far-Infrared Radiation.

V. Shirotov[1,3], Y. Y. Divin[1], M.Liatti[1,3], U. Poppe[1], C.-L. Jia[1], K. Urban[1].
H. Larue[2], E. Zimmermann[2], A. Ahmet[2], H. Halling[2], O. Y. Volkov[3], V.N. Gubankov[3]
[1] *Institut für Festkörperforschung, FZ-Jülich GmbH, D-52425 Jülich, Germany*
[2] *Zentrallabor für Elektronik, FZ-Jülich GmbH, D-52425 Jülich, Germany*
[3] *Institute of Radioengineering and Electronics of Russian Academy of Sciences, 101999 Moscow, Russia*

A prototype of Hilbert spectrometer for operation with pulsed far-infrared radiation has been developed and characterized. The prototype consists from a high-T_c Josephson detector in an optical cryostat, analog electronics with a bandwidth of 14 MHz, and a DSP-based data acquisition system. The spectral range of the spectrometer can be as broad as 30 – 1200 GHz at the junction temperature of 78 K and can be shifted to the higher frequencies by lowering the junction temperature. Tests have been carried out using pulsed 94 GHz radiation with pulse duration of 200 ns and a pulse repetition rate of 1 MHz. A measurement time of 7 ms for a data set of 512 spectral points has been realized. It has been demonstrated, that in broadband (10 MHz) measurements without integration the developed spectrometer could operate in a power dynamic range of FIR radiation of 17 dB, which could be further enhanced by using integration functions.

In the last decade several new approaches have appeared for generation of intensive far infrared (FIR) radiation, e.g. photoconductive or electro-optical terahertz emitters excited by femtosecond laser pulses[1,2], the p-Ge hot hole laser[3] and coherent synchrotron or transition radiation from relativistic electron bunches[4,5]. Essential features of these sources are a high spectral density of radiation and the pulse operation with a high repetition rate in the megahertz range.

Hilbert spectroscopy based on high-T_c Josephson junctions demonstrates good potentials for fast and broadband FIR measurements[6]. This technique with conventional low-frequency electronics has been already used for slow spectral measurements of coherent transition radiation in the range of 100-250 GHz[7]. Here, we present the results of the development and characterization of a Hilbert spectrometer for operation with pulsed far-infrared radiation.

High-quality thin-film $YBa_2Cu_3O_{7-x}$ grain-boundary junctions have been epitaxially grown on the 2x14° (110) $NdGaO_3$ bicrystal substrates and patterned by UV lithography. A TEM image of the grain-boundary region of a fabricated junction and an optical image of the whole junction in polarized reflected light are shown in Fig. 1. The bicrystal boundary is situated horizontally in both images. It could be visualized in the $YBa_2Cu_3O_{7-x}$ thin film by different atomic ordering recovered by TEM (Fig. 1a) and in the substrate by polarization contrast (Fig. 1b). A narrow 2μm-wide $YBa_2Cu_3O_{7-x}$ bridge is patterned across the bicrystal boundary. The $YBa_2Cu_3O_{7-x}$ bridge is integrated into a broadband $Ag/YBa_2Cu_3O_{7-x}$ log-periodic antenna with a designed bandwidth of 30-3000 GHz (Fig. 1b).

The spectral range of Hilbert spectrometer was studied by measuring the frequency-selective responses of fabricated

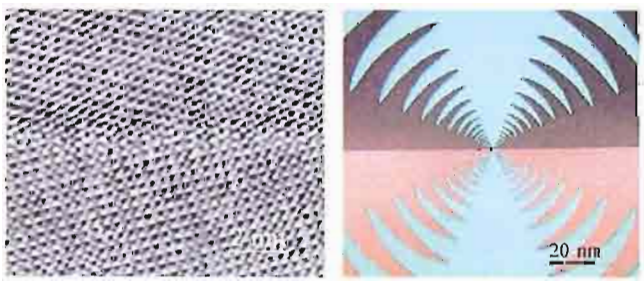

Fig. 1. High-resolution TEM image (a) and optical image (b) of the $YBa_2Cu_3O_{7-x}$ grain-boundary Josephson junction grown on 2x14° (110) $NdGaO_3$ bicrystal substrate.

Josephson junction to monochromatic radiation with the frequencies f_i from 20 GHz to 4 THz. Two sets of the normalized current responses $\Delta I(V)/\Delta I_c$ of the Josephson junction with a normal-state resistance R_n = 0.5 Ohm are shown in Fig. 2 for two junction temperatures of 78 K and 48 K. The ΔI_c is a suppression of a critical current I_c of the junction by monochromatic radiation. With an increase of frequency f, the amplitude of the odd-symmetric resonance at $V=hf/2e$ also increases, then reaches the maximum, and falls down with further increase of frequency. The low-frequency cut-off of the resonances in the responses $\Delta I(V)/\Delta I_c$ in Fig. 1 is in accordance with the RSJ behavior. The high-frequency fall-down of the selective response for low-resistance junctions was attributed to Joule heating. When the junction temperature is decreased from 78 K to 48 K, the bandwidth of the spectrometer shifts to the higher frequencies due to the increase of characteristic frequency $f_c=(2eI_cR_n/h)$.

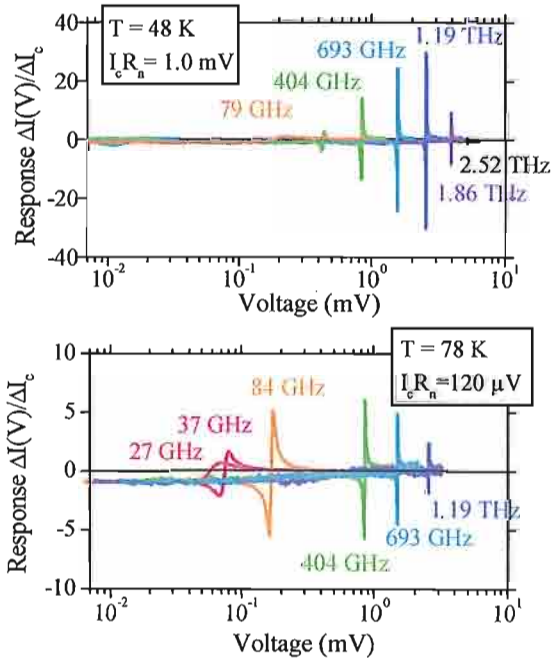

Fig. 2. Two sets of current responses $\Delta I(V)/\Delta I_c$ of the $YBa_2Cu_3O_{7-x}$ Josephson junction with a normal-state resistance R_n = 0.5 Ohm to monochromatic radiation with frequencies in the range 27 GHz – 2.5 THz.

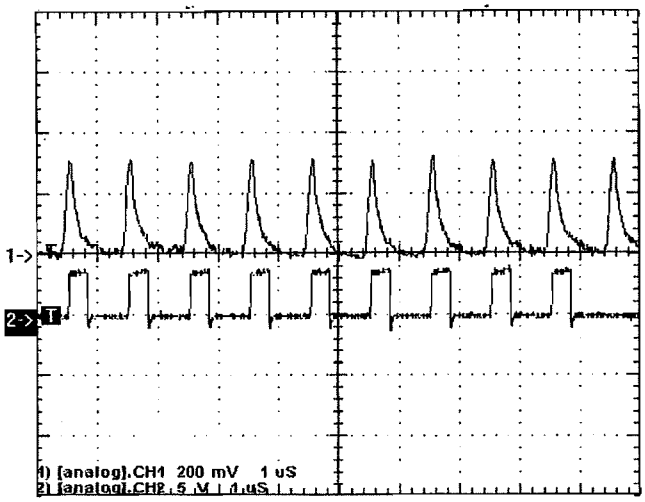

Fig. 3. Trace 1 – The time dependence of the response of the Hilbert spectrometer to pulsed 94 GHz radiation with 1 MHz repetition rate and 200 ns pulse duration. Trace 2 – Example of available integration windows.

A prototype of the Hilbert spectrometer consists from an optical cryostat, an $YBa_2Cu_3O_{7-x}$ grain-boundary Josephson junction as a frequency-selective detector, an analogue electronics, and a digital data acquisition and control system. The junction was placed on a temperature control stage in the optical cryostat. A broadband coupling of the Josephson junction with external radiation has been realized with a silicon hyperhemispherical lens. Josephson junction operation as a frequency-selective detector was accomplished by an analogue electronic scheme with a noise level of 0.16 nV/(Hz)$^{1/2}$ and a bandwidth of 14 MHz.

A specific part of the new Hilbert spectrometer prototype was its digital electronics, which included the experiment control and data acquisition systems. This new specially designed digital electronics differs this prototype from all ever reported before. The characteristic features of used hardware and software are an operation with pulsed signals and a possibility for an optimization of this process. This digital electronics represents a united block, which includes a digital-analogue converter and analogue-digital converters, and whose operation is based on a digital signal processor and a field programmable gate array.

The developed digital electronic system has a special 512-points buffer for a temporal storage of measured data sets. The control channel is able to scan the dc signal with the rate of about $7 \cdot 10^4$ points per second that determines the speed limitation for the experiment performance to around 7 ms for the whole data set. During this scanning, two recording channels take corresponding values in consecutive order (at constant biasing signal) and store them simultaneously.

The W-band has been chosen for the characterization of the new Hilbert spectrometer prototype, because it is the highest frequency range where precision attenuators and fast PIN-switches are available.

A principal suitability of the analogue electronic scheme for fast spectroscopic experiments with pulsed radiation can be seen from Fig. 3. The trace 1 in Fig.3 represents the pulse signal from the irradiated Josephson detector, amplified by the analogue electronic scheme. This figure demonstrates a good reproducibility of the chosen external radiation time structure by the analogue electronic part of the developed prototype. The digital electronics can measure the analog signals either without integration (ADC mode) or with an additional integration (integrator mode). The trace 2 shows an example of the

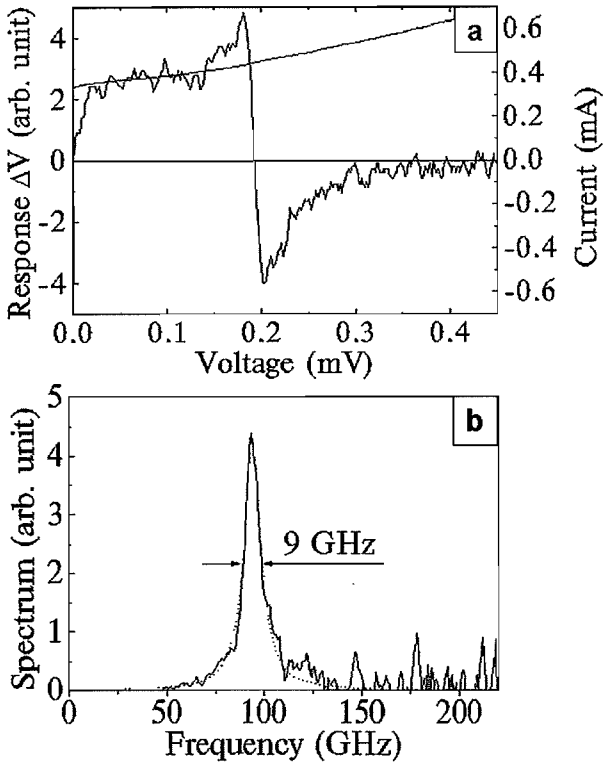

Fig. 4. The measured response to pulsed 94GHz radiation and the *I-V* curve of the Josephson junction (a). Spectrum of pulsed 94GHz radiation, recovered by Hilbert spectrometer (b). The dot line is a lorentzian fit.

integration windows, which are available in the digital electronics of the spectrometer.

Electrical characteristics for the Josephson junction (R_n = 0.85 Ohm, $I_c R_n$ = 315 μV at T = 77 K), i.e. junction *I-V* curve and its response, obtained when the Hilbert spectrometer was irradiated by pulsed monochromatic radiation, are presented in Fig. 4a. The spectrum recovered by Hilbert spectrometer and its lorentzian fit are shown in Fig. 4b. This figure demonstrates good agreement of experimental results and theory prediction. A spectral resolution of 9 GHz is very close to theoretical one. There is no sign of the second line at double frequency of 188 GHz with an experimental accuracy, so the power level of the incident radiation is inside the dynamic range of the spectrometer.

At an operating temperature of 77 K, the power dynamic range of the external W-band power in the ADC mode was equal to 17 dB above the minimal absorbed power of $1 \cdot 10^{-10}$ W (-70 dBm), that can be registered within 10 MHz frequency bandwidth. The corresponding parameters in the integrator mode were shown to be 24 dB and $1.8 \cdot 10^{-11}$ W (-77.5 dBm). Additionally, there is a possibility of a parameter improvement by increasing the measuring time and using an integration function over a large number of pulses or averaging whole data sets.

[1]D. Grischkowsky, in Frontiers in Nonlinear Optics, edited by H. Walther, N. Koroteev, and M. O. Scully (Inst. of Physics, Philadelphia, 1992).
[2]A. Nahata, A. S. Weiling, and T. F. Heinz, Appl. Phys. Lett. 69, 2321, 1996.
[3]E. Gornik and A. A. Andronov, Opt. Quantum Electron. 23, 111, 1991.
[4]T. Nakazato, et al., Phys. Rev. Lett. 63, 1245, 1989.
[5]U. Happek, A. J. Sievers, and E. B. Blum, Phys. Rev. Lett. 67, 2962, 1991.
[6]Y. Divin et al., in: Advaces in Solid State Phys., ed. B.Kramer, v.41, p.301, (Springer, Berlin), 2001.
[7]Y.Y. Divin et al. IEEE Trans. Appl. Supercond., vol. 9, pp. 3346-3349, 1999.

Operation of high-temperature superconductor magnetometers with submicrometer bicrystal junctions

M.I.Faley[1], U.Poppe[1], K.Urban[1], V. Yu. Slobodchikov[2], Yu. V. Maslennikov[2], A. Gapelyuk[3], B. Sawitzki[3], and A. Schirdewan[3]

[1] *Institut für Festkörperforschung, FZ-Jülich GmbH, D-52425 Jülich, Germany*
[2] *Institute of Radio Engineering & Electronics, 101999 Moscow, Russia*
[3] *Franz-Volhard Hospital, D - 13125 Berlin, Germany*

We have investigated the noise properties of dc superconducting quantum interference device flip-chip magnetometers with submicrometer wide bicrystal junctions operating at 77.4 K. The magnetometers demonstrated a modulation voltage V_{pp} up to about 80 μV compared with V_{pp} up to about 30 μV for the magnetometers with 1.5 μm junctions. This increases the slew rate of the magnetometers and improves stability of their operation in noisy environment. The noise of the magnetometers with electronics was about 6 fT/√Hz at frequencies above 100 Hz increasing up to about 20 fT/√Hz at 1 Hz. The operation of the magnetometers was characterized in a HTS dc-SQUID electronic axial first order gradiometer system, which was employed for biomagnetic measurements. The system demonstrated a gradient resolution of about 1 fT/cm√Hz at 77.4 K and a stable operation in a standard magnetically shielded room under clinical conditions[1].
F&E-Nr: 23420

At the present stage of the development of high temperature superconductor (HTS) technology a production of HTS dc superconducting quantum interference device (SQUID) flip-chip magnetometers with a magnetic field resolution of about 6 fT/√Hz at 77.4 K is possible[2]. The sensitivity of dc-SQUIDs can be further improved with Josephson junctions having a higher normal state resistance R_n and I_cR_n product. It was observed[2], that the I_cR_n product of bicrystal junctions is increasing with critical current density J_c like $I_cR_n \propto (J_c)^{0.6}$. In order to keep the critical current I_c fixed optimal for SQUID operation, provide narrow junction conditions, and simultaneously increase J_c and R_n it is necessary to reduce the junction width down to a submicrometer scale. To demonstrate the sensitivity, reproducibility, and stability of the sensors with submicrometer wide Josephson junctions we have constructed a HTS dc-SQUID gradiometric system for biomagnetic measurements, *e.g.*, for magnetocardiography (MCG).

The high-oxygen-pressure dc-sputtering technique was used for the deposition of the $YBa_2Cu_3O_{7-x}$ films on 24° bicrystal $SrTiO_3$ substrates. *C*-oriented 200 nm thick $YBa_2Cu_3O_{7-x}$ films show typical critical current densities J_c of about 6×10^6 A/cm^2 at 77.4 K and a transition temperature T_c above 91 K measured by magnetic susceptibility. Some inclusions of secondary phases served as effective pinning centers. The junctions (see Fig.1) had a width between 0.4 μm and 1 μm, a normal state resistance of about 10 Ω, and a critical current density of about 2×10^4 A/cm^2 (I_cR_n product of about 400 μV) at 77.4 K. The junctions were prepared by optimized conventional photolithography with AZ5214 photoresist, 0.3 μm UV-light exposure, and Ar ion milling.

16-mm flux transformers[1] were prepared with a PMMA-photoresist technique described in Ref. 4 with a $PrBa_2Cu_3O_{7-x}$ insulation layer between the windings of the multiturn input coil and the return strip. The flip-chip SQUID magnetometers demonstrated a modulation voltage V_{pp} up to 80 μV ($\partial V/\partial \Phi \approx$ 250 μV/Φ_0) at 77.4 K. Here Φ is the magnetic flux through the SQUID loop and $\Phi_0 = 2.05 \times 10^{-15}$ T·m^2 is the flux quantum. For comparison, similar magnetometers with 1.5 μm wide junctions showed values of V_{pp} only up to about 30 μV at 77.4 K. The increase of V_{pp} leads to an increase of slew rate of the magnetometers and stability of their operation in noisy environment.

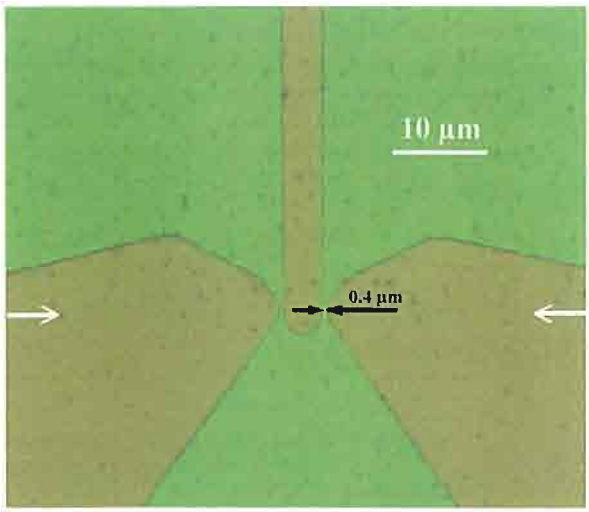

Fig. 1. Optical image of bicrystal junctions, obtained in a combination of transmission and reflective illumination. A magnification of x1000 and a green filter were used. The white arrows indicate the position of the bicrystal boundary. The black arrows determine the width of the 0.4 μm wide junction.

Two encapsulated magnetometers were fixed parallel to each other on a glass-fiber epoxy rod. The gradiometer baseline of 10 cm is determined by the distance between the flux transformers of the magnetometers. A two channel ac-bias electronics (Cryoton) provided a simultaneous operation of the magnetometers and an electronic subtraction of the output signals. The sensors were immersed in liquid nitrogen in a 1.5-liter glass-fiber epoxy cryostat. The cryogen hold time of the cryostat with the gradiometer insert was 10 days. The cold-warm distance at the cryostat bottom is about 10 mm.

The measurements were performed in the magnetically shielded room (MSR) of the Franz-Volhard Hospital. The current shielding factor of the MSR is about 10^4 at 50 Hz and about 10 at 0.1 Hz. A slow variation of the magnetic field in the middle of MSR was observed during daytime. A typical time constant of this drift was about 10 sec and the amplitude up to 5 nT.

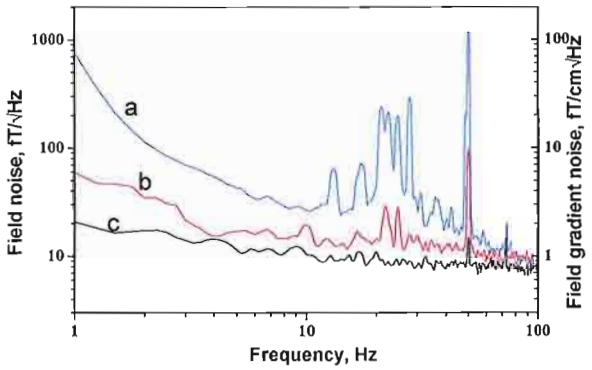

Fig. 2. Noise spectrum of a single magnetometer (a) and the spectrum of the differential signal (b) measured in the MSR of the Franz-Volhard Hospital at 77.4 K. For comparison the noise of the bottom magnetometer measured in a HTS shield is included (c).

The system noise spectrum with one of the individual magnetometer and the spectrum of the differential signal are presented in Fig. 2. The observed increase of the field noise at 1 Hz is associated with the reduced shielding factor of the MSR at low frequencies. The magnetic field signals observed in the frequency range from 10 Hz to 30 Hz (curve a) were mainly caused by building vibrations. In a HTS shield the individual magnetometers demonstrate a field noise below 10 fT/√Hz down to 10 Hz increasing up to 20 fT/√Hz at 1 Hz (curve c).

Taking into account the 10 cm baseline of the electronic gradiometer the spectrum of the differential signal is presented in Fig. 2 with the calibration scale on the right in [fT/cm√Hz] units. The resolution of the gradiometric signal is below 1 fT/cm√Hz at frequencies above 100 Hz and below 2 fT/cm√Hz in the frequency range down to about 4 Hz.

The MCG measurements were performed in the MSR with a volunteer having maximal peak-to-peak amplitude of about 30 pT for the magnetic signal of heart. Both magnetometer signals were measured with a simultaneous recording and processing of the differential signal. A line frequency synchronous filter combined with a bandpass filter suppressed the residues of 50 Hz interference with its harmonics. The measurement frequency bandwidth (0.03 – 125) Hz covered the most significant frequency range of the heart signal. The observed peak-to-peak amplitude of the noise band is about 500 fT. This corresponds to an effective resolution $S_f^{1/2} \sim 1.7$ fT/cm√Hz of the electronic gradiometer in the measurement frequency range.

Stability of the system operation was demonstrated by the measurements of MCG maps. The magnetic field measurements were carried out using a 6 x 6 rectangular grid over the thorax with a distance of 4 cm between neighboring positions of the measurements in both directions. Equiinductional maps of the magnetic field distribution were plotted on the basis of a two-dimensional interpolation at any moment of the heart beat (see Fig.3). The MCG-measurements for one mapping have taken about 30 minutes. The magnetometers have demonstrated a stable operation with no changes in the noise characteristics during the measurements. This has allowed to obtain low noise 2D-plots of the magnetic field distribution. The characteristics of the magnetometers were not changed also after a year of storage and multiple tests accompanied with thermal cyclings.

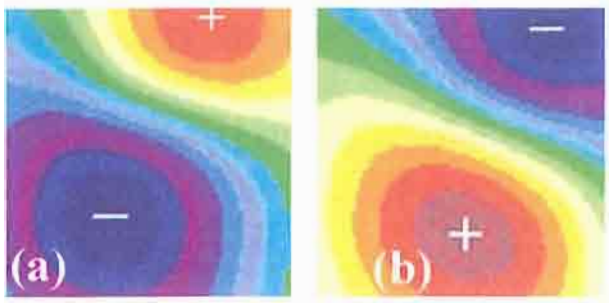

Fig. 3. Magnetic field distribution over the scan area at the moments of the (a) S- and (b) T-peaks of the heart beat.

A demand to improve the parameters of HTS Josephson junctions has determined the present trend of a reduction of the junction width down to a submicrometer scale. In this case the main difficulty is how to maintain the superconducting parameters at 77.4 K in narrow bicrystal junctions preventing degradation during the patterning process. Possible reasons for the degradation are chemical reaction in humid atmosphere and deoxygenating of the $YBa_2Cu_3O_{7-x}$ films, both occur about 100 times faster along the bicrystal boundary compared to single crystalline films in *c*-axis direction. It is important to achieve the highest possible microstructural quality of the $YBa_2Cu_3O_{7-x}$ film and to keep the substrate cold during the ion beam etching process. A subsequent encapsulation then ensures the long-term stability of the sensor. The average size of the growth spirals of the $YBa_2Cu_3O_{7-x}$ films, deposited by high-oxygen-pressure dc-sputtering technique is about 1 μm compared to about 0.3 μm large grains of conventional laser ablated films[5]. This makes it possible for the sputtered films to produce junctions between the individual growth spirals, so contributing to the homogeneity and increasing the tunneling part of the critical current density of the junction[6]. A detailed study of the transport and microstructural properties of submicrometer wide bicrystal Josephson junctions prepared with the sputtered $YBa_2Cu_3O_{7-x}$ films is in progress.

[1]M. I. Faley, U. Poppe, K. Urban, V. Yu. Slobodchikov, Yu. V. Maslennikov, A. Gapelyuk, B. Sawitzki, and A. Schirdewan, Appl. Phys. Lett., **81**, 2406 (2002).
[2]M. I. Faley, U. Poppe, K. Urban, D. N. Paulson, T. Starr, and R. L. Fagaly, IEEE Transactions on Applied Superconductivity **11**, No.1, 1383 (2001).
[3]R. Gross, P. Chaudhari, M. Kawasaki, and A. Gupta, Phys. Rev. B **42**, 10735 (1990).
[4]M. I. Faley, U. Poppe, H. Soltner, C. L. Jia, M. Siegel, and K. Urban, Appl. Phys. Lett. **63**, 2138 (1993).
[5]B. Dam, N. J. Koeman, J. H. Rector, B. Stäuble-Pümpin, U. Poppe, R. Griessen, Physica C **261**, 1 (1996).
[6]E. Sarnelli, G. Testa, Physica C **371**, 10 (2002).

High-T_c dc-SQUID microscope for information technology

U. Poppe[1], M. I. Faley[1], B. Jungbluth[3], H. Soltner[4], I. Breunig[3], R. Speen[1] and K. Urban[1], E. Zimmermann[2], W. Glaas[2], and H. Halling[2]

[1] *Institut für Festkörperforschung, Forschungszentrum Jülich GmbH*
[2] *Zentrallabor für Elektronik, Forschungszentrum Jülich GmbH*
[3] *on leave from Institut für Festkörperforschung, Forschungszentrum Jülich GmbH*
4 Zentralabteilung Technologie

A scanning SQUID microscope based on High Temperature Superconductor (HTS) dc SQUIDs was developed. An extremely soft magnetic antenna was used to guide the flux from room temperature samples to the liquid nitrogen cooled SQUID-sensor. The sample was moved under the cryostat with a computer controlled xy-scanning stage. A lateral resolution of better than 10 µm could be achieved for the determination of the position of current carrying thin wires. This is an improvement of a factor of about five compared to existing commercial SQUID microscopes without flux guide.
F&E-Nr: 23420

In recent years, a number of groups (see, e.g., [1,2,3]) have developed scanning Superconducting Quantum Interference Device (SQUID)- microscopes in which a sample is scanned under a SQUID and the resultant variations in flux are used to construct a magnetic image. Microscopes with High Temperature Superconductor (HTS) SQUIDs operating at 77 K are especially suitable to study the magnetic stray field of room temperature samples [2].
Such SQUID microscopes can be used, *e.g.*, in failure analysis, yield, reliability, and design verification to identify critical defects in high density multilayer printed boards, multilayer structures for magnetoelectronics, multi-chip module substrates, in semiconductor packages, wafers, and processes. The development of the HTS dc-SQUID technology and HTS dc-SQUID measurement systems in Jülich has achieved a level, which allows their application in laboratory prototypes [4].

Compared to other magnetic evaluation methods for microscopic objects the scanning SQUID microscope has higher magnetic field sensitivity and a high linearity over a dynamic range up to about 200 dB. Different SQUID microscope measurement systems are presently under study in IFF FZJ. The goal of this research activity is the creation of a new generation of the high-T_c SQUID microscopes with an improved spatial resolution (< 1 µm) and sensitivity for room temperature samples.

Minimizing SQUID–sample separation for a better field- and spatial resolution becomes a problem for room temperature objects, which are placed outside the cryostat. The typical separation between the SQUID sensor tip and the room temperature sample is about 100 µm. This relatively large distance limits the space resolution of such type of SQUID microscopes to about 50 µm. Examples are commercially available scanning SQUID microscopes of U.S. firms Tristan Technologies Inc. and Neocera [5], which are already used for low spatial resolution failure analysis of multi-chip modules and other semiconductor packaging.

As a SQUID operates at low temperatures the investigation of room temperature samples leads to a loss of spatial resolution due to the required distance between the SQUID loop and the sample. To overcome this drawback different versions of scanning SQUID microscopes where the SQUIDs were combined with magnetic flux guides were investigated [6, 7,8]. Up to now these flux guides usually consisted of extremely soft magnetic several mm long sharp tips. In the case of local magnetic moments like tiny magnetic dipoles as they are provided by the stray field of small magnetic domains in, e.g., magnetic recording media the spatial resolution could be in the submicrometer region. In the other case of non localized fields such as magnetic fields produced by current carrying wires the fields only slowly decay with 1/r (r denotes the distance from the wire) and the whole tip of some mm lengths acts as an antenna for the field of the wire leading to a very poor spatial resolution. Futhermore the decay of the flux transported from the sample at the sharp end of the tip to the SQUID at the other end of the tip is substantial in these designs as no low loss return of magnetic flux to the sample is provided. Both of these difficulties we have substantially deminished by using a specially designed flux guide geometry. Its development is currently under way in the IFF/IMF together with the Zentrallabor für Elektronik (ZEL). This opens up the possibility to image the fields of electrical currents in microelectronic devices with our new flux guide concept (patent pending).

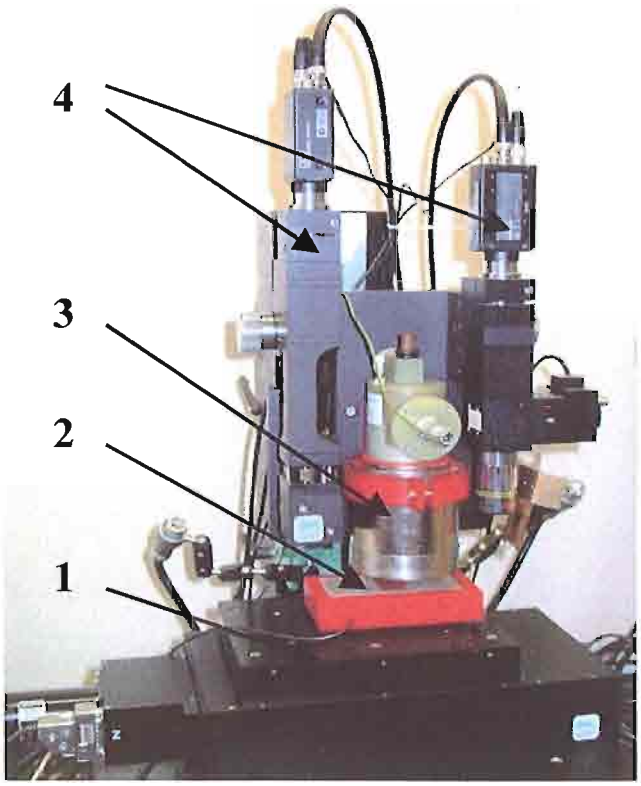

Fig.1. A photo of the SQUID microscope including a xy- scanning stage (1), a sample table (2), a liquid nitrogen cryostat with a HTS dc-SQUID sensor (3) and an optical control of the sensor – sample distance (4). Additional magnetic shielding of the scanning stage and the sensor unit (not shown in the figure) can be provided for sensitive measurements.

The device measures the z-component (direction perpendicular to the sample surface) of the stray field of the sample, which is rastered with submicron precision in xy-direction by a motorized computer controlled scanning stage. In Fig. 1 a photo of the SQUID microscope is presented.

First examples of measurements with new flux guide sensor type, which demonstrates improved spatial resolution are shown in Fig. 2.

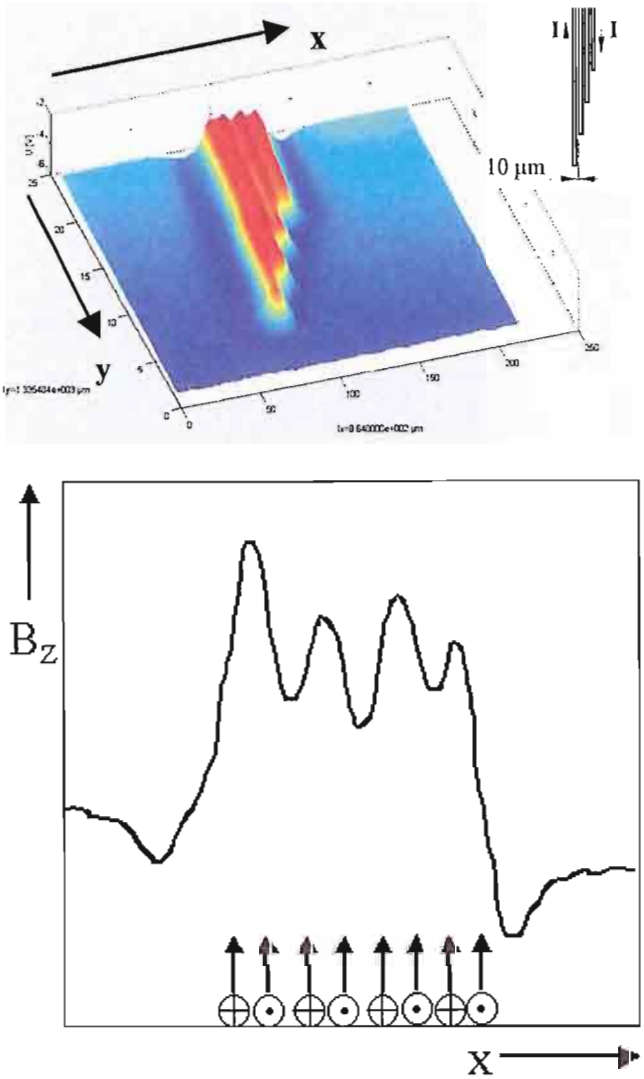

Fig.2. The upper part shows an example of the measurements of a 2D distribution of the magnetic field B_z above a thin-film current-carrying meander, which has 10 µm wide lines separated at 10 µm distance from each other. The total xy scan area was 860 x 1300 µm^2. The lower part shows a single line scan across 8 wires with antiparallel currents.The wire positions are marked by arrows.

The upper part of the picture shows the 2D-distribution of the z-component of the magnetic field B_z above a thin-film current carrying meander test structure. About 200 nm thick and 10 µm wide lines are separated at 10 µm distance by each other carry 63 µA of ac-current. The integration time was 0.3 sec. The current in neighboring lines produces magnetic fields with opposite sign. As indicated in the insert the structure consists of 4 pairs of wires with different length. The single line scan in the lower part of Fig.2 shows that the field of antiparallel currents of 8 neighboring wires can be clearly distinguished. This demonstrates an enhancement by a factor of about 5 in spatial resolution compared to existing state of the art SQUID microscopes for room temperature samples without magnetic flux guides [3].

As a further example, where the gradient $\partial B_z/\partial x$ of the stray fields between domains of magnetic recording material was investigated, is presented in Fig.3. The picture shows three neighboring tracks with ferromagnetically encoded bit-patterns of a floppy disk.

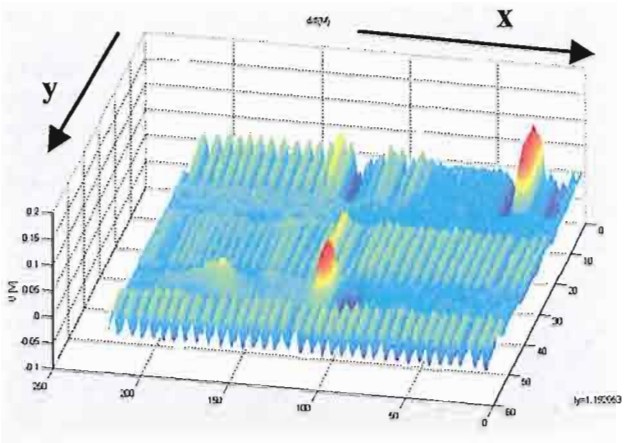

Fig.3. An example of the measurement of a 2D distribution of the field gradient $\partial B_z/\partial x$ above a floppy disk. The xy scan area is 850 x 1200 µm^2.

In conclusion first results of a new type of SQUID microscope with integrated flux guide were presented. An application of the microscope for information technology especially in the field of failure analysis of semiconductor devices or the investigation of magnetic storage devices looks promising. This includes, e.g., the non-destructive detection of package- or chip level shorts of micro-circuits and the analysis of the domain structure in magnetic thin film devices.

Presently we are working on a further improvement of the sensitivity of such instrument. An optimized coupling of the magnetic flux to the SQUID can significantly enhance the sensitivity, which is very important for the measuring speed in failure analysis of low level current distributions.

[1]J. R. Kirtley, Physica C **368**, 55-65, 2002

[2]J. Dechert, M. Mueck and C. Heiden, IEEE Transactions On Applied Superconductivity; vol. **9**, No. 2, 1999

[3]E. F. Fleet, S. Chatraphorn, F. C. Wellstood, L. A. Knauss, and S. M. Green, Rev. Sci. Instrum. **72**, 3281 – 3290, 2001

[4]M. I. Faley, U. Poppe, K. Urban, V. Y. Slobodchikov, Yu. V. Maslennikov, A. Gapelyuk, B. Sawitzki, and A. Schirdewan, Appl. Phys. Lett., **81**, 2406 2002, see also M. I. Faley et al. this issue

[5]http://www.neocera.com/html-files/magma/magma_specs.htm
http://www.tristantech.com/prod_microscop.html

[6]P. Pitzius, V. Dworrak and U. Hartmann, ISEC 97 Extended Abstracts, vol. **3**, pp. 395-398, June 1997

[7]Y. Tavrin and M. Siegel, ISEC 97 Extended Abstracts vol. **3**, pp. 389-391, June 1997

[8]S.A. Gudoshnikov; B.Ya. Liubimov, Yu.V. Deryuzhkina, L.V. Matveets, O.V. Snigirev, A.S. Kalabubukov, M.L. Ranchinski, F. Schmidl, P. Seidel,
Physica C **372-376**, 271-273, 2002

Fabrication process for the growth of large bismuth single crystals for use as neutron filter

K.J. Fischer

Institut für Festkörperforschung, FZ Jülich, D-52425 Jülich, Germany

Single crystals of bismuth of 170 mm diameter and 35 kg weight were grown by directional solidification. The nucleation and orientation of the seed crystal was performed in situ on a graphite sensor. Due to the strong anisotropy in the heat conductivity the better conducting c-plane is aligned with the heat flow nearly parallel to the crucible axis, thus permitting to cut [c]- oriented neutron filter of maximum size. The single crystals are used as windows for subthermic neutrons and filter against γ-rays. The transmission spectra for crystals with weak – and strong – mosaic spread were measured.

Contrary to earlier attempts to grow large bismuth single crystals either by applying steep temperature gradients [1] or using a soft mold of alumina powder [2, 3, 4] or just recovering big grains from a 220 kg slowly solidified melt [5] to obtain 11 x 11 x 10 cm^3 [c]-oriented single crystals the controlled oriented nucleation and growth of 170 mm diameter and 35 kg weight bismuth single crystals by directional solidification is reported.

Due to damage of a bismuth seed crystal even by careful handling by twin formation, in situ seed crystal nucleation was applied without checking whether a damaged seed crystal could have lead to a perfect bulk crystal or not.

To obtain a flat phase boundary necessary for good structural perfection of the crystals grown, a crucible of fire clay, having much lower heat conductivity than those of bismuth, was used. Furthermore, the circumstances for the oriented growth of the nucleus were observed by inventing a sensor permitting to follow its appearance and growth.

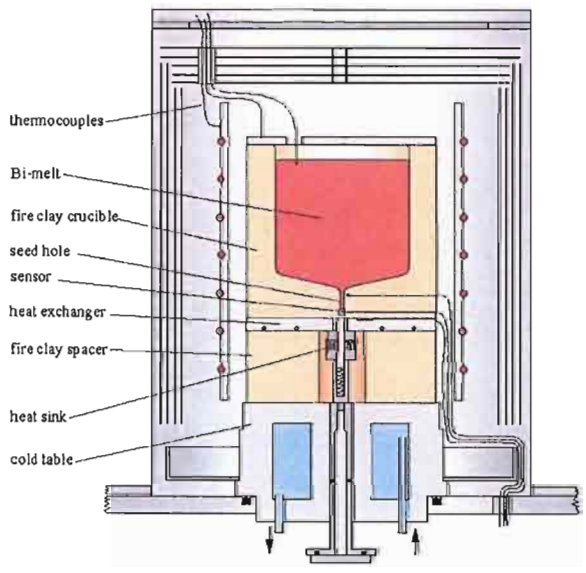

Fig. 1 Scheme of vacuum furnace growth device

A scheme of the growth arrangement is shown in Fig. 1. It consists of a vacuum furnace, a covered fire clay crucible (4 l volume) standing on a heat exchanger, a fire clay spacer and a heat sink. Heat flow towards the bottom is controlled by the heat exchanger which is heated and at the same time variably coupled to the heat sink. A precast bismuth cylinder of about 35 kg fills the crucible after melting with about 3.5 l.

The seed crystal is nucleated in the seed hole in a small undercooled melt volume on the sensor. The sensor is a piece of graphite with a thermocouple hole located in the bottom of the crucible.
By measuring the temperature-time lapse at the sensor during seed formation it was found that the seed aligns nearly parallel with its cleaveable c-plane to the crucible axis if the temperature gradient from the sensor towards the melt is of the order of 2 – 3 K cm^{-1}. The orientation of the seed in this manner is possible due to the anisotropy in heat conductivity. The better conducting c-plane aligns parallel to the heat flow direction. This is advantageous for cutting large in [c]- oriented neutron filter from the single crystal cylinder.
Further directional solidification of the melt is performed by lowering the temperature at the heat exchanger. Before solidification starts the melt has nearly no surplus heat content above latent heat and a temperature gradient of 0.03 K cm^{-1} from bottom to top. This leads to growth times in the range from 120 to 150 hours corresponding to a solidification rate of about 5 g min^{-1}.
The stabilizing temperature gradient at the growth front builds up by the recovered latent heat. The growth front could therefore be described as a "self stabilizing growth front". The low heat conductivities of bismuth in addition to the insulating crucible support this effect.

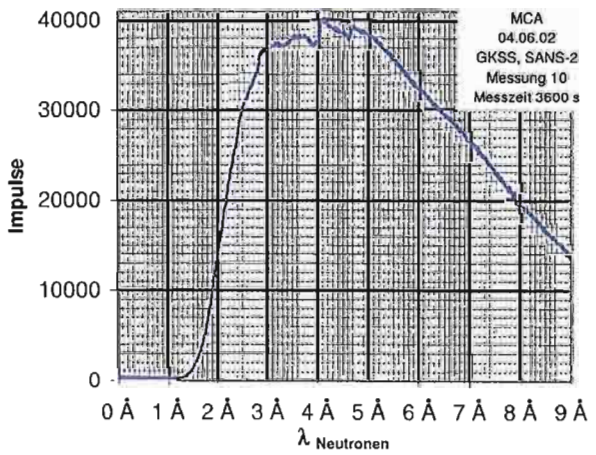

Fig. 2a
Time of flight spectra
Empty measurement

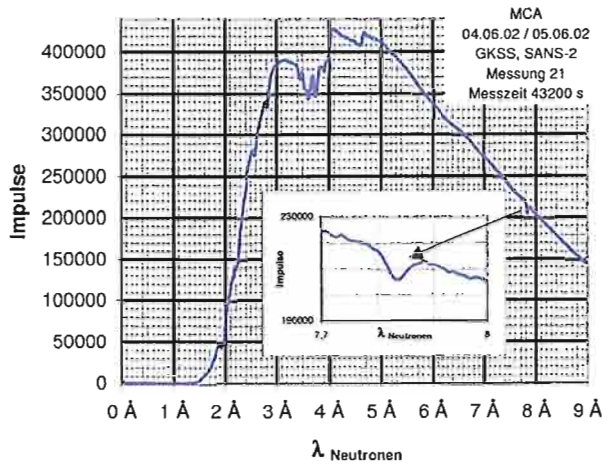

Fig. 2b
Time of flight spectra
Bi – crystal with weak mosaic spread

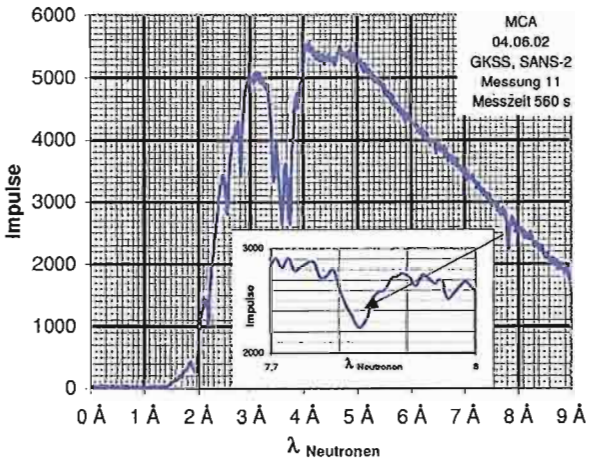

Fig. 2c
Time of flight spectra
Bi – crystal with strong mosaic spread

The influence of the structural perfection of the crystal on the transmission for subthermic neutrons and the appearance of the back reflection peak at 7.89 Å were measured by time of flight measurements at the SANS-2 instrument at the GKSS Forschungszentrum. Figs. 2 a-c show transmission spectra for an empty measurement (2a), for a crystal with weak (2b) – and strong (2c) – mosaic spread.
To see the back reflection peak of structurally perfect crystals at 7.89 Å a sampling time of 12 hours was necessary. Whereas for a crystal with weak mosaic spread a value for the back reflection peak of $\Delta\lambda / \lambda \approx 3 \cdot 10^{-4}$ is estimated, this value rises for a crystal of strong mosaic spread to $\approx 12 \cdot 10^{-4}$. Applying the crystal growth process described, crystals of lowest mosaic spread can reproducibly be grown.

Acknowledgements

I thank all persons that were interested in obtaining neutron filter allowing me to work for a long development time at this growth process. In particular Prof. D. Richter's support in this respect is acknowledged as well as the time of flight measurements of Dr. B. Alefeld, who performed these measurements together with L. Dohmen, J. Thelen, and the GKSS-Team H. Eckerlebe, I. Vollbrandt und G. Kozik at the GKSS Forschungszentrum after retirement.

References

[1.] F. Stöber
Künstliche Darstellung großer, fehlerfreier Kristalle
Zeitschrift für Kristallographie 61, 299-314 (1929)

[2.] T. S. Noggle
A "Soft" Mold Technique for Growing Single Crystals of Aluminium
Rev. Sci. Instr. 24, 184 (1953)

[3.] S. Bednarski
The use of directional freezing of the melt for the preparation of large bismuth single crystals
Phys. Stat. Sol. 9, 839-842 (1965)

[4.] S. Bednarski
Preparation of very large bismuth single crystals for neutron filters
Journal of Crystal Growth 6, 193-194 (1970)

[5.] Bericht der Firma H.M.J. Billiton, Arnheim/NL
Herstellung großer Wismut-Einkristalle
Pressebericht in Atomenergie 11, p. 292 (1969)

Publications in journals

Baier,F.*; Müller,M.A.*; Sprengel,W.*; Grushko,B.; Strertzel,W.*; Assmus,W.*; Schäfer,H.E.*
Atomic defects in Al-Pd-Mn : a study by means of positron annihilation spectroscopy
Materials science forum, 363-365 (2002), S. 179 - 181

Bert,F.*; Belessa,G.*; Grushko,B. C.
Tunneling states anisotropy in a single grain decagonal quasicrystal
Physical review letters, 88 (2002), 25, S. 255901-1 - 255901-9)

Cao,L. X.*; Kremer,R.K.*; Qin,Y.L.; Brötz,J.*; Liu,J. S.*; Zegenhagen,J.*
Stress change in YBa2Cu3O7-delta close to the superconducting transition
Physical review B, 66 (2002), S. 054511

Cao,L. X.*; Qin,Y. L.; Deac,A.*; Snigireva,I.*; Zegenhagen,J.*
Microstructure of YBa2O7-delta/Pb(Zr1-xTix)O3(x=0,0.47) heterostructures
Journal of physics: condensed matter, 14 (2002), S. 3093 - 3097

Chen,J. H.; Jia,C.L.; Urban,K.; Chen,C. L.*
Unusual lattice distortion in Ba0.5Sr0.5TiO3 thin films on a LaAlO3 substrate
Applied physics letters, 81 (2002), S. 1291

Divin,Y. Y.; Volkov,O. Y.*; Laytti,M.; Shirotov,V. V.; Pavlovskii,V. V.*; Poppe,U.; Shadrin,P. M.; Urban,K.
Hilbert spectroscopy from microwave to terahertz frequencies by high-Tc Josephson junctions
Physica C, (2002)

Divin,Y.Y.; Poppe,U.; Jia,C.L.; Shadrin,P.M.*; Urban,K.
Structural and electrical properties of YBa2Cu3O7(100)-tilt grain boundary josephson junctions with large IcRn-products on SrTiO3 bicrystals
Physica C, 372-376 (2002), S. 115 - 118

Divin,Y.Y.; Volkov,O.Y.*; Liatti,M.*; Shirotov,V.V.*; Pavlovskii,V.V.*; Poppe,U.; Shadrin,P.M.*; Urban,K.
Hilbert spectroscopy from gigahertz to terahertz frequencies by high-Tc Josephson junctions
Physica C, 372-376 (2002), S. 416 - 419

Dolinsek,J.*; Apih,T.*; Jeglic,P.*; Feuerbacher,M.; Calvo-Dahlborg,M.*; Dubois,J.M.*
Atomic jumps in quasiperiodic Al72.6Ni10.5Co16.9 and relatad crystalline material
Physical review B, 65 (2002), S. 212203

Döblinger,M.*; Wittmann,R.; Gerthsen,D.; Grushko,B.
Continuous transition between decagonal quasicrystal and approximant by formation and ordering of out-of-phase domains
Physical review B, 65 (2002), S. 224201-1 - 224201-9

Ebert,P.
Defects in III-V semiconductor surfaces
Applied physics letters, A 75 (2002), S. 101 - 112

Faley,M. I.; Poppe,U.; Urban,K.; Paulson,D. N.*; Starr,T. N.*; Fagaly,R. L.*
Sensitive HTS gradiometers for magnetic evalution applications
Physica C, (2002)

Faley,M.I.; Poppe,U.; Urban,K.; Paulson,D.N.*; Fagaly,R.L.*
Sensitive HTS gradiometers for magnetic evaluation applications
Physica C, 372-376 (2002), S. 217 - 220

Faley,M.I.; Poppe,U.; Urban,K.; Slobodchikov,V.Y.*; Maslennikov,Y. V.*; Gapelyuk,A.*; Sawitzki,B.*; Schirdewan,A.*
Operation of high-temperature superconductor magnetometer with submicrometer bicrystal junctions
Applied physics letters, 81 (2002), 13, S. 2406 - 2408

Franke,K. H.*; Sharma,H.R.*; Theis,W.*; Gille,P.*; Ebert,P.; Rieder,H.*
Quasicrystalline epitaxial monolayers grown on icosahedral Al-Pd-Mn and decagonal Al-Ni-Co quasicrystal surfaces
Physical review letters, 89 (2002), S. 156104-1 - 156104-4

Grushko,B. C.; Döblinger,M.*; Wittmann,R.*; Holland-Moritz,D.*
A study of high-Co Al-Ni-Co decagonal phase
Journal of alloys and compounds, 342 (2002), S. 30 - 34

Grushko,B.; Mi,S.; Highfield,J.G.*
A study of the Al-rich region of the Al-Ni-Mo alloy system
Journal of alloys and compounds, 334 (2002), S. 187-191

He,J.Q.; Regnery,S.*; Jia,C.L.; Qin,Y.L.*; Fetsilis,F.*; Erhardt,P.; Waser,R.; Urban,K.; Wang,R.H.*
Interfacial and microstructural properties of SrTiO3 thin films grown on Si(001)

Journal of applied physics, 92 (2002), S. 7200

Heggen,M.; Feuerbacher,M.; Lange,T.; Urban,K.
Microstructural analysis of plastically deformed icosahedral Zn-Mg-Dy single quasicrystals
Journal of alloys and compounds, 342 (2002), S. 330 - 336

Herzog,H.-J.*; Hackbarth,T.*; Seiler,U.*; König,U.*; Holländer,B.; Mantl,S.
Si/SiGe n-MOSFETs on thin SiGe virtual substrates prepared by means of implantation
IEEE electron device letters, 23 (2002), S. 485

Houben,L.; Scholten,C.; Luysberg,M.; Vetterl,O.; Finger,F.; Carius,R.
Growth of microcrystalline nip Si solar cells : role of local epitaxy
Journal of non-crystalline solids, 299 (2002), S. 1189 - 1193

Jia,C.L.; Rodriguez - Contreras,J.*; Poppe,U.; Kohlstedt,H.*; Waser,R.; Urban,K.
Lattice strain and lattice expansion of the SrRuO3 layers in SrRuO3/PbTr0.52Ti0.48O3/SrRuO3 multilayers thin films
Journal of applied physics, 92 (2002), 1, S. 101

Jiang,C.S.*; Yu,H.*; Shih,C.K.*; Ebert,P.
Effect of the substrate structure on the growth of two-dimensional thin Ag films
Surface science, 518 (2002), S. 63 - 71

Jiang,X.*; Jia,C. L.
Structure and defects of vapor-phase-grown diamond nanocrystals
Applied physics letters, 80 (2002), S. 2269

Jiang,X.*; Jia,C.L.; Szyszka,B.*
Manufacture of specific structure of aluminium-doped zinc oxide films by pattering the substrate surface
Applied physics letters, 80 (2002), S. 3090

Jäger,N.D.; Ebert,P.; Urban,K.; Krause-Rehberg,R.*; Weber,E.R.*
Scanning tunneling microscopy and spectroscopy of semiinsulating GaAs
Physical review B, 65 (2002), S. 195318-1 - 195318-8

Jäger,N.D.; Urban,K.; Weber,E.R.*; Ebert,P.
Dopant atom clustering and charge screening induced roughness of electronic interfaces in GaAs p-n multilayers
Physical review B, 65 (2002), S. 235302-1 - 235302-4

Kluge,F.; Yurechko,M.; Urban,K.; Ebert,P.
Influence of growth kinetics and chemical composition on the shape of voids in quasicrystals
Surface science, 519 (2002), S. 33 - 39

Krause,H.J.*; Wolf,W.*; Glaas,W.*; Zimmermann,E.*; Faley,M.I.; Sawade,G.*; Mattheus,R.*; Neudert,G.*; Gampe,U.*; Krieger,J.*
Squid array for magnetic inspection of prestressed concrete bridges
Physica C, 368 (2002), 1-4, S. 91 - 95

Lentzen,M.; Jahnen,B.; Jia,C.L.; Thust,A.; Tillmann,K.; Urban,K.
High-resolution imaging with an aberration-corrected transmission electron microscope
Ultramicroscopy, 92 (2002), S. 233 - 242

Luysberg,M.; Kirch,D.; Trinkaus,H.; Holländer,B.; Lenk,St.; Mantl,S.; Herzog,H.-J.*; Hackbarth,T.*; Fichtner,P.F.P.*
Effect of helium ion implantation and annealing on the relaxation behaviour
of pseudomorphic Si1-xGex/Si(100) buffer layers on Si (100) substrates
Journal of applied physics, 92 (2002), S. 4290 - 4295

Luysberg,M.; Kirch,D.; Trinkaus,H.; Holländer,B.; Lenk,St.; Mantl,S.; Herzog,H.-J.*; Hackbarth,T.*; Fichtner,P.F.P.*
Effect og helium ion implantation and annealing on the relaxation behavior of pseudomorphic Si1-xGex buffer layers on Si (100) substrates
Journal of applied physics, 92 (2002), 8

Messerschmidt,U.*; Petukhov,B.V.*; Bartsch,M.*; Dietzsch,Ch.*; Geyer,B.*; Häussler,L.*; Ledig,L.*; Feuerbacher,M.; Schall,P.; Urban,K.
Dislocation mobility versus dislocation substructure controlled deformation of icosahedral Al-Pd-Mn single quasicrystals
Materials science and engineering A, 319-321 (2002), S. 107

Qin,Y. L.; Jia,C. L.; Urban,K.; Liedtke,R.; Waser,R.
Structural and morphologic evolution of Pt/B007 Sra3 TiO3/Pt capacitors with annealing processes
Applied physics letters, (2002)

Qin,Y.L.; Jia,C.L.; Urban,K.; Liedtke,R.*; Waser,R.
Structural and morphologic evolution of Pt/Ba0.7Sr.0.3TiO3/Pt capacitors with annealing processes
Applied physics letters, 80 (2002), S. 2728 - 2730

Shadrin,P. M.; Jia,C. L.; Divin,Y. Y.
Spread of critical currents in thin-film YBa2Cu3O7-X bicrystal junctions and faceting of grain boundary
Physica C, (2002)

Shadrin,P.*; Jia,C.L.; Divin,Y.
Spread of critical currents in thin-film YBa2Cu3O7-x bycrystal junctions and faceting of grain boundary
Physica C, 372-376 (2002), S. 80 - 82

Shirotov,V. V.; Divin,Y. Y.; Urban,K.
Far-infrared broadband measurements with Hilbert-transform spectroscopy
Physica C, (2002)

Shirotov,V.V.*; Divin,Y.Y.; Urban,K.
Far-infrared broadband measurements with Hilbert spectroscopy
Physica C, 372-376 (2002), S. 454 - 456

Tillmann,K.; Luysberg,M.; Specht,P.*; Weber,E.R.*
Direct compositional analysis of AlGaAs/GaAs heterostructures by the reciprocal space segmentation of high-resolution micrographs
Ultramicroscopy, 93 (2002), S. 123 - 137

Urban,K.; Feuerbacher,M.; Klein,H.
Plasticity of quasicrystalline alloys and their crystalline intermetallix approximants
Radiation effects and defects in solids, 157 (2002), S. 137 - 144

Weidner,E.*; Lei,J. L.; Frey,F.*; Wang,R.*; Grushko,B.
Diffuse scattering in decagonal Al-Ni-Fe
Journal of alloys and compounds, 342 (2002), S. 156 - 158

Wu,J.S.; Jia,C.L.; Urban,K.; Hao,J. H.*; Xi,X. X.*
A new mechanism for misfit dislocation generation : superdislocations associated with Ruddlesden-Popper planar defects
Journal of crystal growth, 234 (2002), S. 603 - 609

Yang,W.*; Feuerbacher,M.; Urban,K.
Cluster structure and low-energy planes in icosahedral Al-Pd-Mn quasicrystals
Journal of alloys and compounds, 342 (2002), S. 164

Yao,Yu.*; Ebert,P.; Li,M.*; Zhang,Zh.*; Wang,E.G.*
Decay characteristics of two-dimensional islands on strongly anisotropic surfaces
Physical review B, 66 (2002), S. 041407-1 - 041407-4

Yu,H.*; Jiang,C.S.*; Ebert,P.; Shilh,C.K.*
Probing the step structure of buried metal/semiconductor interfaces using quantized electron states: the case of Pb on Si(111)6x6-Au
Applied physics letters, 81 (2002), S. 2005 - 2007

Yu,H.*; Jiang,C.S.*; Ebert,P.; Wang,X.D.*; White,J.M.*; Niu,Q.*; Zhang,Zh.*; Shih,C.K.*
Quantitative determination of the metastability of flat Ag overlayers on GaAs(110)
Physical review letters, 88 (2002), S. 016102-1 - 016102-4

Yurechko,M.; Grushko,B.; Velikanova,T.*; Urban,K.
Isothermal sections of the Al-Pd-Co alloy system for 50-100 at.% Al
Journal of alloys and compounds, 337 (2002), S. 172 - 181

Book chapter

Faley,M.I.; Poppe,U.; Urban,K.; Slobodchikov,V.Y.*; Maslennikov,Y. V.*; Gapelyuk,A.*; Sawitzki,B.*; Schirdewan,A.*
Sensitive HTS dc-SQUID system for biomagnetic measurements
Proceedings of the 13th International Conference on Biomagnetism / ed.: H.Nowak ... - VDE, Berlin, 2002. - S. 925 - 927

Jäger,N.D.; Urban,K.; Weber,E.R.*; Ebert,P.
Roughness of electronic interfaces in GaAs p-n multilayers investigated by crossectional scanning tunneling microscopy
Proceedings of the Materials Research Society Spring Meeting, Symposium F : Defect and Impurity Engeneered Semiconductors and Devices III ; F12.4 - F12.4.6 April 1-5 / ed.: S.Ashok ... - San Francisco. - 719 (2002)

Klein,S.; Finger,F.; Carius,R.; Rech,B.; Luysberg,M.; Stutzmann,M.*
High efficiency thin film solar cells with intrinsic microcrystalline silicon by hot-wire CVD
Materials Research Society Symposium proceedings. - 715 (2002). - S. A26.2

Luysberg,M.; Kirch,D.; Trinkaus,H.; Holländer,B.; Lenk,St.; Mantl,S.; Herzog,H.-J.*; Hackbarth,T.*; Fichtner,P.F.P.*
Effect of helium ion implantation and annealing on the relaxation behaviour
of pseudomorphic Si1-xGex/Si(100) buffer layers on Si (100) substrates
Institute of Physics conference series. - 169 (2001). - S. 181

Tillmann,K.; Luysberg,M.; Specht,P.*; Weber,E.R.*
Dopant induced stabilization of LT-grown AlAs/GaAs:Be MQWs against thermally activated Al-Ga intermixing
Proceedings of the 15th International Congress on Electron Microscopy / ed.: R.Cross. - Microscopy Society of Southern Africa. - 1 (2002). - S. 122 - 123

Urban,K.; Feuerbacher,M.; Wollgarten,M.

Mechanical properties of quasicrystals
Quasicrystals : an introduction to structure physical proberties and applications / ed.: J.B.Suck ... - Springer, 2002. - (Materials science series). - S.305

Wollgarten,M.; Franz,V.; Feuerbacher,M.; Urban,K.
Defects
Quasicrystals : an introduction to structure physical properties and applications / ed.: J. B. Suck ... - Springer, 2002. - (Materials science series). - S. 305

Yurechko,M.V.; Velikanova,T.Ya.*; Grushko,B. C.
New ternary phases in the Al-Pd-Co systems.
Reports of the National Academy of Sciences of Ukraine
Reports of the National Academy of Sciences of Ukraine. - 4 (2002). - S. 168 - 172

Invited talks

Baier,F.*; Müller,M.A.*; Sprengel,W.*; Grushko,B.; Strertzel,W.*; Assmus,W.*; Schäfer,H.E.*
Atomic defects in Al-Pd-Mn : a study by means of positron annihilation spectroscopy
12th International Conference on Positron Annihilation
München: 06.08.2000 - 12.08.2000

Divin,Y.Y.; Volkov,O.Y.*; Liatti,M. V.; Gubankov,V. N.*
Spectral range of the ac Josephson effect in (100)-tilt YBa2Cu3O7-x bicrystal junctions
Applied Superconductivity Conference ASC 2002
Houston, Texas: 04.09.2002 - 09.09.2002

Ebert,P.
Atomic scale solid state research using scanning tunneling microscopy
Condensed Matter Seminar : University of Texas ; Prof.Dr.C.K.Shih
Austin, Texas: 15.01.2002

Ebert,P.
From nanostructures to atoms : imaging and measurement methods
Seminar : Institut d'Electronique et de Microelectronique du Nord
Villeneuve d'Ascq, France: 20.06.2002

Ebert,P.; Domke,C.; Urban,K.
Nachweis elektrischer Ladungen und Versetzungen in GaAs mittels Querschnittsrastertunnelmikroskopie
Frühjahrstagung der Deutschen Physikalischen Gesellschaft
Regensburg: 11.03.2002 - 15.03.2002

Feuerbacher,M.
Mechanical properties of large-unit cell intermatallic compounds
Frühjahrstagung der Deutschen Physikalischen Gesellschaft
Regensburg: 10.03.2002 - 15.03.2002

Feuerbacher,M.
Plasticity of quasicrystals and complex intermetallics
Internationale Konferenz : RQ 11
Oxford, GB: 25.08.2002 - 30.08.2002

Franke,K. J.*; Sharma,H.R.*; Theis,W.*; Gille,P.*; Ebert,P.; Rieder,K.H.*
Quasikristalline Sb und Bi Monolagen auf quasikristallinen Oberflächen
Frühjahrstagung der Deutschen Physikalischen Gesellschaft
Regensburg: 11.03.2002 - 15.03.2002

Houben,L.; Luysberg,M.; Brammer,T.*
Holographische Abbildung von Korngrenzen in Silizium in der Transmissionselektronenmikroskopie
Frühjahrstagung der Deutschen Physikalischen Gesellschaft
Regensburg: 10.03.2002 - 15.03.2002

Hüging,N.; Tillmann,K.; Trinkaus,H.; Urban,K.; Holländer,B.; Mantl,S.; Fichtner,P.*; Luysberg,M.
Quantitative TEM analysis on the pressure of helium filled nano-cracks in implanted silicon
Proceedings of the 15th International Congress on Electron Microscopy / ed.: R.Cross. - Microscopy Society of Southern Africa. - 1 (2002). - S. 99 - 100

Jahnen,B.; Luysberg,M.
Interdiffusion in GaSb/AlGaSb heterostructures
15th International Congress on Electron Microscopy
Durban, South Africa: 01.09.2002 - 06.09.2002

Jia,C.L.
Engineering and characterization of the interfaces in electronceramic thin film systems
Euro Conference on Structure and Composition of Interfaces in Solids
Kloster Irsee: 18.08.2002 - 23.08.2002

Jäger,N.-D.; Urban,K.; Weber,E.R.*; Ebert,P.
Dopant atom clustering and charge screening induced roughness of electronic interfaces in GaAs p-n multilayer.
29th Conference on the Physics and Chemistry of Semiconductor Interfaces (PCSI-29)
Santa Fe, New Mexico: 06.01.2002 - 10.01.2002

Jäger,N.D.; Urban,K.; Weber,E.R.*; Ebert,P.
Rauhigkeit an elektronischen p-n Übergängen
Frühjahrstagung der Deutschen Physikalischen Gesellschaft.
Regensburg: 11.03.2002 - 15.03.2002

Jäger,N.D.; Urban,K.; Weber,E.R.*; Ebert,P.
The importance of screening and clustering of dopant atoms in the roughness of electronic interfaces in p-n interfaces in GaAs
Materials Research Society Spring Meeting
San Francisco: 01.04.2002 - 06.04.2002
Klein,S.; Finger,F.; Carius,R.; Rech,B.; Stutzmann,M.*
High efficiency thin film solar cells with intrinsic microcrystalline silicon by hot wire CVD
Materials Research Society Spring Meeting 2002
San Francisco, USA: 02.04.2002 - 05.04.2002

Luysberg,M.; Hüging,N.; Tillmann,K.; Trinkaus,H.; Urban,K.; Holländer,B.; Mantl,S.; Fichtner,P.*
Quantitative TEM analysis on the pressure of helium filled nano.cracks in implanted Si
15th International Congress on Electron Microscopy
Durban, South Africa: 01.09.2002 - 06.09.2002

Luysberg,M.; Kirch,D.; Holländer,B.; Mantl,S.; Lenk,St.; Trinkaus,H.; Hackbarth,Th.*; Herzog,H. J.*; Fichtner,P.*
Strain relaxation of He implanted, pseudomorphic Si1-xGex layers on Si(100)
15th International Congress on Electron Microscopy
Durban, South Africa : 01.09.2002 - 06.09.2002

Luysberg,M.; Kirch,D.; Holländer,D.; Mantl,S.; Lenk,St.; Trinkaus,H.; Hackbarth,Th.*; Herzog,H.-J.*; Fichtner,P.*
Strain relaxation of He implanted, pseudomorphic Si1-xGex layers on Si(100)
Proceedings of the 15th International Congress on Electron Microscopy / ed.: R.Cross. - Microscopy Society of Southern Africa. - 1 (2002). - S. 61

Theis,W.*; Franke,J. K.*; Kury,P.*; Horn-von-Hoegen,M.*; Gille,P.*; Ebert,P.; Rieder,K.H.*
Surfaces of quasicrystals : morphology, epitaxy, and phase transitions
Frühjahrstagung der Deutschen Physikalischen Gesellschaft
Regensburg: 11.03.2002 - 15.03.2002

Tillmann,K.; Luysberg,M.; Specht,P.*; Cich,M.*; Weber,E.R.*
Berryllium dopant induced stabilization against intermixing and precipitation upon annealing of LT/AlAs/GaAs :be multiple quantum wells
3rd Symposium on Non-Stoichiometric III-V Compounds.
Erlangen: 08.10.2001 - 10.10.2001

Tillmann,K.; Luysberg,M.; Specht,P.*; Weber,E.R.*
Dopant induced stabilization of LT-grown Al/As/GaAs:Be MQWs against thermally activated Al-Ga intermixing
15th International Congress on Electron Microscopy ICEM
Durban, Southern Africa: 01.09.2002 - 06.09.2002

Tillmann,K.; Luysberg,M.; Specht,P.*; Weber,E.R.*
Mechanism of interdiffusion and thermal stability upon annealing of AlAs/GaAs:Be quantum wells grown under low temperature conditions.
Institute of Physics Conference : Oxford University
Oxford: 25.03.2001 - 29.03.2001

Other talks

Ebert,P.
Atome sehen mit dem Rastertunnelmikroskop
Bild der Wissenschaft - Forschungscamp : Wissenschaft zum Anfassen für Jugendliche ; Forschungszentrum Jülich
Jülich: 01.04.2002 - 06.04.2002

Ebert,P.; Kreibig,U.*; Mantl,S.; Michely,Th.*; Urban,K.; von Plessen,G.*; Wuttig,M.*
Neue Materialien : vom physikalischen Konzept zur Anwendung
Seminar an der RWTH Aachen : Sommersemester 2002

Luysberg,M.
He implantation in SiGe/Si heterostructures : formation and interaction of defects.
Max-Planck Institut für Mikrostrukturphysik, Halle : invited by P.Werner
Halle

Posters

Faley,M.I.; Poppe,U.; Urban,K.; Slobodchikov,V.Y.*; Maslennikov,Y. V.*; Gapelyuk,A.*; Sawitzki,B.*; Schirdewan,A.*
Sensitive HTS dc-SQUID system for biomagnetic measurements
Biomag 2002 : 13th International Conference on Biomagnetism
Jena, Germany: 10.08.2002 - 14.08.2002

Jäger,N.-D.; Urban,K.; Weber,E.R.*; Ebert,P.
Dopant atom clustering and charge screening induced roughness of electronic interfaces in GaAs p-n multilayer
29th Conference on the Physics and Chemistry of Semiconductor Interfaces (PCSI-29)
Santa Fe, New Mexico: 06.01.2002 - 10.01.2002

Semmler,U.; Ebert,P.; Urban,K.
Quantifizierung der Bildung von Leerstellen aus (110)-Oberflächen von III-V-Halbleitern
Frühjahrstagung der Deutschen Physikalischen Gesellschaft

Regensburg: 11.03.2002 - 15.03.2002

Shirotov,V.*; Divin,Y.; Poppe,U.; Larue,H.*; Zimmermann,E.*; Ahmet,A.*; Halling,H.*; Urban,K.
Application of Hilbert spectroscopy to pulsed far-infrared radiation
Applied Superconductivity Conference
Houston / Texas: 04.09.2002 - 09.09.2002

Patents granted

Faley M.I.; Poppe U., Jia C.L.;
Layered arrangement and component containing the latter
US 6,353,234 B1 (Mar. 5, 2002)
DE 196 34 118 A1 (23.08.1996)
PT 1.1387

Patents applied for

Zimmermann E.1; Poppe U.2; ; Faley M.2; Halling H.1
1ZEL
2IFF
Magnetic flux sensor with a loop-shaped magnetic field conductor, and the production thereof
DE19915226
EP1166139 (02.01.2002)
WO0060370
PCT/DE00/00962
PT 1.1674 PCT

Zimmermann E.1; Glaas W.1; Halling H.1; Faley M.2; Soltner H.3
1ZEL
2IFF
3ESS
SQUID-Mikroskop
EP: 01.125102.2 (23.10.2001) (DE,FR,GB,IT,NL,)
US: (2001)
DE10053034 A (16.05.2002)
EP1202052 (02.05.2002)
PT 1.1838

Institute for Electronic Properties

General Overview

In any condensed matter system, electrons are the "glue" that holds the atoms together. Therefore the electronic structure constitutes a microscopic base for all material properties. The electronic interactions determine whether a solid is metallic, insulating or semiconducting, whether it is transparent or exhibits a distinctive color, whether it is a magnet or a superconductor.

The research program of the Institute for Electronic Properties is devoted towards the investigation of the electronic structure of atoms, clusters, nanostructures, and solids. The ultimate goal is the development of an understanding and thus a base for the control of the properties of new materials.

After the departure of the former institute director Prof. Wolfgang Eberhardt to BESSY in the year 2001 it was decided that in the future the Institute for Electronic Properties should focus on research on magnetic nanostructures. It thus can serve as a nucleus for the various research activities within this field, which exist at the research center. A list of three candidates for the future institute director has been established and negotiations with the first candidate on the list are on the way. We hope that this position can be filled in spring or early summer 2003 so that the institute can resume full operation. In the past year the institute has shrunken considerably due to personnel following Prof. Eberhardt to the BESSY GmbH or taking up an employment in industry. The largest group remaining is the research group on magnetic multilayers, which can well serve as a nucleus for the new "Institute for Electronic Properties of Magnetic Nanostructures". Therefore the activities of this group are highlighted in this overview.

The areas of research of this group can be summarized as follows:

1. Deposition of magnetic thin films and multilayers by various techniques (MBE, ion-beam, and magnetron sputtering).
2. Characterization of magnetic and magnetotransport properties of magnetic thin film and multilayers by LEED, RHEED, MOKE, SQUID, Brillouin light scattering (BLS) and ferromagnetic resonance (FMR), magnetoresistance measurements, I-V characteristics, XPS, AES, XRR, soft x-ray emission (SXE), near-edge x-ray absorption spectroscopy (NEXAFS), AFM, and STM.
3. Definition of stripes and junctions by optical and e-beam lithography down to the 100 nm scale for transport measurements.
4. Instrumental development for (i) an in-situ chemical analysis by XPS and AES in the ion-beam sputtering machine and (ii) electrical transport measurements at low temperature and in a magnetic field with an enhanced sensitivity.

Some important research results in 2002 were:

• The coexistence of strong antiferromagnetic interlayer coupling and electronic transport (in CPP geometry) via tunneling could be shown for epitaxial Fe/Si/Fe(001) trilayers. The existence of a band gap in the Si spacer layer at the Fermi energy providing a tunneling barrier is confirmed by preliminary spectroscopic data (SXE and NEXAFS, in collaboration with S. Eisebitt and A. Zimina, BESSY) and correlates with sharp interfaces observed by TEM (in collaboration with C. Jia). These results are an important piece of information for the theoretical understanding of the coupling mechanism across Si spacers.
• Development of a new theoretical model to calculate BLS spectra and MOKE hysteresis loops for magnetic multilayers with strong antiferromagnetic coupling, for which a twisted magnetization state occurs within each magnetic layer. The excellent agreement between MOKE and BLS measurements and the fits according to the new model confirm the existence of the proposed twisted magnetization state.
• Successful deposition of VITROVAC thin films with good soft magnetic properties by sputtering from targets built from amorphous VITROVAC ribbons (in collaboration with U. Poppe). The magnetic characterization by BLS and FMR indicates preparation and thickness dependent variations of the film magnetization.
• Optimization of the GMR ratio of Co/Cu/Permalloy pseudo spin valves by varying the Ar pressure during magnetron sputter deposition. The dependence is non-monotonic, and a maximum of 4% is achieved at an intermediate pressure.

• The GMR ratio of Co/Cu multilayers strongly depends on the number of bilayers. This dependence can be understood by assuming that the first few bilayers are not significantly contributing to the GMR effect but act as buffer layers which improve the growth quality of the subsequent bilayers.
• The roughness-induced GMR enhancement previously found for pairs of samples with rough and smooth interfaces could be confirmed for a single sample with a wedge-shaped bottom Fe layer: The oscillations of the RHEED intensity (measured along the wedge after deposition) correlate with oscillations of the GMR ratio (measured at different position along the wedge after lithographically defining stripe conductors perpendicular to the wedge slope). These results allow excluding any influence of different buffer layer qualities on the GMR ratios.
• A first series a nanocontacts of epitaxial Fe/Cr/Fe trilayers could be prepared by a combination of e-beam and optical lithography. The contacts with a diameter of about 200 nm show metallic behavior and a currently not understood dependence of the resistance on the current density. A new process for the fabrication of nanopillars of epitaxial Fe/Cr/Fe multilayers has been developed as an alternative route for the observation of current-induced magnetic switching.

Most members of the former cluster group have left the institute and with them the equipment for cluster deposition has been transferred to Berlin. However, the existing cluster beam apperatus is being upgrated with a linear double reflectron. The most important scientific achievement in research on clusters was the interpretation of scanning tunneling spectroscopy data of endohedral fullerenes $Ce@C_{44}$ and $Ce@C_{50}$. Orbitals and orbital symmetries of the fullerene molecules were calculated and assigned.

Work continued on the two soft x-ray beamlines of IFF at DELTA and BESSY. For the latter beamline (UE56/1-SGM) the beam stability was improved by the installation of a more sophisticated mirror chamber. The focus at the sample position could be improved up to a 70 μm vertical spot size. Results obtained on the two beamlines include:

• Investigation of the electronic structure of Co and Cu submonolayers on stepped W(110) surfaces. The dispertion of the electronic states of Co and Cu is compatible with the assumption of quasi on dimensional structures, e.g., monoatomic chains.
• For the Heussler alloy $Co_2Cr_xFe_{1-x}Al$ the electronic structure was investigated by magnetic x-ray circular dichroism (MXCD) and the domains were observed by photoemission electron microscopy (PEEM). The observed magnetic moments of Fe and Cr are considerably larger than those reported in metallic compounds.
• Soft x-ray spectroscopy of fluids. Here first observations of concentration dependent differences in adsorption edges of iron and other 3d metal ions in solution could be made.

In 2002 again some members of the institute received personal awards and achievements:
Dr. S. Blügel has been appointed institute director for the Institute Theory I of the IFF.
Prof. Dr. P. Grünberg received an honorary doctorate from the Ruhr-University Bochum.
Dr. P.S. Bechthold was appointed APL Professor at the University of Cologne.

The following students have been awarded their diploma and Ph.D. degrees in 2002:

Diploma:
Henning Dassow: Herstellung von Nanokontakten zum Nachweis strominduzierten magnetischen Schaltens
Bernd Heitkamp: Charakterisierung magnetischer Materialien mit X-PEEM
Lars Pohlmann: Transporteigenschaften in Fe/Si/Fe Schichtsystemen mit halbleitenden Zwischenschichten

Doctorate:
Jörg Wingbermühle: Transportphänomene in magnetischen Tunnelkontakten unter besonderer Berücksichtigung der Ionenstrahldeposition
Christopher Zilkens: Gestufte Oberflächen und quasieindimensionale Strukturen Photoemission an 3d Metallen auf W(110)
Matthias Buchmeier: Magnetische Schichtsysteme: Veränderung statischer und dynamischer magnetischer Eigenschaften durch starke Zwischenschichtkopplung

I would like to close this report by thanking all members of the institute for their dedicated work during the past year.

Thomas Brückel

Personnel 2002/2003 and areas of activity

Scientists	Research Areas
Dr. L. Baumgarten	F-sec laser photoemission and high resolution photoemission from solids
Prof. P.S. Bechthold	Electronic structure, geometry and materials properties of clusters
Dr. G. Bihlmayer *until 31.10.02*	Electronic structure theory of solids and multilayers
Dr. D.E. Bürgler	Magnetic multilayers for sensors and memory applications
Prof. Dr. Th. Brückel	Interims director
Dr. S. Cramm	Beamlines at DELTA and BESSY II
Dr. R.R. Gareev	Magnetic multilayers for sensors and memory applications
Prof. P. Grünberg	Magnetic multilayers for sensors and memory applications
Dr. J. Morenzin *until 31.08.02*	Development of a magnetic security system
Dr. A. Paul	Magnetic multilayers for sensors and memory applications

Technicians and Engineers

W. Bergs	Cluster beam apparatus
K. Bickmann	Vacuum-Laboratory
J. Gollnick	Secretary
F.-J. Köhne	Magnetic multilayers for sensors and memory applications
B. Küpper	Vacuum-Laboratory
J. Lauer	Electronic-Laboratory
H. Pfeifer	Electronic-Laboratory
C. Schiffer	Electronic-Laboratory
R. Schreiber	Magnetic multilayers for sensors and memory applications

Thesis students

H. Braak (Diploma-student)	Magnetic multilayers for sensors and memory applications
M. Buchmeier (PhD-student)	Magnetic multilayers for sensors and memory applications
M. Breidbach (PhD-student)	Magnetic multilayers for sensors and memory applications
T. Damm (PhD-student)	Magnetic multilayers for sensors and memory applications
H. Dassow (PhD-student)	Magnetic multilayers for sensors and memory applications
M. Heide (PhD-student) *until 31.12.02*	STM-theory
B. Heitkamp (Diploma-student) *until 31.03.02*	Photoelectron microscopy
L. Pohlmann (PhD-student)	Magnetic multilayers for sensors and memory applications
D. Wortmann (PhD-student) *until 31.12.02*	STM-theory
C. Zilkens (PhD-student) *until 31.01.02*	F-sec laser photoemission and high resolution photoemission from solids

Trainees

D. Esser	Electronic-Laboratory

Coexistence of strong antiferromagnetic coupling and transport via tunneling in epitaxial Fe/Si/Fe structures

R.R. Gareev, L.L. Pohlmann, D.E. Bürgler, and P.A. Grünberg
Institute "Electronic Properties"

We prepare epitaxial Fe(5 nm)/Si(0.8-2 nm)/Fe(5 nm) ferromagnetic tunneling junctions with strong antiferromagnetic interlayer coupling. Transport properties in CPP geometry reveal (i) a strong increase of the resistance times area product with spacer thickness, (ii) parabolic *dI/dV-V* characteristics, and (iii) a small and negative temperature coefficient of the zero-bias resistance. Therefore, antiferromagnetic interlayer coupling and transport via tunneling coexists in these junctions.

Recently, we have found very strong antiferromagnetic (AF) interlayer coupling with a total coupling strength in excess of 5 mJ/m^2 in epitaxial Fe/Si/Fe structures [1]. In view of the strong tendency for silicide formation in this system, the question about the nature of the spacer layer arises: Is the coupling mediated by a metallic FeSi alloy [2], by pinholes, or by a non-conductive spacer? The latter would call for a new coupling mechanism to explain the strong AF coupling. Here, we report CPP (current-perpendicular-plane) transport measurements to prove that electronic transport across the spacer proceeds via elastic tunneling and that the coupling is indeed mediated by a non-conductive spacer. To do so, we show the validity of the necessary and sufficient criteria for direct elastic tunneling [3]: (i) strong and exponential increase of the resistance with spacer thickness t, (ii) parabolic dependence of dI/dV on V, and — most decisive — (iii) small and negative temperature coefficient of the zero-bias resistance.

The preparation procedure of Fe(5 nm)/Si(0.8-2 nm)/Fe(5 nm) wedge-type epitaxial samples on Ag(150 nm)/Fe(1 nm)/GaAs(100) buffer systems has been described elsewhere [1,2]. We measure longitudinal magneto-optical Kerr effect (MOKE) and SQUID hysteresis loops to verify the presence of AF coupling. The zero-field antiparallel alignment is observed in the whole range of temperatures (4 –300 K) and for all spacer thicknesses (Fig. 1). After these magnetic characterizations, 10x10 mm^2-sized, wedge-type samples are patterned using photolithography, ion-beam etching, and lift-off to obtain CPP junctions with different spacer thicknesses, which are all deposited under the same

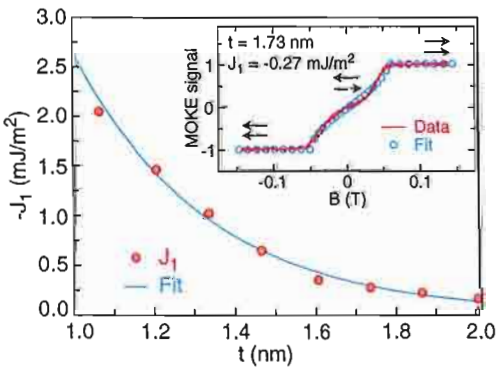

FIG. 1. AF coupling constant J_1 versus spacer thickness t. The fitted curve yields a decay length of 0.33 nm. Inset: Experimental and fitted longitudinal MOKE hysteresis curves clearly show antiparallel alignment due to AF coupling and yield J_1=-0.27 mJ/m^2.

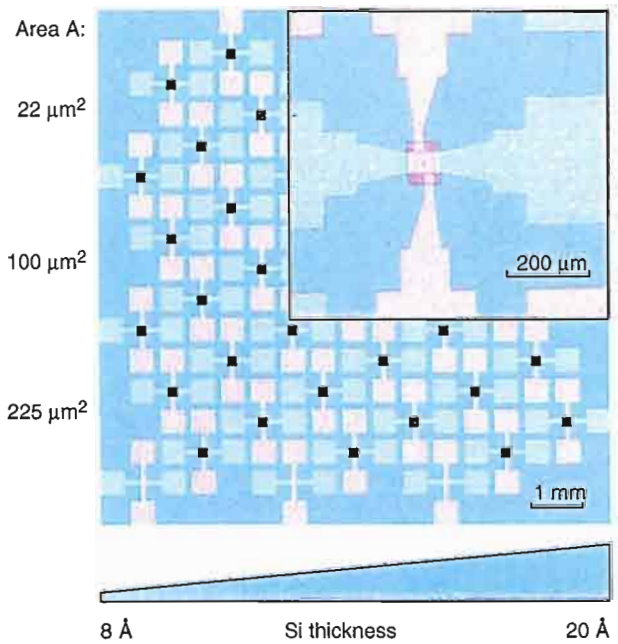

FIG. 2. Layout of the sample with a wedge-type Si spacer layer resulting in junctions with different spacer thicknesses. The inset shows a photograph of a typical patterned junction.

growth conditions. We use crossed contacts, where the upper electrode is formed by depositing a 300 nm-thick Cu layer. The patterned 150 nm-thick silver buffer layer serves as a bottom electrode. Electrical insulation of the electrodes is achieved by deposition of a 250 nm-thick Si-oxide layer. Finally, we define junctions of rectangular shape ranging in area A from 22 to more than 200 µm^2 (Table 1). The layout of the patterned sample is shown in Fig. 2. Voltage and current leads suitable for four-point transport measurements

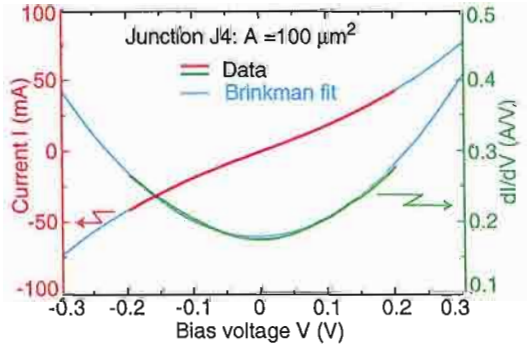

FIG. 3. Measured (red and green) and fitted (blue) I-V and dI/dV curves of junction J4.

Table 1: Junction area A, nominal spacer thickness t, junction resistance R, and the parameters derived from Brinkman fits: mean barrier height ø, barrier asymmetry Δø, and the fitted barrier thickness t_{eff} for various junctions labelled J1 to J6.

Junction	A (μm^2)	t (nm)	R (Ω)	ø (eV)	Δø (eV)	t_{eff} (nm)
J1	22	1.54	307	0.35	-0.35	1.83
J2	22	1.70	23.4	0.54	-0.36	1.22
J3	100	1.48	26.0	0.33	0.05	1.74
J4	100	1.54	5.6	0.43	-0.18	1.35
J5	100	1.64	223	0.78	-0.30	1.44
J6	225	1.70	5.3	0.36	-0.10	1.55

are connected by ultrasonic bonding.

A representative *I-V* curve taken at room temperature and the corresponding *dI/dV-V* curve are presented in Fig. 3 and show typical tunneling-type behaviour. The *dI/dV-V* curve is parabolic with its minimum away from $V=0$. We observe similar curves for all junctions with $t>1.5$ nm, for which the voltage drop is sufficient to reveal the non-linear part of *I-V* characteristics, and we can fit them with the Brinkman formula [4]. The calculated barrier heights ø vary from 0.33 to 0.78 eV and show a definite barrier asymmetry (Table 1). The variation of the barrier heights could be related to locally different Si contents in the Si-rich spacer. The observed barrier asymmetry is most likely caused by different rates of diffusion at Fe/Si and Si/Fe interfaces [1]. The fitted barrier thicknesses t_{eff} are in most cases slightly smaller than the nominal Si indicating some interdiffusion at the interfaces. For junctions J1 and J3, however, the Brinkman fits result in $t_{eff}>t$, which according to Ref. [5] is an indication of a small amount of pin-holes in the spacer layer. In this case, the transport across the pin-holes coexists with the dominating tunneling process and leads to a slightly decreased value of the fitted barrier height [5].

In Fig. 4 we show the resistance times area product *RA* versus t on a semi-logarithmic scale. The value of *RA* increases at room temperature strongly with t by more than 4 orders of magnitude, while t only approximately doubles. The decay length $t_0\approx1$ Å (dashed line in Fig. 4) is of the same order of magnitude as the decay length of the coupling strength given in Fig. 1 and in Ref. [1].

A typical temperature dependence for junctions of the zero-bias resistance for junctions with $t_{eff}<t$ is presented in Fig. 5. The resistance slightly decreases (5-7%) with temperature and thus indicates prevailing direct elastic tunneling. The temperature dependence in this case arises solely from the broadening of Fermi distributions. Elastic but resonant tunneling is much weaker than the direct one

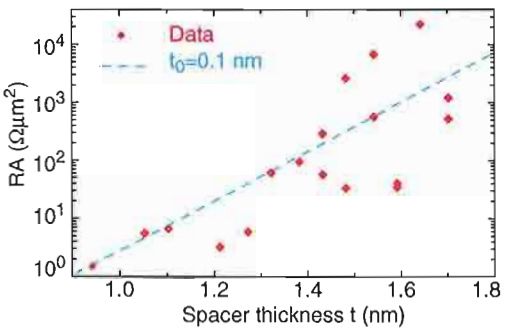

FIG. 4. Dependence of the resistance times area product *RA* on the nominal spacer thickness t obtained from a wedge-type Fe/Si/Fe structure. The blue, dashed line corresponds to a decay length t_0=1 Å.

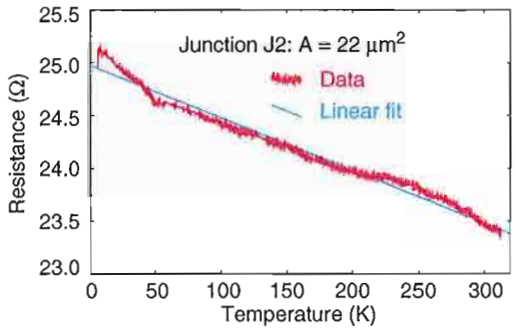

FIG. 5. Dependence of the resistance on temperature for junction J2. The blue line is a linear fit yielding a temperature coefficient of -5×10^{-3} ΩK^{-1}.

and obeys a decay length, which is twice as large as the decay length of direct tunneling. We cannot definitely exclude resonant elastic tunneling for our junctions because of the narrow thickness range ($1.4<t<1.7$ nm). Different weights of the contributions from elastic direct and elastic resonant tunneling could lead to the scattering of the *RA* values in Fig. 4. Next, we consider inelastic tunneling based on thermo-activated hopping across impurity states in the barrier. For this channel a strong decrease of resistance with temperature is expected. Thus, this channel is not dominant in our junctions. Finally, the third criterion for direct tunneling – the negative temperature coefficient of the resistance observed in Fig. 5 – allows us to exclude a significant metallic contribution to the electron transport through pin-holes.

We conclude that epitaxial, AF coupled Fe/Si/Fe junctions fulfil the necessary and sufficient criteria for direct elastic electron tunneling. The experimentally proven coexistence of both strong AF coupling and electron transport via elastic tunneling across nominally pure Si spacers is an important piece of information for the clarification of the so far unknown mechanism of strong AF interlayer exchange coupling across Si spacers.

[1] R.R. Gareev, D.E. Bürgler, M. Buchmeier, R. Schreiber, and P. Grünberg, J. Magn. Magn. Mater. **240**, 237 (2002).

[2] R.R. Gareev, D.E. Bürgler, M. Buchmeier, D. Olligs, R. Schreiber, and P. Grünberg, Phys. Rev. Lett. **87**, 157202 (2001).

[3] D.A. Rabson, B.J. Jönsson-Åkerman, A.H.Romero, R. Escudero, C. Leighton, S.Kim, and I.K.Schuller, J. Appl. Phys. **89**, 2786 (2001).

[4] W.F. Brinkman, R.C. Dynes, and J.M. Rowell, J. Appl. Phys. **41**, 1915 (1970).

[5] J.J. Åkerman, R. Escudero, C. Leighton, S. Kim, D.A. Rabson, R.W. Dave, J.M. Slaughter, and I.K. Schuller, J. Magn. Magn. Mater. **240**, 86 (2002).

Layered magnetic structures: twisted ground state due to strong antiferromagnetic coupling

M. Buchmeier, R. Gareev, D. E. Bürgler and P. Grünberg
Institute "Electronic Properties"

We have investigated the remagnetization behavior of ferromagnetic doublelayers with strong antiferromagnetic interlayer exchange coupling. If the coupling and external field are strong enough a partial Bloch-type domain wall parallel to the interface will form inside the ferromagnetic layers. This twisted groundstate has to be taken into account when extracting the coupling constants from hysteresis loops. Comparing experimental Magneto-Optic-Kerr-Effect (MOKE) and Brillouin Light Scattering (BLS) data obtained from strongly coupled Fe/Si/Fe Samples with a model calculation we find strong evidence for the twisted state.

After the discovery of magnetic interlayer exchange coupling (IEC) in 1986 by Grünberg *et al.* [1] the phenomenon has been explored in much detail and its origin is basically understood. Still some discrepancies remain, for example the large differences between the theoretically predicted and experimentally measured coupling strengths [2]. On the other hand there is an increasing interest in interlayer coupling, in particular in systems showing strong antiferromagnetic (AFM) coupling, due to applications as artificial antiferromagnets or antiferrimagnets in magnetic sensors [3] and more recently in antiferromagnetically coupled (AFC) storage media for hard disk drives [4]. Here we report on the features of the twisted magnetization state encountered in strongly coupled systems and discuss its effect on the remagnetization behavior.

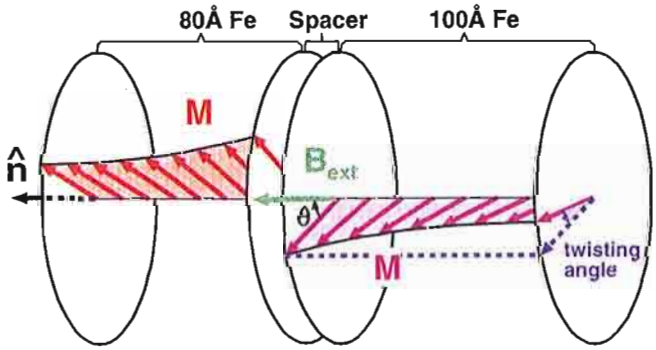

FIG. 1. Schematic view of the twisted magnetization state in a sample with strong AFM coupling. The circles lie in the plane of the interfaces. The in-plane magnetization angle θ varies in direction of the sample normal $\hat{n}$. The picture corresponds to Fe(80Å)/spacer/Fe(100Å) with applied field B_{ext} of 0.5 T and coupling strength $J_1 = -2.6$ mJ/m^2, $J_2 = -0.2$ mJ/m^2 typical for a Si spacer with a thickness of 10Å.

The interlayer exchange coupling can be quantitatively described by the phenomenological bilinear and biquadratic coupling constants J_1 and J_2 respectively, which are defined by their corresponding energy $E_c = -\sum_i J_i \cos^i(\Delta\theta)$ [2]. Generally their determination requires comparing the field dependence of experimental data with a model calculation. In the case of strong coupling special care has to be taken as the commonly used approximation of a rigid magnetization, uniform in each ferromagnetic (FM) layer, will break down. If the AFM interlayer coupling and external field are strong enough compared to the intralayer exchange the magnetizations twist forming a partial Bloch-type domain wall parallel to the interface as sketched in Fig. 1.

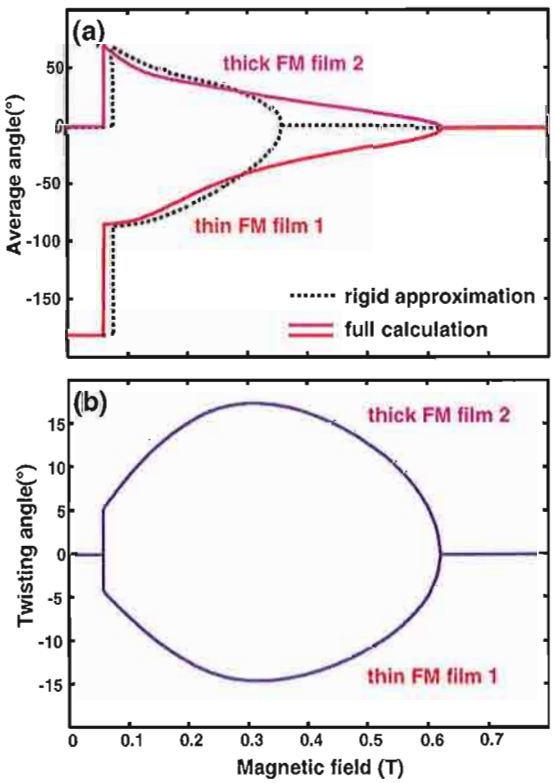

FIG. 2. Calculated field dependence of the twisted state (a) compares the averaged magnetization angles (redd) with the rigid magnetization approximation (black dashed line). In (b) the twisting angle defined as in Fig. 1 is plotted.

The twisted groundstate has been investigated in much detail for the so called exchange springs [5], layered or granular systems with strong direct FM coupling between a hard and soft magnetic material. However, there are only few publications [6–8] treating the twisted groundstate in the case of AFM coupling. The occurrence of the twisted configuration is a result of competing torques exerted at the interface by the coupling and in the bulk by the external field. Its possible lower energy compared to the uniformly magnetized configuration is due

to a reduction of the coupling energy at the cost of intralayer exchange energy, which tends to keep the spins inside the FM layers parallel. A critical AFM coupling strength J_{crit} at which the intralayer exchange and interlayer coupling energy corresponding to a small twist in parallel alignment will cancel out can be estimated to be $J_{crit} \approx -A/d$, where d is the FM layer thickness and A the intralayer exchange constant. For $|J_1| \ll |J_{crit}|$ the twisting effects in a thin film sample can be neglected and the rigid magnetization approximation can be applied as the corresponding intralayer exchange will be bigger than the coupling energy. On the other hand the twist becomes dominant leading to an disproportionate increase of the saturation field with the coupling strength for $|J_1| > |J_{crit}|$ when the anisotropy is negligible.

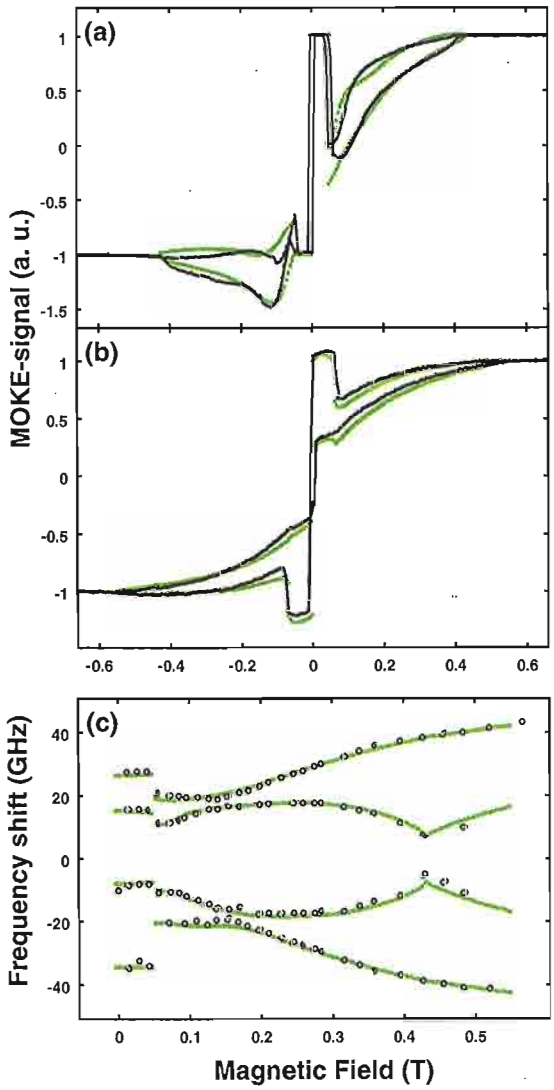

FIG. 3. MOKE loops (a),(b) and BLS data (c) for a Fe(80 Å)/Si(10 Å)/Fe(100 Å) sample. The field is applied along an easy axis in (a) and (c) and a hard axis in (b). Black dotted lines and open circles are the experimental data, the green dotted lines fits including the twisted state.

Using $d = 100$ Å and the literature exchange value for iron of $A = 2 \times 10^{-11}$ J/m yields $J_{crit} = -2$ mJ/m^2. The calculated field dependence in Fig. 2 using parameters typical for Fe(80 Å)/Si(10 Å)/Fe(100 Å) [saturation magnetization $M_s = 1.65 \times 10^6$ A/m, fourfold crystal anisotropy $K_1 = 45000$ J/m^3 and coupling values of $J_1 = -2.6$ mJ/m^2, $J_2 = -0.2$ mJ/m^2], indeed shows pronounced deviations form the uniform state. Although the averaged magnetization angles of the twisted state (solid line in Fig. 2(a)) which approximately determine the MOKE-signal, are close to the result obtained assuming a rigid static magnetization (dotted line) over a wide field range, they clearly deviate for $B_{ext} > 0.3$ T, and the saturation field is about a factor of two bigger. Thus, deriving the coupling strengths from the saturation and spin-flop fields using the rigid approximation will lead to a systematic overestimation of J_1 and especially J_2. The overestimation of J_2 would be as much as by a factor of 3 for the parameters used here. In Fig. 2(b) we plot the the twisting angle defined in Fig. 1 as a measure of the non-uniformity. The twisting angle is not negligible apart from the antiparallel state at low fields ($B_{ext} < 0.07$ T) and the saturated state ($B_{ext} > 0.63$ T) and reaches a maximum value of about 20°.

In Fig. 3 we fit experimental data measured on a epitaxial Fe(80 Å)/Si(10 Å)/Fe(100 Å) sample. This system shows among the largest AFM-coupling values ($|J| > 6$ mJ/m^2) found ever [9]. For the modeling of the MOKE-data [Fig. 3 (a) and (b)] the quadratic MOKE-effects [10] and the twisted state are taken into account approximately by the average magnetization angles. On the other hand the calculation of the spinwave frequencies measured by BLS [Fig. 3 (c)] requires the full magnetic configuration to be included [11]. The coupling values of $J_1 = -1.9$ mJ/m^2 and $J_2 = -0.2$ mJ/m^2 extracted from the different curves are in good agreement and the calculated and experimental curves fits nicely. This shows that the twisted state exists in our sample and is conform to the theory as on the other hand a satisfactory fit assuming a rigid magnetization is not possible.

In conclusion, we have observed the twisted ground-state in strongly AFM coupled doublelayer systems. It has been included in the calculation of MOKE and BLS data, which allows the accurate determination of the coupling constants.

[1] P. Grünberg *et al.*, Phys. Rev. Lett. **57**, 2442 (1986).
[2] D. E. Bürgler *et al.*, Handbook of Magnetic Materials, Vol. 13, p. 14, edited by K. H. J. Buschow, Elsevier Science B. V. (2001).
[3] van den Berg *et al.*, IEEE Trans. Mag. **32**, 4624 (1996).
[4] E. E. Fullerton *et al.*, Appl. Rev. Lett. **77**, 3806 (2000).
[5] E. F. Kneller and R. Hadwig, IEEE Trans. Magn. **27**, 3588 (1991).
[6] W. Folkerts and S. T. Purcell, J. Magn. Mater. **111**, 306 (1992).
[7] J. F. Cochran, J. Magn. Magn. Mater. **147**, 101 (1995).
[8] S. Zoll *et al.*, J. Appl. Phys. **79**, 2601 (1996).
[9] R. R. Gareev *et al.*, J. Magn. Magn. Mater. **240**, 237 (2002).
[10] K. Postava *et al.*, J. Appl. Phys. **91**, 7293 (2002).
[11] M. Buchmeier, thesis, still unpublished

Dynamic properties of sputtered VITROVAC thin films

A.B. Drovosekov, R.R. Gareev, T. Damm, D.E. Bürgler, and P.A. Grünberg
Institute "Electronic Properties"
U. Poppe
Institute "Microstructure Research"

VITROVAC 6025 thin-film samples of different thicknesses are investigated by means of two high-frequency techniques: Ferromagnetic resonance (FMR) and Brillouin light scattering (BLS). FMR measurements are performed by sweeping the frequency from 50 MHz to 40 GHz. In BLS, both the Damon-Eshbach surface mode and multiple standing volume spin wave modes are detected. The combination of FMR and BLS enables us to evaluate the g-factor and the saturation magnetization M_S for film thicknesses down to 4 nm. Thickness and preparation dependent effects are found and discussed.

Amorphous VITROVAC magnetic alloys feature soft magnetic properties such as very low coercivity and anisotropy as well as a high permeability and are therefore used for magnetic field sensors [1]. This application requires the preparation and characterization of sputtered VITROVAC films and motivates our investigation of their magnetic properties. Up to now, there is no report devoted to the high-frequency magnetic properties of sputtered VITROVAC thin films.

Thin films are prepared by ion-beam sputtering in two different deposition setups from VITROVAC 6025 ($Co_{66}Si_{16}B_{12}Fe_4Mo_2$) targets built from 30 µm-thick amorphous, melt-spun ribbons. We perform FMR and BLS for ribbons as well as for a set of thin film samples of different thicknesses t. The sample of 150 nm thickness was sputtered onto a sapphire substrate, all other samples are prepared on oxidized Si wafers. Films with $t \geq 125$ nm are prepared in a small HV chamber using a Kaufmann source, and those with $t \leq 70$ nm in a 4"-compatible UHV system equipped with ECR sources.

In order to study FMR we use a frequency-sweep technique described in Ref. [2]. Our FMR setup is based on a Network Analyser (HP8722ES), which provides the possibility to measure the reflection coefficient S_{11} of a microwave system in a wide range of frequencies from 50 MHz to 40 GHz. We measure the reflected signal in the Corbino geometry where the thin-film sample terminates a coaxial line. The external magnetic field H of up to 6 kOe is applied in the film plane. The microwave magnetic field has radial symmetry according to the modes in the coaxial line. The difference between reflection coefficients obtained at two different external magnetic fields provides information about the resonant losses in the sample.

BLS measurements are carried out in the back-scattering geometry using a Sandercock-type tandem Fabry-Pérot interferometer in (2x3)-pass configuration. An argon laser (λ=532 nm) is used as a light source. The magnetic field (H<6 kOe) is applied in the film plane and perpendicular to the plane defined by the incident and reflected light beam. The magnon spectra are observed at an angle of 45° corresponding to $q_{||} = 1.67 \cdot 10^5$ cm^{-1}.

Figure 1 shows experimental FMR spectra for a 150 nm-thick film. The field dependent minimum reflects the FMR absorption line. Figure 2 depicts the dependencies of the FMR frequencies on H for the ribbon sample as well as for 150 and 70 nm-thick films. The signal from VITROVAC samples with $t \leq 35$ nm is not detectable with our FMR setup based on a Network Analyser.

The theoretical treatment of the experimental FMR spectra is performed on the basis of the formula for the frequency of precession ω in a homogeneously magnetized disk [3]

$$(\omega/\gamma)^2 = H\,(H + 4\pi M_S), \qquad (1)$$

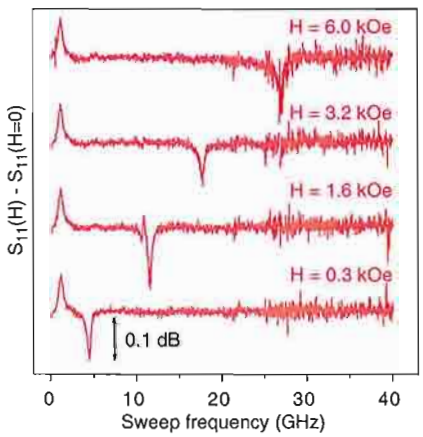

FIG. 1. Experimental FMR spectra of a 150 nm-thick film measured in different magnetic fields H.

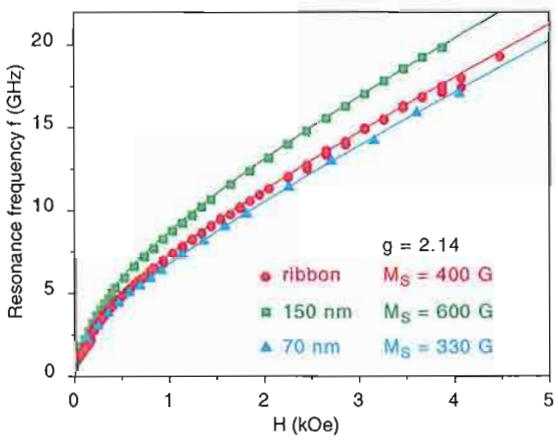

FIG. 2. FMR frequency versus magnetic field for three different samples. Solid lines are fits according to Eq. (1).

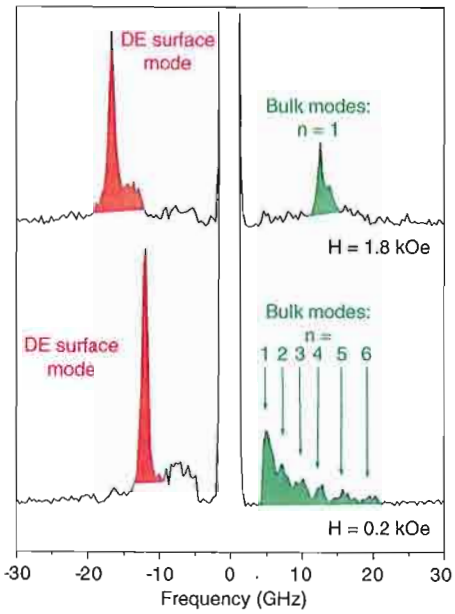

FIG. 3. BLS spectra of a 150 nm film at two different magnetic fields. Arrows indicate positions of bulk modes.

where $\gamma=g\mu_B/\hbar$ with the g-factor g and the saturation magnetization M_S. For all three films the g-factor is constant (g=2.14), while the M_S value is varying.

Figure 3 shows typical experimental BLS spectra taken at two different magnetic fields. The BLS spectra are characterized by the presence of a weak and a strong peak on the Stokes side and up to six peaks on the anti-Stokes side. The resulting field dependence of BLS frequencies for a 150 nm sample is shown in the Fig. 4.

The theoretical treatment of BLS is performed including dipolar interaction and exchange. In this case, the Damon-Eshbach (DE) surface mode frequency is given by [4]

$$(\omega/\gamma)^2 = H(H + 4\pi M_S) + (2\pi M_S)^2[1 - \exp(-2\, q_{||}\, t)], \quad (2)$$

and the volume mode frequencies are given by [5]

$$(\omega/\gamma)^2 = (H+Dq^2)(H+Dq^2+4\pi M_S), \quad (3)$$

where $D=2A/M_S$, $q^2=q_{||}^2+(n\pi/t)^2$ with n= 1,2,3... the number of the standing spin wave mode, and A is the exchange stiffness.

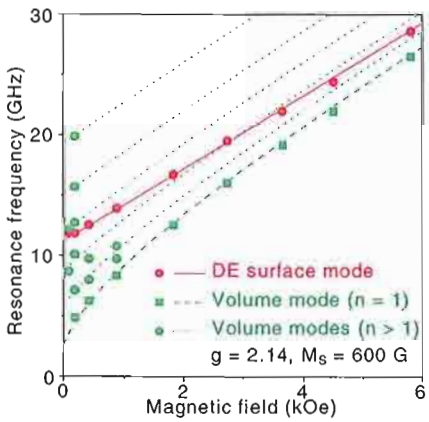

FIG. 4. Dependence of BLS mode frequencies on H for a 150 nm film. Symbols are experimental data and lines indicate calculations according to Eqs. (2) and (3).

Table 1: Summary of fitted parameters for the whole set of samples.

t (nm)	t_{BLS} (nm)	g-factor	M_S (G)	$A\cdot10^7$ (erg/cm)
Ribbon (30 μm)		2.14 ± 0.14[F]	400 ± 80[F]	
150*	150±90[D]	2.14±0.04[F]	620±20[F]	3±3[V]
100*	150±50[D]	2.14±0.07[F]	600±40[F]	6±4[V]
125*	110±110[D]	2.14±0.04[F]	590±10[F]	3±3[V]
70	90±40[D]	2.14±0.14[F]	330±70[F]	5±3[V]
35		2.18±0.10[D]	200±40[D]	
18		2.15±0.10[D]	200±40[D]	
9		2.18±0.10[D]	200±40[D]	
4		2.2±0.2[D]	80±40[D]	

* Estimated, no thickness calibration of the Kaufmann source.
[F] Derived from FMR data.
[D] Derived from the DE mode in BLS.
[V] Derived from BLS volume modes.

Inserting the g-factor and the magnetizations M_S obtained from FMR measurements in Eq. (2) and comparing with experimental BLS spectra enables us to identify the line on the Stokes side of Fig. 3 as the DE mode. Fitting the field dependence of the volume mode frequencies with Eq. (3) allows evaluating the exchange stiffness constant A and the film thickness t_{BLS}, yet with large errors. This procedure could be performed for the t≥70 nm. For thinner films, the volume modes are not observed. However, it is still possible to obtain the g-factor and magnetization M_S from the position of DE modes. The results of the fits are summarized in Table 1.

Our frequency-sweep FMR technique in Corbino geometry provides a simple method to determine the g-factor and M_S, but only for t≥70 nm. For thinner films, these parameters are derived from BLS spectra. The thicknesses determined from the DE mode positions are – within the sizeable error bars – in agreement with the estimated nominal values. We find that the g-factor is rather constant with film thickness. In contrast, M_S shows strong variations: M_S is (i) reduced for all films prepared with the ECR sources (t≤70 nm) and (ii) extremely small for t=4 nm. Possible reasons for this behaviour are (i) different compositions due to preferential sputtering under ECR conditions and (ii) a reduced Curie temperature for the 4 nm film. X-ray reflectivity data indicate the presence of an oxide with a thickness of up to 3 nm, which reduces the effective magnetic thickness of the thinnest film to about 1 nm. Future studies including *in-situ* x-ray photoemission and Auger spectroscopy (XPS/AES) will focus on the dependence of the composition and closely related the saturation magnetization on the sputter conditions and on a precise determination of the effective magnetic thickness of the investigated films.

[1] O.V. Nielsen *et al.*, Sensors and Actuators A **59**, 168 (1997)
[2] J.C. Booth *et al.*, Rev. Sci. Instrum. **65**, 2082 (1994)
[3] C. Kittel, Phys. Rev. **73**, 155 (1948)
[4] R.W. Damon and J.R. Eshbach, J. Phys. Chem. Solids **19**, 308 (1961)
[5] M. Grimsditch *et al.*, Phys. Rev. Lett. **43**, 711 (1979)

Optimizing the GMR effect in NiFe/Cu/Co pseudo spin-valves prepared by magnetron sputtering

Amitesh Paul, Thorsten Damm, Daniel E. Bürgler, and Peter Grünberg
Institute "Electronic Properties"

Simon Stein and Hermann Kohlstedt
Institute "Electroceramic Materials"

We study the dependence of magnetic and magnetotransport properties of NiFe/Cu/Co pseudo spin-valves on the pressure of the Ar sputtering gas during magnetron deposition. The giant magnetoresistance (GMR) ratio as a function of the sputtering pressure behaves non-monotonic with a maximum of about 4% at an intermediate pressure of 0.87×10^{-2} mbar. Atomic force microscopy image reveal a variation of the grain structure with increasing sputtering pressure: The grain size first decreases and then the grains start clustering for highest pressures. These changes influence the spin-independent scattering and thus the GMR ratio via the saturation resistance R_s.

Giant magnetoresistance (GMR) in spin-valves based on different magnetic materials with different coercive fields – so-called pseudo spin-valves – are interesting from the application point of view for developing magnetic sensors and magnetoresistive random access memory (MRAM) technologies [1].

Recently, the influence of the sputtering gas pressure during rf sputtering of the hard CoFe layer in NiFe/Cu/CoFe pseudo spin-valves has been studied [2]. The increase of the GMR ratio with pressure was associated with a small decrease of the grain cluster size [2]. Due to the magnetic confinement of the plasma in magnetron sputtering, the dependence of plasma properties such as the ionization efficiency on pressure are different from that of rf sputtering [3]. Therefore, we attempt to optimize the GMR ratio of NiFe/Cu/Co pseudo spin-valves by changing the sputtering pressure of a magnetron sputtering system.

The pseudo spin-valves studied in the present work are structures of NiFe/Cu/Co prepared by dc magnetron sputtering. The sputtering pressure was controlled by the flow of 99.9999% Ar in the chamber. Trilayer samples labeled S1, S2, and S3 of the structure SiO_2/NiFe(5.0 nm)/Cu(3.0 nm)/Co(3.0 nm) are prepared at three different Ar pressures as listed in Table I.

Magnetoresistance is measured at room temperature (RT) by the conventional four-probe dc technique, and magnetization loops are recorded by means of the magneto-optic Kerr (MOKE) effect at RT. The magnetic field is applied in the plane of the sample for all measurements. Atomic force microscopy (AFM) measurements are performed in tapping mode using a multimode SPM from Digital Instruments.

TABLE I: The GMR ratio, saturation resistance R_s, average feature size, and surface roughness $\sigma_{surface}$ of spin-valves S1, S2, and S3 prepared at different Ar pressures.

Sample	Ar pressure (10^{-2} mbar)	GMR (%)	R_s (Ω)	Feature size (nm)	$\sigma_{surface}$ (nm)
S1	0.34	2.5	0.139	180	1.3
S2	0.87	4.0	0.012	78	0.3
S3	1.70	1.3	0.116	229	2.0

Figure 1(a) shows the MOKE data of the samples. Two distinct separate hysteresis loops corresponding to NiFe (smaller coercivity) and Co (larger coercivity) are seen for S1 and S2, and a weaker, but still well-defined separation for S3. The almost equal vertical position of the plateau due to antialignment for all three samples indicates that the fraction of the sample with antiparallel alignment is approximately the same for all spin-valves. The corresponding magnetoresistance curves are plotted in Fig. 1(b). The GMR ratio is defined as $(R_0 - R_s)/R_s$, where R_s and R_0 are the resistance with and without saturating magnetic field, respectively. The reduced coercivity of S3 is reflected by a narrower field range of the high-resistance state. Note, that the GMR ratio for S2 is higher than that of S1 and S3. Thus, the GMR ratio shows a non-monotonic dependence on the sputtering pressure. This behavior correlates with the different

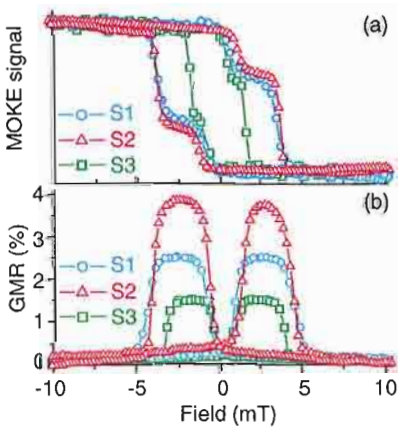

FIG. 1: (a) MOKE hysteresis loops, and (b) magnetoresistance of spin-valves S1, S2, and S3.

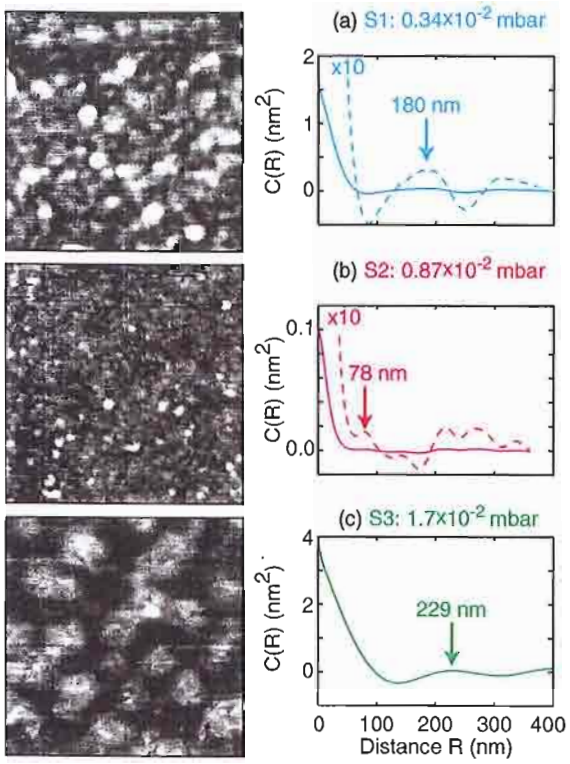

FIG. 2: 1 μm×1 μm AFM micrographs and height-height correlation functions $C(R)$ calculated according to the definition in Eq. (1) from the images of spin-valves (a) S1 (greyscale range 5.0 nm), (b) S2 (greyscale range 2.5 nm), and (c) S3 (greyscale range 10.0 nm). Arrows mark the first correlation maxima which yield a measure for the typical lateral feature size. Dashed curves in (a) and (b) are vertically magnified by a factor of 10.

topographies visible in the AFM micrographs in Fig. 2. The right parts show the height-height correlation function $C(R)$ defined by

$$C(R) := \frac{1}{2\pi A}\int_0^{2\pi} d\vartheta \int_A d^2\rho \; z(\vec{\rho})z(\vec{\rho}+\vec{R}), \qquad (1)$$

where $\vec{R} = (R, \vartheta)$ is an in-plane vector in the integration area A, and $z(\vec{R})$ the height profile. The first correlation maximum allows determining the typical size of the surface features. Evenly distributed grains 180 and 78 nm in size are observed for S1 and S2, respectively. For S3, however, we observe a different surface morphology with larger congeries or clusters of small grains with an average size of 229 nm and voids in between. The rms value of the surface roughness, $\sigma_{surface}$, is given by the relation $C(0) = \sigma^2_{surface}$. The observed variation of $\sigma_{surface}$ (Table I) supports the topological changes from large and small grains in Figs. 2(a) and (b), respectively, to an arrangement of grain clusters in Fig. 2(c). The volume sensitive saturation resistances R_s clearly reflect these structural differences: R_s of sample S2 is about one order of magnitude smaller than those of samples S1 and S3 (Table I).

The deposition rates used in our study (0.037 - 0.056 nm/s) are one order of magnitude lower than usually reported [2, 4], and the substrate heat load is low. Therefore, the temperature is not expected to increase significantly above RT or to vary with Ar pressure. The slight decrease of the deposition rates with increasing Ar pressure (while all other parameters are kept constant) is due to the accumulation of charged particles near the target caused by magnetic confinement and due to more collisions between the ejected particles and the Ar gas. The mean free path varies in the pressure range from 0.34 to 1.70×10^{-2} mbar between about 3.0 and 0.5 cm and is always smaller than the target-substrate separation of 6 cm. Thus, the pressure increase results in a lower average energy and a broader angular distribution of the particles arriving at the substrate [4]. The reduced energy leads to less surface mobility of the deposited adatoms and a higher nucleation density. Therefore, the grain size decreases with pressure and the grain density increases. This behavior is clearly observed for samples S1 and S2 in Figs. 2(a) and (b). The broadening of the angular distribution eventually leads to intergrain shading [4] which gives rise to a morphology with hillocks or clusters and voids on a length scale larger than the grain size. We relate the undulated topography of sample S3 in Fig. 2(c) to this intergrain shading effect. The increase in R_s by almost one order of magnitude for highest and lowest pressures (Table I) supports the described structural changes with voids or high-resistive boundaries between large grains for S1 and between grain clusters for S3. Intergrain magnetic interactions within grain clusters of the NiFe and Co layers may cause incoherent magnetic reversal rotation [5] of the clusters which explains the lower coercivity for sample S3 [Fig. 1(a)].

In conclusion, the GMR ratio of NiFe/Cu/Co pseudo spin-valves prepared by dc magnetron sputtering has been optimized using an intermediate Ar pressure. The non-monotonic dependence of the GMR ratio on the Ar pressure results from (i) the grain size variation and (ii) the onset of grain cluster formation due the intergrain shading. Both effects have an influence on the spin-independent scattering rate as reflected by variations of the saturation resistance.

[1] C. Dupas, P. Beauvillain, C. Chappert, J. P. Renard, F. Trigui, P. Veillet, E. Vélu, and D. Renard , J. Appl. Phys. **67**, 5680 (1990).
[2] S. Bae, J. Li, J. H. Judy, and S. Zurn, Appl. Phys. Lett. **77**, 3435 (2000).
[3] T. E. Sheridan, M. J. Goeckner, and J. Goree, Appl. Phys. Lett. **57**, 2080 (1990).
[4] J. A. Thornton, J. Vac. Sci. Technol. 11, 666 (1974).
[5] R. W. Vook, Int. Met. Rev. **27**, 209 (1982).

The Electronic Structure of Artificial Quasi-One Dimensional Systems

L. Baumgarten, Ch. Zilkens
Institute "Electronic Properties"

The electronic structure of submonolayer coverage of Copper on W(110) stepped surfaces has been investigated using angle resolved photoelectron spectroscopy. For coverages around 0.1 monolayers a Cu related electronic structure near the Fermi edge shows dispersion along and no dispersion perpendicular to the step edge direction. We interpret this behavior as an indication for atomic chain formation of the Copper atoms along the Tungsten steps.

Over the past decade there was great success in the technical application of quasi two-dimensional systems (layers and multilayers). Magnetoresistance devices, based on the exchange interaction of ferromagnetic layers coupled through an intermediate layer are nowadays standard for reading magnetic storage discs. The next step towards an application specific material design is expected from a further reduction of dimensionality. Equivalent to the history of two dimensional systems more recently pure research first paid attention to one and zero dimensional systems (atomic chains and quantum dots). The interest, especially in metallic chains, is of principle character. Such systems should show pronounced instabilities in magnetic and electron phonon interaction as well as a different electron-electron interaction behavior near the Fermi edge, known as "Luttinger liquid". There are mainly three methods in preparing quasi-one-dimensional systems. Lithography is the common technique in semiconductor device applications. In pure research usually two methods are used. The self assembling of adsorbates on single crystalline surfaces [1] (O/Cu(110); Au/Ni(110)) or step edge decoration of vicinal surfaces by molecular beam epitaxy [2]. Especially step edge decoration offers a wide range of choice in materials for preparing metallic chains. The principle of this method is shown in figure 1. A single crystal, slightly miscut towards a low index direction, is used as a substrate for molecular beam epitaxy. The miscut results in the formation of terraces separated by steps. The step density depends on the miscut angle. For specific preparation conditions step flow of the adsorbate is expected. This means, deposited adsorbate atoms move across the terrace towards the step. The aim is to prepare atomic chains along the steps. The difficulty is to find the specific preparation conditions depending on adsorbate and substrate material, step edge orientation, substrate temperature, etc. We investigated the coverage dependant electronic structure of Cu on vicinal W(110) surfaces using angle resolved photoelectron spectroscopy. The choice of tungsten as substrate material was governed by its stability against interdiffusion and alloying as well as the fact that nearly all d-metals can be grown as single crystalline films on a flat W(110) surface.

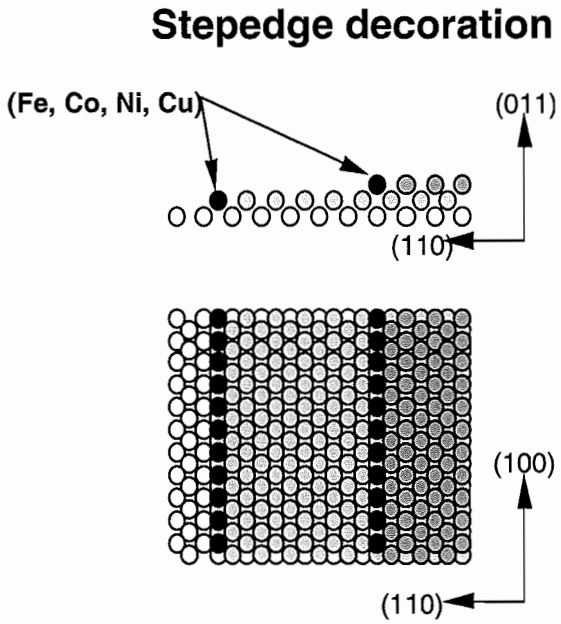

Fig.1: Ideal metal chains on a stepped W(110) surface.

Photoemission experiments are performed at the DELTA storage ring (Dortmund, Germany). Photoelectron spectra are recorded by a Scienta SES 200 analyzer. The samples are prepared by in situ molecular beam epitaxy. From submonolayer to monolayer coverages the gradual development of the electronic structure from a quasi-one to a two dimensional system is analyzed. For coverages around 0.1 monolayer a series of energy and momentum dependent spectra in the vicinity of the Fermi edge are shown in figure 2. The Cu related feature is enhanced by a subtraction of the tungsten background. The Cu related electronic state near the Fermi edge shows dispersion only for electron momenta along the step edge direction. This is expected for a one-dimensional system since the electrons can only move along the chain. Thus, this behavior is the first indication of a quasi-one-dimensional electronic state of Cu on vicinal W(110).

In summary, this work demonstrates that molecular beam epitaxy onto regular stepped substrates can be an

useful method for preparing and investigating a variety of artificial quasi-one dimensional materials. Thus in combination with angle resolved photoelectron spectroscopy experimental electron-electron and electron-phonon interaction parameter should be available for a variety of materials. Finally we acknowledge the help of the DELTA staff. This was one of the first successful experiments at the DELTA storage ring and shows the availability of an additional synchrotron radiation source for user applications.

[1] C. Pampuch et al. Phys. Rev. Lett. **85**, 2561
[2] A. Dallmeyer et al. Phys. Rev. **B61**, R5133

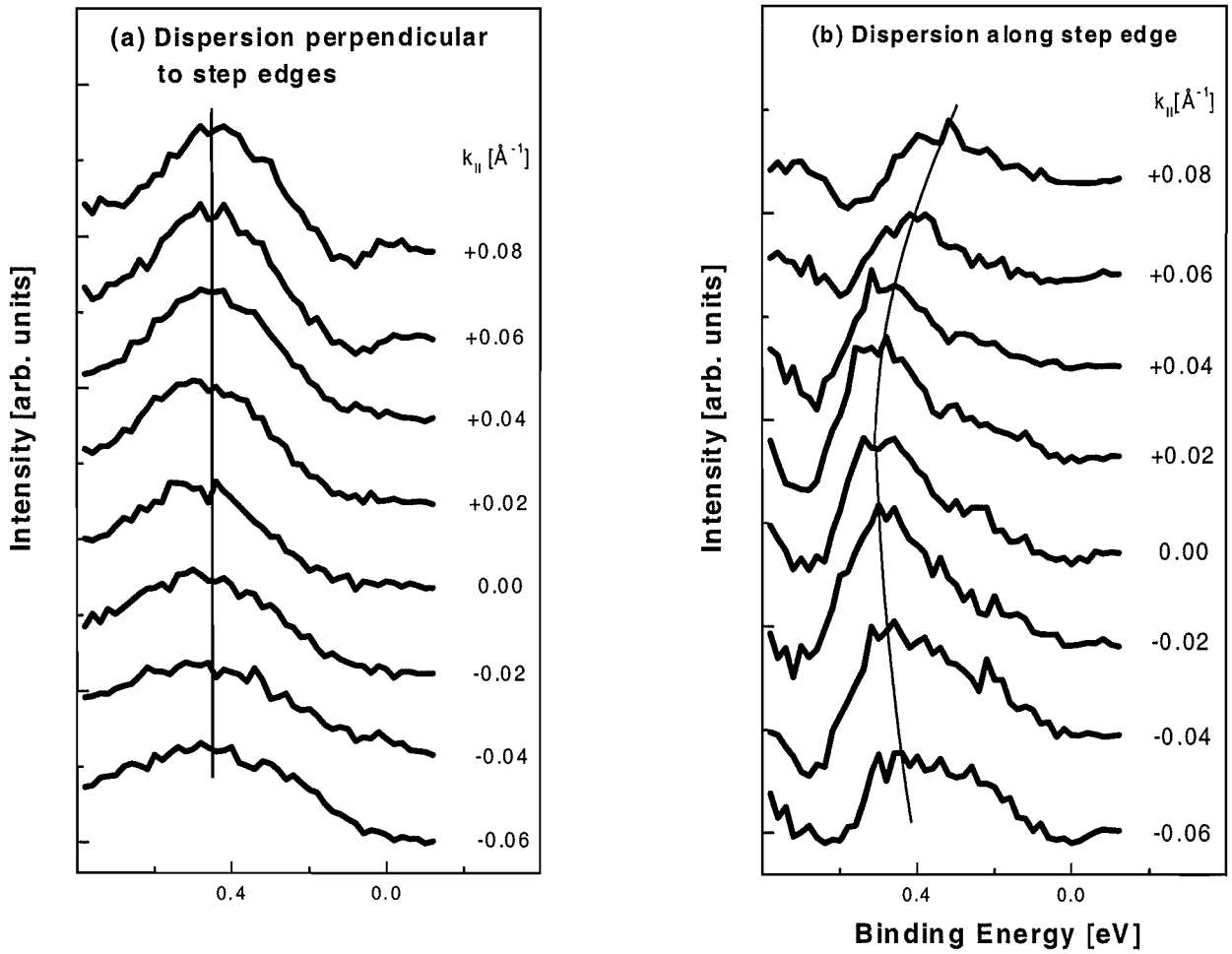

Fig.2: Photoelectron difference spectra of 0.1 monolayer Cu on stepped W(110).
The dispersion of the Cu related state (a) perpendicular and (b) along the step edge direction of the W(110) vicinal surface is shown.

Detection of ferromagnetic spin structure of Manganese in an exchange biased IrMn/CoFe Bilayer

J. Morenzin and S. Cramm,
Institute "Electronic Properties"

D. Schondelmaier, H.A. Dürr and W. Eberhardt
BESSY GmbH, Albert- Einstein-Str.15, D - 12489 Berlin

The magnetic properties of an exchange bias layer system are reported, composed of an antiferromagnetic 85 Å IrMn layer and a ferromagnetic 150 Å CoFe layer. An exchange field H_e of 43 Oe was determined by magneto-optic Kerr effect (MOKE). Measurements of the x-ray magnetic circular dichroism (XMCD) at the $L_{2,3}$ edges of Mn and Co show local magnetic moments not only at the Co atoms in the ferromagnetic layer but also at the Mn atoms in the antiferromagnetic layer. The latter can be assigned to uncompensated spins at a part of the Mn atoms at the interface.

More than 40 years ago Meikeljohn and Bean[1] discovered the exchange bias phenomenon, i.e. a shift of the hysteresis loop by a bias field H_e of a ferromagnetic (FM) layer brought in contact with an antiferromagnetic (AF) layer. The effect is ascribed to an uncompensated amount of ferromagnetic spins at the interface layer in the AF. However, even after a large amount of work a microscopic understanding of the effect is not yet established. Experimentally this may be due to the fact that most of the observation methods can not distinguish the small signal of less than a monolayer of uncompensated spins from the magnetic signal of the FM layer. Using x-ray magnetic circular dichroism (XMCD) at high-brilliance 3rd generation synchrotron light sources such as BESSY we show that it is now possible to obtain element specific information on the magnetic moments and to detect even minute magnetic effects at the interface layers of exchange biased samples.

We have measured the XMCD of Manganese and Cobalt in an exchange biased IrMn/CoFe bilayer. The measurements were performed at the IFF - FZ Jülich beamline UE56/1-SGM at BESSY, Berlin, using circular polarized light with an energy resolution of 0.3 eV.

For this study a 200 Å Cu / 85 Å IrMn / 150 Å CoFe /50 Å Cu. sample was prepared on a 1000Å thick SiN membrane by magnetron sputter deposition. The Cu seed layer was needed to cause a notable exchange biasing of the FM CoFe layer after the whole structure was deposited in an applied magnetic field. The Cu capping layer served as a contamination protection of the sample. The hysteresis loop of the sample obtained using the magneto-optic Kerr effect (MOKE) is shown in Fig. 1.

The magnetic field was applied along the easy magnetization direction. We obtain an exchange

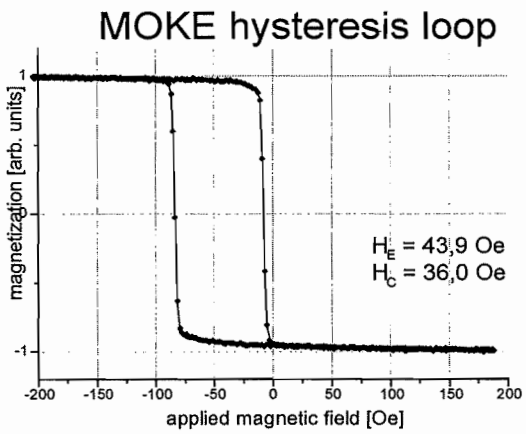

Fig.1 Hysteresis loop of the easy axis of the exchange biased sample.

field of H_e = 43 Oe. The coercivity is H_c = 36 Oe. XMCD spectra were obtained by switching a static magnetic field generated by a pair of permanent magnets mounted in the high-vacuum chamber, switching parallel/ anti-parallel to the easy axis of the sample at each energy step of the spectrum. The sample normal was aligned with a fixed angle of 45° relative to the incident x-rays. The transmitted x-ray intensity, I, was measured with a GaAsP diode mounted behind the sample. The x-ray intensity, I_0, before the sample was measured as the total electron yield of a gold mesh. The normalized absorption spectra at the $L_{2,3}$ edges of Mn and Co are shown in Fig. 2a and Fig. 2c.

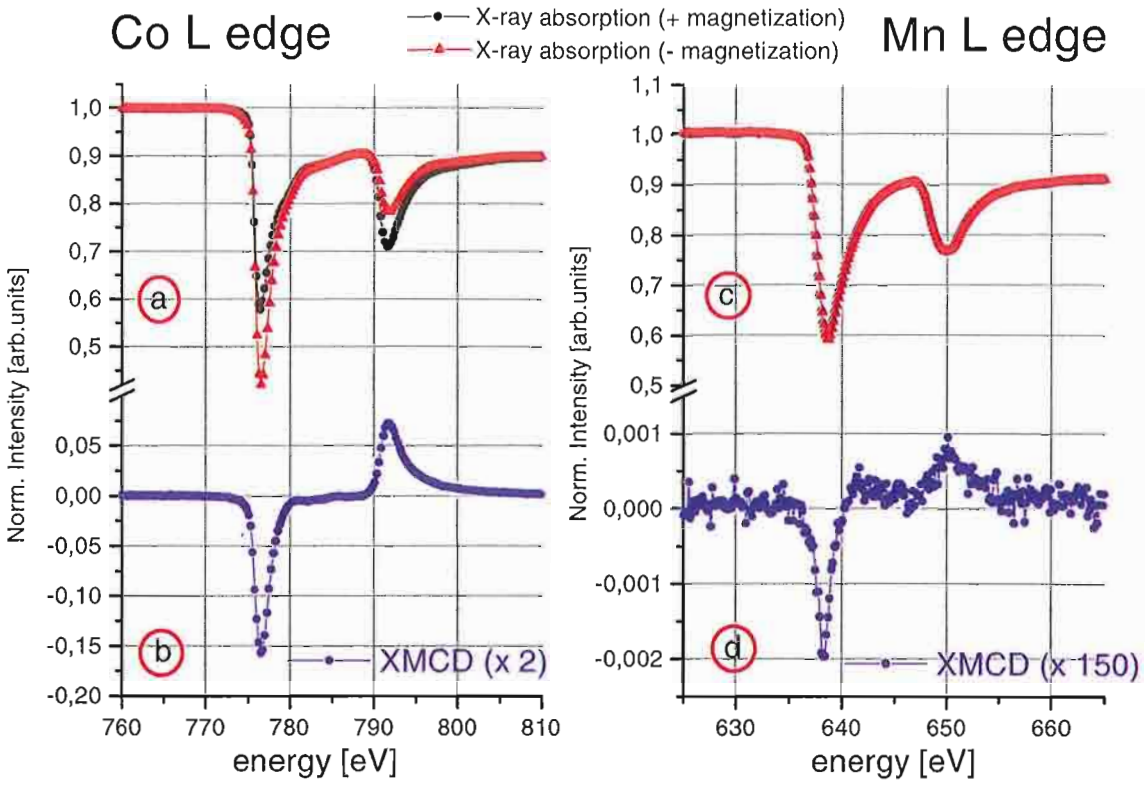

Fig. 2 X-ray absorption (a) & (c) and XMCD (b) & (d) spectra versus photon energy at the $L_{2,3}$ edges of Co and Mn. The XMCD spectra were taken by flipping the magnetization of the sample with help of an applied external field.

The spectra obtained for each magnetization were subtracted from each other to get the XMCD spectra at the Mn and Co L edge respectively. The XMCD spectra are shown in Fig. 2b and Fig. 2d.

We found a strong dichroism of 31% at the Co edge and a dichroism of 0.48% at the Mn edge. For Co a considerable MXCD signal is expected, reflecting a high local magnetic moment around the Co atoms since they are located in a ferromagnetic layer. But in AF IrMn the XMCD signal should be zero.

There are two obvious possible reasons for the non-zero MXCD of Mn: A) Part of the Mn atoms could have diffused into the FM layer, experiencing there a considerable magnetic moment. B) All or part of the interface Mn atoms could be influenced by uncompensated spins. Uncompensated spins are recently discussed to play a key role in the AF/FM coupling in exchange biased systems [2,3].
Other experimental details support explanation B): As mentioned above, a 200 Å Cu seed layer was needed to obtain both exchange bias effect and MXCD signal at the Mn edge. No seed layer or different materials like Ta, Ag or Au resulted in both being much smaller. It is unprobable that the material of the seed layer influences the diffusion of Mn atoms within the Co/Fe layer, while an influence on the growth and morphology at the interface is plausible. Moreover the diffusion is more likely at elevated temperatures rather than at room temperature growth applied here.

We can estimate the number of uncompensated Mn spins assuming that the dichroism is similar on both Mn and Co $L_{2,3}$ edges. Taking into account the thickness of 85 Å of the IrMn and assuming that 3 Å IrMn correspond to one monolayer, the total XMCD signal at the Mn L edge corresponds to a number of Mn atoms from about 13% of a monolayer of IrMn. In conclusion, the data in Fig. 2d support the existence of uncompensated Mn spins at the CoFe/IrMn interface.

---

[1] W.H. Meikeljohn and C.P. Bean, *Phys. Rev.* **102**, 1413 (1956)
[2] K. Takano et. al., *Phys. Rev. Lett.* **79**, 1130 (1997)
[3] W.J. Antel, Jr., F. Perjeru, and G. R. Harp ., *Phys. Rev. Lett.* **83**, 1439 (1999)

Publications in journals

Bode,M.*; Heinze,S.*; Hennefarth,M.*; Pietzsch,O.*; Kubetzka,A.*; Getzlaff,M.*; Wiesendanger,R.*; Nie,X.; Bihlmayer,G.; Blügel,S.
Structural, electronic and magnetic properties of a Mn monolayer on W(110)
Physical review B, 66 (2002), S. 014425

Bode,M.*; Heinze,S.; Kubetzka,A.*; Pietzsch,O.*; Nie,X.; Bihlmayer,G.; Blügel,S.; Wiesendanger,R.*
Magnetization-direction-dependent local electronic structure probed by scanning tunneling spectroscopy
Physical review letters, 89 (2002), S. 237205

Eberhardt,W.
Clusters as new materials
Surface science, 500 (2002), S. 242 - 270

Galanakis,I.; Bihlmayer,G.; Bellini,V.*; Papanikolaou,N.*; Zeller,R.; Blügel,S.; Dederichs,P.H.
Broken bond counting rule for the surface energies of noble metals
Europhysics letters, 58 (2002), S. 751

Gambardella,P.*; Dallmeyer,A.; Maiti,K.; Malagoli,M. C.; Eberhardt,W.; Kern,K.; Carbone,C.
Ferromagnetism in one-dimensional monatomic metal chains
Nature, 416 (2002), S. 301 - 304

Gareev,R. R.; Bürgler,D. E.; Buchmeier,M.; Schreiber,R.; Grünberg,P.
Enhanced antiferromagnetic exchange coupling in Fe/Si/Fe epitaxial trilayers with Fe0.5Si0.5 boundary layers
Applied physics letters, 81 (2002), 7, S. 1264

Gareev,R.R.; Bürgler,D.; Buchmeier,M.; Schreiber,R.; Grünberg,P.
Very strong interlayer exchange coupling in epitaxial Fe/Fe1-xSix/Fe trilayers (x = 0.4-1.0)
Journal of magnetism and magnetic materials, 240 (2002), S. 235 - 237

Grünberg,P.; Bürgler,D.E.; Gareev,R.R.; Olligs,D.; Buchmeier,M.; Breidbach,M.; Kuanr,B.; Schreiber,R.
Experiments on the relation between GMR and interface roughness and on the interlayer exchange coupling across semiconductors
Journal of physics D - applied physics, 35 (2002), S. 2403

Heinze,S.*; Kurz,Ph.; Wortmann,D.; Bihlmayer,G.; Blügel,S.
Complex magnetism in ultra-thin films : atomic-scale spin structures and resolution by the spin-polarized scanning tunneling microscope
Applied physics A, 75 (2002), S. 25

Hoffmann,R.*; Bürgler,D. E.; van Schendel,P.J.A.*; Hug,H. J.*; Martin,S.*; Güntherodt,H.-J.*
Perpendicular magnetic domains of a thin Ag/Fe/Ag film observed by magnetic force microscopy at room temperature
Journal of magnetism and magnetic materials, 250 (2002), S. 32

Klingeler,R.; Bechthold,P. S.; Neeb,M.; Eberhardt,W.
An experimental setup for nondestructive deposition of size-selected clusters
Review of scientific instruments, 73 (2002), 4, S. 1803 - 1808

Klingeler,R.; Pontius,N.; Lüttgens,G.; Bechthold,P. S.; Neeb,M.; Eberhardt,W.
Photoelectron spectroscopy of GdO
Physical review A, 65 (2002), S. 032502

Kuanr,B.; Buchmeier,M.; Bürgler,D.E.; Grünberg,P.
Exchange coupling of MBE grown Fe/Al/Fe trilayers by dynamic techniques
Journal of applied physics, 91 (2002), S. 7209

Kurz,Ph.; Bihlmayer,G.; Hirai,K.*; Blügel,S.
Itinerant magnets on a triangular Cu(111) lattice
Phase transitions, 75 (2002), S. 101 - 112

Kurz,Ph.; Bihlmayer,G.; Blügel,S.
Magnetism and electronic structure of hcp Gd and the Gd(0001) surface
Journal of physics: condensed matter, 14 (2002), S. 6353

Lüttgens,G.; Pontius,N.; Bechthold,P. S.; Neeb,M.; Eberhardt,W.
Photon-induced thermal desorption of CO from small metal-carbonyl clusters
Physical review letters, 88 (2002), S. 076102

Maiti,K.; Malagoli,M. C.; Dallmeyer,A.; Carbone,C.
Finite temperature magnetism in Gd : evidence against a stoner behavior
Physical review letters, 88 (2002), 16, S. 167205

Maus-Friedrichs,W.*; Frerichs,M.*; Gunhold,A.*; Krischok,S.*; Kempter,V.*; Bihlmayer,G.
The characterization of SrTiO3(001) with MIES, UPS(HeI) and first-principles calculations
Surface science, 515 (2002), S. 499 - 506

Olligs,D.; Bürgler,D. E.; Wang,Y. G.; Kentzinger,E.; Rücker,U.; Schreiber,R.; Brückel,Th.; Grünberg,P.
Roughness-induced enhancement of giant magnetoresistance in epitaxial Fe/Cr/Fe(001) trilayers
Europhysics letters, 59 (2002), 3, S. 458 - 464

Paul,A.
Effect of interface roughness on magnetic multilayers of Fe/Tb and Fe/Cr

Journal of magnetism and magnetic materials, 240 (2002), S. 497 - 500

Paul,A.; Lodha,G. S.*
Interface roughness correlation due to changing layer period in Pt/C multilayers
Physical review B, 65 (2002), S. 245426

Pontius,N.; Lüttgens,G.; Bechthold,P. S.; Neeb,M.; Eberhardt,W.
Size dependent hot-electron dynamics in small Pdn-clusters
Journal of chemical physics, 115 (2001), S. 10479

Schondelmaier, D.; Cramm, S.; Klingeler, R.; Eberhardt, W.
Orientation and self-assembly of hydrophobic fluoroalkylsilane
Langmuir, 18 (2002) 16, S. 6242 - 6245

Wortmann,D.; Ishida,H.*; Blügel,S.
An ab initio Green-function formulation of the transfer matrix : application to complex bandstructures
Physical review B, 65 (2002), S. 165103

Wortmann,D.; Ishida,H.*; Blügel,S.
Embedded Green-function approach to the ballistic electron tran sport through an interface
Physical review B, 66 (2002), S. 075113

Wortmann,D.; Kurz,Ph.; Heinze,S.*; Hirai,K.*; Bihlmayer,G.; Blügel,S.
Resolving noncollinear magnetism by spin-polarized scanning tunneling microscopy
Journal of magnetism and magnetic materials, 240 (2002), S. 57 - 63

Wortmann,D.; Kurz,Ph.; Heinze,S.; Hirai,K.*; Bihlmayer,G.; Blügel,S.
Resolving noncollinear magnetism by spin-polarized scanning tunneling microscopy
Journal of magnetism and magnetic materials, 240 (2002), S. 57 - 63

Invited talks

Bihlmayer,G.; Kurz,P.; Blügel,S.
Ab-initio prediction of complex magnetic structures in low dimensions
19th General Conference of the EPS Condensed Matter Division
Brighton: 07.04.2002 - 11.04.2002

Bihlmayer,G.; Kurz,Ph.; Förster,F.; Blügel,S.
Non-collinear ab-initio calculations with the FLAPW-method
ESF/TMR Workshop : Noncollinear Magnetism
Wien: 08.03.2001

Blügel,S.; Heinze,S.*; Wortmann,D.; Bihlmayer,G.
Theorie komplexer magnetischer Strukturen in d¸nnen Schichten und deren Aufl^sung mittels des spin-polarisierten STM
DPG-Frühjahrstagung
Hamburg: 26.03.2001 - 30.03.2001

Bode,M.*; Pietzsch,O.*; Kubetzka,A.*; Heinze,S.*; Kleiber,M.*; Ravlic,R.*; Nie,X.; Blügel,S.; Wiesendanger,R.*
Spin-polarisierte Rastertunnelmikroskopie
DPG-Frühjahrstagung
Hamburg: 26.03.2001 - 30.03.2001

Buchmeier,M.; Kuanr,B.; Gareev,R. R.; Bürgler,D. E.; Grünberg,P.
Studies of strongly coupled epitaxial Fe(001)/Al/Fe trilayers by brillouin light scattering
DPG-Frühjahrstagung
Regensburg: 11.03.2002

Bürgler,D.E.
Interlayer coupling in Fe/Fe-(1-x)Si-x/Fe(001) structures
ICMFS 2002
Kyoto, Japan: 08.03.2002

Förster,F.; Bihlmayer,G.; Blügel,S.
Structure and magnetism of thin Fe films on Cu(100)
Symposium on Surface Science
St. Christoph: 03.03.2002 - 09.03.2002

Förster,F.; Bihlmayer,G.; Blügel,S.
Structure and magnetism of thin Fe films on Cu(100)
Symposium on Surface Science 2002
St. Christoph am Arlberg: 03.03.2002 - 09.03.2002

Gareev,R. R.; Bürgler,D. E.; Buchmeier,M.; Schreiber,R.; Grünberg,P.
Antiferromagnetic interlayer exchange coupling in MBE-grown Fe/Fe1-xSix/Fe structures
DPG-Frühjahrstagung
Regensburg: 11.03.2002

Grünberg,P.; Bürgler,D.E.; Gareev,R.R.; Buchmeier,M.
Magnetic multilayers : exchange coupling of ferromagnetic films across metallic and semiconducting interlayers
281. WE Heraeus Seminar
Wandlitz: 12.06.2002 - 15.06.2002

Heide,M.; Nie,X.; Bihlmayer,G.; Blügel,S.
Ab initio investigations of Fe/W(110) : magnetic structure of domain-walls
DPG-Frühjahrstagung
Regensburg: 11.03.2002 - 15.03.2002

Neeb,M.; Breuer,C.; Klingeler,R.; Blanchard,A.; Wirth,I.; Bechthold,P. S.; Eberhardt,W.

Tunneling spectroscopy on small endohedral metallofullerenes on HOPG
The Electrochemical Society Centennial Meeting
Philadelphia, USA: 12.05.2002 - 17.05.2002

Neeb,M.; Breuer,C.; Klingeler,R.; Blanchard,A.; Wirth,I.; Bechthold,P. S.; Eberhardt,W.
Tunnelspektroskopie an kleinen metalldotierten Fullerenen auf HOPG
DPG-Frühjahrstagung
Regensburg: 11.03.2002 - 15.03.2002

Neeb,M.; Pontius,N.; Lüttgens,G.; Bechthold,P. S.; Eberhardt,W.
Photoelectron spectroscopy on clusters as new materials
New Opportunities in Ultrafast Science using X-rays : Workshop
Napa, CA: 14.04.2002 - 17.04.2002

Wortmann,D.
Spin-polarized ballistic electron transport through an interface by an embedded Green-function method
ESCM 2002 : Electronic Structure and Computational Magnetism
Washington, DC: 14.07.2002 - 17.07.2002

Other talks

Bürgler,D. E.
Zwischenschicht-Kopplung über metallische, amorphe, zusammengesetzte und halbleitende Zwischenschichten
Kolloquium : RWTH Aachen
Aachen: 10.01.2002

Bürgler,D. E.; Grünberg,P.
Structures of thin magnetic films separated by metallic or semiconducting interlayers : growth, structural, magnetic and magnetotransport properties
Seminar : Tohoku University
Sendai, Japan: 12.03.2002

Bürgler,D.E.
Kopplungs- und Transportph‰nomene in magnetischen Nanostrukturen
IFF-Kolloquium : Forschungszentrum Jülich
Jülich: 25.05.2002

Bürgler,D.E.
Magnetische Zwischenschichtkopplung über nicht-metallische Zwischenschichten
SFB-Kolloquium : Universität Bochum
Bochum: 17.10.2002

Bürgler,D.E.; Grünberg,P.
Structures of thin magnetic films separated by metallic or semiconducting interlayers : growth, structural, magnetic and magnetotransport properties
Seminar NTT
Atsugi, Japan: 15.03.2002

Cramm,S.
Installation and first use of the IFF-IEE beamlines
Beiratstreffen im IFF : Forschungszentrum Jülich
Jülich: 21.03.2002

Damm,T.
Fortschritte Ionenstrahl-Sputteranlage
BMBF-Leitprojekt "Magneto-Elektronik"
Bielefeld: 29.05.2002

Grünberg,P.
Experiments on the relation between GMR and interface roughness and on the interlayer exchange coupling across semiconductors
NTT
Tokyo, Japan: 13.03.2002

Grünberg,P.
Interlayer exchange coupling across metals and insulators
Kolloquium : Universite Paris Sud
Paris, France: 31.10.2002

Grünberg,P.
Magnetische Multilagen
Rundgespräch Schichtsysteme
Bad Honnef: 14.02.2002

Grünberg,P.; Bürgler,D.E.
Experiments on the relation between GMR and interface roughness and on the interlayer exchange coupling across semiconductors
Institute for Materials Research
Sendai, Japan: 11.03.2002

Neeb,M.; Pontius,N.; Lüttgens,G.; Bechthold,P. S.; Eberhardt,W.
Time-resolved photoelectron spectroscopy on clusters
BESSY FEL Workshop
Berlin: 04.12.2002

Posters

Breidbach,M.; Olligs,D.; Bürgler,D.E.; Schreiber,R.; Grünberg,P.
Roughness-induced enhancement of giant magnetoresistance in epitaxial Fe/Cr/Fe(001) trilayers
HGF-Workshop 'Kondensierte Materie' : Forschungszentrum Jülich
Jülich: 06.11.2002

Buchmeier,M.; Kuanr,B. K.; Dassow,H.; Bürgler,D. E.; Grünberg,P.
Studies of strongly coupled epitaxial Fe(001)/Al/Fe trilayers by brillouin light scattering
3-Königs-Treffen : WE-Heraeus 2002

07.01.2002 - 09.01.2002

Buchmeier,M.; Kuanr,B.K.; Schreiber,R.; Bürgler,D.E.; Grünberg,P.
Studies of strongly coupled epitaxial Fe(001)/Al/Fe trilayers by Brillouin Light Scattering
ICMFS 2002
Kyoto, Japan: 05.03.2002

Buchmeier,M.; Kuanr,B.K.; Schreiber,R.; Bürgler,D.E.; Grünberg,P.
Studies of strongly coupled epitaxial Fe(001)/Al/Fe trilayers by Brillouin Light Scattering
HGF-Workshop 'Kondensierte Materie' : Forschungszentrum Jülich
Jülich: 06.11.2002

Bürgler,D. E.; Gareev,R. R.; Buchmeier,M.; Schreiber,R.; Grünberg,P.
Interlayer exchange coupling across iron-silicide spacers with varying Si content
Gordon Research Conference on Magnetic Nanostructures
Il Ciocco, Italien: 28.04.2002 - 03.05.2002

Cramm,S.
First experiments and tests at beamline Ue56/1
BESSY User Meeting
Berlin: 09.12.2002

Damm,T.; Paul,A.; Bürgler,D.E.; Grünberg,P.; Jia,C*
Ion-beam and magnetron sputtering for the preparation of magnetic multilayers
HGF-Workshop 'Kondensierte Materie' : Forschungszentrum Jülich
Jülich: 06.11.2002

Dassow,H.; Bürgler,D.E.; Grünberg,P.; Steffen,A.*; Lehmann,R.*; van der Hart,A.*
Fabrication of nanocontacts for current induced remagnetization of Fe/Cr/Fe layers
HGF-Workshop 'Kondensierte Materie' : Forschungszentrum Jülich
Jülich: 06.11.2002
I02

Gareev,R. R.; Bürgler,D. E.; Buchmeier,M.; Schreiber,R.; Grünberg,P.
Interlayer exchange coupling in Fe/FeSi/ /Si/FeSi/Fe structures with combined metallic- and insulating-type spacers
MORIS 02 : Magneto Optical Recording International Symposium
05.05.2002 - 08.05.2002

Gareev,R.R.; Bürgler,D.E.; Pohlmann,L.; Buchmeier,M.; Schreiber,R.; Grünberg,P.; Cramm,S.; Qin,Y.L.*; Jia,C.L.*; Siegel,M.*; Eisebitte,S.*; Zimina,A.
Magnetic interlayer coupling across non-metallic spacer layers
HGF-Workshop Kondensierte Materie : Forschungszentrum Jülich
Jülich: 06.11.2002

Gareev,R.R.; Pohlmann,L. L.; Stein,S.; Bürgler,D.E.; Grünberg,P.
Tunneling across epitaxial Fe/Si/Fe structures with strong antiferromagnetic coupling
MMM 2002 : 47th Annual Conference on Magnetism & Magnetic Materials
Tampa, Fla.: 11.11.2002 - 15.11.2002

Gareev,R.R.; Pohlmann,L.; Stein,S.; Bürgler,D.E.; Grünberg,P. A.
Tunneling across epitaxial Fe/Si/Fe structures with strong antiferromagnetic coupling
47th Annual Conference on Magnetism & Magnetic Materials
Tampa, Florida: 11.11.2002 - 15.11.2002

Heide,M.; Bihlmayer,G.; Blügel,S.
Magnetic structure of domain walls in ultrathin Fe films on the W(110) surface
DPG-Frühjahrstagung
11.03.2002 - 15.03.2002

Heide,M.; Heinze,S.*; Nie,X.; Bihlmayer,G.; Blügel,S.
Ab initio investigation of Fe/W(110) : magnetism, domain-walls, STM-images
3-Königs-Treffen : WE-Heraeus 2002
07.01.2002 - 09.01.2002

Heide,M.; Heinze,S.*; Nie,X.; Bihlmayer,G.; Blügel,S.
Ab initio investigations of Fe/W(110) : magnetism, domain-walls, STM-images 269
WE-Heraeus Seminar on Magnetism on the Sub-Micrometer Scale : Interactions and Microscopy
Bad Honnef: 07.01.2002 - 09.01.2002

Heide,M.; Nie,X.; Bihlmayer,G.; Blügel,S.
Ab initio investigations of Fe/W(110) : magnetic structure of Domain-Walls
WE Heraeus Seminar
Berlin: 11.06.2002 - 15.06.2002

Heide,M.; Nie,X.; Bihlmayer,G.; Blügel,S.
Ab initio investigations of Fe/W(110) : magnetic structure of domain-walls
2nd Annual Meeting of the RTN (Computational Magnetoelectronics)
Oleron Island, France: 05.10.2002 - 09.10.2002
ügel,S.
Ab initio investigations of Fe/W(110) : magnetic structure of domain-walls 281
WE-Heraeus Seminar on Spin-Orbit Interaction and Local Structure
Wandlitz: 12.06.2002 - 15.06.2002

Paul,A.; Damm,T.; Bürgler,D.E.; Stein,S.;
Kohlstedt,H.; Grünberg,P.
Correlation of magnetotransport and structure evolution in sputtered Co/Cu multilayers
HGF-Workshop Kondensierte Materie : Forschungszentrum Jülich
Jülich: 06.11.2002

Wortmann,D.; Bihlmayer,G.; Blügel,S.
A transfer matrix method for ballistic transport : MgO/Fe (001)
19th General Conference of the EPS Condensed Matter Division
Brighton: 07.04.2002 - 11.04.2002

Wortmann,D.; Ishida,H.*; Blügel,S.
A transfer matrix method for ballistic transport : MgO/Fe(001)
Physical Society Meeting of the European Physical Society CMD19CMMP
Brighton, UK: 07.04.2002 - 11.04.2002

Wortmann,D.; Ishida,H.*; Blügel,S.
An embedded Green-function approach to the ballistic electron transport through an interface
RTN Magnetoelectronics Mid-Term Meeting
Oleron, France: 05.10.2002 - 09.10.2002

Wortmann,D.; Ishida,S.*; Blügel,S.
An embedded Green function approach to the ballistic electron transport through an interface
Trends in Nanotechnology Conference
Santiago de Compostela, Spain: 09.09.2002 - 13.09.2002

Pd.D. Theses

Zilkens, C.
Gestufte Oberflächen und Quasieindimensionale Strukturen Photoemission and 3d Metallen auf W(110)
2002
Köln, Univ., Diss., 2002

Institute for Solid State Research (IFF)

Research Center Jülich GmbH

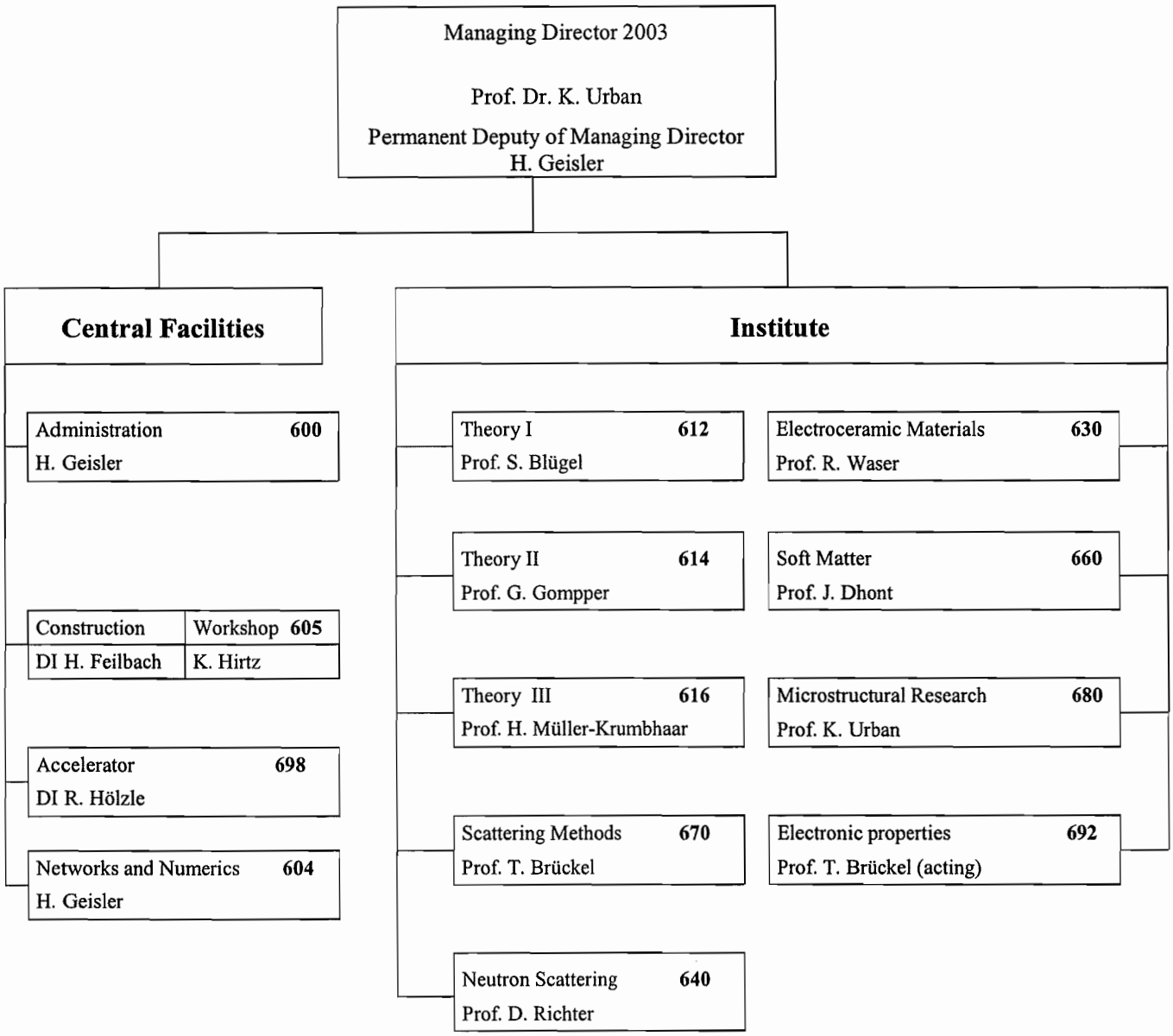

01.01.2003

Scientific Advisory Board 2003

The 2003 meeting of the Scientific Advisory Board will take place on the 03./04. April 2003. Currently, the board consists of the following members:

Dr. C. **Carlile**, Institute Laue-Langevin, Grenoble, France

Prof. R. **Dronskowski**, RWTH Aachen

Prof. K. **Ensslin**, ETH Zürich

Prof. H. **Eschrig**, IFW Dresden **Chairman**

Prof. S. **Hess**, TU Berlin

Prof. H. **Ibach**, ISG-3

Dr. J. **Joosten**, DSM Research, Geleen, NL

Prof. H. **von Löhneysen**, Forschungszentrum Karlsruhe

Prof. M. **Manninen**, University of Jyväskyla, Finland

Prof. T. **Nattermann**, Universität zu Köln

Prof. W. **Press**, Universität Kiel **Vice Chairman**

Dr. J. **Rieger**, BASF, Ludwigshafen

Prof. L. **Singheiser**, Forschungszentrum Jülich, IWV-2

Dr. K. **Sommer**, Bayer AG, Leverkusen

Prof. E. **Umbach**, Universität Würzburg

Prof. M. **Wuttig**, RWTH Aachen

Prof. P. **Wyder**, Centre National de la Recherche Scientifique (MPI), Grenoble, France

Personnel 2002/2003

Staff members (centrally financial)	
- **Scientific Staff**	**98**
including those funded externally	15
- **Technical Staff**	**57**
including those funded externally	2
Post-doc (HGF)	**18**
including those funded externally	3
Staff members of service-groups	**47**
Administrations incl. Secretaries	**17**
Graduate students	**48**
including those funded externally	5
Diploma students	**10**
Trainees	**27**
Guests Scientists staying for two weeks or longer	**65**
Invited lectures	**105**

IFF-Scientists Teaching at Universities

Lecturer:	University:
Dr. A. Baumgärtner	Duisburg
Prof. P.S. Bechthold	Köln
Prof. S. Blügel	Osnabrück
Prof. Th. Brückel	Aachen
Dr. D. Bürgler	Köln
Prof. U. Buchenau	Düsseldorf
Prof. P. Dederichs	Aachen
Prof. J.K.G. Dhont	Düsseldorf
Dr. P. Ebert	Aachen
Dr. P. Ehrhart	Aachen
Prof. E. Eisenriegler	Düsseldorf
Prof. G. Gompper	Köln
Prof. P. Grünberg	Köln
Dr. H. Kohlstedt	Köln
Dr. H. Lustfeld	Duisburg
Prof. H. Müller-Krumbhaar	Aachen
Prof. G. Nägele	Konstanz
Prof. D. Richter	Münster
Prof. T. Schober	Aachen
Dr. H. Schroeder	Aachen
Prof. K. Schroeder	Aachen
Dr. G. Schütz	Bonn
Dr. W. Schweika	Aachen
Prof. K. Urban	Aachen
Prof. R. Waser	Aachen
Dr. S. Wiegand, Frau	Bremen
Prof. R. Winkler	Ulm
Dr. R. Zorn	Münster
Dr. O. Seeck	Kiel (vertretungsweise)

List of IFF-Scientists on leave 2002

Dr. Günter Goerigk	HASYLAB at DESY, Hamburg, Germany
Dr. Dirk Hamann	HASYLAB at DESY, Hamburg, Germany
Dipl.-Ing. György Kali	ILL Grenoble, France
Dr. Winfried Kockelmann	Rutherford Appleton Laboratory, Chilton, England
Dr. Rainer Lässer	Forschungszentrum Karlsruhe, Germany
Matthias Paeßens	Universität Nancy, France
Maikel Christian Rheinstädter	ILL Grenoble, France
Julio Rodriguez y Contreras	Penn State University, Pennsylvannia, USA
Dr. Wolfgang Schmidt	ILL Grenoble, France
Dr. Oliver Hermann Seeck	HASYLAB at DESY, Hamburg, Germany
Richard Willmann	Weizmann Institute, Israel
Daniel Wortmann	Nihon University, Japan

List of IFF-Scientists

(G: Guests; GS: Graduate students)

Akola, Jaakko Eemeli	(Theory I, G)
Allakhiarov, Elchad	(Theory II)
Antons, Armin	(Theory III)
Arbe, Maria	(Neutron Scattering, G)
Atodiresei, Nicolae	(Theory III, GS)
Auth, Thorsten	(Theory II, GS)
Axelrod, Leonid	(Scattering Methods, G)
Babik, Waldemar	(Scattering Methods, GS)
Balanetskyy, Sergiy	(Microstructure Research, GS)
Ballone, Pietro	(Theory I, G)
Baud, Stephanie	(Electronic Properties, G)
Biehl, Ralf	(Neutron Scattering)
Bihlmayer, Gustav	(Theory I)
Blanchard, Ariane Jeanne	(Neutron Scattering, GS)
Bolten, Dierk	(Electroceramic Materials)
Bos, Johanna	(Scattering Methods)
Botti, Alberto	(Neutron Scattering, G)
Breidbach, Michael Peter	(Electronic Properties, GS)
Buitenhuis, Johan	(Soft Matter)
Bukhvalov, Danil	(Theory I, G)
Bürgler, Daniel-Emil	(Electronic Properties)
Burkhardt, Theodore	(Theory II, G)
Byelov, Dmytro	(Neutron Scattering, GS)
Carletto, Philippe	(Soft Matter, G)
Chang, Lieh-Jeng	(Scattering Methods)
Chen, Guangxin	(Neutron Scattering, GS)
Chen, Jiachao	(Scattering Methods)
Cherstvy, Andrey	(Theory II)
Colmenero, Juan	(Neutron Scattering, G)
Corcoran, Derek	(Electroceramic Materials, G)
Da Silva, Juarez L.F.	(Theory III)
Damm, Thorsten	(Electronic Properties, GS)
Dassow, Henning	(Electronic Properties, GS)
di Napoli, Solange	(Theory I, G)
Dittmann, Regina	(Electroceramic Materials)
Drovosekov, Alexey	(Electronic Properties, G)
Eliashberg, Guerassim	(Electroceramic Materials, G)

Elsebrock, Ralf	(Electroceramic Materials)
Fetters, Lewis J.	(Neutron Scattering, G)
Fitsilis, Fotios	(Electroceramic Materials)
Fitsilis, Michael	(Electroceramic Materials, GS)
Freiwald, Mirko	(Electronic Properties, GS)
Frielinghaus, Heinrich	(Neutron Scattering)
Galanakis, Iosif	(Theory III, G)
Gareev, Rashid	(Electronic Properties, G)
Gerber, Andreas Alexander	(Electroceramic Materials)
Goerigk, Günter	(Scattering Methods)
Guo, Xin	(Electroceramic Materials)
Gurevich, Vadim	(Theory III, G)
Gutheim, Frank	(Theory III, GS)
Gwan, Jean-Feng	(Theory II, G)
Hamann, Dirk	(Scattering Methods)
Hartmann, Miks Jan	(Theory III, GS)
He, Jiaqing	(Microstructure Research, GS)
Heggen, Marc	(Microstructure Research, GS)
Heide, Marcus	(Electronic Properties, GS)
Heil, Marco	(Neutron Scattering, GS)
Heinrich, Martine	(Neutron Scattering)
Hermes, Helen	(Neutron Scattering)
Hilbrand, Nicole	(Administration)
Hoffmann-Eifert, Susanne	(Electroceramic Materials)
Höhler, Holger	(Theory III)
Holderer, Olaf	(Neutron Scattering)
Houben, Lothar	(Microstructure Research)
Hüging, Norbert Johann	(Microstructure Research, GS)
Hur, Kahyun	(Theory II, G)
Ioffe, Alexander	(Scattering Methods)
Iordanski, Sergei	(Theory III, G)
Iosselevitch, Alexei S.	(Administration, G)
Istomin, Konstantin	(Scattering Methods, GS)
Kahle, Stefan	(Neutron Scattering)
Kali, György	(Neutron Scattering)
Karthäuser, Silvia	(Electroceramic Materials)
Kirstein, Oliver	(Neutron Scattering)
Kockelmann, Winfried	(Scattering Methods)
Kollmann, Markus	(Soft Matter)
Koroteev, Iouri	(Electronic Properties, G)
Kriegs, Hartmut Oskar Kurt	(Soft Matter)

Kukhar, Vladimir G.	(Electroceramic Materials, G)
Lamura, Antonio	(Theory II, G)
Lang, Peter	(Soft Matter)
Laurati, Marco	(Neutron Scattering, GS)
Lenstra, Tjerk	(Soft Matter, G)
Lettinga, Minne Paul	(Soft Matter)
Lezaic, Marjana	(Theory I, GS)
Liatti, Matvei	(Microstructure Research, GS)
Liu, Yi	(Theory I, G)
Lund, Reidar	(Neutron Scattering, GS)
Lüttgens, Gunnar	(Electronic Properties)
Luysberg, Martina	(Microstructure Research)
Maassen, Ralph	(Theory I, GS)
Machkina, Elena	(Neutron Scattering, G)
Magrez, Arnaud	(Electroceramic Materials, G)
Malinin, Sergey	(Theory III, G)
Marchenko, Vladimir	(Theory III, G)
Massalovitch, Serguei	(Scattering Methods, G)
Mavropoulos, Phivos	(Theory III)
Meier, Gerhard	(Soft Matter)
Mi, Shaobo	(Microstructure Research, GS)
Mihaylova, Milena	(Scattering Methods, GS)
Minar, Jan	(Theory III)
Mokrousov, Yuriy	(Theory I, GS)
Morenzin, Jan	(Electronic Properties)
Murthy, Kalpathy Narayana	(Theory II, G)
Mussawisade, Kiaresch	(Theory II)
Mustafa, Yacoub	(Electroceramic Materials, GS)
Nägele, Gerhard	(Soft Matter)
Niu, Aizhen	(Neutron Scattering, G)
Ohl, Michael	(Neutron Scattering)
Ohly, Christian Andreas	(Electroceramic Materials, GS)
Ohwaki, Tsukuru	(Theory I, G)
Paeßens, Matthias	(Theory II, GS)
Parshin, Dimitrii	(Theory III, G)
Paul, Amitech	(Electronic Properties)
Perßon, Jörg	(Scattering Methods)
Pertsev, Nicholas	(Electroceramic Materials, G)
Pipich, Vitaliy	(Neutron Scattering, GS)
Pithan, Christian	(Electroceramic Materials)
Plakhty, Vladimir	(Scattering Methods, G)

Pohl, Christoph	(Scattering Methods, GS)
Pohlmann, Lars	(Electronic Properties, GS)
Popkov, Vladislav	(Theory II, G)
Qin, Yueling	(Microstructure Research)
Radulescu, Aurel	(Neutron Scattering)
Rathgeber, Silke	(Soft Matter)
Regnery, Stephan	(Electroceramic Materials)
Rheinstädter, Maikel Christian	(Neutron Scattering)
Ripoll Hernando, Marisol	(Theory II)
Ritter, Sigrun	(Electroceramic Materials)
Rodriguez y Contreras, Julio	(Electroceramic Materials, GS)
Rother, Gernot	(Neutron Scattering)
Rottländer, Johannes Peter	(Neutron Scattering)
Sager, Wiebke	(Soft Matter)
Sato, Kazunori	(Theory III, G)
Schlapp, Michael	(Scattering Methods, GS)
Schmitz, Sam	(Electroceramic Materials)
Schütz, Gunter-Markus	(Theory II)
Schwahn, Dietmar	(Neutron Scattering)
Seeck, Oliver Hermann	(Scattering Methods)
Semmler, Ulrich	(Microstructure Research, GS)
Shadrin, Pavel	(Microstructure Research, G)
Shirotov, Vadim	(Microstructure Research, GS)
Stein, Simon	(Electroceramic Materials, GS)
Straube, Ekkehard	(Neutron Scattering, G)
Su, Yixi	(Scattering Methods)
Teren, Andrew R.	(Electroceramic Materials, G)
Tillmann, Karsten	(Microstructure Research)
Toperverg, Boris	(Scattering Methods, G)
Trinkaus, Helmut	(Theory III)
Tuinier, Remco	(Soft Matter)
Vad, Thomas	(Scattering Methods)
Vasco Matías, Enriquo	(Electroceramic Materials, G)
Velikanova, Tamara	(Microstructure Research, G)
Vliegenthart, Gerard Adriaan	(Theory II)
Voigt, Jörg Jakob	(Scattering Methods, GS)
Volokitin, Alexander	(Theory I, G)
Vos, Wessel	(Theory II, G)
Wang, Hao	(Soft Matter, G)
Willmann, Richard	(Theory II, GS)
Wingbermuehle, Jörg	(Electronic Properties, GS)

Winkler, Roland	(Theory II)
Wirth, Ingo	(Electronic Properties, GS)
Wortmann, Daniel	(Electronic Properties, GS)
Wunnicke, Olaf	(Theory III, GS)
Yao, Zhenyu	(Scattering Methods, G)
Zamponi, Michaela	(Neutron Scattering, GS)
Zeiske, Thomas	(Scattering Methods)
Zhang, Haiyan	(Soft Matter, G)
Zhang, Ze	(Microstructure Research, G)
Zilkens, Christopher	(Electronic Properties, GS)

Guest Scientists

Dr. Jaakko Eemeli Akola	University of Jyväskylä, Finnland
Dr. Maria Arbe	Universidad Pais Vasco, Spanien
Dr. Leonid Axelrod	Petersburg Nuclear Physics Institute, Rußland
Prof. Dr. Pietro Ballone	Universität Messina, Italien
Stephanie Baud	Labor de Physics Moleculaire, France
Dr. Alberto Botti	Universität Salerno, Italien
Danil Bukhvalov	Institute of Metal Physics, Ekaterinburg, Rußland
Prof. Theodore Burkhardt	Temple University, Philadelphia, USA
Dr. Philippe Carletto	Universität Nizza-Sophia Antipolis, Frankreich
Prof. Juan Colmenero	Universität San Sebastian, Spanien
Derek Corcoran	University of St. Andrews, Scotland
Solange di Napoli	Universität Salerno, France
Alexey Drovosekov	Landau Institute for Theoretical Phy., Rußland
Dr. Iosif Galanakis	University Louis Pasteuer, France
Dr. Rashid Gareev	Russian Academy of Sciences, GUS
Dr. Gennady P. Gordeev	Petersburg Nuclear Physics Institute, Rußland
Stefan Grosskinsky	TU München,
Prof. Vadim Gurevich	IOFFE-Institut, St. Petersburg, Rußland
Jean-Feng Gwan	National Center for High Performance, Taiwan
Kahyun Hur	Universität Salerno, Korea
Prof. Sergei Iordanski	Landau Institut für Theor. Physik, Rußland
Dr. Satoshi Koizumi	Japan Atomic Energy Research Institute, Japan
Dr. Iouri Koroteev	Universität San Sebastian, Spanien
Dr. Vladimir G. Kukhar	Universität Salerno, Russland
Dr. Antonio Lamura	Universität Salerno, Italien
Hans-Jochen Lauter	ILL Grenoble,
Valeria Lauter	ILL Grenoble, Frankreich
Dr. Yi Liu	Nagoya Technical University, Japan
Dr. Gary W. Lynn	Oak Ridge International Laboratory, USA
Dr. Elena Machkina	Universität Erlangen,
Dr. Arnaud Magrez	Université de Nantes, France

Dr. Sergey Malinin	Landau Institut für theoretische Physik, Rußland
Prof. Vladimir Marchenko	Akademie der Wissenschaften, GUS
Dr. Serguei Massalovitch	Kurchatov Institut, Rußland
Dr. Yuri B. Melnichenko	Oak Ridge International Laboratory, USA
Dr. Kalpathy Narayana Murthy	Indira Gandhi Centre for Atomic Research, Indien
Klaus-Ulrich Neumann	Loughborough University of Technology, England
Dr. Aizhen Niu	Nankai Universität, China
Dr. Tsukuru Ohwaki	University of Tokyo, Japan
Prof. Dr. Dimitrii Parshin	Technische Staatsuniv. St. Petersburg, GUS
Dr. Nicholas Pertsev	Russian Academy of Sciences, Rußland
Dr. Yuri Petrusenko	Inst. of Physics and Technology, Ukraine
Prof. Vladimir Plakhty	Sankt Petersburg Nuclear Physics Inst., GUS
Dr. Vladislav Popkov	Institut for Low Temperature Physics, Ukraine
Dr. Kazunori Sato	Osaka University, Japan
Dr. Pavel Shadrin	Inst. of Radioengineering & Electronics, Rußland
Ion Sivebak	Technical University of Denmark, Dänemark
Prof. Ekkehard Straube	Universität Merseburg, Deutschland
Dr. Jacek Szade	Universität Kattowice,
Dr. Andrew R. Teren	University Chicago, USA
Dr. Boris Toperverg	Petersburg Nuclear Physics Institute, Rußland
Dr. Enriquo Vasco Matías	Universität Salerno, Spanien
Prof. Tamara Velikanova	National Academy of Sciences of Ukraine, Ukraine
Prof. Alexander Volokitin	State Technical University Samara, Rußland
Wessel Vos	Universität Wagenigen, Niederlande
Prof. Enge Wang	Institut of Physics, China
Dr. Hao Wang	Nankai Universität, China
Zhenyu Yao	China Institute of Atomic Energy, China
Prof. Dr. Haiyan Zhang	Universität Salerno, China
Prof. Dr. Ze Zhang	Beijing University, China

Spring Schools of the IFF

Beginning in 1970, our institute has organized an annual two-week Spring School on modern topics in solid state physics.

The topics of the Spring Schools over the past 14 years were:

1990	Solid State research for Information Technology
1991	Physics of Polymers
1992	Synchrotron Radiation for investigating Condensed Matter
1993	Magnetism of Solids and Boundaries
1994	Complex Systems between Atoms and Solids
1995	Electroceramics – Basics and Applications
1996	Scattering Methods for investigating Condensed Matter
1997	Dynamics and Pattern Formation in Condensed Matter
1998	Physics of Nanostructures
1999	Magnetic Layer Structures
2000	Fsec and neV: Dynamics of Condensed Matter
2001	New materials for the information technology
2002	Soft Matter – Complex Materials on Mesoscopic scales
2003	Fundamentals of Nanoelectronics

Spring School 2003 on "Fundamentals of Nanoelectronics"

This event was the 34. spring school offered by the IFF. It took place from 10.-21. March 2003 and included the latest developments in the fields of spectroscopic investigations of the dynamics in condensed matter.

The following lectures were presented (in chronological order):

R. Waser	Introduction
H. Lüth	Basics of Solid State Physics
J. van Delft	Scattering Theory of Conductance
H. Hardtdegen	Atomic Layer Deposition I
R.W. Siegel	Opening Lecture
D. Pfannkuche	Tunneling of Electrons
P. Ebert	Scanning Tunneling Microscopy
S. Blügel	Spin-dependent transport
B. Voigtländer	Self Organization I
B. Beschoten	Spintronic
C. Sotomayor-Torres	Non-Optical Lithography
T. Noll	Future Integrated Circuits
U. Simon	Self Organization III
A. Förster	Atomic Layer Deposition I
A. Thust	High-Resolution Transmission Electron Microscopy
J. Mayer	Electron Spectroscopy
R. Zorn	Atomic Layer Deposition III
F. Gießibl	Atomic Force Microscopy
S. Karthäuser	Self Organisation II
M. Mayor	Molecular Electronics
H. Weber	Transport in Molecular Structures
K. Takayanagi	Metallic Nanowires
M. Indlekofer	Resonant Tunneling Barrier Systems
M. Indlekofer	Semiconductor Nanodots
J. Weis	Single Electron Devices
J. Hoeckstra	Single Electron Tunneling
V. Derycke	C-Nanotubes
R. Waser	Scaling Effects of Memory Principles
Th. Schäpers	Quantum Communication
G. Meyer	Scanning Probe Manipulation Techniques
Th. Wandlowski	Nanostructure Manipulation at Solid Liquid Interfaces

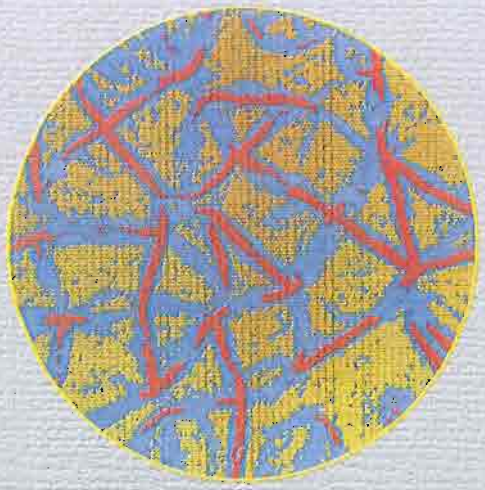

When a thin elastic foil with high shear modulus and low bending rigidity is crumpled by an external force, the stretching and bending energies are not distributed uniformly, but condense into localized folds and conical dislocations. A familiar example for such a material is paper. The crumpling process can be studied very well by computer simulations. The picture shows a circular piece of an originally flat, thin elastic sheet, which has been compressed by a constant isotropic force to about a third of its original (linear) size. A characteristic pattern of folds has formed, which is shown here in the flat reference state. Coloring is used to indicate the sharpness of the folds where yellow means a nearly flat surface, blue indicates weakly curved regions while strongly curved folds are shown in red.

Forschungszentrum Jülich
in der Helmholtz-Gemeinschaft